Design and Synthesis of Selective Butyrylcholinesterase (BChE) Inhibitors for the Development of Radiotracers to Investigate the Role of BChE in Alzheimer's Disease

Dissertation

zur Erlangung des naturwissenschaftlichen Doktorgrades der

Julius-Maximilians-Universität Würzburg

vorgelegt von

Edgar Sawatzky

aus Darmstadt

Würzburg 2016

Eingereicht bei der Fakultät für Chemie und Pharmazie am

_____

Gutachter der schriftlichen Arbeit

1. Gutachter:_____

2. Gutachter:_____

Prüfer des öffentlichen Promotionskolloquiums

1. Prüfer:_____

2. Prüfer:_____

3. Prüfer:_____

Datum des öffentlichen Promotionskolloquiums

_____

Doktorurkunde ausgehändigt am

_____

The presented work has been carried out under supervision of Professor Michael Decker in Pharmaceutical and Medicinal Chemistry at the Institute of Pharmacy and Food Chemistry of the Julius Maximilian University Würzburg between January 2013 and February 2016.

The great tragedy of Science:

The slaying of a beautiful hypothesis

by an ugly fact.

Thomas Henry Huxley (1825-1895)

Publications

Sawatzky, E.; Al-Momani, E.; Kobayashi, R.; Higuchi, T.; Samnick, S.; Decker, M. A Novel Way to Radiolabel Human Butyrylcholinesterase for Positron Emission Tomography through Irreversible Transfer of the Radiolabelled Moiety. *ChemMedChem* **2016**, *11*, 1540-1550. (*cf.* **Appendix 1**)

Sawatzky, E.; Wehle, S.; Kling, B.; Wendrich, J.; Bringmann, G.; Sotriffer, C. A.; Heilmann, J.; Decker, M. Discovery of Highly Selective and Nanomolar Carbamate-Based Butyrylcholinesterase Inhibitors by Rational Investigation into Their Inhibition Mode. *J. Med. Chem.* **2016**, *59*, 2067-2082. (*cf.* **Appendix 2**)

Dolles, D.; Nimczick, M.; Scheiner, M.; Ramler, J.; Stadtmüller, P.; **Sawatzky, E.**; Drakopoulos, A.; Sotriffer, C.; Wittmann, H.-J.; Strasser, A.; Decker, M. Aminobenzimidazoles and Structural Isomers as Templates for Dual-Acting Butyrylcholinesterase Inhibitors and *h*CB2R Ligands to Combat Neurodegenerative Disorders. *ChemMedChem* **2016**, *11*,1270-1283.

Darras, F. H.; Kling, B.; **Sawatzky, E.**; Heilmann, J.; Decker, M. Cyclic Acyl Guanidines Bearing Carbamate Moieties Allow Potent and Dirigible Cholinesterase Inhibition of either Acetyl- or Butyrylcholinesterase. B*ioorg. Med. Chem.* **2014**, *22*, 5020-5034.

Sawatzky, E.; Bukowczan, J.; Decker, M. Investigation into Selective Debenzylation and Ring Cleavage of Quinazoline Based Heterocycles. *Tetrahedron Lett.* **2014**, *55*, 2973-2976. (*cf.* **Appendix 3**)

Sawatzky, E.; Drakopoulos, A.; Rölz, M.; Sotriffer, C. A.; Engels, B.; Decker, M. Experimental and Theoretical Investigations into the Stability of Cyclic Aminals. *Beilstein J. Org Chem.*, Accepted. (*cf.* **Appendix 4**)

Copyrights

Parts of this work have been published previously and are reproduced, adapted and/or modified with permission from:

Documentation of Authorship

All individual contributions for each author to the publications reprinted in this thesis as well as unpublished manuscripts are listed below:

Chapter 3 (Appendix 1)	Sawatzky, E. (1); Al-Momani, E. (2); Kobayashi , R. (3); Higuchi, T. (4); Samnick, S. (5); Decker, M. (6) A Novel Way to Radiolabel Human Butyrylcholinesterase for Positron Emission Tomography through Irreversible Transfer of the Radiolabeled Moiety. *ChemMedChem* **2016**, *11*, 1540-1550.							
Author	**1**	**2**	**3**	**4**	**5**	**6**	**Jeßberger, S.**	**Högger, P.**
Study design/concept development	x					x		
Synthesis of intermediates and precursors	x							
Analytical characterization of intermediates and precursors	x							
IC$_{50}$ determination of reference compounds on *h*BChE and *h*AChE	x							
Time and concentration dependent inhibition of reference compounds on *h*BChE	x							
Plasma stability test of reference compounds	x						x	x
Radiosynthesis of radiotracers		x			x			
Purification and formulation of radiotracers		x			x			
Ex vivo Autoradiography experiments			x	x				
Manuscript writing and correction	x					x		
Supervision of Edgar Sawatzky						x		

Chapter 4 (Appendix 2)	Sawatzky, E. (1); Wehle, S. (2); Kling, B. (3); Wendrich, J. (4); Bringmann, G. (5); Sotriffer, C. A. (6); Heilmann, J. (7); Decker, M. (8) Discovery of Highly Selective and Nanomolar Carbamate-Based Butyrylcholinesterase Inhibitors by Rational Investigation into Their Inhibition Mode. *J. Med. Chem.* **2016**, *59*, 2067-2082.													
Author	**1**	**2**	**3**	**4**	**5**	**6**	**7**	**8**						
Study design/concept development	x							x						
Synthesis of intermediates and test compounds	x													
Analytical characterization of intermediates and test compounds	x													
Enzyme inhibition determination of test compounds on *eq*BChE, *h*BChE and *h*AChE	x													
Time and concentration dependent inhibition of reference compounds on *h*BChE and *eq*BChE	x													
Computational studies/Moleculat modeling studies		x				x								
Sequence comparison of AChE and BChE		x				x								
ORAC Assay			x			x								
Neurotoxicity and –protection of test compounds on murine HT-22 cell line			x			x								
Enantiomeric resolution of the most active compound				x	x									
Manuscript writing	x	x				x	x							
Manuscript correction	x	x			x	x	x							
Supervision of Edgar Sawatzky							x							

Chapter 5	Sawatzky, E. (1); Decker, M. (2) Dual Addressing of Butyrylcholinesterase by Targeting the Catalytic Active Site (CAS) and the Peripheral Anionic Site (PAS). Unpublished.		
Author		1	2
Study design/concept development		x	x
Synthesis of intermediates and test compounds		x	
Analytical characterization of intermediates and test compounds		x	
Enzyme inhibition determination of test compounds on *eq*BChE		x	
Supervision of Edgar Sawatzky			x

Chapter 6 (Appendix 3)	Sawatzky, E. (1); Bukowczan, J. (2); Decker, M. (3) Investigation into Selective Debenzylation and Ring Cleavage of Quinazoline Based Heterocycles. *Tetrahedron Lett.* **2014**, *55*, 2973-2976.			
Author		1	2	3
Study design/concept development		x		x
Synthesis of intermediates and compounds		x	x	
Analytical characterization of intermediates and compounds		x		
Evaluation of reduction conditions		x	x	
Manuscript writing		x		x
Manuscript correction		x		x
Supervision of Edgar Sawatzky				x

Chapter 7 (Appendix 4)	Sawatzky, E. (1); Drakopoulos, A. (2); Rölz, M. (3); Sotriffer, C. A. (4); Engels, B. (5); Decker, M. (6) Experimental and Theoretical Investigations into the Stability of Cyclic Aminals. *Beilstein J. Org Chem.*, Accepted.						
Author		1	2	3	4	5	6
Study design/concept development		x					x
Synthesis of intermediates and test compounds		x		x			
Analytical characterization of intermediates and test compounds		x		x			
Conducting calibration lines of test compounds on HPLC		x					
pH-dependent hydrolysis experiments of test compounds		x					
condensation experiments of test compounds		x					
MoKa calculations of test compounds			x		x		
Quantum mechanics calculations of test compounds			x			x	
Conformational search of test compounds			x		x		
Molecular mechanics ring strain comparison of test compounds			x		x	x	
Manuscript writing		x	x				x
Manuscript correction		x	x		x	x	x
Supervision of Edgar Sawatzky							x

Declaration of Copyrights and Author Contributions

Prof. Dr. Michael Decker   Würzburg, 2016

Edgar Sawatzky   Würzburg, 2016

Acknowledgement

Table of Contents

1. Introduction

1.1 Ageing and Diseases

Until the mid of the 20th century, human mortality in developed countries and industrial nations was often caused by infectious diseases with bacterial, viral or fungal pathogens. Although infectious diseases still exist today, several developments in the medical sector, e.g. vaccination agents or antibiotics, enabled the preventive and curative treatment of these diseases; and in part led to the (almost) entire extinction of several infectious diseases like pox, measles or polio.

However, the challenge in drug development, especially in industrial nations, has a new focus. Continuous improvements in the medical sector as well as the increasing general prosperity in developed countries have caused a vast prolongation of life expectance. In consequence of this demographic change, diseases associated with ageing have become one of the major burdens of the modern society in nowadays. Within the top 10 causes of death reported by the World Health Organization (WHO) in 2012,[1] age related diseases (when excluding cancer as an age related disease) were stated to be the main reasons for mortality in developed countries; with disorders of the cardiovascular system like ischemic heart diseases (ranking 1) and hypertension (ranking 9), stroke (ranking 2), Alzheimer's disease and other forms of dementia (ranking 4), and diabetes mellitus (ranking 8). In addition, age-related non-lethal diseases, like those affecting the locomotory system (e.g. rheumatism, osteoarthritis or osteoporosis) or disorders of the sensory organs (e.g. deafness or blindness) are a vast economical problem causing immense costs for the health care system. Accordingly, the treatment of such diseases has become a hot topic in different interdisciplinary research fields in the last decades. Although symptomatic treatments are partially achieved to some degree, a curative therapy often fails in the majority of cases as the underlying causes are still not yet thoroughly clarified regarding the complex and multi factorial characteristics of age related diseases. Due to this lack of knowledge on the initial pathophysological changes, there is a strong requirement for basic research on the pathogenesis of these diseases in order to understand the triggering, pivotal and preliminary biochemical alterations of disorders. Only such information can help to realize a curative treatment and therefore to increase life quality during aging.

1.2   Alzheimer's Disease

Alzheimer's disease (AD) was reported for the first time in literature in 1907 by the German psychiatrist and neuropathologist Alois Alzheimer.[2] Alzheimer described the clinical patient Auguste Deter to suffer on several psychic symptoms including disorientation, distinct mood changes and loss of her memories. After her death, postmortem studies revealed the deposition of neurofibrilliar bundles as well as senile plaques in her brain (**Figure 1.1**) which were unknown until this date.
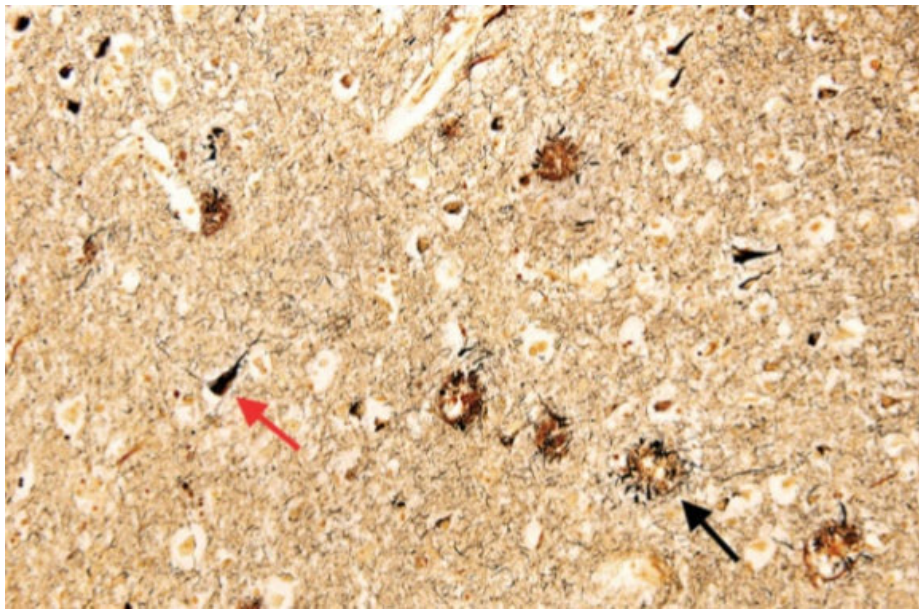
Figure 1.1. Photomicrograph of a temporal cortex postmortem section of a patient with AD indicating the occurrence of senile plaques (black arrow) and neurofibrillary tangles (red arrow). Reproduced with permission from ref. [3], Copyright John Wiley and Sons.

Today, AD is known to be the most common form of dementia (50-75% of all known types of dementia[4]) with aging as the major risk factor.[5-7] In fact, the incidence rate for dementia increases exponentially with age, with the most pronounced increase occurring through the 7th and 8th decades of life.[5] Regarding the general increased prosperity in society in the last few decades and in consequence the resulting longer life expectance, it is not surprising, that the World Alzheimer's Report estimated the prevalence of dementia to triple from 46.8 million cases in 2015 to 131.5 million cases in 2050 (**Figure 1.2**).[8] And further, the world wide societal costs of dementia are estimated to have reached already 818 billion dollars and will dramatically multiply in the future.[8]
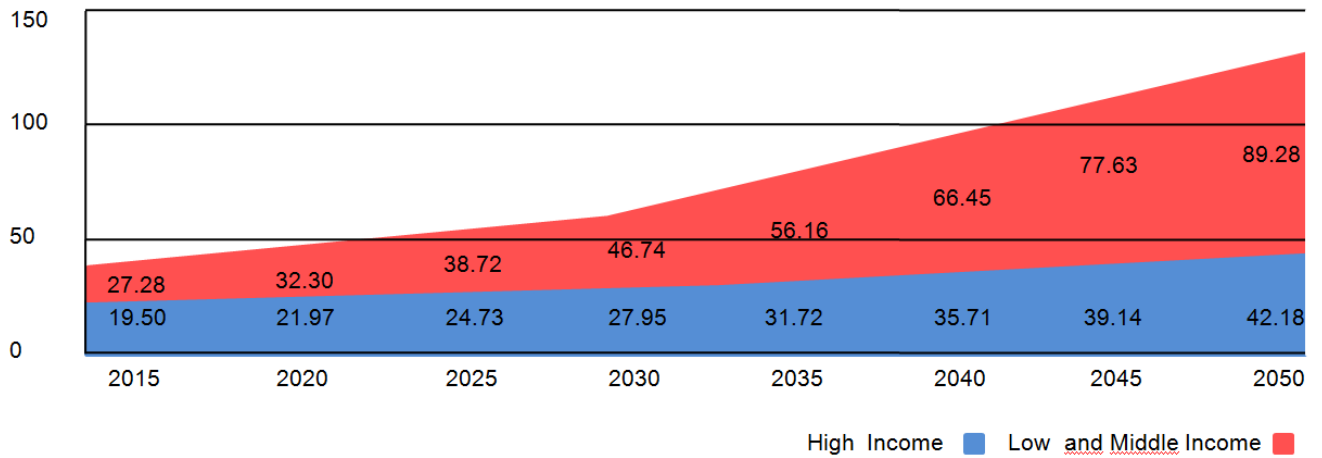
Figure 1.2. The growth in numbers of people with dementia (millions) in high income (HIC) and low and middle income countries (LMIC).[8]

Although the impact of AD is dramatically increasing and several interdisciplinary research fields have intensively focused on the biochemical mechanisms in the development of AD, cure of AD is still impossible to date. Nevertheless, the pathogenesis of AD is mainly determined by specific biochemical changes, including the formation of amyloid-β plaques, the hyperphosphorylation of τ-proteins and their aggregation into neurotoxic fibrillary tangles, oxidative stress caused cell death, neuroinflammations and the synaptic failure due to the imbalance of several neurotransmitter like acetylcholine (ACh) or glutamate.[9-11] The most important biochemical changes as well as their therapeutic consequences will be discussed in the following sections.

1.2.1 Amyloid-β Hypothesis

Since Alois Alzheimer observed in his studies the disposition of neurotic plaques in AD patient's brain, their molecular decomposition and especially their biochemical synthesis have been widely investigated and led to the development to one of the most important theories for the pathogenesis of AD, the amyloid-β (Aβ) cascade hypothesis.[9,11-16]

The amyloid precursor protein (APP) is an integral type I transmembrane protein of neuronal cells with a single transmembrane domain, a large extracellular ectodomain, and a short cytoplasmic tail.[17] The physiological function of APP is not yet completely understood but it is known to be involved in the cell adhesion and to have

a trophic function in neurons.[17-19] Physiological processing of APP (*cf.* nonamyloidogenic pathway in **Figure 1.3**) is mostly mediated on the surface of the cell through the proteolytic enzyme α-secretase, which cleaves APP into the membrane bound C83-fragment and the soluble sAPPα-fragment. The C83-fragment is further cleaved by the integral membrane protein γ-secretease into the p3-fragment and a short C-terminal peptide known as the APP intracellular domain (AICD).[9,20] In addition, APP processing is also possible through a second pathway. In this so called amyloidogenic pathway (**Figure 1.3**), cleavage of APP takes place by β-secretease (often also termed as beta-site amyloid precursor protein cleaving enzyme 1 (BACE-1)) under formation of a sAPPβ-fragment. Successive cleavage of the remaining membrane bound C99-fragment by γ-secretease leads to the release of a 40 to 42 amino acid long peptide segment, called Aβ40 or Aβ42 (depending on its length), respectively.[10,16] Normally, the production of Aβ and its clearance is balanced through the cleavage of Aβ by different proteins,[21-23] but in the course of AD this system is disturbed either by the over expression of Aβ and/or a reduced clearance rate. In consequence, the amount of Aβ is continuously increasing in the extracellular space.
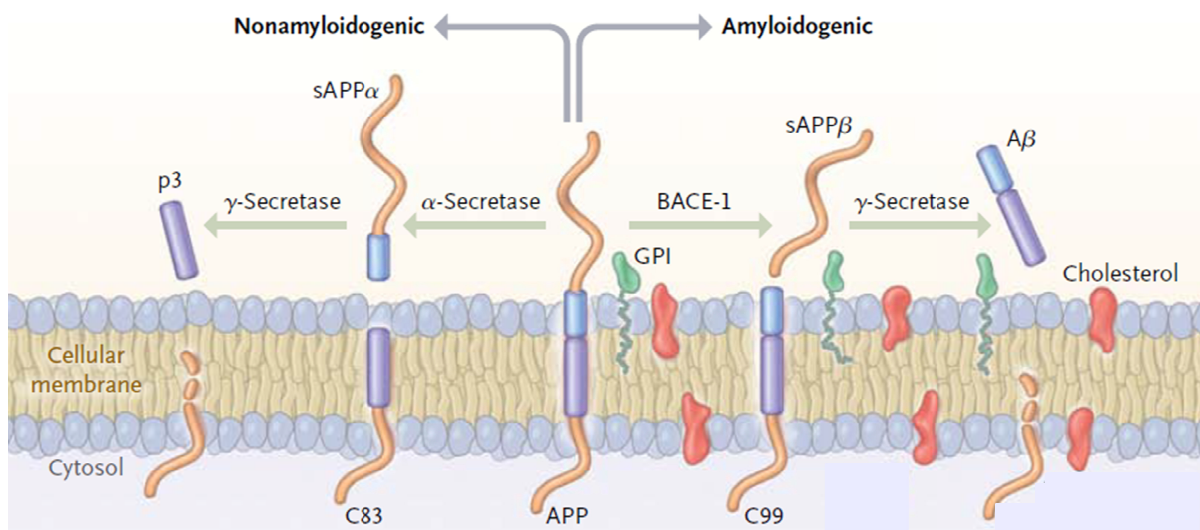
Figure 1.3. Physiological processing pathways of APP. For details see the main text. Reproduced with permission from ref. [9], Copyright Massachusetts Medical Society.

Once the Aβ-system is imbalanced, single Aβ-monomers can self-aggregate into soluble oligomers which further congregate into insoluble Aβ-fibrils and plaques. These insoluble forms of Aβ were long considered to be responsible for neuronal cell death, but recent studies showed an increasing evidence for the pathogenic role of soluble Aβ-oligomers instead of the insoluble plaques.[13] Aβ-oligomers cause synaptic dysfunction by inducing the internalization of the ionotropic *N*-methyl-*D*-aspartate receptor (NMDAR)[24,25] and by interactions

with distinct types of plasma membrane bound receptors.[9,26] Furthermore, several studies showed that Aβ-oligomers can release Ca^{2+} from the endoplasmic reticulum causing mitochondrial dysfunction and mitochondrial induced apoptosis.[27-29]

In the course of AD, the Aβ-cascade hypothesis offers a diversity of feasible therapeutic approaches to reduce the levels of Aβ: 1) Down regulation of APP processing by inhibiting the function of β-secretease or γ-secretease, 2) reduction of the APP biosynthesis on the RNA site, 3) increasing the clearance rate of Aβ, e.g. by antibodies, or 4) interruption of the Aβ-induced signal pathways.[10,12,15] To date, numerous experimental therapeutics have been developed targeting all possibilities of Aβ-oligomer formation and their pathophysological roles in Aβ, but none of them have passed phase 3 clinical trials due to their little clinical benefits.[12,30]

1.2.2 Tau-Protein Hypothesis

Tau (τ) proteins are microtubule associated proteins (MAP). These proteins are localized in the axons of neuronal cells and regulate microtubules assembly to stabilize the cytoskeleton, facilitate axonal transport (e.g. of organelles) and mediate cell signaling.[31-33] The function of τ-proteins is mainly regulated through their phosphorylation (the largest isoforms has 79 putative phosphorylation sites) by a large set of kinases such as tau protein kinase I (GSK3), tau protein kinase II (cdk5), MAP kinase (p38), protein kinase C (PKC), etc..[31] In the healthy neuron, τ-proteins are only little phosphorylated as several phosphatases are balancing this system by dephosphorylation. However, during AD this equilibrium is interrupted resulting in the hyperphosphorylation of τ-proteins (**Figure 1.4**).[32,34]

At the current state, there is an increasing evidence, that hyperphosphorylation of τ-proteins triggers a conformational change resulting in the detachment of τ-proteins from the microtubules.[35,36] Consequently, the integrity of microtubules is impaired followed by a breakdown of intracellular axon transport in neurons.[34] And further, soluble hyperphsophorylated τ-proteins aggregate in the neuronal intracellular space to form filaments and insoluble neurofibrillary tangles (NFT) which both are causing neuronal dysfunction with successive neuronal cell death.[37-39]

Thorough description in literature regarding pathophysological changes associated with tau-proteins enables different therapeutic approaches to prevent τ-protein mediated toxicity: 1) Modulating the τ-protein phosphorylation by inhibiting specific kinases or by increasing the phosphatase activity, 2) inhibition of τ-protein aggregation into toxic oligomers and NFTs, 3) down regulation of τ-protein expression, or 4)

stabilizing of the microtubules.[40,41] However, similar to Aβ-treatment strategies, none of the drug candidates targeting τ-protein pathology were approved to date.
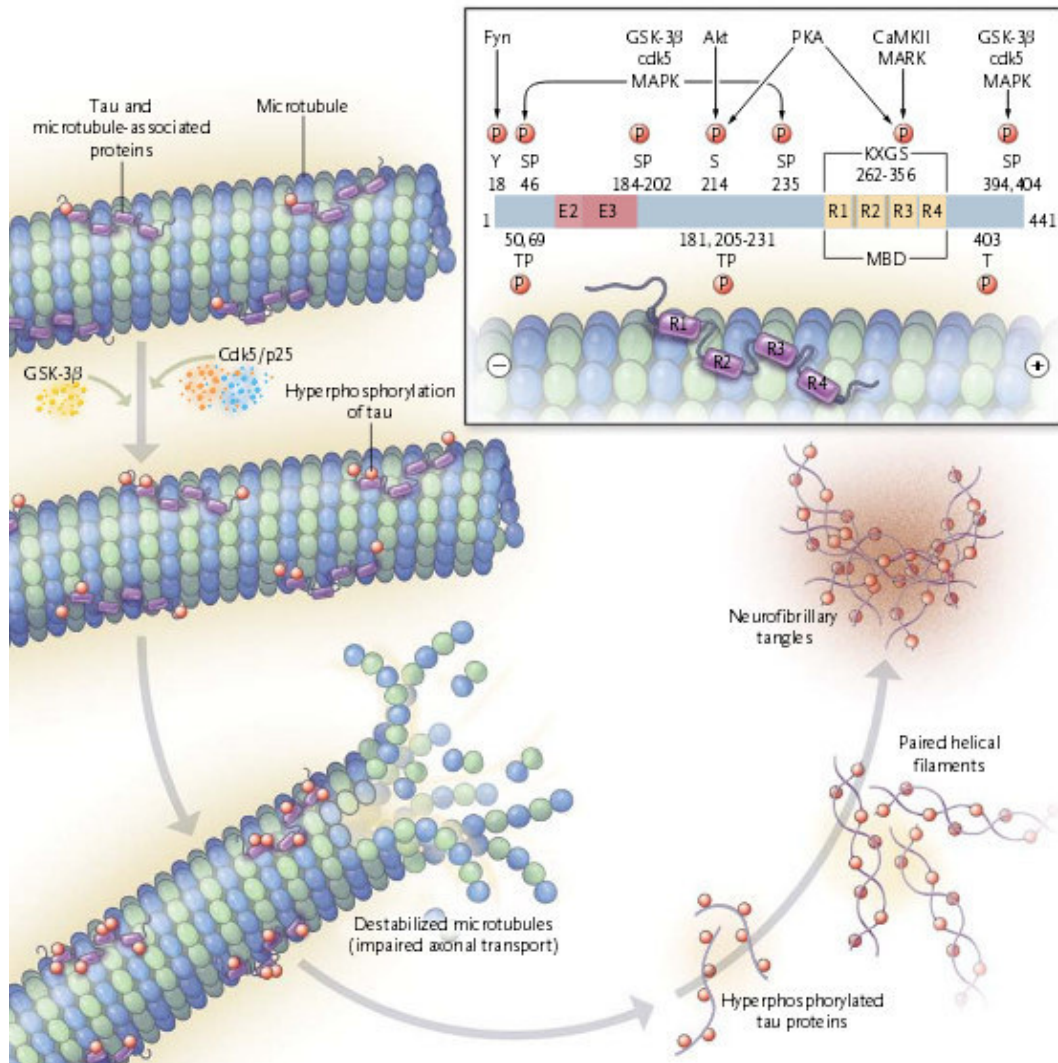
Figure 1.4. Hyperphosphorylation of τ-proteins is triggering the formation of neurofibrillary tangles. Reproduced with permission from ref. [9], Copyright Massachusetts Medical Society.

1.2.3 Oxidative Stress

In a healthy biological system, the formation of reactive oxygen species (ROS) and reactive nitrogen species (RNS) is mainly intracellular induced by complexes I and III of the electron transport chain of mitochondria during metabolism. Not only, but also exogenous sources like UV-light or ionizing irradiations as well as

several endogenous factors are in part responsible for an increased oxidative stress burden.[42,43] Under normal physiological conditions, the ROS production is balanced by an intricate antioxidant defense system including the enzymatic scavengers superoxide dismutase (SOD), catalase (CAT), glutathione peroxidase (GPx) and peroxiredoxins, as well as several low molecular weight ROS scavengers like glutathione or ascorbate.[42,43] Nevertheless, certain physiological levels of ROS are recognized to regulate cell signaling in terms of propagation of cytokine mediated proinflammatory signals, growth-stimulation or induction of apoptosis.[44-46]

During AD, ROS-regulation is disturbed by a defect of mitochondria, in particular a dysfunction of cytochrome-*c* oxidase in complex IV of the electron transport chain. These defects trigger the release of ROS and might further reduce the energy resources. In consequence, free ROS can oxidize and/or peroxidize physiologic important proteins of several cell compartments, thus causing dysfunction and cell damage through toxic oxidation products.[47,48] Beyond the physical damage due to high ROS levels, several signal cascades were activated by oxidative stress inducing cell apoptosis.[49,50] Interestingly, oxidative stress was also reported to be induced by low concentrations of Aβ,[51-53] probably as a result of Aβ's ability to reduce physiological occurring Cu^{II} and Fe^{III} into Cu^{I} and Fe^{II}, respectively, which in turn are the source for ROS formation due to their redox potential.[54,55] Therefore, increased oxidative stress might be directly correlated to the pathogenic APP processing in the course of AD.

Nevertheless, although the involvement of oxidative stress in the pathogenesis of AD is well accepted today, increased cellular damage through ROS is not necessarily a disease inducing cause. Instead, it is normally the result of aging and therefore this process can takes place independently or even much earlier as the first pathological symptoms correlated with AD. It should therefore be noted, that this process is not a rapid development, rather more a continuous progress in the pathological altered as well as the healthy physiological system.

1.2.4 Cholinergic Hypothesis

The cholinergic system is one of the major signal transduction pathways in the central nervous system (CNS), comprising a stimulating function which is essential for cognition abilities, e.g. by encoding new memories or by modulating learning processes.[56-58] Signaling of this system is mediated through the neurotransmitter acetylcholine (ACh), which is biosynthesized in the cytosol of specific neurons, the so called cholinergic neurons, where choline acetyltransferase (ChAT) transfers an acyl group from acetyl-CoA onto choline. During neuronal signaling, ACh is released from vehicles of the presynaptic neuron into the synaptic cleft, where it binds onto two classes of postsynaptic receptors, the muscarinic receptors (mAChR) and the nicotinic receptor (nAChR), both named after their selective agonists muscarine and nicotine, respectively. (**Figure 1.5**)

mAChR are G protein-coupled receptors (GPCRs) which are divided into two groups depending on their downstream signal cascades after activation. Binding of ACh to either M1, M3 or M5-mAChR activates phospholipase C (PLC), which in turn hydrolyses phosphoinositol-1,4,5-biphosphate (PIP2) into two second messengers inositol-1,4,5-triphosphate (IP3) and diacylglycerol (DAG).[59] These second messengers cause Ca^{2+}-influx from the extracellular space as well as Ca^{2+}-release from the endoplasmic reticulum into the cytosol thereby triggering a broad spectra of actions depending on the cell type and the muscarinic receptor subtype.[59-61] Binding of ACh to either M2 or M4-mAChR activates inward rectifying K^+-channels and induces inhibition of the adenyl cyclase (AC) which regulates the molecular amounts of the second messenger cAMP. In general, binding of ACh at the mAChR in the CNS, especially at the M_1-subtype which is the predominant form in the brain, induces the modulation of neurotransmitter release into the cortex and hippocampus as well as the reorganization of functional connectivity.[59,62]
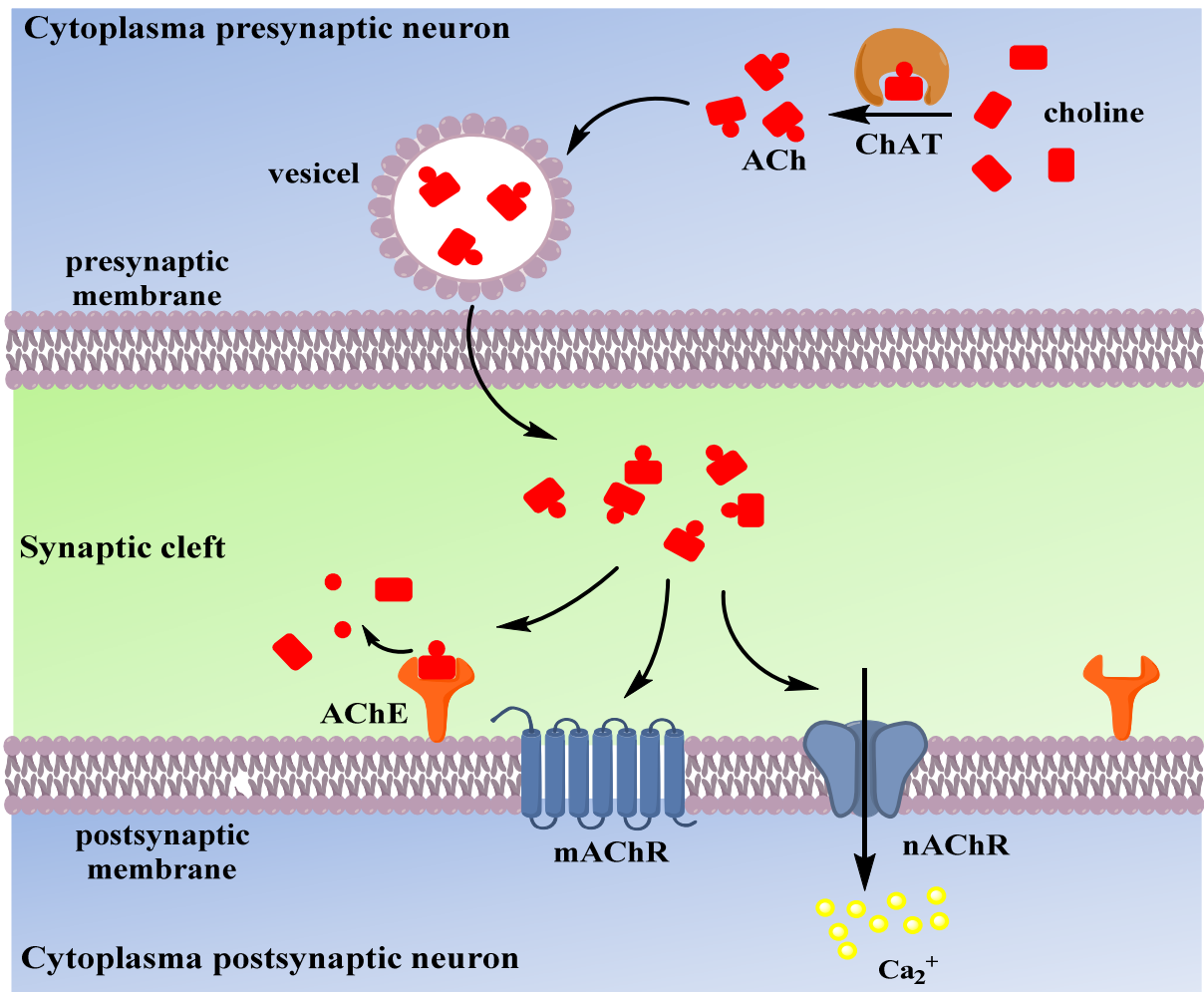
Figure 1.5. Signal pathways of the cholinergic system.

On the other hand, activation of the ligand-gated ionotropic nAChR by ACh induces increased cytoplasmic Ca^{2+}-levels over three mechanisms: 1) Direct influx of Ca^{2+} through the nAChR, 2) indirect Ca^{2+}-influx by voltage dependent calcium channels (VDCCs) and 3) release of Ca^{2+} from the endoplasmic reticulum. These nAChR induced signals are reported to cause the release of several neurotransmitters at the presynaptic neuron and a fast excitatory signal transmission at the postsynaptic neuron.[63,64]

To regulate ACh-mediated neurotransmission, ACh is decomposed in the synaptic cleft into choline and acetate by acetylcholinesterase (AChE). AChE can occur in a monomeric, dimeric and tetrameric soluble form, but in the CNS a hydrophobic tetramer (70-90%) anchored to the plasma membrane of pre- and post-synaptic neurons is predominant.[65,66] It is quite remarkably, that AChE is reported to have a hydrolysis rate of more than 10000 molecules of ACh per second and per molecule of AChE, which is close to the diffusion limitation of ACh to AChE's active site.[67] Therefore, ACh-mediated signaling in the cholinergic system - including its release, its interactions with the mAChR and the nAChR as well as its cleavage by AChE - is a process which takes place in a few milliseconds.

Pathological alterations in the cholinergic system linked to neuronal disorders led to the development of the cholinergic hypothesis in the early 80s.[68-71] This theory states the impairment of cognitive abilities, in terms of memory loss and reduced learning abilities, to be the result of a disruption of the cholinergic system in distinct brain areas. By using muscarinic antagonis, like scopolamine,[72] or nicotinic antagonist,[73,74] several experiments could support this hypothesis as suppression of ACh-mediated signal transduction through these signal pathways causes memory deficits. Historically, the first indication for AD development as a consequence of impairments of the cholinergic system was attributed to a significantly reduced activity of ChAT in specific brain areas of AD patients.[75-77] Although deficits in ChAT activity might well cause a cognitive decline, different reports disproved a causal correlation between a reduced ChAT-activity as the triggering event for AD pathogenesis as no physiological alterations in ChAT levels were found at early stages of AD or during mild cognitive impairment (MCI).[78,79] Also a reduced activity of the vesicular acetylcholine transporter (VAChT) or cell death of cholinergic neurons were investigated regarding their involvement in the development of AD. Similar to ChAT, pathological changes of these biomarkers were only found in progressed AD but none of them was proven to be a triggering event for an impaired cholinergic signal transmission.[68,69,78] Interestingly, several clinical studies indicated, that even if cholinergic neurons are maintained in early stages of AD, a reduced cell volume and alterations in the cell morphology of these neurons are observed while several non-AD associated biomarkers were up regulated.[80-82] It might be well possible, that there is an underlying event in the cholinergic system which induces impairments in the neuronal integrity and in consequence triggers AD pathogenesis. Nevertheless, such an event is not yet found to date.

In summary, although the impairment of the cholinergic system is well accepted for the decline in memory and learning abilities during AD, the initial biochemical alterations of this system are still unknown. Nevertheless, ay abnormal cell morphology of cholinergic neurons as well as several biochemical indicators strongly suggest a

shift of biochemical processes which might impair the neuronal integrity and in turn lead to a dysfunction of the cholinergic system in early AD.

However, it is doubtless proven that during the course of AD cholinergic neurons, especially those of the basal forebrain (most important brain region for ACh biosynthesis), undergo a selective degeneration, and in consequence patients suffer from ACh deficits and cognitive impairments.[83-85] Based on these findings, therapeutic approaches were followed up in which ACh deficits were counteracted either by supporting cholinergic signaling with suitable mAChR and nAChR agonists or by increasing the available amount of ACh to a normal level. Although it is clear, that such approaches are only symptomatic and cannot cure AD, to date three out of the four approved drugs for AD treatment focus on increasing brain ACh levels by inhibiting AChE:

1) Donepezil (Aricept®) is marketed in the USA since 1996 and was approved by the US Food and Drug Administration (FDA) in 2006 as a selective and reversible AChE inhibitor for the treatment of mild and moderate dementia. Today, Donepezil is the best-selling drug for AD treatment due to its effectiveness to improve cognitive impairments of AD patients compared to placebo groups.[86]
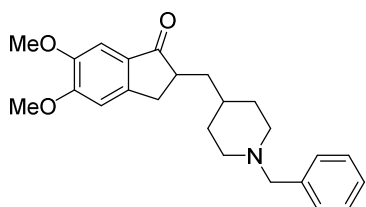
2) Rivastigmine (Exelon®) was initially approved in 2000 for the treatment of mild to moderate AD and later for the syptomatic treatment of Parkinsons's disease in 2006. Rivastigmine is a non-selective pseudo-irreversible cholinesterase inhibitor for both, AChE as well as for butyrylcholinesterase (BChE). It transfers its carbamate moiety directly onto the enzymes active site providing pseudo-irreversible inhibition of the target enzyme. In a second step, the transferred carbamate moiety is hydrolyzed off thus releasing the intact enzyme.
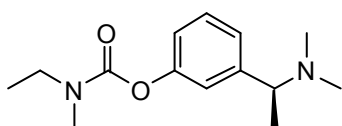
3) Galantamine (Reminyl®) is a naturally occuring alkaloid which was first isolated by Bulgarian pharmacologists from the flowers and bulbs of the wild Caucasian snow-drop *Galanthus nivalis*.[87] In 2001 galantamine was approved by the FDA for the treatment of mild and moderate AD due to its ability to selectively inhibit AChE. In addition to its inhibitory potency, galantamine was reported to act as an allosteric modulator of the nAChR by potentiating the agonistic response of neurons.[88]
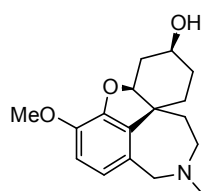
Although AD patients benefit from a symptomatic treatment with AChE inhibitors during mild to moderate AD, clinical studies in severe AD are controversy.[86] In fact, in progressed AD inhibition of AChE as therapeutic

strategy is highly questionable, as the AChE concentration is drastically decreased by 90%[89,90] making AChE probably impractical as physiological target.

In summary, the cholinergic hypothesis was the first theory stateing a causal correlation between the progress of AD and impairments of the cholinergic system. Although distinct biological changes in the cholinergic system were observed, none of them could be proven to be a triggering event for the development of AD so far. Nevertheless, an improved cholinergic signal transmission through increased ACh levels in the brain can well be considered as a therapeutic strategy. It is clear, that such a strategy can act only symptomatically; but on the other hand, clinical studies revealed a positive effect against early cognitive declines by increasing ACh levels. More important, in the preclinical phase of AD the cholinergic system might already be impaired as indicated by several biomarkers, but unfortunately, a fundamental cause for this pre-pathological and clinical changes is not yet found. Therefore, the research on this system is still in progress.

1.3 Butyrylcholinesterase

1.3.1 Involvement in the Cholinergic System during AD Pathogenesis

Butyrylcholinesterase (BChE) is a functional and structural isoforms of AChE which's exact physiological function is unknown to date. Nevertheless, BChE is found to be one of the major detoxification agents in human plasma by cleaving the ester or carbamate moieties of xenobiotics.[91] Furthermore, it is described to have aryl acylamidase and peptidase activities.[92,93]

In the non-pathological human brain, BChE occurs mainly in endothelial and glia cells of the amygdala and the hippocampal formation[94,95] where it has only a minor function (10-20%) in regulation of the cholinergic system by hydrolyzing ACh.[96,97] However, in the course of AD, BChE levels of different brain areas are described to be significantly increased up to 90%[96] with a remarkable increase of the BChE:AChE ratio from 0.6 to as high as 11.[96,97] To date, some theories state that BChE can adopt the function of AChE in later stages of AD, when the amount of AChE is dramatically reduced (*cf.* **Chapter 1.2.4**), to regulate cholinergic signal transmission in the brain. This hypothesis is supported by several AChE -/- knock out animal models showing survival of the test subjects even in the absence of AChE as BChE takes over AChE's function.[98-101] Nevertheless, such animals suffer on a general massive cholinergic hyper activation with up to 60 fold increased ACh levels compared to AChE +/+ subjects, which in consequence causes a delay in the postnatal development, tremor and an overall high mortality.[98,100] Moreover, selective inhibition of BChE in the AChE -/- model further increased the high ACh levels in the brain and led to severe cholinergic symptoms with successive death. Such results were not observed in wild type mice containing AChE and BChE as AChE was still able to cleave ACh.[98,101,102]

These reports clearly indicate a function of BChE in the regulation of the neuronal cholinergic system when AChE levels are reduced or in the absence of AChE. In fact, in a study using wild type mice treated with a selective BChE inhibitor, an enhanced synaptic connectivity and improved cognitive performances was determined, probably due to increased ACh levels.[103] And furthermore, studies with -/- BChE knockout mice revealed augmented learning capacities and lowered vulnerability to Aβ toxicity compared to wild type mice.[104] Although animal models are not necessarily transferable to human subjects due to different species dependent systemic effects, a positive effect in cognitive abilities in both models was proven in the absence of BChE. Therefore, BChE might well be considered as a clinical target in the course of AD as it might take over AChE's function in the regulation of cholinergic signal transmission. Indeed, clinical studies comparing the effect of the two approved drugs donepezil (only AChE inhibition) and rivastigmine (AChE and BChE inhibition), revealed a greater benefit in daily living and global function for rivastigmine in those patients having the BChE allele due to the dual inhibition of AChE and BChE.[105,106]

Besides BChE's potential involvement in cholinergic signaling, neurofibrillary tangles as well as amyloid β-plaques were found to be colocalized with BChE supporting the potential involvement for BChE in plaque formation.[107-112] However, the relationship between BChE and the occurrence of plaques is not yet fully understood to date. Literature is controversy at this point: While BChE inhibition and BChE knockout mice were reported to feature a lower Aβ burden,[103,110] Diamant *et al.* described BChE to attenuate Aβ fibril formation.[113]

In summary, the function of BChE in the course of AD is not yet determined to date, but it is found to be remarkably increased in AD patient's brain. Several animal studies showed, that BChE might adopt the function of AChE and therefore becomes responsible for the regulation of cholinergic signal transmission. Furthermore, inhibition of BChE has shown to increase ACh brain levels. These observations suggest that BChE targeting might become a therapeutic strategy in the symptomatic treatment of AD. Nevertheless, before such a therapy can be realized, basic research on BChE's involvement in the cholinergic system during AD and its role in plaque formation has to be further carried on to understand the underlying biochemical processes.

1.3.2 Association with Various Diseases

In recent years, an increasing number of reports revealed the association of BChE with a set of diseases, all connected to each other over the metabolic syndrome. A brief description of these diseases will be given in the following:

Obesity: Several clinical studies linked obesity and a high body mass index (BMI) to an increased activity of all molecular forms of serum BChE compared to none obese patients.[114-117] In contrast, losing weight as well as physical exercises lead to a significant reduction of BChE serum levels.[118,119] It is not clear, whether BChE is the initiator for obesity or if its increased expression is a result of a physiological shift during obesity. However, BChE knockout mice fed with a 11% fat diet were found to increase body weight up to 30% whereas in wild type mice the body weight remained constant on such a diet.[120-122] The authors contributed this effect to the involvement of BChE in the lipid and fat-metabolism. More interestingly, Chen *et al.*[121] was able to demonstrate a restored resistance against high fat diet induced obesity when BChE was transferred into BChE knockout mice by an adeno-associated virus vector. Therefore, literature remains controversy on the role of BChE as protector or inducer for obesity.

Diseases of the cardiovascular system: Risk factors of the cardiovascular system are biochemical attributed to increased cholesterol, triglycerides and serum lipid levels. Although the role of BChE for the development in cardiovascular diseases is not investigated to date, BChE levels are reported to proceed inverse to mortality caused by cardiovascular events.[123-126] Therefore, a reduced BChE activity might be considered as a non-specific risk factor for cardiovascular caused mortality.

Diabetes mellitus type 2: Several studies reported the correlation of BChE with hyperglycemia, insulin resistance and an altered lipoprotein metabolism in hypertriglyceridemia.[114,127-129] These biomarkers are all reported to be risk factors and indicators of diabetes mellitus type 2. In consequence, BChE might also serve as an indicator during the diagnosis of diabetes. Nevertheless, due to little available reports in literature, the role of BChE in diabetes mellitus is widely unknown in the pathological development of this disease.

1.4   References

[1]   WHO| World Health Organization Home Page. The Top 10 Causes of Death. http://www.who.int/mediacentre/factsheets/fs310/en/index4.html. (Accessed April 20, 2016).

[2] Alzheimer, A. Über eine Eigenartige Erkrankung der Hirnrinde. *Allgemeine Zeitschrift für Psychiatrie und Psychisch-gerichtliche Medizin* **1907**, *64,146-148.*

[3] Daniel, P. P. Neuropathology of Alzheimer's Disease. *Mt. Sinai J. Med.* **2010**, *77*, 32-42.

[4] Prince, M.; Albanese, E.; Guerchet, M.; Prina, M. *World Alzheimer Report 2014. Dementia and Risk Reduction.* Alzheimer's Disease International, **2014**.

[5] Reitz, C.; Mayeux, R. Alzheimer Disease: Epidemiology, Diagnostic Criteria, Risk Factors and Biomarkers. *Biochem. Pharmacol.* **2014**, *88*, 640-651.

[6] Reeve, A.; Simcox, E.; Turnbull, D. Ageing and Parkinson's Disease: Why is Advancing Age the Biggest Risk Factor? *Ageing Res. Rev.* **2014**, *14*, 19-30.

[7] Deak, F.; Freeman, W. M.; Ungvari, Z.; Csiszar, A.; Sonntag, W. E. Recent Developments in Understanding Brain Aging: Implications for Alzheimer's Disease and Vascular Cognitive Impairment. *J. Gerontol. A Biol. Sci. Med. Sci.* **2016**, *71*, 13-20.

[8] Prince, M.; Wimo, A.; Guerchet, M.; A., G.-C.; Wu, Y.-T.; Prina, M. *World Alzheimer Report 2015. The Global Impact of Demenzia. An Analysis of Prevalence, Incidence, Cost and Trends.* Alzheimer's Disease International, **2015**.

[9] Querfurth, H. W.; La Ferla, F. M. Alzheimer's Disease. *New Engl. J. Med.* **2010**, *362*, 329-344.

[10] Crews, L.; Masliah, E. Molecular Mechanisms of Neurodegeneration in Alzheimer's Disease. *Hum. Mol. Genet.* **2010**, *19*, 12-20.

[11] Maccioni, R. B.; Muñoza, J. P.; Barbeitob, L. The Molecular Bases of Alzheimer's Disease and Other Neurodegenerative Disorders. *Arch. Med. Res.* **2001**, *32*, 367-381.

[12] Selkoe, D. J.; Hardy, J. The Amyloid Hypothesis of Alzheimer's Disease at 25 Years. *EMBO Mol. Med.* **2016**, *8*, 595-608.

[13] Musiek, E. S.; Holtzman, D. M. Three Dimensions of the Amyloid Hypothesis: Time, Space and 'Wingmen'. *Nat. Neurosci.* **2015**, *18*, 800-806.

[14] Pimplikar, S. W. Reassessing the Amyloid Cascade Hypothesis of Alzheimer's Disease. *Int. J. Biochem. Cell Biol.* **2009**, *41*, 1261-1268.

[15] Hardy, J.; Selkoe, D. J. The Amyloid Hypothesis of Alzheimer's Disease: Progress and Problems on the Road to Therapeutics. *Science* **2002**, *297*, 353-356.

[16] Haass, C.; Selkoe, D. J. Soluble Protein Oligomers in Neurodegeneration: Lessons from the Alzheimer's Amyloid *β*-peptide. *Nat. Rev. Mol. Cell Biol.* **2007**, *8*, 101-112.

[17] Müller, U. C.; Zheng, H. Physiological Functions of APP Family Proteins. *Cold Spring Harb. Perspect. Med.* **2012**, *2*, a006288.

[18] Thinakaran, G.; Koo, E. H. Amyloid Precursor Protein Trafficking, Processing, and Function. *J. Biol. Chem.* **2008**, *283*, 29615-29619.

[19] Bignante, E. A.; Heredia, F.; Morfini, G.; Lorenzo, A. Amyloid β Precursor Protein as a Molecular Target for Amyloid β-Induced Neuronal Degeneration in Alzheimer's Disease. *Neurobiol. Aging* **2013**, *34*, 2525-2537.

[20] Dawkins, E.; Small, D. H. Insights into the Physiological Function of the β-Amyloid Precursor Protein: Beyond Alzheimer's Disease. *J. Neurochem.* **2014**, *129*, 756-769.

[21] Mawuenyega, K. G.; Sigurdson, W.; Ovod, V.; Munsell, L.; Kasten, T.; Morris, J. C.; Yarasheski, K. E.; Bateman, R. J. Decreased Clearance of CNS β-Amyloid in Alzheimer's Disease. *Science* **2010**, *330*, 1774.

[22] Wang, Y.-J.; Zhou, H.-D.; Zhou, X. F. Clearance of Amyloid-Beta in Alzheimer's Disease: Progress, Problems and Perspectives. *Drug Discovery Today* **2006**, *11*, 931-938.

[23] Sagare, A.; Deane, R.; Bell, R. D.; Johnson, B.; Hamm, K.; Pendu, R.; Marky, A.; Lenting, P. J.; Wu, Z.; Zarcone, T.; Goate, A.; Mayo, K.; Perlmutter, D.; Coma, M.; Zhong, Z.; Zlokovic, B. V. Clearance of Amyloid-β by Circulating Lipoprotein Receptors. *Nat. Med.* **2007**, *13*, 1029-1031.

[24] Snyder, E. M.; Nong, Y.; Almeida, C. G.; Paul, S.; Moran, T.; Choi, E. Y.; Nairn, A. C.; Salter, M. W.; Lombroso, P. J.; Gouras, G. K.; Greengard, P. Regulation of NMDA Receptor Trafficking by Amyloid-β. *Nat. Neurosci.* **2005**, *8*, 1051-1058.

[25] Tanzi, R. E. The Synaptic Aβ Hypothesis of Alzheimer Disease. *Nat. Neurosci.* **2005**, *8*, 977-979.

[26] Mucke, L.; Selkoe, D. J. Neurotoxicity of Amyloid β-Protein: Synaptic and Network Dysfunction. *Cold Spring Harb. Perspect. Med.* **2012**, *2*, a006338.

[27] Ferreiro, E.; Resende, R.; Costa, R.; Oliveira, C. R.; Pereira, C. M. F. An Endoplasmic-Reticulum-Specific Apoptotic Pathway is Involved in Prion and Amyloid-Beta Peptides Neurotoxicity. *Neurobiol. Dis.* **2006**, *23*, 669-678.

[28] Resende, R.; Ferreiro, E.; Pereira, C.; Resende de Oliveira, C. Neurotoxic Effect of Oligomeric and Fibrillar Species of Amyloid-Beta Peptide 1-42: Involvement of Endoplasmic Reticulum Calcium Release in Oligomer-Induced Cell Death. *Neurosci.* **2008**, *155*, 725-737.

[29] Ferreiro, E.; Resende de Oliveira, C.; Pereira, C. M. F. The Release of Calcium from the Endoplasmic Reticulum Induced by Amyloid-Beta and Prion Peptides Activates the Mitochondrial Apoptotic Pathway. *Neurobiol. Dis.* **2008**, *30*, 331-342.

[30] Mangialasche, F.; Solomon, A.; Winblad, B.; Mecocci, P.; Kivipelto, M. Alzheimer's Disease: Clinical Trials and Drug Development. *Lancet Neurol.* **2010**, *9*, 702-716.

[31] Avila, J.; Lucas, J. J.; Pérez, M.; Hernández, F. Role of Tau Protein in Both Physiological and Pathological Conditions. *Physiol. Rev.* **2004**, *84*, 361-384.

[32] Ballatore, C.; Lee, V. M.-Y.; Trojanowsk, J. Q. Tau-Mediated Neurodegeneration in Alzheimer's Disease and Related Disorders. *Nat. Rev. Neurosci.* **2007**, *8*, 663-672.

[33] Maina, M. B.; Al-Hilaly, Y. K.; Serpell, L. C. Nuclear Tau and Its Potential Role in Alzheimer's Disease. *Biomolecules* **2016**, *6*, 9.

[34] Mandelkow, E.-M.; Mandelkow, E. Tau in Alzheimer's Disease. *Cell Biol.* **1998**, *8*, 425-427.

[35] Mondragón-Rodríguez, S.; Perry, G.; Luna-Muñoz, J.; Acevedo-Aquino, M. C.; Willi, S. Phosphorylation of Tau Protein at Sites Ser$^{396-404}$ is one of the Earliest Events in Alzheimer's Disease and Down Syndrome. *Neuropathol. Appl. Neurobiol.* **2014**, *40*, 121-135.

[36] Mondragón-Rodríguez, S.; Basurto-Islas, G.; Santa-Maria, I.; Mena, R.; Binder, L. I.; Avila, J.; Smith, M. A.; Perry, G.; García-Sierr, F. Cleavage and Conformational Changes of Tau Protein Follow Phosphorylation During Alzheimer's Disease. *Int. J. Exp. Path.* **2008**, *89*, 81-90.

[37] Spires-Jones, T. L.; Stoothoff, W. H.; de Calignon, A.; Jones, P. B.; Hyman, B. T. Tau Pathophysiology in Neurodegeneration: A Tangled Issue. *Trends Neurosci.* **2009**, *32*, 150-159.

[38] Pritchard, S. M.; Dolan, P. J.; Vitkus, A.; Johnso, G. V. W. The Toxicity of Tau in Alzheimer Disease: Turnover, Targets and Potential Therapeutics. *J. Cell. Mol. Med.* **2011**, *15*, 1621-1635.

[39] Ward, S. M.; Himmelstein, D. S.; Lancia, J. K.; Binder, L. I. Tau Oligomers and Tau Toxicity in Neurodegenerative Disease. *Biochem. Soc. Trans.* **2012**, *40*, 667-671.

[40] Medina, M.; Avila, J. New Perspectives on the Role of Tau in Alzheimer's Disease. Implications for Therapy. *Biochem. Pharmacol.* **2014**, *88*, 540-547.

[41] Wischik, C. M.; Harrington, C. R.; Storey, J. M. D. Tau-Aggregation Inhibitor Therapy for Alzheimer's Disease. *Biochem. Pharmacol.* **2014**, *88*, 529-539.

[42] Finkel, T.; Holbrook, N. J. Oxidants, Oxidative Stress and the Biology of Ageing. *Nature* **2000**, *408*, 239-247.

[43] Dai, D.-F.; Chiao, Y. A.; Marcinek, D. J.; Szeto, H. H.; Rabinovitch, P. S. Mitochondrial Oxidative Stress in Aging and Healthspan. *Longev. Healthspan* **2014**, *3*, 6.

[44] Thannickal, V. J.; Fanburg, B. L. Reactive Oxygen Species in Cell Signaling. *Am. J. Physiol. Lung Cell. Mol. Physiol.* **2000**, *279*, L1005-L1028.

[45] Hensley, K.; Robinson, K. A.; Gabbita, S. P.; Salsman, S.; Floyd, R. A. Reactive Oxygen Species, Cell Signaling, and Cell Injury. *Free Radical Biol. Med.* **2000**, *28*, 1456-1462.

[46] Ray, P. D.; Huang, B.-W.; Tsuji, Y. Reactive Oxygen Species (ROS) Homeostasis and Redox Regulation in Cellular Signaling. *Cell. Signalling* **2012**, *24*, 981-990.

[47] Christen, Y. Oxidative Stress and Alzheimer Disease. *Am. J. Clin. Nutr.* **2000**, *71*, 621S-629S.

[48] Lin, M. T.; Beal, M. F. Mitochondrial Dysfunction and Oxidative Stress in Neurodegenerative Diseases. *Nature* **2006**, *443*, 787-795.

[49] Kannan, K.; Jain, S. K. Oxidative Stress and Apoptosis. *Pathophysiology* **2000**, *7*, 153-163.

[50] Buttke, T. M.; Sandstrom, P. A. Oxidative Stress as a Mediator of Apoptosis. *Immunol. Today* **1994**, *15*, 7-10.

[51] Butterfield, D. A.; Drake, J.; Pocernich, C.; Castegna, A. Evidence of Oxidative Damage in Alzheimer's Disease Brain: Central Role for Amyloid *β*-Peptide. *Trends Mol. Med.* **2001**, *7*, 548-554.

[52] Miranda, S.; Opazo, C.; Larrondo, L. F.; Munoz, F. J.; Ruiz, F.; Leighton, F.; Inestrosa, N. C. The Role of Oxidative Stress in the Toxicity Induced by Amyloid *β*-Peptide in Alzheimer's Disease. *Prog. Neurobiol.* **2000**, *62*, 633-648.

[53] Varadarajan, S.; Yatin, S.; Aksenova, M.; Butterfield, D. A. Review: Alzheimer's Amyloid *β*-Peptide-Associated Free Radical Oxidative Stress and Neurotoxicity. *J. Struct. Biol.* **2000**, *130*, 184-208.

[54] Jomova, K.; Vondrakova, D.; Lawson, M.; Valko, M. Metals, Oxidative Stress and Neurodegenerative Disorders. *Mol. Cell Biochem.* **2010**, *345*, 91-104.

[55] Zhu, X.; Su, B.; Wang, X.; Smith, M. A.; Perry, G. Causes of Oxidative Stress in Alzheimer Disease. *Cell. Mol. Life Sci.* **2007**, *64*, 2202-2210.

[56] Gold, P. E. Acetylcholine Modulation of Neural Systems Involved in Learning and Memory. *Neurobiol. Learn. Mem.* **2003**, *80*, 194-210.

[57] Hasselmo, M. E. The Role of Acetylcholine in Learning and Memory. *Curr. Opin. Neurobiol.* **2006**, *16*, 710-715.

[58] Blokland, A. Acetylcholine: A Neurotransmitter for Learning and Memory? *Brain Res. Rev.* **1996**, *21*, 285-300.

[59] Thiele, A. Muscarinic Signaling in the Brain. *Annu. Rev. Neurosci.* **2013**, *36*, 271-294.

[60] Lanzafame, A. A.; Christopoulos, A.; Mitchelson, F. Cellular Signaling Mechanisms for Muscarinic Acetylcholine Receptors. *Recept. Channels* **2003**, *9*, 241-260.

[61] Felder, C. C. Muscarinic Acetylcholine Receptors: Signal Transduction Through Multiple Effectors. *FASEB J.* **1995**, *9*, 619-625.

[62] Bymaster, F. P.; McKinzie, D. L.; Felder, C. C.; Wess, J. Use of M1–M5 Muscarinic Receptor Knockout Mice as Novel Tools to Delineate the Physiological Roles of the Muscarinic Cholinergic System. *Neurochem. Res.* **2003**, *28*, 437-442.

[63] Shen, J.-X.; Yakel, J. L. Nicotinic Acetylcholine Receptor-Mediated Calcium Signaling in the Nervous System. *Acta Pharmacol. Sin.* **2009**, *30*, 673-680.

[64] Dajas-Bailador, F.; Wonnacott, S. Nicotinic Acetylcholine Receptors and the Regulation of Neuronal Signalling. *Trends Pharmacol. Sci.* **2004**, *25*, 317-324.

[65] Rotundo, R. L. Expression and Localization of Acetylcholinesterase at the Neuromuscular Junction. *J. Neurocyt.* **2003**, *32*, 743-766.

[66] Legay, C. Why so Many Forms of Acetylcholinesterase? *Micros. Res. Techniq.* **2000**, *49*, 56-72.

[67] Quinn, D. M. Acetylcholinesterase: Enzyme Structure, Reaction Dynamics, and Virtual Transition States. *Chem. Rev.* **1987**, *87*, 955-979.

[68] Craig, L. A.; Hong, N. S.; McDonald, R. J. Revisiting the Cholinergic Hypothesis in the Development of Alzheimer's Disease. *Neurosci. Biobehav. Rev.* **2011**, *35*, 1397-1409.

[69] Contestabile, A. The History of the Cholinergic Hypothesis. *Behav. Brain Res.* **2011**, *221*, 334-340.

[70] Terry Jr., A. V.; Buccafusco, J. J. The Cholinergic Hypothesis of Age and Alzheimer's Disease-Related Cognitive Deficits: Recent Challenges and Their Implications for Novel Drug Development. *J. Pharmacol. Exp. Ther.* **2003**, *306*, 821-827.

[71] Gallagher, M.; Colombo, P. J. Ageing: The Cholinergic Hypothesis of Cognitive Decline. *Curr. Opin. Neurobiol.* **1995**, *2*, 161-168.

[72] Newman, L. A.; Gold, P. E. Attenuation in Rats of Impairments of Memory by Scopolamine, a Muscarinic Receptor Antagonist, by Mecamylamine, a Nicotinic Receptor Antagonist. *Psychopharmacol.* **2016**, *233*, 925-932.

[73] Levin, E. D.; Bradley, A.; Addy, N.; Sigurani, N. Hippocampal α7 and α4ß2 Nicotinic Receptors and Working Memory. *Neuroscience* **2002**, *109*, 757-765.

[74] Levin, E. D. Nicotinic Receptor Subtypes and Cognitive Function. *J. Neurobiol.* **2002**, *53*, 633-640.

[75] Bowen, D. M.; Smith, C. B.; White, P.; Davison, A. N. Neurotransmitter-Related Enzymes and Indices of Hypoxia in Senile Dementia and Other Abiotrophies. *Brain* **1976**, *99*, 459-496.

[76] Davies, P.; Maloney, A. J. F. Selective Loss of Central Cholinergic Neurons in Alzheimer's Disease. *Lancet* **1976**, *2*, 1403.

[77] Perry, E. K.; Perry, R. H.; Blessed, G.; Tomlinson, B. E. Necropsy Evidence of Central Cholinergic Deficits in Senile Dementia. *Lancet* **1977**, *1*, 189.

[78] Gilmor, M. L.; Erickson, J. D.; Varoqui, H.; Hersh, L. B.; Bennett, D. A.; Cochran, E. J.; Mufson, E. J.; Levey, A. I. Preservation of Nucleus Basalis Neurons Containing Choline Acetyltransferase and the Vesicular Acetylcholine Transporter in the Elderly with Mild Cognitive Impairment and Early Alzheimer's Disease. *J. Comp. Neurol.* **1999**, *411*, 693-704.

[79] Kenneth, L. D.; Mohs, R. C.; Marin, D.; Purohit, D. P.; Perl, D. P.; Lantz, M.; Austin; G.; Haroutunian, V. Cholinergic Markers in Elderly Patients with Early Signs of Alzheimer Disease. *JAMA.* **1999**, *281*, 1401-1406.

[80] Mufson, E. J.; Counts, S. E.; Fahnestock, M.; Ginsberg, S. D. Cholinotrophic Molecular Substrates of Mild Cognitive Impairment in the Elderly. *Curr. Alzheimer Res.* **2007**, *4*, 340-350.

[81] Sassin, I.; Schultz, C.; Thal, D. R.; Rub, U.; Arai, K.; Braak, E.; Braak, H. Evolution of Alzheimer's Disease-Related Cytoskeletal Changes in the Basal Nucleus of Meynert. *Acta Neuropathol.* **2000**, *100*, 259-269.

[82] Mesulam, M. The Cholinergic Lesion of Alzheimer's Disease: Pivotal Factor or Side Show? *Learn. Mem.* **2004**, *11*, 43-49.

[83] Arendt, T.; Brückner, M. K.; Morawski, M.; Jäger, C.; Gertz, H.-J. Early Neurone Loss in Alzheimer's Disease: Cortical or Subcortical? *Acta Neuropathol. Commun.* **2015**, *3*, 10.

[84] Muir, J. L. Acetylcholine, Aging, and Alzheimer's Disease. *Pharmacol. Biochem. Behav.* **1997**, *56*, 687-696.

[85] Whitehouse, P. J.; Price, D. L.; Struble, R. G.; Clark, A. W.; Coyle, J. T.; Delon, M. R. Alzheimer's Disease and Senile Dementia: Loss of Neurons in the Basal Forebrain. *Science* **1982**, *215*, 1237-1239.

[86] Schneider, L. S.; Mangialasche, F.; Andreasen, N.; Feldman, H.; Giacobini, E.; Jones, R.; Mantua, V.; Mecocci, P.; Pani, L.; Winblad, B.; Kivipelto, M. Clinical Trials and Late-Stage Drug Development for Alzheimer's Disease: An Appraisal from 1984 to 2014. *J. Intern. Med.* **2014**, *275*, 251-283.

[87] Cronin, J. R. The Plant Alkaloid Galantamine: Approved as a Drug; Sold as a Supplement. *J. Altern. Complement. Med.* **2001**, *7*, 380-383.

[88] Samochocki, M.; Höffle, A.; Fehrenbacher, A.; Jostock, R.; Ludwig, J.; Christner, C.; Radina, M.; Zerlin, M.; Ullmer, C.; Pereira, E. F. R.; Lübbert, H.; Albuquerque, E. X.; Maelicke, A. Galantamine is an Allosterically Potentiating Ligand of Neuronal Nicotinic but not of Muscarinic Acetylcholine Receptors. *J. Pharmacol. Exp. Ther.* **2003**, *305*, 1024-1036.

[89] Nordberg, A.; Ballard, C.; Bullock, R.; Darreh-Shori, T.; Somogyi, M. A Review of Butyrylcholinesterase as a Therapeutic Target in the Treatment of Alzheimer's Disease. *Prim. Care Companion CNS Disord.* **2013**, *15*; doi:10.4088/PCC.12r01412.

[90] Giacobini, E. Cholinergic Function and Alzheimer's Disease. *Int. J. Geriatr. Psych.* **2003**, *18*, 1-5.

[91] Li, B.; Sedlacek, M.; Manoharan, I.; Boopathy, R.; Duysen, E. G.; Masson, P.; Lockridge, O. Butyrylcholinesterase, Paraoxonase, and Albumin Esterase, but not Carboxylesterase, are Present in Human Plasma. *Biochem. Pharmacol.* **2005**, *70*, 1673-1684.

[92] Balasubramanian, A. S.; Bhanumathy, C. D. Noncholinergic Functions of Cholinesterases. *FASEB J.* **1993**, *14*, 1354-1358.

[93] Çokuğraş, A. N. Butyrylcholinesterase: Structure and Physiological Importance. *Turk. J. Biochem.* **2003**, *28*, 54-61.

[94] Darvesh, S.; Hopkins, D. A.; Geula, C. Neurobiology of Butyrylcholinesterase. *Nat. Rev. Neurosci.* **2003**, *4*, 131-138.

[95] Darvesh, S.; Grantham, D. L.; Hopkins, D. A. Distribution of Butyrylcholinesterase in the Human Amygdala and Hippocampal Formation. *J. Comp. Neurol.* **1998**, *393*, 374-390.

[96] Greig, N. H.; Lahiri, D. K.; Sambamurti, K. Butyrylcholinesterase: An Important New Target in Alzheimer's Disease Therapy. *Int. Psychogeriatr.* **2002**, *14*, 77-91.

[97] Greig, N. H.; Utsuki, T.; Yu, X.-S.; Zhu, X.; Holloway, H. W.; Perry, T.; Lee, B.; Ingram, D. K.; Lahiri, D. K. A New Therapeutic Target in Alzheimer's Disease Treatment: Attention to Butyrylcholinesterase. *Curr. Med. Res. Opin.* **2001**, *17*, 159-165.

[98] Hartmann, J.; Kiewert, C.; Duysen, E. G.; Lockridge, O.; Greig, N. H.; Klein, J. Excessive Hippocampal Acetylcholine Levels in Acetylcholinesterase-Deficient Mice are Moderated by Butyrylcholinesterase Activity. *J. Neurochem.* **2007**, *100*, 1421-1429.

[99] Mesulam, M.-M.; Guillozet, A.; Shaw, P.; Levey, A.; Duysen, E. G.; Lockridge, O. Acetylcholinesterase Knockouts Establish Central Cholinergic Pathways and can Use Butyrylcholinesterase to Hydrolyze Acetylcholine. *Neuroscience* **2002**, *110*, 627-639.

[100] Xie, W.; Stribley, J. A.; Chatonnet, A.; Wilder, P. J.; Rizzino, A.; McComb, R. D.; Taylor, P.; Hinrichs, S. H.; Lockridge, O. Postnatal Developmental Delay and Supersensitivity to Organophosphate in Gene-Targeted Mice Lacking Acetylcholinesterase. *J. Pharmacol. Exp. Ther.* **2000**, *293*, 896-902.

[101] Naik, R. S.; Hartmann, J.; Kiewert, C.; Duysen, E. G.; Lockridge, O.; Klein, J. Effects of Rivastigmine and Donepezil on Brain Acetylcholine Levels in Acetylcholinesterase-Deficient Mice. *J. Pharm. Pharmaceut. Sci.* **2009**, *12*, 79-85.

[102] Duysen, E. G.; Li, B.; Darvesh, S.; Lockridge, O. Sensitivity of Butyrylcholinesterase Knockout Mice to (−)-Huperzine A and Donepezil Suggests Humans with Butyrylcholinesterase Deficiency May not Tolerate These Alzheimer's Disease Drugs and Indicates Butyrylcholinesterase Function in Neurotransmission. *Toxicology* **2007**, *233*, 60-69.

[103] Greig, N. H.; Utsuki, T.; Ingram, D. K.; Wang, Y.; Pepeu, G.; Scali, C.; Yu, Q.-S.; Mamczarz, J.; Holloway, H. W.; Giordano, T.; Chen, D.; Furukawa, K.; Sambamurti, K.; Brossi, A.; Lahiri, D. K. Selective Butyrylcholinesterase Inhibition Elevates Brain Acetylcholine, Augments Learning and Lowers Alzheimer *β*-Amyloid Peptide in Roden. *PNAS* **2005**, *102*, 17213-17218.

[104] Maurice, T.; Strehaiano, M.; Siméon, N.; Bertrand, C.; Chatonnet, A. Learning Performances and Vulnerability to Amyloid Toxicity in the Butyrylcholinesterase Knockout Mouse. *Behav. Brain Res.* **2016**, *296*, 351-360.

[105] Bullock, R.; Touchon, J.; Bergman, H.; Gambina, G.; He, Y.; Rapatz, G.; Nagel, J.; Lane, R. Rivastigmine and Donepezil Treatment in Moderate to Moderately-Severe Alzheimer's Disease over a 2-Year Period. *Curr. Med. Res. Opin.* **2005**, *21*, 1317-1327.

[106] Bullock, R.; Bergman, H.; Touchon, J.; Gambina, G.; He, Y.; Nagel, J.; Lane, R. Effect of Age on Response to Rivastigmine or Donepezil in Patients with Alzheimer's Disease. *Curr. Med. Res. Opin.* **2006**, *22*, 483-494.

[107] Mizukami, K.; Akatsu, H.; Abrahamson, E. E.; Mi, Z.; Ikonomovic, M. D. Immunohistochemical Analysis of Hippocampal Butyrylcholinesterase: Implications for Regional Vulnerability in Alzheimer's Disease. *Neuropathology* **2016**, *36*, 135-145.

[108] Darvesh, S. Butyrylcholinesterase Radioligands to Image Alzheimer's Disease Brain. *Chem. Biol. Interact.* **2013**, *203*, 354-357.

[109] Darvesh, S.; Cash, M. K.; Reid, G. A.; Martin, E.; Mitnitski, A.; Geula, C. Butyrylcholinesterase is Associated with *β*-Amyloid Plaques in the Transgenic APP_{SWE}/PSEN1dE9 Mouse Model of Alzheimer Disease. *J. Neuropathol. Exp. Neurol.* **2012**, *71*, 2-14.

[110] Reid, G. A.; Darvesh, S. Butyrylcholinesterase-Knockout Reduces Brain Deposition of Fibrillar *β*-Amyloid in an Alzheimer Mouse Model. *Neuroscience* **2015**, *298*, 424-435.

[111] Guillozet, A. L.; Smiley, J. F.; Mash, D. C.; Mesulam, M.-M. Butyrylcholinesterase in the Life Cycle of Amyloid Plaques. *Ann. Neurol.* **1997**, *42*, 909-918.

[112] Gómez-Ramos, P.; Bouras, C.; Morán, M. A. Ultrastructural Localization of Butyrylcholinesterase on Neurofibrillary Degeneration Sites in the Brains of Aged and Alzheimer's Disease Patients. *Brain Res.* **1994**, *640*, 17-24.

[113] Diamant, S.; Podoly, E.; Friedler, A.; Ligumsky, H.; Livnah, O.; Soreq, H. Butyrylcholinesterase Attenuates Amyloid Fibril Formation *in vitro*. *PNAS* **2006**, *103*, 8628-8633.

[114] Iwasaki, T.; Yoneda, M.; Nakajima, A.; Terauchi, Y. Serum Butyrylcholinesterase is Strongly Associated with Adiposity, the Serum Lipid Profile and Insulin Resistance. *Intern. Med.* **2007**, *46*, 1633-1639.

[115] Randell, E. W.; Mathews, M. S.; Zhang, H.; Seraj, J. S.; Sun, G. Relationship Between Serum Butyrylcholinesterase and the Metabolic Syndrome. *Clin. Biochem.* **2005**, *38*, 799-805.

[116] Boberg, D. R.; Furtado-Alle, L.; Souza, R. L. R.; Chautard-Freire-Maia, E. A. Molecular Forms of Butyrylcholinesterase and Obesity. *Genet. Mol. Biol.* **2010**, *33*, 452-454.

[117] Alcântara, V. M.; Oliveira, L. C.; Réa, R. R.; Suplicy, H. L.; Chautard-Freire-Maia, E. A. Butyrylcholinesterase Activity and Metabolic Syndrome in Obese Patients. *Clin. Chem. Lab. Med.* **2005**, *43*, 285-288.

[118] Tvarijonaviciute, A.; Ceron, J. J.; Tecles, F. Acetylcholinesterase and Butyrylcholinesterase Activities in Obese Beagle Dogs Before and After Weight Loss. *Vet. Clin. Pathol.* **2013**, *42*, 207-211.

[119] Silva, I. M. W.; Leite, N.; Boberg, D.; Chaves, T. J.; Eisfeld, G. M.; Eisfeld, G. M.; Bono, G. F.; Souza, R. L. R.; Furtado-Alle, L. Effects of Physical Exercise on Butyrylcholinesterase in Obese Adolescents. *Genet. Mol. Biol.* **2012**, *35*, 741-742.

[120] Li , B.; Duysen, E. G.; Lockridge, O. The Butyrylcholinesterase Knockout Mouse is Obese on a High-Fat Diet. *Chem. Biol. Interact.* **2008**, *175*, 88-91.

[121] Chen, V. P.; Gao, Y.; Geng, L.; Stout, M. B.; Jensen, M. D.; Brimijoin, S. Butyrylcholinesterase Deficiency Promotes Adipose Tissue Growth and Hepatic Lipid Accumulation in Male Mice on High-Fat Diet. *Endocrinology* **2016**, *157*, 3086-3095.

[122] Duysen, E. G.; Li, B.; Lockridge, O. The Butyrylcholinesterase Knockout Mouse a Research Tool in the Study of Drug Sensitivity, Biodistribution, Obesity and Alzheimer's Disease. *Expert Opin. Drug Metab. Toxicol.* **2009**, *5*, 523-528.

[123] Goliasch, G.; Haschemi, A.; Marculescu, R.; Endler, G.; Maurer, G.; Wagner, O.; Huber, K.; Mannhalter, C.; Niessner, A. Butyrylcholinesterase Activity Predicts Long-Term Survival in Patients with Coronary Artery Disease. *Clin. Chem.* **2012**, *58*, 1055-1058.

[124] Calderon-Margalit, R.; Adler, B.; Abramson, J. H.; Gofin, J.; Kark, J. D. Butyrylcholinesterase Activity, Cardiovascular Risk Factors, and Mortality in Middle-Aged and Elderly Men and Women in Jerusalem. *Clin. Chem.* **2006**, *52*, 845-852.

[125] Distelmaier, K.; Winter, M.-P.; Rützler, K.; Heinz, G.; Lang, I. M.; Maurer, G.; Koinig, H.; Steinlechner, B.; Niessner, A.; Goliasch, G. Serum Butyrylcholinesterase Predicts Survival after Extracorporeal Membrane Oxygenation after Cardiovascular Surgery. *Crit. Care* **2014**, *18*, R24.

[126] Sulzgruber, P.; Koller, L.; Reiberger, T.; El-Hamid, F.; Forster, S.; Rothgerber, D.-J.; Goliasch, G.; Wojta, J.; Niessner, A. Butyrylcholinesterase Predicts Cardiac Mortality in Young Patients with Acute Coronary Syndrome. *PLoS One* **2015**, *10*, e0123948.

[127] Umar, R. A.; Hassan, S. W.; Ndukwe, O. F. Butyrylcholinesterase Activity in Nigerian Type 2 Diabetics with and without Metabolic Syndrome. *Afr. J. Biotechnol.* **2010**, *9*, 4110-4113.

[128] Rustemeijer, C.; Schouten, J. A.; Voerman, H. J.; Beynen, A. C.; Donker, A. J. M.; Heine, R. J. Is Pseudocholinesterase Activity Related to Markers of Triacylglycerol Synthesis in Type II Diabetes Mellitus? *Clin. Sci.* **2001**, *101*, 29-35.

[129] Abbott, C. A.; Mackness, M. I.; Kumar, S.; Olukoga, A. O.; Gordon, C.; Arrol, S.; Bhatnagar, D.; Boulton, A. J.; Durrington, P. N. Relationship Between Serum Butyrylcholinesterase Activity, Hypertriglyceridaemia and Insulin Sensitivity in Diabetes Mellitus. *Clin. Sci.* **1993**, *85*, 77-81.

2. Scope and Objective

Regarding the relevance of butyrylcholinesterase (BChE) in diseases associated with this enzyme (*cf.* introduction **Chapter 1.3**) and especially its putative involvement in the progress of AD, the development of selective BChE inhibitors can help to enable new medication strategies and to determine the role of BChE with pathophysological alterations in these diseases.

Decker *et al.*[1,2] used the natural occurring indoloalkaloid dehydroevodiamine (DHED) from the Chinese herb *evodia rutaecarpa* as a lead structure for the design of selective cholinesterase inhibitors. DHED has been described as a moderately active cholinesterase (ChE) inhibitor[3], and replacement of its indole moiety by a smaller phenyl system provided benzodehydroevodiamine with a high selectivity towards AChE compared to the non-selective DHED (**Scheme 2.1**). Interestingly, reduction of the quinazolinonium core in benzodehydroevodiamine into its corresponding tetrahydroquinazoline **1** gave a reversed selectivity towards BChE. In the following years, several investigations used the tetrahydroquinazoline template **1** for the synthesis of potent BChE as well as AChE inhibitors.[4-8] Darras *et al.*[4] as well as Huang *et al.*[5] adopted the concept of (pseudo-)irreversible inhibition (concept will be explained later), which is known for many ChE inhibitors including the approved drug Rivastigmine (Exelon®), and incorporated diverse carbamate moieties into the tetrahydroquinazoline scaffold. Both investigations showed that a heptyl-residue at the carbamate site (compound **2** and **3**) led to a high selectivity and affinity on BChE with IC_{50}-values in the two digit nanomolar range.
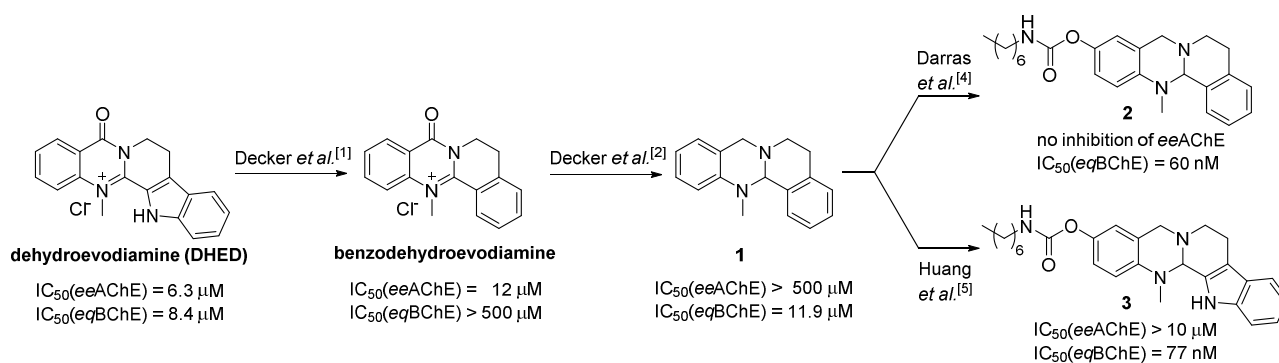
Scheme 2.1. Development of tetrahydroquinazoline based BChE inhibitors **2** and **3** from DHED.

Regarding the previously described studies, the current semi-cumulative work progresses on the development of tetrahydroquinazoline derived carbamate based BChE inhibitors with focus on two general parts. (Some chapters are only briefly summarized but can be found in a full version in the respective appendix.)

The first part extends the basic comprehension of the molecular, pharmacological and biological properties of tetrahydroquinazoline based BChE inhibitors:

1) Methods were developed in which the positron emission tomography (PET) radioisotopes ^{11}C and ^{18}F were introduced into the carbamate moiety of inhibitor **2**. The resulting radiotracers can be used to determine the pharmacokinetic profile of tetrahydroquinazoline derived inhibitors, to map the BChE distribution *in vivo* and to enable investigations of the pathophysological mechanisms in diseases associated with alterations in BChE levels and distribution (**Chapter 3**, **Appendix 1**).

2) A library of different tetrahydroquinazoline based carbamates was systematically designed, synthesized and analyzed to determine the structure activity relationship (SAR) between BChE and tetrahydroquinazoline based inhibitors. Using this data, a binding model for such inhibitors within the active site of BChE was postulated to assist the rational design of new BChE selective inhibitors (**Chapter 4**, **Appendix 2**).

3) Targeting of a second peripheral binding pocket in BChE was exploratively investigated to enable the design of new inhibitors with advanced properties (**Chapter 5**).

The second part of this work is set apart from the biological activity of tetrahydroquinazolines and focuses on the chemical and physical properties of this scaffold. In literature, the tetrahydroquinazoline core is fairly well documented in terms of its synthesis[4,5,9-14] as well as its selective oxidation towards quinazolinones, 3,4-dihydroquinazolines and quinazolines.[9,13,15-17] To supplement the known reaction properties of the tetrahydroquinazoline system two approaches were followed up:

1) Regarding the well described oxidations of tetrahydroquinazolines, several reductive conditions were applied onto this scaffold to extend the knowledge on the reaction behavior of tetrahydroquinazolines (**Chapter 6**, **Appendix 3**).

2) The stability of the aminal core of the tetrahydroquinazoline system towards hydrolysis was systematically investigated in dependency of the pH-value. Literature is lacking to a large degree of such information which are important e.g. to prevent degradation of compounds by applying the wrong conditions during biological studies, reaction set up or work up (**Chapter 7**, **Appendix 4**).

2.1 References

[1] Decker, M. Novel Inhibitors of Acetyl- and Butyrylcholinesterase Derived from the Alkaloids Dehydroevodiamine and Rutaecarpine. *Eur. J. Med. Chem.* **2005**, *40*, 305-313.

[2] Decker, M.; Krauth, F.; Lehmann, J. Novel Tricyclic Quinazolinimines and Related Tetracyclic Nitrogen Bridgehead Compounds as Cholinesterase Inhibitors with Selectivity Towards Butyrylcholinesterase. *Bioorg. Med. Chem.* **2006**, *14*, 1966-1977.

[3] Park, C. H.; Kim, S.-H.; Choi, W.; Lee, Y.-L.; Kim, J. S.; Kang, S. S.; Suh, Y.-H. Novel Anticholinesterase and Antiamnesic Activities of Dehydroevodiamine, a Constituent of *Evodia Rutaecarpa. Planta Med.* **1996**, *62*, 405-409.

[4] Darras, F. H.; Kling, B.; Heilmann J.; Decker, M. Neuroprotective Tri- and Tetracyclic BChE Inhibitors Releasing Reversible Inhibitors upon Carbamate Transfer. *ACS Med. Chem. Lett.* **2012**, *3*, 914-919.

[5] Huang, G.; Kling, B.; Darras, F. H.; Heilmann, J.; Decker, M. Identification of a Neuroprotective and Selective Butyrylcholinesterase Inhibitor Derived from the Natural Alkaloid Evodiamine. *Eur. J. Med.Chem.* **2014**, *81*, 15-21.

[6] Darras, F. H.; Pockes, S.; Huang, G.; Wehle, S.; Strasser, A.; Wittmann, H.-J.; Nimczick, M.; Sotriffer, C. A.; Decker, M. Synthesis, Biological Evaluation, and Computational Studies of Tri- and Tetracyclic Nitrogen-Bridgehead Compounds as Potent Dual-Acting AChE Inhibitors and hH$_3$ Receptor Antagonists. *ACS Chem. Neurosci.* **2014**, *5*, 225-242.

[7] Darras, F. H.; Wehle, S.; Huang, G.; Sotriffer, C. A.; Decker, M. Amine Substitution of Quinazolinones Leads to Selective Nanomolar AChE Inhibitors with 'Inverted' Binding Mode. *Bioorg. Med. Chem.* **2014**, *22*, 4867-4881.

[8] Decker, M. Homobivalent Quinazolinimines as Novel Nanomolar Inhibitors of Cholinesterases with Dirigible Selectivity Toward Butyrylcholinesterase. *J. Med. Chem.* **2006**, *49*, 5411-5413.

[9] Richers, M. T.; Deb, I.; Platonova, A. Y.; Zhang, C.; Seidel, D. Facile Access to Ring-Fused Aminals *via* Direct α-Amination of Secondary Amines with *o*-Aminobenzaldehydes: Synthesis of Vasicine, Deoxyvasicine, Deoxyvasicinone, Mackinazolinone, and Ruteacarpine. *Synthesis* **2013**, *45*, 1730-1748.

[10] Dieckmann, A.; Richers, M. T.; Platonova, A. Y.; Zhang, C.; Seidel, D.; Houk, K. N. Metal-Free α-Amination of Secondary Amines: Computational and Experimental Evidence for Azaquinone Methide and Azomethine Ylide Intermediates. *J. Org. Chem.* **2013**, *78*, 4132-4144.

[11] Zhang, C.; De, C. K.; Mal, R.; Seidel, D. α-Amination of Nitrogen Heterocycles: Ring-Fused Aminals. *J. Am. Chem. Soc.* **2008**, *130*, 416-417.

[12] Sinkkonen, J.; Zelenin, K. N.; Potapov, A.-K. A.; Lagoda, I. V.; Alekseyev, V. V.; Pihlaja, K. Ring-Chain Tautomerism in 2-Substituted 1,2,3,4-Tetrahydroquinazolines A ^{1}H, ^{13}C and ^{15}N NMR Study. *Tetrahedron* **2003**, *59*, 1939-1950.

[13] Fan, X.; Li, B.; Guo, S.; Wang, Y.; Zhang, X. Synthesis of Quinazolines and Tetrahydroquinazolines: Copper-Catalyzed Tandem Reactions of 2-Bromobenzyl Bromides with Aldehydes and Aqueous Ammonia or Amines. *Chem. Asian J.* **2014**, *9*, 739-743.

[14] Schiedler, D. A.; Vellucci, J. K.; Beaudry, C. M. Formation of Carbon-Carbon Bonds Using Aminal Radicals. *Org. Lett.* **2012**, *14*, 6092-6095.

[15] Richers, M. T.; Zhao, C.; Seidel, D. Selective Copper(II) Acetate and Potassium Iodide Catalyzed Oxidation of Aminals to Dihydroquinazoline and Quinazolinone Alkaloids. *Beilstein J. Org. Chem.* **2013**, *9*, 1194-1201.

[16] Han, B.; Yang, X.-L.; Wang, C.; Bai, Y.-W.; Pan, T.-C.; Chen, X.; Yu, W. CuCl/DABCO/4-HO-TEMPO-Catalyzed Aerobic Oxidative Synthesis of 2-Substituted Quinazolines and 4*H*-3,1-Benzoxazines. *J. Org. Chem.* **2012**, *77*, 1136-1142.

[17] Maheswari, C. U.; Kumar, G. S.; Venkateshwar, M.; Kumar, R. A.; Kantam, M. L.; Reddy, K. R. Highly Efficient One-Pot Synthesis of 2-Substituted Quinazolines and 4*H*-Benzo[*d*][1,3]oxazines *via* Cross Dehydrogenative Coupling using Sodium Hypochlorite. *Adv. Synth. Catal.* **2010**, *352*, 341-346.

3. A Novel Way to Radiolabel Human Butyrylcholinesterase for PET through Irreversible Transfer of the Radiolabeled Moiety[1]

A Novel Way To Radiolabel Human Butyrylcholinesterase for Positron Emission Tomography through Irreversible Transfer of the Radiolabeled Moiety

Edgar Sawatzky,[a] Ehab Al-Momani,[b] Ryohei Kobayashi,[b] Takahiro Higuchi,[b] Samuel Samnick,[b] and Michael Decker*[a]

The enzyme butyrylcholinesterase (BChE) is known to be involved in the detoxification of xenobiotics in blood plasma and is associated with the progress of neurodegenerative disorders, diabetes type 2, obesity, and diseases of the cardiovascular system. In the present study, we developed carbamate-based inhibitors serving as positron emission tomography (PET) radiotracers with ^{18}F and ^{11}C as radioisotopes to visualize BChE distribution. These inhibitors are radiolabeled at the carbamate site and transfer this moiety onto BChE, which thus results in covalent and permanent radiolabeling of the enzyme. There are no comparable radiotracers for cholinesterases described to date. By ex vivo autoradiography experiments on mice brain slices and kinetic investigations, selective and covalent transfer of the radiolabeled carbamate moiety onto BChE was proven. These tracers might provide high resolution of BChE distribution in vivo to enable investigations into the pathophysiological mechanisms of diseases associated with alterations in BChE occurrence.

Author contributions:

Edgar Sawatzky, under supervision of Prof. Dr. Michael Decker, performed the design and the synthesis of all test compounds and precursors as well as their biological evaluation on BChE and AChE (IC$_{50}$-values and kinetic studies).

Edgar Sawatzky and Steffen Jeßberger, under supervision of Prof. Dr. Petra Högger, were responsible for the plasma stability test.

Dr. Ehab Al-Momani and Prof. Dr. Samuel Samnick preformed the radiosynthesis of the radiotracers.

Ryohei Kobayashi and Prof. Dr. Takahiro Higuchi were responsible for the *ex vivo* autoradiography experiments on mice brain slices.

3.1   Introduction

The clinical diagnosis of AD is challenging as it requires the proper distinction between pathophysological changes caused by AD and those caused by other neurodegenerative disorders, e.g. Parkinson's disease, or during the process of aging itself. Therefore, radiotracers applicable in positron emission spectroscopy (PET) can be used as a simple non-invasive tool to detect abnormal levels as well as unusual distribution of specific biological markers to ensure correct AD diagnosis. A typical biomarker is the occurrence of neurotoxic amyloid *β*-plaques in the brain; often described as the neuropathological hallmark of AD. Therefore, the development of suitable radiotracers for plaque visualization has continuously proceeded[2,3] resulting into three tracers ([^{18}F]Florbetapir (Amyvid; 2012), [^{18}F]Flutemetamol (Vizamyl; 2013) and [^{18}F]Florbetaben (Neuraceq; 2014), *cf.* **Figure 3.1**) approved by the US Food and Drug Administration (FDA) for AD diagnosis.[4,5] However, results with these tracers have to be carefully rated as amyloid *β*-plaque formation is common in AD but can also occur in healthy subjects.[6-9]
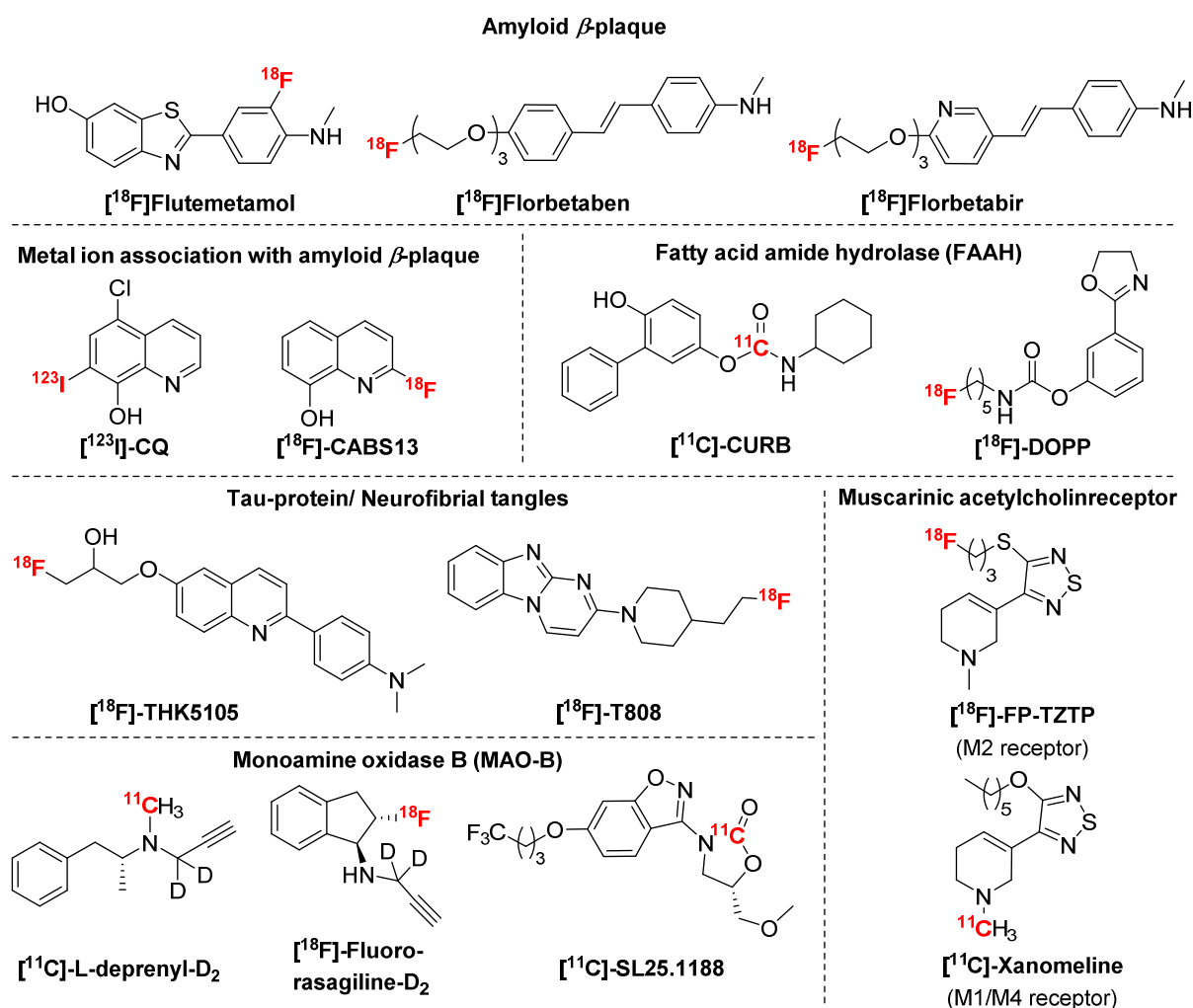
Figure 3.1. Structures of several prominent ^{11}C-labeled and ^{18}F-labeled PET radiotracers for imaging of different biological targets in Alzheimer's disease pathology. Radioisotopes are highlighted in red.[10,11]

Regarding the complex multifactorial nature of AD (*cf.* **Chapter 1.2**), besides amyloid *β*-plaques diverse proteins, receptors and enzymes are described in literature as potential target for PET tracer development to determine pathological changes associated with AD.[10,11] Some of the most prominent tracers are summarized in **Figure 3.1**. Also imaging of ChE is possible for AD diagnosis: In progressed AD the AChE concentration is known to be lost up to 90%[12-15] due to neuronal cell death. Therefore, selective PET tracers were developed to visualize these reduced AChE levels to assist AD diagnosis and to investigate the pathophysological role of AChE in the brain.[16] For this purpose, two general strategies have been pursued using substrate- or ligand-type radiotracers.[1] Substrate-type radiotracers (**Figure 3.2a**) are penetrating the brain and are hydrolyzed by AChE. The resulting radioactive metabolites cannot pass the blood brain barrier (BBB) because of their polar character, and in consequence radioactivity is accumulating in AChE rich brain regions (principle of metabolic trapping).[17-22] Ligand-type radio tracers are reversibly binding AChE inhibitors which are modified to incorporate a suitable radioisotope to non-covalently label the enzyme (**Figure 3.2b**).[16,23-28] Besides the described general types of radiotracers, a few irreversibly acting ChE inhibitors were reported that transfer a radiolabeled group covalently onto the enzyme thus labeling it irreversibly (**Figure 1c**).[29-31]
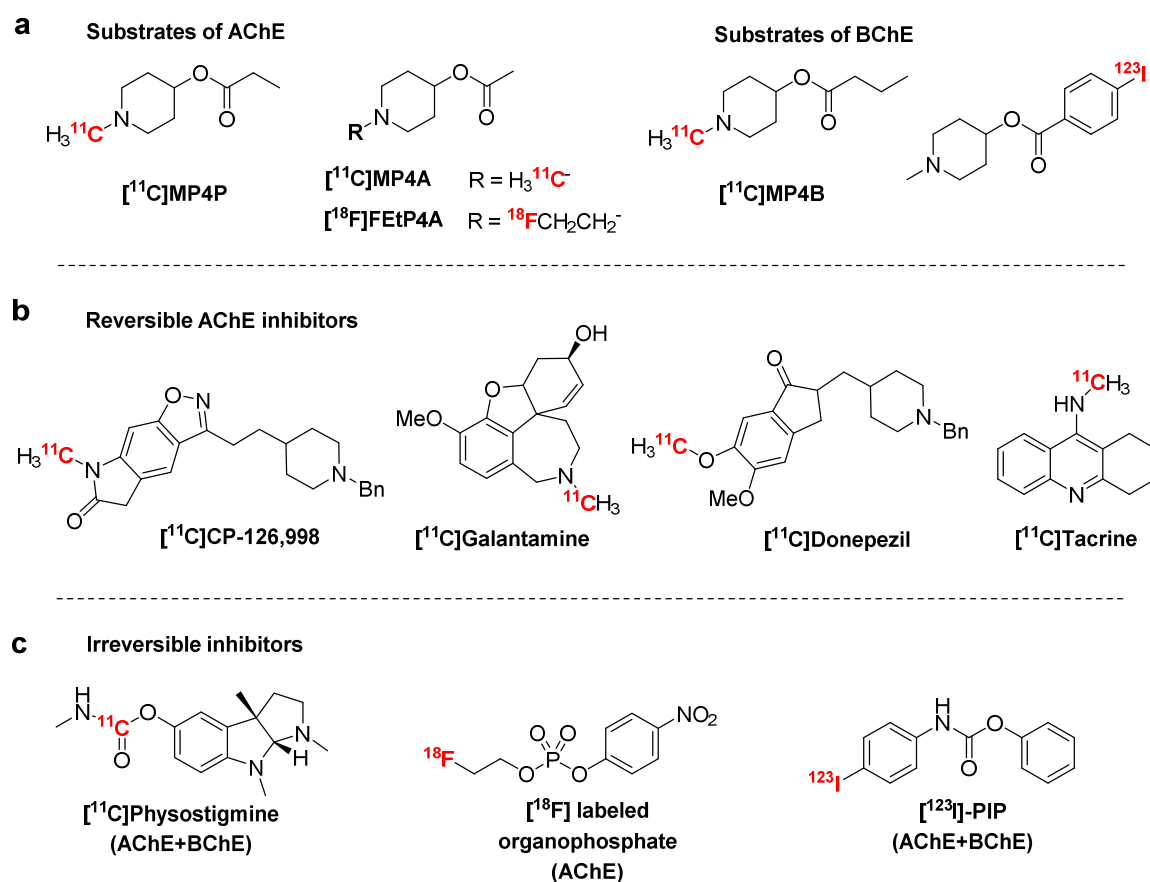
Figure 3.2. Radiotracers developed for ChE visualization: (**a**) Substrates for AChE and BChE using the principle of metabolic trapping, (**b**) reversible AChE inhibitors and (**c**) irreversible AChE inhibitors.[1]

However, in contrast to the decrease of AChE, the levels of some molecular forms of BChE are reported to be significantly increased up to 30-60%[32] and 40-90%[33] (values are reported in dependency of literature source) in several brain areas during AD resulting in a drastic increase of the BChE:AChE ratio, e.g. in cortical regions from 0.6 to as high as 11.[12,13,32,33] Furthermore, neurofibrillary tangles as well as amyloid β-plaques often were found to be colocalized with BChE[34-38] supporting the potential involvement of BChE in plaque formation and its role for decreased cognitive performance associated with plaques.[39-41]

Regarding the distinct pathological changes of increased BChE levels and its colocalization in neurotoxic plaques during AD, it is quite remarkable that there is little attention on BChE as a physiological marker for AD diagnosis. To date, only a few selective substrate-type tracers (**Figure 3.2a**) have been developed for BChE imaging.[36,42-45] To overcome the lack of such BChE tracer, this chapter will describe the development of selective carbamate based BChE inhibitors as suitable PET tracer by the introduction of ^{18}F and ^{11}C as possible radionuclids. These tracers might offer new possibilities for AD diagnosis and can help to investigate pathophysological changes, expression levels and locations of BChE to understand the molecular mechanisms in AD and diseases associated with this enzyme (*cf.* **Chapter 1.3**).[1]

3.2   Design and Development of PET Radiotracers

For the design of new PET tracers, the highly potent BChE inhibitor **1** (**Figure 3.3**) was chosen because of its good affinity and selectivity on BChE over AChE.[46] In contrast to the typically applied concepts of ChE radiotracers (**Figure 3.2a** and **b**), the irreversible labeling approach reported for fatty acid amide hydrolase (FAAH)[47-50] and monoacylglycerol lipase (MAGL)[51,52] was adopted and incorporation of the radio isotopes was performed at the carbamate site.[1] The resulting tracer can transfer its radio labeled moiety covalently onto BChE under release of the tetrahydroquinazoline carrier scaffold **2** thus BChE radio labeling occurs directly and permanently at the enzymes active site (**Figure 3.3**).
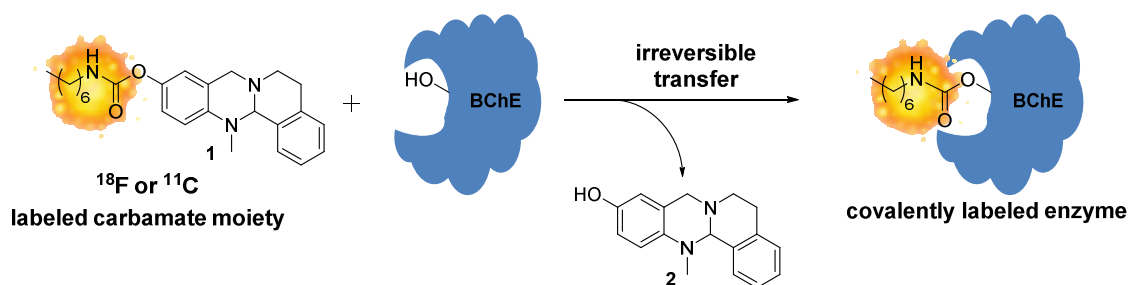
Figure 3.3. Covalent labeling of BChE with the irreversible inhibitor **1** by carbamate transfer.[1]

In general, the direct introduction of a radioisotope in the last reaction step during synthesis is desirable to prevent time dependent decay of the radioisotope as well as undesired side reactions.[1] Therefore, for ^{18}F-introduction at the carbamate site of inhibitor **1**, precursor **9** was synthesized bearing an iodine leaving group which can easily be replaced by [18]F (**Scheme 3.1a**): For this purpose, amino alcohol **4** was synthesized *via* a Gabriel synthesis from 7-bromoheptan-1-ol. Further activation of **4** with 4-nitrophenyl chloroformate gave intermediate **5** which was coupled with the phenolic tetrahydroquinazoline **2** (synthesis described in literature[53]) to yield carbamate **6**. Although the activation of the alcohol moiety in **6** with *p*-toluenesulfonyl chloride towards compound **7** failed in an initial attempt, precursor **8** and the unlabeled fluorinated compound **9** (necessary as reference compound to identify [**18**F]**9** during HPLC purification) could easily be synthesized directly from carbamate **6**.

a

b
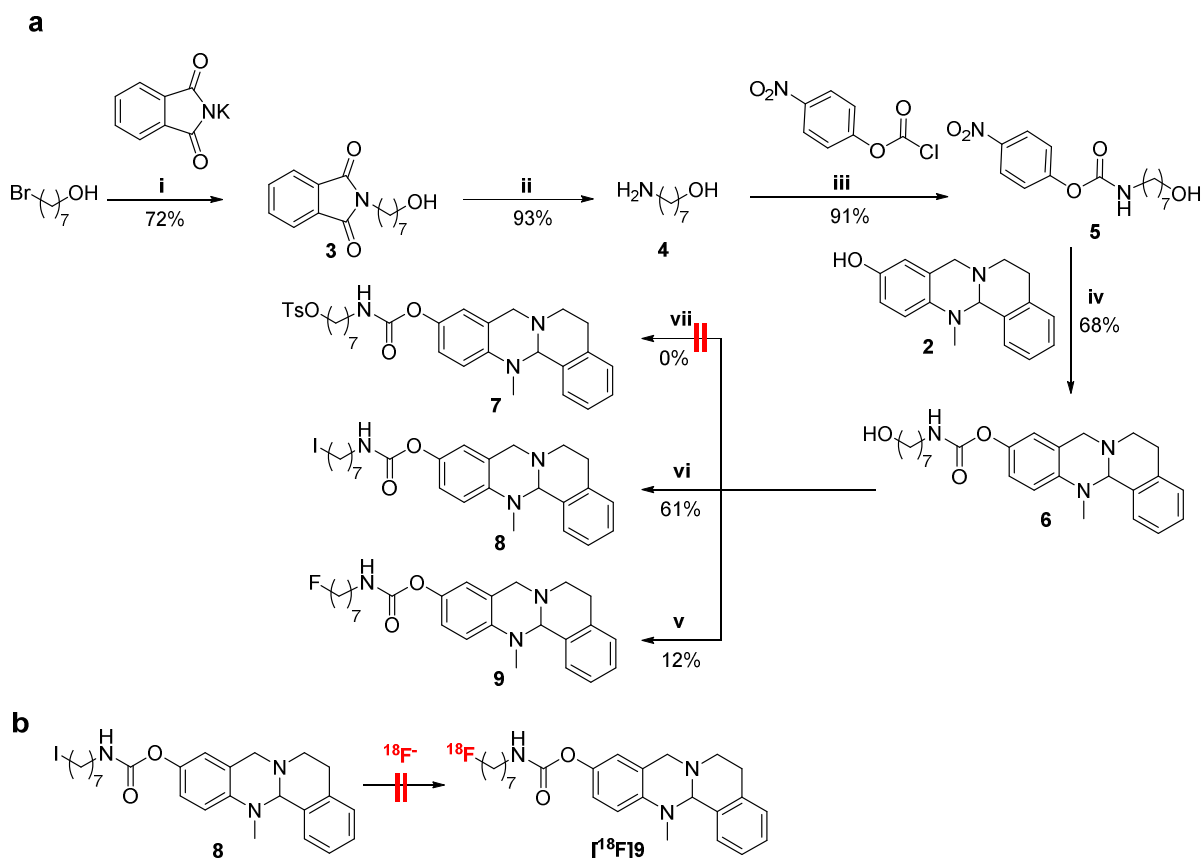
Scheme 3.1. Reagents and conditions: (i) DMF, 3 h, 120 °C; (ii) H_2N-$NH_2 \cdot H_2O$, EtOH, 5 h, reflux; (iii) Et_3N, DCM, 2 h, rt; (iv) NaH, THF, 1 h, rt; (v) DAST, DCM, 6 h, rt; (vi) PPh_3, I_2, THF, 2 h, rt, (vii) TsCl, DCM.[1]

Unfortunately, the direct ^{18}F-labeling of precursor **8** towards radiotracer [**18**F]**9** failed (**Scheme 3.1b**). Sadovski *et al.*[49] reported similar difficulties for the synthesis of [18F]DOPP (*cf.* **Figure 3.1**) as the carbamate moiety undergoes a fast E1cb elimination due to the basic labeling conditions. Therefore, the synthesis strategy was

altered and precursor **11** was smoothly synthesized starting with amino alcohol **4** (**Scheme 3.2a**). In a four step reaction sequence 1) precursor **11** was radiolabeled with $^{18}F^-$, 2) Boc-deprotected under acidic conditions, 3) activated with 4-nitrophenyl chloroformate towards **[^{18}F]12** and 4) coupled with phenol **2** to obtain the desired radiotracer **[^{18}F]9** in a radiochemical yield of 17-22% (n = 5, corrected decay) and a radiochemical purity of >98% after purification by reversed phase HPLC (**Scheme 3.2b**).[1]

a

b
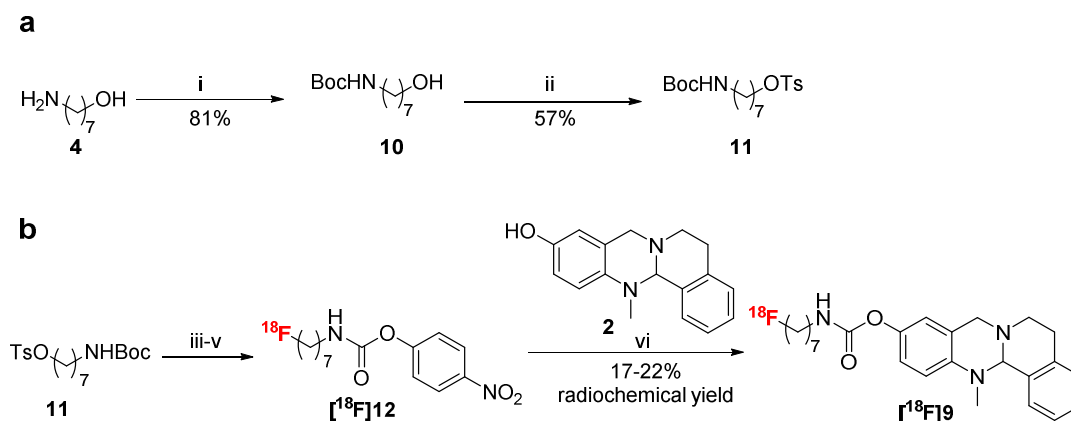
Scheme 3.2. Reagents and conditions: (i) (*t*Boc)$_2$O, K$_2$CO$_3$, MeOH/H$_2$O, 4 h, rt; (ii) TsCl, Et$_3$N, K$_2$CO$_3$, DCM, 3 d, rt; (iii) [^{18}F]F$^-$, Kryptofix 222, K$_2$CO$_3$, 10 min, 90 °C; (iv) TFA, 10 min, rt; (v) Et$_3$N, CH$_3$CN, 4-NO$_2$-Ph-O(C=O)Cl, 90 °C, 7 min; (vi) 10 min, 90 °C.[1]

Introduction of ^{11}C into an aliphatic carbamate is even more challenging regarding the little possibilities to incorporate the radioisotope without altering the chemical structure. Wilson and coworkers[48,54,55] developed a method to incorporate ^{11}C at the carbonyl carbon in carbamate and urea based derivatives by applying ^{11}CO$_2$, 2-*tert*-butylimino-2-diethylamino-1,3-dimethylperhydro-1,3,2-diazaphosphorine (BEMP) and POCl$_3$ in three reaction steps. Although this method is well described, a different approach was performed to avoid multiple steps with the radioisotope: Precursor **14** was synthesized in two steps using triphenylphosphine and heptylamine (**Scheme 3.3**). When treating a mixture of precursor **14** and tetracyclic phenol **2** in the presence of DBU with ^{11}CO$_2$, followed by heating to 60 °C for 6 min, the desired radiotracer **[^{11}C]1** was obtained in only one reaction step with a radiochemical yield of 30-36% (n = 4, corrected decay) and a radiochemical purity of 98% after purification by reversed phase HPLC (**Scheme 3.3**).[1]
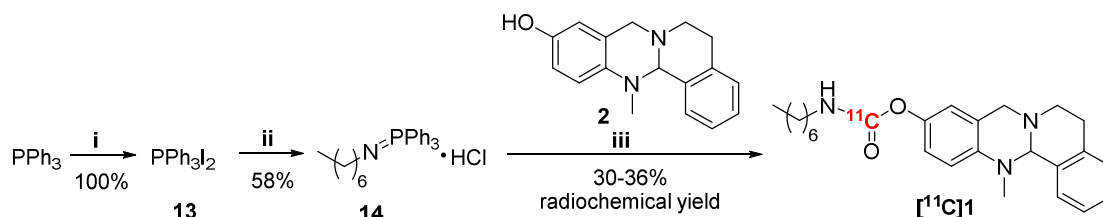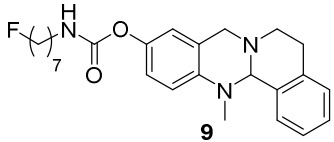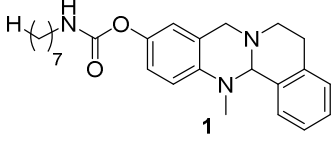
Scheme 3.3. Reagents and conditions: (i) I$_2$, Et$_2$O, 1 h, rt; (ii) CH$_3$(CH$_2$)$_6$NH$_2$, DCM, 5 h, rt; (iii) 1) DBU, ^{11}CO$_2$, THF, 10 min, -78 °C; 2) 6 min, 60 °C.

3.3   Enzyme Inhibition and Kinetic Studies

To prove irreversibility of radiolabelling by carbamate transfer of the described radiotracer, kinetic investigations were performed with the non-labeled analogues **1** (synthesis described by Darras *et al.*[46]) and **9**. Initial determination of IC$_{50}$-values for both compounds revealed inhibition of *h*BChE in the low nanomolar range with a high selectivity over *h*AChE (**Table 3.1**). However, carbamate based pseudo-irreversible inhibitors are known to undergo a three step kinetic process (**Table 3.1**): In an initial step, the inhibitor (I) binds reversibly to the enzyme (E) forming an enzyme-inhibitor-complex (EI) described in equilibrium by the constant K$_C$. In the second step, the carbamate moiety is transferred covalently onto the enzyme (E-C) thus inhibiting the enzyme irreversibly with k$_3$ as the carbamoylation rate constant. Finally, the carbamate moiety is hydrolyzed off over time while recovering the intact enzyme (E) and k$_4$ as the decarbamoylation rate constant (A detailed description of this study as well as the calculation of the kinetic parameters can be found in **Appendix 1**[1] and **Appendix 2**[56]).

Table 3.1. Inhibition and kinetic data on human AChE and BChE for compound **9** and **1**. Experiments were performed in triplicate.[1]

	IC$_{50}$(*h*AChE) [µM] (pIC$_{50}$ ±SEM)	IC$_{50}$(*h*BChE) [nM] (pIC$_{50}$ ±SEM)	K$_C$(*h*BChE) ±SEM [nM]	k$_3$(*h*BChE) ±SEM [min^{-1}]	k$_4$(*h*BChE) ±SEM [h^{-1}]
9	3.6 (5.44 ± 0.05)	5.2 (8.28 ± 0.02)	24.3 ± 19.3	0.78 ± 0.48	0.81 ± 0.04
1	3.8 (5.42 ± 0.02)	6.4 (8.19 ± 0.02)	28.5 ± 17.2	0.66 ± 0.32	0.62 ± 0.04

Carbamate transfer onto the enzyme is a comparable slow reaction, thus enzyme inhibition by carbamate based inhibitors is time dependent. Compounds **1** and **9** caused such a time dependent inhibition (**Figure 3.4a** and **3.4b**) with high affinity (K_C-values in **Table 3.1**) on *h*BChE and a high carbamoylation rate constant (k_3-values in **Table 3.1**). Also decarbamoylation experiments (**Figure 3.4c** and **3.4d**) were performed and revealed a slow recovery of the enzyme with a half-life time of the carbamoylated enzyme (E-C) of approximately 1 h before cleavage of the carbamate moiety. Therefore, carbamoylation kinetics as well as decarbamoylation kinetics proved carbamate transfer of the reference compounds **1** and **9** onto the enzyme showing that radiotracers **[11C]1** and **[18F]9** act irreversibly.
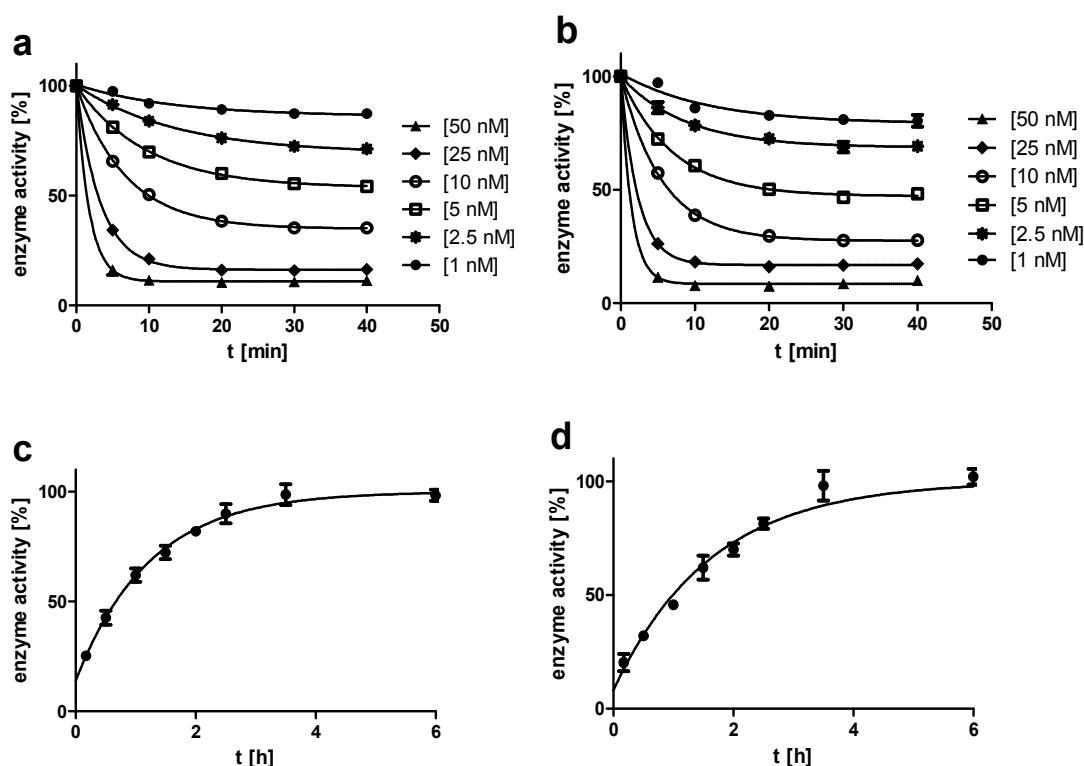
Figure 3.4. Time dependent inhibition of *h*BChE by different concentrations of (**a**) compound **9** and (**b**) compound **1**. Recovery of *h*BChE activity after inhibition with (**c**) compound **9** and 1000fold dilution and (**d**) with compound **1** and 1000fold dilution. Experiments were performed in triplicate (means±SD).[1]

3.4 Plasma Stability Analyzes

Plasma stability is an important factor for PET tracer development, especially as BChE is one of the major detoxification enzymes in human plasma.[57] Therefore, plasma stability analyses on human pooled plasma samples were carried out with the non-labeled reference compounds **1** and **9**. Only slow degradation of both

compounds was observed (blue and black in **Figure 3.5**) with less than 50% decomposition even after 2 h;[1] and also preinhibition of BChE with a high tacrine concentration (50 μM) led to similar results (yellow and purple in **Figure 3.5**). Only when precipitating the plasma proteins beforehand, no degradation of compound **9** was observed (red in **Figure 3.5**). These results show:

1) Plasma stability of the test compounds is sufficient high for PET investigations.
2) The test compounds are not only cleaved by BChE as preinhibition of BChE with tacrine did not alter their cleavage.
3) Degradation is enzyme mediated as no cleavage of the test compounds was observed when removing the plasma proteins beforehand.
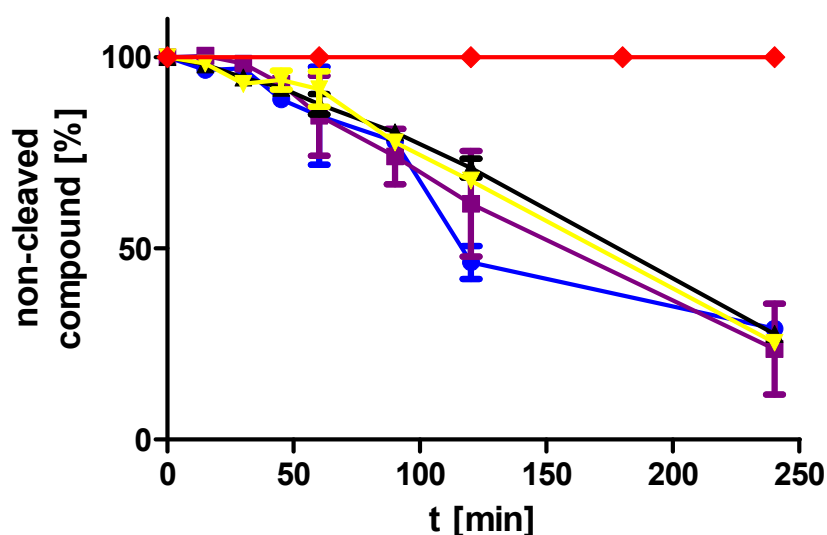
Figure 3.5. Time-dependent plasma stability of compounds **9** (black) and **1** (blue) and stability after pretreatment with a tacrine concentration of 50 μM (**9** yellow; **1** purple). Stability of compound **9** was also measured when proteins had been precipitated beforehand (red). Experiments were performed in triplicate (means±SEM). [1]

3.5   *Ex vivo* Autoradiography

To show specific binding of the developed radiotracer, *ex vivo* brain-autoradiography experiments with healthy mouse brain slices were performed using [18F]**9** (**Figure 3.6**). When applying radio tracer [18F]**9** onto brain tissue, good binding of the radio tracer was observed in all brain areas (**Figure 3.6a**). Pre-blocking of BChE with the known selective BChE inhibitor ethopropazine followed by the addition of [18F]**9** caused only little binding of the radiotracer onto the tissue samples, thus proving that binding of [18F]**9** on brain tissue is selective for BChE.
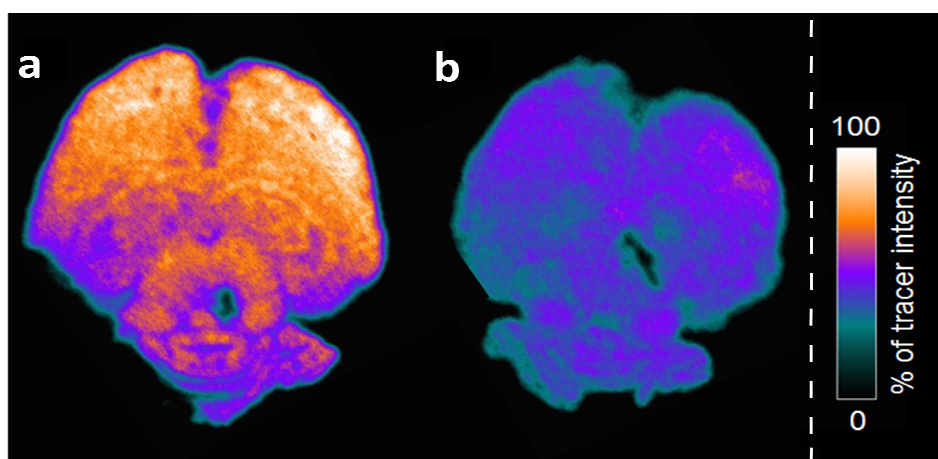
Figure 3.6. Autoradiography of **[^{18}F]9** on a healthy mouse brain (**a**) without and (**b**) with ethopropazine hydrochloride pre-incubation. Intensity (arbitrary unit) is given in percentage of the maximum tracer activity.[1]

3.6   Conclusion

To date, the proper diagnosis of AD is challenging and is supported by using selective PET radiotracers targeting amyloid β-plaques as physiological marker. However, also BChE levels are remarkably increased during AD and BChE is found to be colocalized with toxic amyloid β-plaques. Therefore, targeting of BChE with PET tracers can help to enable the diagnosis of AD and to investigate pathophysological alterations associated with this enzyme. Compounds **[^{11}C]1** and **[^{18}F]9** were developed as such selective BChE tracers. These tracers are labeled at the carbamate site and transfer their carbamate moiety onto the active site of BChE thus radiolabeling the enzyme covalently. Kinetic investigations could prove that carbamate transfer is rapidly taking place and revealed a high stability of the transferred moiety at the enzyme. First *ex vivo* autoradiography experiments combined with blocking studies on mice brain slices could show that binding of these tracers occurs selectively at BChE. Taking these results together, the described radiotracers have encouraging properties for further *in vivo* experiments with the overall aim to develop new PET tracers to reveal physiological alterations of BChE levels and distribution. Such tracers might be used as a diagnostic tool to improve proper AD diagnosis.

The detailed results of this chapter as well as experimental data were previously published[1] and can be found in **Appendix 1**.

3.7 References

[1] Sawatzky, E.; Al-Momani, E.; Kobayashi, R.; Higuchi, T.; Samnick, S.; Decker, M. A Novel Way to Radiolabel Human Butyrylcholinesterase for Positron Emission Tomography through Irreversible Transfer of the Radiolabeled Moiety. *ChemMedChem* **2016**, *11*, 1540-1550.

[2] Mason, N. S.; Mathis, C. A.; Klunk, W. E. Positron Emission Tomography Radioligands for *in vivo* Imaging of Aβ Plaques. *J. Label. Compd. Radiopharm.* **2013**, *56*, 89-95.

[3] Promteangtrong, C.; Kolber, M.; Ramchandra, P.; Moghbel, M.; Houshmand, S.; Schöll, M.; Werner, T. J.; Alavi, A.; Buchpiguel, C. Multimodality Imaging Approaches in Alzheimer's Disease Part II: 1H MR Spectroscopy, FDG PET and Amyloid PET. *Dement. Neuropsychol.* **2015**, *9*, 330-342.

[4] FDA| US Food and Drug Administration Home Page. Drugs@FDA: FDA Approved Drug Products. http://www.accessdata.fda.gov/scripts/cder/drugsatfda/index.cfm. (Accessed May 12, 2016).

[5] Morris, E.; Chalkidou, A.; Hammers, A.; Peacock, J.; Summers, J.; Keevil, S. Diagnostic Accuracy of ^{18}F Amyloid PET Tracers for the Diagnosis of Alzheimer's Disease: A Systematic Review and Meta-Analysis. *Eur. J. Nucl. Med. Mol. Imaging* **2016**, *43*, 374-385.

[6] Morris, J. C.; Storandt, M.; McKeel, D. W.; Rubin, E. H.; Price, J. L.; Grant, E. A.; Berg, L. Cerebral Amyloid Deposition and Diffuse Plaques in "Normal" Aging: Evidence for Presymptomatic and Very Mild Alzheimer's Disease. *Neurol.* **1996**, *46*, 707-719.

[7] Villain, N.; Chételat, G.; Grassiot, B.; Bourgeat, P.; Jones, G.; Ellis, K. A.; Ames, D.; Martins, R. N.; Eustache, F.; Salvado, O.; Masters, C. L.; Rowe, C. C.; Villemagne, V. L.; AIBL Research Group Regional Dynamics of Amyloid-β Deposition in Healthy Elderly, Mild Cognitive Impairment and Alzheimer's Disease: A Voxelwise PiB–PET Longitudinal Study. *Brain* **2012**, *135*, 2126-2139.

[8] Villemagne, V. L.; Pike, K. E.; Chételat, G.; Ellis, K. A.; Mulligan, R. S.; Bourgeat, P.; Ackermann, U.; Jones, G.; Szoeke, C.; Salvado, O.; Martins, R.; O'Keefe, G.; Mathis, C. A.; Klunk, W. E.; Ames, D.; Masters, C. L.; Rowe, C. C. Longitudinal Assessment of Aβ and Cognition in Aging and Alzheimer Disease. *Ann. Neurol.* **2011**, *69*, 181-192.

[9] Sojkova, J.; Zhou, Y.; An, Y.; Kraut, M. A.; Ferrucci, L.; Wong, D. F.; Resnick, S. M. Longitudinal Patterns of β-Amyloid Deposition in Nondemented Older Adults. *Arch. Neurol.* **2011**, *68*, 644-649.

[10] Holland, J. P.; Liang, S. H.; Rotstein, B. H.; Collier, T. L.; Stephenson, N. A.; Greguric, I.; Vasdev, N. Alternative Approaches for PET Radiotracer Development in Alzheimer's Disease: Imaging Beyond Plaque. *J. Label Compd. Radiopharm.* **2014**, *57*, 323-331.

[11] McConathy, J.; Sheline, Y. I. Imaging Biomarkers Associated With Cognitive Decline: A Review. *Biol. Psychiatry* **2015**, *77*, 685-692.

[12] Nordberg, A.; Ballard, C.; Bullock, R.; Darreh-Shori, T.; Somogyi, M. A Review of Butyrylcholinesterase as a Therapeutic Target in the Treatment of Alzheimer's Disease. *Prim. Care Companion CNS Disord.* **2013**, *15*; doi:10.4088/PCC.12r01412.

[13] Giacobini, E. Cholinergic Function and Alzheimer's Disease. *Int. J. Geriatr. Psych.* **2003**, *18*, 1-5.

[14] Shinotoh, H.; Namba, H.; Fukushi, K.; Nagatsuka, S.; Tanaka, N.; Aotsuka, A.; Ota, T.; Tanada, S.; Irie, T. Progressive Loss of Cortical Acetylcholinesterase Activity in Association with Cognitive Decline in Alzheimer's Disease: A Positron Emission Tomography Study. *Ann. Neurol.* **2000**, *48*, 194-200.

[15] Rinne, J. O.; Kaasinen, V.; Järvenpää, T.; Någren, K.; Roivainen, A.; Yu, M.; Oikonen, V.; Kurki, T. Brain Acetylcholinesterase Activity in Mild Cognitive Impairment and Early Alzheimer's Disease. *J. Neurol. Neurosurg. Psychiatry* **2003**, *74*, 113-115.

[16] Kikuchi, T.; Okamura, T.; Zhang, M.-R.; Irie, T. PET Probes for Imaging Brain Acetylcholinesterase. *J. Label. Compd. Radiopharm.* **2013**, *56*, 172-179.

[17] Haense, C.; Kalbe, E.; Herholz, K.; Hohmann, C.; Neumaiera, B.; Kraisa, R.; Heiss, W.-D. Cholinergic System Function and Cognition in Mild Cognitive Impairment. *Neurobiol. Aging* **2012**, *33*, 867-877.

[18] Namba, H.; Fukushi, K.; Nagatsuka, S.; Iyo, M.; Shinotoh, H.; Tanada, S.; Irie, T. Positron Emission Tomography: Quantitative Measurement of Brain Acetylcholinesterase Activity Using Radiolabeled Substrates. *Methods* **2002**, *27*, 242-250.

[19] Herholz, K. Acetylcholine Esterase Activity in Mild Cognitive Impairment and Alzheimer's Disease. *Eur. J. Nucl. Med. Mol. Imaging* **2008**, *35*, 25-29.

[20] Iyo, M.; Namba, H.; Fukushi, K.; Shinotoh, H.; Nagatsuka, S.; Suhara, T.; Sudo, Y.; Suzuki, K.; Irie, T. Measurement of Acetylcholinesterase by Positron Emission Tomography in the Brains of Healthy Controls and Patients with Alzheimer's Disease. *Lancet* **1997**, *349*, 1805-1809.

[21] Nagatsuka, S.; Fukushi, K.; Shinotoh, H.; Namba, H.; Iyo, M.; Tanaka, N.; Aotsuka, A.; Ota, T.; Tanada, S.; Irie, T. Kinetic Analysis of [11C]MP4A Using a High-Radioactivity Brain Region that Represents an Integrated Input Function for Measurement of Cerebral Acetylcholinesterase Activity Without Arterial Blood Sampling. *J. Cereb. Blood Flow Metab.* **2001**, *21*, 1354-1366.

[22] Shao, X.; Koeppe, R. A.; Butch, E. R.; Kilbourn, M. R.; Snyder, S. E. Evaluation of ^{18}F-Labeled Acetylcholinesterase Substrates as PET Radiotracers. *Bioorg. Med. Chem.* **2005**, *13*, 869-875.

[23] Musachio, J. L.; Flesher, J. E.; Scheffel, U. A.; Rauseo, P.; Hilton, J.; Mathews, W. B.; Ravert, H. T.; Dannals, R. F.; Frost J. J. Radiosynthesis and Mouse Brain Distribution Studies of [11C]CP-126,998: a PET Ligand for *in vivo* Study of Acetylcholinesterase. *Nucl. Med. Biol.* **2002**, *29*, 547-552.

[24] Kim, D. H.; Choe, Y. S.; Choi, J. Y.; Lee, K.-H.; Kim, B.-T. Binding of 2-[18F]fluoro-CP-118,954 to Mouse Acetylcholinesterase: MicroPET and *ex vivo* Cerenkov Luminescence Imaging Studies. *Nucl. Med. Biol.* **2011**, *38*, 541-547.

[25] Ryu, E. K.; Choe, Y. S.; Park, E. Y.; Paik, J.-Y.; Kim, Y. R.; Lee, K.-H.; Choi, Y.; Kim, S. E.; Kim, B.-T. Synthesis and Evaluation of 2-[18F]fluoro-CP-118,954 for the *in vivo* Mapping of Acetylcholinesterase. *Nucl. Med. Biol.* **2005**, *32*, 185-191.

[26] Kimura, H.; Kawai, T.; Hamashima, Y.; Kawashima, H.; Miura, K.; Nakaya, Y.; Hirasawa, M.; Arimitsu, K.; Kajimoto, T.; Ohmomo, Y.; Ono, M.; Node, M.; Saji, H. Synthesis and Evaluation of (-)- and (+)-[11C]Galanthamine as PET Tracers for Cerebral Acetylcholinesterase Imaging. *Bioorg. Med. Chem.* **2014**, *22*, 285-291.

[27] De Vos, F.; Santens, P.; Vermeirsch, H.; Dewolf, I.; Dumont, F.; Slegers, G.; Dierckx, R. A.; De Reuck, J. Pharmacological Evaluation of [11C]Donepezil as Tracer for Visualization of Acetylcholinesterase by PET. *Nucl. Med. Biol.* **2000**, *27*, 745-747.

[28] Tavitian, B.; Pappata, S.; Bonnot-Lours, S.; Prenant, C.; Jobert, A.; Crouzel, C.; Di Giamberardino, L. Positron Emission Tomography Study of [11C]Methyl-Tetrahydroaminoacridine (Methyl-Tacrine) in Baboon Brain. *Eur. J. Pharmacol.* **1993**, *236*, 229-238.

[29] James, S. L.; Ahmed, S. K.; Murphy, S.; Braden, M. R.; Belabassi, Y.; VanBrocklin, H. F.; Thompson, C. M.; Gerdes, J. M. A Novel Fluorine-18 *β*-Fluoroethoxy Organophosphate Positron Emission Tomography Imaging Tracer Targeted to Central Nervous System Acetylcholinesterase. *ACS Chem. Neurosci.* **2014**, *5*, 519-524.

[30] Blomqvist, G.; Tavitian, B.; Pappata, S.; Crouzel, C.; Jobert, A.; Doignon, I.; Di Giamberardino, L. Quantitative Measurement of Cerebral Acetylcholinesterase Using [11C]Physostigmine and Positron Emission Tomography. *J. Cereb. Blood Flow Metab.* **2001**, *21*, 114-131.

[31] Macdonald, I. R.; Reid, G. A.; Pottie, I. R.; Martin, E.; Darvesh, S. Synthesis and Preliminary Evaluation of Phenyl 4-^{123}I-Iodophenylcarbamate for Visualization of Cholinesterases Associated with Alzheimer Disease Pathology. *J. Nucl. Med.* **2016**, *57*, 297-302.

[32] Greig, N. H.; Utsuki, T.; Yu, X.-S.; Zhu, X.; Holloway, H. W.; Perry, T.; Lee, B.; Ingram, D. K.; Lahiri, D. K. A New Therapeutic Target in Alzheimer's Disease Treatment: Attention to Butyrylcholinesterase. *Curr. Med. Res. Opin.* **2001**, *17*, 159-165.

[33] Greig, N. H.; Lahiri, D. K.; Sambamurti, K. Butyrylcholinesterase: An Important New Target in Alzheimer's Disease Therapy. *Int. Psychogeriatr.* **2002**, *14*, 77-91.

[34] Darvesh, S.; Hopkins, D. A.; Geula, C. Neurobiology of Butyrylcholinesterase. *Nat. Rev. Neurosci.* **2003**, *4*, 131-138.

[35] Mizukami, K.; Akatsu, H.; Abrahamson, E. E.; Mi, Z.; Ikonomovic, M. D. Immunohistochemical Analysis of Hippocampal Butyrylcholinesterase: Implications for Regional Vulnerability in Alzheimer's Disease. *Neuropathology* **2016**, *36*, 135-145.

[36] Darvesh, S. Butyrylcholinesterase Radioligands to Image Alzheimer's Disease Brain. *Chem. Biol. Interact.* **2013**, *203*, 354-357.

[37] Darvesh, S.; Cash, M. K.; Reid, G. A.; Martin, E.; Mitnitski, A.; Geula, C. Butyrylcholinesterase is Associated with β-Amyloid Plaques in the Transgenic APP$_{SWE}$/PSEN1dE9 Mouse Model of Alzheimer Disease. *J. Neuropathol. Exp. Neurol.* **2012**, *71*, 2-14.

[38] Reid, G. A.; Darvesh, S. Butyrylcholinesterase-Knockout Reduces Brain Deposition of Fibrillar β-Amyloid in an Alzheimer Mouse Model. *Neuroscience* **2015**, *298*, 424-435.

[39] Furukawa-Hibi, Y.; Alkam, T.; Nitt, A.; Matsuyama, A.; Mizoguchi, H.; Suzuki, K.; Moussaoui, S.; Yu, Q.-S.; Greig, N. H.; Nagai, T.; Yamada, K. Butyrylcholinesterase Inhibitors Ameliorate Cognitive Dysfunction Induced by Amyloid-β Peptide in Mice. *Behav. Brain Res.* **2011**, *225*, 222-229.

[40] Greig, N. H.; Utsuki, T.; Ingram, D. K.; Wang, Y.; Pepeu, G.; Scali, C.; Yu, Q.-S.; Mamczarz, J.; Holloway, H. W.; Giordano, T.; Chen, D.; Furukawa, K.; Sambamurti, K.; Brossi, A.; Lahiri, D. K. Selective Butyrylcholinesterase Inhibition Elevates Brain Acetylcholine, Augments Learning and Lowers Alzheimer β-Amyloid Peptide in Roden. *PNAS* **2005**, *102*, 17213-17218.

[41] Maurice, T.; Strehaiano, M.; Siméon, N.; Bertrand, C.; Chatonnet, A. Learning Performances and Vulnerability to Amyloid Toxicity in the Butyrylcholinesterase Knockout Mouse. *Behav. Brain. Res.* **2016**, *296*, 351-360.

[42] Macdonald, I. R.; Reid, G. A.; Joy, E. E.; Pottie, I. R.; Matte, G.; Burrell, S.; Mawko, G.; Martin, E.; Darvesh, S. Synthesis and Preliminary Evaluation of Piperidinyl and Pyrrolidinyl Iodobenzoates as Imaging Agents for Butyrylcholinesterase. *Mol. Imaging Biol.* **2011**, *13*, 1250-1261.

[43] Snyder, S. E.; Gunupudi, N.; Sherman, P. S.; Butch, E. R.; Skaddan, M. B.; Kilbourn, M. R.; Koeppe, R. A.; Kuhl, D. E. Radiolabeled Cholinesterase Substrates: *In Vitro* Methods for Determining Structure-Activity Relationships and Identification of a Positron Emission Tomography Radiopharmaceutical for *in vivo* Measurement of Butyrylcholinesterase Activity. *J. Cereb. Blood Flow Metab.* **2001**, *21*, 132-143.

[44] Roivainen, A.; Rinne, J.; Virta, J.; Järvenpää, T.; Salomäki, S.; Yu, M.; Någren, K. Biodistribution and Blood Metabolism of 1-^{11}C-Methyl-4-Piperidinyl *n*-Butyrate in Humans: An Imaging Agent for *in vivo* Assessment of Butyrylcholinesterase Activity with PET. *J. Nucl. Med.* **2004**, *45*, 2023-2039.

[45] Virta, J. R.; Tolvanen, T.; Någren, K.; Brück, A.; Roivainen, A.; Rinne, J. O. 1-^{11}C-Methyl-4-Piperidinyl-*N*-Butyrate Radiation Dosimetry in Humans by Dynamic Organ-Specific Evaluation. *J. Nucl. Med.* **2008**, *49*, 347-353.

[46] Darras, F. H.; Kling, B.; Heilmann J.; Decker, M. Neuroprotective Tri- and Tetracyclic BChE Inhibitors Releasing Reversible Inhibitors upon Carbamate Transfer. *ACS Med. Chem. Lett.* **2012**, *3*, 914-919.

[47] Rusjan, P. M.; Wilson, A. A.; Mizrahi, R.; Boileau, I.; Chavez, S. E.; Lobaugh, N. J.; Kish, S. J.; Houle, S.; Tong, J. Mapping Human Brain Fatty Acid Amide Hydrolase Activity with PET. *J. Cereb. Blood Flow Metab.* **2013**, *33*, 407-414.

[48] Wilson, A. A.; Hicks, J. W.; Sadovski, O.; Parkes, J.; Tong, J.; Houle, S.; Fowler, C. J.; Vasdev, N. Radiosynthesis and Evaluation of ^{11}C-Carbonyl]-Labeled Carbamates as Fatty Acid Amide Hydrolase Radiotracers for Positron Emission Tomography. *J. Med. Chem.* **2013**, *56*, 201-209.

[49] Sadovski, O.; Hicks, J. W.; Parkes, J.; Raymond, R.; Nobrega, J.; Houle, S.; Cipriano, M.; Fowler, C. J.; Vasdev, N.; Wilson, A. A. Development and Characterization of a Promising Fluorine-18 Labelled Radiopharmaceutical for *in vivo* Imaging of Fatty Acid Amide Hydrolase. *Bioorg. Med. Chem.* **2013**, *21*, 4351-4357.

[50] Rotstein, B. H.; Wey, H.-Y.; Shoup, T. M.; Wilson, A. A.; Liang, S. H.; Hooker, J. M.; Vasdev, N. PET Imaging of Fatty Acid Amide Hydrolase with [^{18}F]DOPP in Nonhuman Primates. *Mol. Pharmaceutics* **2014**, *11*, 3832-3838.

[51] Wang, C.; Placzek, M. S.; Van de Bittner, G. C.; Schroeder, F. A.; Hooker, J. M. A Novel Radiotracer for Imaging Monoacylglycerol Lipase in the Brain Using Positron Emission Tomography. *ACS Chem. Neurosci.* **2016**, *7*, 484-489.

[52] Hicks, J. W.; Parkes, J.; Tong, J.; Houle, S.; Vasdev, N.; Wilson, A. A. Radiosynthesis and *ex vivo* Evaluation of ^{11}C-Carbonyl]Carbamate- and Urea-Based Monoacylglycerol Lipase Inhibitors. *Nucl. Med. Biol.* **2014**, *41*, 688-694.

[53] Sawatzky, E.; Bukowczan, J.; Decker, M. Investigation into Selective Debenzylation and Ring Cleavage of Quinazoline Based Heterocycles. *Tetrahedron Lett.* **2014**, *55*, 2973-2976.

[54] Wilson, A. A.; Garcia, A.; Houle, S.; Sadovski, O.; Vasdev, N. Synthesis and Application of Isocyanates Radiolabeled with Carbon-11. *Chem. Eur. J.* **2011**, *17*, 259-264.

[55] Rotstein, B. H.; Liang, S. H.; Holland, J. P.; Lee Collier, T.; Hooker, J. M.; Wilson A. A.; Vasdev, N. $^{11}CO_2$ Fixation: A Renaissance in PET Radiochemistry. *Chem. Commun.* **2013**, *49*, 5621-5629.

[56] Sawatzky, E.; Wehle, S.; Kling, B.; Wendrich, J.; Bringmann, G.; Sotriffer, C. A.; Heilmann, J.; Decker, M. Discovery of Highly Selective and Nanomolar Carbamate-Based Butyrylcholinesterase Inhibitors by Rational Investigation into Their Inhibition Mode. *J. Med. Chem.* **2016**, *59*, 2067-2082.

[57] Li, B.; Sedlacek, M.; Manoharan, I.; Boopathy, R.; Duysen, E. G.; Masson, P.; Lockridge, O. Butyrylcholinesterase, Paraoxonase, and Albumin Esterase, but not Carboxylesterase, are Present in Human Plasma. *Biochem. Pharmacol.* **2005**, *70*, 1673-1684.

4. Discovery of Highly Selective and Nanomolar Carbamate-Based Butyrylcholinesterase Inhibitors by Rational Investigation into Their Inhibition Mode[1]

Discovery of Highly Selective and Nanomolar Carbamate-Based Butyrylcholinesterase Inhibitors by Rational Investigation into Their Inhibition Mode

Edgar Sawatzky,[†] Sarah Wehle,[†] Beata Kling,[‡] Jan Wendrich,[§] Gerhard Bringmann,[§] Christoph A. Sotriffer,[†] Jörg Heilmann,[‡] and Michael Decker*[,†]

[†]Pharmazeutische und Medizinische Chemie, Institut für Pharmazie und Lebensmittelchemie, Universität Würzburg, Am Hubland, D-97074 Würzburg, Germany

[‡]Lehrstuhl für Pharmazeutische Biologie, Institut für Pharmazie, Universität Regensburg, Universitätsstraße 31, D-93053 Regensburg, Germany

[§]Lehrstuhl für Organische Chemie I, Institut für Organische Chemie, Universität Würzburg, Am Hubland, D-97074 Würzburg, Germany

🅢 *Supporting Information*

ABSTRACT: Butyrylcholinesterase (BChE) is a promising target for the treatment of later stage cognitive decline in Alzheimer's disease. A set of pseudo-irreversible BChE inhibitors with high selectivity over hAChE was synthesized based on carbamates attached to tetrahydroquinazoline scaffolds with the 2-thiophenyl compound **2p** as the most potent inhibitor of eqBChE ($K_C = 14.3$ nM) and also of hBChE ($K_C = 19.7$ nM). The inhibitors transfer the carbamate moiety onto the active site under release of the phenolic tetrahydroquinazoline scaffolds that themselves act as neuro-

2p
IC$_{50}$ (hBChE) = 13 nM
$K_C = 19.7 \pm 0.9$ nM
$k_3 = 0.32 \pm 0.01$ min^{-1}
$k_3/K_C = 16.24 \pm 0.64$ µM^{-1}min^{-1}

protectants. By combination of kinetic data with molecular docking studies, a plausible binding model was probed describing how the tetrahydroquinazoline scaffold guides the carbamate into a close position to the active site. The model explains the influence of the carrier scaffold onto the affinity of an inhibitor just before carbamate transfer. This strategy can be used to utilize the binding mode of other carbamate-based inhibitors.

Author contributions:

Edgar Sawatzky, under supervision of Prof. Dr. Michael Decker, performed the design and the synthesis of all test compounds as well as their biological evaluation on BChE and AChE (IC$_{50}$-values and kinetic studies).

Computational studies were performed by Sarah Wehle under supervision of Prof. Dr. Christoph A. Sotriffer.

Dr. Beata Kling was responsible for the neuroprotection and -toxicity assays under supervision of Prof. Dr. Jörg Heilmann.

Jan Wendrich was responsible for the separation of the enantiomers under supervision of Prof. Dr. Gerhard Bringmann.

4.1 Introduction

In the last decades, the majority of designed ChE inhibitors mainly focused on AChE as target or the non-selective inhibition of AChE as well as BChE; resulting into a comparable rare number of reports for BChE inhibitors. With regard to the increasing relevance of BChE in different diseases (*cf.* **Chapter 3.1**), there is a strong requirement for selective and highly potent inhibitors of BChE a) to investigate its physiological function in the described diseases and b) to offer new therapeutic approaches. The design of these inhibitors is challenging as *h*BChE and *h*AChE share an identity of approximately 49% and a similarity of 66%.[1] Although several structural features between both enzymes are highly conserved, there are notably differences in the available space for binding of substrates or inhibitors. Especially the replacement of bulky aromatic residues at the entrance of the gorge as well as the replacement of aromatic residues at the acyl binding pocket in AChE against smaller aliphatic residues in BChE allows BChE to bind significant larger substrates and inhibitors.[2,3]

However, targeting of BChE is often achieved by addressing the catalytic active site (CAS) with carbamate based inhibitors. These inhibitors transfer their carbamate moiety onto the serine of the catalytic triade thus deactivating the enzyme pseudo-irreversibly. In this context, the term "pseudo" indicates a slow reactivation of the enzyme through hydrolysis of the carbamate moiety over time. Carbamate based inhibitors normally consist of a carrier scaffold and a respective carbamate moiety. The carrier scaffold binds near the active site of the enzyme and guides the carbamate moiety into a favorable position to enable carbamate transfer onto the serine of the CAS. This scaffold is not necessarily involved in enzyme inhibition to a significant extent but it is essential for the affinity of the whole inhibitor to the enzyme. Enzyme inhibition itself is majorly mediated through transfer of the carbamate moiety onto the CAS (**Figure 4.1 a**).

In literature, the development of such carbamate based ChE inhibitors is often limited to modifications of the carbamate moiety (**Figure 4.1 c**)[4-7] and there is only little information available on the structure activity relationships (SARs) between a modified carrier scaffold and the enzyme (**Figure 4.1 b**).[8-11] This is quite remarkable, as the rational design of new inhibitors requires extended knowledge about the binding mode of the carrier scaffold next to the CAS in the preliminary step before inhibition itself can take place. Only a well bound carrier scaffold at the correct position within the enzyme allows carbamate transfer and therefore is the pivotal source of enzyme inhibition. To overcome the lack of knowledge onto the binding mode of the carrier scaffold of carbamate based inhibitors, this chapter focuses on the development of a suitable binding model for tetrahydroquinazoline derived carbamates.

a

b

Inhibitors designed by modifying
the carrier scaffold

c

Inhibitors designed by modifying
the carbamate moiety
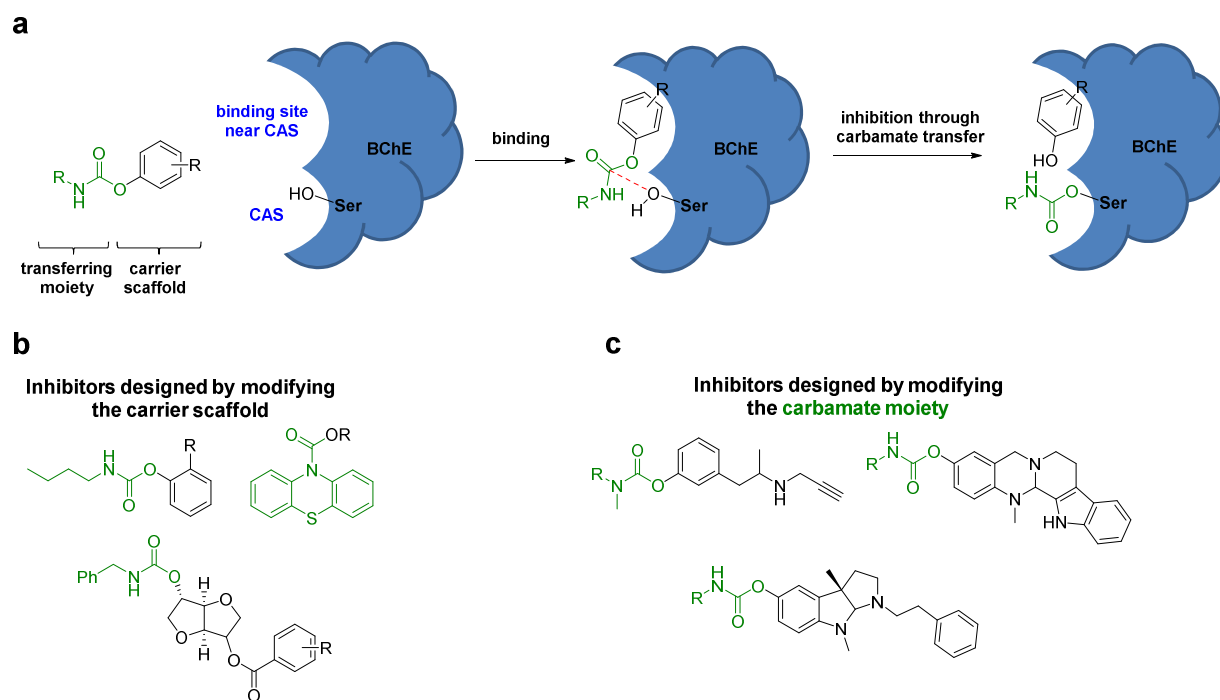
Figure 4.1. (**a**) Schematic description of BChE inhibition by carbamate based inhibitors. For details of the single steps see the main text. (**b**) Previously described carbamate-based structures investigated as ChE inhibitors by altering the carrier scaffold[8-11] and (**c**) by altering the carbamate moiety.[4-7] Carrier scaffolds are shown in black, carbamate moieties in green.[1]

4.2   Compound Design and Synthesis

Previous studies have found the carbamate based tetrahydroquinazoline **1** to be a highly potent BChE inhibitor in the nanomolar range with an excellent selectivity on *eq*BChE over *ee*AChE.[12] Similar to other carbamate based inhibitors (*cf.* **Chapter 4.1**), the tetrahydroquinazoline scaffold binds close to the CAS to enable transfer of the carbamate moiety onto the active site of the enzyme, thus inhibiting BChE pseudo-irreversibly (**Figure 4.2**). Additionally, this mode of action leads to the release of the tetrahydroquinazoline carrier scaffold **2**, which acts as neuroprotectant and prevents oxidative-stress-induced cell death due to the radical scavenging properties of its *para*-aminophenol moiety.
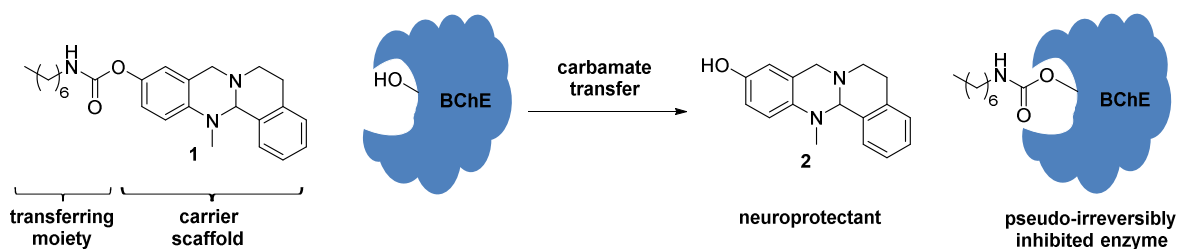
Figure 4.2. Pseudo-irreversible inhibition of BChE by carbamate based inhibitor **1** under release of tetrahydroquinazoline scaffold **2** which acts as neuroprotectant.

However, a detailed binding mode of inhibitor **1** and related tetrahydroquinazoline based carbamates[4,12,13] on BChE is not available to date. To investigate the interactions between such inhibitors with BChE systematically, SAR studies on the tetrahydroquinazoline scaffold are necessary with regard to the impacting importance of the scaffold for inhibitor binding at the enzyme (*cf.* **Figure 4.1 a**). Therefore, to conduct SARs studies and to enable the design of diverse tetrahydroquinazoline carrier scaffolds, the rigid ring structure of lead compound **1** was "opened" to give access to compound series **3** and **4** which can easily be modified at the aryl site (series **3**) as well as at the aliphatic nitrogen (series **4**) of the carrier scaffold (**Figure 4.3**).
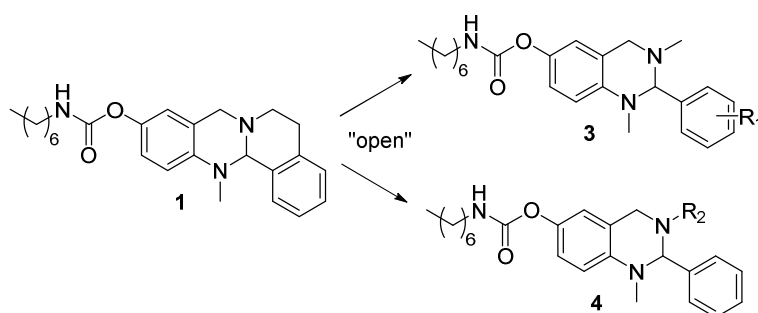
Figure 4.3. "Opening" of the ring structure of lead compound **1** to give compound series **3** and **4**.

The synthesis of both series was performed as shown in **Scheme 4.1**. Briefly, 6-hydroxy isatoic anhydride **5** was obtained quantitatively from 3-hydroxy anthranilic acid and triphosgene, followed by the selective *N*-methylation towards compound **6**.[14] Nucleophile substitution with free amines or their corresponding hydrochlorides was performed to give amides **7a-d** which were further cyclized with benzaldehyde or substituted benzaldehyde derivatives to yield 1,2-dihydroquinazolinones **8a-u** and **9a-c**. Reduction of 1,2-dihydroquinazolinones **8a-u** and **9a-c** with LiAlH$_4$ towards tetrahydroquinazolines **10a-u** and **11a-c**, and successive introduction of the carbamate moiety gave the desired target compound series **3a-u** and **4a-c**. The substitution pattern of these compounds will be discussed later (**Chapter 4.3**) as their synthesis and SAR investigations were performed in parallel.
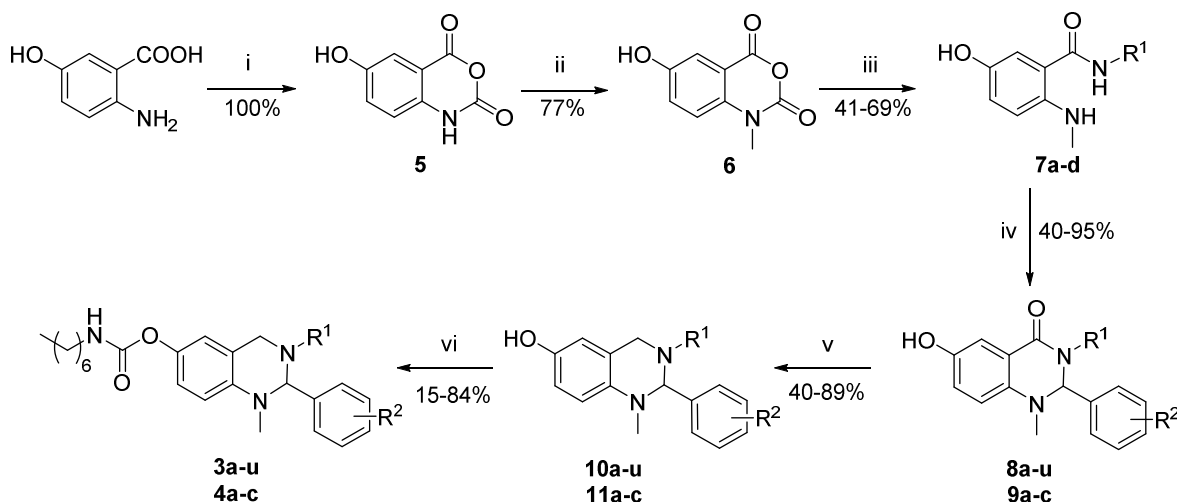
Scheme 4.1. Synthesis of aryl and *N*-alkyl substituted target compounds **3a-u** and **4a-c**. For substitution pattern of R^1 and R^2 see **Table 4.1** in **Chapter 4.3**. Reagents and conditions: (i) $CO(OCCl_3)_2$, THF, 70 °C, 3.5 h; (ii) MeI, DIPEA, DMAc, 40 °C, 24 h; (iii) R^1-NH_2 or $MeNH_3Cl$ and Et_3N, DMF, 40-120 °C, 4-5 h; (iv) R^2-PhCHO, AcOH, 70 °C, 1-3 h; (v) $LiAlH_4$, THF, reflux, 1-3 h; (vi) $(4-NO_2)PhO(C=O)NH$-nHept, NaH, THF, rt, 2 h or n-Hept-NCO, Et_3N, rt, 6 h for **3o,p**.[1]

To investigate the influence of a bicyclic aromatic system onto the binding behavior of the carrier scaffold at the enzyme, also quinazoline **17** was synthesized (**Scheme 4.2**). Starting with 5-hydroxy-2-nitrobenzaldehyde, *O*-benzyl protection towards compound **12** and successive reduction of the nitro moiety gave compound **13**. After the formation of amide **14** by using benzoyl chloride, quinazoline **15** was synthesized applying aqueous ammonia in a sealed tube under microwave irradiation.[15] Finally, removal of the benzyl protection group and introduction of the carbamate moiety gave the desired target compound **17**.
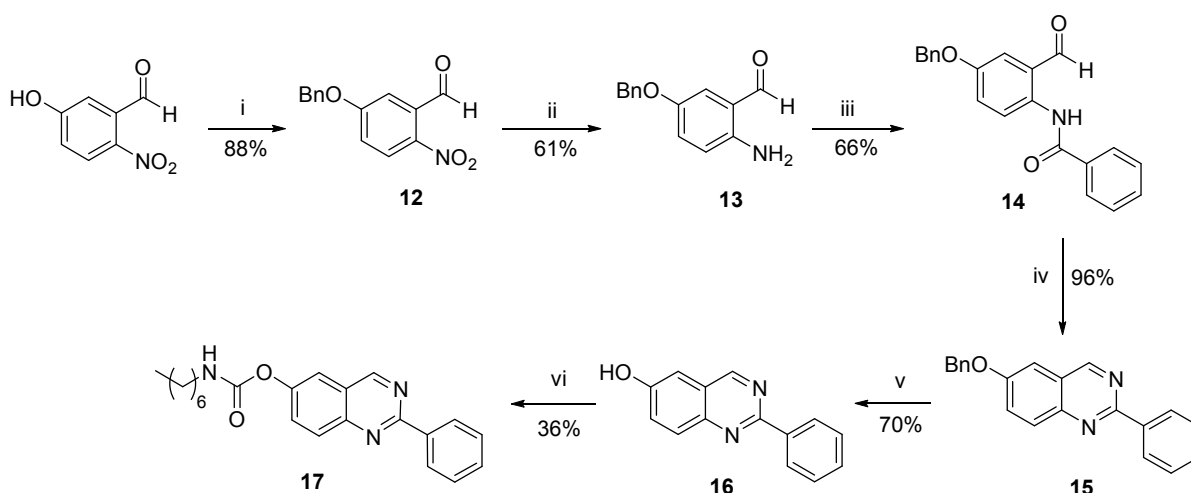
Scheme 4.2. Reagents and conditions: (i) BnBr, K_2CO_3, DMF, 40 °C, 24 h; (ii) Fe, HCl, EtOH/H_2O, reflux, 1 h; (iii) Ph(C=O)Cl, Et_3N, DCM, rt, 4 h; (iv) conc. NH_3, *i*-PrOH, MW, 90 °C, 6 h; (v) Pd/C, H_2, MeOH, 50 °C, 3 h; (vi) $(4-NO_2)PhO(C=O)NH$-*n*-Hept, NaH, THF, rt, 2 h.[1]

4.3 Enzyme Inhibition and SAR

To investigate the potency of the synthesized compounds in dependency of their carrier scaffolds, the unsubstituted target compound **3a** (*cf.* **Table 4.1** at the end of this chapter) was initially synthesized as reference compound for further scaffold development. This compound showed good inhibition of BChE ($IC_{50}(eqBChE) = 106$ nM) and, similar to the lead structure **1**, no pronounced inhibition of *h*AChE. Interestingly, it's simple phenolic tetrahydroquinazoline analog **10a** showed a ~400-fold decrease in potency towards BChE ($IC_{50}(BChE) = 39.9$ μM). This results support the general concept described for carbamate based inhibitors (**Figure 4.1**) as the carrier scaffold **10a** is supposed to play part only for inhibitor binding but is not the intrinsic source of enzyme inhibition. As all phenolic carrier scaffolds of series **10** and **11** (left columns in **Table 4.1**) feature a similar behavior in terms of BChE inhibition, only the carbamate based inhibitor series **3** and **4** (right columns of **Table 4.1**) will be discussed in the following paragraphs.

To explore the space available at the tetrahydroquinazoline binding site and to find more potent inhibitors, different approaches were realized for alteration of the substitution pattern of the aromatic residue (compound series **3**):

1) Topliss decision tree:[16,17] The topliss decision tree advices the systematic modification of the steric, hydrophobic and electronic properties of a compound by introduction of different substitution pattern into an aromatic system with the aim to improve the affinity to a biological target. This approach led to the synthesis of compounds **3b-k**; and also compound **3l** (4-CF_3) was synthesized although not being advised by the classical topliss tree.

2) Bioisosterism:[18.19] Bioisosters are expected to improve different physical properties of a compound while maintaining its biologic activity. Therefore, replacement of the whole phenyl residue with different bioisosteric heterocycles was performed resulting in the synthesis of compounds **3m-r**.

3) Sterical influence: To investigate the influence of sterical demanding groups, compounds **3s,t** (naphthyl residues) as well as the disubstituted compound **3u** (2,6-dichloro) were synthesized.

Interestingly, the majority of the introduced groups within compound series **3** showed no significant differences in inhibition compared to the reference compound **3a**; and in most cases the affinity towards BChE was slightly decreased. Only non-polar compounds with a comparable size or a smaller residue than the phenyl system improved the affinity of these inhibitors (4-F group in **3k** with $IC_{50}(eqBChE) = 44$ nM; thiophene residues in **3o** and **3p** with $IC_{50}(eqBChE) = 22$ nM and 14 nM; furryl residue in **3q** with $IC_{50}(eqBChE) = 83$ nM; pyrrolyl residue in **3r** with $IC_{50}(eqBChE) = 23$ nM). Also compounds with larger site groups at the nitrogen showed improved potency towards BChE ($IC_{50}(eqBChE) = 21$ nM (**4a**), 40 nM (**4b**) and 34 nM (**4c**)) revealing available space close to the tertiary nitrogen at the binding site of BChE. In contrast, only three compounds showed little inhibition of BChE in the micro molar range: The 1-naphthyl substituted compound **3s** ($IC_{50}(eqBChE) =$

36.2 μM), the 4-CF$_3$ bearing compound **3l** (IC$_{50}$(*eq*BChE) = 2.7 μM) and also the planar compound **17** (IC$_{50}$(*eq*BChE) = 1.8 μM). Beyond the mentioned decrease in affinity, it is remarkable that the IC$_{50}$-curves of these three compounds showed Hill slopes around 0.5 compared to all the other inhibitors with Hill slopes ≥ 1. These differences are exemplarily shown in **Figure 4.4** for the most potent compound **3p** and the 4-CF$_3$ compound **3l**.
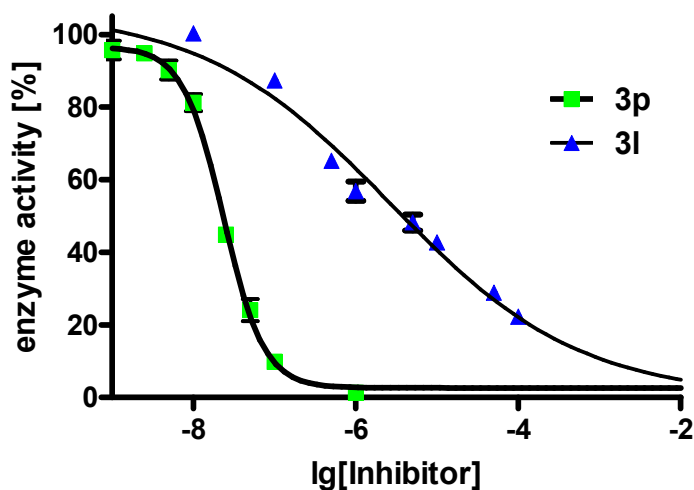
Figure 4.4. IC$_{50}$-curves of thiophene **3p** (green) and the 4-CF$_3$ compound **3l** (blue) with significant differences in their Hill slopes (means ± SD).

Even if the differences in potency (expressed by IC$_{50}$ values) can support SAR investigations and are a useful first indication for the establishment of a plausible binding model of the tetrahydroquinazoline carrier scaffold, the inhibition mode of pseudo-irreversible inhibitors is much more complex. Therefore, a more detailed view into the kinetic mode of action of these inhibitors will be discussed in **Chapter 4.4**.[1]

Table 4.1. Cholinesterase inhibition of the synthesized test compounds.[a] [1]
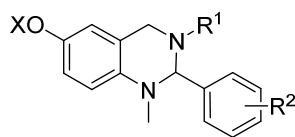
Moiety	X = H	IC$_{50}$ [µM] or % inhibition		X = (C=O)NH-nHept	IC$_{50}$ [µM] or % inhibition	
		*eq*BChE	*h*AChE		*eq*BChE	*h*AChE
R^1 = Me; R^2 =						
H	**10a**	39.9	327.0	**3a**	0.106	4%[d]
4-Cl-Ph-	**10b**	13.8	235.6	**3b**	0.115	24%[d]
3-Cl-Ph-	**10c**	2.1	242.4	**3c**	0.096	39%[d]
2-Cl-Ph-	**10d**	56.0	60%[b]	**3d**	0.474	48%[e]
4-Me-Ph-	**10e**	22.6	109.9	**3e**	0.231	9%[d]
3-Me-Ph-	**10f**	17.4	437.0	**3f**	0.199	27%[d]
2-Me-Ph-	**10g**	92.4	143.4	**3g**	0.251	18%[e]
4-MeO-Ph-	**10h**	39.5	103.8	**3h**	0.875	14%[d]
3-MeO-Ph-	**10i**	7.8	61%[b]	**3i**	0.208	10%[d]
2-MeO-Ph-	**10j**	9.9	192.8	**3j**	0.238	47%[e]
4-F-Ph-	**10k**	58.9	143.4	**3k**	0.044	1.61
4-CF$_3$-Ph-	**10l**	64.6	nd[c]	**3l**	2.7	59%[d]
4-pyridyl-	**10m**	2.1	242.4	**3m**	0.723	16%[d]
3-pyridyl-	**10n**	70.7	61%[b]	**3n**	0.565	18%[d]
3-thiophenyl-	**10o**	193.7	52%[b]	**3o**	0.022	13%[d]
2-thiophenyl	**10p**	63.2	225.8	**3p**	0.014 0.013*	0%[d]
3-furyl-	**10q**	196.1	341.7	**3q**	0.083	12%[d]
3-pyrrolyl-	**10r**	15.3	115.9	**3r**	0.023	0.852
1-naphthyl-	**10s**	2.8	341.7	**3s**	36.2	8%[e]
2-naphthyl-	**10t**	16.5	9%[c]	**3t**	0.374	5%[e]
2,6-dichloro	**10u**	7.1	13.5	**3u**	0.531	33%[e]
R^2 = Ph; R^1 =						
i-Pr-	**11a**	55.8	253.0	**4a**	0.021	33%[d]
n-Pr-	**11b**	22.8	279.3	**4b**	0.040	46%[d]
benzyl-	**11c**	14.8	16%[c]	**4c**	0.034	17%[e]
	16	98.1	20%[b]	**17**	1.8	22%[d]
				physostigmine	0.078	0.032

[a]Experiments were performed in triplicate at AChE from human erythrocytes and BChE from equine serum. Phenols were pre-incubated for 4.5 min and carbamates for 30 min. [b-e] % Inhibition at a concentration of [b]500 µM; [c]50 µM; [d]100 µM; [e]10 µM. * Values determined at human BChE.

4.4   Kinetic Investigations

Carbamate based pseudo-irreversible inhibitors are known to undergo a three step kinetic (**Figure 4.5**): In an initial step, the inhibitor (I) binds reversibly to the enzyme (E) forming an enzyme-inhibitor-complex (EI) described in equilibrium by the constant K_C. In the second step, the carbamate moiety is transferred covalently onto the enzyme thus inhibiting the enzyme irreversibly (E-C) with k_3 as the carbamoylation rate constant. Finally, the carbamate moiety is hydrolyzed over time while recovering the intact enzyme (E) and k_4 as the decarbamoylation rate constant.

$$\text{E} + \text{I} \underset{k_2}{\overset{k_1}{\rightleftharpoons}} \text{(EI)} \xrightarrow[-R]{k_3} \text{E-C} \xrightarrow{k_4} \text{E} + \text{C}'$$
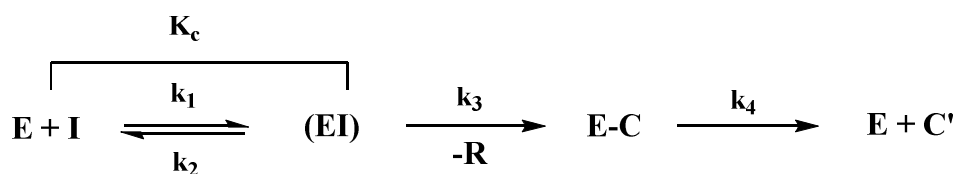
Figure 4.5. Kinetic model of pseudo-irreversible inhibitors. For description of the single steps see the main text.[1]
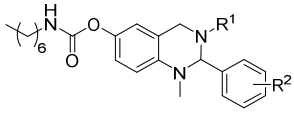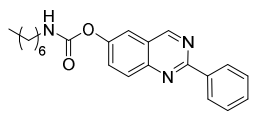
To investigate the influence of the tetrahydroquinazoline carrier scaffold for binding onto BChE (first step in **Figure 4.5**) and therefore to postulate a suitable binding model for this class of compounds, time-dependent studies are necessary to determine the K_C-values (**Table 4.2**). These values quantify the reversible interactions of the test compounds before inhibition through enzyme-carbamoylation takes place. As the heptyl-carbamate moiety was kept for all compounds constant, differences in the K_C-values are attributed to differences of the substitution patterns of the carrier scaffold due to altered interactions between the enzyme and the tetrahydroquinazoline system.

The kinetic studies revealed:

1) The affinity (K_C-values in **Table 4.2**) of the test compounds showed a similar trend when compared to the IC_{50}-values (**Table 4.1**).

2) Most compounds showed a comparable carbamoylation rate constant (k_3-values) between 0.13 and 0.24 min^{-1} with exceptions for the 4-CF$_3$ compound **3l** and the naphthyl compound **3s**. It can be assumed, that a similar carbamoylation rate constant has its origin in the same orientation of the carbamate moiety with respect to the serine of the CAS supporting a conserved binding mode for these inhibitors.[1]

Table 4.2. Kinetic values for carbamoylation and decarbamoylation on *eq*BChE for selected compounds. Experiments were performed in triplicate (means±SEM)[1]

			$K_C \pm SEM$ [nM]	$k_3 \pm SEM$ [min^{-1}]	$k_3/K_C \pm SEM$ [µM^{-1}min^{-1}]	$k_4 \pm SEM$ [h^{-1}]
	R^1	R^2				
3a	Me	Ph-	226.2 ± 82.8	0.13 ± 0.04	0.57 ± 0.27	0.14 ± 0.003
3p	Me	2-thiophenyl-	14.3 ± 6.2 19.7 ± 0.9*	0.14 ± 0.04 0.32 ± 0.01*	9.79 ± 5.08 16.24 ± 0.64*	0.14 ± 0.003
3k	Me	4-F-Ph-	24.5 ± 12.7	0.14 ± 0.04	5.71 ± 3.38	
3c	Me	3-Cl-Ph-	227.3 ± 120.5	0.16 ± 0.05	0.7 ± 0.43	
3h	Me	4-MeO-Ph-	1203.6 ± 118.7	0.24 ± 0.01	0.2 ± 0.02	
3i	Me	3-MeO-Ph-	622 ± 234.5	0.18 ± 0.05	0.29 ± 0.14	
3l	Me	4-CF$_3$-Ph-	*756.5 ± 251.7**	*0.05 ± 0.01**	*0.07 ± 0.03**	
3s	Me	1-naphthyl-	*15.6 ± 17.6**	*0.03 ± 0.002*	*1.92 ± 2.17**	
3u	Me	2,6-Cl-Ph	4118 ± 1204	0.23 ± 0.063	0.06 ± 0.02	
4a	*i*-Pr	Ph-	185.8 ± 115.1	0.16 ± 0.07	0.86 ± 0.65	
17			*1057.9 ± 577.7**	*0.14 ± 0.06*	*0.13 ± 0.09**	
physostigmine			280.3 ± 130.0	0.3 ± 0.1	0.3 ± 0.1	0.25 ± 0.01

* Values measured for human BChE.

** Values are calculated under the assumption of a pseudo-irreversible inhibition. They have to be carefully rated as the inhibition mode might be different from those of other inhibitors.

Interestingly, the time and concentration dependent inhibition curves for inhibitors **3l**, **3s** and **17** showed remarkable differences in their shape compared to the other inhibitors. This is exemplarily shown for the most active compound **3p** (**Figure 4.6 a**) and the 4-CF$_3$ compound **3l** (**Figure 4.6 b**). While **3p** showed a clear separation of its concentration-dependent inhibition curves over time, the 4-CF$_3$ compound **3l** showed even after

40 min bundling of all curves at different inhibitor concentrations. Although the underlying reason for the altered kinetics of these three compounds remains unclear, this result supports the hypothesis of a different binding mode for **3l**, **3s** and **17**.
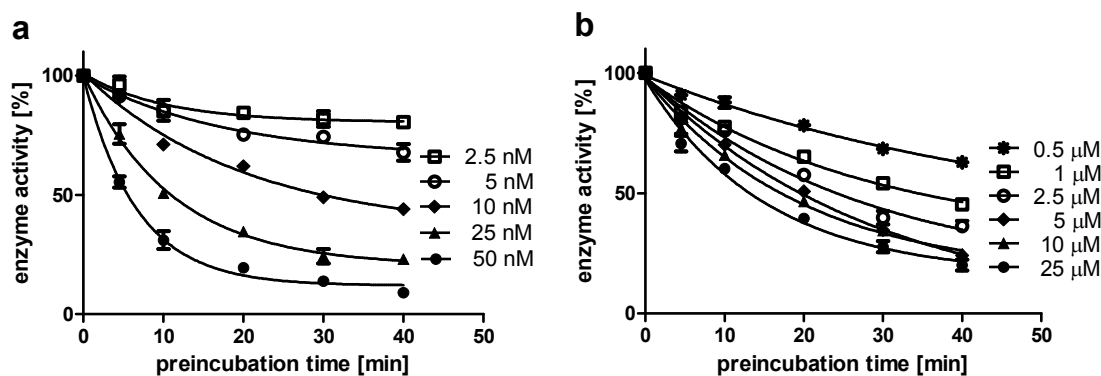
Figure 4.6. Time dependent inhibition of BChE (**a**) by compound **3p** and (**b**) by the 4-CF$_3$ compound **3l** at different inhibitor concentrations. Experiments were performed in triplicate (means±SD).

A detailed description of this study as well as the calculation of the kinetic parameters can be found in **Appendix 2**.

4.5 Binding Model of Tetrahydroquinazoline Based Carbamates

Regarding the obtained results for the IC$_{50}$-values (**chapter 4.3**) and the kinetic investigations (**chapter 4.4**), several requirements for a reasonable binding model of the inhibitors described have to be considered:

1) Kinetic studies have shown that enzyme inhibition is time dependent indicating a pseudo-irreversible reaction mechanism. Therefore, the carbamate moiety of a non-covalently and reversibly bound inhibitor has to be in a close position and in a correct orientation to the serine of the CAS to enable carbamate transfer.

2) Non-polar compounds with a small residue at the aromatic site are preferred compared to those with polar groups and increased size.

3) Most of the inhibitors undergo a general conserved binding mode indicated by similar carbamoylation rate constants (k$_3$) only differing in their affinity (K$_c$).

4) Compounds **3l**, **3s** and **17** showed significant differences compared to the other test compounds regarding their low IC$_{50}$-values in the micro molar range, the shape of the IC$_{50}$-curves (**Figure 4.4**),

the shape of the time-dependent curves **(Figure 4.6)** as well as low k_3 values. Taking these data together, it can be assumed that these inhibitors adhere to a different binding mode or act as slow reversible binding inhibitors and should not fit into a proposed binding model.

Considering these requirements, docking studies were conducted (for details see **Appendix 2**) to reveal a binding model for the inhibitors described: Ser198 of the CAS was found to be in close proximity to the carbonyl carbon of the carbamate moiety offering the possibility for carbamate transfer onto this residue and in consequence for pseudo-irreversible inhibition. The aromatic residues (with their different substituent pattern) are positioned in a side cavity next to the CAS but showed no further interactions to residues of the enzyme. This binding mode was found to be conserved for almost all inhibitors and is exemplarily shown for the two
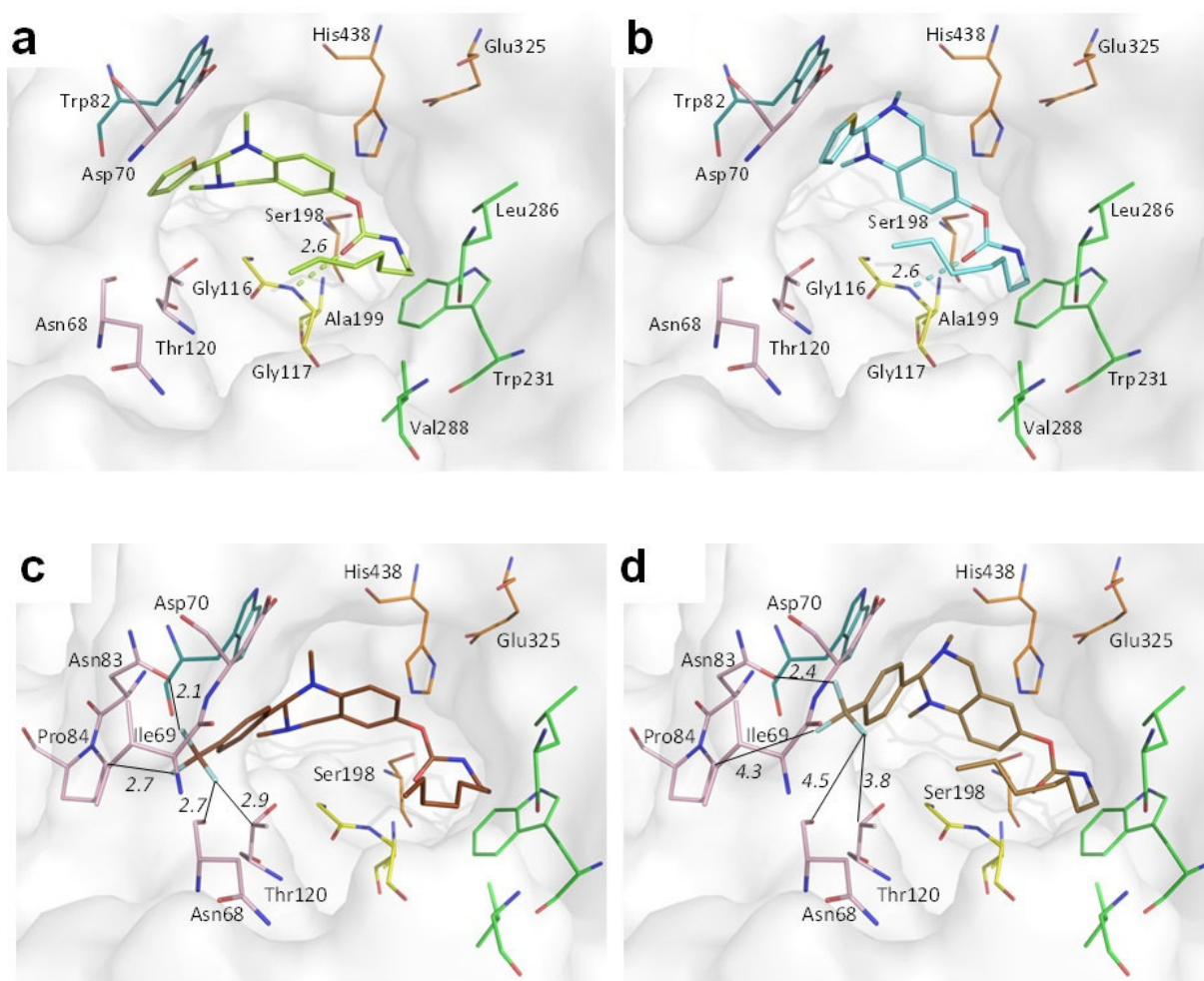
Figure 4.7 (**a**) Representation of the preferred binding mode of **3p** as *R*-enantiomer (light green) and (**b**) *S*-enantiomer (light blue) at BChE's binding site. (**c**) Representation of the binding mode of **3l** (dark brown) in the *R*-enantiomeric form when forced to an analogous binding mode as the most active compound **3p** (**d**) and of the *S*-enantiomer (light brown). Residues of the acyl pocket are shown in green, the oxyanion hole in yellow, the CAS in orange, the choline binding site (Trp82) in turquoise, and parts of the side cavity in pink. Distances in Å are given in italics.[1]

enantiomers of the thophene **3p** in **Figure 4.7a** and **b**. Interestingly, although an explanation for the altered affinity of the described inhibitors cannot be revealed with this binding model as no distinct interactions of the aromatic residues were found, the exceptions **3l** (4-CF$_3$) and **17** (planar system) did not fit to it. When forcing these inhibitors into a comparable binding mode like the most active compound **3p**, several unfavorable sterical interactions can be observed indicating that this binding mode is unlikely for these compounds. These observations are exemplarily shown in **Figure 4.7 c** and **d** for the two enantiomers of **3l** whose CF$_3$-group leads to clashes with residues of the enzyme (distances are less than 3 Å).

Taken together, the proposed model describes the reversible binding mode of the tetrahydroquinazoline scaffold in relation to different substitution patterns. Furthermore, this model supports the hypothesis that compounds with irregular kinetics (**3l**, **3s** and **17**) do not fit into the described side cavity due to sterical interactions between the aromatic residues of the inhibitors with the enzyme; at least for compounds **3l** and **17**. Therefore, the model can explain in part the influence of the tetrahydroquinazoline carrier scaffold for binding of the whole inhibitor before inhibition through carbamate transfer occurs.

4.6 Neuroprotection and –toxicity

Due to the pseudo-irreversible inhibition mechanism of the described inhibitors, the tetrahydroquinazoline carrier scaffold is released after the carbamate transfer (*cf.* **Figure 4.2**). This carrier scaffold can act as a neuroprotectant due to the radical scavenging properties of its *para*-aminophenol moiety and therefore prevents oxidative stress induced cell death. To prove this concept, murine hippocampal HT-22 cells were used to determine the self-toxicity and the neuroprotective abilities against oxidative stress of several carbamate based inhibitors (series **3** and **4**) as well as their phenolic analogs (series **10** and **11**) (**Figure 4.8**).

All carbamates (series **3** and **4**) showed only little self-toxicity up to a concentration of 25 μM while maintaining the cell viability above 50% and also their corresponding phenols (series **10** and **11**) did not reduce cell viability significantly up to a concentration of 5 μM (**Figure 4.8a**). When inducing oxidative stress through addition of a high concentration of glutamate (**Figure 4.8b**), the phenolic compounds effectively counteracted oxycytosis at a concentration of 5 μM while maintaining the cell viability. Cell death at higher concentrations was found to proceed parallel to the self-toxicity of these compounds and therefore oxidative stress can be excluded as the source for decreased cell viability at higher concentrations.

Interestingly, also the carbamate based compounds (series **3** and **4**) where able to prevent oxidative stress induced cell death as all compounds maintained cell viability to a significant extent at concentrations above 5 μM. This is quite remarkable, as neuroprotective abilities are observable already for the carbamate based

compounds and hydrolysis to the corresponding phenols is not obligatory necessary for neuroprotection.[1] It might be possible that the benzyl positions can act as radical scavengers as it is known that benzyl radicals are highly stable structures.
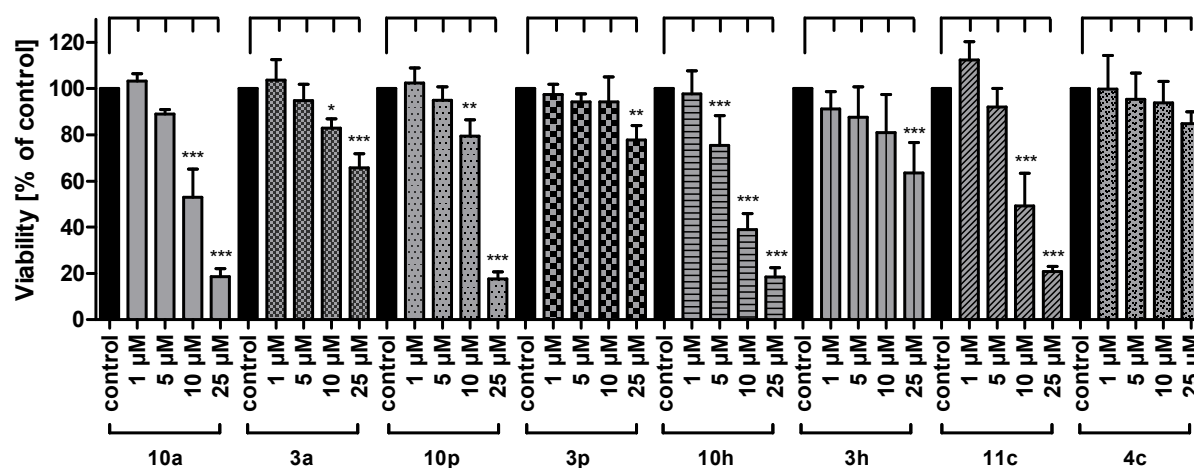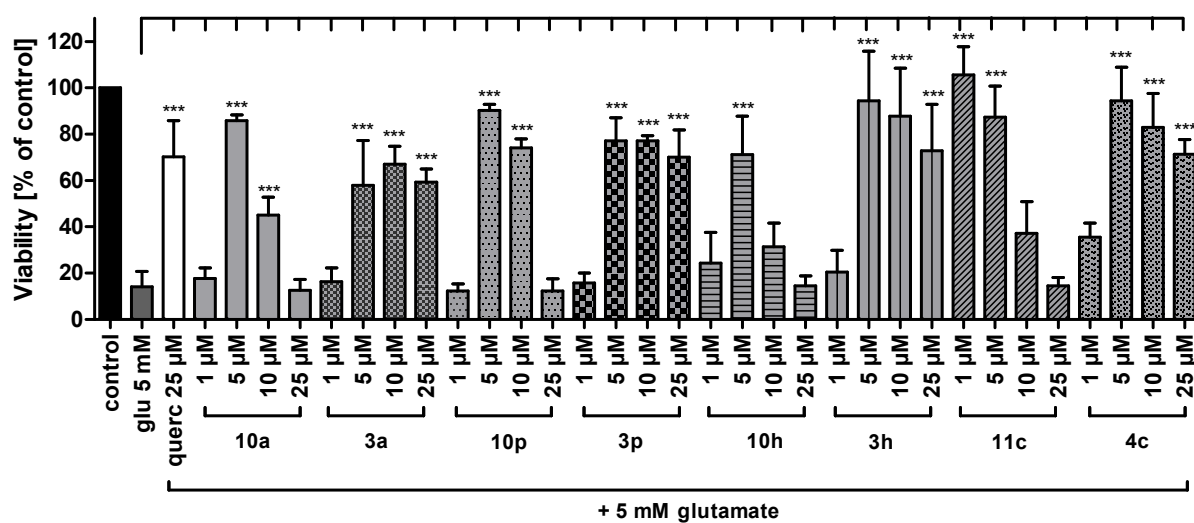
Figure 4.8 (**a**) Neurotoxicity tests for target compounds on HT-22 cells. (**b**) Neuroprotection tests against glutamate induced oxidative stress for target compounds on HT-22 cells.[1]

4.7 Conclusion

Pseudo-irreversible ChE inhibitors consist of a carrier scaffold and a carbamate moiety. The carrier scaffold binds near the CAS and guides the carbamate moiety into a close position to enable carbamate transfer onto the CAS thus inhibiting the enzyme. Therefore, information about the binding mode of the carrier scaffold is essential for the design of new inhibitors as only a well bound carrier scaffold in the correct orientation to the CAS offers the possibility for pronounced pseudo-irreversible inhibition. To investigate the influence of tetrahydroquinazoline based carrier scaffolds for binding on BChE, carbamate based inhibitors of the series **3** and **4** were synthesized by applying different rational approaches such as the topliss decision tree or bioisosterism. Kinetic investigations revealed that the compounds synthesized inhibit BChE pseudo-irreversibly through carbamate transfer while binding in a conserved manner with some exceptions (**3l**, **3s** and **17**). Based on these data a plausible binding model was postulated explaining the influence of the carrier scaffold for binding at BChE's active site just before carbamate transfer takes place. Additionally, these compounds feature neuroprotective properties and prevent oxidative stress induced cell death in their carbamate form as well as after the release of the tetrahydroquinazoline carrier scaffold.

The detailed results of this chapter as well as experimental data were previously published[1] and can be found in **Appendix 2**.

4.8 References

[1] Sawatzky, E.; Wehle, S.; Kling, B.; Wendrich, J.; Bringmann, G.; Sotriffer, C. A.; Heilmann, J.; Decker, M. Discovery of Highly Selective and Nanomolar Carbamate-Based Butyrylcholinesterase Inhibitors by Rational Investigation into Their Inhibition Mode. *J. Med. Chem.* **2016**, *59*, 2067-2082.

[2] Radic, Z.; Pickering, N. A.; Vellom, D. C.; Camp, S.; Taylor, P. Three Distinct Domains in the Cholinesterase Molecule Confer Selectivity for Acetyl- and Butyrylcholinesterase Inhibitors. *Biochem.* **1993**, *32*, 12074-12084.

[3] Vellom, D. C.; Radic, Z.; Li, Y.; Pickering, N. A.; Camp, S.; Taylor, P. Amino Acid Residues Controlling Acetylcholinesterase and Butyrylcholinesterase Specificity. *Biochem.* **1993**, *32*, 12-17.

[4] Huang, G.; Kling, B.; Darras, F. H.; Heilmann, J.; Decker, M. Identification of a Neuroprotective and Selective Butyrylcholinesterase Inhibitor Derived from the Natural Alkaloid Evodiamine. *Eur. J. Med.Chem.* **2014**, *81*, 15-21.

[5] Takahashi, J.; Hijikuro, I.; Kihara, T.; Murugesh, M. G.; Fuse, S.; Tsumura, Y.; Akaike, A.; Niidome, T.; Takahashi, T.; Sugimoto, H. Design, Synthesis and Evaluation of Carbamate-Modified (-)-N^1-Phenethylnorphysostigmine Derivatives as Selective Butyrylcholinesterase Inhibitors. *Bioorg. Med. Chem. Lett.* **2010**, *20*, 1721-1723.

[6] Groner, E.; Ashani, Y.; Schorer-Apelbaum, D.; Sterling, J.; Herzig, Y.; Weinstock, M. The Kinetics of Inhibition of Human Acetylcholinesterase and Butyrylcholinesterase by Two Series of Novel Carbamates. *Mol. Pharmacol.* **2007**, *71*, 1610-1617.

[7] Yu, Q.; Greig, N. H.; Holloway, H. W.; Brossi A. Syntheses and Anticholinesterase Activities of (3aS)-*N*1, *N*8-Bisnorphenserine, (3aS)-*N*1,*N*8-Bisnorphysostigmine, their Antipodal Isomers, and Other Potential Metabolites of Phenserine. *J. Med. Chem.* **1998**, *41*, 2371-2379.

[8] Darvesh, S.; Darvesh, K. V.; McDonald, R. S.; Mataija, D.; Walsh, R.; Mothana, S.; Lockridge, O.; Martin, E. Carbamates with Differential Mechanism of Inhibition Toward Acetylcholinesterase and Butyrylcholinesterase. *J. Med. Chem.* **2008**, *51*, 4200-4212.

[9] Chiou, S.-Y.; Huang, C.-F.; Hwang, M.-T.; Lin, G. Comparison of Active Sites of Butyrylcholinesterase and Acetylcholinesterase Based on Inhibition by Geometric Isomers of Benzene-di-*N*-Substituted Carbamates. *J. Biochem. Mol. Tox.* **2009**, *23*, 303-308.

[10] Lin, G.; Lee, Y.-R.; Liu, Y.-C.; Wu, Y.-G. *Ortho* Effects for Inhibition Mechanisms of Butyrylcholinesterase by *o*-Substituted Phenyl *N*-Butyl Carbamates and Comparison with Acetylcholinesterase, Cholesterol Esterase, and Lipase. *Chem. Res. Toxicol.* **2005**, *18*, 1124-1131.

[11] Carolan, C. G.; Dillon, G. P.; Khan, D.; Ryder, S. A.; Gaynor, J. M.; Reidy, S.; Marquez, J. F.; Jones, M.; Holland, V.; Gilmer, J. F. Isosorbide-2-benzyl Carbamate-5-salicylate, A Peripheral Anionic Site Binding Subnanomolar Selective Butyrylcholinesterase Inhibitor. *J. Med. Chem.* **2010**, *53*, 1190-1199.

[12] Darras, F. H.; Kling, B.; Heilmann J.; Decker, M. Neuroprotective Tri- and Tetracyclic BChE Inhibitors Releasing Reversible Inhibitors upon Carbamate Transfer. *ACS Med. Chem. Lett.* **2012**, *3*, 914-919.

[13] Darras, F. H.; Kling, B.; Sawatzky, E.; Heilmann, J.; Decker, M. Cyclic Acyl Guanidines Bearing Carbamate Moieties Allow Potent and Dirigible Cholinesterase Inhibition of either Acetyl- or Butyrylcholinesterase. *Bioorg. Med. Chem.* **2014**, *22*, 5020-5034.

[14] Sawatzky, E.; Bukowczan, J.; Decker, M. Investigation into Selective Debenzylation and Ring Cleavage of Quinazoline Based Heterocycles. *Tetrahedron Lett.* **2014**, *55*, 2973-2976.

[15] Zhao, D.; Shen, Q.; Zhou, Y.-R.; Li, J.-X. KO*t*Bu-Mediated Stereoselective Addition of Quinazolines to Alkynes Under Mild Conditions. *Org. Biomol. Chem.* **2013**, *11*, 5908-5912.

[16] Topliss, J. G. Utilization of Operational Schemes for Analog Synthesis in Drug Design. *J. Med. Chem.* **1972**, *15*, 1006-1011.

[17] O'Boyle, N. M.; Bostrom, J.; Sayle, R. A.; Gill, A. Using Matched Molecular Series as a Predictive Tool to Optimize Biological Activity. *J. Med. Chem.* **2014**, *57*, 2704-2713.

[18] Kier, L. B.; Hall, L. H. Bioisosterism: Quantitation of Structure and Property Effects. *Chem. Biodiv.* **2004**, *1*, 138-151.

[19] Sheridan, R. P. The Most Common Chemical Replacements in Drug-Like Compounds. *J. Chem. Inf. Comp. Sci.* **2002**, *42*, 103-108.

5. Dual Addressing of Butyrylcholinesterase by Targeting the Catalytic Active Site (CAS) and the Peripheral Anionic Site (PAS)

Project in progress.

Author contributions:

Edgar Sawatzky, under supervision of Prof. Dr. Michael Decker, is responsible for the project idea, performed the design and the synthesis of the test compounds as well as their biological evaluation on BChE and AChE.

5.1   Introduction

As discussed before in **Chapter 4**, *h*BChE and *h*AChE share an identity of 49% and a similarity of 66%,[1] making selective targeting of these enzymes challenging. Nevertheless, BChE offers specific differences in its structure:[2-4] In contrast to AChE which is forged by 14 aromatic residues, in BChE six of them are replaced against aliphatic hydrophobic amino acid residues.[5,6] BChE features a catalytic active site (CAS) consisting a catalytical triade (Ser198, His438, Glu325), which is buried at the end of a 20 Å deep gorge (*cf.* **Figure 5.1**). The catalytic triade is flanked by a large acyl binding pocket (Leu286, Val288) where the acyl part of substrates binds and by an anionic site (Trp82), also called the choline binding site, that interacts with positively charged substrates by cation-π interactions. Especially the wide acyl pocket in BChE allows binding of bulky substrates and inhibitors compared to AChE and therefore can be exploited for the design of selective BChE inhibitors. At the entrance of the hydrophobic gorge a peripheral anionic site (PAS) is located (Asp70, Tyr332) which is connect by an Ω-loop to the choline binding site. The peripheral site is necessary for initial binding of substrates[7] and in the case of AChE it was found to promote amyloid-*β* aggregation.[8,9]
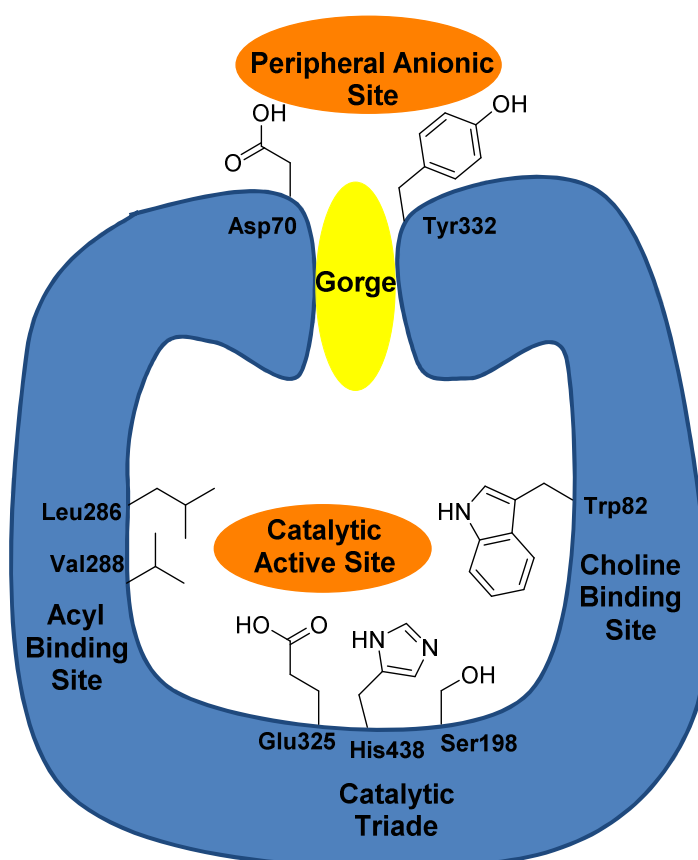
Figure 5.1. Schematic description of BChE's binding sites.

While for AChE numerous inhibitors are known addressing the different subsides of the enzyme,[10-25] the number of selective BChE inhibitors is comparable small in literature. Highly potent and selective targeting of BChE often is contributed to inhibitors binding at the CAS (**Figure 5.2a**);[26-27] in most cases with carbamates but also with organophosphates or reversibly acting inhibitors like ethopropazine. Further, targeting the CAS and additional binding to amino acid residues at the PAS or at the gorge is described for bivalent compounds like homo- and heterobivalent tacrine dimers (**Figure 5.2b**).[2,5,28-30] Carolan *et al.*[31] and Lin *et al.*[32] combined these two concepts and developed pseudo-irreversible carbamate based inhibitors (**Figure 5.2c**) which interact with their carrier scaffold (for description of the binding concept of carbamates *cf.* **Chapter 4**) with residues at the PAS and in addition can transfer the carbamate moiety onto the serine of the catalytic triade at the CAS. Carolan *et al.* proved with enzyme mutant studies that inhibitors binding at the CAS which additional interact with residues of the PAS, like Asp70 or Tyr332, are the source for a significantly increased BChE inhibition leading to inhibition values from the nanomolar range to those in the picomolar range.[31]
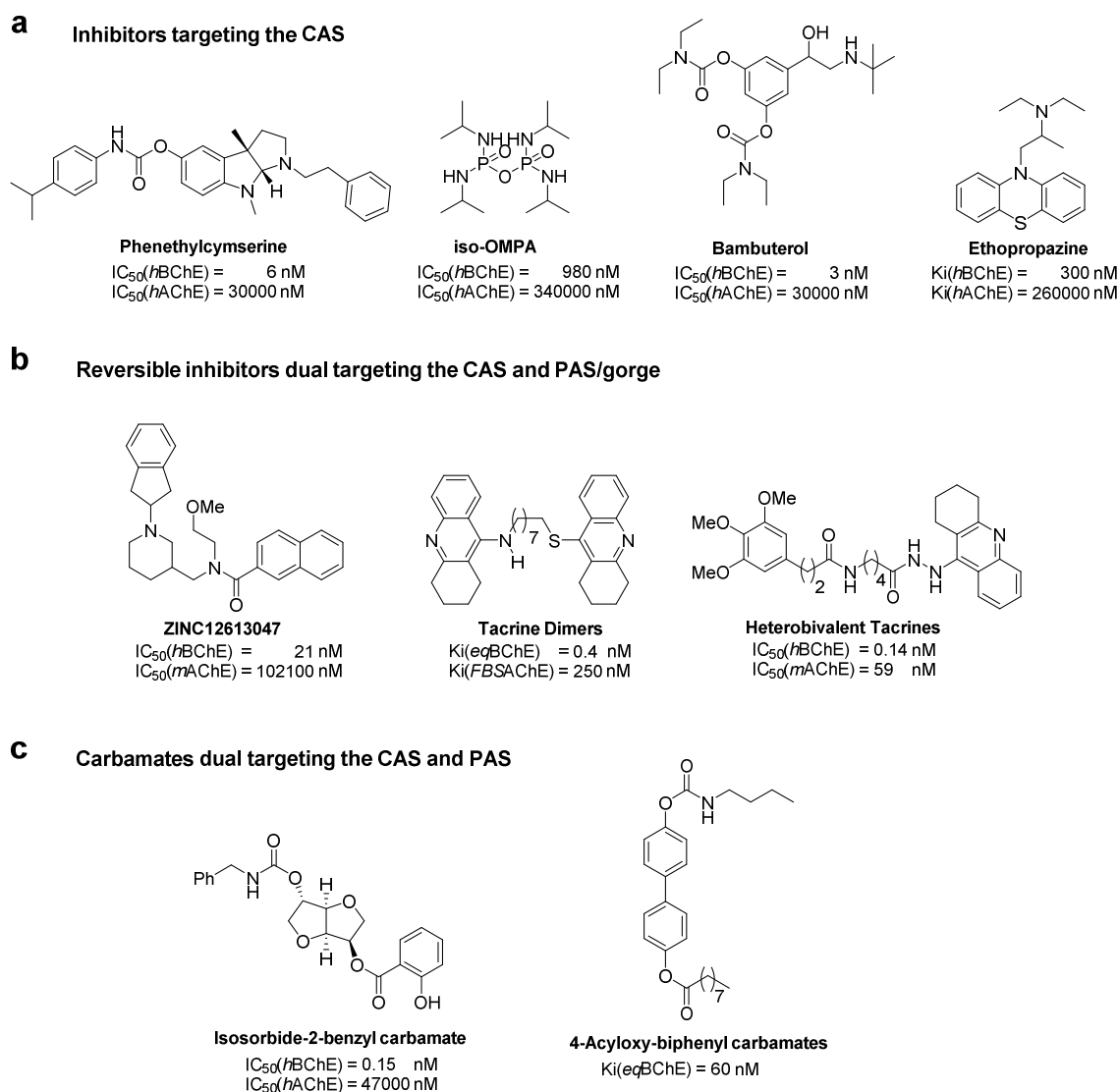
Figure 5.2. Selective high affinity inhibitors for BChE targeting (**a**) the CAS,[26,27] (**b**) the CAS and PAS/gorge with reversible inhibitors[2,5,28-29] and (**c**) the CAS and PAS with carbamates.[31,32]

However, structural features of BChE's PAS are not yet fully explored, especially due to the little number of available crystal structures with inhibitors binding to this site.[2,33] Therefore, the current chapter focuses on the development of carbamate based inhibitors targeting the CAS and the PAS at the same time. These inhibitors can help to identify further amino acid residues within the PAS which can be exploited to gain affinity when designing new compounds.

5.2   Compound Design and Synthesis

To identify a compound which is dual targeting the CAS and the PAS, the tetrahydroquinazoline template was chosen for the synthesis of carbamate based inhibitors as it plays only a minor part in inhibition of BChE itself (*cf.* **Chapter 4**). In contrast to the carbamates shown in **Figure 5.2c** which are targeting the PAS with their carrier scaffold, the herein planned compounds are modified at the carbamate residue to further explore the possibilities of targeting different binding sites of BChE, especially the PAS, with suitable chemical motifs (**Figure 5.3**). Therefore, the concept of enzyme inhibition described in **Chapter 4** can be expanded as follows: The tetrahydroquinazoline template binds to a subsite close to the catalytic triad guiding the carbamate moiety into a favorable position to enable carbamate transfer onto the enzyme's catalytic triad thus deactivating the enzyme pseudo-irreversibly (*cf.* **Chapter 4**). In addition, the transferred carbamate moiety is connected *via* a
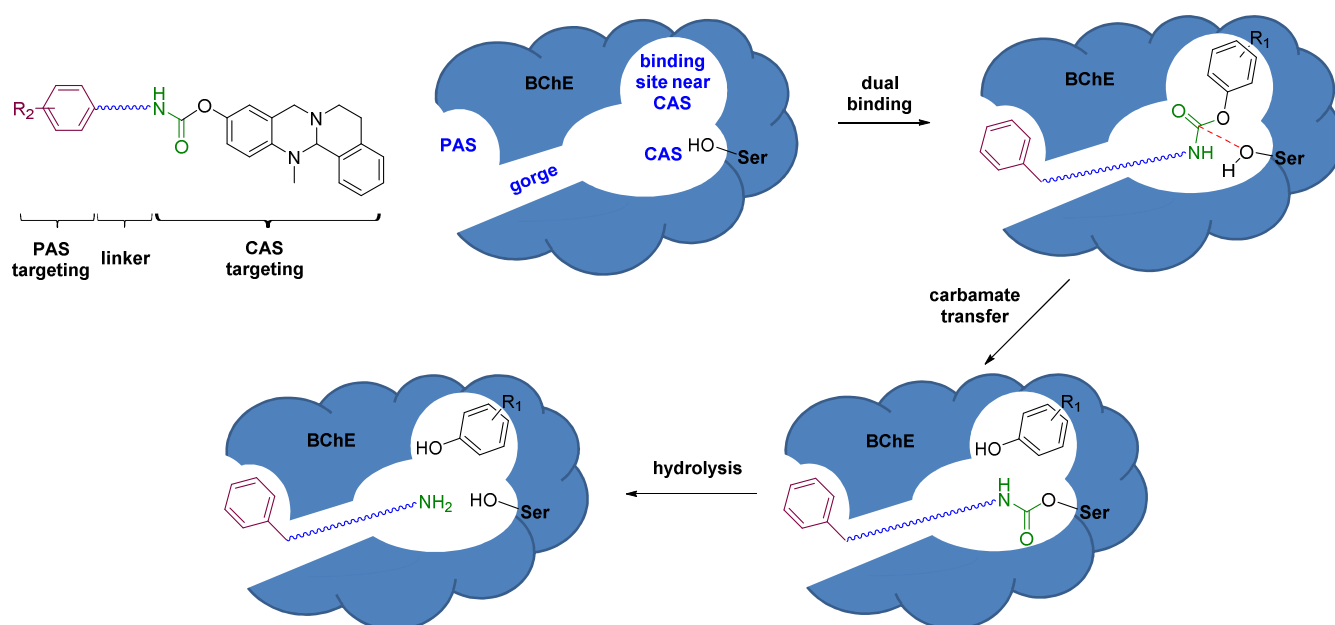
Figure 5.3. Carbamate based inhibition of BChE by targeting the CAS and the PAS concomitantly. The tetrahydroquinazoline scaffold is shown in black, the carbamate moiety in green, the linker in blue and the PAS binding moiety in purple. For description of the single steps see the main text.

linker to a second pharmacophore targeting the PAS at the same time. This additional interaction can help to improve the affinity of carbamate based compounds and is expected to have inhibitory potency even after time dependent hydrolysis of the carbamate moiety from the serine as it plugs the entrance of the gorge preventing entry of substrate and in consequence leads to BChE inhibition (**Figure 5.3**).

The discovery of an additional binding site with such compounds has to be performed in several steps. The first step is the exploration of a suitable linker length to bridge the distance between the CAS and the PAS to enable bivalent binding of the carbamate residue. For such an investigation, a phthalimide moiety was chosen as PAS binder as it is described in literature for the case of AChE to interact with amino acid residues at the PAS and the gorge.[20,34-36] For this purpose, inhibitors of the structure **5** with a functionalized carbamate chain are desirable (**Scheme 5.1**): Starting with dibromo alkanes and potassium phthalimide the alkylated compounds **1a** and **1b** were synthesized in moderate yields, followed by the substitution of the second bromine atom using sodium azide towards **2a** and **2b**. Unfortunately, the reduction of the azide group in the presence of the phthalimide moiety was unsuccessful by hydrogenation with Pd/C,[37,38] or under Staudinger conditions using PPh$_3$.[39,40] Interestingly, although reduction of an azide group in presence of the phthalimide moiety is claimed in literature[37,38] to work well, Villemin *et al.*[41] reported similar difficulties for such a reaction.
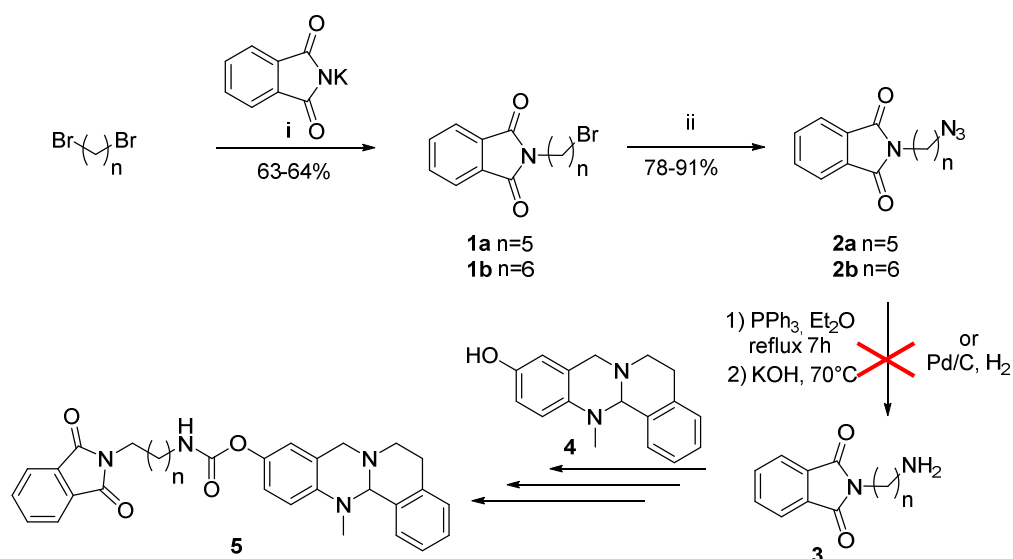
Scheme 5.1. Reagents and conditions: (i) DMF, 120 °C, 5 h; (ii) NaN$_3$, DMF, rt, 6 h.

Therefore, the compound design strategy was altered and a simple unsubstituted phenyl system was chosen as an alternative group for PAS binding (**Scheme 5.2a** and **b**). Starting with dibromoalkanes and phenol, compounds **6a-c** were synthesized. Substitution of the bromine atom by an azide group toward compounds **7a-c**, successfully followed by reduction with LiAlH$_4$ gave amines **8a-c**. Finally, activation of these amines with 4-

nitrophenyl chloroformate and coupling with the phenolic tetrahydroquinazoline **4** (synthesis described in literature[42]) gave the desired target compounds **10 a-c** with different linker lengths between the carbamate moiety and the supposed PAS binding phenyl system. In addition, also compound **11** (**Scheme 5.2b**) with one methylene unit between the mentioned residues was synthesized although it might be expected that only one linking atom is significantly too short to reach the PAS with the phenyl system while targeting the CAS with the carbamate moiety.
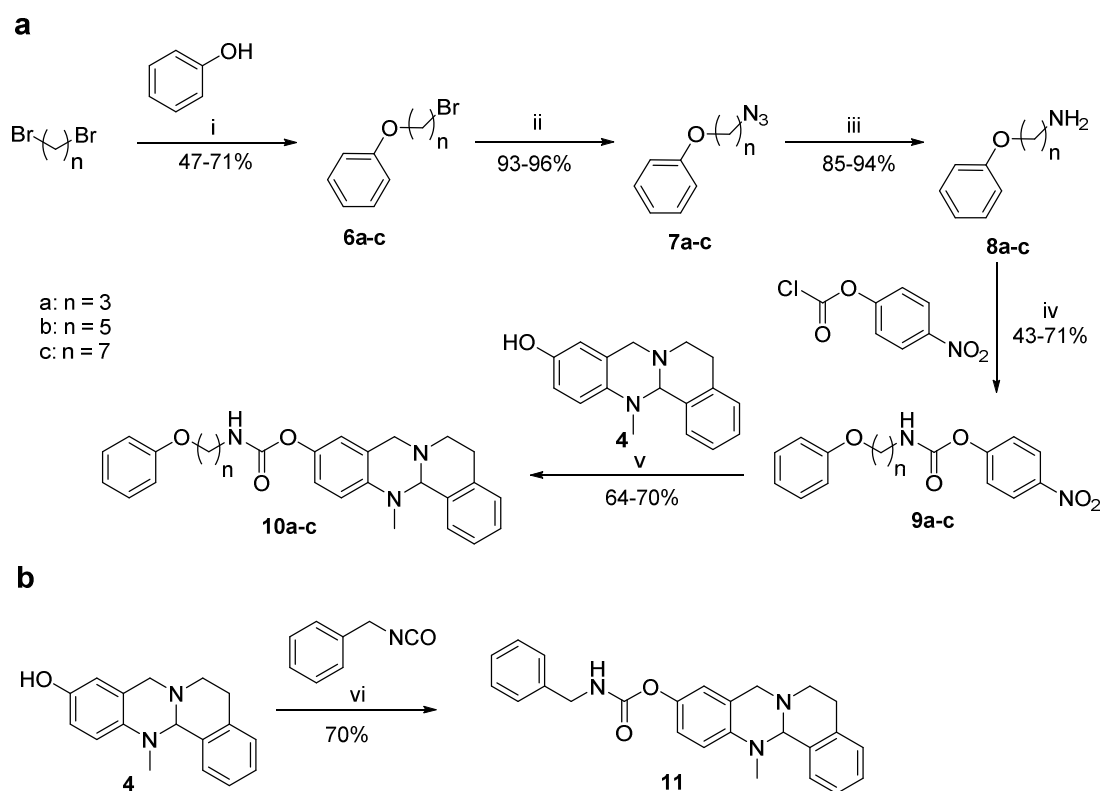
Scheme 5.2. Reagents and conditions: (i) DMF, K$_2$CO$_3$, rt, 24 h; (ii) NaN$_3$, DMF, rt, 6 h; (iii) LiAlH$_4$, THF, rt, 2 h; (iv) Et$_3$N, DCM, rt, 4 h; (v) NaH, DCM, rt, 3 h; (vi) Et$_3$N, DCM, rt, 5 h.

Besides, also the possibility of a more polar linker was investigated to improve the solubility of the test compounds. Therefore, the PEG-chain bearing compound **15** (**Scheme 5.3**) was synthesized: Starting with 1-bromo-2-(2-ethoxyethoxy)ethane a Gabriel synthesis was performed to give amine **13** in two steps. Activation of **13** with 4-nitrophenyl chloroformate gave compound **14** which was finally used to introduce the PEG-chain into compound **4** yielding the desired target compound **15**.
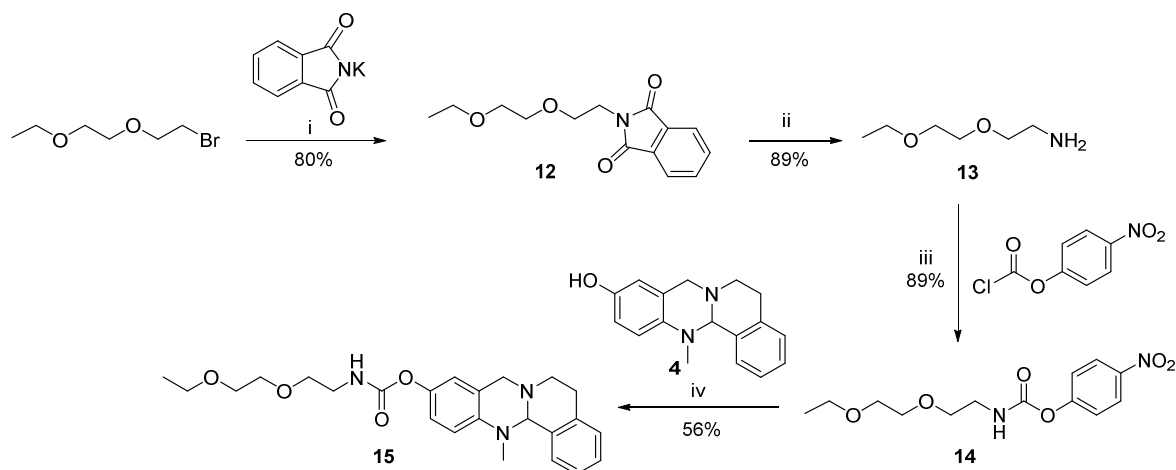
Scheme 5.3. Reagents and conditions: (i) DMF, 120 °C, 3 h; (ii) H$_2$N-NH$_2$·H$_2$O, EtOH, reflux, 4h; (iii) Et$_3$N, THF, rt, 4 h; (iv) NaH, THF, rt, 1h.

5.3 Enzyme Inhibition

To indicate binding of the synthesized target compounds to the PAS while inhibiting the CAS, IC$_{50}$-values were determined on BChE with the previously described heptyl carbamate **16** as reference compound[43] (**Table 5.1**). Interestingly, while compound **11** with only one atom as spacer between the carbamate moiety as CAS binding residue and the phenyl system as PAS binder showed almost 10 fold decrease in inhibition compared to the heptyl reference compound, all compounds of series **10** with 4 to 8 spacer atoms (counting oxygen and carbons) showed nearly identical inhibition of BChE as reference compound **16**. In contrast, the polar PEG-chain bearing compound **15** was the least active compound with ~60 fold decrease in inhibition; still being a very potent inhibitor.

These results indicate:

1) A polar carbamate group (**15**) as well as large groups connected *via* a short linker to the carbamate moiety (**11**) might not be able to interact with the unpolar acyl binding pocket due unfavorable electrostatic repulsion or steric interactions and might impede carbamoylation and BChE inhibition.

2) Extending the length of the linker (**10a-c**) eradicates unfavorable interactions between the PAS binding part of the compound and the acyl binding pocket resulting in similar inhibition compared to a heptyl carbamate moiety.

3) No additional PAS interactions could be identified so far as no changes in BChE inhibition within compound series **10** was detected.

Table 5.1. Cholinesterase inhibition of the synthesized test compounds.[a]
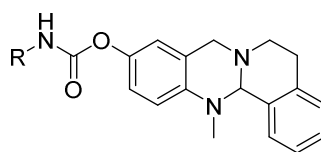
Compound	R =	IC$_{50}$(eqBChE) [nM] (pIC$_{50}$ ±SEM)
16[b]		14.8 (7.83 ± 0.03)
11		129.7 (6.89 ± 0.03)
10a		12.3 (7.91 ± 0.05)
10b		23.6 (7.63 ± 0.02)
10c		13.2 (7.88 ± 0.02)
15		929.9 (6.03 ± 0.04)

[a]Experiments were performed in triplicate with BChE from equine serum and 30 min of pre-incubation time.

[b]Compound resynthesized as described in Ref[44].

5.4   Conclusion

Dual-targeting of AChE's CAS and the PAS is well described in literature. Although the existence and the role of the PAS in BChE is discussed controversially, several investigations[28,31,44] have indicated such a binding site that might be exploited additionally for the design of new inhibitors. However, inhibitors targeting the CAS and the PAS have been rarely described for BChE (*cf.* **Figure 5.2**); but those compounds, that have adopted the concept of dual targeting BChE, are the most potent and selective BChE inhibitors to date with inhibition values in the picomolar range. The current chapter describes the modification of previously reported tetrahydroquinazoline based carbamates targeting the CAS of BChE[1,43] to find an additional interaction site with residues of the PAS. In an initial step, the linker length was investigated which is necessary to bridge the distance between the CAS and the PAS. Interestingly, no pronounced differences in inhibition between linker lengths of 4 to 8 atoms were found, proving an empty, large space in BChE for carbamate groups. This space might be exploited for further modifications, e.g. longer linker or other functional groups as PAS binder.

Due to limitations in time, the current project could not be finished and therefore only the basic ideas and the initial syntheses are presented. Nevertheless, to successfully proceed the development of dual CAS-PAS binding inhibitors, this project has to progress in three steps:

1) The linker length has to be further investigated, as to the current state no changes in BChE inhibition were found. These changes might be an increase or decrease in inhibition while it is not known if the phenyl ring as PAS binder leads to favorable or unfavorable interactions with residues of the PAS.

2) When a suitable linker length is found, the PAS binding moiety has to be systematically altered to find the best fitting moiety to the PAS. Therefore, it might be helpful to introduce moieties which are known to interact with AChE's PAS like the mentioned phthalimide moiety due to the high similarity of AChE and BChE.

3) Binding of these inhibitors at BChE's PAS has to be proven. Macdonald *et al.*[44] showed that a combination of mutant studies altered at BChE's PAS and competition studies with inhibitors known to bind to the PAS can help to determine if binding of the herein described compounds occurs specific at the PAS. Using these techniques and additional docking experiments might help to predict a suitable binding model.

5.5   Experimental Section

Chemistry.

General.

Common reagents and solvents were obtained from commercial suppliers and used without any further purification. Tetrahydrofurane (THF) was distilled from sodium/benzophenone under argon atmosphere. Reaction progress was monitored using analytical thin layer chromatography (TLC) on precoated silica gel GF_{254} plates (Macherey-Nagel GmbH & Co. KG) and spots were detected under UV light (254 nm) or through staining with iodine. Nuclear magnetic resonance spectra were performed with a Bruker AV-400 NMR instrument (Bruker, Karlsruhe, Germany) in DMSO-d_6 or CDCl$_3$. Chemical shifts are expressed in ppm relative to CDCl$_3$ or DMSO-d_6 (7.26/2.50 and 77.16/39.52 ppm for ^{1}H and ^{13}C NMR, respectively). Melting points were determined in open capillaries on a Büchi B-540 without any further correction. For purity of target compounds, analytic HPLC was performed on a system from Shimadzu equipped with a DGU-20A3R controller, LC20AB liquid chromatograph, and a SPD-20A UV/Vis detector. Stationary phase was a Synergi 4U fusion-RP (150 x 4.6 mm) column (Phenomenex, Aschaffenburg, Germany). As mobile phase, water (phase A) and MeOH (phase B) were used with 1 mL/min: conc. B: 5% → 90% from 0 to 8 min; 90% from 8 to 13 min;

90% → 5% from 13 to 15 min; 5% from 15 to 18 min. ESI mass spectral data were acquired on a Simadzu LCMS-2020.

2-(5-Bromopentyl)isoindoline-1,3-dione **1a**: 1,5-Dibromopentan (731 μL, 5.40 mmol, 2 equiv.) was dissolved in dry DMF (40 mL) and treated with potassium phthalate (500 mg, 2.70 mmol, 1 equiv.). The mixture was stirred for 5 h at 120 °C. Then, the precipitated solid was filtered and the filtrate was diluted with water (30 mL). The aqueous phase was extracted with ethyl acetate (3 x 50 mL). The combined organic layer was washed with brine (30 mL) and dried over Na_2SO_4. After removal of the solvent under reduced pressure, the residue was purified by column chromatography (petroleum ether:EtOAc = 9:1) to yield 2-(5-bromopentyl)isoindoline-1,3-dione **1a** (514 mg, 64%) as clear oil; ^{1}H NMR (400 MHz, $CDCl_3$): δ = 7.86 (dd, J = 5.5, 3.0 Hz, 2H), 7.73 (dd, J = 5.5, 3.0 Hz, 2H), 3.72 (t, J = 7.2 Hz, 2H), 3.42 (t, J = 6.8 Hz, 2H), 2.00 - 1.88 (m, 2H), 1.80 - 1.68 (m, 2H), 1.58 - 1.45 (m, 2H) ppm. ^{13}C NMR (101 MHz, $CDCl_3$): δ = 168.4 (2C), 133.9 (2C), 132.1 (2C), 123.2 (2C), 37.7, 33.4, 32.2, 27.7, 25.4 ppm.

2-(6-Bromohexyl)isoindoline-1,3-dione **1b**: 1,6-Dibromohexan (831 μL, 5.40 mmol, 2 equiv.) was dissolved in dry DMF (40 mL) and treated with potassium phthalate (500 mg, 2.70 mmol, 1 equiv.). The mixture was stirred for 5 h at 120 °C. Then, the precipitated solid was filtered and the filtrate was diluted with water (30 mL). The aqueous phase was extracted with ethyl acetate (3 x 50 mL). The combined organic layer was washed with brine (30 mL) and dried over Na_2SO_4. After removal of the solvent under reduced pressure, the residue was purified by column chromatography (petroleum ether:EtOAc = 9:1) to yield 2-(6-bromohexyl)isoindoline-1,3-dione **1b** (524 mg, 63%) as clear oil; ^{1}H NMR (400 MHz, $CDCl_3$): δ = 7.86 (dd, J = 5.5, 3.0 Hz, 2H), 7.73 (dd, J = 5.5, 3.0 Hz, 2H), 3.76 - 3.65 (m, 2H), 3.41 (t, J = 6.8 Hz, 2H), 1.94 - 1.82 (m, 2H), 1.72 (p, J = 7.4 Hz, 2H), 1.54 - 1.46 (m, 2H), 1.46 - 1.32 (m, 2H) ppm. ^{13}C NMR (101 MHz, $CDCl_3$): δ = 168.4 (2C), 133.9 (2C), 132.2 (2C), 123.2 (2C), 37.8, 33.7, 32.6, 28.4, 27.7, 26.0 ppm.

2-(5-Azidopentyl)isoindoline-1,3-dione **2a**: Referring to literature[39], 2-(5-bromopentyl)isoindoline-1,3-dione **1a** (500 mg, 1.69 mmol, 1 equiv.) was dissolved in dry DMF (40 mL) and treated with sodium azide (138 mg, 2.12 mmol, 1.25 equiv.) under argon atmosphere. The mixture was stirred for 5 h at room temperature. Then the mixture was diluted with water (30 mL) and extracted with ethyl acetate (2 x 50 mL). The organic phase was washed with water (3 x 30 mL), dried over Na_2SO_4 and the solvent was removed under reduced pressure to yield 2-(5-azidopentyl)isoindoline-1,3-dione **2a** (339 mg, 78%) as yellow oil; ^{1}H NMR (400 MHz, $CDCl_3$): δ = 7.84 (dd, J = 5.5, 3.0 Hz, 2H), 7.71 (dd, J = 5.5, 3.0 Hz, 2H), 3.74 - 3.61 (m, 2H), 3.26 (t, J = 6.9 Hz, 2H), 1.77 -

1.68 (m, 2H), 1.68 - 1.59 (m, 2H), 1.48 - 1.35 (m, 2H) ppm. ^{13}C NMR (101 MHz, CDCl$_3$): δ = 168.4 (2C), 133.9 (2C), 132.1 (2C), 123.2 (2C), 51.2, 37.7, 28.4, 28.1, 24.0 ppm.

<u>2-(6-Azidohexyl)isoindoline-1,3-dione **2b**</u>: Referring to literature[38], 2-(5-bromohexyl)isoindoline-1,3-dione **1b** (500 mg, 1.62 mmol, 1 equiv.) was dissolved in dry DMF (40 mL) and treated with sodium azide (132 mg, 2.03 mmol, 1.25 equiv.) under argon atmosphere. The mixture was stirred for 5 h at room temperature. Then the mixture was diluted with water (30 mL) and extracted with ethyl acetate (2 x 50 mL). The organic phase was washed with water (3 x 30 mL), dried over Na$_2$SO$_4$ and the solvent was removed under reduced pressure to yield 2-(6-azidohexyl)isoindoline-1,3-dione **2b** (399 mg, 91%) as yellow oil; ^{1}H NMR (400 MHz, CDCl$_3$): δ = 7.84 (dd, J = 5.5, 3.0 Hz, 2H), 7.70 (dd, J = 5.5, 3.0 Hz, 2H), 3.77 - 3.56 (m, 2H), 3.25 (t, J = 6.9 Hz, 2H), 1.74 - 1.65 (m, 2H), 1.63 - 1.54 (m, 2H), 1.48 - 1.30 (m, 4H) ppm. ^{13}C NMR (101 MHz, CDCl$_3$): δ = 168.4 (2C), 133.9 (2C), 132.2 (2C), 123.2 (2C), 51.3, 37.8, 28.7, 28.4, 26.4, 26.3 ppm.

<u>(3-Bromopropoxy)benzene **6a**</u>: Referring to literature[45], 1,3-dibromopropan (1.08 mL, 10.64 mmol, 2 equiv.), phenol (500 mg, 5.32 mmol, 1 equiv.) and potassium carbonate (734 mg, 5.32 mmol, 1 equiv.) in dry DMF (40 mL) were stirred for 24 h. Then, the precipitated solid was filtered and the filtrate was diluted with water (100 mL). The aqueous phase was extracted with ethyl acetate (3 x 50 mL). The combined organic layer was washed with brine (30 mL) and dried over Na$_2$SO$_4$. After removal of the solvent under reduced pressure, the residue was purified by column chromatography (cyclohexane 1 L, then cyclohexane:EtOAc = 10:1) to yield (3-bromopropoxy)benzene **6a** (534 mg, 47%) as clear liquid; ^{1}H NMR (400 MHz, CDCl$_3$): δ = 7.33 - 7.26 (m, 2H), 7.00 - 6.90 (m, 3H), 4.12 (t, J = 5.8 Hz, 2H), 3.62 (t, J = 6.5 Hz, 2H), 2.38 - 2.30 (m, 2H) ppm. ^{13}C NMR (101 MHz, CDCl$_3$): δ = 158.7, 129.5 (2C), 121.0, 114.6 (2C), 65.2, 32.4, 30.1 ppm.

<u>((5-Bromopentyl)oxy)benzene **6b**</u>: Referring to literature[45], 1,5-dibromopentan (1.44 mL, 10.64 mmol, 2 equiv.), phenol (500 mg, 5.32 mmol, 1 equiv.) and potassium carbonate (734 mg, 5.32 mmol, 1 equiv.) in dry DMF (40 mL) were stirred for 24 h. Then, the precipitated solid was filtered and the filtrate was diluted with water (100 mL). The aqueous phase was extracted with ethyl acetate (3 x 50 mL). The combined organic layer was washed with brine (30 mL) and dried over Na$_2$SO$_4$. After removal of the solvent under reduced pressure, the residue was purified by column chromatography (cyclohexane 1 L, then cyclohexane:EtOAc = 10:1) to yield ((5-bromopentyl)oxy)benzene **6b** (646 mg, 50%) as clear liquid; ^{1}H NMR (400 MHz, CDCl$_3$): δ = 7.24 - 7.16 (m, 2H), 6.89 - 6.78 (m, 3H), 3.90 (t, J = 6.3 Hz, 2H), 3.36 (t, J = 6.8 Hz, 2H), 1.91 - 1.82 (m, 2H), 1.80 - 1.70 (m, 2H), 1.61 - 1.50 (m, 2H) ppm. ^{13}C NMR (101 MHz, CDCl$_3$): δ = 159.0, 129.5 (2C), 120.6, 114.5 (2C), 67.5, 33.6, 32.5, 28.5, 24.9 ppm.

((7-Bromoheptyl)oxy)benzene **6c**: Referring to literature[45], 1,7-dibromoheptan (1.91 mL, 10.64 mmol, 2 equiv.), phenol (500 mg, 5.32 mmol, 1 equiv.) and potassium carbonate (734 mg, 5.32 mmol, 1 equiv.) in dry DMF (40 mL) were stirred for 24 h. Then, the precipitated solid was filtered and the filtrate was diluted with water (100 mL). The aqueous phase was extracted with ethyl acetate (3 x 50 mL). The combined organic layer was washed with brine (30 mL) and dried over Na_2SO_4. After removal of the solvent under reduced pressure, the residue was purified by column chromatography (cyclohexane 1 L, then cyclohexane:EtOAc = 10:1) to yield ((7-bromoheptyl)oxy)benzene **6c** (1028 mg, 71%) as clear liquid; ^{1}H NMR (400 MHz, $CDCl_3$): δ = 7.34 - 7.27 (m, 2H), 6.99 - 6.90 (m, 3H), 3.99 (t, J = 6.5 Hz, 2H), 3.45 (t, J = 6.8 Hz, 2H), 1.95 - 1.87 (m, 2H), 1.87 - 1.77 (m, 2H), 1.57 - 1.37 (m, 6H) ppm. ^{13}C NMR (101 MHz, $CDCl_3$): δ = 159.1, 129.4 (2C), 120.5, 114.5 (2C), 67.7, 33.9, 32.7, 29.2, 28.5, 28.1, 25.9 ppm.

(3-Azidopropoxy)benzene **7a**: Referring to literature[46], (3-bromopropoxy)benzene **6a** (500 mg, 2.34 mmol, 1 equiv.) and sodium azide (190 mg, 2.92 mmol, 1.25 equiv.) in dry DMF (20 mL) were stirred for 6 h. The solution was diluted with water (100 mL) and extracted with ethyl acetate (3 x 20 mL). The combined organic layer was washed with water (3 x 50 mL) and brine (50 mL). The organic phase was dried over Na_2SO_4 and the solvent was removed under reduced pressure to yield (3-azidopropoxy)benzene **7a** (389 mg, 94%) as yellow oil; ^{1}H NMR (400 MHz, $CDCl_3$): δ = 7.33 - 7.26 (m, 2H), 6.99 - 6.88 (m, 3H), 4.06 (t, J = 5.9 Hz, 2H), 3.53 (t, J = 6.7 Hz, 2H), 2.11 - 2.00 (m, 2H) ppm. ^{13}C NMR (101 MHz, $CDCl_3$): δ = 158.7, 129.5 (2C), 120.9 (2C), 114.5, 64.4, 48.3, 28.8 ppm.

((5-Azidopentyl)oxy)benzene **7b**: Referring to literature[46], ((5-bromopentyl)oxy)benzene **6b** (600 mg, 2.47 mmol, 1 equiv.) and sodium azide (201 mg, 3.09 mmol, 1.25 equiv.) in dry DMF (20 mL) were stirred for 6 h. The solution was diluted with water (100 mL) and extracted with ethyl acetate (3 x 20 mL). The combined organic layer was washed with water (3 x 50 mL) and brine (50 mL). The organic phase was dried over Na_2SO_4 and the solvent was removed under reduced pressure to yield ((5-azidopentyl)oxy)benzene **7b** (471 mg, 93%) as clear oil; ^{1}H NMR (400 MHz, $CDCl_3$): δ = 7.32 - 7.23 (m, 2H), 6.97 - 6.87 (m, 3H), 3.98 (t, J = 6.3 Hz, 2H), 3.31 (t, J = 6.8 Hz, 2H), 1.89 - 1.77 (m, 2H), 1.73 - 1.63 (m, 2H), 1.63 - 1.53 (m, 2H) ppm. ^{13}C NMR (101 MHz, $CDCl_3$): δ = 159.0, 129.5 (2C), 120.6, 114.5 (2C), 67.4, 51.4, 28.9, 28.7, 23.4 ppm.

((7-Azidoheptyl)oxy)benzene **7c**: Referring to literature[46], ((7-bromoheptyl)oxy)benzene **6c** (980 mg, 3.62 mmol, 1 equiv.) and sodium azide (294 mg, 4.52 mmol, 1.25 equiv.) in dry DMF (20 mL) were stirred for 6 h. The solution was diluted with water (100 mL) and extracted with ethyl acetate (3 x 20 mL). The combined

organic layer was washed with water (3 x 50 mL) and brine (50 mL). The organic phase was dried over Na_2SO_4 and the solvent was removed under reduced pressure to yield ((7-azidoheptyl)oxy)benzene **7c** (807 mg, 96%) as clear oil; ^{1}H NMR (400 MHz, $CDCl_3$): δ = 7.33 - 7.22 (m, 2H), 6.98 - 6.81 (m, 3H), 3.96 (t, J = 6.5 Hz, 2H), 3.27 (t, J = 6.9 Hz, 2H), 1.85 - 1.74 (m, 2H), 1.68 - 1.56 (m, 2H), 1.56 - 1.34 (m, 6H) ppm. ^{13}C NMR (101 MHz, $CDCl_3$): δ = 159.1, 129.4 (2C), 120.5, 114.5 (2C), 67.7, 51.5, 29.2, 28.9, 28.8, 26.7, 26.0 ppm.

3-Phenoxypropan-1-amine **8a**: In modification to literature[46], (3-azidopropoxy)benzene **7a** (370 mg, 2.09 mmol, 1 equiv.) was dissolved in dry THF (20 mL) and treated portion wise with $LiAlH_4$ (318 mg, 8.36 mmol, 4 equiv.) under ice cooling. Then, the mixture was stirred for 2 h at room temperature. The reaction mixture was quenched with water (50 mL) and ethyl acetate (50 mL) was added. The phases were separated and the aqueous phase was back extracted with ethyl acetate (2 x 30 mL). The combined organic layer was dried over Na_2SO_4 and the solvent was removed under reduced pressure to yield 3-phenoxypropan-1-amine **8a** (288 mg, 91%) as yellow oil; ^{1}H NMR (400 MHz, $CDCl_3$): δ = 7.32 - 7.24 (m, 2H), 6.97 - 6.87 (m, 3H), 4.06 (t, J = 6.1 Hz, 2H), 2.92 (t, J = 6.8 Hz, 2H), 1.97 - 1.89 (m, 2H), 1.28 (br, NH_2) ppm. ^{13}C NMR (101 MHz, $CDCl_3$): δ = 159.0, 129.4 (2C), 120.6, 114.5 (2C), 65.8, 39.3, 33.1 ppm. ESI-MS: m/z calc.: 151.10, found: 152.1 [M+H][+].

5-Phenoxypentan-1-amine **8b**: In modification to literature[46], ((5-azidopentyl)oxy)benzene **7b** (450 mg, 2.16 mmol, 1 equiv.) was dissolved in dry THF (20 mL) and treated portion wise with $LiAlH_4$ (334 mg, 8.78 mmol, 4 equiv.) under ice cooling. Then, the mixture was stirred for 2 h at room temperature. The reaction mixture was quenched with water (50 mL) and ethyl acetate (50 mL) was added. The phases were separated and the aqueous phase was back extracted with ethyl acetate (2 x 30 mL). The combined organic layer was dried over Na_2SO_4 and the solvent was removed under reduced pressure to yield 5-phenoxypentan-1-amine **8b** (378 mg, 96%) as clear oil; ^{1}H NMR (400 MHz, $CDCl_3$): δ = 7.18 - 7.09 (m, 2H), 6.82 - 6.77 (m, 1H), 6.77 - 6.72 (m, 2H), 3.83 (t, J = 6.5 Hz, 2H), 2.59 (t, J = 6.7 Hz, 2H), 1.74 - 1.63 (m, 2H), 1.42 - 1.33 (m, 2H), 1.04 (br, NH_2) ppm. ^{13}C NMR (101 MHz, $CDCl_3$): δ = 159.1, 129.4 (2C), 120.5, 114.5 (2C), 67.7, 42.2, 33.6, 29.2, 23.4 ppm. ESI-MS: m/z calc.: 179.13, found: 180.1 [M+H][+].

7-Phenoxyheptan-1-amine **8c**: In modification to literature[46], ((7-azidoheptyl)oxy)benzene **7c** (780 mg, 3.35 mmol, 1 equiv.) was dissolved in dry THF (20 mL) and treated portion wise with $LiAlH_4$ (509 mg, 13.39 mmol, 4 equiv.) under ice cooling. Then, the mixture was stirred for 2 h at room temperature. The reaction mixture was quenched with water (50 mL) and ethyl acetate (50 mL) was added. The phases were separated and the aqueous phase was back extracted with ethyl acetate (2 x 30 mL). The combined organic layer was dried over Na_2SO_4 and the solvent was removed under reduced pressure to yield 7-phenoxyheptan-1-amine **8c**

(591 mg, 85%) as white solid; ^{1}H NMR (400 MHz, CDCl$_3$): δ = 7.24 - 7.15 (m, 2H), 6.88 - 6.78 (m, 3H), 3.88 (t, J = 6.5 Hz, 2H), 2.65 - 2.55 (m, 2H), 1.75 - 1.67 (m, 2H), 1.47 - 1.34 (m, 4H), 1.34 - 1.22 (m, 4H), 1.15 - 0.99 (br, NH$_2$) ppm. ^{13}C NMR (101 MHz, CDCl$_3$): δ = 159.1, 129.4 (2C), 120.5, 114.5 (2C), 67.8, 42.3, 33.8, 29.3(2C), 26.8, 26.1 ppm. ESI-MS: m/z calc.: 207.16, found: 208.1 [M+H]$^{+}$.

4-Nitrophenyl (3-phenoxypropyl)carbamate 9a: 3-Phenoxypropan-1-amine **8a** (270 mg, 1.79 mmol, 1 equiv.) in DCM (10 mL) was added drop wise into a mixture of 4-nitrophenyl chloroformate (395 mg, 1.97 mmol, 1.1 equiv.) and triethylamine (272 μL, 1.97 mmol, 1.1 equiv.) in DCM (20 mL). The mixture was stirred for 4 h. Then, the mixture was diluted with DCM (50 mL) and washed with water (3 x 50 mL) and brine (30 mL). The organic layer was dried over Na$_2$SO$_4$ and the solvent was removed under reduced pressure. The crude residue was purified by column chromatography (petroleum ether:EtOAc = 5:1) to obtain 4-nitrophenyl (3-phenoxypropyl)carbamate **9a** (275 mg, 49%) as white solid; mp: 90-94 °C. ^{1}H NMR (400 MHz, CDCl$_3$): δ = 8.21 - 8.11 (m, 2H), 7.29 - 7.20 (m, 4H), 6.95 - 6.88 (m, 1H), 6.88 - 6.83 (m, 2H), 5.43 (br, NH), 4.04 (t, J = 5.7 Hz, 2H), 3.46 (dd, J = 12.5, 6.3 Hz, 2H), 2.03 (dt, J = 11.9, 6.1 Hz, 2H) ppm. ^{13}C NMR (101 MHz, CDCl$_3$): δ = 158.5, 156.0, 153.2, 144.8, 129.6 (2C), 125.1 (2C), 122.0 (2C), 121.2, 114.5 (2C), 66.0, 39.4, 29.0 ppm. ESI-MS: m/z calc.: 316.11, found: 317.0 [M+H]$^{+}$.

4-Nitrophenyl (5-phenoxypentyl)carbamate 9b: 5-Phenoxypentan-1-amine **8b** (350 mg, 1.96 mmol, 1 equiv.) in DCM (10 mL) was added drop wise into a mixture of 4-nitrophenyl chloroformate (432 mg, 2.15 mmol, 1.1 equiv.) and triethylamine (298 μL, 2.15 mmol, 1.1 equiv.) in DCM (20 mL). The mixture was stirred for 4 h. Then, the mixture was diluted with DCM (50 mL) and washed with water (3 x 50 mL) and brine (30 mL). The organic layer was dried over Na$_2$SO$_4$ and the solvent was removed under reduced pressure. The crude residue was purified by column chromatography (petroleum ether:EtOAc = 5:1) to obtain 4-nitrophenyl (5-phenoxypentyl)carbamate **9b** (291 mg, 43%) as white solid; mp: 92-94 °C. ^{1}H NMR (400 MHz, CDCl$_3$): δ = 8.11 - 8.04 (m, 2H), 7.20 - 7.09 (m, 4H), 6.83 - 6.77 (m, 1H), 6.77 - 6.72 (m, 2H), 5.03 (s, NH), 3.83 (t, J = 6.2 Hz, 2H), 3.18 (dd, J = 13.1, 6.8 Hz, 2H), 1.75 - 1.63 (m, 2H), 1.59 - 1.49 (m, 2H), 1.49 - 1.36 (m, 2H) ppm. ^{13}C NMR (101 MHz, CDCl$_3$): δ = 159.0, 156.0, 153.1, 144.7, 129.5 (2C), 125.1 (2C), 121.9 (2C), 120.7, 114.5 (2C), 67.4, 41.3, 29. 5, 28.9, 23.4 ppm. ESI-MS: m/z calc.: 344.14, found: 345.1 [M+H]$^{+}$.

4-Nitrophenyl (7-phenoxyheptyl)carbamate 9c: 7-Phenoxyheptan-1-amine **8c** (570 mg, 2.75 mmol, 1 equiv.) in DCM (15 mL) was added drop wise into a mixture of 4-nitrophenyl chloroformate (609 mg, 3.03 mmol, 1.1 equiv.) and triethylamine (419 μL, 2.15 mmol, 1.1 equiv.) in DCM (20 mL). The mixture was stirred for 4 h. Then, the mixture was diluted with DCM (50 mL) and washed with water (3 x 50 mL) and brine (30 mL). The

organic layer was dried over Na_2SO_4 and the solvent was removed under reduced pressure. The crude residue was purified by column chromatography (petroleum ether:DCM = 1:2) to obtain 4-nitrophenyl (7-phenoxyheptyl)carbamate **9c** (721 mg, 71%) as white solid; mp: 99-120 °C. ^{1}H NMR (400 MHz, CDCl$_3$): δ = 8.32 - 8.22 (m, 2H), 7.38 - 7.25 (m, 4H), 6.99 - 6.93 (m, 1H), 6.93 - 6.87 (m, 2H), 5.11 (s, NH), 3.99 (t, J = 6.4 Hz, 2H), 3.32 (dd, J = 13.3, 7.0 Hz, 2H), 1.88 - 1.75 (m, 2H), 1.69 - 1.58 (m, 2H), 1.57 - 1.47 (m, 2H), 1.47 - 1.38 (m, 4H) ppm. ^{13}C NMR (101 MHz, CDCl$_3$): δ = 159.1, 156.0, 153.1, 144.7, 129.4 (2C), 125.1 (2C), 121.9 (2C), 120.6, 114.5 (2C), 67.7, 41.4, 29.7, 29.2, 29.0, 26.6, 26.0 ppm. ESI-MS: *m/z* calc.: 372.17, found: 373.1 [M+H]+.

13-Methyl-5,8,13,13a-tetrahydro-6*H*-isoquinolino[1,2-*b*]quinazolin-10-yl (3-phenoxypropyl) carbamate **10a**:
13-Methyl-5,8,13,13a-tetrahydro-6*H*-isoquinolino[1,2-*b*]quinazolin-10-ol **4** (120 mg, 0.45 mmol, 1 equiv.) in DCM (5 mL) was treated with NaH in parafine oil (60 wt%, 22 mg, 0.54 mmol, 1.2 equiv.) followed by 4-nitrophenyl (3-phenoxypropyl)carbamate **9a** (171 mg, 0.54 mmol, 1.2 equiv.). The mixture was stirred for 3 h and then diluted with DCM (30 mL). The organic phase was washed with water (30 mL), brine (30 mL) and dried over Na_2SO_4. The solvent was removed under reduced pressure and the crude residue was purified by column chromatography (petroleum ether:EtOAc = 1:1) to obtain 13-methyl-5,8,13,13a-tetrahydro-6*H*-isoquinolino[1,2-*b*]quinazolin-10-yl (3-phenoxypropyl) carbamate **10a** (127 mg, 64%) as clear oil; ^{1}H NMR (400 MHz, CDCl$_3$): δ = 7.72 (t, J = 5.6 Hz, NH), 7.37 - 7.16 (m, 6H), 6.93 (dd, J = 15.8, 8.1 Hz, 4H), 6.83 (dd, J = 8.7, 2.5 Hz, 1H), 6.75 (d, J = 2.4 Hz, 1H), 4.78 (s, 1H), 4.03 (t, J = 6.2 Hz, 2H), 3.90 (d, J = 15.8 Hz, 1H), 3.84 (d, J = 15.9 Hz, 1H), 3.22 (dt, J = 8.3, 4.1 Hz, 2H), 3.18 (dd, J = 10.9, 5.4 Hz, 1H), 3.03 - 2.92 (m, 1H), 2.78 (dt, J = 16.3, 4.7 Hz, 1H), 2.67 (ddd, J = 13.5, 8.7, 4.9 Hz, 1H), 2.50 (s, 3H), 1.97 - 1.87 (m, 2H) ppm. ^{13}C NMR (101 MHz, CDCl$_3$): δ = 159.0, 155.3, 145.5, 144.7, 136.4, 134.4, 129.9 (2C), 129.2, 128.7, 127.8, 126.1, 125.8, 121.0, 120.8, 120.2, 120.0, 114.9 (2C), 76.2, 65.4, 55.6, 47.6, 38.2, 38.0, 29.5, 28.3 ppm. ESI-MS: *m/z* calc.: 443.22, found: 444.3 [M+H]+. HPLC: 96%.

13-Methyl-5,8,13,13a-tetrahydro-6*H*-isoquinolino[1,2-*b*]quinazolin-10-yl (5-phenoxypentyl) carbamate **10b**:
13-Methyl-5,8,13,13a-tetrahydro-6*H*-isoquinolino[1,2-*b*]quinazolin-10-ol **4** (120 mg, 0.45 mmol, 1 equiv.) in DCM (5 mL) was treated with NaH in parafine oil (60 wt%, 22 mg, 0.54 mmol, 1.2 equiv.) followed by 4-nitrophenyl (5-phenoxypentyl)carbamate **9b** (186 mg, 0.54 mmol, 1.2 equiv.). The mixture was stirred for 3 h and then diluted with DCM (30 mL). The organic phase was washed with water (30 mL), brine (30 mL) and dried over Na_2SO_4. The solvent was removed under reduced pressure and the crude residue was purified by column chromatography (petroleum ether:EtOAc = 1:1) to obtain 13-methyl-5,8,13,13a-tetrahydro-6*H*-isoquinolino[1,2-*b*]quinazolin-10-yl (5-phenoxypentyl) carbamate **10b** (138 mg, 65%) as clear oil; ^{1}H NMR (400 MHz, CDCl$_3$): δ = 7.64 (t, J = 5.7 Hz, NH), 7.37 - 7.31 (m, 1H), 7.31 - 7.22 (m, 4H), 7.21 - 7.15 (m, 1H),

6.97 - 6.87 (m, 4H), 6.83 (dd, J = 8.7, 2.7 Hz, 1H), 6.74 (d, J = 2.6 Hz, 1H), 4.77 (s, 1H), 3.97 (t, J = 6.4 Hz, 2H), 3.90 (d, J = 15.8 Hz, 1H), 3.84 (d, J = 15.9 Hz, 1H), 3.23 - 3.13 (m, 1H), 3.08 (q, J = 6.5 Hz, 2H), 3.04 - 2.93 (m, 1H), 2.78 (dt, J = 16.3, 4.7 Hz, 1H), 2.66 (ddd, J = 11.2, 8.9, 4.9 Hz, 1H), 2.50 (s, 3H), 1.80 - 1.67 (m, 2H), 1.60 - 1.40 (m, 4H) ppm. ^{13}C NMR (101 MHz, CDCl$_3$): δ = 159.1, 155.3, 145.5, 144.7, 136.4, 134.4, 129.9 (2C), 129.2, 128.7, 127.8, 126.1, 125.8, 120.8, 120.8, 120.2, 120.0, 114.9 (2C), 76.2, 67.7, 55.6, 47.6, 40.8, 38.3, 29.5, 28.9, 28.3, 23.3 ppm. ESI-MS: m/z calc.: 471.25, found: 472.3 [M+H]$^+$. HPLC: 95%.

13-Methyl-5,8,13,13a-tetrahydro-6*H*-isoquinolino[1,2-*b*]quinazolin-10-yl (7-phenoxyheptyl) carbamate **10c**: 13-Methyl-5,8,13,13a-tetrahydro-6*H*-isoquinolino[1,2-*b*]quinazolin-10-ol **4** (120 mg, 0.45 mmol, 1 equiv.) in DCM (5 mL) was treated with NaH in parafine oil (60 wt%, 22 mg, 0.54 mmol, 1.2 equiv.) followed by 4-nitrophenyl (7-phenoxyheptyl)carbamate **9c** (201 mg, 0.54 mmol, 1.2 equiv.). The mixture was stirred for 3 h and then diluted with DCM (30 mL). The organic phase was washed with water (30 mL), brine (30 mL) and dried over Na$_2$SO$_4$. The solvent was removed under reduced pressure and the crude residue was purified by column chromatography (petroleum ether:EtOAc = 1:1) to obtain 13-methyl-5,8,13,13a-tetrahydro-6*H*-isoquinolino[1,2-*b*]quinazolin-10-yl (7-phenoxyheptyl)carbamate **10c** (158 mg, 70%) as clear oil; ^{1}H NMR (400 MHz, CDCl$_3$): δ = 7.61 (t, J = 5.6 Hz, NH), 7.38 - 7.31 (m, 1H), 7.31 - 7.22 (m, 4H), 7.22 - 7.15 (m, 1H), 6.96 - 6.88 (m, 4H), 6.83 (dd, J = 8.7, 2.4 Hz, 1H), 6.74 (d, J = 2.3 Hz, 1H), 4.77 (s, CH), 3.96 (t, J = 6.5 Hz, 2H), 3.90 (d, J = 15.9 Hz, 1H), 3.84 (d, J = 15.9 Hz, 1H), 3.22 - 3.11 (m, 1H), 3.05 (dd, J = 12.9, 6.7 Hz, 2H), 3.01 - 2.91 (m, 1H), 2.78 (dt, J = 16.2, 4.5 Hz, 1H), 2.72 - 2.61 (m, 1H), 2.50 (s, 3H), 1.80 - 1.65 (m, 2H), 1.56 - 1.26 (m, 8H) ppm. ^{13}C NMR (101 MHz, CDCl$_3$): δ = 159.1, 155.3, 145.5, 144.7, 136.4, 134.4, 129.9 (2C), 129.2, 128.7, 127.8, 126.1, 125.8, 120.8, 120.8, 120.3, 120.0, 114.9 (2C), 76.2, 67.7, 55.6, 47.6, 40.9, 38.3, 29.7, 29.1, 28.9, 28.3, 26.7, 26.0 ppm. ESI-MS: m/z calc.: 499.28, found: 500.3 [M+H]$^+$. HPLC: 97%

13-Methyl-5,8,13,13a-tetrahydro-6*H*-isoquinolino[1,2-*b*]quinazolin-10-yl benzylcarbamate **11**: A mixture of 13-methyl-5,8,13,13a-tetrahydro-6*H*-isoquinolino[1,2-*b*]quinazolin-10-ol **4** (120 mg, 0.45 mmol, 1 equiv.), triethylamine (67 µL, 0.54 mmol, 1.2 equiv.) and benzyl isocyanate (99 µL, 0.54 mmol, 1.2 equiv.) in DCM (15 mL) was stirred for 5 h at room temperature. The reaction mixture was diluted with DCM (35 mL), washed with water (2 x 20 mL) and brine (20 mL) and finally dried over Na$_2$SO$_4$. After purification with column chromatography (petroleum ether:EtOAc = 1:1) 13-methyl-5,8,13,13a-tetrahydro-6*H*-isoquinolino[1,2-*b*]quinazolin-10-yl benzylcarbamate **11** (126 mg, 70%) was isolated; ^{1}H NMR (400 MHz, DMSO-d$_6$): δ = 8.19 (t, J = 6.1 Hz, 1H), 7.40 - 7.16 (m, 9H), 6.92 (d, J = 8.8 Hz, 1H), 6.86 (dd, J = 8.7, 2.6 Hz, 1H), 6.78 (d, J = 2.4 Hz, 1H), 4.78 (s, 1H), 4.27 (d, J = 6.1 Hz, 2H), 3.92 (d, J = 15.9 Hz, 1H), 3.85 (d, J = 15.9 Hz, 1H), 3.23 - 3.13 (m, 1H), 3.05 - 2.91 (m, 1H), 2.78 (dt, J = 16.3, 4.7 Hz, 1H), 2.73 - 2.62 (m, 1H), 2.50 (s, 3H) ppm. ^{13}C NMR (101 MHz, DMSO-d$_6$): δ = 155.6, 145.6, 144.6, 139.9, 136.4, 134.4, 129.2, 128.8 (2C), 128.7, 127.8, 127.6

(2C), 127.4, 126.1, 125.8, 120.8, 120.1, 120.1, 76.1, 55.6, 47.5, 44.4, 38.2, 28.3 ppm. ESI-MS: *m/z* calc.: 399.19, found: 400.2 [M+H]$^+$. HPLC: 98%.

2-(2-(2-Ethoxyethoxy)ethyl)isoindoline-1,3-dione **12**: 1-Bromo-2-(2-ethoxyethoxy)ethane (770 µL, 4.97 mmol, 1 equiv.) was dissolved in dry DMF (15 mL) and treated with potassium phthalate (966 mg, 5.22 mmol, 1.05 equiv.). The mixture was stirred for 3 h at 120 °C. Then, the precipitated solid was filtered and the filtrate was diluted with water (30 mL). The aqueous phase was extracted with ethyl acetate (3 x 50 mL). The combined organic layer was washed with brine (30 mL) and dried over Na$_2$SO$_4$. After removal of the solvent under reduced pressure, the residue was purified by column chromatography (petroleum ether:EtOAc = 1:1) to yield 2-(2-(2-ethoxyethoxy)ethyl)isoindoline-1,3-dione **12** (1046 mg, 80%) as clear oil; ^{1}H NMR (400 MHz, CDCl$_3$): δ = 7.89 - 7.81 (m, 2H), 7.75 - 7.69 (m, 2H), 3.92 (t, *J* = 5.9 Hz, 2H), 3.76 (dd, *J* = 7.5, 4.2 Hz, 2H), 3.68 - 3.61 (m, 2H), 3.55 (dd, *J* = 5.7, 3.8 Hz, 2H), 3.47 (q, *J* = 7.0 Hz, 2H), 1.14 (t, *J* = 7.0 Hz, 3H) ppm. ^{13}C NMR (101 MHz, CDCl$_3$): δ = 168.2 (2C), 133.9 (2C), 132.2 (2C), 123.2 (2C), 70.1, 69.8, 67.9, 66.6, 37.2, 15.1 ppm. ESI-MS: *m/z* calc.: 263.12, found: 286.2 [M+Na]$^+$.

2-(2-Ethoxyethoxy)ethanamine **13**: 2-(2-(2-Ethoxyethoxy)ethyl)isoindoline-1,3-dione **12** (3130 mg, 11.9 mmol, 1 equiv.) was dissolved in ethanol (50 mL) and treated with hydrazine hydrate (1.13 mL, 23.8 mmol, 2 equiv.). The mixture was refluxed for 4 h during which a white precipitate has formed. The reaction mixture was filtered and the filtrate was evaporated to dryness. The resulting residue was suspended in diethyl ether (300 mL) and filtered again. The filtration cake was washed with diethyl ether (3 x 100 mL) and the combined filtrates were evaporated to dryness to obtain 2-(2-ethoxyethoxy)ethanamine **13** (1402 mg, 88%) as pale yellow liquid; ^{1}H NMR (400 MHz, DMSO-d$_6$): δ = 3.52 - 3.46 (m, 4H), 3.43 (q, *J* = 7.0 Hz, 2H), 3.37 (t, *J* = 5.8 Hz, 2H), 2.95 (br, NH$_2$), 2.66 (t, *J* = 5.8 Hz, 2H), 1.10 (t, *J* = 7.0 Hz, 3H) ppm. ^{13}C NMR (101 MHz, DMSO-d$_6$): δ = 73.3, 70.1, 69.7, 66.0, 41.7, 15.6 ppm. ESI-MS: *m/z* calc.: 133.11, found: 134.3 [M+H]$^+$.

4-Nitrophenyl 2-(2-ethoxyethoxy)ethylcarbamate **14**: 4-Nitrophenyl chloroformate (4.25 g, 21.05 mmol, 2 equiv.) was dissolved in dry THF (30 mL) and treated with triethylamine (2.9 mL, 21.05 mmol, 2 equiv.). Then, 2-(2-ethoxyethoxy)ethanamine **13** (1.4 g, 10.52 mmol, 1 equiv.) in dry THF (10 mL) was added drop wise over 30 min and the reaction mixture was stirred for 4 h at room temperature. The mixture was diluted with ethyl acetate (50 mL), washed with 1 M HCl-solution (3 x 10 mL) and washed with brine (10 mL). Then, the organic layer was dried over Na$_2$SO$_4$, followed by the removal of the solvent under reduced pressure. The crude product was purified by column chromatography (DCM:MeOH = 15:1) to yield 4-nitrophenyl 2-(2-ethoxyethoxy)ethylcarbamate **14** (1328 mg, 42%) as yellow oil; ^{1}H NMR (400 MHz, CDCl$_3$): δ = 8.30 - 8.22

(m, 2H), 7.38 - 7.29 (m, 2H), 3.72 - 3.66 (m, 4H), 3.66 - 3.62 (m, 2H), 3.59 (q, J = 7.0 Hz, 2H), 3.51 (dd, J = 10.6, 5.1 Hz, 2H), 1.27 (t, J = 7.0 Hz, 3H) ppm. ^{13}C NMR (101 MHz, CDCl$_3$): δ = 156.0, 153.2, 144.7, 125.1 (2C), 122.0 (2C), 70.4, 69.8, 69.6, 66.8, 41.1, 15.1 ppm. ESI-MS: m/z calc.: 298.12, found: 321.2 [M+Na]$^+$.

13-methyl-6,8,13,13a-tetrahydro-5*H*-isoquinolino[1,2-*b*]quinazolin-10-yl-2-(2-ethoxyethoxy)-ethyl   carbamate **15**: A solution of 13-methyl-6,8,13,13a-tetrahydro-5*H*-isoquinolino[1,2-*b*]quinazolin-10-ol **4** (200 mg, 0.75 mmol, 1 equiv.) in dry THF (5 mL) was treated with NaH in parafine oil (60%, 36 mg, 0,9 mmol, 1.2 equiv.). The mixture was stirred until the formation of gas stopped. Then, 4-nitrophenyl 2-(2-ethoxyethoxy)ethylcarbamate **14** (269 mg, 0.90 mmol, 1.2 equiv.) was added and the mixture was stirred for 1 h. The mixture was diluted with ethyl acetate (20 mL) and washed with water (10 mL) and brine (10 mL). The organic phase was dried over Na$_2$SO$_4$ and concentrated in vacuum to dryness. The crude product was purified by column chromatography (petroleum ether: EtOAc = 1:5) to yield 13-methyl-6,8,13,13a-tetrahydro-5*H*-isoquinolino[1,2-*b*]quinazolin-10-yl-2-(2-ethoxyethoxy)-ethyl carbamate **15** (178 mg, 56%) as yellow oil; ^{1}H-NMR (400 MHz, DMSO-d$_6$): δ = 7.64 (t, J = 5.6 Hz, 1H), 7.38 - 7.30 (m, 1H), 7.28 - 7.21 (m, 2H), 7.21 - 7.12 (m, 1H), 6.91 (d, J = 8.8 Hz, 1H), 6.83 (dd, J = 8.7, 2.5 Hz, 1H), 6.75 (d, J = 2.4 Hz, 1H), 4.78 (s, 1H), 3.91 (d, J = 15.8 Hz, 1H), 3.85 (d, J = 15.9 Hz, 1H), 3.57 - 3.52 (m, 2H), 3.52 - 3.41 (m, 6H), 3.25 - 3.14 (m, 3H), 3.05 - 2.91 (m, 1H), 2.78 (dt, J = 16.3, 4.6 Hz, 1H), 2.67 (ddd, J = 13.4, 8.9, 4.9 Hz, 1H), 2.50 (s, 3H), 1.12 (t, J = 7.0 Hz, 3H) ppm. ^{13}C-NMR (101 MHz, DMSO-d$_6$): δ = 155.4, 145.5, 144.6, 136.4, 134.4, 129.2, 128.7, 127.8, 126.1, 125.8, 120.7, 120.2, 120.0, 76.2, 70.1, 69.7, 69.4, 66.0, 55.6, 47.6, 40.8, 38.2, 28.3, 15.6 ppm. ESI-MS: m/z calc.: 425.23, found: 426.3 [M+H]$^+$. HPLC: 97%.

Enzyme Inhibition.

BChE (E.C.3.1.1.8, from equine serum) was purchased from Sigma Aldrich (Steinheim, Germany). DTNB (Ellman's reagent), BTC iodide was obtained from Fluka (Buchs, Switzerland). The stock solutions of the test compounds were prepared in ethanol with a concentration of 33.3 mM (1 mM in assay) and step wise diluted with ethanol to a concentration of 33.3 nM (1 nM in assay). For assay buffer preparation, 3.12 g of potassium dihydrogen phosphate were dissolved in 500 mL of water and adjusted with a NaOH-solution (0.2 M) to pH = 8.0. Enzyme solutions were prepared with buffer to give 2.5 units/mL and stabilized with 2 mg albumin bovine (SERVA, Heidelberg, Germany) per mL of enzyme solution. 396 mg of DTNB were dissolved in 100 mL of buffer to give a 10 mM solution (0.3 mM in assay). BTC solution was prepared in buffer with a concentration of 75 mM (452 μM in assay). The assay was performed at 25 °C as described in the following: Into a cuvette containing 1.5 mL of buffer, 50 μL BChE solution, 50 μL of DTNB solution, the test compound solution (50 μL) was added and the mixture was mixed. The mixture was incubated for 30 min, before 10 μL of BTC was added. The mixture was incubated for further 2.5 min before the absorption at 412 nm was determined with a

Shimadzu UVmini-1240 spectrophotometer. To measure full enzyme activity, the compound solution was replaced by ethanol. Each compound concentration was tested three times. The enzyme activity in percentage was plotted against the logarithm of the compound concentrations from which the IC_{50} values were calculated by using the software GraphPad Prism 4.0.[1]

5.6   References

[1] Sawatzky, E.; Wehle, S.; Kling, B.; Wendrich, J.; Bringmann, G.; Sotriffer, C. A.; Heilmann, J.; Decker, M. Discovery of Highly Selective and Nanomolar Carbamate-Based Butyrylcholinesterase Inhibitors by Rational Investigation into Their Inhibition Mode. *J. Med. Chem.* **2016**, *59*, 2067-2082.

[2] Brus, B.; Kosak, U.; Turk, S.; Pislar, A.; Coquelle, N.; Kos, J.; Stojan, J.; Colletier, J.-P.; Gobec, S. Discovery, Biological Evaluation, and Crystal Structure of a Novel Nanomolar Selective Butyrylcholinesterase Inhibitor. *J. Med. Chem.* **2014**, *57*, 8167-8179.

[3] Nachon, F.; Carletti, E.; Ronco, C.; Trovaslet, M.; Nicolet, Y.; Jean, L.; Renaed, P.-Y. Crystal Structures of Human Cholinesterases in Complex with Huprine W and Tacrine: Elements of Specificity for Anti-Alzheimer's Drugs Targeting Acetyl- and Butyrylcholinesterase. *Biochem. J.* **2013**, *453*, 393-399.

[4] Nicolet, Y.; Lockridge, O.; Masson, P.; Fontecilla-Camps, J.-C.; Nachon, F. Crystal Structure of Human Butyrylcholinesterase and of Its Complexes with Substrate and Products. *J. Biol. Chem.* **2003**, *278*, 41141-41147.

[5] Savini, L.; Gaeta, A.; Fattorusso, C.; Catalanotti, B.; Campiani, G.; Chiasserini, L.; Pellerano, C.; Novellino, E.; McKissic, D.; Saxena, A. Specific Targeting of Acetylcholinesterase and Butyrylcholinesterase Recognition Sites. Rational Design of Novel, Selective, and Highly Potent Cholinesterase Inhibitors. *J. Med. Chem.* **2003**, *46*, 1-4.

[6] Bosak, A.; Gazić Smilović, I.; Štimac, A.; Vinković, V.; Šinko, G.; Kovarik, Z. Peripheral Site and Acyl Pocket Define Selective Inhibition of Mouse Butyrylcholinesterase by two Biscarbamates. *Arch. Biochem. Biophys.* **2013**, *529*, 140-145.

[7] Masson, P.; Xie, W.; Froment, M.-T.; Levitsky, V.; Fortier, P.-L.; Albaret, C.; Lockridge, O. Interaction Between the Peripheral Site Residues of Human Butyrylcholinesterase, D70 and Y332, in Binding and Hydrolysis of Substrates. *Biochim. Biophys. Acta* **1999**, *1433*, 281-293.

[8] Inestrosa, N. C.; Dinamarca, M. C.; Alvarez, A. Amyloid-Cholinesterase Interactions. Implications for Alzheimer's Disease. *FEBS J.* **2008**, *275*, 625-632.

[9] Bartolini, M.; Bertucci, C.; Cavrini, V.; Andrisano, V. *β*-Amyloid Aggregation Induced by Human Acetylcholinesterase: Inhibition Studies. *Biochem. Pharmacol.* **2003**, *65*, 407-416.

[10] Dorronsoro, I.; Castro, A.; Martinez, A. Peripheral and Dual Binding Site Inhibitors of Acetylcholinesterase as Neurodegenerative Disease Modifying Agents. *Expert Opin. Ther. Pat.* **2003**, *13*, 1725-1732.

[11] Bourne, Y.; Taylor, P.; Radic, Z.; Marchot, P.; Structural Insights into Ligand Interactions at the Acetylcholinesterase Peripheral Anionic Site. *EMBO J.* **2003**, *22*, 1-12.

[12] Beri, V.; Wildman, S. A.; Shiomi, K.; Al-Rashid, Z. F.; Cheung, J.; Rosenberry, T. L. The Natural Product Dihydrotanshinone I Provides a Prototype for Uncharged Inhibitors That Bind Specifically to the Acetylcholinesterase Peripheral Site with Nanomolar Affinity. *Biochemistry* **2013**, *52*, 7486-7499.

[13] Di Pietro, O.; Viayna, E.; Vicente-García, E.; Bartolini, M.; Ramón, R.; Juárez-Jiménez, J.; Clos, M. V.; Pérez, B.; Andrisano, V.; Luque, F. J.; Lavilla, R.; Muñoz-Torrero, D. 1,2,3,4-Tetrahydrobenzo[*h*][1,6]naphthyridines as a New Family of Potent Peripheral-to-Midgorge-Site Inhibitors of Acetylcholinesterase: Synthesis, Pharmacological Evaluation and Mechanistic Studies. *Eur. J. Med Chem.* **2014**, *73*, 141-152.

[14] Pejchal, V.; Štěpánková, S.; Pejchalová, M.; Královec, K.; Havelek, R.; Růžičková, Z.; Ajani, H.; Lo, R.; Lepšík, M. Synthesis, Structural Characterization, Docking, Lipophilicity and Cytotoxicity of 1-[(1*R*)-1-(6-Fluoro-1,3-benzothiazol-2-yl)ethyl]-3-alkyl Carbamates, Novel Acetylcholinesterase and Butyrylcholinesterase Pseudo-Irreversible Inhibitors. *Bioorg. Med. Chem.* **2016**, *24*, 1560-1572.

[15] Darvesh, S.; Darvesh, K. V.; McDonald, R. S.; Mataija, D.; Walsh, R.; Mothana, S.; Lockridge, O.; Martin, E. Carbamates with Differential Mechanism of Inhibition Toward Acetylcholinesterase and Butyrylcholinesterase. *J. Med. Chem.* **2008**, *51*, 4200-4212.

[16] Camerino, E.; Wong, D. M.; Tong, F.; Körber, F.; Gross, A. D.; Islam, R.; Viayna, E.; Mutunga, J. M.; Li, J.; Totrov, M. M.; Bloomquist, J. R.; Carlier, P. R. Difluoromethyl Ketones: Potent Inhibitors of Wild Type and Carbamate-Insensitive G119S Mutant *Anopheles Gambiae* Acetylcholinesterase. *Bioorg. Med. Chem. Lett.* **2015**, *25*, 4405-4411.

[17] Camps, P.; Formosa, X.; Galdeano, C.; Muñoz -Torrero, D.; Ramírez, L.; Gómez, E.; Isambert, N.; Lavilla, R.; Badia, A.; Clos, M. V.; Bartolini, M.; Mancini, F.; Andrisano, V.; Arce, M. P.; Rodriguez-Franco, M. I.; Huertas, O.; Dafni, T.; Luque, F. J. Pyrano [3,2-*c*]quinoline-6-chlorotacrine Hybrids as a Novel Family of

Acetylcholinesterase- and *β*-Amyloid-Directed Anti-Alzheimer Compounds. *J. Med. Chem.* **2009**, *52*, 5365-5379.

[18] Mantoani, S. P.; Chierrito, T. P. C.; Vilela, A. F. L.; Cardoso, C. L.; Martínez, A.; Carvalho, I. Novel Triazole-Quinoline Derivatives as Selective Dual Binding Site Acetylcholinesterase Inhibitors *Molecules* **2016**, *21,* 193; doi:10.3390/molecules21020193.

[19] Wang, C.; Wu, Z.; Cai, H.; Xu, S.; Liu, J.; Jiang, J.; Yao, H.; Wu, X.; Xu, J. Design, Synthesis, Biological Evaluation and Docking Study of 4-Isochromanone Hybrids Bearing *N*-Benzyl Pyridinium Moiety as Dual Binding Site Acetylcholinesterase Inhibitors. *Bioorg. Med. Chem. Lett.* **2015**, *25*, 5212-5216.

[20] Alonso, D.; Dorronsoro, I.; Rubio, L.; Muñoz, P.; García-Palomero, E.; Del Monte, M.; Bidon-Chanal, A.; Orozco, M.; Luque, F. J.; Castro, A.; Medina, M.; Martínez, A. Donepezil-Tacrine Hybrid Related Derivatives as New Dual Binding Site Inhibitors of AChE. *Bioorg. Med. Chem.* **2005**, *13*, 6588-6597.

[21] Dorronsoro, I.; Alonso, D.; Castro, A.; del Monte, M.; García-Palomero, E.; Martínez, A. Synthesis and Biological Evaluation of Tacrine-Thiadiazolidinone Hybrids as Dual Acetylcholinesterase Inhibitors. *Arch. Pharm. Chem. Life Sci.* **2005**, *338*, 18-23.

[22] Camps, P.; Formosa, X.; Muñoz-Torrero, D.; Petrignet, J.; Badia, A.; Clos, M. V. Synthesis and Pharmacological Evaluation of Huprine-Tacrine Heterodimers: Subnanomolar Dual Binding Site Acetylcholinesterase Inhibitors. *J. Med. Chem.* **2005**, *48*, 1701-1704.

[23] Bolognesi, M. L.; Cavalli, A.; Valgimigli, L.; Bartolini, M.; Rosini, M.; Andrisano, V.; Recanatini, M.; Melchiorre, C. Multi-Target-Directed Drug Design Strategy: From a Dual Binding Site Acetylcholinesterase Inhibitor to a Trifunctional Compound against Alzheimer's Disease. *J. Med. Chem.* **2007**, *50*, 6446-6449.

[24] Nunes Lemes, L. F.; de Andrade Ramos, G.; de Oliveira, A. S.; da Silva, F. M. R.; de Castro Couto, G.; da Silva Boni, M.; Guimaraes, M. J. R.; Souza, I. N. O.; Bartolini, M.; Andrisano, V.; do Nascimento Nogueira, P. C.; Silveira, E. R; Brand, G. D.; Soukup, O.; Korabecný, J.; Romeiro, N. C.; Castro, N. G.; Bolognesi, M. L.; Soares Romeiro, L. A. Cardanol-Derived AChE Inhibitors: Towards the Development of Dual Binding Derivatives for Alzheimer's Disease. *Eur. J. Med. Chem.* **2016**, *108*, 687-700.

[25] He, X.-C.; Feng, S.; Wang, Z. F.; Shi, Y.; Zheng, S.; Xia, Y.; Jiang, H.; Tang, X.-C.; Bai, D. Study on Dual-Site Inhibitors of Acetylcholinesterase: Highly Potent Derivatives of Bis- and Bifunctional Huperzine B. *Bioorg. Med. Chem.* **2007**, *15*, 1394-1408.

[26] Giacobini, E.; Cholinesterase Inhibitors: New Roles and Therapeutic Alternatives. *Pharmacol. Res.* **2004**, *50*, 433-440.

[27] Atack, J. A.; Vu, Q.-S.; Soncrant, T. T.; Brossi, A.; Rapoport, S. I. Comparative Inhibitory Effects of Various Physostigmine Analogs against Acetyl- and Butyryicholinesterases. *J. Pharmacol. Exp. Ther.* **1989**, *249*, 194-202.

[28] Campiani, G.; Fattorusso, C.; Butini, S.; Gaeta, A.; Agnusdei, M.; Gemma, S.; Persico, M.; Catalanotti, B.; Savini, L.; Nacci, V.; Novellino, E.; Holloway, H. W.; Greig, N. H.; Belinskaya, T.; Fedorko, J. M.; Saxena, A. Development of Molecular Probes for the Identification of Extra Interaction Sites in the Mid-Gorge and Peripheral Sites of Butyrylcholinesterase (BuChE). Rational Design of Novel, Selective, and Highly Potent BuChE Inhibitors. *J. Med. Chem.* **2005**, *48*, 1919-1929.

[29] Elsinghorst, P. W.; González Tanarro, C. M., Gütschow, M. Novel Heterobivalent Tacrine Derivatives as Cholinesterase Inhibitors with Notable Selectivity Toward Butyrylcholinesterase. *J. Med. Chem.* **2006,** *49*, 7540-7544.

[30] Chen, X.; Tikhonova, I. G.; Decker, M. Probing the Mid-Gorge of Cholinesterases with Spacer-Modified Bivalent Quinazolinimines Leads to Highly Potent and Selective Butyrylcholinesterase Inhibitors. *Bioorg. Med. Chem.* **2011**, *19*, 1222-1235.

[31] Carolan, C. G.; Dillon, G. P.; Khan, D.; Ryder, S. A.; Gaynor, J. M.; Reidy, S.; Marquez, J. F.; Jones, M.; Holland, V.; Gilmer, J. F. Isosorbide-2-benzyl Carbamate-5-salicylate, A Peripheral Anionic Site Binding Subnanomolar Selective Butyrylcholinesterase Inhibitor. *J. Med. Chem.* **2010**, *53*, 1190-1199.

[32] Lin, G.; Chen, G.-H.; Lu, C.-P.; Yeh, S.-C. QSARs for Peripheral Anionic Site of Butyrylcholinesterase with Inhibitions by 4-Acyloxy-biphenyl-4'-*N*-butylcarbamate. *QSAR Comb. Sci.* **2005**, *24*, 943-952.

[33] Knez, D.; Brus, B.; Coquelle, N.; Sosic, I.; Šink, R.; Brazzolotto, X.; Mravljak, J.; Colletier, J.-P.; Gobec, S. Structure-Based Development of Nitroxoline Derivatives as Potential Multifunctional Anti-Alzheimer Agents. *Bioorg. Med. Chem.* **2015**, *23*, 4442-4452.

[34] Ignasik, M.; Bajda, M.; Guzior, N.; Prinz, M.; Holzgrabe, U.; Malawska, B. Design, Synthesis and Evaluation of Novel 2-(Aminoalkyl)-isoindoline-1,3-dione Derivatives as Dual-Binding Site Acetylcholinesterase Inhibitors. *Arch. Pharm. Chem. Life Sci.* **2012**, *345*, 509-516.

[35] Guzior, N.; Bajda, M.; Rakoczy, J.; Brus, B.; Gobec, S.; Malawska, B. Isoindoline-1,3-dione Derivatives Targeting Cholinesterases: Design, Synthesis and Biological Evaluation of Potential Anti-Alzheimer's Agents. *Bioorg. Med. Chem.* **2015**, *23*, 1629-1637.

[36] Zhao, Q.; Xie, R.; Zhang, T.; Fang, J.; Mei, X.; Ning, J.; Tang, Y. Homo- and Hetero-Dimers of Inactive Organophosphorous Group Binding at Dual Sites of AChE. *Bioorg. Med. Chem. Lett.* **2011**, *21*, 6404-6408.

[37] Rawe, S. L.; Doyle, D.; Zaric, V.; Rozas, I.; McMahon, K.; Tosin, M.; Müller Bunz, H.; Murphy, E. P.; O' Boyleb, K. M.; Murphy, P. V. *N*-Glycosyl-thiophene-2-carboxamides: Synthesis, Structure and Effects on the Growth of Diverse Cell Types. *Carbohydr. Res.* **2006**, *341*, 1370-1390.

[38] Varghese, S.; Gupta, D.; Baran, T.; Jiemjit, A.; Gore, S. D.; Casero, R. A.; Woster, P. M. Alkyl-Substituted Polyaminohydroxamic Acids: A Novel Class of Targeted Histone Deacetylase Inhibitors. *J. Med. Chem.* **2005**, *48,* 6350-6365.

[39] Katritzky, A. R.; Mazurkiewicz, R.; Stevens, C. V.; Gordeev, M. F.; Steel, P. J. Convenient Two-Pot Conversion of Aldehydes to Sec-Alkyl Primary Amines: Reactions of *α*-(Benzotriazol-1-yl) Alkyliminophosphoranes with Organocerium (III) or Grignard Reagents. *Synth. Commun.* **1994**, *24*, 2955-2972.

[40] Hankovszky, H. O.; Hideg, K.; Lex, L. Nitroxyls; VIII[1]. Synthesis of Nitroxylphosphinimines; A Convenient Route to Amine, Isothiocyanate, Aminocarbonylaziridine, and Carbodiimide Nitroxyls. *Synthesis* **1981**, *2*, 147-149.

[41] Villemin, E.; Herent, M.-F.; Marchand-Brynaert, J. Functionalized Phosphonated Half-Cage Molecules as Ligands for Metal Complexes. *Eur. J. Org. Chem.* **2012**, 6165-6178.

[42] Sawatzky, E.; Bukowczan, J.; Decker, M. Investigation into Selective Debenzylation and Ring Cleavage of Quinazoline Based Heterocycles. *Tetrahedron Lett.* **2014**, *55*, 2973-2976.

[43] Darras, F. H.; Kling, B.; Heilmann J.; Decker, M. Neuroprotective Tri- and Tetracyclic BChE Inhibitors Releasing Reversible Inhibitors upon Carbamate Transfer. *ACS Med. Chem. Lett.* **2012**, *3*, 914-919.

[44] Macdonald, I. R.; Martin, E.; Rosenberry, T. L.; Darvesh, S. Probing the Peripheral Site of Human Butyrylcholinesterase. *Biochemistry* **2012**, *51*, 7046-7053.

[45] Wang, S.; Jin, G.; Wang, W.; Zhu, L.; Zhang, Y.; Dong, G.; Liu, Y.; Zhuang, C.; Miao, Z.; Yao, J.; Zhang, W.; Sheng, C. Design, Synthesis and Structure Activity Relationships of New Triazole Derivatives Containing *N*-Substituted Phenoxypropylamino Side Chains. *Eur. J. Med. Chem.* **2012**, *53*, 292-299.

[46] Crotti, P.; Renzi, G.; Roselli, G.; Di Bussolo, V.; Giuli, S.; Tsitsigia, S.; Romano, M. R. Regiochemical Control of the Ring-Opening of Aziridines by Means of Chelating Processes. Part 4: Regioselectivity of the Opening Reactions with MeOH of 1-(Benzyloxy)-2,3- and -3,4-*N*-(methoxycarbonyl)aziridoalkanes Under Condensed and Gas-Phase Operating Conditions. *Tetrahedron* **2007**, *63*, 5501-5509.

6. Investigation into Selective Debenzylation and Ring Cleavage of Quinazoline based Heterocycles[1]

Investigation into selective debenzylation and ring cleavage of quinazoline based heterocycles

Edgar Sawatzky, Jerzy Bukowczan, Michael Decker *

Institut für Pharmazie und Lebensmittelchemie, Universität Würzburg, Am Hubland, 97074 Würzburg, Germany

ABSTRACT

The selective cleavage of different benzyl bonds within tetrahydroquinazoline and dihydroquinazolinone derived structures can be achieved by the usage of different reduction and debenzylation conditions thereby providing selective removal of O-benzyl protection groups as well as the cleavage of the ring structure within the quinazoline and quinazolinone systems.

Author contributions:

Edgar Sawatzky, under supervision of Prof. Dr. Michael Decker, performed the development of the project and was responsible for the synthesis.

Jerzy Bukowczan assisted the synthesis under supervision of Edgar Sawatzky.

6.1   Introduction

In literature the quinazolinone moiety has gained the status of a "privileged structure" due to its occurrence in various synthetic and non-synthetic compounds for numerous applications in medicinal chemistry.[2,3] This structure is known as a common element in several natural products[4,5] (**Figure 6.1a**), and has been widely used for the development of therapeutic agents acting as anticonvulsants,[6] in the treatment of cancer,[7,8] as cholinesterase inhibitors for Alzheimer's disease treatment,[9-12] vasodilators,[13] anti-inflammatory agents,[14] as retrograde transport inhibitor for Shiga toxin treatment[15] or as ligands for the serotonin receptor 7 (5-HT$_7$ receptor),[16] the thyroid stimulating hormone (TSH) receptor[17] as well as the histamine H$_3$ receptor[18,19] (**Figure 6.1b**).[1]
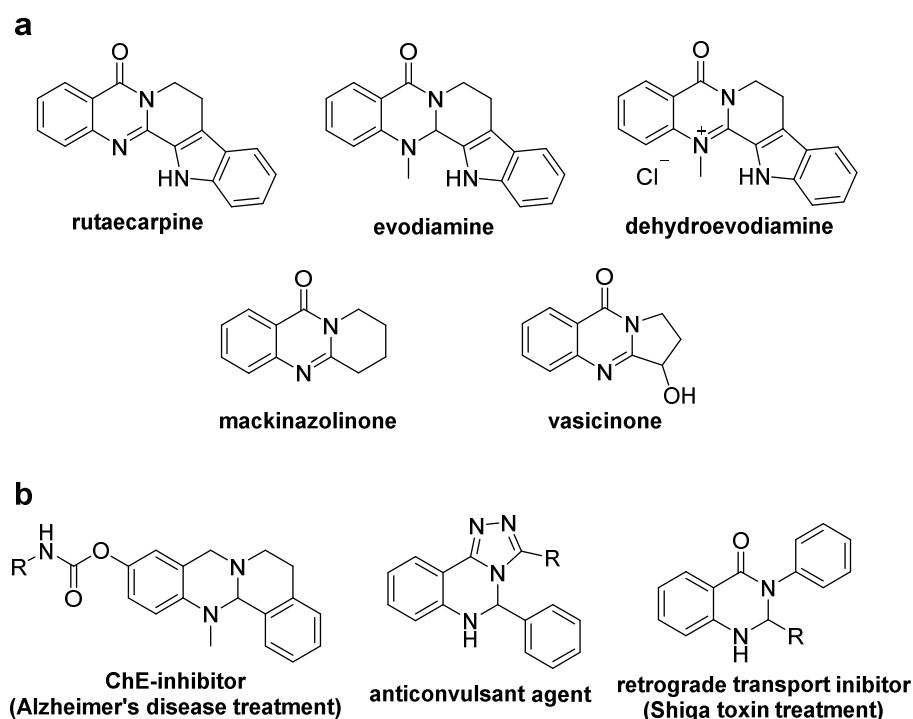
Figure 6.1. Molecules bearing a quinazoline derived core: (**a**) Several naturally occurring alkaloids and (**b**) examples of synthetic experimental therapeutics with related chemical structures.[1]

One important class of compounds derived from the quinazolinone core are tetrahydroquinazolines. The synthesis of tetrahydroquinazolines is well described by condensation of diamines with aldehydes or ketones yielding bicyclic structures,[20-22] by the direct α-amination of *ortho*-aminobenzaldehydes,[23-25] or by the reduction of the corresponding dihydroquinazolinones.[9,26,27] (**Scheme 6.1**)[28]
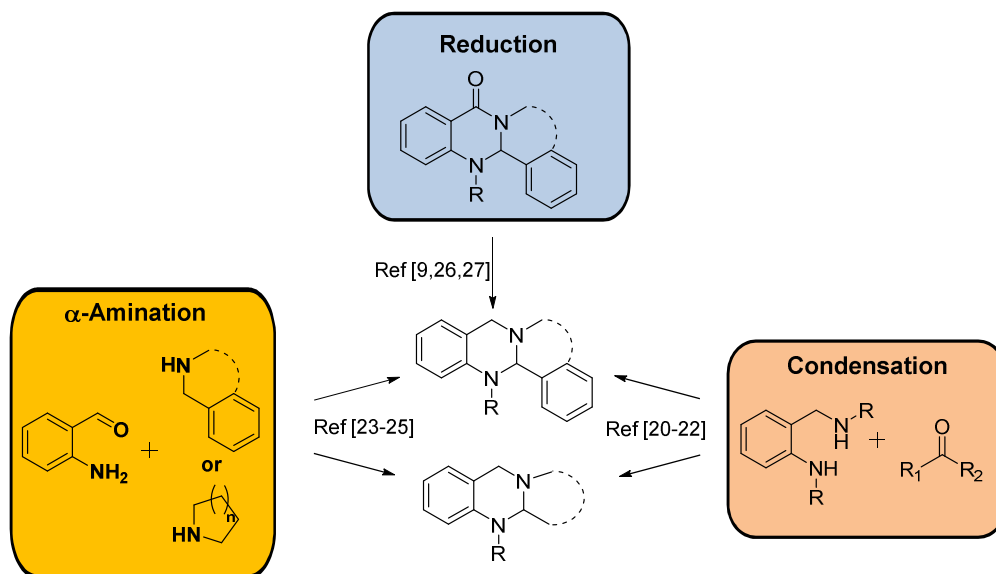
Scheme 6.1. Synthetic approaches for the formation of the tetrahydroquinazoline moiety. Dashed lines indicate cyclized and non-cyclized compounds.[28]

And also oxidative conditions applied onto the tetrahydroquinazoline core are thoroughly investigated yielding (**Scheme 6.2**)[28]

1) 3,4-dihydroquinazolines like the partially unsaturated alkaloids vasicine or deoxyvasicine,[23,29]
2) quinazolinones like the naturally occurring alkaloids deoxyvasicinone, mackinazolinone or rutaecarpine,[23,29]
3) and aromatic quinazolines.[21,30,31]
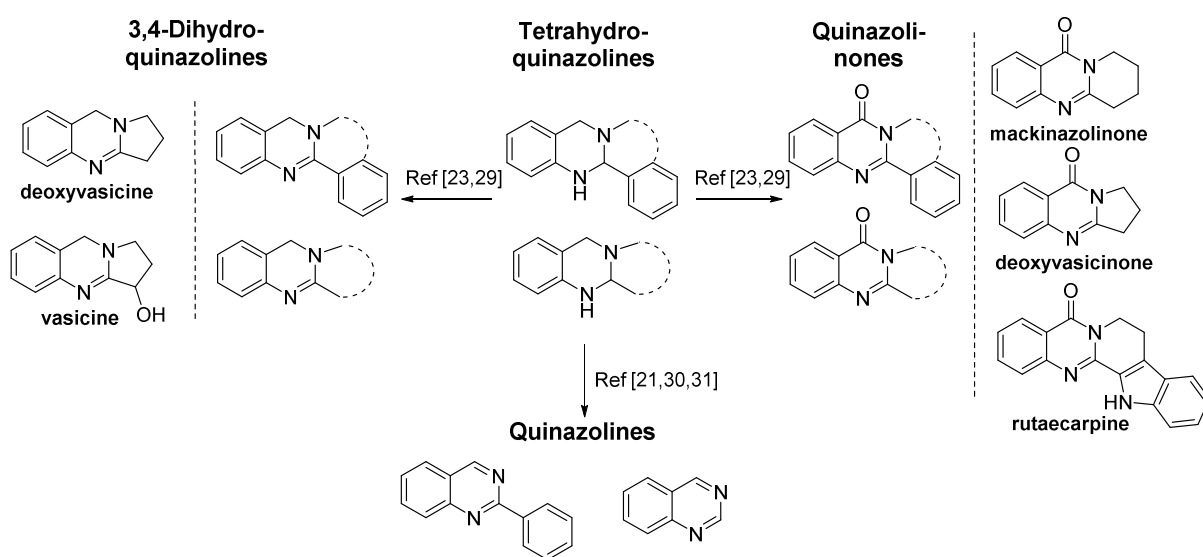
Scheme 6.2. Oxidation reactions of tetrahydroquinazolines. Dashed lines indicate cyclized and non-cyclized compounds.[28]

Regarding the well described synthesis of tetrahydroquinazolines (**Scheme 6.1**) and their selective oxidation into related structures (**Scheme 6.2**), it is quite remarkable that the reactivity of this system is not yet completely explored. Especially for this work, information about the reactivity are of high importance as the tetrahydroquinazoline scaffold was used in the previous chapters as a template for the design of selective BChE inhibitors (**Chapter 3-5**). Therefore, knowledge about the reactivity of the tetrahydroquinazoline system is of impacting interest to prevent undesired side reactions when chemically altering this scaffold. Such information can help to plan and optimize new synthetic routes for the design of new inhibitors based on the tetrahydroquinazoline template and are the source of a successful synthesis. To further explore and extend the knowledge of the chemical reactivity of the tetrahydroquinazoline core beyond the thoroughly known oxidations, the current chapter focuses on reductive conditions applied onto the tetrahydroquinazoline system by using typical reduction reagents.

6.2   Reduction of Tetrahydroquinazolines and Dihydroquinazolinones

Starting point of this investigation was the synthesis of dihydroquinazolinone **1** (**Scheme 6.3**): 5-Hydroxy anthranilic acid and triphosgene were used to synthesize isatoic anhydride derivative **2**, followed by the methylation towards dihydroquinazolinone **3**. In a two step one pot synthesis, compound **3** was first benzylated using BnBr and then fused with 3,4-dihydroisoquinoline towards compound **1** in moderate yield. Interestingly, fusion of compound **3** and 3,4-dihydroisoquinoline without prior benzyl protection is also possible, but was reported to give a yield of only 23%.[9]
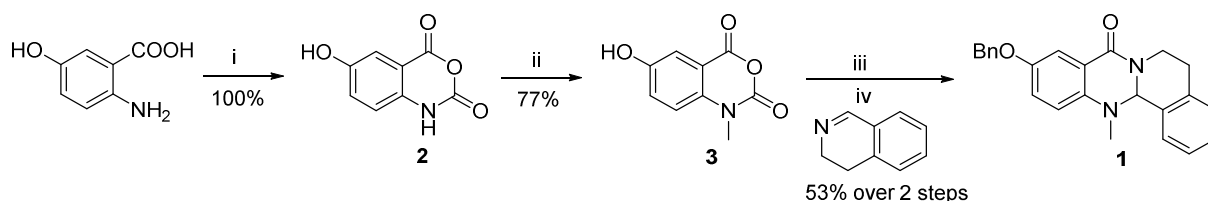
Scheme 6.3. Reagents and conditions: (i) CO(OCCl$_3$)$_2$,THF, 3.5 h, 70 °C; (ii) MeI, DIPEA, DMAc, 24 h, 40 °C; (iii) BnBr, K$_2$CO$_3$, DMF, 3.5 h, 40 °C; (iv) DMF, 5 h, 120 °C.

To synthesize tetrahydroquinazoline **5**, which was used (**Chapter 3-5**) as a template for carbamate based inhibitors, dihydroquinazolinone **1** was debenzylated using Pd/C and H$_2$ in methanol towards compound **4**, followed by the reduction with LiAlH$_4$ to the tetracyclic tetrahydroquinazoline **5** (**Scheme 6.4**, **Table 6.1**, reaction pathway *a,* followed by *b*). Interestingly, changing the reaction sequence did not give access to

compound **5** but yielded the non-cyclized compound **7** *via* tetrahydroquinazoline **6** (reaction pathway *b* followed by *a*). This is quite remarkable, as LiAlH$_4$ as a strong reduction agent does only reduce the amide bonds of dihydroquinazolinones **4** and **1** but did not further affect the tetrahydroquinazoline core of the isolated tetrahydroquinazolines **5** and **6** indicated by high yields (>90%). In contrast, comparable mild hydrogenation conditions using Pd/C as catalyst resulted for the case of tetrahydroquinazolines **5** and **6** the opening of the tetrahydroquinazoline core yielding compound **7** (reaction pathway *a* for **6** and *c* for **5**). However, to find a synthesis strategy in which the *O*Bn protection group of **6** can be removed without affecting the tetrahydroquinazoline core to access the deprotected compound **5**, different conditions were investigated. The influence of solvent and catalyst for a hydrogenation was systematically altered. Using Pd/C as catalyst and methanol, ethanol or acetic acid as solvent caused removal of the *O*Bn protection group in all cases but also opened the tetrahydroquinazoline core yielding compound **7** (pathways *a*, *d*, *e*). Interestingly, using Pd/C as catalyst and THF as solvent (pathway *f*) or PtO$_2$ as catalyst and methanol as solvent (pathway *g*) did not remove the *O*Bn protection group but selectively opened the tetrahydroquinazoline system towards compound **8**. Similar results were also found when applying NaBH$_4$ or BH$_3$ as reduction agents onto compound **6** (pathways *h* and *i*). Opening of the tetrahydroquinazoline core yielding compounds **7** and **8** under different conditions might result from the underlying benzyl position character of the C-N bond within the tetrahydroquinazoline system explaining the increased sensitivity of this bond, especially when applying typical debenzylation conditions
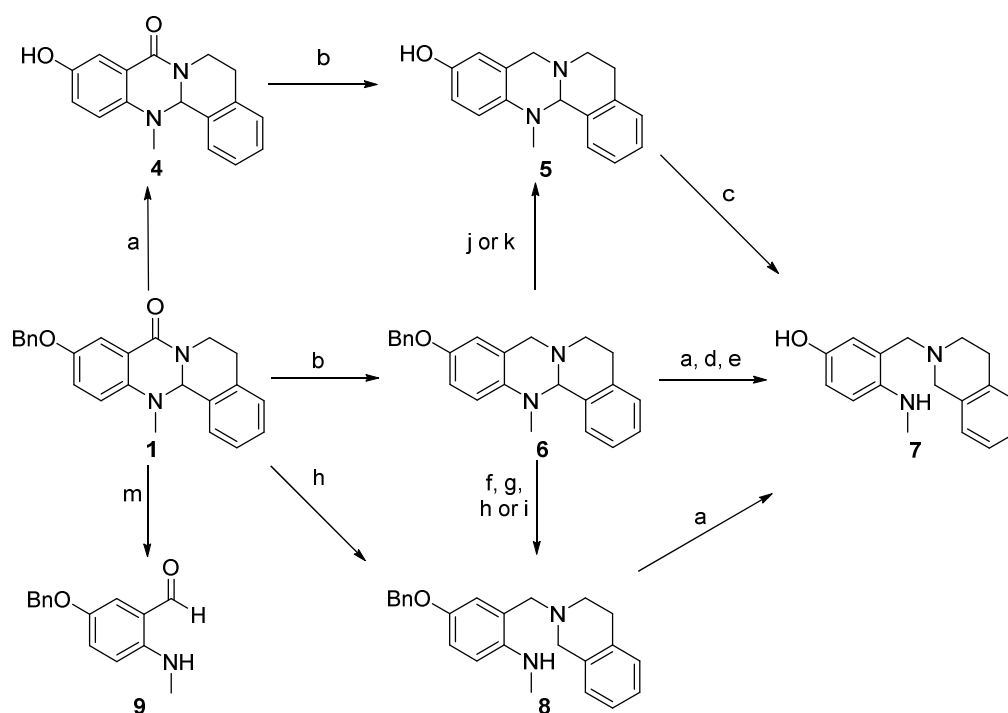
Scheme 6.4. Reaction pathways during reduction reactions of dihydroquinazolinone **1** and tetrahydroquinazoline **6** towards different products.[1]

like hydrogenation with Pd/C or PtO$_2$. In addition, the cyclic structure might cause tension making the whole system striving to a lower energy through opening of the structure which might further explain the weak C-N bond character compared to the C-O character of the benzyl protection group. However, selective *O*Bn deprotection of tetrahydroquinazoline **6** without opening the cyclic structure was possible when using AlCl$_3$ as Lewis acid (pathway *j*) or under reflux conditions in concentrated acid (pathway *k*) to yield the tetracyclic compound **5**.

Table 6.1. Applied reduction conditions *via* **Scheme 6.4**.[1]

Pathway	Starting-material	Product	Conditions	Yield /%
a	**1**	**4**	H$_2$, Pd/C, methanol, 50°C	100
a	**8**	**7**	H$_2$, Pd/C, methanol, 50°C	49
a	**6**	**7**	H$_2$, Pd/C, methanol, 50°C	44
b	**4**	**5**	LiAlH$_4$, THF, reflux	98
b	**1**	**6**	LiAlH$_4$, THF, reflux	93
c	**5**	**7**	H$_2$, Pd/C, methanol, rt	28
d	**6**	**7**	H$_2$, Pd/C, acetic acid, 50°C	14
e	**6**	**7**	H$_2$, Pd/C, ethanol, 50°C	37
f	**6**	**8**	H$_2$, Pd/C, THF, rt	93
g	**6**	**8**	H$_2$, PtO$_2$, methanol, 50°C	80
h	**6**	**8**	BH$_3$·THF, THF, reflux	42
h	**1**	**8**	BH$_3$·THF, THF, reflux	47
i	**1**	-	NaBH$_4$, ethanol, reflux	-
i	**6**	**8**	NaBH$_4$, ethanol, reflux	60
j	**6**	**5**	AlCl$_3$, PhNMe$_2$ CH$_2$Cl$_2$, rt	65
k	**6**	**5**	conc. HCl, reflux	80
l	**1**	-	NaCNBH$_3$, acetic acid, 50°C	-
m	**1**	**9**	LiAlH$_4$, THF, rt	19

6.3   Conclusion

Tetrahydroquinazolines are an important class of compounds due to their potential use as precursors for the synthesis of several natural occurring alkaloids. The syntheses of tetrahydroquinazolines as well as their oxidations are well documented in literature but to date knowledge about the reactivity of this system is not yet fully explored. Therefore, tetrahydroquinazoline **6** as well as its precursor dihydroquinazolinone **1** were synthesized and systematically exposed to different reduction conditions. These experiments revealed a high sensitivity of the tetrahydroquinazoline core towards several reduction agents resulting in the opening of the cyclic core. In conclusion, knowledge of the chemical reactivity, including reduction and oxidation conditions, of the tetrahydroquinazoline core is essential for the design of compounds derived from this template and can help to prevent undesired side reactions during synthesis.

The detailed results of this chapter as well as experimental data were previously published[1] and can be found in **Appendix 3**.

6.4   References

[1] Sawatzky, E.; Bukowczan, J.; Decker, M. Investigation into Selective Debenzylation and Ring Cleavage of Quinazoline Based Heterocycles. *Tetrahedron Lett.* **2014**, *55*, 2973-2976.

[2] Khan, I.; Ibrar, A.; Abbas, N.; Saeed, A. Recent Advances in the Structural Library of Functionalized Quinazoline and Quinazolinone Scaffolds: Synthetic Approaches and Multifarious Applications. *Eur. J. Med. Chem.* **2014**, *76*, 193-244.

[3] Khan, I.; Ibrar, A.; Ahmed, W.; Saeed, A. Synthetic Approaches, Functionalization and Therapeutic Potential of Quinazoline and Quinazolinone Skeletons: The Advances Continue. *Eur. J. Med. Chem.* **2015**, *90*, 124-169.

[4] Lee, S. H.; Son, J.-K.; Jeong, B. S.; Jeong, T.-C.; Chang, H. W.; Lee, E.-S.; Jahng, Y. Progress in the Studies on Rutaecarpine. *Molecules* **2008**, *13*, 272-300.

[5] Mhaske, S. B.; Argade, N. P. The Chemistry of Recently Isolated Naturally Occurring Quinazolinone Alkaloids. *Tetrahedron* **2006**, *62*, 9787-9826.

[6] Zheng, Y.; Bian, M.; Deng, X.-Q.; Wang, S.-B.; Quan, Z.-S. Synthesis and Anticonvulsant Activity Evaluation of 5-Phenyl-[1,2,4]triazolo[4,3-c]quinazolin-3-amine. *Arch. Pharm. Chem. Life Sci.* **2013**, *346*, 119-126.

[7] Cao, S.-L.; Feng, Y.-P.; Jiang, Y.-Y.; Liu, S.-Y.; Ding, G.-Y.; Li, R.-T. Synthesis and *in vitro* Antitumor Activity of 4(3*H*)-Quinazolinone Derivatives with Dithiocarbamate Side Chains. *Bioorg. Med. Chem. Lett.* **2005**, *15*, 1915-1917.

[8] Dong, G.; Wang, S.; Miao, Z.; Yao, J.; Zhang, Y.; Guo, Z.; Zhang, W.; Sheng, C. New Tricks for an Old Natural Product: Discovery of Highly Potent Evodiamine Derivatives as Novel Antitumor Agents by Systemic Structure–Activity Relationship Analysis and Biological Evaluations. *J. Med. Chem.* **2012**, *55*, 7593-7613.

[9] Darras, F. H.; Kling, B.; Heilmann J.; Decker, M. Neuroprotective Tri- and Tetracyclic BChE Inhibitors Releasing Reversible Inhibitors upon Carbamate Transfer. *ACS Med. Chem. Lett.* **2012**, *3*, 914-919.

[10] Decker, M.; Kraus, B.; Heilmann, J. Design, Synthesis and Pharmacological Evaluation of Hybrid Molecules out of Quinazolinimines and Lipoic Acid Lead to Highly Potent and Selective Butyrylcholinesterase Inhibitors with Antioxidant Properties. *Bioorg. Med. Chem.* **2008**, *16*, 4252-4261.

[11] Wang, B.; Mai, Y.-C.; Li, Y.; Hou, J.-Q.; Huang, S.-L.; Ou, T.-M.; Tan, J.-H.; An, L.-K.; Li, D.; Gu, L.-Q.; Huang, Z.-S. Synthesis and Evaluation of Novel Rutaecarpine Derivatives and Related Alkaloids Derivatives as Selective Acetylcholinesterase Inhibitors. *Eur. J. Med. Chem.* **2010**, *45*, 1415-1423.

[12] Chen, X.; Tikhonova, I. G.; Decker, M. Probing the Mid-Gorge of Cholinesterases with Spacer-Modified Bivalent Quinazolinimines Leads to Highly Potent and Selective Butyrylcholinesterase Inhibitors. *Bioorg. Med. Chem.* **2011**, *19*, 1222-1235.

[13] Chen, Z.; Hua, G.; Li, D.; Chen, J.; Li, Y.; Zhou, H.; Xie, Y. Synthesis and Vasodilator Effects of Rutaecarpine Analogues Which Might be Involved Transient Receptor Potential Vanilloid Subfamily, Member 1 (TRPV1). *Bioorg. Med. Chem.* **2009**, *17*, 2351-2359.

[14] Bubenyák, M.; Noszál, B.; Kóczián, K.; Takács, M.; Béni, S.; Hermecz, I.; Kökösi, J. Bioisosteric Hybrids of Two Anti-Inflammatory Agents, Rutaecarpine and Piroxicam. *Tetrahedron Lett.* **2008**, *49*, 5711-5713.

[15] Noel, R.; Gupta, N.; Pons, V.; Goudet, A.; Garcia-Castillo, M. D.; Michau, A.; Martinez, J.; Buisson, D.-A.; Johannes, L.; Gillet, D.; Barbier, J.; Cintrat, J.-C. *N*-Methyldihydroquinazolinone Derivatives of Retro-2 with Enhanced Efficacy against Shiga Toxin. *J. Med. Chem.* **2013**, *56*, 3404-3413.

[16] Na, Y. H.; Hong, S. H.; Lee, J. H.; Park, W.-K.; Baek, D.-J.; Koh, H. Y.; Cho, Y. S.; Chooa, H.; Paea, A. N. Novel Quinazolinone Derivatives as 5-HT$_7$ Receptor Ligands. *Bioorg. Med. Chem.* **2008**, *16*, 2570-2578.

[17] Englund, E. E.; Neumann, S.; Eliseeva, E.; McCoy, J. G.; Titus, S.; Zheng, W.; Southall, N.; Shinn, P.; Leister, W.; Thomas, C. J.; Inglese, J.; Austin, C. P.; Gershengorn, M. C.; Huang, W. The Synthesis and Evaluation of Dihydroquinazolin-4-ones and Quinazolin-4-ones as Thyroid Stimulating Hormone Receptor Agonists. *Med. Chem. Commun.* **2011**, *2*, 1016-1020.

[18] Nagase, T.; Mizutani, T.; Ishikawa, S.; Sekino, E.; Sasaki, T.; Fujimura, T.; Ito, S.; Mitobe, Y.; Miyamoto, Y.; Yoshimoto, R.; Tanaka, T.; Ishihara, A.; Takenaga, N.; Tokita, S.; Fukami, T.; Sato, N. Synthesis, Structure-Activity Relationships, and Biological Profiles of a Quinazolinone Class of Histamine H_3 Receptor Inverse Agonists. *J. Med. Chem.* **2008**, *51,* 4780-4789.

[19] Darras, F. H.; Pockes, S.; Huang, G.; Wehle, S.; Strasser, A.; Wittmann, H.-J.; Nimczick, M.; Sotriffer, C. A.; Decker, M. Synthesis, Biological Evaluation, and Computational Studies of Tri- and Tetracyclic Nitrogen-Bridgehead Compounds as Potent Dual-Acting AChE Inhibitors and *h*H_3 Receptor Antagonists. *ACS Chem. Neurosci.* **2014**, *5*, 225-242.

[20] Sinkkonen, J.; Zelenin, K. N.; Potapov, A.-K. A.; Lagoda, I. V.; Alekseyev, V. V.; Pihlaja, K. Ring-Chain Tautomerism in 2-Substituted 1,2,3,4-Tetrahydroquinazolines A ^{1}H, ^{13}C and ^{15}N NMR Study. *Tetrahedron* **2003**, *59*, 1939-1950.

[21] Fan, X.; Li, B.; Guo, S.; Wang, Y.; Zhang, X.; Synthesis of Quinazolines and Tetrahydroquinazolines: Copper-Catalyzed Tandem Reactions of 2-Bromobenzyl Bromides with Aldehydes and Aqueous Ammonia or Amines. *Chem. Asian J.* **2014**, *9*, 739-743.

[22] Schiedler, D. A.; Vellucci, J. K.; Beaudry, C. M. Formation of Carbon-Carbon Bonds Using Aminal Radicals. *Org. Lett.* **2012**, *14*, 6092-6095.

[23] Richers, M. T.; Deb, I.; Platonova, A. Y.; Zhang, C.; Seidel, D. Facilet Access to Ring-Fused Aminals *via* Direct α-Amination of Secondary Amines with *o*-Aminobenzaldehydes: Synthesis of Vasicine, Deoxyvasicine, Deoxyvasicinone, Mackinazolinone, and Ruteacarpine. *Synthesis* **2013**, *45*, 1730-1748.

[24] Dieckmann, A.; Richers, M. T.; Platonova, A. Y.; Zhang, C.; Seidel, D.; Houk, K. N. Metal-Free *α*-Amination of Secondary Amines: Computational and Experimental Evidence for Azaquinone Methide and Azomethine Ylide Intermediates. *J. Org. Chem.* **2013**, *78*, 4132-4144.

[25] Zhang, C.; De, C. K.; Mal, R.; Seidel, D. *α*-Amination of Nitrogen Heterocycles: Ring-Fused Aminals. *J. Am. Chem. Soc.* **2008**, *130*, 416-417.

[26] Huang, G.; Kling, B.; Darras, F. H.; Heilmann, J.; Decker, M. Identification of a Neuroprotective and Selective Butyrylcholinesterase Inhibitor Derived from the Natural Alkaloid Evodiamine. *Eur. J. Med. Chem.* **2014**, *81*, 15-21.

[27] Sawatzky, E.; Wehle, S.; Kling, B.; Wendrich, J.; Bringmann, G.; Sotriffer, C. A.; Heilmann, J. Decker, M. Discovery of Highly Selective and Nanomolar Carbamate-Based Butyrylcholinesterase Inhibitors by Rational Investigation into Their Inhibition Mode. *J. Med. Chem.* **2016**, *59*, 2067-2082.

[28] Sawatzky, E.; Drakopoulos, A.; Rölz, M.; Sotriffer, C. A.; Engels, B.; Decker, M. Experimental and Theoretical Investigations into the Stability of Cyclic Aminals. *Beilstein J. Org Chem.*, Accepted.

[29] Richers, M. T.; Zhao, C.; Seidel, D. Selective Copper(II) Acetate and Potassium Iodide Catalyzed Oxidation of Aminals to Dihydroquinazoline and Quinazolinone Alkaloids. *Beilstein J. Org. Chem.* **2013**, *9,* 1194-1201.

[30] Han, B.; Yang, X.-L.; Wang, C.; Bai, Y.-W.; Pan, T.-C.; Chen, X.; Yu, W. CuCl/DABCO/4-HO-TEMPO-Catalyzed Aerobic Oxidative Synthesis of 2-Substituted Quinazolines and 4*H*-3,1-Benzoxazines. *J. Org. Chem.* **2012**, *77*, 1136-1142.

[31] Maheswari, C. U.; Kumar, G. S.; Venkateshwar, M.; Kumar, R. A.; Kantam, M. L.; Reddy, K. R. Highly Efficient One-Pot Synthesis of 2-Substituted Quinazolines and 4*H*-Benzo[*d*][1,3]oxazines *via* Cross Dehydrogenative Coupling using Sodium Hypochlorite. *Adv. Synth. Catal.* **2010**, *352*, 341-346.

7. Experimental and Theoretical Investigation into the Stability of Cyclic Aminals[1]

Sawatzky, E.; Drakopoulos, A.; Rölz, M.; Sotriffer, C.; Engels, B.; Decker, M. Experimental and Theoretical Investigations into the Stability of Cyclic Aminals. *Beilstein J. Org. Chem.*, Accepted.

Author contributions:

Edgar Sawatzky, under supervision of Prof. Dr. Michael Decker, performed the development of the project, the synthesis of the test compounds and the stability tests.

Martin Rölz, under supervision of Edgar Sawatzky, synthesized compounds **8a,e**, **9a-c** and **13a,c** in his Bachelor's Thesis.

Computational studies were performed by Antonios Drakopoulos under supervision of Prof. Dr. Christoph A. Sotriffer and Prof. Dr. Bernd Engels

7.1   Introduction

In literature, the aminal-system is a common structure motive in various compounds, e. g. in the naturally occurring alkaloids tetraponerine T1 to T8 from the venom of the New Guinean ant *tetraponera sp.*,[2,3] in ligands of ruthenium based catalysts for metathesis,[4] in imidazolidines acting as anti-protozoan and -bacterial agents,[5,6] in Tröger's base derivatives applied in diverse research fields[7-15] or ChE inhibitors based on the scaffold of the naturally occurring alkaloid physostigmine from the calabar bean *physostigma venenosum* (**Figure 7.1a**).[16,17] And also the tetrahydroquinazoline system used in the previous chapters as template for the design of BChE inhibitors contains the aminal moiety (**Figure 7.1b**).[1]
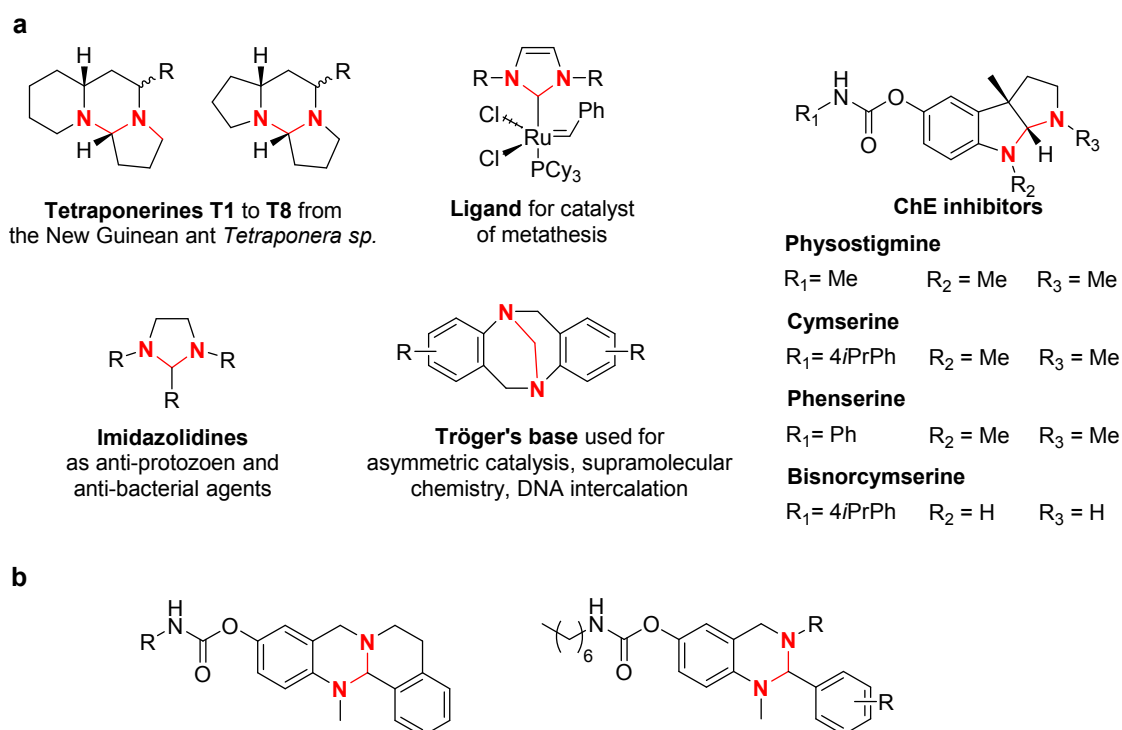
Figure 7.1. (**a**) Compounds described in literature containing an aminal core for various applications.[1] (**b**) Compounds designed in this work containing an animal core. The aminal structure is highlighted in red.

However, similar to *O,O*-acetals the aminal system is known to be sensitive to acidic hydrolysis in aqueous media. This is of special importance for compounds that are exposed to an acidic environment, e. g. orally applied drugs which are in direct contact with gastric acid. Although this fact seems obvious, there is only little information available describing the hydrolysis of the aminal system in detail.[18,19] Considering the tetrahydroquinazoline based inhibitors synthesized in the previous chapters (**Chapter 3-5**, **Figure 7.1b**), the current chapter focus on a systematic report determining the influence of the pH-value on hydrolysis of the

aminal structure within the tetrahydroquinazoline system in dependency of different parameters. This information is not only of importance for medicinal applications, it will also help to optimize reaction- or workup-conditions during synthesis to prevent degradation of compounds bearing an aminal system. Therefore, the current chapter represents a further extension on the exploration of the physical and chemical properties of tetrahydroquinazolines described in **Chapter 6**.

7.2   Compound Design and Synthesis

With regard to compound design, tetrahydroquinazolines of the general structure **1** were chosen bearing different substitution pattern at the 1-*N* and 3-*N* nitrogen atoms as well as the aromatic residue in position 2 of the tetrahydroquinazoline system (**Scheme 7.1**) to investigate their hydrolysis into the two respective fragments **2** and **3**. For this purpose, two residues were always kept constant while altering the third one. As substituents for both the 1-*N* and 3-*N* nitrogen atoms *i*Pr, *n*Pr, Me-, and Ph-residues were chosen, respectively, to investigate the effect of decreasing electron density at the nitrogen sites onto the stability of the aminal core; and at the same time the *i*Pr- and Ph-residue served as bulkier substituents for investigations into steric effects. Similar to the 1-*N* and 3-*N* nitrogen atoms, 4-*t*Bu, 4-Me-, 4-F- and 4-CF$_3$-groups were incorporated into the aromatic site to investigate the influence of decreasing electron density at this position. These substituents were chosen as they provide only inductive effects onto the aromatic system and no pronounced mesomeric effects. Also a disubstituted 2,6-dichloro compound was chosen to study the influence of steric interactions at this site of the structure.[1]
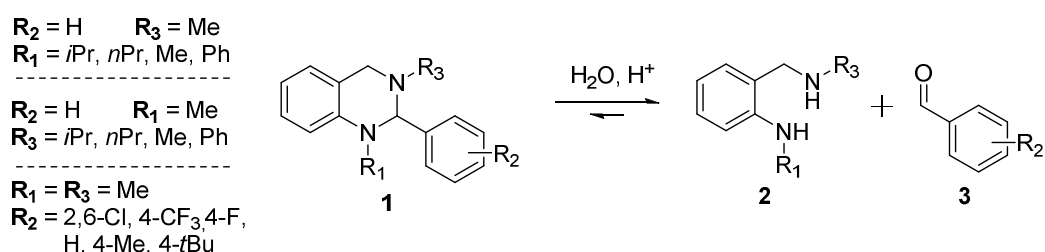
Scheme 7.1: Hydrolysis of the aminal core of tetrahydroquinazolines **1** into the corresponding diamines **2** and aldehydes **3**.[1]

The synthesis of tetrahydroquinazolines substituted at the phenyl ring as well as at the 3-*N* nitrogen atom was achieved in 4 steps (**Scheme 7.2**). Briefly, isatoic anhydride was methylated in good yield using MeI towards compound **4**, followed by formation of amides **5a-d** using the corresponding amines or their salts. Cyclization

towards dihydroquinazolinones **6a-f** and **7a-c** was performed using benzaldehyde derivatives under acidic conditions in moderate to excellent yields. The tetrahydroquinazoline target compounds **8a-f** and **9a-c** were finally obtained by reduction of **6a-f** and **7a-c** with LiAlH$_4$.[1]
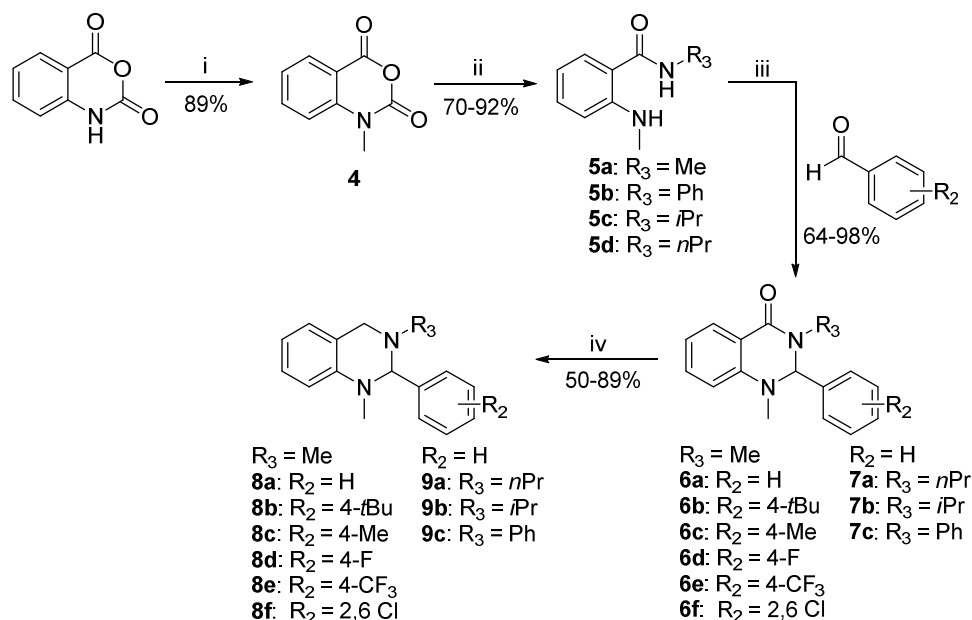
Scheme 7.2. Reagents and conditions: (i) MeI, DMAc, rt, 24h; (ii) R^1-NH$_2$ or MeNH$_3$Cl and Et$_3$N, DMF, 40-120 °C, 3-6 h; (iii) AcOH, 70 °C, 1-4 h; (iv) LiAlH$_4$, THF, 70 °C, 1-3 h.[1]

Because direct alkylation of isatoic anhydride in the first reaction step with different alkyl halides failed, the reaction strategy was changed to access compounds with different substitution patterns at the *N*-1 position (**Scheme 7.3**). For this purpose, amide **10** was synthesized using isatoic anhydride and methyl-ammonium hydrochloride (**Scheme 7.3a**) followed by the cyclization under acidic conditions with benzaldehyde to yield dihydroquinazolinone **11**. Unfortunately, introduction of substituents at the *N*-1 nitrogen in **11** by applying alkyl haildes was only successful when using *n*-PrBr and the strong non-nucleophilic base *t*BuOK to give compound **12a** and failed in the case of *i*-PrI. However, target compound **13a** was finally obtained by reduction of dihydroquinazolinone **12a** with LiAlH$_4$.

Since the synthesis of **12b** failed by applying *i*-PrI onto compound **11**, a second synthetic pathway was pursued to alter the substituents at the *N*-1 nitrogen atom of the tetrahydroquinazoline core (**Scheme 7.3b**): Anthranilic acid was alkylated by reductive amination with acetone and NaBH$_4$ in two steps to yield the *i*-Pr substituted derivative **14**. Derivative **14** and the commercially available *N*-phenyl anthranilic acid were used to synthesize amides **15a,b** under standard conditions, successively followed by the cyclization with benzaldehyde towards

dihydroquinazolinones **12b,c**. Tetrahydroquinazolines **13b,c** were finally obtained by reduction of **12b,c** with LiAlH$_4$.[1]
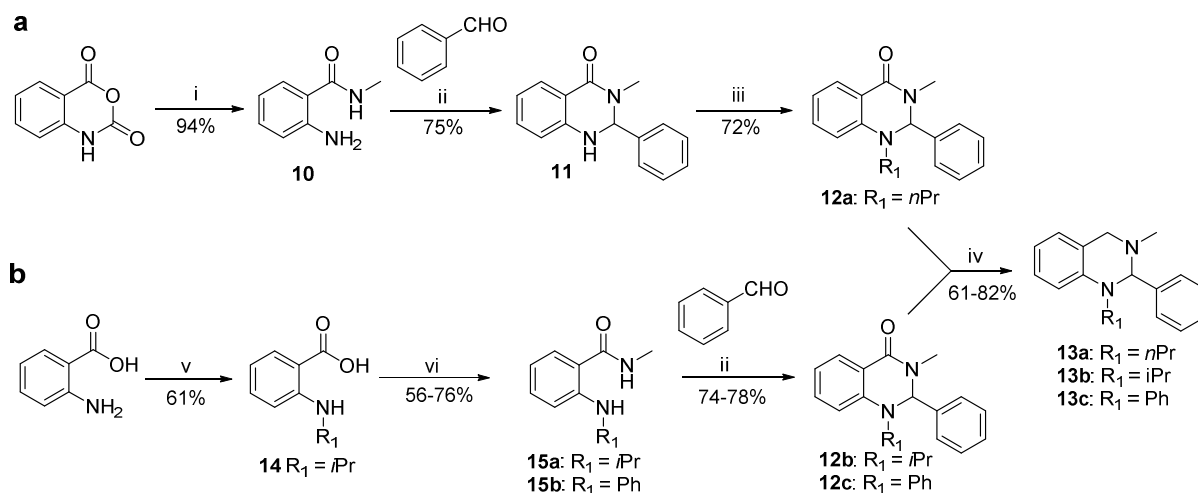
Scheme 7.3. Reagents and conditions: (i) MeNH$_3$Cl, Et$_3$N, DMF, 70 °C, 3 h; (ii) AcOH, 70 °C, 4 h; (iii) *n*PrBr, *t*BuOK, 110°C, 16 h; (iv) LiAlH$_4$, THF, 70 °C, 2-3 h; (v) 1) (CH$_3$)$_2$CO, MeOH, 80 °C, 5h; 2) NaBH$_4$, rt, 3 h; (vi) MeNH$_3$Cl, Et$_3$N, EDCI, HOBt, DMF, 70 °C, 8-14 h.[1]

7.3   pH-Stability Test

All compounds synthesized were exposed to phosphate buffered aqueous systems with defined pH-values between pH = 2 and pH = 12 for 1 h to investigate hydrolysis of the aminal core. After hydrolysis subsequent reversed phase HPLC analyses were performed to determine the ratio of intact tetrahydroquinazoline **1** and the corresponding aldehyde **3** (*cf.* **Scheme 7.1**) as cleavage product by using calibration lines (a detailed description can be found in **Appendix 4**). The results of this study are summarized in **Figure 7.2 a-c**.
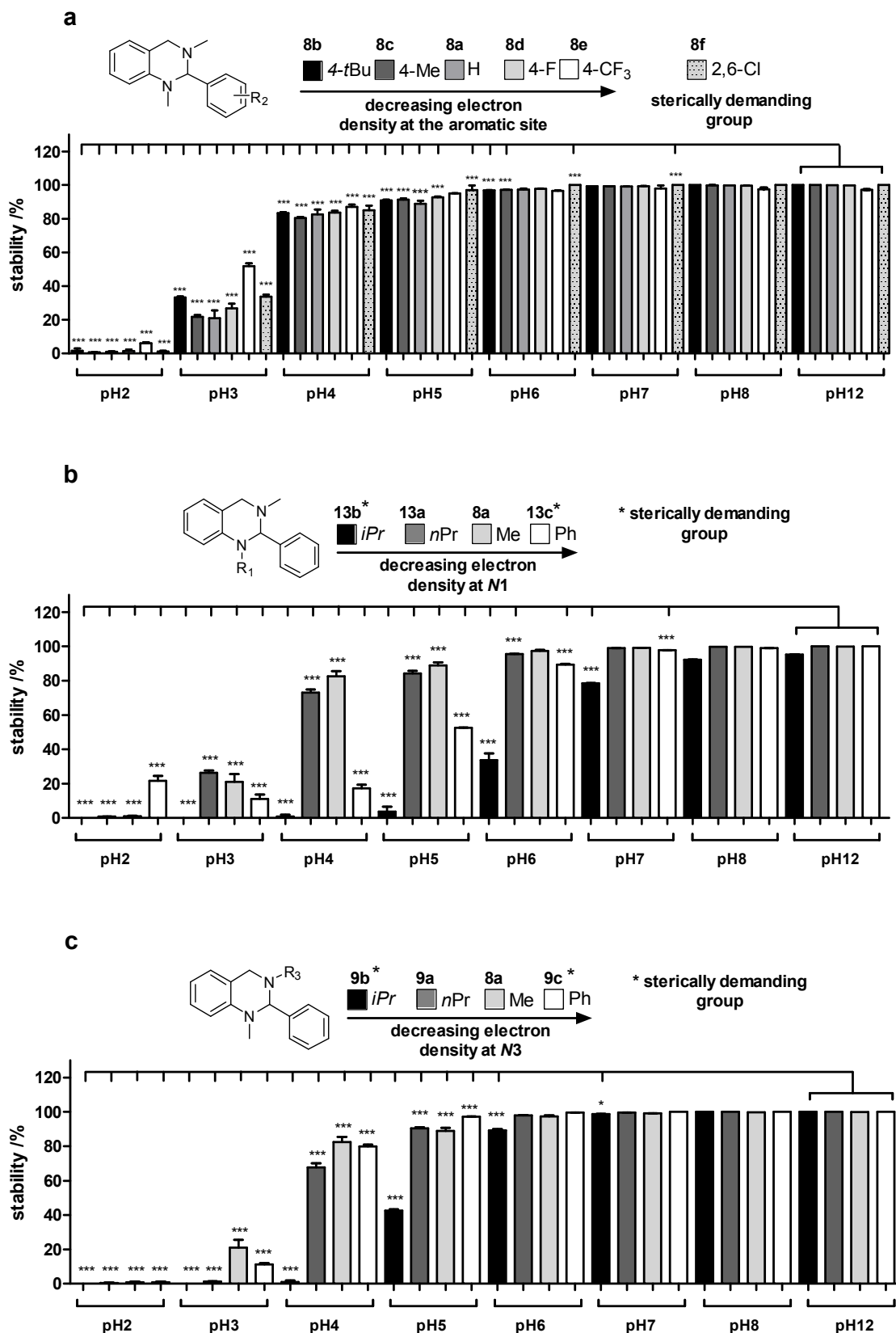
Figure 7.2. Stability test of the aminal core toward hydrolysis in dependency of different substitution pattern at (**a**) the phenyl residue, (**b**) the *N*-1 position and (**c**) the *N*-3 position. Each experiment was performed in triplicate (means+SD).[1]

7.4 Computational Studies and Discussion

Compounds of series **8** as well as compounds **9a**,**c** and compound **13a** showed the same tendency for their pH dependent hydrolysis: All of the aforementioned compounds are stable in basic and neutral conditions until pH = 6 while they slowly start to decompose at pH = 4 and 5. At pH = 3 these compounds are hydrolyzed to more than 50% while being completely cleaved at pH = 2. Interestingly, there are three compounds (**9b** and **13b**,**c**) providing an accelerated hydrolysis rate with compound **13b** as the least stable compound which completely decomposes at pH = 5 and which is even significantly hydrolyzed at pH = 7. The results obtained for the stability test lead to two fundamental questions: 1) Why does an increasing acidic environment drastically increase the hydrolysis rate? 2) Why do some compounds (**9b** and **13b**,**c**) decompose even faster compared to most of the others?

Initially, the protonation pattern of the test compounds was predicted using the empirical algorithm of MoKa and density functional theory (DFT) energy calculations (*cf.* **Appendix 4**). Protonation of all compounds was determined to occur at the aliphatic *N*-3 nitrogen with exception of compound **9c**. Prediction of the protonation pattern is necessary for ongoing calculation due to the fact that hydrolysis takes place in acidic media and therefore compounds are expected to be protonated. However, to explore the influence of the pH-value on hydrolysis of the test compounds, DFT single point energy calculations for the hydrolysis of compound **8a** and the least stable compound **13b** were carried out. Therefore, the absolute energy of the neutral compounds **8a** and **13b** as well as the *N*-3 protonated compounds **8a'** and **13b'** (-'- indicates *N*-3 protonation in the following) were predicted in water including NH_4^+ as proton donor and one molecule water for stoichiometrical reasons. The obtained data revealed, that hydrolysis of compound **8a'** (II in **Figure 7.3a**) into its respective protonated diamine and aldehyde (III in **Figure 7.3a**) is exothermic with -6.7 kcal/mol while the hydrolysis of the neutral form of **8a** (I in **Figure 7.3a**) into the neutral fragments (IV in **Figure 7.3a**) is an endothermic reaction with 3.1 kcal/mol. Therefore, it might be expected, that the hydrolysis of tetrahydroquinazoline **8a** is favored in acidic media and in contrast its formation is favored in neutral or basic conditions. Indeed, data from literature indicated that the synthesis of tetrahydroquinazolines takes place in organic solvent[20-22] as well as in non-acidic aqueous media.[23] Therefore, the condensation of the respective diamine with benzaldehyde towards compound **8a** was experimentally investigated in water, acetonitrile and a 1:1 mixture of both. Interestingly, complete formation of **8a** was observed in all cases proving reversibility of the reaction. In consequence, the hydrolysis of tetrahydroquinazolines can be shifted to their condensation by changing the reaction conditions from an acidic to a basic environment. Furthermore, for the case of the least stable compound **13b** the exothermicity of the reaction of the protonated tetrahydroquinazoline **13b'** (II in **Figure 7.3b**) into its fragments (III in **Figure 7.3b**) increased to -11 kcal/mol, explaining the increased hydrolysis rate of this compound in acidic media compared to compound **8a'**. More interestingly, the hydrolysis of the neutral tetrahydroquinazoline **13b** (I in **Figure 7.3b**) into its neutral fragments (IV in **Figure 7.3b**) was predicted to be exothermic with -4.9 kcal/mol indicating the hydrolysis to take place even in a neutral environment. These observations are in agreement with the described

stability experiments of compound **13b**, which was found to degrade in neutral environment at pH = 7 (*cf.* **Figure 7.2b**).[1]
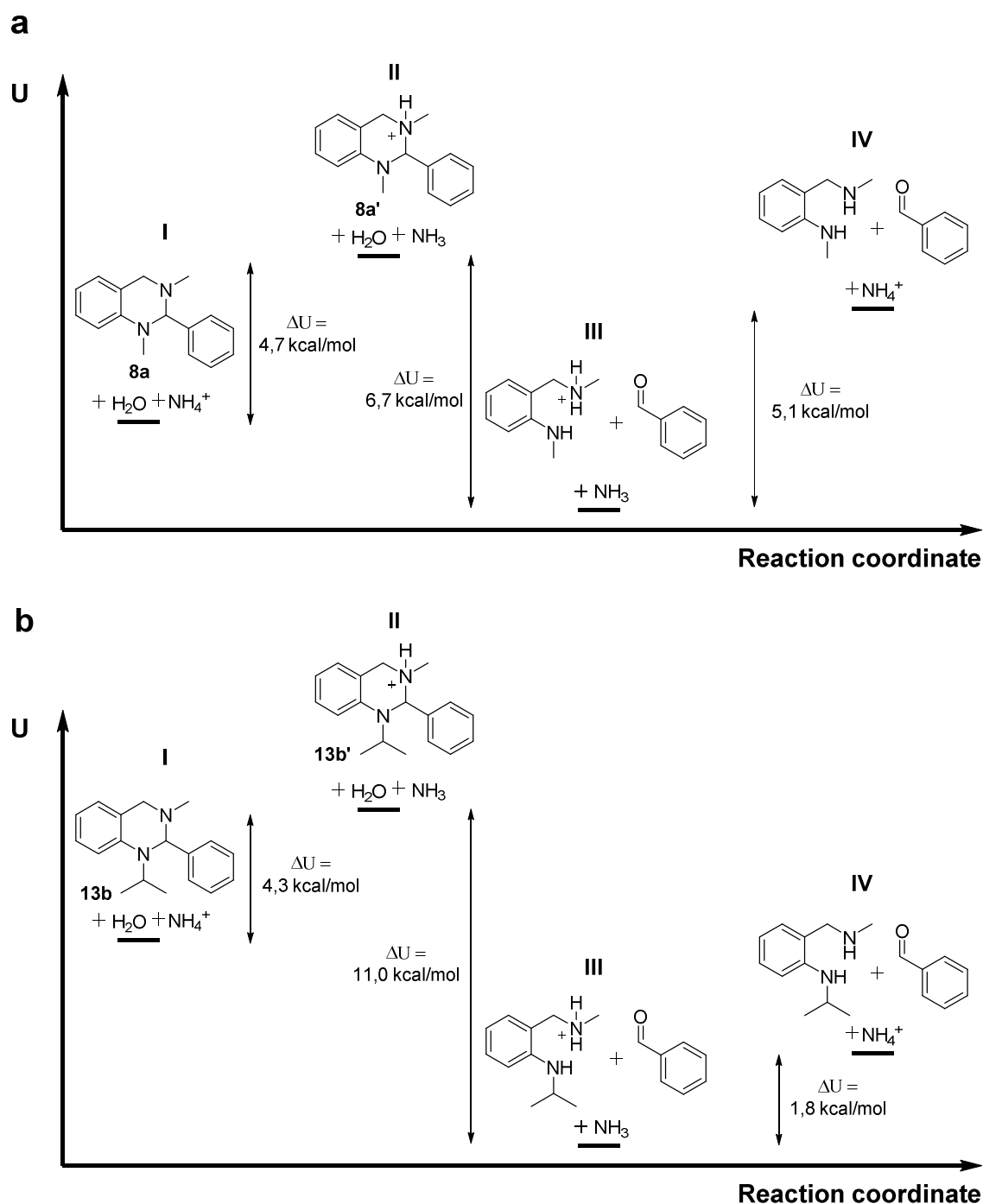
Figure 7.3. Differences in energy along the reaction coordinate for the hydrolysis of (**a**) compound **8a** and (**b**) compound **13b** in water.[1]

In summary, computational studies and experimentally data proved that basic reaction conditions shift the equilibrium towards the formation of tetrahydroquinazolines of the general structure **1**, while acidic conditions induces the hydrolysis of the protonated tetrahydroquinazolines **1'** (**Scheme 7.4**).

basic or neutral solvent
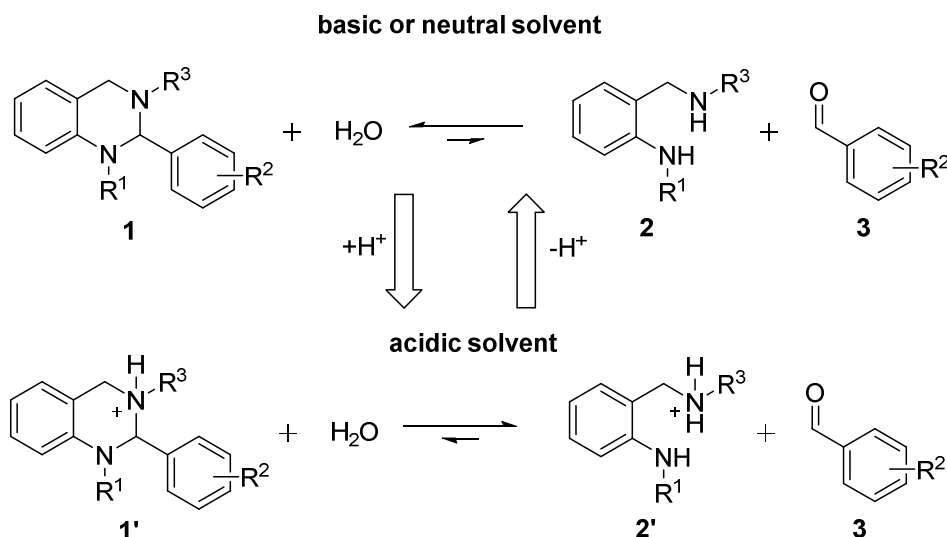
Scheme 7.4: Reaction equilibrium between tetrahydroquinazoline **1**, the corresponding diamine **2** and aldehyde **3** in basic or neutral media as well as the protonated tetrahydroquinazoline **1'** and the corresponding diamine **2'** and aldehyde **3** in acidic media.[1]

To determine the influence of different substitution patterns for an accelerated hydrolysis rate of compounds **9b** and **13b,c** a systematic conformational search was executed for all of the test compounds to determine differences in the minimum energy conformation of both, their neutral and protonated forms. However, no correlation was found as **9b** and **13b**,**c** as well as all of the other compounds were found to share the same two sorts of minimum energy conformers. Therefore, differences in the conformation were excluded as possible reason for an increased instability of the mentioned compounds (for details *cf.* **Appendix 4**). Further energy differences caused by conformational energy of the tetrahydroquinazoline core were investigated. For this purpose, the minimum energy conformers of **9b** and **13b,c** were kept frozen and the substituents at the nitrogen atoms were replaced by simple methyl groups giving a comparable structure like the one of compound **8a**. Subsequently, energy calculations using Molecular Mechanics (MM) revealed that this modified compounds showed in all cases a higher potential energy compared to compound **8a** (**Table 7.1**, for details *cf.* **Appendix 4**).

Table 7.1. Calculated differences in potential energy (U) of the mutated compounds compared to compound **8a** in water and gas phase with MM. Differences were calculated by $\Delta U = U(\textbf{Cpd\_mod}) - U(\textbf{8a})$.[1]

	ΔU [kcal/mol]					
	9b_mod water	**9b_mod** gas	**13b_mod** water	**13b_mod** gas	**13c_mod** water	**13c_mod** gas
neutral	2.09	3.74	3.05	3.09	5.27	4.90
protonated	2.46	0.74	3.5	3.6	5.22	5.84

Due to the fact, that this modified compounds share the same substitution pattern as compound **8a** the energy differences have to be contributed to the conformational energy of the aminal core, e. g. strain within the tetrahydroquinazoline system, strain in the respective angles or other geometric effects. Repetto *et al.*[24] reported a similar trend for the hydrolysis of cyclic geminal ethers. Sterical demanding groups were found to drastically accelerate the hydrolysis of geminal ethers through reduction of the activation barrier. These results support the herein reported data and therefore sterical demanding groups might cause an increase of conformational enegry of the tetrahydroquinazoline system which in consequence accelerate the hydrolysis of these compounds.

A detailed description of all computational analyzes can be found in **Appendix 4**.

7.5   Conclusion

The aminal system is a common moiety of diverse synthetic and naturally occurring compounds with various applications. This moiety can degrade in an acidic environment through hydrolysis but no systematic investigation had been carried out to determine this effect. The current chapter described the synthesis of the aminal bearing tetrahydroquinazolines of the general structure **1** which were modified at both nitrogen atoms as well as at the aromatic site with different substituents. These compounds were exposed to phosphate buffered systems with defined pH-values and a clear relationship between an increased hydrolysis rate and an increasing acidic environment was found. Interestingly, this reaction was predicted to be reversible and indeed experiments could prove that the formation of tetrahydroquinazoline **8a** from the respective diamine and aldehyde takes place in a neutral environment. Furthermore, computational studies suggested an increased conformational energy to increase the sensitivity of some compounds towards hydrolysis which is consistent with the experimental data. In conclusion, the herein described sensitivity towards hydrolysis of tetrahydroquinazolines is important to prevent degradation of such compounds in acidic media during reactions or reaction work up.

The detailed results of this chapter as well as experimental data will be published soon and can be found in **Appendix 4**.

7.6   References

[1] Sawatzky, E.; Drakopoulos, A.; Rölz, M.; Sotriffer, C. A.; Engels, B.; Decker, M. Experimental and Theoretical Investigations into the Stability of Cyclic Aminals. *Beilstein J. Org Chem.*, Accepted.

[2] Kim, J. T.; Gevorgyan, V. Double Cycloisomerization as a Novel and Expeditious Route to Tricyclic Heteroaromatic Compounds: Short and Highly Diastereoselective Synthesis of (±)-Tetraponerine T6. *Org. Lett.* **2002**, *4*, 4697-4699.

[3] Bosque, I.; Gonzalez-Gomez, J. C.; Loza, M. I.; Brea, J. Natural Tetraponerines: A General Synthesis and Antiproliferative Activity. *J. Org. Chem.* **2014**, *79*, 3982-3991.

[4] Scholl, M.; Trnka, T. M.; Morgan, J. P.; Grubbs, R. H. Increased Ring Closing Metathesis Activity of Ruthenium-Based Oiefin Metathesis Catalysts Coordinated with Imidazolin-2-ylidene Ligands. *Tetrahedron Lett.* **1999**, *40*, 2247-2250.

[5] Sharma, V.; Khan, M. S. Y. Synthesis of Novel Tetrahydroimidazole Derivatives and Studies for Their Biological Properties. *Eur. J. Med. Chem.* **2001**, *36*, 651-658.

[6] Caterina, M. C.; Perillo, I. A.; Boiani, L.; Pezaroglo, H.; Cerecetto, H.; González, M.; Salerno, A. Imidazolidines as New Anti-Trypanosoma Cruzi Agents: Biological Evaluation and Structure-Activity Relationships. *Bioorg. Med. Chem.* **2008**, *16*, 2226-2234.

[7] Veale, E. B.; Frimannsson, D. O.; Lawler, M.; Gunnlaugsson, T. 4-Amino-1,8-naphthalimide-Based Tröger's Bases As High Affinity DNA Targeting Fluorescent Supramolecular Scaffolds. *Org. Lett.* **2009**, *11*, 4040-4043.

[8] Baldeyrou, B.; Tardy, C.; Bailly, C.; Colson, P.; Houssier, C.; Charmantray, F.; Demeunynck, M. Synthesis and DNA Interaction of a Mixed Proflavine-Phenanthroline Tröger Base. *Eur. J. Med. Chem.* **2002**, *37*, 315-322.

[9] Johnson, R. A.; Gorman, R. R.; Wnuk, R. J.; Crittenden, N. J.; Aiken, J. W. Tröger's Base. An Alternate Synthesis and a Structural Analog with Thromboxane A_2 Synthetase Inhibitory Activity. *J. Med. Chem.* **1993**, *36*, 3202-3206.

[10] Goswami, S.; Ghosh, K.; Dasgupta, S. Tröger's Base Molecular Scaffolds in Dicarboxylic Acid Recognition. *J. Org. Chem.* **2000**, *65*, 1907-1914.

[11] Wu, H.; Chen, X.; Wan, Y.; Ye, L.; Xin, H.; Xu, H.; Yue, C.; Pang, L.; Ma, R.; Shi, D. Stereoselective Mannich Reactions Catalyzed by Tröger's Base Derivatives in Aqueous Media. *Tetrahedron Lett.* **2009**, *50*, 1062-1065.

[12] Harmata, M.; Kahraman, M. Congeners of Troeger's Base as Chiral Ligands. *Tetrahedron: Asymmetry* **2000**, *11*, 2875-2879.

[13] Pardo, C.; Sesmilo, E.; Gutiérrez-Puebla, E.; Monge, A.; Elguero, J.; Fruchier, A. New Chiral Molecular Tweezers with a Bis-Tröger's Base Skeleton. *J. Org. Chem.* **2001**, *66*, 1607-1611.

[14] Valik, M.; Dolenski, B.; Petrickova, H.; Vasek, P.; Kral, V. Novel Heterocyclic Tröger's Base Derivatives Containing *N*-Methylpyrrole Units. *Tetrahedron Lett.* **2003**, *44*, 2083-2086.

[15] Paul, A.; Maji, B.; Misra, S. K.; Jain, A. K.; Muniyappa, K.; Bhattacharya, S. Stabilization and Structural Alteration of the G-Quadruplex DNA Made from the Human Telomeric Repeat Mediated by Tröger's Base Based Novel Benzimidazole Derivatives. *J. Med. Chem.* **2012**, *55*, 7460-7471.

[16] Kamal M. A.; Qu, X.; Yu, Q.-S.; Tweedie, D.; Holloway, H. W.; Li, Y.; Tan, Y.; Greig, N. H. Tetrahydrofurobenzofuran Cymserine, a Potent Butyrylcholinesterase Inhibitor and Experimental Alzheimer Drug Candidate, Enzyme Kinetic Analysis. *J. Neural. Transm.* **2008**, *115*, 889-898.

[17] Tasso, B.; Catto, M.; Nicolotti, O.; Novelli, F.; Tonelli, M.; Giangreco, I.; Pisani, L.; Sparatore, A.; Boido, V.; Carotti, A.; Sparatore, F. Quinolizidinyl Derivatives of Bi- and Tricyclic Systems as Potent Inhibitors of Acetyl- and Butyrylcholinesterase with Potential in Alzheimer's Disease. *Eur. J. Med. Chem.* **2011**, *46*, 2170-2184.

[18] Greenberg, A.; Molinaro, N.; Lang, M. Structure and Dynamics of Tröger's Base and Simple Derivatives in Acidic Media. *J. Org. Chem.* **1984**, *49*, 1127-1130.

[19] Taylor, P. D. Potentiometric Determinations of Aminal Stability Constants. *Talanta* **1995**, *42*, 243-248.

[20] Sinkkonen, J.; Zelenin, K. N.; Potapov, A.-K. A.; Lagoda, I. V.; Alekseyev, V. V.; Pihlaja, K. Ring-Chain Tautomerism in 2-Substituted 1,2,3,4-Tetrahydroquinazolines A ^{1}H, ^{13}C and ^{15}N NMR Study. *Tetrahedron* **2003**, *59*, 1939-1950.

[21] Fan, X.; Li, B.; Guo, S.; Wang, Y.; Zhang, X. Synthesis of Quinazolines and Tetrahydroquinazolines: Copper-Catalyzed Tandem Reactions of 2-Bromobenzyl Bromides with Aldehydes and Aqueous Ammonia or Amines. *Chem. Asian J.* **2014**, *9*, 739-743.

[22] Schiedler, D. A.; Vellucci, J. K.; Beaudry, C. M. Formation of Carbon-Carbon Bonds Using Aminal Radicals. *Org. Lett.* **2012**, *14*, 6092-6095.

[23] Correa, W. H.; Papadopoulos, S.; Radnidge, P.; Roberts, B. A.; Scott, J. L. Direct, Efficient, Solvent-Free Synthesis of 2-Aryl-1,2,3,4-Tetrahydroquinazolines. *Green Chem.* **2002**, *4*, 245-251.

[24] Repetto, S. L.; Costello, J. F.; Butts, C. P.; Lam, J. K. W.; Ratcliffe, N. M. The Hydrolysis of Geminal Ethers: A Kinetic Appraisal of Orthoesters and Ketals. *Beilstein J. Org. Chem.* **2016**, *12*, 1467-1475.

8. Summary and Outlook

Although the physiological roles of BChE are not yet determined to date, the importance of this enzyme is continuously increasing as it was found to be associated with several disorders like diabetes mellitus type 2, cardiovascular diseases, obesity and especially with Alzheimer's disease (AD). In consequence, for investigations of BChE's pathological role in these diseases and to find new medication strategies, the development of selective and potent inhibitors is necessary.

For this purpose, the current work progresses in five chapters on the exploration of the chemical, physical and biochemical properties of tetrahydroquinazoline based carbamates which were previously reported to be selective BChE inhibitors with potency in the low nanomolar range:

1) A Novel Way to Radiolabel Human Butyrylcholinesterase for PET through Irreversible Transfer of the Radiolabeled Moiety:

PET-radiotracers represent an innovative tool to determine the distribution and the expression of a biological target *in vivo*. BChE lacks to a large degree of such tracers with a few exceptions. In this work, methods were developed to incorporate the radioisotopes ^{11}C and ^{18}F into the carbamate moiety of inhibitor **1** resulting into the two radiotracers **[^{18}F]2** and **[^{11}C]1** (**Figure 8.1**). In contrast to reversibly acting PET-probes, the described radiotracers were proven by kinetic studies to transfer the radioisotope covalently onto the active site of BChE, thus labeling the enzyme directly and permanently. *Ex vivo* autoradiography experiments on healthy mice brain slices revealed binding of **[^{18}F]2** on brain tissue (**Figure 8.1**) with selectivity for BChE. The developed radiotracers **[^{18}F]2** and **[^{11}C]1** might be used for further *in vivo* studies to detect and quantify abnormal changes of the physiological occurrence of BChE to investigate its role in the pathogenesis of diseases.
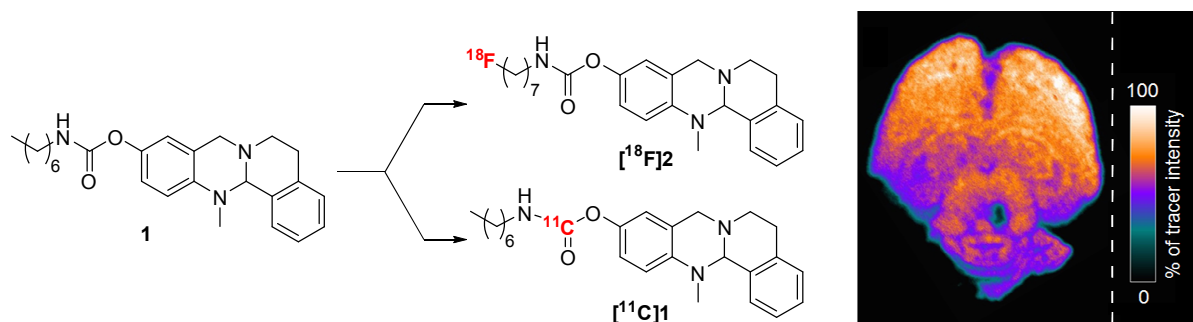
Figure 8.1. Development of PET-radiotracers that transfer the radioisotope covalently onto BChE (left) and *ex vivo* autoradiography experiment of **[^{18}F]2** on a healthy mouse brain (right).

2) <u>Discovery of Highly Selective and Nanomolar Carbamate-Based Butyrylcholinesterase Inhibitors by Rational Investigation into Their Inhibition Mode:</u>

To investigate the role of the tetrahydroquinazoline carrier scaffold on BChE inhibition, carbamate based inhibitor **1** was formally "opened" to give access to compound series **3** and **4** (**Figure 8.2**). The synthesized compounds were successively used to perform kinetic investigations to determine their inhibition mode. Based on these data, a plausible binding model was postulated explaining the influence of the tetrahydroquinazoline carrier scaffold for binding at BChE's active site just before carbamate transfer takes place (**Figure 8.2**). Additionally, these compounds feature neuroprotective properties and prevent oxidative stress induced cell death in their carbamate form as well as after the release of the tetrahydroquinazoline carrier scaffold. The data obtained as well as the postulated binding model might help to improve the computer assisted design of inhibitors based on the tetrahydroquinazoline scaffold.
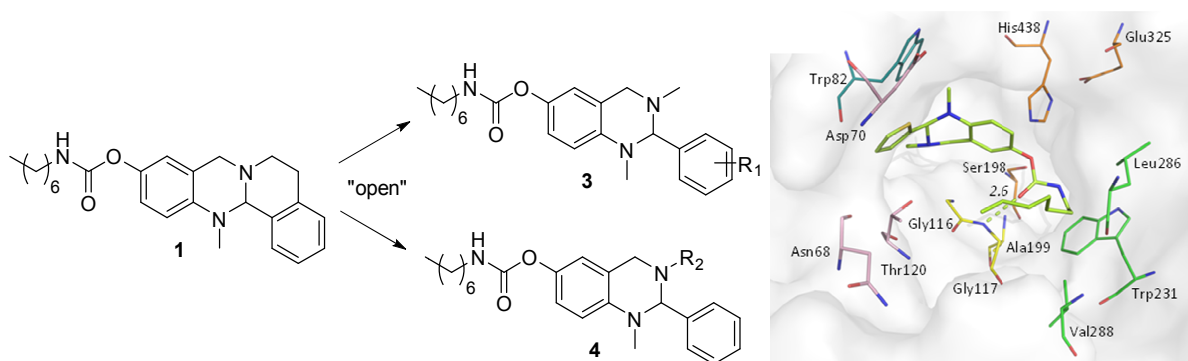
Figure 8.2. Development of compound series **3** and **4** (left) which were analyzed to postulate a suitable binding model for tetrahydroquinazolines based inhibitors (right).

3) <u>Dual Addressing of Butyrylcholinesterase by Targeting the Catalytic Active Site (CAS) and the Peripheral Anionic Site (PAS):</u>

Compounds which are dual-targeting the CAS and the PAS of BChE are the most potent and selective BChE inhibitors to date with inhibition values in the picomolar range. In this work, a strategy is described how to turn tetrahydroquinazoline based carbamates into dual binding BChE inhibitors. These inhibitors feature a carbamate moiety which is covalently transferred onto the CAS of BChE, and in addition provide a second pharmacophore connected *via* a linker to the carbamate moiety which is proposed to target the PAS (**Figure 8.3**). Preliminary results reveal a high tolerance of BChE towards different linker lengths without decrease in affinity. Future studies will show if dual-targeting of the CAS and the PAS with such compounds is possible.
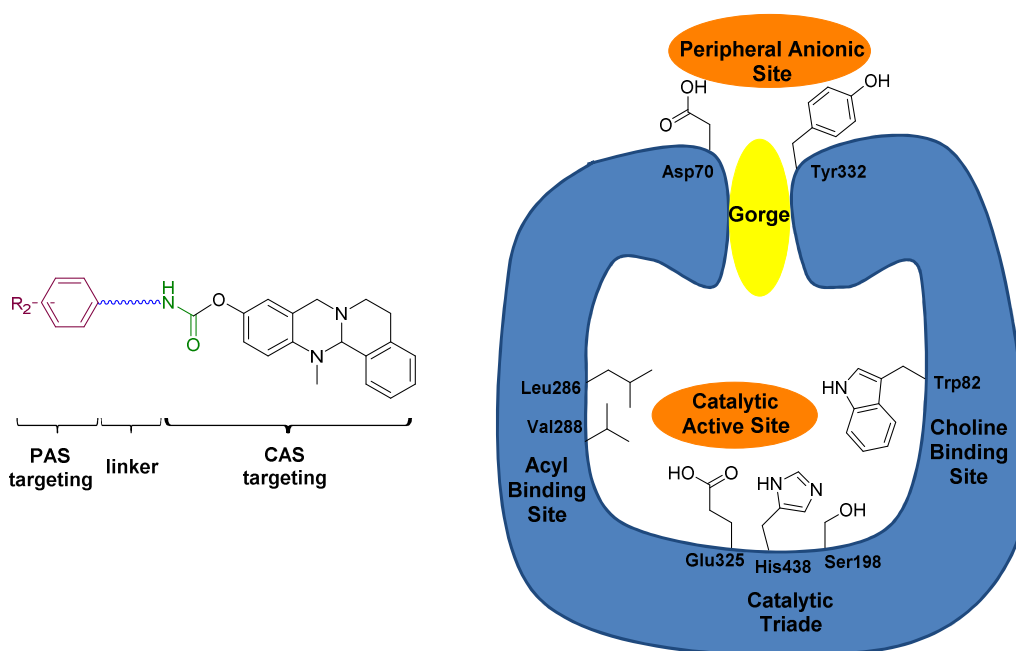
Figure 8.3. Structure of tetrahydroquinazoline based carbamates targeting the CAS and the PAS (left) and cartoon showing BChE's structural features (right).

4) <u>Investigation into Selective Debenzylation and Ring Cleavage of Quinazoline based Heterocycles:</u>

The tetrahydroquinazoline system is well investigated in terms of its synthesis and its selective oxidation. To explore the reactivity of this system, tetrahydroquinazoline **5**, which was used as precursor for the design of BChE-inhibitors, was exposed to common reduction agents. These experiments revealed a high sensitivity of the tetrahydroquinazoline core towards several reduction conditions resulting into compounds **6-9** (**Figure 8.4**). Knowledge about the chemical reactivity of tetrahydroquinazolines is essential for the design of compounds derived from this template and can help to prevent undesired site reactions during synthesis.
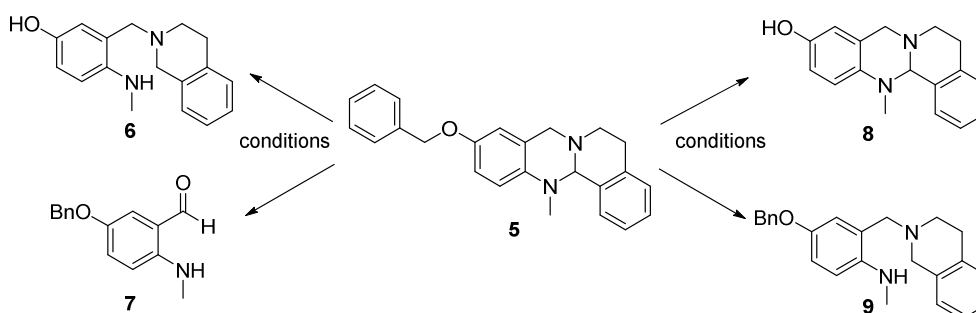
Figure 8.4. Reduction of tetrahydroquinazoline **5** towards compound **6-9** in dependency of different reduction conditions.

5) <u>Experimental and Theoretical Investigation into the Stability of Cyclic Aminals:</u> Tetrahydroquinazolines are known to degrade in acidic media through hydrolysis of their aminal system; but literature is lacking of a systematic investigation into this behavior. Therefore, compounds of the general structure **10** were synthesized and exposed to phosphate buffered systems with defined pH-values (**Figure 8.5**). A clear increase of the hydrolysis rate of the aminal system was determined in dependency of an increasing acidic media. Computational studies predicted and experimental studies proved that hydrolysis of **10** only takes place in an acidic environment while the condensation of tetrahydroquinazoline **10** is preferred in neutral or basic aqueous media.
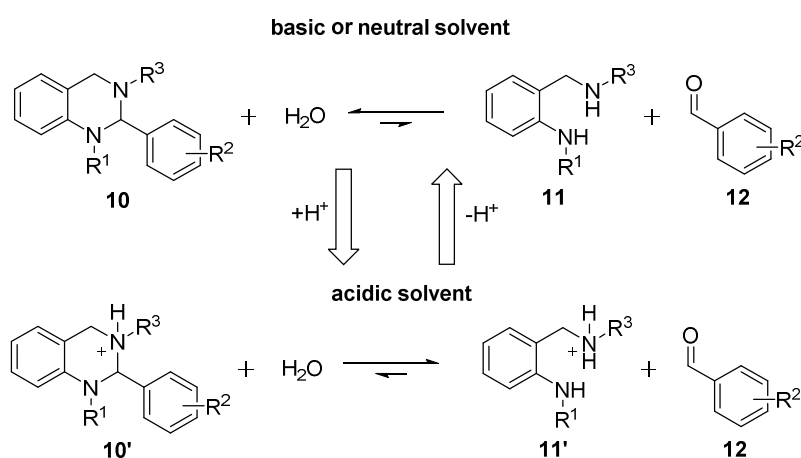
Figure 8.5. Reaction equilibrium between tetrahydroquinazoline **10**, the corresponding diamine **11** and aldehyde **12** in basic or neutral media as well as the protonated tetrahydroquinazoline **11** and the corresponding diamine **11'** and aldehyde **12** in acidic media.

In conclusion, the tetrahydroquinazoline system is an interesting template in terms of its chemical reactivity as well as for its use for the design of pseudo-irreversible BChE inhibitors. Nevertheless, regarding the overall aim to investigate BChE's role in the pathogenesis of AD, future *in vivo* studies have to show

a) if it is possible to map BChE with the described PET-radiotracers in AD patient's brain. Successful radiolabelling of BChE can serve as a diagnostic tool for AD diagnosis and help to determine pathological changes of BChE occurrence.

b) if inhibition of BChE with the described inhibitors can be used as a therapeutic strategy in the symptomatic treatment of AD.

9. Zusammenfassung und Ausblick

Obwohl die physiologische Funktion der BChE zum aktuellen Zeitpunkt noch nicht vollständig aufgeklärt ist, so ist die Bedeutung dieses Enzyms hinsichtlich seiner möglichen Involvierung bei Diabetes mellitus Typ 2, kardiovaskulären Erkrankungen, Übergewicht und der Alzheimer-Erkrankung stetig steigend. Die Entwicklung von selektiven und hochwirksamen Inhibitoren ist daher notwendig um die Rolle der BChE im pathologischen Verlauf dieser Erkrankungen beurteilen zu können und ggf. neue Therapiemöglichkeiten zu eröffnen.

In der hier durchgeführten Arbeit wurde in fünf Kapiteln die chemischen, physikalischen und pharmakologischen Eigenschaften von Tetrahydrochinazolin basierten Carbamaten untersucht.

1) <u>Eine neuartige Methode zur PET-Radiomarkierung der menschlichen BChE durch den irreversiblen Transfer eines radioaktiv markierten Carbamatrestes:</u>

PET-Radiopharmaka (auch Radiotracer genannt) werden häufig verwendet, um die Verteilung biologischer Zielmoleküle *in vivo* bestimmen zu können. In der hier präsentierten Arbeit wurden Methoden entwickelt, um die beiden PET-Radioisotope ^{11}C und ^{18}F in den Carbamatrest von Inhibitor **1** zu integrieren, sodass die beiden radioaktiv markierten Inhibitoren **[^{18}F]2** und **[^{11}C]1** erhalten werden konnten (**Abbildung 9.1**). Im Gegensatz zu herkömmlichen, reversibel agierenden PET-Radiotracern konnte bei den hier beschriebenen Radiotracern mittels kinetischer Untersuchungen gezeigt werden, dass sie den radioaktiv markierten Rest kovalent auf die BChE übertragen können, sodass das Enzym direkt und kontinuierlich radioaktiv markiert wird. Darüberhinaus konnten erste *ex vivo* Autoradiographie Untersuchungen an Maushirnschnitten zeigen, dass der Radiotracer **[^{18}F]2** eine gute Bindung und hohe Selektivität zur Gewebe-BChE aufweist. Zukünftige *in vivo* Untersuchungen könnten die beiden Radiotracer **[^{18}F]2** und **[^{11}C]1** nutzen um die physiologische Verteilung der BChE und ihre pathologischen Veränderungen im Verlauf einer Erkrankung zu quantifizieren.
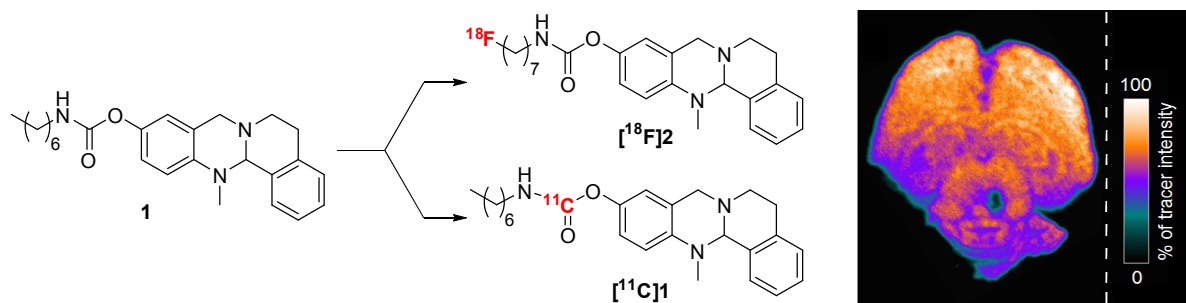
Abbildung 9.1. Entwicklung der PET-Radiotracer **[^{11}C]1** und **[^{18}F]2** (links) sowie ein *ex vivo* Autoradiographie Experiment zur Bindung von **[^{18}F]2** an Maushirnschnitten (rechts).

2) Entwicklung hochselektiver Carbamat-basierter BChE Inhibitoren durch rationale Untersuchung ihres Bindemoduses:

Um den Einflusses des Tetrahydrochinazolingerüstes zur Hemmung der BChE untersuchen zu können, wurde ausgehend von Inhibitor **1** die beiden Verbindungsreihen **3** und **4** synthetisiert (**Abbildung 9.2**). Der Bindemodus dieser Verbindungen wurde dabei eingehend mittels ihrer Inhibitionskinetik untersucht. Auf Grundlage der dabei erhaltenen Daten konnte mithilfe computergestützter Methoden ein Bindemodell entwickelt werden, welches den Einfluss des Tetrahydrochinazolingerüstes zur Bindung des gesamten Inhibitors in das aktive Zentrum der BChE qualitativ wiederspiegelt bevor die eigentliche Inhibition durch den Carbamattransfer auf das aktive Zentrum stattfindet (**Abbildung 9.2**). Zusätzlich konnte gezeigt werden, dass die hier synthetisierten Verbindungen neuroprotektive Eigenschaften aufweisen, indem sie oxidativem Stress entgegenwirken.
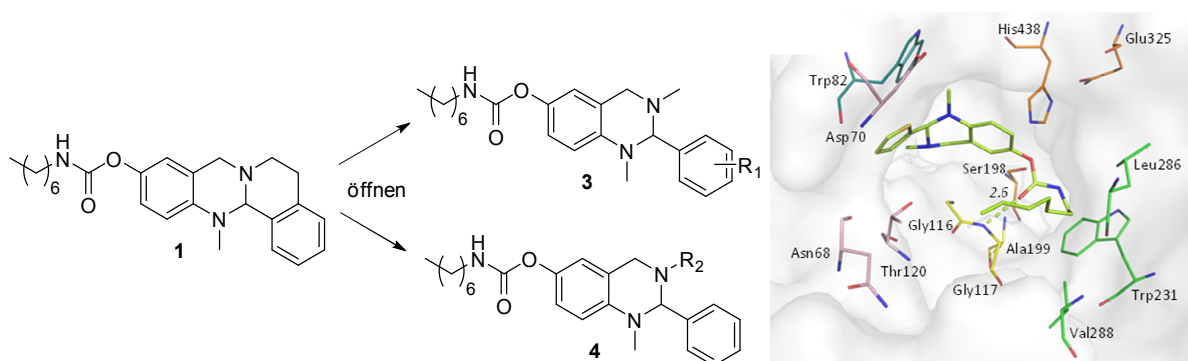
Abbildung 9.2. Entwicklung der Verbindungsreihen **3** und **4** (links), welche zur Entwicklung eines geeigneten Bindemodells (rechts) untersucht wurden.

3) Duale Adressierung des katalytisch aktivem Zentrums (CAS) und der peripheren anionischen Bindestelle (PAS) der Butyrylcholinesterase:

Verbindungen, welche sowohl die CAS als auch die PAS der BChE simultan adressieren, gehören zu den potentesten und selektivsten BChE Inhibitoren mit Inhibitionswerten im pikomolarem Bereich. In der hier vorliegenden Arbeit wurde eine Strategie entwickelt, wie Tetrahydrochinazolin basierte Inhibitoren so modifiziert werden müssen, damit diese ebenfalls als dual-aktive Inhibitoren wirksam werden. Diese Inhibitoren weisen eine Carbamatfunktionalität auf, welche kovalent auf die CAS der BChE übertragen wird, und besitzen darüber hinaus ein zweites Pharmakophor, welches über einen Linker mit dem Carbamatrest chemisch verknüpft ist und an die PAS bindet (**Abbildung 9.3**). Erste Untersuchungen haben gezeigt, dass die BChE gegenüber verschiedenen Linkerlängen weitestgehend tolerant ist, ohne einen Aktivitätsverlust der Verbindungen aufzuweisen. Weitere Studien werden zeigen, ob die duale Adressierung der CAS und der PAS mit solchen Substanzen möglich ist.
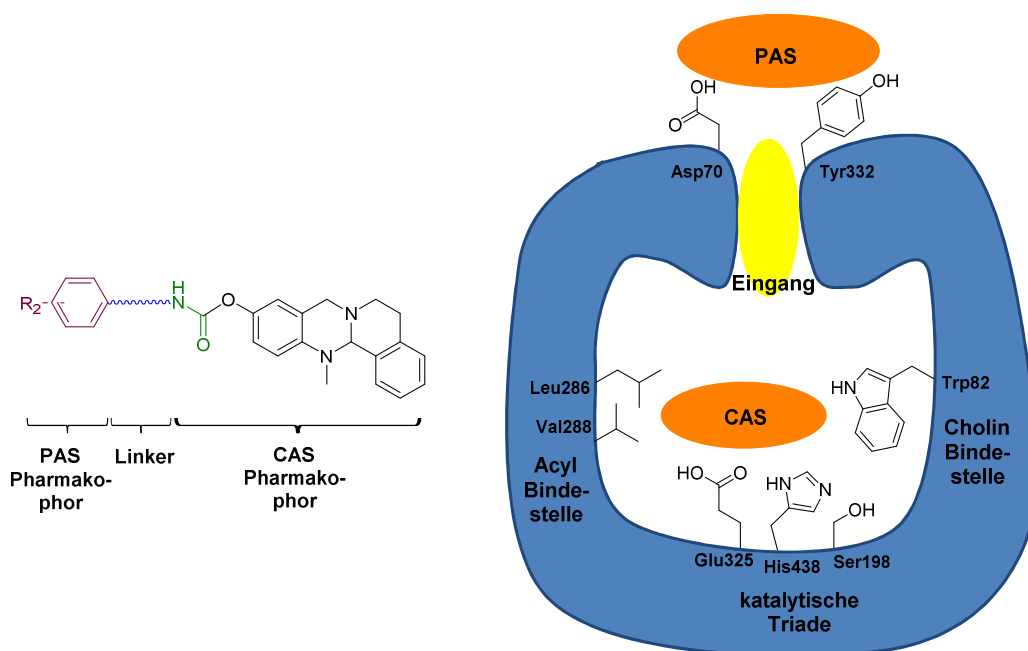
Abbildung 9.3. Chemische Struktur Tetrahydrochinazolin basierter Inhibitoren, welche die CAS und PAS adressieren (links) und schematische Darstellung der verschiedenen Bindestellen der BChE (rechts).

4) <u>Untersuchungen zur selektiven Debenzylierung und Ringspaltung von Chinazolin basierten Heterozyklen:</u>

Das Tetrahydrochinazolinsystem ist in der Literatur ausgiebig hinsichtlich seiner Synthese und selektiven Oxidation beschrieben worden. Um den Einfluss reduktiver Bedingungen auf dieses System zu untersuchen, wurde Tetrahydrochinazolin **5** (Vorstufe der in dieser Arbeit hergestellten Inhibitoren) gezielt mit verschiedenen Reduktionsmitteln umgesetzt, wobei Verbindungen **6-9** (**Abbildung 9.4**) selektiv erhalten werden konnten. Informationen über die Reaktivität des Tetrahydrochinazolinsystems sind unumgänglich bei der Entwicklung neuer Verbindungen auf Grundlage dieses Systems, um Nebenreaktionen zu vermeiden.
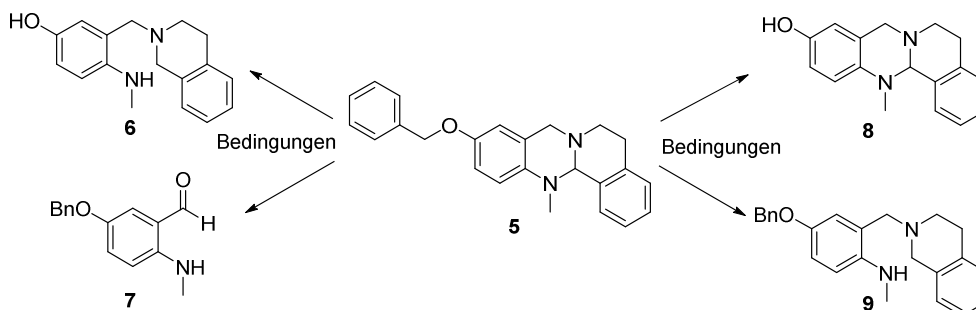
Abbildung 9.4. Reduktion von Tetrahydrochinazolin **5** zu Verbindung **6-9** in Abhängigkeit des verwendeten Reduktionsmittels.

5) <u>Experimentelle und Theoretische Untersuchungen zur Stabilität zyklischer Aminale:</u>

Tetrahydrochinazoline weisen ein Aminalsystem auf, welches im sauren Milieu hydrolytisch gespalten werden kann. Um die Stabilität dieses Systems systematisch zu untersuchen, wurden Tetrahydrochinazoline mit der generellen Struktur **10** synthetisiert und in einem wässrigen Phosphat-gepuffertem System mit definiertem pH-Wert inkubiert (**Abbildung 9.5**). Bei diesen Untersuchungen konnte ein klarer Zusammenhang zwischen einem sinkendem pH-Wert und einer beschleunigten Zersetzung der Testsubstanzen beobachtet werden. Außerdem konnte mittels quantenmechanischen Berechnungen und weiteren Experimenten gezeigt werden, dass diese Reaktion im alkalischen oder neutralem Milieu reversibel ist und die Kondensation der Tetrahydroquinazolin Derivate **10** aus den jeweiligen Benzaldehyden **12** und Diaminen **11** unter solchen Bedingungen bevorzugt wird.
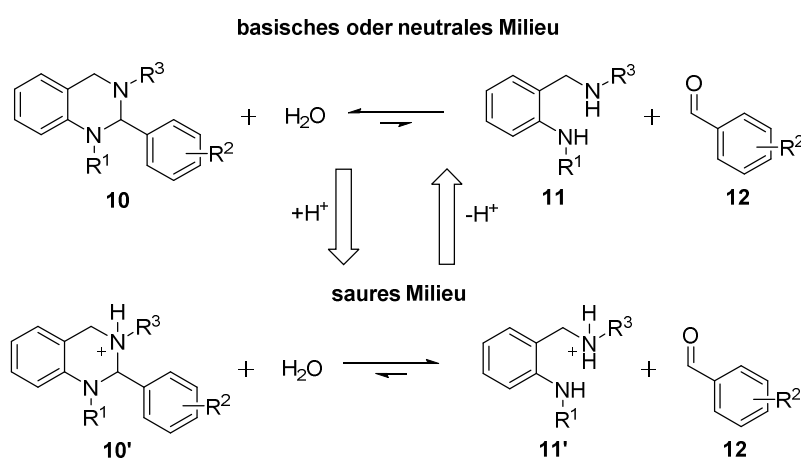
Abbildung 9.5. Gleichgewichtsreaktion der Hydrolyse von Tetrahydrochinazolin **10** in das entsprechende Diamin **11** und Benzaldehyd **12** im basischem bzw. neutralem Milieu (oben) und im sauren Milieu (unten).

Tetrahydrochinazoline sind interessante Verbindungen hinsichtlich ihrer chemischen und physikalischen Eigenschaften, und darüber hinaus als Grundgerüst bei der Entwicklung von selektiven BChE Inhibitoren. Im Hinblick auf die Ausgangsfragestellung, der Funktion der BChE in der Pathogenese bei der Alzheimer-Erkrankung, sind jedoch noch weitere *in vivo* Studien notwendig, um

a) zu beweisen, dass die Visualisierung der BChE-Verteilung im Gehirn mittels der beschriebenen PET-Radiotracer möglich ist und

b) zu zeigen, ob die Inhibition der BChE mit den hier gezeigten Verbindungen ein therapeutischer Ansatzpunkt bei der symptomatischen Behandlung der Alzheimer-Erkrankung sein könnte.

10. Abbreviations

Å	-	Angström
Aß	-	Amyloid beta
AC	-	Adenylyl cyclase
ACh	-	Acetylcholine
AChE	-	Acetylcholinesterase
AD	-	Alzheimer 's disease
AICD	-	APP intracellular domain
APP	-	Amyloid precursor protein
ATC	-	Acetlythiocholine
BACE-1	-	Beta-site amyloid precursor protein cleaving enzyme 1
BBB	-	Blood brain barrier
BChE	-	Butyrylcholinesterase
BEMP	-	2-*t*-Butylimino-2-diethylamino-1,3-dimethylperhydro-1,3,2-diazaphosphorine
BMI	-	Body mass index
BTC	-	Butyrylthiocholine
Calc.	-	Calculated
cAMP	-	cyclic adenosine monophosphate
CAS	-	Catalytic active site
CAT	-	Catalase
Cdk 5	-	Cyclin-dependent kinase 5 <u>or</u> tau protein kinase II
ChAT	-	Choline acetyltransferase
ChE	-	Cholinesterase
CNS	-	Central nervous system
CoA	-	Coenzyme A
DAG	-	Diacylglycerol
DAST	-	Diethylaminosulfur trifluoride
DBU	-	1,8-Diazabicyclo[5.4.0]undec-7-ene
DCM	-	Dichlormethane
DFT	-	Density functional theory
DHED	-	Dehydroevodiamine
DIPEA	-	*N,N*-Diisopropylethylamine
DMAc	-	Dimethylacetamide
DMF	-	Dimethylformamide
DMSO	-	Dimethylsulfoxide

Abbreviations

DTNB	-	5,5'-Dithiobis-(2-nitrobenzoic acid)
*ee*AChE	-	Acetylcholinesterase from *Electrophorus electricus*
EI	-	Enzyme-inhibitor complex
*eq*BChE	-	Butyrylcholinesterase from equine serum
ESI-MS	-	Electrospray ionization-mass spectrometry
E-C	-	Carbamoylated enzyme
FAAH	-	Fatty acid amide hydrolase
FBSAChE	-	Acetylcholinesterase from fetal bovine serum
FDA	-	U.S. Food and Drug Administration
GSK 3	-	Glycogen synthase kinase 3 or tau protein kinase I
GPCR	-	G-Protein coupled receptor
GPx	-	Glutathione peroxidase
hAChE	-	humane Acetylcholinesterase
hBChE	-	humane Butyrylcholinesterase
HIC	-	High income countries
HPLC	-	High-performance liquid chromatography
I	-	Inhibitor
IC_{50}	-	Inhibitory concentration 50
Iso-OMPA	-	Tetra(monoisopropyl)pyrophosphortetramide
IP3	-	Inositol-1,4,5-triphosphate
LIC	-	Low income countries
mAChE	-	Acetylcholinesterase from mice
mAChR	-	Muscarinic acetylcholine receptor
MAGL	-	Monoacylglycerol lipase
MAP	-	Microtubule associated protein
MCI	-	Mild cognitive impairment
MM	-	Molecular mechanics
mp	-	Melting point
MW	-	Microwave
nAChR	-	Nicotinic acetylcholine receptor
NMDAR	-	*N*-Methyl-*D*-aspartate receptor
NFT	-	Neurofibrillary tangles
NMR	-	Nuclear magnetic resonance spectroscopy
PAS	-	Peripheral anionic site
PEG	-	Polyethylene glycol
PET	-	Positron emission tomography
PIP2	-	Phosphoinositol-1,4,5-biphosphate

PKC	-	Protein kinase C
RNA	-	Ribonucleic acid
RNS	-	Reactive nitrogen species
ROS	-	Reactive oxygen species
RP	-	Reversed phase
rt	-	Room temperature
SAR	-	Structure activity relationships
SEM	-	Standard error of the means
SD	-	Standard deviation
SOD	-	Superoxide dismutase
TFA	-	Trifluoroacetic acid
THF	-	Tetrahydrofurane
TLC	-	Thin-layer chromatography
TsCl	-	4-Toluenesulfonyl chloride
TSH	-	Thyroid stimulating hormone
τ-protein	-	tau-protein
UV	-	Ultraviolet
VAChT	-	Vesicular acetylcholine transporter
Vis	-	Visible
VDCC	-	Voltage dependent calcium channels
WHO	-	World Health Organization

11. Appendix

<u>Appendix 1:</u> A Novel Way to Radiolabel Human Butyrylcholinesterase for Positron Emission Tomography through Irreversible Transfer of the Radiolabeled Moiety.

Sawatzky, E.; Al-Momani, E.; Kobayashi, R.; Higuchi, T.; Samnick, S.; Decker, M. A Novel Way to Radiolabel Human Butyrylcholinesterase for Positron Emission Tomography through Irreversible Transfer of the Radiolabelled Moiety. *ChemMedChem* **2016**, *11*, 1540-1550. Copyright (2016) John Wiley and Sons.
http://onlinelibrary.wiley.com/doi/10.1002/cmdc.201600223/abstract

<u>Appendix 2:</u> Discovery of Highly Selective and Nanomolar Carbamate-Based Butyrylcholinesterase Inhibitors by Rational Investigation into Their Inhibition Mode.

Sawatzky, E.; Wehle, S.; Kling, B.; Wendrich, J.; Bringmann, G.; Sotriffer, C. A.; Heilmann, J.; Decker, M. Discovery of Highly Selective and Nanomolar Carbamate-Based Butyrylcholinesterase Inhibitors by Rational Investigation into Their Inhibition Mode. *J. Med. Chem.* **2016**, *59*, 2067-2082. Copyright (2016) American Chemical Society.
http://pubs.acs.org/doi/abs/10.1021/acs.jmedchem.5b01674

<u>Appendix 3:</u> Investigation into Selective Debenzylation and Ring Cleavage of Quinazoline Based Heterocycles.

Sawatzky, E.; Bukowczan, J.; Decker, M. Investigation into Selective Debenzylation and Ring Cleavage of Quinazoline Based Heterocycles. *Tetrahedron Lett.* **2014**, *55*, 2973-2976. Copyright (2014) Elsevier.
http://www.sciencedirect.com/science/article/pii/S0040403914005413

<u>Appendix 4:</u> Experimental and Theoretical Investigations into the Stability of Cyclic Aminals.

Sawatzky, E.; Drakopoulos, A.; Rölz, M.; Sotriffer, C.; Engels, B.; Decker, M. Experimental and Theoretical Investigations into the Stability of Cyclic Aminals. *Beilstein J. Org Chem.*, Accepted.
https://www.beilstein-journals.org/bjoc/home/home.htm

Appendix 1

A Novel Way to Radiolabel Human Butyrylcholinesterase for Positron Emission Tomography through Irreversible Transfer of the Radiolabeled Moiety.

A Novel Way To Radiolabel Human Butyrylcholinesterase for Positron Emission Tomography through Irreversible Transfer of the Radiolabeled Moiety

Edgar Sawatzky,[a] Ehab Al-Momani,[b] Ryohei Kobayashi,[b] Takahiro Higuchi,[b] Samuel Samnick,[b] and Michael Decker*[a]

The enzyme butyrylcholinesterase (BChE) is known to be involved in the detoxification of xenobiotics in blood plasma and is associated with the progress of neurodegenerative disorders, diabetes type 2, obesity, and diseases of the cardiovascular system. In the present study, we developed carbamate-based inhibitors serving as positron emission tomography (PET) radiotracers with ^{18}F and ^{11}C as radioisotopes to visualize BChE distribution. These inhibitors are radiolabeled at the carbamate site and transfer this moiety onto BChE, which thus results in covalent and permanent radiolabeling of the enzyme. There are no comparable radiotracers for cholinesterases described to date. By ex vivo autoradiography experiments on mice brain slices and kinetic investigations, selective and covalent transfer of the radiolabeled carbamate moiety onto BChE was proven. These tracers might provide high resolution of BChE distribution in vivo to enable investigations into the pathophysiological mechanisms of diseases associated with alterations in BChE occurrence.

Introduction

The decline of memory and cognitive abilities during Alzheimer's disease (AD) and other neurodegenerative disorders, such as Parkinson's disease (PD) or dementia with Lewy bodies, is strongly attributed to pathological changes in the cholinergic system with decreased levels of the neurotransmitter acetylcholine (ACh).[1] In AD, progressive loss of cholinergic neurons is responsible for this deficit. Consequently, acetylcholinesterase (AChE) inhibitors, that is, compounds inhibiting the enzyme responsible for inactivation of ACh, were developed to increase the levels of ACh and, therefore, to improve cognitive abilities. Unfortunately, in advanced AD the level of AChE dramatically drops by 90%,[2] which makes this enzyme inefficient as a therapeutic target in later stages of the disease. In contrast, the level of its isoenzyme butyrylcholinesterase (BChE) is significantly increased by approximately 30% during later stages of AD.[2,3] Although the physiological role of BChE has not yet been fully investigated, BChE can compensate the loss of neuronal AChE in progressed AD and, therefore, takes over the function of AChE. Several studies have shown a positive correlation between BChE inactivation and improved cognition.[4] Therefore, inhibition of BChE might well constitute a therapeutic target for clinical use in progressed AD when

AChE inhibitors fail. Interestingly, BChE was also found to be colocalized with neurotoxic amyloid β-plaques[5] in the brains of AD patients and might promote amyloid β-toxicity.[4c–e, 6] Increased levels of BChE in cortical brain regions and especially its occurrence with amyloid β-plaques might, therefore, be a suitable marker to enable AD diagnostics. Besides its potential role in AD pathogenesis, BChE is known to be involved in 1) serum metabolism in context with the detoxification of naturally occurring and pharmacologically active compounds by ester or carbamate cleavage,[7] 2) obesity,[8] 3) diabetes mellitus type 2,[8b,9] and 4) cardiovascular risk factors.[10] Accordingly, to investigate the role of BChE in these research fields the development of highly potent and selective positron emission tomography (PET) radiotracers is highly desirable to visualize BChE in vivo. Such a tracer might be used as a diagnostic tool in AD to determine unusual BChE distribution and help to investigate pathophysiological changes, expression levels, and location of BChE to understand the molecular mechanisms in the diseases mentioned.

Several cholinesterase (ChE) PET radiotracers have been described in the literature mainly focusing on brain and/or peripheral AChE as target.[11] Thereby, two main strategies have been pursued by using substrate- or ligand-type radiotracers. Substrate-type radiotracers pass the blood–brain barrier (BBB) and are hydrolyzed by AChE within the brain. The resulting radioactive metabolites have low BBB permeability, and thus, radioactivity accumulates in brain regions in which AChE is localized. This method allows quantification of AChE distribution and gives additional information about the catalytic activity of AChE in different brain areas. Examples of such tracers are [^{11}C]MP4P, [^{11}C]MP4A, and [^{18}F]FEtP4A (Figure 1A).[12] Besides these substrate-type radiotracers, several reversibly binding

[a] E. Sawatzky, Prof. Dr. M. Decker
Pharmaceutical and Medicinal Chemistry, Institute of Pharmacy and Food Chemistry, Julius Maximilian University Würzburg, Am Hubland, 97074 Würzburg (Germany)
E-mail: Michael.Decker@uni-wuerzburg.de

[b] Dr. E. Al-Momani, R. Kobayashi, Prof. Dr. T. Higuchi, Prof. Dr. S. Samnick
Experimental Nuclear Medicine, Center of Inner Medicine, University Hospital Würzburg, OberdürrbacherStrasse 6, 97080 Würzburg (Germany)

⬚ Supporting Information for this article can be found under http://dx.doi.org/10.1002/cmdc.201600223.
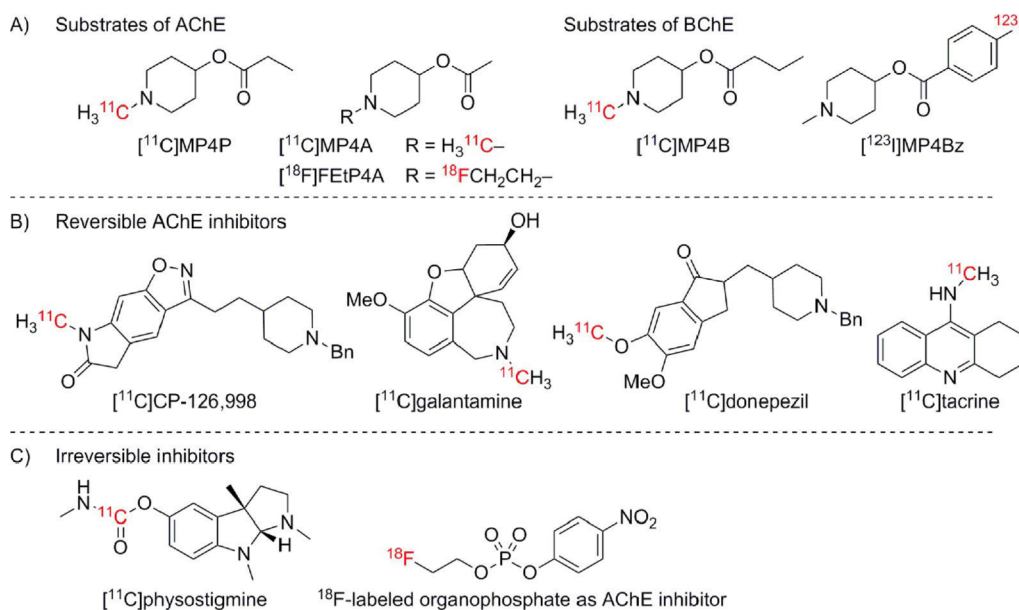
Figure 1. Radiotracers developed for ChE visualization: A) substrates for AChE and BChE by using the principle of metabolic trapping, B) reversible AChE inhibitors, and C) irreversible AChE inhibitors.

AChE inhibitors (Figure 1 B) were developed as ligand-type radiotracers for enzyme labeling.[13] Beyond the mentioned two major radiotracer concepts for ChE labeling, to our knowledge only two irreversibly acting ChE inhibitors have been developed ([11C]physostigmine and an AChE-selective ^{18}F-labeled organophosphate) that can transfer the radioisotope covalently onto the enzyme, which thus results in irreversible labeling (Figure 1 C).[14] However, [11C]physostigmine lacks selectivity for either ChE, and organophosphates are well known to be highly toxic nerve agents, which putatively limits their use.

Although the concept of irreversible labeling is well documented for various biological targets {e.g., imaging of monoamine oxidase (MAO) with [11C]deprenyl, [11C]deprenyl-D2, or [18F]fluororasasagiline-D2;[15] different carbamate-based inhibitors for monoacylglycerol lipase (MAGL) imaging;[16] and carbamate-based inhibitors such as [11C]CURB and [18F]DOPP for fatty acid amide hydrolase (FAAH) visualization[17]}, currently only little attention has been focused on such tracers for ChE imaging.

As possible limitations for the application of irreversible radiotracers in PET, two issues are often considered: 1) the often-complex mechanism of enzyme inactivation as well as difficulties in the exact determination of in vivo kinetics and distribution and 2) such inhibitors might reflect the plasma delivery rate of the radiotracer into the tissue (flow limitation) rather than the regional enzyme distribution.[18] The latter issue also applies to both reversibly binding competitive PET tracers of high affinity and substrate-type radiotracers, as delivery limitations into the tissue and quick hydrolysis of the substrate are limiting factors for radiotracers. This is exemplarily the case for the widely used radiosubstrate [11C]MP4A.[11a, 19] On the other hand, Fowler and others have demonstrated for MAO imaging that suicide PET radiotracers can well quantify and map the physiological distribution of a target enzyme.[20]

Regarding the increasing relevance of BChE for treatment and diagnosis of the diseases mentioned above, it is remarkable that for BChE only a few selective tracers—and all of them of the substrate type—have been reported (Figure 1 A).[5c, 21] To overcome the lack of suitable BChE radiotracers, in the present study we developed a selective and highly potent BChE inhibitor incorporating either ^{11}C or ^{18}F as a radioisotope. These tracers might be used in PET studies to investigate the role of BChE and are, to our knowledge, the first radiotracers reported for BChE of the inhibitor type. The starting point of our investigation was a tetracyclic carbamate that we found in previous studies to be a promising candidate because of its excellent inhibitory potency and selectivity toward BChE over AChE (Figure 2).[22] For PET tracer development, the irreversible labeling approach reported for FAAH and MAGL was adopted,[16, 17] and incorporation of the radioisotopes was performed at the carbamate site to achieve covalent transfer of the radioisotope onto the enzyme (Figure 2). For these tracers, the in vitro kinetics of enzyme inhibition were determined in detail, and a first ex vivo autoradiography experiment was performed showing selective binding of the tracers on tissue BChE.

Results and Discussion

Most efficient ^{18}F labeling is achieved by direct introduction of [18]F$^-$ into a suitable precursor in the last or one of the last reaction steps. This prevents complicated reaction processing with the radioisotope and gives access to higher radiochemical yields, as time-dependent decay of the radioisotope and undesired side reactions are minimized. Therefore, precursor **7** was synthesized in five steps (Scheme 1 A): Starting with 7-bromoheptan-1-ol, a Gabriel synthesis was applied to yield 7-amino-heptan-1-ol (**2**) in two steps via phthalimide **1**. Amino alcohol
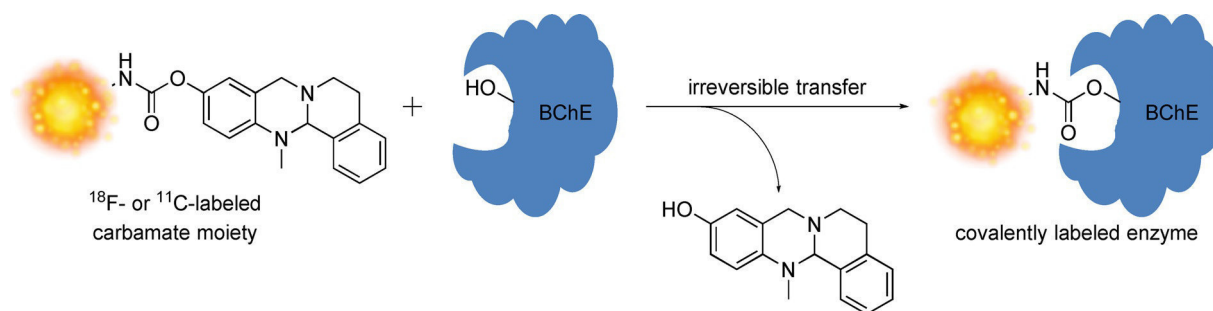
Figure 2. Covalent labeling of BChE with an irreversible inhibitor by carbamate transfer.
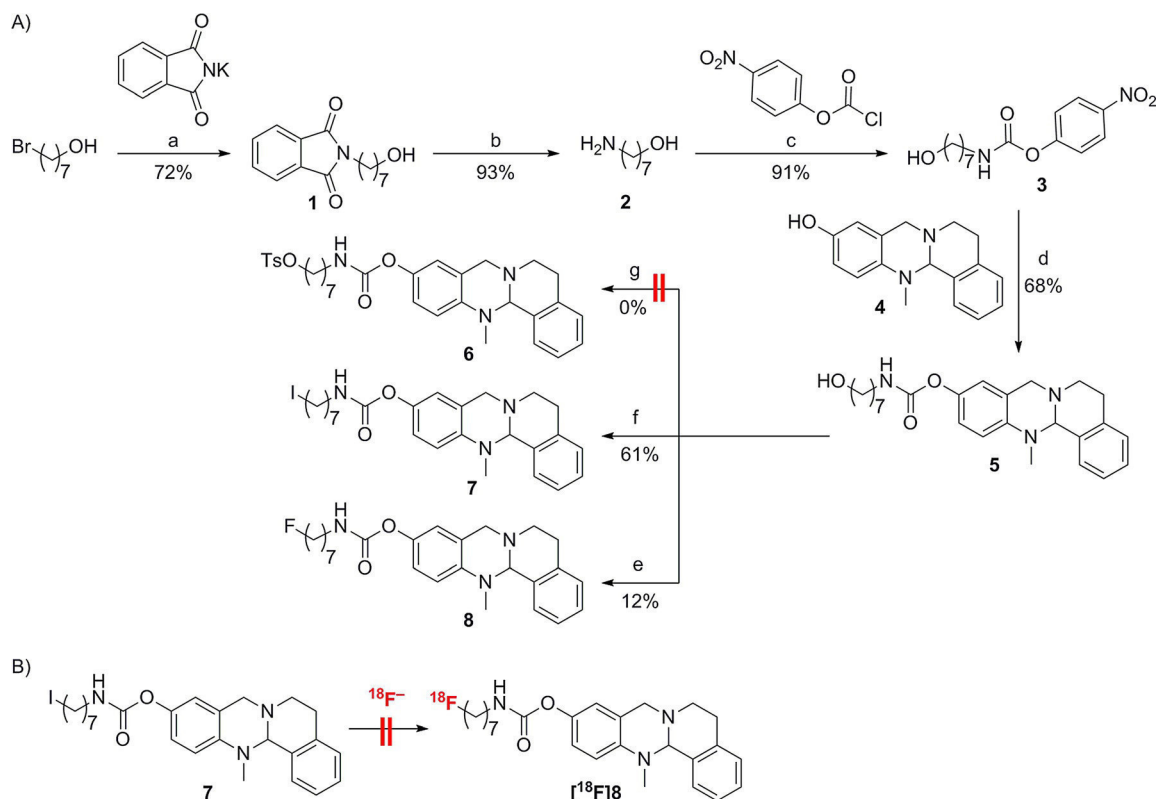
Scheme 1. *Reagents and conditions*: a) DMF, 3 h, 120 °C; b) H₂NNH₂·H₂O, EtOH, 5 h, reflux; c) Et₃N, CH₂Cl₂, 2 h, RT; d) NaH, THF, RT, 1 h; e) DAST, CH₂Cl₂, 6 h, RT; f) PPh₃, I₂, THF, 2 h, RT, g) TsCl, CH₂Cl₂.

2 was then activated with 4-nitrophenyl chloroformate toward carbamate **3**, followed by coupling with tetracyclic phenol **4** (synthesis of **4** was described recently[23]) to give carbamate **5**. Initial introduction of a suitable leaving group by applying *p*-toluenesulfonyl (Ts) chloride toward compound **6** failed, as the nucleophilic character of the aliphatic nitrogen atom in the tetrahydroquinazoline core led to unfavorable side reactions that resulted in complete degradation. Therefore, an iodine leaving group was introduced by applying triphenylphosphine and elementary iodine to yield compound **7**. Besides, the use of the fluorination reagent diethylaminosulfur trifluoride (DAST) yielded unlabeled ("cold") fluorinated compound **8**, which was an indispensable compound as a reference for the radiolabeling process.

Unfortunately, direct ¹⁸F labeling toward [¹⁸F]**8** failed with precursor **7** (Scheme 1B), as the carbamate moiety itself degraded under the applied labeling conditions. Similar behavior was previously reported for the FAAH radiotracer [¹⁸F]DOPP,[24] for which the carbamate moiety underwent fast E1cB elimination into the corresponding phenol and isocyanate during labeling.

Therefore, we adopted and modified the protocol reported by Sadovski et al.[24] and synthesized precursor **10** smoothly via intermediate **9** from amino alcohol **2** (Scheme 2A). In a four-step reaction sequence, precursor **10** was first radiolabeled with ¹⁸F⁻, then *tert*-butoxycarbonyl (Boc)-deprotected under acidic conditions, then activated with 4-nitrophenyl chloroformate toward [¹⁸F]**11**, and finally coupled with phenol **4** toward
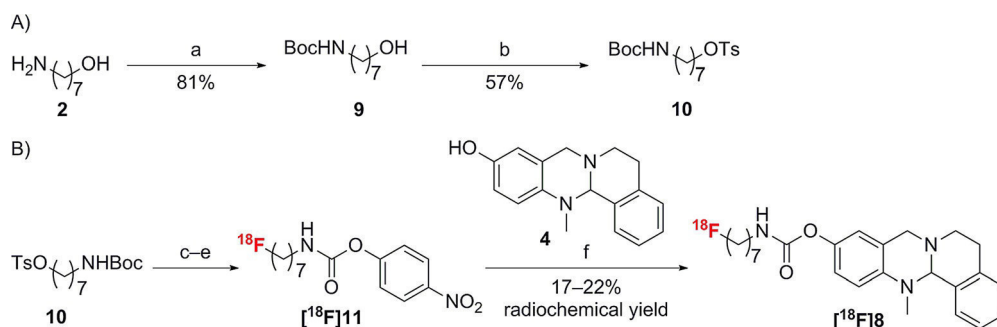
Scheme 2. Reagents and conditions: a) (Boc)$_2$O, K$_2$CO$_3$, MeOH/H$_2$O, 4 h, RT; b) TsCl, Et$_3$N, K$_2$CO$_3$, CH$_2$Cl$_2$, 3 d, RT; c) Kryptofix 222, K$_2$CO$_3$, 10 min, 90 °C; d) TFA, 10 min, RT; e) Et$_3$N, MeCN, 4-NO$_2$-C$_6$H$_4$-O(C=O)Cl, 90 °C, 7 min; f) 7 min, 90 °C.

desired radiotracer [18F]**8** in a radiochemical yield of 18–22% (n = 5, corrected decay) and a radiochemical purity of > 98% after purification by reversed-phase HPLC (Scheme 2B). The specific activity after radiosynthesis was determined to be 400 MBq μmol^{-1}. The identity of [18F]**8** was confirmed by HPLC through co-injection of [18F]**8** with unlabeled analogue **8**. Notably, Sadovski et al.[24] reported a protocol for labeling that prevents activation of the labeled precursor toward [18F]**11** by using an activated phenol, but for the heterocycles applied herein, the synthesis of such a phenol was not successful (see the Supporting Information).

Besides introducing ^{18}F into the carbamate residue, incorporation of ^{11}C as a common alternative radioisotope for PET was investigated. Regarding the limited possibilities for radioisotope introduction into an aliphatic, chemically nonfunctionalized chain, a method was chosen in which labeling occurs directly at the carbonyl carbon atom of the carbamate moiety. Wilson and co-workers developed a method that easily allows the formation of ^{11}C-labeled carbamate and urea derivatives by using ^{11}CO$_2$, 2-tert-butylimino-2-diethylamino-1,3-dimethylperhydro-1,3,2-diazaphosphorine (BEMP) and POCl$_3$ in a three-step reaction sequence.[17d, 25] Although in our case this method led to satisfying results in terms of carbamate formation upon applying nonradioactive CO$_2$ (data not shown), we chose to develop a simpler method to avoid this multistep sequence with radioactive intermediates. Therefore, an approach reported for aromatic triphenylphosphinimines[26] was modified, and heptylphosphinimine hydrochloride (**13**) was synthesized in two steps (Scheme 3). Upon treating a mixture of precursor **13** and tetracyclic phenol **4** in the presence of 1,8-diazabicyclo[5.4.0]undec-7-ene (DBU) with ^{11}CO$_2$, followed by heating to 60 °C for 6 min, desired radiotracer [11C]**14** was obtained in a good radiochemical yield of 30–36% (n = 4, corrected decay)

and a radiochemical purity of 98% after purification by reversed-phase HPLC (Scheme 3). The identity of [11C]**14** was confirmed by HPLC through co-injection with unlabeled analogue **14** (synthesis described previously[22b]). This method allows easy access to carbamates labeled at the carbonyl carbon atom by using ^{11}CO$_2$ in only one reaction step.

To prove carbamate transfer and therefore irreversibility of radiolabeling of BChE, in vitro enzyme kinetic investigations for unlabeled reference compounds **8** and **14** were performed. First, IC$_{50}$ values for human AChE and BChE (hAChE and hBChE) were determined after 30 min, and both compounds showed inhibition of hBChE in the single-digit nanomolar range with a 600- to 700-fold selectivity for hBChE over hAChE (Table 1).

Time-dependent evaluation of the carbamoylation process was also necessary, as carbamate-mediated enzyme inhibition is known to undergo a three-step kinetic process (see equation in Table 1):[22a] The inhibitor 1) binds reversibly to the enzyme (E) thus to form a EI complex quantified in equilibrium by K_C, 2) the carbamate group is transferred covalently onto the enzyme to form the irreversibly inhibited enzyme E−C under release of the phenolic carrier (R) with k_3 as the carbamoylation rate constant, and 3) E−C is slowly hydrolyzed under reactivation of E and k_4 as decarbamoylation constant. Transferring the carbamate moiety onto the enzyme is a comparably slow chemical reaction (in terms of enzymatic catalysis), and therefore, carbamate-mediated enzyme inhibition is time dependent. Knowing the exact kinetic profile of in vitro enzyme inhibition is a prerequisite before studying in vivo (pharmaco)kinetics, especially because carbamate-based inhibitors do not necessarily act irreversibly.[27] Therefore, careful kinetic monitoring of the inhibition mechanism was performed. Compounds **8** and **14** caused time-dependent inhibition (Figure 3 A,B) and showed a high affinity in the nanomolar range on hBChE (K_C
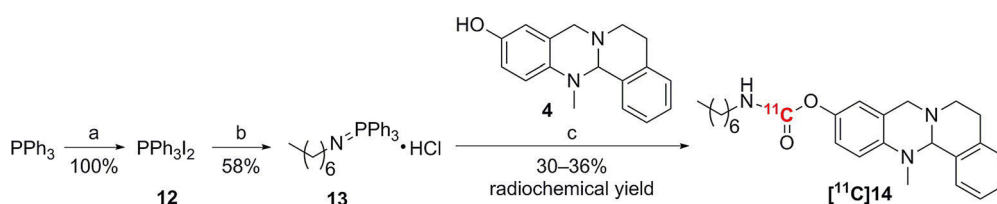
Scheme 3. Reagents and conditions: a) I$_2$, Et$_2$O, RT, 1 h; b) CH$_3$(CH$_2$)$_6$NH$_2$, CH$_2$Cl$_2$, RT, 5 h; c) 1. DBU, ^{11}CO$_2$, THF, 10 min, −78 °C; 2. 60 °C, 6 min.

Table 1. Inhibition and kinetic data on human AChE and BChE for compounds **8** and **14**.

$$E + I \underset{k_2}{\overset{k_1}{\rightleftharpoons}} (EI) \overset{k_3}{\underset{-R}{\longrightarrow}} E\text{--}C \overset{k_4}{\longrightarrow} E + C'$$

with K_C spanning the first equilibrium.

Compd	$IC_{50}(h\text{AChE})$ [µM] ($pIC_{50} \pm$ SEM)	$IC_{50}(h\text{BChE})$ [nM] ($pIC_{50} \pm$ SEM)	$K_C(h\text{BChE}) \pm$ SEM [nM]	$k_3(h\text{BChE}) \pm$ SEM [min^{-1}]	$k_4(h\text{BChE}) \pm$ SEM [h^{-1}]
8	3.6 (5.44 ± 0.05)	5.2 (8.28 ± 0.02)	24.3 ± 19.3	0.78 ± 0.48	0.81 ± 0.04
14	3.8 (5.42 ± 0.02)	6.4 (8.19 ± 0.02)	28.5 ± 17.2	0.66 ± 0.32	0.62 ± 0.04
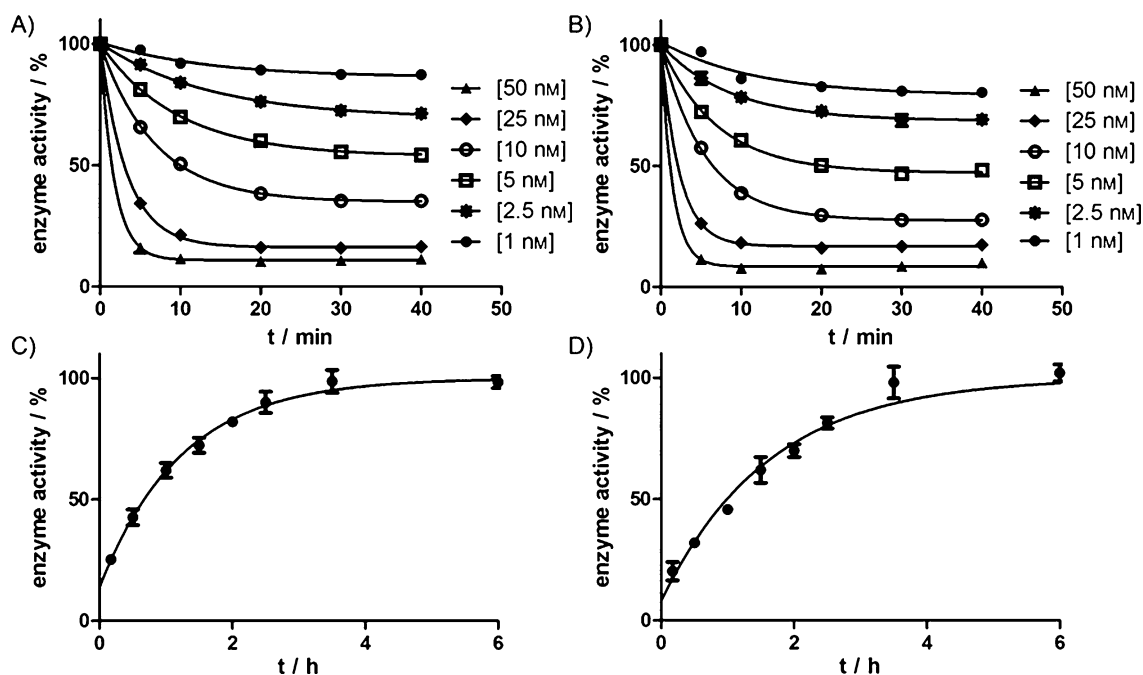
Figure 3. Time-dependent inhibition of hBChE by different concentrations of A) compound **8** and B) compound **14**. Recovery of hBChE activity after inhibition with C) compound **8** and 1000-fold dilution and D) with compound **14** and 1000-fold dilution. Each experiment was performed in triplicate (mean ± SD).

values are presented in Table 1) in addition to a high carbamoylation rate of the enzyme (k_3 values). Also, the decarbamoylation rate constant (k_4) was determined in dilution experiments: both derivatives were incubated with the enzyme for 1 h to completely inhibit the enzyme before 1000-fold dilution to an inhibitor concentration at which no further enzyme inhibition occurs. Recovery of enzyme activity was determined after certain time points. For reversible inhibitors, enzyme recovery occurs immediately after dilution and only irreversible inhibitors show slow first-order enzyme recovery kinetics, as inhibition occurs covalently and therefore is independent of the inhibitor concentration of the assay media after dilution. Compounds **8** and **14** caused slow regeneration of enzyme activity after dilution (Scheme 3 C,D), which revealed the high stability of the carbamoylated enzyme E–C with a decarbamoylation half-life of approximately 1 h (calculated from k_4). Carbamoylation (K_C and k_3) as well as decarbamoylation kinetics (k_4) proved irreversible transfer of the carbamate moiety, which

makes these compounds suitable for further PET investigations. Kinetic data for the single steps are reported in Table 1.

For in vivo evaluations, metabolic stability in plasma is of special importance for radiotracers targeting BChE, as it is one of the major detoxification enzymes in human plasma hydrolyzing xenobiotic substrates by cleaving carbamate or ester bonds.[7c] Therefore, the stability of unlabeled reference compounds **8** and **14** was investigated in vitro by using human pooled plasma samples. Only slow degradation of both compounds was observed with less than 50% decomposition even after 2 h (blue and black lines in Figure 4). Given that the compounds are supposed to be cleaved by BChE over time, the stability analysis was repeated with plasma samples pre-incubated for 1 h with a high concentration of the known unselective ChE inhibitor tacrine. Tacrine inhibits both AChE and BChE and, therefore, prevents ChE-mediated degradation of the test compounds. Surprisingly, no differences were detected in stability (purple and yellow lines in Figure 4) relative to the non-
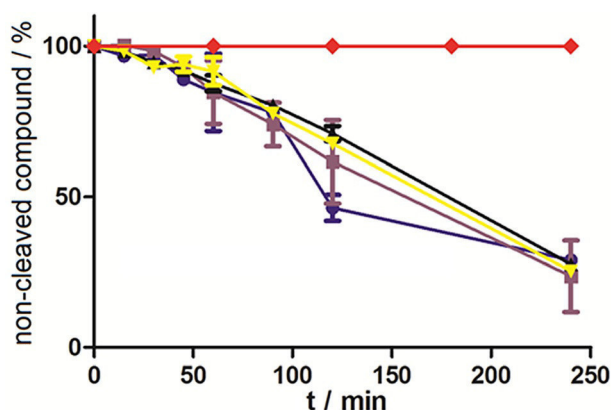
Figure 4. Time-dependent plasma stability of compounds **8** (black) and **14** (blue) and stability after pretreatment with a tacrine concentration of 50 μM (**8**, yellow; **14**, purple). Stability of compound **8** was also measured when proteins had been precipitated beforehand (red). Each experiment was performed in triplicate (mean ± SEM).

pre-incubated samples. Subsequently, the plasma proteins were first precipitated, and the remaining solution was used to incubate compound **8** without proteins to investigate whether degradation of the compounds was enzyme mediated or if the compounds were chemically unstable in the buffered solution (red line in Figure 4). HPLC showed no decomposition in buffer solution; thus, it was concluded that compounds **8** and **14** were cleaved enzymatically and were stable in aqueous media. This is in agreement with the literature, as in addition to BChE, paraoxonase and albumin are also known as plasma proteins with esterase activity. Therefore, cleavage of compounds **8** and **14** in human plasma might be catalyzed by such mechanisms.[7c]

Finally, binding of [18F]**8** was investigated by ex vivo brain autoradiography with healthy mouse brain slices. Accumulation of high radioactivity in all relevant brain areas was found, which proved good binding of [18F]**8** to brain tissue (Figure 5 A).[6] In parallel, inhibition experiments were performed on brain slices after pre-incubation with ethopropazine hydrochloride, known as a selective BChE inhibitor, to confirm the specificity of [18F]**8** binding (Figure 5 B). Ethopropazine selectively blocks the active site of BChE and prevents any binding
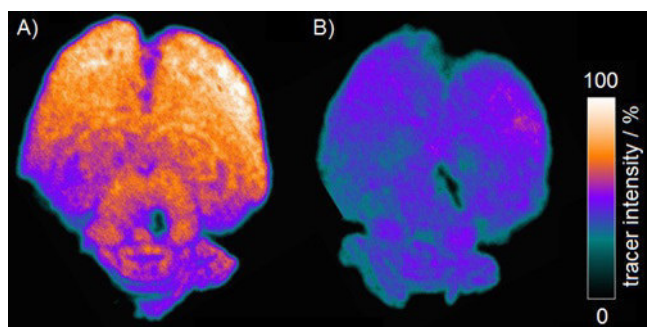
Figure 5. Autoradiography of [18F]**8** on a healthy mouse brain A) without and B) with ethopropazine hydrochloride pre-incubation. Intensity (arbitrary unit) is given in percentage of the maximum tracer activity.

of other BChE inhibitors or substrates. As expected, in this blocking experiment only little binding of [18F]**8** was found on the tissue relative to that on the control slices, which suggests specific binding of [18F]**8** to BChE.[6]

Conclusions

In summary, butyrylcholinesterase (BChE) constitutes an enzyme with high relevance for Alzheimer's disease diagnostics. To investigate its role in AD, we developed the first selective BChE inhibitors acting as potential positron emission tomography (PET) radiotracers to image human BChE after labeling with the positron emitters 18F and 11C. These radiotracers were labeled at the carbamate site, which thus made covalent and direct labeling of the enzyme through carbamate transfer possible. By applying kinetic investigations and decarbamoylation experiments of the reference compounds, 13-methyl-6,8,13,13a-tetrahydro-5H-isoquinolino[1,2-b]quinazolin-10-yl 7-fluoroheptylcarbamate (**8**) and carbonyltetrahydro-13-methyl-5H-isoquinolino[1,2-b]quinazolin-10-yl heptylcarbamate (**14**), we showed that carbamate transfer onto the enzyme rapidly took place and proved irreversible transfer of the carbamate moiety, thus offering the possibility for covalent and irreversible labeling upon using [18F]**8** and [11C]**14**. To our knowledge, no comparable BChE radiotracers have been developed to date. The herein described radiotracers showed high stability in human plasma with less than 50% degradation after 2 h, and preliminary autoradiography experiments on mice brain slices combined with blocking studies by using the known BChE-selective inhibitor ethopropazine revealed rapid and selective binding of the tracers on BChE at the brain. Taking these results together, the concept of irreversible labeling was applied for a carbamate-based BChE inhibitor, and the first ex vivo and in vitro studies showed promising results for further studies. Of course, in vivo studies are now necessary to evaluate the distribution, stability, and pharmacokinetics of the developed tracer in a suitable mouse model.

We consider the strategy of irreversible labeling for radioimaging to be a promising approach. Although the concept has already been applied on several targets, for example, monoamine oxidase imaging, many more irreversible inhibitors are known[28] that might be turned into suitable irreversible PET radiotracers by the chemical and biological methods described herein, which would thereby enable the investigation of more biological targets.

Experimental Section

Chemistry

Common reagents and solvents were obtained from commercial suppliers and were used without any further purification. Tetrahydrofuran (THF) was distilled from sodium/benzophenone under an argon atmosphere. Reaction progress was monitored by using analytical thin-layer chromatography (TLC) on precoated silica gel GF254 plates (Macherey–Nagel GmbH & Co. KG, Düren, Germany), and spots were detected under UV light ($\lambda = 254$ nm) or by staining with iodine. Nuclear magnetic resonance spectra were per-

formed with a Bruker AV-400 NMR instrument (Bruker, Karlsruhe, Germany) in [D$_6$]DMSO or CDCl$_3$. Chemical shifts are expressed in ppm relative to CHCl$_3$/DMSO ($\delta = 7.26/2.50$ and $77.16/39.52$ ppm for ^{1}H and ^{13}C NMR, respectively). Melting points were determined in open capillaries with a Büchi B-540 without any further correction. For purity and reaction analyzes, analytical HPLC analysis was performed with a system from Shimadzu equipped with a DGU-20A3R controller, LC20AB liquid chromatograph, and a SPD-20A UV/Vis detector. Stationary phase was a Synergi 4 μm fusion-RP (150×4.6 mm) column (Phenomenex, Aschaffenburg, Germany). As mobile phase, H$_2$O (phase A) and MeOH (phase B) were used with 1 mL min^{-1} (conc. B: 5→90% from 0 to 8 min; 90% from 8 to 13 min; 90→5% from 13 to 15 min; 5% from 15 to 18 min). ESI mass spectral data were acquired with a Shimadzu LCMS-2020.

2-(7-Hydroxyheptyl)isoindoline-1,3-dione (1): 7-Dibromoheptan-1-ol (1 g, 5.13 mmol, 1 equiv) was dissolved in dry DMF (20 mL) and treated with potassium phthalate (996 mg, 5.38 mmol, 1.05 equiv). The mixture was stirred at 120 °C for 3 h. Then, the precipitated solid was filtered off, and the filtrate was diluted with H$_2$O (30 mL). The aqueous phase was extracted with ethyl acetate (3×50 mL). The combined organic layers were washed with brine (30 mL) and dried (Na$_2$SO$_4$). After removal of the solvent under reduced pressure, the residue was purified by column chromatography (petroleum ether/EtOAc 1:1) to yield **1** (960 mg, 72%) as a clear oil that crystallized over time; mp: 56–60 °C. ^{1}H NMR (400 MHz, CDCl$_3$): $\delta = 7.87–7.79$ (m, 2H), 7.73–7.65 (m, 2H), 3.69–3.64 (m, 2H), 3.62 (t, $J = 6.6$ Hz, 2H), 1.72–1.62 (m, 2H), 1.59–1.50 (m, 2H), 1.42 (s, OH), 1.39–1.30 ppm (m, 6H); ^{13}C NMR (101 MHz, CDCl$_3$): $\delta = 168.5$, 133.9 (2C), 132.2 (2C), 123.2, 62.9, 38.0, 32.6, 28.9, 28.5, 26.8, 25.6 ppm; MS (ESI): m/z: 262.2 $[M+H]^+$.

7-Aminoheptan-1-ol (2): 2-(7-Hydroxyheptyl)isoindoline-1,3-dione (1; 2.05 g, 7.85 mmol, 1 equiv) was dissolved in EtOH (30 mL) and treated with hydrazine hydrate (1.57 g, 31 mmol, 4 equiv). The mixture was heated at reflux for 4 h, during which a white precipitate formed. The mixture was filtered, and the filtrate was evaporated to dryness. The resulting residue was suspended in diethyl ether (100 mL) and filtered again. The filtration cake was washed with diethyl ether (3×100 mL), and the combined filtrate was evaporated to dryness to obtain **2** (953 mg, 93%) as a pale-yellow solid; mp: 43–47 °C. ^{1}H NMR (400 MHz, CDCl$_3$): $\delta = 3.55$ (t, $J = 6.6$ Hz, 2H), 2.61 (t, $J = 7.0$ Hz, 2H), 1.74 (br, 3H), 1.54–1.45 (m, 2H), 1.42–1.34 (m, 2H), 1.32–1.22 ppm (m, 6H); ^{13}C NMR (101 MHz, CDCl$_3$): $\delta = 62.7$, 42.1, 33.6, 32.8, 29.2, 26.8, 25.8 ppm; MS (ESI): m/z: 132.3 $[M+H]^+$.

4-Nitrophenyl 7-hydroxyheptylcarbamate (3): 4-Nitrophenyl chloroformate (505 mg, 2.50 mmol, 1.1 equiv) was dissolved in CH$_2$Cl$_2$ (30 mL) and treated with triethylamine (346 μL, 2.50 mmol, 1.1 equiv). Then, a solution of 7-aminoheptan-1-ol (2; 298 mg, 2.27 mmol, 1 equiv) in CH$_2$Cl$_2$ (20 mL) was added dropwise over 30 min, and the mixture was stirred for 4 h at RT. The mixture was then diluted with CH$_2$Cl$_2$ (30 mL), washed with 1 M HCl solution (3×10 mL), and washed with brine (10 mL). Then, the organic layer was dried (Na$_2$SO$_4$), which was followed by removal of the solvent under reduced pressure. The crude product was purified by column chromatography (petroleum ether/EtOAc 1:1) to yield **3** (673 mg, 91%) as a white solid; mp: 75–77 °C. ^{1}H NMR (400 MHz, CDCl$_3$): $\delta = 8.28–8.20$ (m, 2H), 7.36–7.27 (m, 2H), 5.13 (s, NH), 3.68–3.61 (m, 2H), 3.28 (dd, $J = 13.3$, 7.0 Hz, 2H), 1.67–1.51 (m, 4H), 1.45–1.33 (m, 6H), 1.30 ppm (s, OH); ^{13}C NMR (101 MHz, CDCl$_3$): $\delta = 156.0$, 153.1, 144.7, 125.1 (2C), 121.9 (2C), 62.9, 41.4, 32.6, 29.6, 29.0, 26.6, 25.6 ppm; MS (ESI): m/z: 297.2 $[M+H]^+$.

13-Methyl-6,8,13,13a-tetrahydro-5H-isoquinolino[1,2-b]quinazolin-10-yl 7-hydroxyheptylcarbamate (5): A solution of 13-methyl-6,8,13,13a-tetrahydro-5H-isoquinolino[1,2-b]quinazolin-10-ol (4; 445 mg, 1.5 mmol, 1 equiv) in dry THF (5 mL) was treated with NaH in paraffin oil (60%, 66 mg, 1,65 mmol, 1.1 equiv). The mixture was stirred until the formation of gas stopped. Then, 4-nitrophenyl 7-hydroxyheptylcarbamate (3; 400 mg, 1.5 mmol, 1 equiv) was added, and the mixture was stirred for 1 h. The mixture was diluted with ethyl acetate (20 mL) and washed with H$_2$O (10 mL) and brine (10 mL). The organic phase was dried (Na$_2$SO$_4$) and concentrated to dryness. The crude product was purified by column chromatography (100% EtOAc) to yield **5** (416 mg, 68%) as a pale-yellow oil. ^{1}H NMR (400 MHz, [D$_6$]DMSO): $\delta = 7.60$ (t, $J = 5.6$ Hz, NH), 7.38–7.32 (m, 1H), 7.27–7.22 (m, 2H), 7.20–7.15 (m, 1H), 6.91 (d, $J = 8.8$ Hz, 1H), 6.83 (dd, $J = 8.7$, 2.6 Hz, 1H), 6.75 (d, $J = 2.5$ Hz, 1H), 4.77 (s, 1H), 4.34 (t, $J = 5.1$ Hz, OH), 3.96–3.80 (m, 2H), 3.40 (dd, $J = 11.5$, 6.4 Hz, 2H), 3.23–3.14 (m, 1H), 3.03 (dt, $J = 10.8$, 5.4 Hz, 2H), 2.97 (dd, $J = 15.2$, 6.7 Hz, 1H), 2.78 (dt, $J = 16.2$, 4.5 Hz, 1H), 2.72–2.62 (m, 1H), 2.50 (s, 3H), 1.50–1.37 (m, 4H), 1.34–1.25 ppm (m, 6H); ^{13}C NMR (101 MHz, [D$_6$]DMSO): $\delta = 154.8$, 145.0, 144.3, 135.9, 133.9, 128.7, 128.2, 127.3, 125.6, 125.3, 120.3, 119.8, 119.5, 75.7, 60.7, 55.2, 47.1, 40.4, 37.8, 32.5, 29.2, 28.6, 27.8, 26.3, 25.4 ppm; MS (ESI): m/z: 424.3 $[M+H]^+$.

13-Methyl-6,8,13,13a-tetrahydro-5H-isoquinolino[1,2-b]quinazolin-10-yl 7-iodoheptylcarbamate (7): A solution of iodine (125 mg, 0.49 mmol, 2 equiv) in CH$_2$Cl$_2$ (2 mL) was added dropwise to a solution of triphenylphosphane (129 mg, 0.49 mmol, 2 equiv) in CH$_2$Cl$_2$ (2 mL). Then, a solution of imidazole (24 mg, 0.34 mmol, 1.4 equiv) and 13-methyl-6,8,13,13a-tetrahydro-5H-isoquinolino[1,2-b]quinazolin-10-yl 7-hydroxyheptylcarbamate (5; 100 mg, 0.25 mmol, 1 equiv) in CH$_2$Cl$_2$ (5 mL) was added dropwise. The mixture was stirred at room temperature for 2 h. The mixture was then washed with H$_2$O (5 mL) and brine (5 mL) and dried (Na$_2$SO$_4$), and the solvent was removed under reduced pressure. The crude product was purified by column chromatography (petroleum ether/EtOAc 2:1) to yield **7** (80 mg, 61%) as a yellow oil. ^{1}H NMR (400 MHz, [D$_6$]DMSO): $\delta = 7.61$ (t, $J = 5.6$ Hz, NH), 7.38–7.32 (m, 1H), 7.27–7.21 (m, 2H), 7.21–7.14 (m, 1H), 6.91 (d, $J = 8.8$ Hz, 1H), 6.83 (dd, $J = 8.7$, 2.6 Hz, 1H), 6.75 (d, $J = 2.6$ Hz, 1H), 4.77 (s, 1H), 3.95–3.79 (m, 2H), 3.27 (t, $J = 6.7$ Hz, 2H), 3.22–3.15 (m, 1H), 3.04 (dd, $J = 12.9$, 6.7 Hz, 2H), 3.01–2.93 (m, 1H), 2.78 (dt, $J = 16.3$, 4.6 Hz, 1H), 2.71–2.62 (m, 1H), 2.50 (s, 3H), 1.81–1.70 (m, 2H), 1.53–1.42 (m, 2H), 1.39–1.22 ppm (m, 6H); ^{13}C NMR (101 MHz, [D$_6$]DMSO): $\delta = 154.8$, 145.0, 144.2, 135.9, 133.9, 128.7, 128.2, 127.3, 125.6, 125.3, 120.3, 119.8, 119.5, 75.7, 55.2, 47.1, 40.4, 37.8, 32.8, 29.8, 29.1, 27.8, 27.5, 26.1, 9.0 ppm; MS (ESI): m/z: 534.3 $[M+H]^+$.

13-Methyl-6,8,13,13a-tetrahydro-5H-isoquinolino[1,2-b]quinazolin-10-yl 7-fluoroheptylcarbamate (8): A solution of 13-methyl-6,8,13,13a-tetrahydro-5H-isoquinolino[1,2-b]quinazolin-10-yl 7-hydroxyheptylcarbamate (5; 100 mg, 0.24 mmol, 1 equiv) in CH$_2$Cl$_2$ (3 mL) was cooled to 0 °C and then diethylaminosulfur trifluoride (65 μL, 0.49 mmol, 2 equiv) was added dropwise over a period of 5 min. The mixture was allowed to reach RT and was then stirred for another 6 h. The mixture was diluted with a saturated solution of NaHCO$_3$ (10 mL). The layers were separated, and the aqueous phase was extracted with CH$_2$Cl$_2$ (3×15 mL). The combined organic layer was dried (Na$_2$SO$_4$), and the solvent was removed under reduced pressure. The crude product was purified by column chromatography (petroleum ether/EtOAc 1:1) to yield **8** (12 mg, 12%) as a yellow solid; mp: 92–95 °C. ^{1}H NMR (400 MHz, [D$_6$]DMSO): $\delta = 7.60$ (t, $J = 5.7$ Hz, NH), 7.38–7.31 (m, 1H), 7.26–7.20 (m, 2H), 7.19–7.15 (m, 1H), 6.90 (d, $J = 8.8$ Hz, 1H), 6.82 (dd, $J = 8.7$, 2.7 Hz, 1H),

6.74 (d, $J = 2.6$ Hz, 1H), 4.76 (s, 1H), 4.49 (t, $J = 6.1$ Hz, 1H), 4.37 (t, $J = 6.1$ Hz, 1H), 3.89 (d, $J = 15.8$ Hz, 1H), 3.84 (d, $J = 15.9$ Hz, 1H), 3.21–3.14 (m, 1H), 3.03 (dd, $J = 13.0$, 6.7 Hz, 2H), 3.00–2.92 (m, 1H), 2.77 (dt, $J = 16.3$, 4.7 Hz, 1H), 2.66 (ddd, $J = 11.2$, 8.8, 4.9 Hz, 1H), 1.70–1.55 (m, 2H), 1.51–1.41 (m, 2H), 1.38–1.26 ppm (m, 6H); ^{13}C NMR (101 MHz, [D$_6$]DMSO): $\delta = 155.3$, 145.5, 144.7, 136.4, 134.4, 129.2, 128.7, 127.8, 126.1, 125.8, 120.8, 120.2, 120.0, 84.3 (d, $J = 161.7$ Hz), 76.2, 55.6, 47.6, 40.9, 38.3, 30.2 (d, $J = 19.1$ Hz), 29.6, 28.7, 28.3, 26.6, 25.1 ppm (d, $J = 5.4$ Hz). MS (ESI): m/z: 426.3 $[M+H]^+$.

tert-Butyl 7-hydroxyheptylcarbamate (9): A mixture of 7-amino-heptan-1-ol (**2**; 460 mg, 3.51 mmol, 1 equiv), di-tert-butyl dicarbonate (0.9 mL, 4.21 mmol, 1.2 equiv), and K$_2$CO$_3$ (581 mg, 4.21 mmol, 1.2 equiv) in MeOH/H$_2$O (1:1, 25 mL) was stirred for 4 h. Then, the organic solvent was removed under reduced pressure, and the aqueous phase was diluted with H$_2$O (25 mL) and extracted with ethyl acetate (3×35 mL). The combined organic phase was washed with H$_2$O (25 mL) and brine (25 mL), dried (Na$_2$SO$_4$), and concentrated under reduced pressure to obtain **9** (653 mg, 81%) as a clear oil. ^{1}H NMR (400 MHz, CDCl$_3$): $\delta = 4.50$ (br, NH), 3.63 (t, $J = 6.6$ Hz, 2H), 3.10 (td, $J = 12.9$, 6.4 Hz, 2H), 1.60–1.46 (m, 4H), 1.44 (s, 9H), 1.32 ppm (d, $J = 9.2$ Hz, 7H); ^{13}C NMR (101 MHz, CDCl$_3$): $\delta = 156.2$, 77.4, 63.1, 40.7, 32.8, 30.1, 29.1, 28.6 (3C), 26.9, 25.8 ppm; MS (ESI): m/z: 254.2 $[M+Na]^+$.

7-(tert-Butoxycarbonylamino)heptyl-p-tolyl sulfate (10): A mixture of tert-butyl 7-hydroxyheptylcarbamate (**9**; 310 mg, 1.34 mmol, 1 equiv), K$_2$CO$_3$ (370 mg, 2.68 mmol, 2 equiv), triethylamine (18 µL, 0.14 mmol, 0.1 equiv) and p-toluenesulfonyl chloride (280 mg, 1.48 mmol, 1.1 equiv) in CH$_2$Cl$_2$ (10 mL) was stirred for 3 days at ambient temperature. Then, H$_2$O (30 mL) was added, and the mixture was extracted with ethyl acetate (3×30 mL). The combined organic layer was washed with brine (30 mL), dried (Na$_2$SO$_4$), and concentrated under reduced pressure. The crude product was purified by column chromatography (petroleum ether/EtOAc 5:1) to obtain **10** (296 mg, 57%) as a clear oil. ^{1}H NMR (400 MHz, CDCl$_3$): $\delta = 7.85$–7.71 (m, 2H), 7.39–7.29 (m, 2H), 4.48 (br, NH), 4.01 (t, $J = 6.5$ Hz, 2H), 3.07 (dd, $J = 13.1$, 6.5 Hz, 2H), 2.44 (s, 3H), 1.69–1.58 (m, 2H), 1.43 (s, 9H), 1.42–1.14 ppm (m, 8H); ^{13}C NMR (101 MHz, CDCl$_3$): $\delta = 156.1$, 144.8, 133.4, 129.9 (2C), 128.0 (2C), 79.2, 70.7, 40.6, 30.1, 28.9, 28.7, 28.6 (3C), 26.7, 25.4, 21.8 ppm; MS (ESI): m/z: 408.3 $[M+Na]^+$.

Diiodotriphenylphosphane (12): Solid iodine (1.07 g, 4.2 mmol, 1.1 equiv) was added to a solution of triphenylphosphine (1 g, 3.82 mmol, 1 equiv) in diethyl ether (100 mL). The mixture was stirred for 1 h. The precipitated solid was filtered off and washed with diethyl ether (3×20 mL). The solid was then dried in vacuo to afford **12** (1.97 g, 100%) as a yellow-brown solid; mp: decomposition. ^{1}H NMR (400 MHz, CDCl$_3$): $\delta = 7.80$–7.74 (m, 3H), 7.70–7.55 ppm (m, 12H); ^{13}C NMR (101 MHz, CDCl$_3$): $\delta = 134.8$ (d, $J = 2.9$ Hz, 3C), 132.8 (d, $J = 11.5$ Hz, 6C), 129.7 ppm (d, $J = 13.4$ Hz, 6C).

N-Heptyl-1,1,1-triphenylphosphanimine hydrochloride (13): A mixture of heptylamine (143 µL, 0.97 mmol 1 equiv) and triethylamine (268 µL, 1.94 mmol 2 equiv) in CH$_2$Cl$_2$ (30 mL) was added dropwise to a solution of diiodotriphenylphosphane (**12**; 500 mg, 0.97 mmol, 1 equiv) in CH$_2$Cl$_2$ (50 mL) under ice cooling. After complete addition, the mixture was allowed to reach room temperature and was stirred for another 5 h. The solution was then washed with brine (30 mL), dried (Na$_2$SO$_4$), and concentrated under reduced pressure. The crude product was purified by column chromatography (CH$_2$Cl$_2$/MeOH 19:1) to yield **13** (233 mg, 58%) as a brown oil. ^{1}H NMR (400 MHz, CDCl$_3$): $\delta = 7.83$–7.74 (m, 6H), 7.74–7.66 (m, 3H), 7.62–7.54 (m, 6H), 7.04 (dt, $J = 15.9$, 7.1 Hz, N$^+$H),

3.02–2.90 (m, 2H), 1.64–1.54 (m, 2H), 1.16–0.98 (m, 8H), 0.75 ppm (t, $J = 7.1$ Hz, 3H); ^{13}C NMR (101 MHz, CDCl$_3$): $\delta = 134.8$ (d, $J = 2.9$ Hz, 3C), 133.8 (d, $J = 11.0$ Hz, 6C), 129.9 (d, $J = 13.1$ Hz, 6C), 121.5 (d, $J = 102.8$ Hz, 3C), 42.5 (d, $J = 2.8$ Hz), 31.6, 31.4 (d, $J = 5.9$ Hz), 28.6, 26.6, 22.5, 14.0 ppm; MS (ESI): m/z: 376.2 $[M+H]^+$.

Radiochemistry

All chemicals and solvents were purchased commercially from Aldrich and were used directly without further purification. [^{18}F]F$^-$ and [^{11}C]CO$_2$ were produced on the PETtrace cyclotron (GE Medical Systems, Uppsala) at the interdisciplinary PET center of the University of Würzburg. [^{18}F]Fluoride was produced by a ^{18}O(p,n)^{18}F reaction by irradiating 95% enriched [^{18}O]H$_2$O (3.0 mL) with protons (16.5 MeV), whereas [^{11}C]CO$_2$ was produced according to the ^{14}N(p,α)^{11}C nuclear reaction by irradiation of nitrogen gas containing 1% oxygen with a proton beam (16.5 MeV). Automatic synthesis module TRACERlab (FX-M, GE) was used for trapping the ^{11}CO$_2$ radioactivity and the following radiosynthesis, whereas radio fluorination was performed manually. Purification and analyses of the radioactive mixtures were performed by high-performance liquid chromatography (HPLC) with a Shimadzu system (Shimadzu, Duisburg, Germany) equipped with a UV detector ($\lambda = 220$ and 254 nm) and a γ-detector for radioactivity. The HPLC-purified radiotracers were diluted with injectable saline for further evaluation.

13-Methyl-5,8,13,13a-tetrahydro-6H-isoquinolino[1,2-b]quinazolin-10-yl (7-[^{18}F]fluoroheptyl)carbamate {[^{18}F]8}: [^{18}F]Fluoride was separated from enriched [^{18}O]H$_2$O by solid-phase extraction (SPE) using an anion-exchange cartridge (Sep-Pak Accell QMA light) and was then eluted with a solution of potassium carbonate (10 mg mL^{-1}, 400 µL) into a 5 mL conical vial containing a solution of kryptofix (12 mg) in dry MeCN (0.7 mL). The mixture was dried by the addition of dry MeCN (2×700 µL) under argon flow at 90°C. To the dried [^{18}F]fluoride, tosylate precursor **10** (4 mg) in MeCN (600 µL) was added, and the mixture was heated at 90°C for 10 min in the sealed vial. The mixture was cooled for 2 min, diluted with H$_2$O (2 mL) and injected into the HPLC system with a Synergi 4 µm Fusion-RP80 C$_{18}$ column (Phenomenex, 10×250 mm) and a mobile phase of MeCN/H$_2$O (50:50 v/v) at 4 mL min^{-1} ($t_R = $ 12.4 min). The collected product was diluted with H$_2$O (20 mL) and purified by SPE using a C$_{18}$ cartridge (Sep-Pak Plus C$_{18}$, Waters). After washing with H$_2$O (5 mL) and drying with argon, the radiolabeled precursor was eluted with MeCN, followed by addition of trifluoroacetic acid (TFA, 500 µL) at room temperature for 10 min. After evaporation of TFA, a solution of 4-nitrophenyl chloroformate (3 mg) in MeCN (200 µL) was added, which was followed by Et$_3$N (15 µL), and the mixture was heated at 90°C for 7 min. Afterward, a solution of phenol **4** (5 mg) in MeCN (100 µL) was added, and heating was continued for another 10 min. Purification was performed by radio-HPLC with a Synergi 4 µm Fusion-RP80 C$_{18}$ column (Phenomenex, 10×250 mm) and a mobile phase of 80:20 v/v MeOH/H$_2$O at 4 mL min^{-1}. The collected product was evaporated and formulated in 10% v/v EtOH in saline. The identity and radiochemical purity (98%) of the radiotracer were confirmed by co-injection with the corresponding standard by using reversed-phase HPLC with a Synergi 4 µm Fusion-RP80 C$_{18}$ column (Phenomenex, 4.6×150 mm) and a mobile phase of 80:20 v/v MeOH/H$_2$O at 1 mL min^{-1} ($t_R = 10.6$ min). Radiochemical yield: 17–22% ($n = 5$).

[^{11}C-Carbonyl]tetrahydro-13-methyl-5H-isoquinolino[1,2-b]quinazolin-10-yl heptylcarbamate {[^{11}C]14}: ^{11}CO$_2$ was dispensed in a stream of He into a target vial charged with n-heptyl-1,1,1-triphenyl-phosphanimine hydrochloride (**13**, 5 mg), DBU (4 mg), and

phenol **4** (3.6 mg) in anhydrous THF (100 μL) at −78 °C for 5 min. After $^{11}CO_2$ trapping, the mixture was heated at 60 °C for 10 min. Afterward, the solution was cooled to 40 °C and diluted with HPLC eluent (800 μL). The quenched mixture was purified by reversed-phase HPLC with a Synergi 4 μm Fusion-RP80 C_{18} column (Phenomenex, 10×250 mm) and a mobile phase of 80:20 *v/v* MeOH/H_2O at 4 mL min^{-1}. The desired product was collected, evaporated, and formulated in 10 % *v/v* EtOH in saline. The identity and radio-chemical purity (98 %) of the radiotracer were verified by co-injection with the corresponding standard by using reversed-phase HPLC with a Synergi 4 μm Fusion-RP80 C_{18} column (Phenomenex, 4.6×150 mm) and a mobile phase of 80:20 *v/v* MeOH/H_2O at 1 mL min^{-1} (t_R = 10.4 min). Radiochemical yield: 30–36 % (n = 4).

Enzyme inhibition

Enzyme inhibition and kinetics were investigated as recently described in detail.[22] AChE (EC 3.1.1.7, from human erythrocytes) was purchased from Sigma–Aldrich (Steinheim, Germany) and BChE (EC 3.1.1.8, from human serum) was kindly donated by Dr. Oksana Lockridge (University of Nebraska Medical Center). DTNB (Ellman's reagent) and ATC and BTC iodides were obtained from Fluka (Buchs, Switzerland). The stock solutions of the test compounds were prepared in EtOH with a concentration of $3.33×10^{-2}$ M (1 mM in assay) and were stepwise diluted with EtOH to a concentration at $3.33×10^{-8}$ M (1 nM in assay). For assay buffer preparation, potassium dihydrogen phosphate (3.12 g) was dissolved in H_2O (500 mL) and adjusted with a NaOH solution (0.2 M) to pH 8.0. Enzyme solutions were prepared with buffer to give 2.5 units mL^{-1}. DTNB (0.396 g) was dissolved in buffer (100 mL) to give a 0.01 M solution (0.3 mM in assay). ATC and BTC solutions were prepared in buffer with a concentration of 0.075 M (452 μM in assay).

The assay was performed at 25 °C as described in the following: A cuvette containing buffer (1.5 mL), the respective enzyme solution (50 μL), and DTNB solution (50 μL) was mixed with the test compound solution (50 μL). The mixture was incubated for 30 min, before ATC or BTC (depending on the enzyme, 10 μL) was added. The mixture was incubated for another 2.5 min before the absorption at λ = 412 nm was determined with a Shimadzu UVmini-1240 spectrophotometer. To measure full enzyme activity, the compound solution was replaced by EtOH. Each compound concentration was tested three times. The enzyme activity in percentage was plotted against the logarithm of the compound concentrations, from which the IC_{50} values were calculated by GraphPad Prism 5 Software.

Enzyme kinetics

Carbamoylation kinetics were investigated by following the protocol above by using the method described by Hosie et al. and Feaster et al.[29] The enzyme was pre-incubated for 5, 10, 20, 30, and 40 min of different inhibitor concentrations before addition of the substrate. Plotting the enzyme activity in percentage as a function of time for each inhibitor concentration gave nonlinear time-dependent inhibition curves, from which the apparent first-order constant k_{obs} was determined according to Equation (1):

$$A = A_0 e^{-k_{obs}×t} + A_\infty \tag{1}$$

in which A is the activity of the enzyme at a specific time t, A_0 is the activity at t = 0, A_∞ is the activity at t = ∞, and k_{obs} represents

the apparent first-order rate constant. By double reciprocal plotting of k_{obs}^{-1} against $[I]^{-1}$, K_C and k_3 can be obtained from Equation (2):

$$\frac{1}{k_{obs}} = \frac{K_c}{k_3} × \frac{1}{[I]} + \frac{1}{k_3} \tag{2}$$

Decarbamoylation kinetics were measured by incubating the enzyme with an inhibitor concentration that fully inhibited the enzyme for 1 h. This mixture was then diluted 1:1000 with assay buffer to prevent further enzyme inhibition. The assay was performed as described in the enzyme inhibition protocol at different time points after the dilution to determine recovery of enzyme activity. Uninhibited enzyme was treated by the same procedure to access control values for enzyme activity after dilution. Plotting the enzyme activity against different time points after dilution gave an exponential first-order kinetics, from which k_4 was calculated by Equation (3):

$$A = (1 - e^{k_4×t}) × (1 - A_0) + A_0 \tag{3}$$

in which A is the activity of the enzyme at a specific time t and A_0 is the activity at t = 0. All kinetic values were determined by using GraphPad Prism 5 Software.

Plasma stability

Compounds **8** (50 μM) and **14** (5 μM) were dissolved in human pooled plasma (n = 3) and placed at 37 °C with 5 % CO_2 in an incubator (Thermo Scientific) while shaking with 100 rpm (Unimax 1010 Schüttler, Heidolph, Schwalbach, Germany). Samples of 1 mL were taken after t = 0, 15, 30, 45, 60, 90, 120, and 240 min and were treated with ice-cold MeCN (1 mL). Precipitated proteins were removed by centrifugation (Microfuge 22R centrifuge, Beckman Coulter GmbH, Krefeld, Germany) with 8000 g for 10 min at 4 °C. The obtained clear solution was directly analyzed by reversed-phase HPLC (see the General section), and signal areas for compounds **8** and **14** were compared with the signal area at t = 0 min to investigate degradation of the compounds. To determine whether degradation of the compounds was ChE mediated, plasma samples were pre-incubated for 1 h with tacrine (50 μM) before the addition of the compounds. The samples were then treated as described above. To determine whether degradation of the compounds was enzymatic mediated, proteins were precipitated, and the remaining solution was used to determine the stability of **8** (50 μM). Each experiment was repeated three times. GraphPad Prism 5 Software was used to evaluate the data obtained.

Ex vivo autoradiography

The ex vivo tissue binding assay was conducted by using tissue slices of a healthy mouse brain (male, BALB/c). The frozen brain sample was sectioned in a cryostat at transverse 20 μm thickness and dried overnight at −20 °C. After 30 min of pre-incubation with assay media containing 150 mM NaCl, 5 mM EDTA, 0.1 mM bacitracin, and 50 mM Na_2HPO_4 at room temperature, tissue sections were incubated for 30 min with the assay media containing [^{18}F]**8** (cold mass dose = 301 nM, calculated from specific activity). To see the binding specificity, one section was incubated with the butyryl-cholinesterase inhibitor ethopropazine hydrochloride (60 μM) in assay media, and as control another section was incubated without inhibitor. The sections were rinsed in water, dried under cool air

stream, and finally exposed to a phosphor imaging plate for 3 h. Using a digital autoradiography system (CR 35 bio, Raytest), the binding distribution of the ^{18}F-labeled tracer was visualized as a digitalized image.

Acknowledgements

[1] a) E. J. Mufson, S. E. Counts, S. E. Perez, S. D. Ginsberg, *Expert Rev. Neurother.* **2008**, *8*, 1703; b) N. I. Bohnen, R. L. Albin, *Behav. Brain Res.* **2011**, *221*, 564; c) R. Schliebs, T. Arendt, *Behav. Brain Res.* **2011**, *221*, 555.

[2] a) A. Nordberg, C. Ballard, R. Bullock, T. Darreh-Shori, M. A. Somogyi, *Prim. Care Companion CNS Disord.* **2013**, *15*, 12r01412; b) A. V. Terry, Jr., J. J. Buccafusco, *J. Pharmacol. Exp. Ther.* **2003**, *306*, 821; c) E. Giacobini, *Int. J. Geriatr. Psychopharmacol.* **2003**, *18*, S1; d) H. Shinotoh, H. Namba, K. Fukushi, S. Nagatsuka, N. Tanaka, A. Aotsuka, T. Ota, S. Tanada, T. Irie, *Ann. Neurol.* **2000**, *48*, 194.

[3] a) N. H. Greig, T. Utsuki, Q.-S. Yu, X. Zhu, H. W. Holloway, T. Perry, B. Lee, D. K. Ingram, D. K. Lahiri, *Curr. Med. Res. Opin.* **2001**, *17*, 159; b) S. Darvesh, D. A. Hopkins, C. Geula, *Nat. Rev. Neurosci.* **2003**, *4*, 131.

[4] a) M.-M. Mesulam, A. Guillozet, P. Shaw, A. Levey, E. G. Duysen, O. Lockridge, *Neuroscience* **2002**, *110*, 627; b) J. Hartmann, C. Kiewert, E. G. Duysen, O. Lockridge, N. H. Greig, J. Klein, *J. Neurochem.* **2007**, *100*, 1421; c) Y. Furukawa-Hibi, T. Alkam, A. Nitt, A. Matsuyama, H. Mizoguchi, K. Suzuki, S. Moussaoui, Q.-S. Yu, N. H. Greig, T. Nagai, K. Yamada, *Behav. Brain Res.* **2011**, *225*, 222; d) N. H. Greig, T. Utsuki, D. K. Ingram, Y. Wang, G. Pepeu, C. Scali, Q.-S. Yu, J. Mamczarz, H. W. Holloway, T. Giordano, D. Chen, K. Furukawa, K. Sambamurti, A. Brossi, D. K. Lahiri, *Proc. Natl. Acad. Sci. USA* **2005**, *102*, 17213; e) T. Maurice, M. Strehaiano, N. Siméon, C. Bertrand, A. Chatonne, *Behav. Brain Res.* **2016**, *296*, 351; f) R. S. Naik, J. Hartmann, C. Kiewert, E. G. Duysen, O. Lockridge, J. Klein, *J. Pharm. Pharm. Sci.* **2009**, *12*, 79; g) T. Darreh-Shori, S. Brimijoin, A. Kadir, O. Almkvist, A. Nordberg, *Neurobiol. Dis.* **2006**, *24*, 326.

[5] a) K. Mizukami, H. Akatsu, E. E. Abrahamson, Z. Mi, M. D. Ikonomovic, *Neuropathology* **2016**, *36*, 135–145; b) M. A. Morán, E. J. Mufson, P. Gómez-Ramos, *Acta Neuropathol.* **1993**, *85*, 362; c) S. Darvesh, *Chem.-Biol. Interact.* **2013**, *203*, 354; d) S. Darvesh, M. K. Cash, G. A. Reid, E. Martin, A. Mitnitski, C. Geula, *J. Neuropathol. Exp. Neurol.* **2012**, *71*, 2.

[6] G. A. Reid, S. Darvesh, *Neuroscience* **2015**, *298*, 424.

[7] a) O. Lockridge, *Pharmacol. Ther.* **2015**, *148*, 34; b) Y. Ashani, *Drug Dev. Res.* **2000**, *50*, 298; c) B. Li, M. Sedlacek, I. Manoharan, R. Boopathy, E. G. Duysen, P. Masson, O. Lockridge, *Biochem. Pharmacol.* **2005**, *70*, 1673.

[8] a) B. Li, E. G. Duysen, O. Lockridge, *Chem.-Biol. Interact.* **2008**, *175*, 88; b) T. Iwasaki, M. Yoneda, A. Nakajima, Y. Terauchi, *Intern. Med.* **2007**, *46*, 1633.

[9] K. K. Sato, T. Hayashi, I. Maeda, H. Koh, N. Harita, S. Uehara, Y. Onishi, K. Oue, Y. Nakamura, G. Endo, H. Kambe, K. Fukuda, *Clin. Endocrinol.* **2014**, *80*, 362.

[10] a) M. Stojanov, A. Stefanović, G. Džingalašević, S. Mandić-Radić, M. Prostran, *Clin. Biochem.* **2011**, *44*, 623; b) V. M. Alcântara, E. A. Chautard-Freire-Maia, M. Scartezini, M. S. J. Cerci, K. Braun-Prado, G. Picheth, *Scand. J. Clin. Lab. Invest.* **2002**, *62*, 399.

[11] a) T. Kikuchi, T. Okamura, M.-R. Zhang, T. Irie, *J. Labelled Compd. Radiopharm.* **2013**, *56*, 172; b) J. P. Holland, S. H. Liang, B. H. Rotstein, T. L. Collier, N. A. Stephenson, I. Greguric, N. Vasdev, *J. Labelled Compd. Radiopharm.* **2014**, *57*, 323.

[12] a) C. Haense, E. Kalbe, K. Herholz, C. Hohmann, B. Neumaiera, R. Kraisa, W.-D. Heiss, *Neurobiol. Aging* **2012**, *33*, 867; b) H. Namba, K. Fukushi, S. Nagatsuka, M. Iyo, H. Shinotoh, S. Tanada, T. Irie, *Methods* **2002**, *27*, 242; c) K. Herholz, *Eur. J. Nucl. Med. Mol. Imaging* **2008**, *35*, 25; d) M. Iyo, H. Namba, K. Fukushi, H. Shinotoh, S. Nagatsuka, T. Suhara, Y. Sudo, K. Suzuki, T. Irie, *Lancet* **1997**, *349*, 1805; e) S. Nagatsuka, K. Fukushi, H. Shinotoh, H. Namba, M. Iyo, N. Tanaka, A. Aotsuka, T. Ota, S. Tanada, T. Irie, *J. Cereb. Blood Flow Metab.* **2001**, *21*, 1354.

[13] a) J. L. Musachio, J. E. Flesher, U. A. Scheffel, P. Rauseo, J. Hilton, W. B. Mathews, H. T. Ravert, R. F. Dannals, J. J. Frost, *Nucl. Med. Biol.* **2002**, *29*, 547; b) D. H. Kim, Y. S. Choe, J. Y. Choi, K.-H. Lee, B.-T. Kim, *Nucl. Med. Biol.* **2011**, *38*, 541; c) E. K. Ryu, Y. S. Choe, E. Y. Park, J.-Y. Paik, Y. R. Kim, K.-H. Lee, Y. Choi, S. E. Kim, B.-T. Kim, *Nucl. Med. Biol.* **2005**, *32*, 185; d) H. Kimura, T. Kawai, Y. Hamashima, H. Kawashima, K. Miura, Y. Nakaya, M. Hirasawa, K. Arimitsu, T. Kajimoto, Y. Ohmomo, *Bioorg. Med. Chem.* **2014**, *22*, 285; e) F. De Vos, P. Santens, H. Vermeirsch, I. Dewolf, F. Dumont, G. Slegers, R. A. Dierckx, J. De Reuck, *Nucl. Med. Biol.* **2000**, *27*, 745; f) B. Tavitian, S. Pappata, S. Bonnot-Lours, C. Prenant, A. Jobert, C. Crouzel, L. Di Giamberardino, *Eur. J. Pharmacol.* **1993**, *236*, 229.

[14] a) S. L. James, S. K. Ahmed, S. Murphy, M. R. Braden, Y. Belabassi, H. F. VanBrocklin, C. M. Thompson, J. M. Gerdes, *ACS Chem. Neurosci.* **2014**, *5*, 519; b) G. Blomqvist, B. Tavitian, S. Pappata, C. Crouzel, A. Jobert, I. Doignon, L. Di Giamberardino, *J. Cereb. Blood Flow Metab.* **2001**, *21*, 114.

[15] a) S. Nag, L. Lehmann, G. Kettschau, M. Toth, T. Heinrich, A. Thiele, A. Varrone, C. Halldin, *Bioorg. Med. Chem.* **2013**, *21*, 6634; b) S. Nag, L. Lehmann, G. Kettschau, T. Heinrich, A. Thiele, A. Varrone, B. Gulyas, C. Halldin, *Bioorg. Med. Chem.* **2012**, *20*, 3065; c) B. Gulyás, E. Pavlova, P. Kása, K. Gulya, L. Bakota, S. Várszegi, E. Keller, M. Csilla Horváth, S. Nag, I. Hermecz, K. Magyar, C. Halldin, *Neurochem. Int.* **2011**, *58*, 60; d) S. Nag, P. Fazio, L. Lehmann, G. Kettschau, T. Heinrich, A. Thiele, M. Svedberg, N. Amini, S. Leesch, A. Catafau, J. Hannestad, A. Varrone, C. Halldin, *J. Nucl. Med.* **2016**, *57*, 315–320; e) J. S. Fowler, J. Logan, G.-J. Wang, N. D. Volkow, W. Zhu, D. Franceschi, N. Pappas, R. Ferrieri, C. Shea, V. Garza, Y. Xu, R. R. MacGregor, D. Schlyer, S. J. Gatley, Y.S. Ding, D. Alexoff, *J. Nucl. Med.* **2002**, *43*, 1331.

[16] a) C. Wang, M. S. Placzek, G. C. Van de Bittner, F. A. Schroeder, J. M. Hooker, *ACS Chem. Neurosci.* **2016**, *7*, 484–489; b) J. W. Hicks, J. Parkes, J. Tong, S. Houle, N. Vasdev, A. A. Wilson, *Nucl. Med. Biol.* **2014**, *41*, 688.

[17] a) P. M. Rusjan, A. A. Wilson, I. Mizrahi, I. Boileau, S. E. Chavez, N. J. Lobaugh, S. J. Kish, S. Houle, J. Tong, *J. Cereb. Blood Flow Metab.* **2013**, *33*, 407; b) A. A. Wilson, A. Garcia, J. Parkes, S. Houle, J. Tong, N. Vasdev, *Nucl. Med. Biol.* **2011**, *38*, 247; c) B. H. Rotstein, H.-Y. Wey, T. M. Shoup, A. A. Wilson, S. H. Liang, J. M. Hooker, N. Vasdev, *Mol. Pharm.* **2014**, *11*, 3832; d) A. A. Wilson, J. W. Hicks, O. Sadovski, J. Parkes, J. Tong, S. Houle, C. J. Fowler, N. Vasdev, *J. Med. Chem.* **2013**, *56*, 201.

[18] a) J. S. Fowler, J. Logan, N. D. Volkow, G.-J. Wang, R. R. MacGregor, Y.-S. Ding, *Methods* **2002**, *27*, 263; b) J. Logan, J. S. Fowler, Y.-S. Ding, D. Franceschi, G.-J. Wang, N. D. Volkow, C. Felder, D. Alexoff, *J. Cereb. Blood Flow Metab.* **2002**, *22*, 1367.

[19] M. R. Kilbourn, S. E. Snyder, P. S. Sherman, D. E. Kuhl, *Synapse* **1996**, *22*, 123.

[20] a) J. S. Fowler, R. R. MacGregor, A. P. Wolf, C. D. Arnett, S. L. Dewey, D. Schlyer, D. Christman, J. Logan, M. Smith, H. Sachs, S. M. Aquilonius, P. Bjurling, C. Halldin, P. Hartvig, K. L. Leenders, L. Lundqvist, L. Oreland, C.-G. Stalnacke, B. Langström, *Science* **1987**, *235*, 481; b) J. S. Fowler, N. D. Volkow, G.-J. Wang, J. Logan, N. Pappas, C. Shea, R. MacGregor, *Neurobiol. Aging* **1997**, *18*, 431; c) J. Logan, J. S. Fowler, N. D. Volkow, G.-J. Wang, R. R. MacGregor, C. Shea, *Nucl. Med. Biol.* **2000**, *27*, 43.

[21] a) S. E. Snyder, N. Gunupudi, P. S. Sherman, E. R. Butch, M. B. Skaddan, M. R. Kilbourn, R. A. Koeppe, D. E. Kuhl, *J. Cereb. Blood Flow Metab.* **2001**, *21*, 132; b) A. Roivainen, J. Rinne, J. Virta, T. Järvenpää, S. Salomäki, M. Yu, K. Någren, *J. Nucl. Med.* **2004**, *45*, 2032; c) J. R. Virta, T. Tolvanen, K. Någren, A. Brück, A. Roivainen, J. O. Rinne, *J. Nucl. Med.* **2008**, *49*, 347; d) D. E. Kuhl, R. A. Koeppe, S. E. Snyder, S. Minoshima, K. A. Frey, M. R. Kilbourn, *Ann. Neurol.* **2006**, *59*, 13; e) I. R. Macdonald, G. A. Reid, E. E. Joy, I. R. Pottie, G. Matte, S. Burrell, G. Mawko, E. Martin, S. Darvesh, *Mol. Imaging Biol.* **2011**, *13*, 1250.

[22] a) E. Sawatzky, S. Wehle, B. Kling, G. Bringmann, C. A. Sotriffer, *J. Med. Chem.* **2016**, *59*, 2067; b) F. H. Darras, B. Kling, J. Heilmann, M. Decker,

ACS Med. Chem. Lett. **2012**, *3*, 914; c) G. Huang, B. Kling, F. H. Darras, J. Heilmann, M. Decker, *Eur. J. Med. Chem.* **2014**, *81*, 15.

[23] E. Sawatzky, J. Bukowczan, M. Decker, *Tetrahedron Lett.* **2014**, *55*, 2973.

[24] O. Sadovski, J. W. Hicks, J. Parkes, R. Raymond, J. Nobrega, S. Houle, M. Cipriano, C. J. Fowler, N. Vasdev, A. A. Wilson, *Bioorg. Med. Chem.* **2013**, *21*, 4351.

[25] a) J. W. Hicks, J. Parkes, O. Sadovski, J. Tong, S. Houle, N. Vasdev, A. A. Wilson, *Nucl. Med. Biol.* **2013**, *40*, 740; b) B. H. Rotstein, S. H. Liang, J. P. Holland, T. Lee Collier, J. M. Hooker, A. A. Wilson, N. Vasdev, *Chem. Commun.* **2013**, *49*, 5621; c) A. A. Wilson, A. Garcia, S. Houle, O. Sadovski, N. Vasdev, *Chem. Eur. J.* **2011**, *17*, 259.

[26] E. W. Van Tilburg, A. D. Windhorst, M. van der Mey, J. D. M. Herscheid, *J. Labelled Compd. Radiopharm.* **2006**, *49*, 321.

[27] a) C. G. Carolan, G. P. Dillon, J. M. Gaynor, S. Reidy, S. A. Ryder, D. Khan, J. F. Marquez, J. F. Gilmer, *J. Med. Chem.* **2008**, *51*, 6400; b) S. Darvesh, K. V. Darvesh, R. S. McDonald, D. Mataija, R. Walsh, S. Mothana, O. Lockridge, E. Martin, *J. Med. Chem.* **2008**, *51*, 4200.

[28] a) A. K. Ghosh, M. Brindisi, *J. Med. Chem.* **2015**, *58*, 2895; b) J. C. Powers, J. L. Asgian, Ö. D. Ekici, K. E. James, *Chem. Rev.* **2002**, *102*, 4639.

[29] a) L. Hosie, L. D. Sutton, D. M. Quinn, *J. Biol. Chem.* **1987**, *262*, 260; b) S. R. Feaster, K. Lee, N. Baker, D. Y. Hui, D. M. Quinn, *Biochemistry* **1996**, *35*, 16723.

CHEMMEDCHEM

Chemistry & Drug Discovery

Supporting Information

A Novel Way To Radiolabel Human Butyrylcholinesterase for Positron Emission Tomography through Irreversible Transfer of the Radiolabeled Moiety

Edgar Sawatzky,[a] Ehab Al-Momani,[b] Ryohei Kobayashi,[b] Takahiro Higuchi,[b] Samuel Samnick,[b] and Michael Decker*[a]

cmdc_201600223_sm_miscellaneous_information.pdf

Contents:

^{18}F-labelling approach reported by Sadovski et al.

1) Development of precursors

In the original protocol for ^{18}F-labelling reported by Sadovski *et al.*,[1] an *N*-Boc protected precursor was labeled and fused with an activated phenol to yield the carbamate based radiotracer in three steps (**Scheme S1A**). To synthesize radiotracer **[^{18}F]8** following this approach, precursor **10** and an activated phenol of the general structure **15** were necessary (**Scheme S1B**).
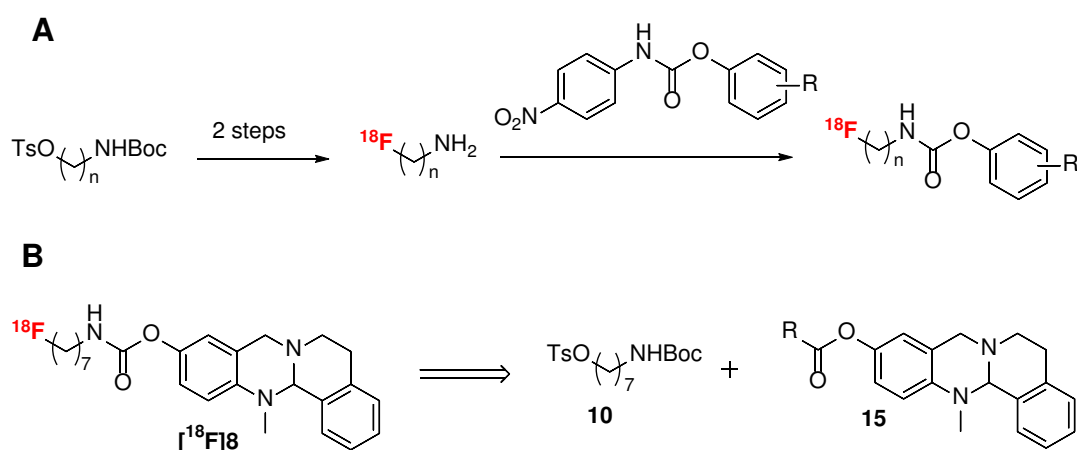
Scheme S1. (A) Approach reported by Sadovski *et al.*[1]. (B) Retrosynthesis of **[^{18}F]8** using the reported approach.

The synthesis of **10** was performed smoothly as described in the main text of the manuscript. Unfortunately, the activation of phenol **4** with nitrophenyl chloroformate as well as with triphosgene towards compound **16** and **18** failed (**Scheme S2**). In general we observed, that strong electrophiles applied on phenol **4** always caused degradation of the reaction mixture resulting in failure of the reaction (compare compound **6** in the main text); probably as a result of the high reactivity of the tertiary nitrogen in the tetrahydroquinazoline system. Only activation with CDI towards **17** was conducted successfully without any degradation. As a common method to further increase the leaving group character of the imidazole moiety in compound **17**, selective *N*-methylation of the aromatic nitrogen is described in literature.[2] Interestingly, such an methylation did not yield the expected compound **19** rather than compound **20** being methylated at the tertiary nitrogen of the tetrahydroquinazoline core as

revealed by 2D-NMR. This finding supports the hypothesis for the high reactivity of the tertiary nitrogen which causes problems when applying strong electrophiles.
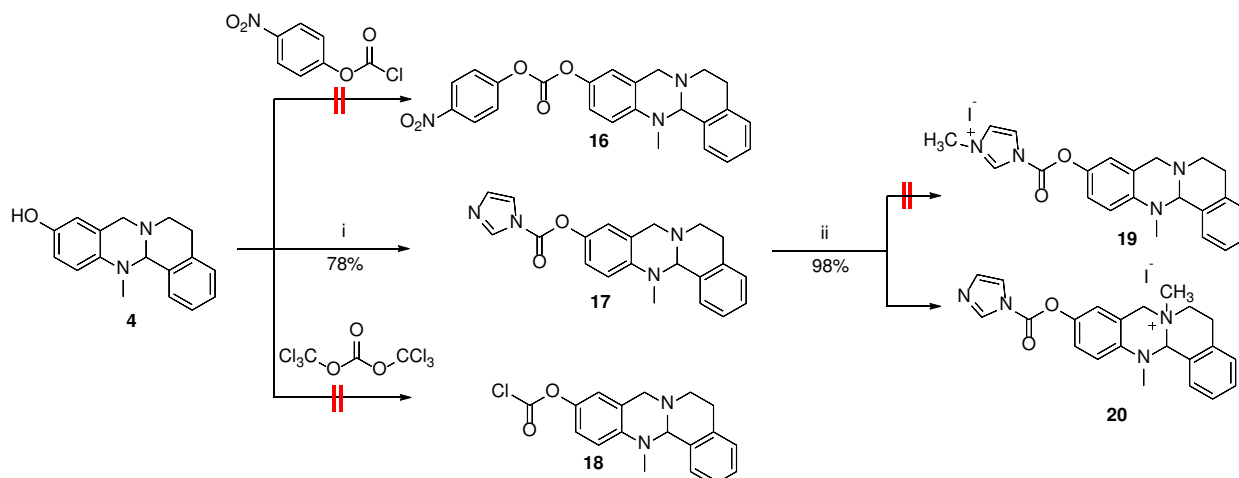
Scheme S2. Reagents and conditions: (i) CDI, CH₃CN/H₂O, 1 h, rt, (ii) CH₃I, CH₃CN, 24 h, rt.

However, fusing compound **17** with a simple heptylamine in test reactions did not yield carbamate **14** but resulted in the release of **4** under the conditions applied (**Scheme S3**). Therefore we did not follow up the original protocol reported by Sadovski *et al.*[1] (**Scheme S1A**) as the synthesis of a suitable activated phenol with the general structure **15** (**Scheme S1B**) was not achieved.
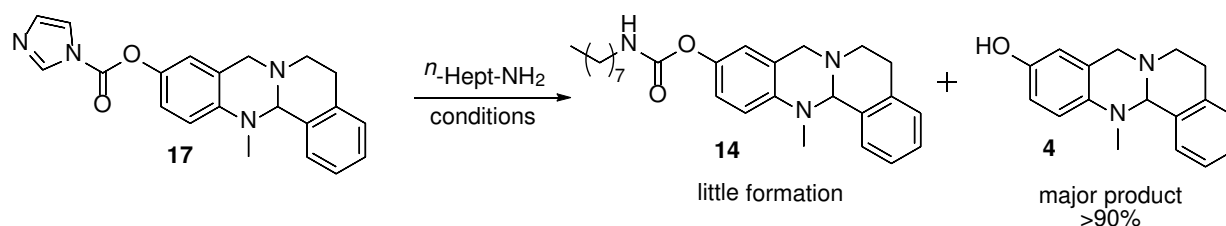
Scheme S3. Test reactions for carbamate formation using the activated phenol **17**.

2) Syntheses and spectral data

13-Methyl-6,8,13,13a-tetrahydro-5H-isoquinolino[1,2-b]quinazolin-10-yl   1H-imidazole-1-carboxylate **17**: A solution of 13-methyl-6,8,13,13a-tetrahydro-5H-isoquinolino[1,2-b]quinazolin-10-ol **4** (100 mg, 0.38 mmol, 1 eq.) in $CH_3CN:H_2O$ (1:1) was treated with CDI (73 mg, 0.45 mmol, 1.2 eq.). The mixture was stirred for 1 h at room temperature. Subsequently, water was added and the precipitated solid was filtered. The solid was dries in an air stream to obtain 13-methyl-6,8,13,13a-tetrahydro-5H-isoquinolino[1,2-b]quinazolin-10-yl 1H-imidazole-1-carboxylate **17** (105 mg, 78%) as white solid; mp 82-84 °C. ^{1}H-NMR (400 MHz, DMSO-d_6): δ = 8.45 - 8.40 (m, 1H), 7.75 (t, J = 1.5 Hz, 1H), 7.35 - 7.30 (m, 1H), 7.28 - 7.22 (m, 2H), 7.22 - 7.17 (m, 1H), 7.17 - 7.10 (m, 2H), 7.06 (d, J = 2.7 Hz, 1H), 6.97 (d, J = 8.9 Hz, 1H), 4.90 (s, 1H), 4.03 (d, J = 16.0 Hz, 1H), 3.85 (d, J = 16.1 Hz, 1H), 3.19 (dt, J = 11.1, 5.4 Hz, 1H), 3.03 - 2.91 (m, 1H), 2.81 (dt, J = 16.2, 5.3 Hz, 1H), 2.78 - 2.65 (m, 1H), 2.58 (s, 3H) ppm. ^{13}C-NMR (101 MHz, DMSO-d_6): δ = 147.5, 146.0, 142.3, 137.7, 135.7, 133.8, 130.5, 128.8, 128.4, 127.5, 125.5, 124.7, 119.9, 119.2, 118.4, 117.9, 75.1, 54.6, 46.4, 37.2, 27.6 ppm. ESI-MS: m/z: calcd: 360.2, found: 361.2 [M+H]$^+$.

10-((1H-Imidazole-1-carbonyl)oxy)-7,13-dimethyl-5,6,7,8,13,13a-hexahydroisoquinolino [1,2-b]quinazolin-7-ium iodide **20**: 13-Methyl-6,8,13,13a-tetrahydro-5H-isoquinolino[1,2-b]quinazolin-10-yl 1H-imidazole-1-carboxylate **17** (100 mg, 0.28 mmol, 1 eq.) was dissolved in CH_3CN (2 mL) and treated with MeI (61 µL, 0.97 mmol, 3.5 eq.). The mixture was stirred for 24 h at room temperature. The reaction mixture was evaporated to dryness to obtain 10-((1H-imidazole-1-carbonyl)oxy)-7,13-dimethyl-5,6,7,8,13,13a-hexahydroisoquinolino[1,2-b]quinazolin-7-ium iodide **20** (136 mg, 98%) as white solid; mp 200-206 °C. ^{1}H-NMR (400 MHz, DMSO-d_6): δ = 8.38 (s, 1H), 7.70 (t, J = 1.4 Hz, 1H), 7.46 - 7.31 (m, 3H), 7.27 (t, J = 7.4 Hz, 1H), 7.21 (d, J = 9.0 Hz, 1H), 7.14 (dt, J = 3.3, 2.7 Hz, 2H), 7.06 (d, J = 2.6 Hz, 1H), 6.34 (s, 1H), 4.57 (d, J = 16.7 Hz, 1H), 4.44 (d, J = 16.6 Hz, 1H), 4.19 - 4.04 (m, 2H), 3.52 (s, 3H), 3.49 - 3.38 (m, 1H), 3.28 (dd, J = 18.8, 5.3 Hz, 1H), 3.21 (s, 3H) ppm. ^{13}C-NMR (101 MHz, DMSO-d_6): δ = 147.7, 142.8, 138.2, 137.9, 132.6, 131.3, 131.0, 129.9, 127.9, 126.7, 122.8, 120.6, 118.4, 116.0, 115.1, 82.3, 58.2, 53.5, 49.3, 41.1, 23.2 ppm. ESI-MS m/z: calcd: 375.1, found: 375.1 [M]$^+$.

Additional References

[1] O. Sadovski, J. W. Hicks, J. Parkes, R. Raymond, J. Nobrega, S. Houle, M. Cipriano, C. J. Fowler, N. Vasdev, A. A. Wilson, *Bioorg. Med. Chem.* **2013**, *21*, 4351.

[2] V. A. Vaillard, M. González, J. P. Perotti, R. J. A. Grau, S. E. Vaillard, *RSC Adv.* **2014**, *4*, 13012.

Appendix 2

Discovery of Highly Selective and Nanomolar Carbamate-Based Butyrylcholinesterase Inhibitors by Rational Investigation into Their Inhibition Mode.

Article published at:

http://pubs.acs.org/doi/abs/10.1021/acs.jmedchem.5b01674

Discovery of Highly Selective and Nanomolar Carbamate-Based Butyrylcholinesterase Inhibitors by Rational Investigation into Their Inhibition Mode

Edgar Sawatzky,[†] Sarah Wehle,[†] Beata Kling,[‡] Jan Wendrich,[§] Gerhard Bringmann,[§] Christoph A. Sotriffer,[†] Jörg Heilmann,[‡] and Michael Decker*[,†]

[†]Pharmazeutische und Medizinische Chemie, Institut für Pharmazie und Lebensmittelchemie, Universität Würzburg, Am Hubland, D-97074 Würzburg, Germany

[‡]Lehrstuhl für Pharmazeutische Biologie, Institut für Pharmazie, Universität Regensburg, Universitätsstraße 31, D-93053 Regensburg, Germany

[§]Lehrstuhl für Organische Chemie I, Institut für Organische Chemie, Universität Würzburg, Am Hubland, D-97074 Würzburg, Germany

🅢 Supporting Information

ABSTRACT: Butyrylcholinesterase (BChE) is a promising target for the treatment of later stage cognitive decline in Alzheimer's disease. A set of pseudo-irreversible BChE inhibitors with high selectivity over hAChE was synthesized based on carbamates attached to tetrahydroquinazoline scaffolds with the 2-thiophenyl compound **2p** as the most potent inhibitor of eqBChE (K_C = 14.3 nM) and also of hBChE (K_C = 19.7 nM). The inhibitors transfer the carbamate moiety onto the active site under release of the phenolic tetrahydroquinazoline scaffolds that themselves act as neuro-

2p
IC$_{50}$ (hBChE) = 13 nM
K_C = 19.7 ± 0.9 nM
k_3 = 0.32 ± 0.01 min^{-1}
k_3/K_C = 16.24 ± 0.64 μM^{-1}min^{-1}

protectants. By combination of kinetic data with molecular docking studies, a plausible binding model was probed describing how the tetrahydroquinazoline scaffold guides the carbamate into a close position to the active site. The model explains the influence of the carrier scaffold onto the affinity of an inhibitor just before carbamate transfer. This strategy can be used to utilize the binding mode of other carbamate-based inhibitors.

■ INTRODUCTION

In 2010 the World Alzheimer Report[1,2] estimated the worldwide societal costs of dementia to a value of 604 billion dollars with an increase of prevalence from 35 million people in 2010 to 115 million people in 2050. The most common form of dementia is Alzheimer's disease (AD), a progressive neurodegenerative disorder of multifactorial nature characterized by the loss of cognitive abilities through the death of central neuronal cells.

Although the initial pathophysiological reasons in AD are still not yet fully understood, the pathogenesis is mainly determined by several specific biochemical changes,[3,4] namely, (i) aggregation of toxic β-amyloid oligomers[5,6] followed by deposition of larger insoluble fibers in advanced amyloid plaques,[7] (ii) hyperphosphorylation of tau proteins and their aggregation into toxic neurofibrillary tangles,[8–10] (iii) oxidative stress with subsequent cell death,[11,12] and (iv) the imbalance of the two major neurotransmitters acetylcholine (ACh) and glutamate which are necessary for cognition.[13–15] Although these multifactorial changes provide a broad spectrum of possible therapeutic targets, there are only four approved drugs on the market, all targeting the neurotransmitter systems. The non-competitive antagonist memantine targets the glutamatergic system through binding at the ionotropic glutamate receptor

NMDA. Besides, the cholinergic system is affected by the acetylcholinesterase (AChE) inhibitors rivastigmine, donepezil, and galantamine. Several clinical studies on these cholinesterase inhibitors[16–18] have proven their positive effectiveness with regard to cognition, global cognitive functions, and daily activities, but due to their (only) symptomatic mode of action, no curative treatment is achieved.

The decline of cognition during AD is attributed to the progressive loss of cholinergic neurons and therefore to a deficit of ACh. This deficit is permanently enhanced through the decomposition of available ACh in the synaptic gap of neuronal cells by AChE that normally regulates the amount of ACh in healthy brain. Therefore, inhibition of AChE can compensate the lack of ACh and in consequence improve cognitive abilities. In advanced AD the level of AChE drops down to 90% compared to the healthy brain,[19–21] making it impractical as a target for therapeutic use in later stages of AD. Clinical trials are in striking accordance with the lack of effectiveness of AChE inhibitors in these stages of AD. On the other hand, several studies[20–23] have shown increased levels of the isoenzyme butyrylcholinesterase

(BChE) in AD patients in brain areas that are relevant for cognition. Although the role of BChE for ACh hydrolysis in healthy brain is only of minor impact, there is strong evidence that BChE compensates the loss of neuronal AChE in progressed AD and therefore takes over the function of AChE. This hypothesis is supported by an AChE knockout mouse model[24] in which mice did not suffer on cholinergic hyperactivation in the absence of AChE as ACh hydrolysis is controlled by BChE. These data are in agreement with other reports[18,25−28] showing a positive correlation between selective BChE inhibition, improved cognitive performance, and memory acquisition. In a recent in vivo study with BChE knockout mice it was shown that in contrast to wild-type mice, lipid peroxidation and ACh levels were not changed after treatment with amyloid-β_{25-35} and learning capacities were attenuated.[28] Therefore, inhibition of BChE might well constitute a therapeutic target for clinical use in progressed AD, where AChE inhibitors fail.

And further, BChE might be of clinical interest not only for AD treatment, as it was found to be involved in the regulation of the serum metabolism in context with obesity,[29,30] insulin resistance and diabetes mellitus,[30,31] and cardiovascular risk factors.[32,33] Accordingly, for investigation into the role of BChE in these research fields, the search for highly active and selective inhibitors and their development are of high importance.

Selective targeting of BChE over AChE is a challenging task, as sequence comparison of the two isoforms *h*AChE and *h*BChE shows an identity of 49% and a similarity of 66% (see Supporting Information). Although the catalytic active site (CAS), where hydrolysis of the neurotransmitter is mediated,[34] of both enzymes is highly conserved, the two enzymes show differences in the space they provide for a substrate or inhibitor, respectively. These differences are notably seen in the amino acids forming the gorge of the binding site and the acyl binding pocket (for a more detailed comparison see ref 35).

However, selective inhibition of BChE can be achieved by targeting the CAS with carbamate-based inhibitors. These inhibitors generally feature a carrier scaffold guiding a carbamate moiety into the correct position in the enzyme, successively followed by the transfer of the carbamate moiety onto the serine of the CAS under release of the carrier scaffold (see Figure 1). In the literature the development of pseudo-irreversible ChE

inhibitors is in most cases limited to the modification of the transferable carbamate moiety,[36−39] but at the current stage only very limited information with regard to the binding mode of the carrier scaffold itself is available (Figure 1).[40−43]

For rational design of carbamate-based BChE inhibitors there is a strong requirement for enhanced knowledge of the interactions between the carrier scaffold and the enzyme. Only a well bound carrier in the correct position offers the possibility for carbamate transfer and thus for enzyme inhibition. Concise knowledge about an appropriate experimental approach will of course also be useful for the development of other types of pseudo-irreversible inhibitors. Surprisingly, to our knowledge such experimental investigations are lacking to a large degree. In the present study we designed, synthesized, and investigated a set of bicyclic compounds as selective BChE inhibitors to explore the binding mode of the carrier scaffold into the active center of BChE by chemical modifications of the carrier scaffold. Subsequently and in part parallel to these efforts, a molecular docking model was established that describes a suitable binding mode.

Starting point of our investigation were tetrahydroquinazo-line-derived scaffolds that can be used as templates for the synthesis of potent AChE and BChE inhibitors.[44−48] Further incorporation of a carbamate moiety into these molecular templates resulted in highly selective and nanomolar active BChE inhibitors with the tetracyclic *n*-heptyl carbamate **1** as the most potent one (Figure 2a).[36,47] This inhibitor binds to the active site of BChE with its tetrahydroquinazoline scaffold followed by the pseudo-irreversible transfer of the carbamate moiety onto the serine of the CAS ("pseudo" because the carbamate moiety slowly hydrolyzes off from the serine and enzyme activity is reconstituted). In consequence, this mode of action leads to release of the heterocyclic carrier scaffold which itself acts with its *p*-aminohydroquinoline moiety as an antioxidant preventing oxidative-stress-induced cell death (Figure 2b).[36,47]

Since the tetracyclic moiety of compound **1** is difficult to be modified comprehensively and systematically in a chemical sense with regard to SARs, the tetrahydroquinazoline-based scaffold was "opened" to access compound series **2** and **3** (Figure 2a), which enables the conduction of SARs. These compounds can be modified at the aryl residue site, and they can also be further exploited by introduction of suitable bulky *N*-site groups. In a previous study,[47] we had already investigated the role of the carbamate moiety on BChE inhibition by introducing the carbamate group of several known selective BChE inhibitors, like eptastigmine bearing a *n*-heptyl residue, rivastigmine bearing an ethylmethyl residue, or cymserine bearing a 4-*i*-Pr-phenyl residue at the carbamate site. We found that a *n*-heptyl residue incorporated into the carrier scaffold leads to the most affine and BChE-selective inhibitor in this series (compound **1**), and therefore we decided for compound series **2** and **3** to keep this residue constant for SAR investigations.[47]

With the target structures synthesized we performed kinetic studies to evaluate the mode of action and computational studies. We combined the kinetic data with the molecular docking studies and established a model for binding of these inhibitors to the enzyme. This model describes the binding mode of the tetrahydroquinazoline scaffolds just before carbamate transfer occurs onto BChE and therefore explains altered affinity and potency of these inhibitors based on the carrier scaffold. The scaffolds themselves take only little part in BChE inhibition, but they are guiding the carbamate moiety into the correct position

Inhibitors investigated by changing the carrier scaffold
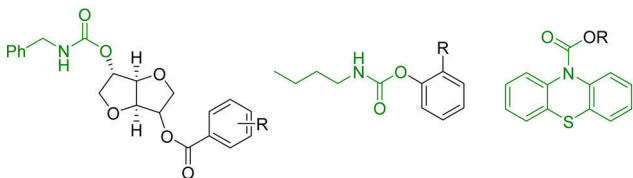
Inhibitors investigated by changing the carbamate moiety
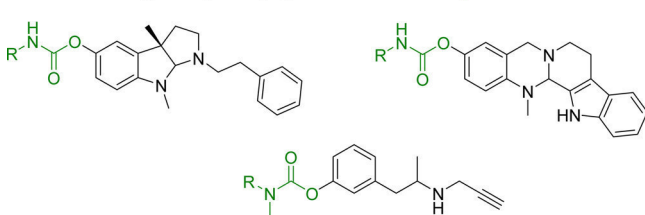
Figure 1. Previously described carbamate-based structures investigated as ChE inhibitors by altering the carrier scaffold[40,42,43] (top) and by altering the carbamate moiety.[36−38] Carrier scaffolds are shown in black, carbamate moieties in green.

2a

previous work   this work

IC$_{50}$(AChE) > 500 μM
IC$_{50}$(BChE) = 11.9 μM

no inhibition of AChE
IC$_{50}$(BChE) = 60 nM

2b

moiety to be transferred

carrier scaffold

enzyme

neuroprotectant

pseudo-irreversibly inhibited enzyme
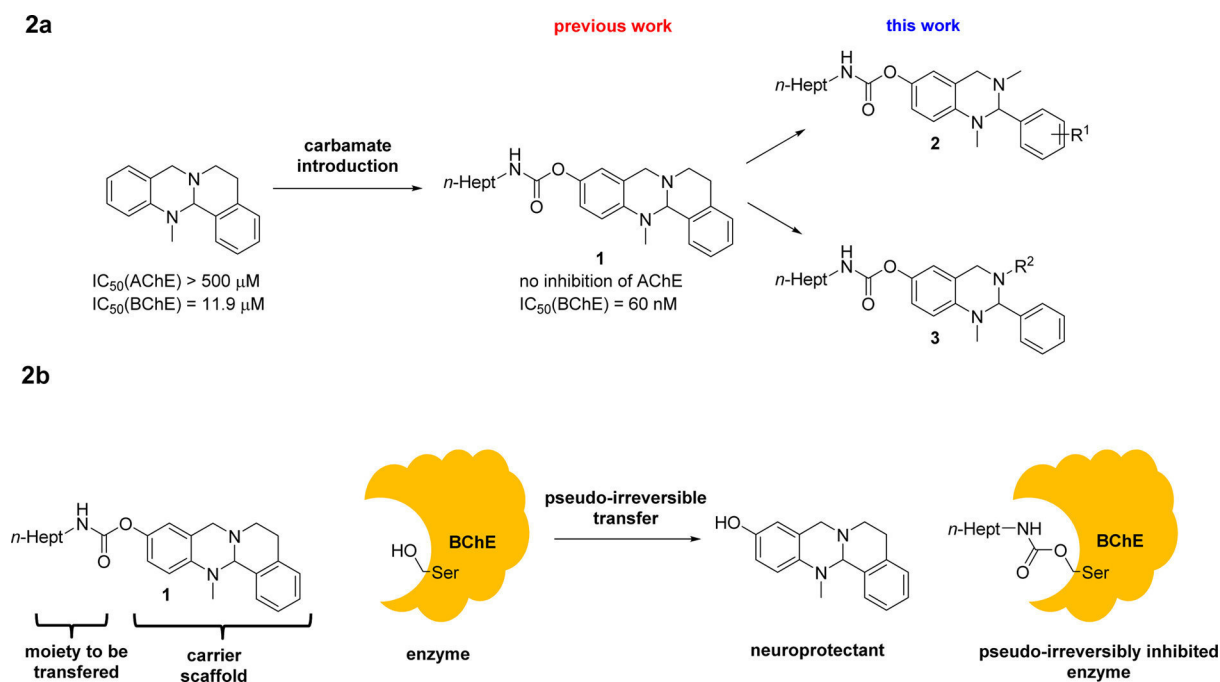
Figure 2. (a) Development of carbamate-based inhibitor **1** and modifications toward compounds **2** and **3** for SAR investigations of tetrahydroquinazoline-based carbamates. (b) Mode of inhibition of BChE by tetrahydroquinazoline-based carbamate **1**.[47]

Scheme 1. Synthesis of Aryl and N-Alkyl Substituted Target Compounds 2a–u and 3a–c[a]
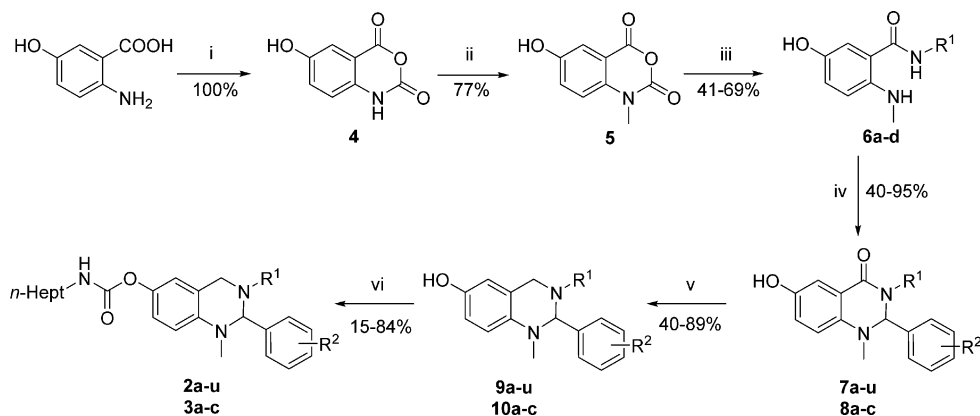
[a]For substitution pattern of R^1 and R^2 see Table 1. Reagents and conditions: (i) CO(OCCl$_3$)$_2$, THF, 70 °C, 3.5 h; (ii) MeI, DIPEA, DMAc, 40 °C, 24 h; (iii) R^1-NH$_2$ or MeNH$_3$Cl and Et$_3$N, DMF, 40–120 °C, 4–5 h; (iv) R^2-PhCHO, AcOH, 70 °C, 1–3 h; (v) LiAlH$_4$, THF, reflux, 1–3 h; (vi) (4-NO$_2$)PhO(C=O)NHn-Hept , NaH, THF, rt, 2 h or n-Hept-NCO, Et$_3$N, rt, 6 h for **2o,p**.

toward the active site to enable carbamate transfer and therefore enzyme inhibition. By application of this general strategy, the binding mode of carbamate based inhibitors bearing transferable moieties can easily be investigated also for other biological targets through the combination of kinetic data and computational studies. This is possible as the general mechanism for carbamate-based pseudo-irreversible inhibitors is similar for all targets.

■ RESULTS AND DISCUSSION

Chemistry. Tetrahydroquinazoline substituted carbamates of the series **2** and **3** were synthesized as outlined in Scheme 1. The first two steps were described recently.[49] Briefly, 3-hydroxyanthranilic acid and triphosgene were heated in THF to yield 6-hydroxyisatoic anhydride **4** quantitatively. Subsequently, the selective N-methylation yielded compound **5**. Free amines or corresponding hydrochlorides were used to synthesize amides

6a–d in moderate yields. These amides were cyclized with either benzaldehyde or substituted derivatives to yield dihydroquina-zolinones **7a–u** and **8a–c** which were reduced with LiAlH$_4$ to give tetrahydroquinazolines **9a–u** and **10a–c**, respectively. In the last step, the n-heptyl carbamate moiety bearing compounds **2a–u** and **3a–c** were synthesized using 4-nitrophenyl-n-heptylcarbamate instead of the previously applied commercially available n-heptyl isocyanate, as its use led in some cases to the formation of the symmetric n-heptylurea which is difficult to remove.

Besides the target compounds above, also the fully aromatic compound **16** was synthesized in six steps (Scheme 2). 5-Hydroxy-2-nitrobenzaldehyde was O-benzyl protected, then the nitro moiety was reduced with iron using a catalytical amount of conc HCl solution toward **12**, and finally the amide bond of **13** was formed with benzoyl chloride. The cyclization was achieved

Scheme 2. Synthesis of Quinazoline 16[a]
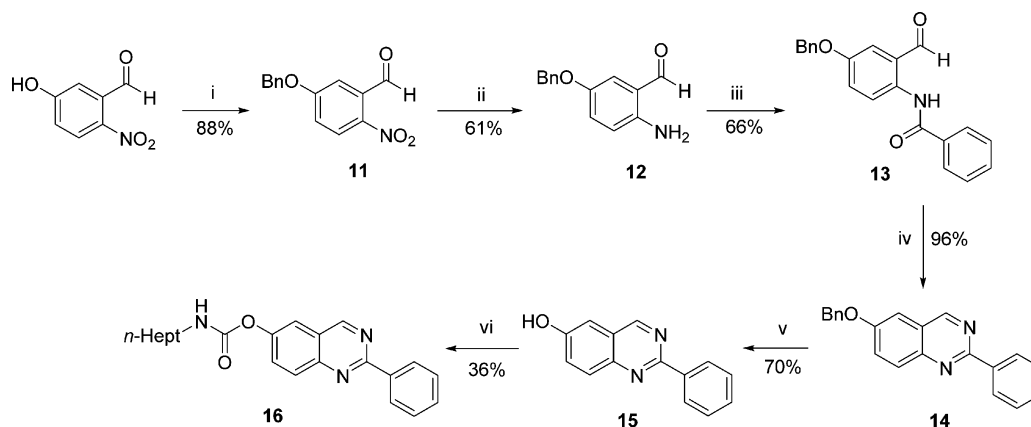
[a]Reagents and conditions: (i) BnBr, K$_2$CO$_3$, DMF, 40 °C, 24 h; (ii) Fe, HCl, EtOH/H$_2$O, reflux, 1 h; (iii) Ph(C=O)Cl, Et$_3$N, DCM, rt, 4 h; (iv) conc NH$_3$, i-PrOH, MW, 90 °C, 6 h; (v) Pd/C, H$_2$, MeOH, 50 °C, 3 h; (vi) (4-NO$_2$)PhO(C=O)NHn-Hept , NaH, THF, rt, 2 h.

Table 1. Cholinesterase Inhibition of the Synthesized Test Compounds[a]

		IC$_{50}$ [μM] or % inhibition			IC$_{50}$ [μM] or % inhibition	
moiety	X = H	eqBChE	hAChE	X = (C=O)NHn-Hept	eqBChE	hAChE
R^1 = Me; R^2 =						
H	9a	39.9	327.0	2a	0.106	4%[d]
4-Cl-Ph-	9b	13.8	235.6	2b	0.115	24%[d]
3-Cl-Ph-	9c	2.1	242.4	2c	0.096	39%[d]
2-Cl-Ph-	9d	56.0	60%[b]	2d	0.474	48%[e]
4-Me-Ph-	9e	22.6	109.9	2e	0.231	9%[d]
3-Me-Ph-	9f	17.4	437.0	2f	0.199	27%[d]
2-Me-Ph-	9g	92.4	143.4	2g	0.251	18%[e]
4-MeO-Ph-	9h	39.5	103.8	2h	0.875	14%[d]
3-MeO-Ph-	9i	7.8	61%[b]	2i	0.208	10%[d]
2-MeO-Ph-	9j	9.9	192.8	2j	0.238	47%[e]
4-F-Ph-	9k	58.9	143.4	2k	0.044	1.61
4-CF$_3$-Ph-	9l	64.6	nd[c]	2l	2.7	59%[d]
4-pyridyl-	9m	2.1	242.4	2m	0.723	16%[d]
3-pyridyl-	9n	70.7	61%[b]	2n	0.565	18%[d]
3-thiophenyl-	9o	193.7	52%[b]	2o	0.022	13%[d]
2-thiophenyl	9p	63.2	225.8	2p	0.014, 0.013[f]	0%[d]
3-furyl-	9q	196.1	341.7	2q	0.083	12%[d]
3-pyrrolyl-	9r	15.3	115.9	2r	0.023	0.852
1-naphthyl-	9s	2.8	341.7	2s	36.2	8%[e]
2-naphthyl-	9t	16.5	9%[c]	2t	0.374	5%[e]
2,6-dichloro	9u	7.1	13.5	2u	0.531	33%[e]
R^2 = Ph; R^1 =						
i-Pr-	10a	55.8	253.0	3a	0.021	33%[d]
n-Pr-	10b	22.8	279.3	3b	0.040	46%[d]
benzyl-	10c	14.8	16%[c]	3c	0.034	17%[e]
	15	98.1	20%[b]	16	1.8	22%[d]
				physostigmine	0.078	0.032

[a]Phenols were incubated for 4.5 min and carbamates for 30 min. Experiments were performed in triplicate at AChE from human erythrocytes and BChE from equine serum. [b–e]Percent inhibition at a concentration of [b]500 μM, [c]50 μM, [d]100 μM, [e]10 μM. Table with confidence intervals is available in Supporting Information. [f]Values determined at human BChE.

in a modified procedure[50] by treatment of **13** with ammonia in a sealed tube under microwave irradiation to obtain **14**. In the last steps the benzyl protection group was removed under standard conditions using Pd/C and H$_2$ and the carbamate moiety was formed with 4-nitrophenyl-n-heptylcarbamate as mentioned above to obtain the quinazoline-based carbamate **16**.

Enzyme Inhibition and SARs. For evaluation and quantification of enzyme inhibition, Ellman's spectrophotomet-

ric method[45,51,52] was applied using AChE from human erythrocytes (EC 3.1.1.7) and BChE from equine serum (EC 3.1.1.8). BChE from horse serum was chosen, as it shows a sequence identity of 90% and a homology of 94% compared to the human analog.[53] Acetylthiocholine and butyrylthiocholine were used as substrates for *h*AChE and *eq*BChE inhibition, respectively. In short, the enzymes were preincubated with different concentrations of the synthesized phenols for 4.5 min or the corresponding carbamates for 30 min to enable time-dependent carbamate transfer onto the serine of the active site, before substrate was added to determine the remaining enzyme activity.

Only few highly selective and potent BChE inhibitors are described in the literature (and even fewer with the carbamate structure; see Figure 1), and only limited information on SARs regarding the carrier scaffold is reported. Therefore, the aromatic system in the target compounds was systematically altered. The unsubstituted target structure **2a** was synthesized as the reference compound and tested for the inhibition of *h*AChE and *eq*BChE (Table 1). This structure is a highly potent inhibitor with an IC$_{50}$ value of 106 nM on *eq*BChE and no significant inhibition on *h*AChE, proving its *eq*BChE selectivity. By contrast, its unsubstituted phenolic analog **9a** shows weak inhibition on *h*AChE with IC$_{50}$ = 327 μM and a value of 39.9 μM for *eq*BChE inhibition, corresponding to an approximately 400-fold decrease in inhibition of *eq*BChE compared to the carbamate **2a**. These results already support the hypothesis that BChE inhibition mainly occurs by carbamate transfer and that the tetrahydroquinazoline scaffold is only the carrier for the carbamate moiety lacking pronounced inhibition of the enzyme. Therefore, in the subsequent SARs analysis only the carbamate based compounds (right columns of Table 1) will be discussed, as their phenolic carrier scaffolds showed no pronounced inhibition (left columns of Table 1) in most cases on neither enzyme.

Optimization of the substitution pattern of the aromatic moiety was conducted by various approaches starting with the Topliss tree approach.[54,55] Within this approach the hydrophobic, electronic, and steric properties of an aromatic system are systematically altered by the introduction of different substituents with the aim to improve activity toward a biological target. In our case the Topliss tree approach guided to the synthesis of Cl- (**2b–d**), Me- (**2e–g**), and MeO- (**2h–j**) substituted aromatic systems in ortho, meta, and para positions and finally to the 4-fluorine substituted system **2k**. Interestingly, none of these groups improved affinity except for the fluorinated compound **2k** with the fluorine atom as the smallest substituent in this series with IC$_{50}$(BChE) = 44 nM. Compound **2l** bearing a strong electron withdrawing 4-CF$_3$ group was synthesized although not being recommended in the classical Topliss tree approach and showed strongly decreased BChE inhibition by a factor of 25 (IC$_{50}$ = 2.7 μM). In addition to the Topliss tree approach, bioisosteric replacements for the phenyl system were investigated with pyridines **2m–n** and thiophenes **2o–p**.[56,57] Surprisingly, the pyridyl residues as more polar bioisosteres of the phenyl residue decreased inhibition and the thiophene residues as less polar bioisosteres increased inhibition more than 5-fold to IC$_{50}$(BChE) of 22 nM for **2o** and 14 nM for **2p**. With regard to these results, further similarity replacements of the thiophenyl system were investigated leading to the furyl compound **2q** with decreased activity (IC$_{50}$(BChE) = 83 nM) and the pyrrolyl compound **2r** (IC$_{50}$(BChE) = 23 nM) with BChE inhibition similar to that of the thiophenyl compound **2o**. Finally, the phenyl system was replaced by sterically demanding

aromatic substituents; here the 1-naphthyl and the 2-naphthyl substituted compounds **2s,t** were investigated. Interestingly, inhibition of BChE by the 1-naphthyl substituted compound **2s** dropped to IC$_{50}$(BChE) = 36.2 μM (i.e., by a factor of approximately 300 compared to reference compound **2a**). To further investigate steric influence on the affinity toward BChE, the 2,6-disubstituted chlorine compound **2u** was synthesized which has to undergo a twist caused by its ortho-substitution pattern, thus leading to a almost perpendicular arrangement of the aryl ring and the bicyclic core. This compound shows an IC$_{50}$ value of 531 nM, which is lower than for all three monosubstituted chlorine compounds (**2b,c,d**).

Beyond the mentioned introduction of different substitution patterns into the aromatic system, also the space close to the tertiary nitrogen was exploited by the replacement of the methyl group with other side groups (**3a–c**) with the best results for the *i*-Pr group with IC$_{50}$(BChE) = 21 nM. For the bicyclic aromatic quinazoline **16** a strongly decreased inhibition was observed meaning that either a bent system or a more basic nitrogen within the core structure is necessary for binding, comparable to many AChE inhibitors.[58−61]

As the 2-thiophenyl compound **2p** was found to be the most potent and selective compound toward *eq*BChE, its potency on *h*BChE was also investigated. The IC$_{50}$ value on *h*BChE was determined to 13 nM and is comparable to the one on *eq*BChE (14 nM), proving that the results obtained on *eq*BChE can be used as an approximation for *h*BChE.

Even if the IC$_{50}$ values of the compounds described in Table 1 (a respective table with confidence intervals is provided in the Supporting Information) are a useful first hint to establish a binding model for these inhibitors, the inhibition mode of pseudo-irreversible inhibitors is much more complex. Therefore, a more detailed view into the kinetic mode of action is necessary to determine the influence of substituents on enzyme inhibition. At this point, it should also be mentioned that the inhibition curves of the weakest active compounds **2l**, **2s**, and **16** show a Hill slope of around 0.5 (data not shown). These slopes are remarkably different from those of all other inhibitors (slope of ≥1). This fact might be a strong hint for a different mode of action for these three inhibitors.

Kinetic Investigations into the Mode of BChE Inhibition. The mechanism of pseudo-irreversible enzyme inhibition by carbamates can be described by three pivotal steps as shown in Figure 3. First, the enzyme E forms a reversible enzyme−
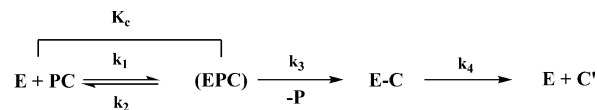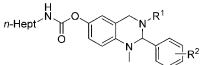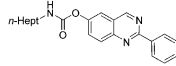
Figure 3. Pseudo-irreversible inhibition of an enzyme E by carbamates PC. For description see the main text.

inhibitor complex (EPC) with the carbamate-based inhibitor PC (PC for phenol carbamate) comparable to reversible competitive inhibitors. This reversible inhibition is quantified by K_C which describes the apparent affinity between the enzyme and the inhibitor in an equilibrium state. In the second step, the carbamate moiety itself is transferred onto the enzyme with release of the carrier scaffold P (P for phenol), resulting in the carbamoylated enzyme E−C. The constant k_3 represents the carbamolyation rate of the inhibitor from the reversible complex (EPC) to the carbamoylated enzyme E−C. The last step is the recovery of the enzyme through slow hydrolysis of E−C and

Table 2. Kinetic Values for Carbamoylation and Decarbamoylation on *eq*BChE for Selected Compounds[a]

	R^1	R^2	K_C [nM]	k_3 [min^{-1}]	k_3/K_C [μM^{-1}min^{-1}]	k_4 [h^{-1}]
2a	Me	Ph-	226.2 ± 82.8	0.13 ± 0.04	0.57 ± 0.27	0.14 ± 0.003
2p	Me	2-thiophenyl-	14.3 ± 6.2 19.7 ± 0.9*	0.14 ± 0.04 0.32 ± 0.01*	9.79 ± 5.08 16.24 ± 0.64*	0.14 ± 0.003
2k	Me	4-F-Ph-	24.5 ± 12.7	0.14 ± 0.04	5.71 ± 3.38	
2c	Me	3-Cl-Ph-	227.3 ± 120.5	0.16 ± 0.05	0.7 ± 0.43	
2h	Me	4-MeO-Ph-	1203.6 ± 118.7	0.24 ± 0.01	0.2 ± 0.02	
2i	Me	3-MeO-Ph-	622 ± 234.5	0.18 ± 0.05	0.29 ± 0.14	
2l	Me	4-CF$_3$-Ph-	*756.5 ± 251.7***	*0.05 ± 0.01***	*0.07 ± 0.03***	
2s	Me	1-naphthyl-	*15.6 ± 17.6***	*0.03 ± 0.002***	*1.92 ± 2.17***	
2u	Me	2,6-Cl-Ph	4118 ± 1204	0.23 ± 0.063	0.06 ± 0.02	
3a	*i*-Pr	Ph-	185.8 ± 115.1	0.16 ± 0.07	0.86 ± 0.65	
16			*1057.9 ± 577.7***	*0.14 ± 0.06***	*0.13 ± 0.09***	
physostigmine			280.3 ± 130.0	0.3 ± 0.1	0.3 ± 0.1	0.25 ± 0.01

[a]Asterisks indicate the following: (*) Values are measured for human BChE. (**) Values are calculated under the assumption of a pseudo-irreversible inhibition; they have to be carefully rated, as the inhibition mode might be different from that of the other inhibitors.

release of the carbamate C′ with k_4 as the decarbamoylation rate constant. Normally, k_4 is significantly lower than k_3 due to the fact that carbamoylation occurs much faster than decarbamoylation because of the high stability of E−C toward hydrolysis.

The values of K_C and k_3 can be quantified applying the method described by Hosie et al.[62] and Feaster et al.[63] Following this approach, the carbamate-mediated inhibition described in Figure 3 is known to undergo apparent first order kinetics:

$$A = A_0 \, e^{-k_{obs}t} + A_\infty \qquad (1)$$

in which A is the activity of the enzyme at a specific time t, A_0 the activity at $t = 0$, A_∞ the activity at $t = \infty$ and k_{obs} represents the apparent first order rate constant. Plotting of k_{obs} against the inhibitor concentration [PC] yields a hyperbolic curve described by

$$k_{obs} = \frac{k_3[PC]}{K_C\left(1 + \frac{[S]}{K_M}\right) + [PC]} \qquad (2)$$

Rearrangement of eq 2 into a double reciprocal form with $1/k_{obs}$ as a function of $1/[PC]$ results in a linear plot:

$$\frac{1}{k_{obs}} = \frac{K_C\left(1 + \frac{[S]}{K_M}\right)}{k_3} \frac{1}{[PC]} + \frac{1}{k_3} \qquad (3)$$

in which k_3 can be determined from the y-intercept and K_C from the slope. From these data also the second order rate constant k_3/K_C can be calculated describing the overall carbamoylation efficacy to evaluate differences in inhibitory potency. For the case, that substrate is not added from the beginning of the preincubation between inhibitor and enzyme, [S] becomes equal to zero because substrate and inhibitor are not competing for the binding pocket, and the substrate only adopts a function as reporter for remaining enzyme activity. In this case, eq 3 is simplified to

$$\frac{1}{k_{obs}} = \frac{K_C}{k_3} \frac{1}{[PC]} + \frac{1}{k_3} \qquad (4)$$

On the basis of this method, we investigated kinetic parameters (Table 2) of a selected set of compounds including the reference compound **2a** and the highly potent inhibitors **2p** and **2k** as well as those compounds that showed differences in the Hill slopes of their IC$_{50}$ curves compared to the other inhibitors (**2l**, **2s**, and **16**). The alkaloid physostigmine served as the external reference compound. In this series the thiophene compound **2p** was found as the most affine inhibitor with K_C = 14.3 nM and the one with the highest carbamoylation efficacy (k_3/K_C = 9.79 μM^{-1} min^{-1}). The fluorine substituted compound **2k** showed a comparably high affinity and carbamoylation efficacy. Interestingly, the twisted 2,6-dichloro compound **2u** displayed the lowest affinity to the enzyme with K_C = 4118 nM. This finding supports the hypothesis that a twist of the aromatic residue leads to decreased affinity toward the binding pocket (for details see Computational Studies). But even with this twist the carbamate is transferred to the serine. The only major exception for IC$_{50}$ and K_C correlation was measured for the 1-naphthyl compound **2s** which showed a high affinity to the enzyme with K_C = 15.6 nM but an IC$_{50}$ value in the micromolar range. Similar to the curves for determination of IC$_{50}$ values, the shape of the obtained time-dependent inhibition curves was much less steep for compounds **2l**, **2s**, and **16** compared to all other inhibitors, indicating a different binding interaction.

For all compounds high carbamoylation rate constants k_3 were observed with similar values between 0.13 and 0.24 min^{-1}; exceptions were, as mentioned, the 1-naphthyl substituted derivative **2s** and also the 4-CF$_3$ analog **2l**. Apart from the exceptions, it can be assumed that similar values for k_3 have their origin in a similar orientation of the carbamate moiety with respect to the serine of the CAS, supporting a conserved binding mode of these inhibitors (see Computational Studies).

Enzyme recovery was measured exemplarily for the reference compound **2a** and the thiophenyl analog **2p**. For this purpose,
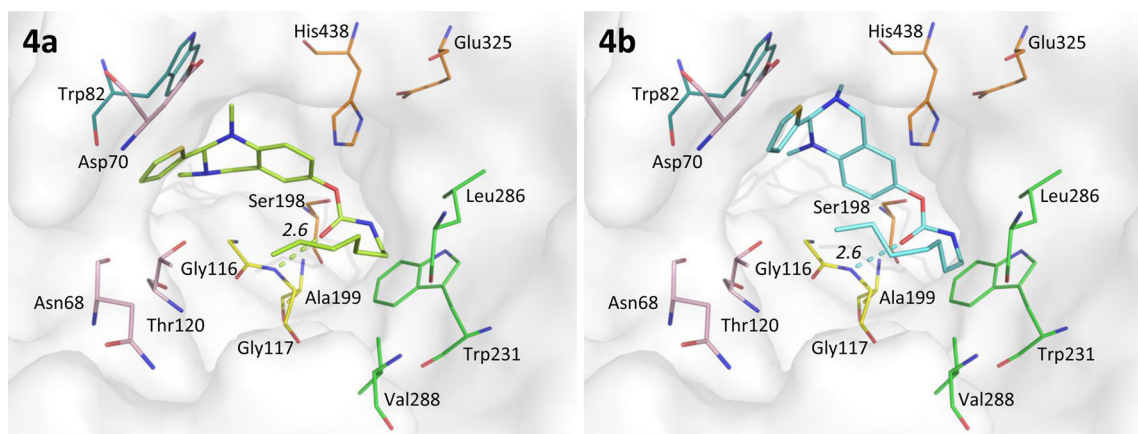
Figure 4. (a) Representation of the preferred binding mode for **2p** as *R*-enantiomer (light green) and (b) *S*-enantiomer (light blue) in the BChE binding site. Residues of the acyl pocket are shown in green, the oxyanion hole is in yellow, the CAS is in orange, the choline binding site (Trp82) is in turquoise, and parts of the side cavity are in pink. Distances in Å are given in italics. The figure was created with Pymol.[72]

the derivatives were incubated for 1 h with the enzyme at a concentration where complete inhibition was achieved and then successively 1000-fold diluted to a concentration where no carbamoylation was observed anymore. The recovery of the enzyme through hydrolysis of the carbamate residue was monitored after certain time points after dilution, showing first order kinetics with $k_4 = 0.14$ h^{-1} or a half-life for the carbamoylated enzyme of approximately 5 h. This value is identical for both compounds, as in both cases an *n*-heptyl carbamate is cleaved from the serine.

Taken together, the kinetic parameters reveal that (a) most inhibitors follow a conserved inhibition mode indicated by a similar carbamoylation rate constant k_3 and (b) they are only differing in their affinity expressed as K_C. It was observed that the exceptions **2l**, **2s**, and **16** probably do not adhere to this conserved binding mode, as shown by significant differences in the slope of their IC$_{50}$ curves and kinetic parameters. Therefore, the results for these three inhibitors should be carefully rated, as the kinetic parameters were determined under the assumption of a pseudo-irreversible inhibition model, although the exact inhibition mode might in fact be different. These observations need to be further investigated.

We further investigated the most potent compound **2p** by performing enantiomeric resolution with HPLC on a chiral phase and chiroptical analysis by CD spectroscopy. Although both enantiomers could be obtained after preparative chiral HPLC in their pure form (revealed by CD spectroscopy), they underwent rapid isomerization back into the racemic mixture (conditions and chromatograms are provided in the Supporting Information). It seems that racemization at the chiral center occurs by opening of the ring system into an imine structure which in turn reacts nonstereoselectively back to the ring system, thereby producing the racemate. Even though resolution of enantiomers was achieved, it can be assumed that isomerization of pure enantiomers into the racemate will occur at least in aqueous media during the biological testing of the compound. Assuming that the postulated binding modes (see Computational Studies) are correct, conformational energies and intermolecular scores of the respective binding poses suggest that in general the *S*-enantiomers might be more active than the *R*-enantiomers (see Supporting Information for further details).

We also investigated the kinetic properties of **2p** on human BChE (Table 2). We found this compound to have similar

inhibitory activity on *h*BChE (as reported above for the IC$_{50}$ values) compared to *eq*BChE with slightly decreased affinity (K_C = 19.7 nM), a higher carbamoylation rate ($k_3 = 0.32$ min^{-1}), and a higher carbamoylation efficacy ($k_3/K_C = 16.24$ μM^{-1} min^{-1}). With regard to the high similarity in inhibition and kinetic values of **2p** on *h*BChE and *eq*BChE, it can be assumed that all compounds synthesized will bind on *h*BChE and *eq*BChE in a similar manner.

Computational Studies. Modeling studies were performed in a combined docking and minimization approach with GOLD[64] and MiniMuDS.[65] For this purpose, the human BChE crystal structure 1P0I was used,[66] which possesses the highest resolution (2.0 Å) of BChE structures in the PDB.[67] Docking studies of reversible ligands of BChE had also been carried out by other groups.[43,68−70]

As the inhibitors were tested as racemic mixtures in the assay, both enantiomeric forms were built up and used for docking. All ligands of the series examined by detailed kinetic measurements (Table 2) as well as ligand **1** were used for docking studies.

For pseudo-irreversible inhibition, three different states may be addressed with classical docking methods: (1) A covalent docking can be carried out representing the carbamoylated serine (corresponding to E−C in Figure 3). As the carbamate stays the same throughout the data set, this approach was not performed here. (2) The tetrahedral transition state that occurs during the carbamoylation can be docked covalently to the serine. This method had been chosen by Carolan et al.[43] However, in this case a generally applicable interpretation for a set of compounds in light of the inhibition and kinetic data was not possible. Therefore, (3) the inhibitor structures were docked non-covalently to BChE to mimic reversible inhibition by formation of the initial noncovalent complex ((EPC) in Figure 3). These docking data can be analyzed in relation to the experimentally determined K_C values.

Docking poses of inhibitor **1** showed the same binding mode for both enantiomeric forms on the top (*S*-enantiomer) and the second-best rank (*R*-enantiomer) (see Experimental Section for a detailed description of pose selection). These poses were taken as reference poses to model the binding mode of the other inhibitor structures by deletion and addition of the corresponding functional groups and subsequent local minimization in the binding site using MiniMuDS. The methyl group on the benzylic nitrogen can adopt a pseudo-equatorial or pseudo-axial

orientation. The herein displayed structures show the methyl group in the pseudo-equatorial position for the *R*-enantiomer and in the pseudo-axial position for the *S*-enantiomer, as these orientations were found to be preferred.

The binding mode of the compounds is characterized by the following features: The *n*-heptyl chain is placed over the acyl binding site (mainly formed by Trp231, Leu286, and Val288). The carbamate moiety is positioned near His438 and Ser198 (together with Glu325 the CAS comprising amino acids), showing distances of the carbamate carbon to the serine oxygen of 2.9−3.0 Å and 3.6−4.1 Å for the *R*- and *S*-enantiomers, respectively. The oxygen of the carbamate moiety is oriented toward Gly117-NH in hydrogen bond distances of 2.6−2.9 Å and 2.6−3.0 Å for the *R*- and *S*-enantiomers, respectively. Gly116, Gly117, and Ala119 form the oxyanion hole. These residues are important in stabilizing the negative charge formed at the carbonyl oxygen during substrate hydrolysis.[71]

The tetrahydroquinazoline is placed "above" the oxyanion hole, and the aromatic ring is in π−π interaction distances of 3.4 and 3.8 Å to His438 (measured for *S*- and *R*-**2p**, respectively). The aryl rings (the substituents R² of Table 2) are placed in a cavity "below" Trp82, formed by Asn68, Asp70, and Thr120 (colored in pink in Figure 4).

The ligand poses derived from ligand **1** show the aryl ring "in plane" with the tetrahydroquinazoline (more precisely, the bond between the aryl ring and the tetrahydroquinazoline shows a dihedral angle of approximately 0°). However, a twisted conformation with a ∼90° dihedral, similar as in ortho-substituted biaryls,[73] would also be possible. To test whether the "in plane" or "twisted" orientation of the aryl ring is favored, compound **2u**, a 2,6-dichloro derivative, was therefore synthesized. Due to steric hindrance of the ortho-chloro substituents and the methyl groups on the quinazoline core, the aryl ring needs to adopt the twisted conformation. As the affinity of this compound (K_C = 4118 nM) is the lowest in the tested series, the twisted conformation is apparently not favorable for high-affinity binders. As the modeled ligand pose shows, without a displacement from the generally preferred binding mode, this conformation would lead to clashes with the protein. Thus, except for **2u**, the aryl ring can be assumed to be "in plane" with the tetrahydroquinazoline core as shown in Figure 4.
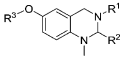
Although a quantitative correlation between the docking scores and the activity of the compounds cannot be expected (primarily due to the well-known accuracy limitations of scoring functions and the uncertain contribution of the enantiomers to the experimentally measured affinities of the racemic compounds), some differences in affinity (in terms of K_C) can qualitatively be explained by the structural differences of the inhibitors in this binding model. Compared to the thiophene derivative **2p** as the smallest compound, the significantly weaker affinity of compounds with sterically demanding para-substituents (**2h**, **2l**) is in line with the steric restrictions imposed by the side cavity (formed by Ile69, Asn83, and Pro84) to which these para-substituents point. Especially the para-CF₃ compound **2l** leads to clashes with the protein when forcing it into a similar binding mode as identified for thiophene derivative **2p** (see Figure S5 in the Supporting Information). This is in agreement with the different kinetic profile and supports the hypothesis of a different binding mode for this compound. Although not forming particularly favorable interactions, meta-substituents (cf. **2c**, **2i**) are better tolerated because they point "upward" to a more accessible area. Additional interactions in this region can be

formed by the 1-naphthyl group (**2s**), which might overall lead to the similarly favorable affinity as observed for **2p**. However, because of the different kinetic characteristics described above, caution is warranted in interpreting the results for compound **2s** (as well as for **2l**). This also applies to the achiral compound **16**, which served as a test compound to confirm the binding mode without the uncertainty of enantiomeric forms. However, docking showed that the planar shape of the ligand cannot be accommodated in the common binding mode adopted by the other inhibitors. This could indicate a different mode of action, as suggested also by the kinetic data.

Antioxidant Capacity, Neuroprotection, and Neurotoxicity. Neuronal cell death induced by reactive oxygen species (ROS) is prevented by antioxidants that contain radical scavenging structures. The determination of these antioxidant capacities can be achieved by the oxygen radical absorbance capacity (ORAC) assay in which the ability of an antioxidant to reduce the amount of induced peroxylradicals is determined. This test therefore describes direct physiochemical radical scavenging properties of compounds but does not necessarily directly relate to results from cell-based methods,[36,47] although often claimed in the literature. Results in this assay are expressed in relation to the radical scavenging properties of 6-hydroxy-2,5,7,8-tetramethylchroman-2-carboxylic acid (also called Trolox, a water-soluble vitamin E analog) yielding the Trolox equivalents (TE) unit.

In this work, the synthesized carbamates release the corresponding carrier phenols after carbamate transfer onto BChE (compare Figure 2b),[36,47] which can act as potent radical scavengers with their *p*-aminohydroquinone moiety. Therefore, we chose pairs of compounds (carbamates and corresponding phenols) to investigate and correlate their antioxdative properties, including the unsubstituted compound **2a**, the thiophene bearing compound **2p** as a highly potent BChE inhibitor, the 4-MeO bearing compound **2h** as a relatively weak BChE inhibitors, and the *N*-benzyl containing compound **3c** as well as their phenolic analogs **9a,p,h** and **10c**. The results for the ORAC assay are summarized in Table 3. All of the tested carbamates show by

Table 3. Antioxidant Capacities of Target Compounds Expressed as Trolox Equivalents (TE)

R¹	R²		R³		
				H	*n*-Hept-NHC(O)-
Me	Ph	**9a**	3.0 ± 0.3	**2a**	0.2 ± 0.1
Me	2-thiophenyl-	**9p**	3.4 ± 0.1	**2p**	0.2 ± 0.1
Me	4-MeO-Ph-	**9h**	3.7 ± 0.3	**2h**	0.5 ± 0.2
Bn	Ph	**10c**	3.9 ± 0.4	**3c**	1.7 ± 0.2

themselves radical scavenging properties with antioxidant capacities between 0.2 and 0.5 TE. A remarkable difference can be observed for the *N*-benzyl bearing compound **3c** with an antioxidant capacity of 1.7 which might be explained by the possibility to form stable benzyl radicals, thereby acting as a strong antioxidant exceeding Trolox already in its carbamate form.

As expected, the antioxidant capacities of the hydroxy compounds **9** and **10** were significantly higher than those of their corresponding carbamates and of the positive control and reference Trolox, itself ranging from 3.0 to 3.9 TE. The *N*-benzyl bearing tetrahydroquinazoline **10c** shows the highest antioxidant capacity with 3.9 TE in this series, as it might be able to trap radicals with its *p*-aminohydroquinone core and additionally with
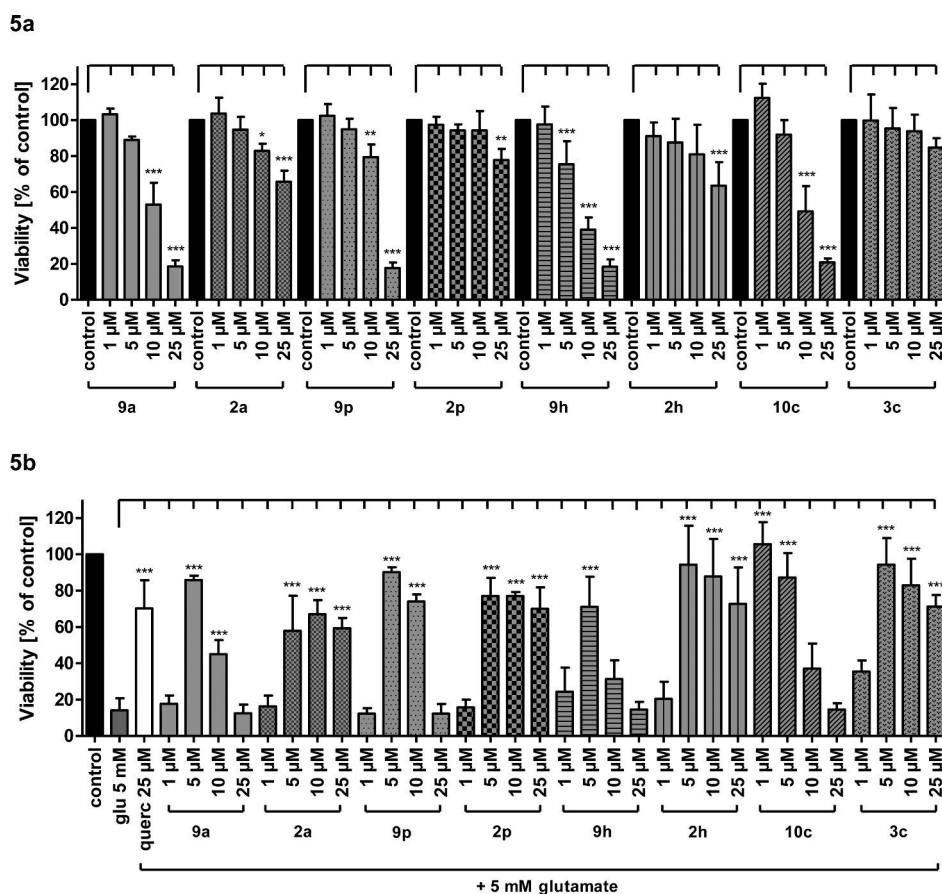
Figure 5. (a) Neurotoxicity tests for target compounds on HT-22 cells. (b) Neuroprotection tests against glutamate induced oxidative stress for target compounds on HT-22 cells.

the benzyl group as mentioned before for the carbamate **10c**. In summary, it was observed that the carbamates by themselves show already antioxidant capacities, albeit only moderate ones, and their corresponding phenols released after carbamate transfer onto the active site of BChE represent highly potent radical scavengers with 3- to 4-fold higher antioxidant capacities than Trolox.

As mentioned above, evaluation of compounds in a cellular neuronal assay provides additional information with respect to therapeutic applications, since it enables assessment of how well physicochemical properties translate into biological settings. In fact correlating both methods is most meaningful. Therefore, to evaluate the ability of the target compounds to prevent oxycytotic cell death after glutamate exposure, the compounds were applied onto a model system with the glutamate sensitive murine hippocampal HT-22 cells which lack an ionotropic glutamate receptor. These cells contain a glutamate−cysteine antiporter that is necessary for the cysteine uptake from the extracellular side under physiological conditions and at the same time transports glutamate out of the cytosol.[74] When HT-22 cells are exposed to high glutamate concentrations, this transporter is blocked by extracellular glutamate. In consequence, no cysteine is uptaken for glutathione (GSH) synthesis, the antioxidant protecting from intracellular ROS induced cell death.[75−77]

The same compounds evaluated in the ORAC assay were tested for neuroprotection on HT-22 cell line with the natural product quercetin as the antioxidant reference. Cells were incubated with the compounds in different concentrations either with 5 mM glutamate to induce oxycytosis or without glutamate

to determine self-toxicity toward the cells (Figure 5). In general, all tested hydroxy compounds (series **9** and **10**) showed similar effects on HT-22 cells with no or only little toxicity at concentrations of 1 and 5 μM (Figure 5a). The carbamates (series **2** and **3**) are even less neurotoxic compared to the corresponding phenols. The cell viability was maintained above 80% for all carbamates up to a concentration of 10 μM. Interestingly the N-benzyl carbamate **3c** showed no significant decrease in cell viability even at the highest concentration of 25 μM.

When glutamate was added to induce oxidative stress (Figure 5b), the phenols very effectively counteracted glutamate-induced neurotoxicity already at a concentration of 5 μM as the cell viability was maintained. Decreasing viability at higher concentrations relates to neurotoxic effects for compounds like **9h** and **10c** but is only significant at 25 μM. Furthermore, the N-benzyl containing phenol **10c** maintained cell viability at already 1 μM, proving its high neuroprotectivity already at low concentrations.

It is remarkable that also the carbamate-based structures (series **2** and **3**) showed at concentrations above 5 μM that cell viability is comparable to the one of the reference compound quercetin at 25 μM, proving their neuroprotective effect. This finding is quite of interest, since hydrolysis to the phenol is not necessary for cell-based neuroprotective effects.

However, neuroprotection assays suffer from the drawback that the concentrations needed to be applied in such assays are much higher than what is expected for a ligand/inhibitor to be effective in vivo. This is because respective assays are not

sensitive enough and the data therefore have to be correlated to the positive control (in our case Trolox in the ORAC assay and quercetin in the HT-22 assay). Compared to quercetin (applied at 25 μM) the compounds are more active even at lower concentrations than for quercetin.

In summary, the compounds described are not only very potent and selective BChE inhibitors but also act as highly active neuroprotectants both by themselves and after release of the phenolic carrier.

■ CONCLUSION

In this report we identified a set of pseudo-irreversible carbamate-based inhibitors of BChE (**2a–u**, **3a–c**, and **16**) by applying rational approaches to conduct SARs of the tetrahydroquinazoline carrier scaffold. Although the corresponding phenolic tetrahydroquinazolines **9a–u**, **10a–c**, and **15** showed BChE inhibition in the micromolar range lacking significant selectivity over hAChE, they are the source of the modulated affinity of the carbamate series. In this series we found thiophene compound **2p** as the most potent inhibitor with regard to both affinity (K_C = 14.3 nM) and carbamoylation efficacy (k_3/K_C = 9.79 μM^{-1} min^{-1}) toward the enzyme. To our knowledge, this compound represents by far one of the most active and selective inhibitors of BChE described to date.

By combining kinetic investigations with computational studies, we established a model for binding of the tetrahydroquinazoline scaffold and therefore for modulated affinity of the inhibitors toward the enzyme. In the computational studies, the heterocyclic inhibitors place their carbamate moieties in close proximity to the serine of the CAS. This accounts for appropriate preorientation for the subsequent transfer of the carbamate. Substituents on the aryl ring that are responsible for affinity of this set of compounds bind to a side cavity of BChE's active site located next to the entrance of the binding site. Both kinetic data and computational studies support a conserved binding mode for the described inhibitors, with the exception of the 4-CF$_3$-substituted compounds **2l**, 1-naphthyl compound **2s**, and the planar quinazoline **16**. Combining computational studies with kinetic values can be considered as a general approach to investigate the binding mode of carbamate-based pseudo-irreversible inhibitors, as the binding mode of these inhibitors is similar.

Neuroprotective abilities for a subset of carbamates and their corresponding phenols were determined in an ORAC assay and a neuronal cell-based one and revealed high radical scavenging properties of the phenolic heterocycle carrier scaffold formed after transfer of the carbamate moiety to the enzyme. Pronounced neuroprotection comparable to quercetin was seen when intracellular oxidative stress was triggered through glutamate exposure in neuronal cells.

In addition to the development of improved and neuroprotective BChE inhibitors, our results might be of relevance for a general methodology to be applied for development of other pseudo-irreversible enzyme inhibitors.

■ EXPERIMENTAL SECTION

Chemistry. General. Common reagents and solvents were obtained from commercial suppliers and used without any further purification. Tetrahydrofuran (THF) was distilled from sodium/benzophenone under argon atmosphere. Reaction progress was monitored using analytical thin layer chromatography (TLC) on precoated silica gel GF$_{254}$ plates (Macherey-Nagel GmbH & Co. KG, Düren, Germany), and spots were detected under UV light (254 nm) or through staining with iodine. Nuclear magnetic resonance spectra were performed with a Bruker AV-400 NMR instrument (Bruker, Karlsruhe, Germany) in DMSO-d_6 or CDCl$_3$. Chemical shifts are expressed in ppm relative to CDCl$_3$ or DMSO-d_6 (7.26/2.50 and 77.16/39.52 ppm for ^{1}H and ^{13}C NMR, respectively). Melting points were determined in open capillaries on a Büchi B-540 without any further correction except for the phenolic tetrahydroquinazolines, as they undergo rapid decomposition during heating. For purity of target compounds, analytic HPLC was performed on a system from Shimadzu equipped with a DGU-20A3R controller, LC20AB liquid chromatograph, and a SPD-20A UV/vis detector. Stationary phase was a Synergi 4U fusion-RP (150 mm × 4.6 mm) column (Phenomenex, Aschaffenburg, Germany). As mobile phase, water (phase A) and MeOH (phase B) were used with 1 mL/min. (Method A: conc B, 5% → 90% from 0 to 8 min; 90% from 8 to 13 min; 90% → 5% from 13 to 15 min; 5% from 15 to 18 min. Method B: conc B, 10% → 80% from 0 to 8 min; 80% from 8 to 13 min; 80% → 10% from 13 to 15 min; 10% from 15 to 18 min. Method C: conc B, 30% → 90% from 0 to 8 min; 90% from 8 to 13 min; 90% → 30% from 13 to 15 min; 30% from 15 to 18 min) Target compounds were ≥95% pure. Purities of **9r** and **10a** were determined by CHN analysis on a Vario MICRO CUBE (Elementar Analysesysteme GmbH, Hanau, Germany) because of their low stability on HPLC. ESI mass spectral data were acquired on a Simadzu LCMS-2020.

General Reactions. General Amide Formation Procedure (GP1). 6-Hydroxy-1-methyl-2H-benzo[d][1,3]oxazine-2,4(1H)-dione **5** was dissolved in dry DMF (30 mL) and treated with the corresponding amine (5 equiv) or a mixture of the amine hydrochloride (5 equiv) and triethylamine (5 equiv). The mixture was heated to 40–120 °C (depending on the amine) for 4–5 h. For workup, the mixture was poured into water (100 mL) and the product was extracted with ethyl acetate (5 × 100 mL). The combined organic layers were washed with brine (50 mL), dried over Na$_2$SO$_4$, and evaporated to dryness. The crude product was purified by column chromatography to obtain 5-hydroxy-N-methyl-2-(alkylamino)benzamides **6a–d**.

General Cyclization Procedure (GP2). 5-Hydroxy-N-methyl-2-(alkylamino)benzamides **6a–d** were dissolved in glacial acetic acid (20 mL). The mixture was treated with the corresponding aldehyde (1.2 equiv) and heated to 70 °C for 1–3 h. Then the mixture was poured onto ice–water (20 mL), basified with a NaOH solution (2 M) and the pH was adjusted to 9 with sat. NH$_4$Cl solution. The product was extracted with ethyl acetate (3 × 40 mL), the combined organic layers were washed with brine (30 mL), dried over Na$_2$SO$_4$, and the solvent was evaporated under reduced pressure. The crude product was either recrystallized or purified by column chromatography to obtain dihydroquinazolinones **7a–u** and **8a–c**.

General Reduction Procedure (GP3). Dihydroquinazolinones **7a–u** and **8a–c** were dissolved in dry THF (30 mL) at 0 °C, and LiAlH$_4$ (4 equiv) was added. The mixture was allowed to reach rt and was then heated to reflux temperature for 1–3 h. After cooling to rt, the mixture was poured into ice–water (50 mL) followed by the addition of saturated NH$_4$Cl solution until pH = 9. The aqueous phase was then extracted with ethyl acetate (3 × 80 mL). The combined organic layers were washed with brine (50 mL), dried over Na$_2$SO$_4$, and the solvent was evaporated under reduced pressure. The crude product was purified by column chromatography to obtain the corresponding tetrahydroquinazolines **9a–u** and **10a–c**.

General Carbamate Formation Procedure (GP4). A solution of tetrahydroquinazolines **9a–n**, **9q–u**, and **10a–c** in dry THF (5 mL) was treated with NaH in paraffin oil (60%, 1.2 equiv). The mixture was stirred until the formation of gas stopped. Then, a solution of 4-nitrophenyl-n-heptylcarbamate (1.2 equiv) in dry THF (3 mL) was added at once. The mixture was stirred for 2 h. For workup, the mixture was diluted with ethyl acetate (30 mL), washed with water (10 mL), and washed with brine (10 mL). The organic phase was dried over Na$_2$SO$_4$, and the solvent was evaporated under reduced pressure. The crude product was purified by column chromatography to obtain the corresponding n-heptylcarbamate **2a–n**, **2q–u**, and **3a–c**.

Synthesis and Spectral Data. Syntheses of **4** and **5** were performed as described.[49] The synthesis of target compound **2a** is

exemplarily given in the following. For synthetic procedures and spectral data of **2b−u** and **3a−c** see Supporting Information.

5-Hydroxy-*N*-methyl-2-(methylamino)benzamide 6a. According to GP1, 6-hydroxy-1-methyl-1*H*-benzo[*d*][1,3]oxazine-2,4-dione **5** (500 mg, 2.59 mmol, 1 equiv), methylamine hydrochloride (874 mg, 12.95 mmol, 5 equiv), and triethylamine (1.79 mL, 12.95 mmol, 5 equiv) were used to obtain 5-hydroxy-*N*-methyl-2-(methylamino)benzamide **6a** (321 mg, 69%) after column chromatography (petroleum ether/EtOAc = 1:4) as a yellow-brown solid; mp 164−166 °C. ^{1}H NMR (400 MHz, DMSO-d_6): δ = 8.59 (s, OH), 8.15 (q, J = 4.2 Hz, NH), 6.92 (d, J = 2.8 Hz, 1H), 6.85 (q, J = 4.3 Hz, NH), 6.80 (dd, J = 8.8, 2.8 Hz, 1H), 6.49 (d, J = 8.8 Hz, 1H), 2.71 (d, J = 1.3 Hz, 3H), 2.70 (d, J = 2.0 Hz, 3H) ppm. ^{13}C NMR (101 MHz, DMSO-d_6): δ = 169.4, 146.5, 143.3, 119.6, 116.7, 114.6, 111.6, 30.0, 26.0 ppm. ESI-MS: m/z calcd, 180.09; found, 181.2 [M + H]$^+$.

6-Hydroxy-1,3-dimethyl-2-phenyl-2,3-dihydroquinazolin-4(1*H*)-one 7a. According to GP2, 5-hydroxy-*N*-methyl-2-(methylamino)benzamide **6a** (170 mg, 0.94 mmol, 1 equiv) and benzaldehyde (114 μL, 1.13 mmol, 1.2 equiv) were used to obtain 6-hydroxy-1,3-dimethyl-2-phenyl-2,3-dihydroquinazolin-4(1*H*)-one **7a** (167 mg, 66%) after column chromatography (petroleum ether/EtOAc = 1:2) as a yellow solid; mp 205−207 °C. ^{1}H NMR (400 MHz, DMSO-d_6): δ = 8.99 (s, OH), 7.35−7.27 (m, 3H), 7.22 (d, J = 2.9 Hz, 1H), 7.19−7.09 (m, 2H), 6.80 (dd, J = 8.7, 3.0 Hz, 1H), 6.46 (d, J = 8.7 Hz, 1H), 5.67 (s, 1H), 2.90 (s, 3H), 2.73 (s, 3H) ppm. ^{13}C NMR (101 MHz, DMSO-d_6): δ = 161.7, 149.6, 139.4, 136.8, 128.6, 128.5 (2C), 126.2 (2C), 120.9, 117.6, 114.1, 113.4, 78.6, 35.7, 32.1 ppm. ESI-MS: m/z calcd, 268.12; found, 559.25 [2M + Na]$^+$.

1,3-Dimethyl-2-phenyl-1,2,3,4-tetrahydroquinazolin-6-ol 9a. According to GP3, starting from 6-hydroxy-1,3-dimethyl-2-phenyl-2,3-dihydroquinazolin-4(1*H*)-one **7a** (160 mg, 0.6 mmol, 1 equiv) the title compound 1,3-dimethyl-2-phenyl-1,2,3,4-tetrahydroquinazolin-6-ol **9a** (79 mg, 52%) was obtained as a pale yellow solid. ^{1}H NMR (400 MHz, DMSO-d_6): δ = 8.42 (s, OH), 7.34−7.27 (m, 2H), 7.27−7.21 (m, 1H), 7.18−7.08 (m, 2H), 6.56 (dd, J = 8.6, 2.7 Hz, 1H), 6.51 (d, J = 8.7 Hz, 1H), 6.32 (d, J = 2.6 Hz, 1H), 4.83 (s, 1H), 3.50 (d, J = 16.2 Hz, 1H), 3.27 (d, J = 16.1 Hz, 1H), 2.84 (s, 3H), 2.36 (s, 3H) ppm. ^{13}C NMR (101 MHz, DMSO-d_6): δ = 147.8, 141.1, 136.7, 128.1 (2C), 127.3, 126.9 (2C), 119.1, 114.1, 113.9, 110.1, 80.7, 49.2, 41.6, 36.8 ppm. ESI-MS: m/z calcd, 254.14; found, 255.2 [M + H]$^+$. HPLC (method A): 98%.

1,3-Dimethyl-2-phenyl-1,2,3,4-tetrahydroquinazolin-6-yl *n*-Heptylcarbamate 2a. According to GP4, starting from 1,3-dimethyl-2-phenyl-1,2,3,4-tetrahydroquinazolin-6-ol **9a** (120 mg, 0.47 mmol, 1 equiv) the title compound 1,3-dimethyl-2-phenyl-1,2,3,4-tetrahydroquinazolin-6-yl *n*-heptylcarbamate **2a** (95 mg, 51%) was obtained after column chromatography (DCM/MeOH = 95:5) as white solid; mp 93−95 °C. ^{1}H NMR (400 MHz, DMSO-d_6): δ = 7.51 (t, J = 5.7 Hz, NH), 7.36−7.29 (m, 2H), 7.29−7.23 (m, 1H), 7.15 (d, J = 7.1 Hz, 2H), 6.82 (dd, J = 8.7, 2.7 Hz, 1H), 6.62 (d, J = 8.9 Hz, 1H), 6.60 (d, J = 2.7 Hz, 1H), 4.96 (s, 1H), 3.56−3.49 (m, 1H), 3.36−3.30 (m, 1H), 3.01 (dd, J = 13.0, 6.7 Hz, 2H), 2.92 (s, 3H), 2.40 (s, 3H), 1.50−1.38 (m, 2H), 1.27 (s, 8H), 0.87 (t, J = 6.8 Hz, 3H) ppm. ^{13}C NMR (101 MHz, DMSO-d_6): δ = 155.1, 141.0, 140.9, 140.6, 128.2 (2C), 127.5, 126.7 (2C), 120.6, 120.1, 118.0, 108.8, 80.5, 48.5, 41.6, 40.4, 36.7, 31.2, 29.2, 28.4, 26.2, 22.0, 13.9 ppm. ESI-MS: m/z calcd, 395.26; found, 396.3 [M + H]$^+$. HPLC (method B): 100%.

5-(Benzyloxy)-2-nitrobenzaldehyde 11. A solution of 5-hydroxy-2-nitrobenzaldehyde (2 g, 11.98 mmol, 1 equiv) in dry DMF (40 mL) was treated with benzyl bromide (2.85 mL, 23.95 mmol, 2 equiv) and potassium carbonate (3.3 g, 23.95 mmol, 2 equiv). The reaction mixture was stirred for 48 h at 40 °C. Then ice cold water (100 mL) was added and the mixture was stirred for further 15 min. The precipitated solid was filtered and washed with petroleum ether (20 mL) to obtain 5-(benzyloxy)-2-nitrobenzaldehyde **11** (2.86 g, 88%) as a yellow solid; mp 68−70 °C. ^{1}H NMR (400 MHz, CDCl$_3$): δ = 10.48 (s, 1H), 8.16 (d, J = 9.1 Hz, 1H), 7.46−7.30 (m, 6H), 7.21 (dd, J = 9.1, 2.9 Hz, 1H), 5.20 (s, 2H). ^{13}C NMR (101 MHz, CDCl$_3$): δ = 188.4, 163.1, 142. 5, 135.0, 134.3, 128.9 (2C), 128.7, 127.6 (2C), 127.3, 119.3, 114.2, 71.1 ppm.

2-Amino-5-(benzyloxy)benzaldehyde 12. 5-(Benzyloxy)-2-nitrobenzaldehyde **11** (2.83 g, 10.44 mmol, 1 equiv) was dissolved in EtOH/H$_2$O (4:1, 50 mL) and treated with elementary iron (5.85 g, 104.4 mmol, 10 equiv) and a catalytic amount of conc HCl solution (50 μL). The mixture was heated to reflux temperature for 1 h. The product was then extracted with ethyl acetate (3 × 100 mL), and the combined organic layers were washed with brine (50 mL) and dried over Na$_2$SO$_4$. After removal of the solvent under reduced pressure, 2-amino-5-(benzyloxy)benzaldehyde **12** (1.44 g, 61%) was obtained as a yellow solid; mp 83 °C. ^{1}H NMR (400 MHz, CDCl$_3$): δ = 9.74 (d, J = 0.5 Hz, 1H), 7.38−7.21 (m, 5H), 6.99 (dd, J = 8.7, 2.9 Hz, 1H), 6.96 (d, J = 2.8 Hz, 1H), 6.54 (d, J = 8.7 Hz, 1H), 5.77 (s, NH$_2$), 4.95 (s, 2H) ppm. ^{13}C NMR (101 MHz, CDCl$_3$): δ = 193.5, 149.9, 145.0, 137.0, 128.6 (2C), 128.1, 127.5 (2C), 125.5, 118.7, 118.5, 117.6, 71.1 ppm. ESI-MS: m/z calcd, 227.09; found, 228.10 [M + H]$^+$.

N-(4-(Benzyloxy)-2-formylphenyl)benzamide 13. A mixture of 2-amino-5-(benzyloxy)benzaldehyde **12** (1022 mg, 4.49 mmol, 1 equiv) and triethylamine (934 μL, 4.63 mmol, 1.2 equiv) was dissolved in DCM (50 mL) and treated dropwise with benzoyl chloride (784 μL, 6.75 mmol, 1.5 equiv). After stirring for 4 h, the reaction mixture was diluted with DCM (100 mL) and washed with 2 M HCl (50 mL), sat. NaHCO$_3$ (50 mL), and brine (50 mL). The solvent was removed under reduced pressure and the crude product was purified by column chromatography (DCM/petroleum ether = 1:1) to obtain *N*-(4-(benzyloxy)-2-formylphenyl)benzamide **13** (986 mg, 66%) as a yellow solid; mp 131−133 °C. ^{1}H NMR (400 MHz, CDCl$_3$): δ = 11.84 (s, NH), 9.94 (d, J = 0.6 Hz, 1H), 8.92 (d, J = 9.1 Hz, 1H), 8.12−8.03 (m, 2H), 7.60−7.50 (m, 3H), 7.48−7.38 (m, 4H), 7.38−7.34 (m, 1H), 7.32 (dd, J = 9.0, 3.0 Hz, 1H), 7.29 (d, J = 2.9 Hz, 1H), 5.14 (s, 2H) ppm. ^{13}C NMR (101 MHz, CDCl$_3$): δ = 195.5, 165.8, 154.3, 136.3, 135.2, 134.5, 132.0, 128.9 (2C), 128.7 (2C), 128.3, 127.5 (2C), 127.4 (2C), 123.3, 122.9, 121.8, 121.1, 70.7 ppm. ESI-MS: m/z calcd, 331.12; found, 332.15 [M + H]$^+$.

6-(Benzyloxy)-2-phenylquinazoline 14. According to the literature,[50] *N*-(4-(benzyloxy)-2-formylphenyl)benzamide **13** (980 mg, 2.96 mmol, 1 equiv) was suspended in *i*-PrOH/conc ammonia (1:1, 30 mL) and heated to 90 °C for 6 h under microwave irradiation. Then the product was extracted with ethyl acetate (2 × 100 mL), the combined organic layers were washed with brine (50 mL) and dried over Na$_2$SO$_4$. After removal of the solvent, 6-(benzyloxy)-2-phenylquinazoline **14** (889 mg, 96%) was obtained as a beige solid; mp 119−120 °C. ^{1}H NMR (400 MHz, CDCl$_3$): δ = 9.38 (d, J = 0.7 Hz, 1H), 8.63−8.56 (m, 2H), 8.04 (d, J = 9.2 Hz, 1H), 7.66 (dd, J = 9.2, 2.8 Hz, 1H), 7.58−7.51 (m, 5H), 7.51−7.43 (m, 2H), 7.43−7.36 (m, 1H), 7.27 (d, J = 2.8 Hz, 1H), 5.25 (s, 2H) ppm. ^{13}C NMR (101 MHz, CDCl$_3$): δ = 159.6, 158.9, 157.3, 147.1, 138.2, 136.1, 130.3, 130.2, 128.8 (2C), 128.6 (2C), 128.4, 128.2 (2C), 127.6 (2C), 127.5, 124.5, 105.3, 70.6 ppm. ESI-MS: m/z calcd, 312.13; found, 313.20 [M + H]$^+$.

2-Phenylquinazolin-6-ol 15. 6-(Benzyloxy)-2-phenylquinazoline **14** (870 mg, 2.79 mmol, 1 equiv) was dissolved in MeOH (50 mL), and Pd/C (87 mg, 10 wt %) was added. The atmosphere of the reaction vessel was removed under reduced pressure, and then the vessel was purged with hydrogen. The mixture was heated to 50 °C for 3 h. Then the mixture was filtered over a short silica column to obtain 2-phenylquinazolin-6-ol **15** (435 mg, 70%) as a white solid; mp 233−235 °C. ^{1}H NMR (400 MHz, DMSO-d_6): δ = 10.44 (br, OH), 9.50 (d, J = 0.7 Hz, 1H), 8.58−8.43 (m, 2H), 7.95 (d, J = 9.1 Hz, 1H), 7.61−7.48 (m, 4H), 7.32 (d, J = 2.6 Hz, 1H) ppm. ^{13}C NMR (101 MHz, DMSO-d_6): δ = 159.7, 157.7, 156.9, 145.4, 138.3, 130.6, 130.1, 129.1 (2C), 128.1 (2C), 127.7, 125.2, 108.2 ppm. ESI-MS: m/z calcd, 222.08; found, 223.15 [M + H]$^+$. HPLC (method A): 100%.

2-Phenylquinazolin-6-yl *n*-Heptylcarbamate 16. According to GP4, starting from 2-phenylquinazolin-6-ol **15** (60 mg, 0.27 mmol, 1 equiv) the title compound 2-phenylquinazolin-6-yl heptylcarbamate **16** (35 mg, 36%) was obtained after column chromatography (petroleum ether/EtOAc = 3:1) as white powder; mp 141−144 °C. ^{1}H NMR (400 MHz, CDCl$_3$): δ = 9.41 (s, 1H), 8.64−8.55 (m, 2H), 8.07 (d, J = 9.1 Hz, 1H), 7.71 (d, J = 2.4 Hz, 1H), 7.66 (dd, J = 9.1, 2.6 Hz, 1H), 7.58−7.48 (m, 3H), 5.20 (t, J = 5.6 Hz, NH), 3.29 (dd, J = 13.3, 7.0 Hz, 2H), 1.67−1.49 (m, 2H), 1.44−1.23 (m, 8H), 0.90 (t, J = 6.9 Hz, 3H) ppm. ^{13}C NMR (101 MHz, CDCl$_3$): δ = 160.8, 160.0, 154.0, 149.3, 148.5, 137.9,

130.6, 130.0, 129.7, 128.6 (2C), 128.5 (2C), 123.7, 117.3, 41.4, 31.7, 29.8, 28.9, 26.7, 22.6, 14.1 ppm. ESI-MS: m/z calcd, 363.19; found, 364.25 $[M + H]^+$. HPLC (method B): 100%.

Enzyme Inhibition. AChE (EC 3.1.1.7, from human erythrocytes) and BChE (EC 3.1.1.8, from equine serum and from human serum) were purchased from Sigma-Aldrich (Steinheim, Germany). DTNB (Ellman's reagent), ATC and BTC iodides were obtained from Fluka (Buchs, Switzerland). The stock solutions of the test compounds were prepared in ethanol with a concentration of 33.3 mM (1 mM in assay) and stepwise diluted with ethanol to a concentration of 33.3 nM (1 nM in assay). For assay buffer preparation, an amount of 3.12 g of potassium dihydrogen phosphate was dissolved in 500 mL of water and adjusted with a NaOH solution (0.2 M) to pH = 8.0. Enzyme solutions were prepared with buffer to give 2.5 units/mL and stabilized with 2 mg of albumin bovine (SERVA, Heidelberg, Germany) per mL of enzyme solution. An amount of 396 mg of DTNB was dissolved in 100 mL of buffer to give a 10 mM solution (0.3 mM in assay). ATC and BTC solutions were prepared in buffer with a concentration of 75 mM (452 μM in assay). The assay was performed at 25 °C as described in the following: Into a cuvette containing 1.5 mL of buffer, 50 μL of the respective enzyme, and 50 μL of DTNB solution, the test compound solution (50 μL) was added, and the mixture was mixed. The mixture was incubated for 4.5 min (phenols) or 30 min (carbamates), before an amount of 10 μL of ATC or BTC (depending on the enzyme) was added. The mixture was incubated for further 2.5 min before the absorption at 412 nm was determined with a Shimadzu UVmini-1240 spectrophotometer. To measure full enzyme activity, the compound solution was replaced by ethanol. Each compound concentration was tested three times. The enzyme activity in percentage was plotted against the logarithm of the compound concentrations from which the IC_{50} values were calculated by the software GraphPad Prism 4.

Enzyme Kinetics. Carbamoylation kinetics were measured following the enzyme inhibition protocol. For this purpose, the enzyme was 5, 10, 20, 30, and 40 min preincubated with different inhibitor concentrations before the addition of substrate. Plotting the enzyme activity in percentage as a function of time for each inhibitor concentration gave nonlinear time dependent inhibition curves from which k_{obs} was determined by eq 1. Double reciprocal plot of $1/k_{obs}$ against $1/c$(inhibitor) gave a linear plot from which k_3 and K_C were determined by eq 4. Decarbamoylation kinetics were measured by incubating the enzyme with an inhibitor concentration that fully inhibits the enzyme for 1 h. This mixture was then diluted 1:1000 with assay buffer to prevent further enzyme inhibition. The assay was then performed as described in the enzyme inhibition protocol at different time points after the dilution to determine recovery of enzyme activity. Uninhibited enzyme was treated by the same procedure to access control values for enzyme activity after dilution. Plotting the enzyme activity against different time points after dilution gave an exponential first order kinetics from which k_4 was calculated. All kinetic values were determined using the software GraphPad Prism 4.

Molecular Modeling Studies. To derive a common binding-mode hypothesis, a combined docking and minimization approach was applied.

Docking studies were conducted with the program GOLD, version 5.2.2 (CCDC Software, http://www.ccdc.cam.ac.uk)[64] using the crystal structure PDB code 1P0I of human BChE (resolution 2.0 Å).[66] Prior to docking, all water molecules and non-protein atoms were removed and the amino acids were protonated with Protonate 3D in MOE[78] (version 2013.0801) at pH = 8 as the assay pH value. The binding site corresponding to the search region in the docking was defined by the following residues: Asn68, Asp70, Ser79, Trp82, Asn83, Gly115, Gly116, Gly117, Gln119, Thr120, Gly121, Thr122, Leu125, Tyr128, Glu197, Ser198, Ala199, Trp231, Leu286, Val288, Glu325, Ala328, Phe329, Tyr332, Trp430, His438, Gly439, Tyr440, Ile442.

Ligand structures were built in MOE or extracted from the crystal structure (ligand for redocking experiment, see below). The ligands were energy minimized in MOE with the MMFF94x force field to an rms gradient of 0.001 kcal/(mol·Å).

A redocking test was performed with the BChE crystal structure 4BDS (resolution, 2.10 Å) and tacrine as a reversible ligand. Tacrine was

protonated at the acridinic N at pH = 8, according to a calculation with MoKa.[79] Fifty independent docking runs were carried out, with the number of operations set to 1 million to improve docking pose clustering. Among the four tested scoring functions, Goldscore[80,81] found the pose with the lowest rmsd (0.45 Å) to the crystal structure on higher ranks (rank 14) than the other functions (rank >40) and in a cluster containing 21 poses. The top pose showed an rmsd of 0.76 Å and was in a cluster with 27 poses. The Goldscore scoring function had previously proven to be applicable also in docking studies with AChE.[45,48]

Docking was performed with the same parameters (as used in the redocking test) for the kinetically investigated ligands listed in Table 2 (i.e., **2a**, **2c**, **2h**, **2i**, **2k**, **2l**, **2p**, **2s**, **2u**, **3a**, and **16**) as well as for ligand **1**, which possesses the most rigid structure. Chiral ligands were handled in both enantiomeric forms. The Goldscore value provided the first ranking criterion for the poses of a given ligand. In addition, rescoring with DSX[82] and CSD potentials were used as a second evaluation criterion. Moreover, docking poses were visually inspected, in particular the position of the carbamate moiety with respect to the catalytic serine and the orientation of the C═O group with respect to the oxyanion hole. Only poses showing a suitable orientation for the transfer of the carbamate to the serine were further considered.[83]

Ligand **1** as the most rigid compound showed well-clustered results and reasonable positions for carbamate transfer in both enantiomeric forms. The top rank for the *S*-enantiomer (second best in rescoring the top-five poses with DSX/CSD) and the second-best rank for the *R*-enantiomer (top rank in rescoring the top-five poses with DSX/CSD) showed the carbonyl oxygen of the carbamate pointing toward the oxyanion hole with distances of 2.7 and 2.8 Å between C═O and Gln117-N for the *S*- and the *R*-enantiomer, respectively. These poses were chosen as a reference for the binding modes of the studied class of compounds.

Because of the large size of the BChE binding pocket and the higher flexibility of the compounds in comparison to **1**, docking of all other investigated ligands resulted in more diverse and energetically rather degenerate poses besides the reference binding mode. To generate a more consistent binding-mode hypothesis, a modeling approach was followed for these structurally very similar ligands, in which the reference poses of compound **1** were used to construct the ligands in the binding site. Essentially, this was done with MOE 2014.0901 by deleting the methylene bridge of the tetracyclic structure of **1** and adding the required substituents to the aryl ring. The obtained structures were relaxed in the binding pocket with MiniMuDS[65] and scored with DSX/CSD.

For both enantiomers, the methyl group at the benzylic nitrogen was initially modeled in both the pseudo-equatorial and the pseudo-axial form. All *R*-enantiomers showed unfavorable distances of 2.1−2.4 Å between the axial methyl group and Gly116-Cα and were, hence, scored lower than the poses with the equatorial methyl. Thus, the *R*-enantiomers are presented with the methyl group in equatorial orientation. For the *S*-enantiomers, the methyl group in the axial position is much more favorable because it points to a small cavity between Trp82 of the choline binding site and His438 of the CAS. The conformer with the equatorial methyl group also fits to the binding site but corresponds to an energetically less favorable conformation, as investigated by force field calculations with the MMFF94s force field[84] in MOE. Accordingly, the *S*-enantiomers are presented with the methyl group in an axial orientation.

All figures of docking poses and enzyme structures were made with Pymol.[72]

Antioxidant Capacities (ORAC Assay). The antioxidant activity was determined by the oxygen radical absorbance capacity fluorescein (ORAC-FL) assay, modified by Dávalos et al.[85] The ORAC assay measures antioxidant scavenging activity against peroxyl radicals, their formation induced by 2,2′-azobis(2-amidinopropane) dihydrochloride (AAPH) at 37 °C. The reaction was carried out in 75 mM phosphate buffer (pH 7.4), and the final reaction mixture was 200 μL. Antioxidant (20 μL) and fluorescein (120 μL; 300 nM final concentration) were placed in the wells of a 96-well plate, and the mixture was incubated for 15 min at 37 °C. Then AAPH (Sigma, Steinheim, Germany) solution

(60 μL; 12 mM final concentration) was added rapidly. The plate was immediately placed into a SpectraFluor Plus plate reader (Tecan, Crailsheim, Germany) and fluorescence measured every 60 s for 90 min with excitation at 485 nm and emission at 535 nm. 6-Hydroxy-2,5,7,8-tetramethylchroman-2-carboxylic acid (Trolox, Sigma, Steinheim, Germany) was used as a standard (1–8 μM, final concentration). A blank (FL + AAPH) using phosphate buffer instead of antioxidant and Trolox calibration were carried out in each assay. The samples were measured at different concentrations (1–5 μM). All reaction mixtures were prepared 4-fold, and at least four independent runs were performed for each sample. Fluorescence measurements were normalized to the curve of the blank (without antioxidant). From the normalized curves, the area under the fluorescence decay curve (AUC) was calculated as

$$AUC = 1 + \sum_{i=1}^{i=90} f_i/f_0$$

where f_0 is the initial fluorescence at 0 min and f_i is the fluorescence at time i. The net AUC for a sample was calculated as follows:

$$net\ AUC = AUC\ antioxidant - AUC\ blank$$

The ORAC-FL values were calculated:

$$\left[\frac{(AUC\ sample) - (AUC\ blank)}{(AUC\ Trolox) - (AUC\ blank)}\right]\left[\frac{concentration\ of\ Trolox}{concentration\ of\ sample}\right]$$

and expressed as Trolox equivalents by using the standard curve calculated for each assay. Final results were in μM of Trolox equivalent/μM of compound.

Neurotoxicity and Neuroprotection. Neurotoxicity and neuroprotection were done as described before.[47] HT 22 cells were derived from murine hippocampal tissue, kindly provided by the Max Planck Institute of Psychiatry, Munich, and were grown in high glucose Dulbecco's modified Eagle medium (DMEM, Invitrogen, Karlsruhe, Germany) supplemented with 10% (v/v) heat inactivated fetal calf serum (FCS) (Biochrom, Berlin, Germany). Cells were kept under standard cell culture conditions at 37 °C under 5% CO_2 in a humidified incubator and were subcultured every 2 d. Cell viability was determined by 3-(4,5-dimethylthiazol-2-yl)-2,5-diphenyltetrazolium bromide (MTT) assay. Briefly, cells were seeded in 96-well plates at a densitiy of 5 × 10 per well and cultured for 24 h. Subsequently cells were incubated for another 24 h with medium, compounds, or solvent in presence (neuroprotection assay) or absence (neurotoxicity assay) of 5 mM glutamate (monosodium L-glutamate, Merck, Darmstadt, Germany). Quercetin (Sigma, Steinheim, Germany) in a concentration of 25 μM served as the positive control in the neuroprotection assay. MTT (Sigma, Steinheim, Germany) solution (4 mg/mL in PBS) was diluted 1:10 with medium, and the mixture was added to the wells after removal of previous medium. The plates were then incubated for another 3 h. The supernatants were removed, and 100 μL of lysis buffer (10% SDS, pH 4.1) was added to the wells. Absorbance at 560 nM was determined on the next day with a multiwall plate photometer (Spectra Fluor Plus, Crailsheim, Germany). Results of cell viability are expressed as percentage to untreated control cells. All compounds were dissolved in DMSO and diluted with fresh medium. DMSO concentration in final dilutions was ≤0.1%. Data are expressed as the mean ± SD of at least three different independent experiments. Data were subjected to one way ANOVA followed by Dunnett's multiple comparison post-test using GraphPad Prism 4 software (levels of significance: (∗) $p < 0.05$; (∗∗) $p < 0.01$; (∗∗∗) $p < 0.001$).

ASSOCIATED CONTENT

Ⓢ Supporting Information

The Supporting Information is available free of charge on the ACS Publications website at DOI: 10.1021/acs.jmedchem.5b01674.

> Sequence comparison, IC_{50} values with confidence intervals, description and chromatograms of the enantiomeric separation of **2p**, energetic comparison of the

enantiomeres, the postulated binding mode of **2l**, synthetic procedures and spectral data for **6b–d**, **7b–u**, **8a–c**, **9b–u**, **10a–c**, **2b–u**, and **3a–c** (PDF)
Molecular formula strings (CSV)

AUTHOR INFORMATION

Corresponding Author
*M.D.: phone, +0049-931 31-89676; fax, +0049-931 31-85494; e-mail, Michael.Decker@uni-wuerzburg.de.

Author Contributions
The manuscript was written with contributions of all authors. E.S. performed the synthesis and biological testing on AChE and BChE as well as the kinetic studies on BChE. S.W., under the supervision of C.S., was responsible for the molecular docking studies on BChE. B.K., under the supervision of J.H., tested the antioxidant capacity, neuroprotection, and toxicity of the synthesized compounds. J.W. performed the separation of enantiomers of **2p** under the supervision of G.B. M.D. was responsible for the supervision and development of the whole project.

Notes
The authors declare no competing financial interest.

ABBREVIATIONS USED

AAPH, 2,2′-azobis(2-amidinopropane) dihydrochloride; ATC, acetylthiocholine iodide; BTC, butyrylthiocholine iodide; CAS, catalytic active site; CD, circular dichroism; DIPEA, N,N-diisopropylethylamine; DMAc, dimethylacetamide; DTNB, 5,5′-dithiobis(2-nitrobenzoic acid); EC, Enzyme Commission number; eqBChE, equine butyrylcholinesterase; FL, fluorescein; GSH, glutathione; hAChE, human acetylcholinesterase; hBChE, human butyrylcholinesterase; MW, microwave; ORAC, oxygen radical absorbance capacity; rmsd, root mean square deviation; SAR, structure–activity relationship; TE, Trolox equivalent; Trolox, 6-hydroxy-2,5,7,8-tetramethylchroman-2-carboxylic acid

REFERENCES

(1) Wimo, A.; Prince, M. *World Alzheimer Report 2010. The Global Economic Impact of Dementia*; Alzheimer's Disease International, 2010.

(2) Prince, M.; Prina, M.; Guerchet, M. *World Alzheimer Report 2013. Journey of Caring. An Analysis of Long-Term Care for Dementia*; Alzheimer's Disease International, 2013.

(3) Querfurth, H. W.; LaFerla, F. M. Alzheimer's Disease. *N. Engl. J. Med.* **2010**, *362*, 329–344.

(4) Hensley, K. Neuroinflammation in Alzheimer's Disease: Mechanisms, Pathologic Consequences, and Potential for Therapeutic Manipulation. *J. Alzheimer's Dis.* **2010**, *21*, 1–14.

(5) Larson, M. E.; Lesné, S. E. Soluble Aβ Oligomer Production and Toxicity. *J. Neurochem.* **2012**, *120*, 125–139.

(6) Walsh, D. M.; Townsend, M.; Podlisny, M. B.; Shankar, G. M.; Fadeeva, J. V.; El Agnaf, O.; Hartley, D. M.; Selkoe, D. J. Certain Inhibitors of Synthetic Amyloidβ-Peptide (Aβ) Fibrillogenesis Block Oligomerization of Natural Aβ and Thereby Rescue Long-Term Potentiation. *J. Neurosci.* **2005**, *25*, 2455–2462.

(7) De Calignon, A.; Polydoro, M.; Suárez-Calvet, M.; William, C.; Adamowicz, D. H.; Kopeikina, K. J.; Pitstick, R.; Sahara, N.; Ashe, K. H.; Carlson, G. A.; Spires-Jones, T. L.; Hyman, B. T. Propagation of Tau Pathology in a Model of Early Alzheimer's Disease. *Neuron* **2012**, *73*, 685−697.

(8) Lee, H.; Perry, G.; Moreira, P. I.; Garrett, M. R.; Liu, Q.; Zhu, X.; Takeda, A.; Nunomura, A.; Smith, M. A. Tau Phosphorylation in Alzheimer's Disease: Pathogen or Protector? *Trends Mol. Med.* **2005**, *11*, 164−169.

(9) Eidenmüller, J.; Fath, T.; Hellwig, A.; Reed, J.; Sontag, E.; Brandt, R. Structural and Functional Implications of Tau Hyperphosphorylation: Information from Phosphorylation-Mimicking Mutated Tau Proteins. *Biochemistry* **2000**, *39*, 13166−13175.

(10) Khlistunova, I.; Biernat, J.; Wang, Y.; Pickhardt, M.; von Bergen, M.; Gazova, Z.; Mandelkow, E.; Mandelkow, E.-M. Inducible Expression of Tau Repeat Domain in Cell Models of Tauopathy. Aggregation is Toxic to Cells but can be Reversed by Inhibitor Drugs. *J. Biol. Chem.* **2006**, *281*, 1205−1214.

(11) Varadarajan, S.; Yatin, S.; Aksenova, M.; Butterfield, D. A. Review: Alzheimer's Amyloid β-Peptide-Associated Free Radical Oxidative Stress and Neurotoxicity. *J. Struct. Biol.* **2000**, *130*, 184−208.

(12) Wang, X.; Wang, W.; Li, Li.; Perry, G.; Lee, H.; Zhu, X. Oxidative Stress and Mitochondrial Dysfunction in Alzheimer's Disease. *Biochim. Biophys. Acta, Mol. Basis Dis.* **2014**, *1842*, 1240−1247.

(13) Francis, P. T. Glutamatergic Systems in Alzheimer's Disease. *Int. J. Geriatr. Psych.* **2003**, *18*, 15−21.

(14) Wenk, G. L. Neuropathologic Changes in Alzheimer's Disease: Potential Targets for Treatment. *J. Clin. Psychiatry* **2006**, *67*, 3−7.

(15) Francis, P. T.; Palmer, A. M.; Snape, M.; Wilcock, G. K. The Cholinergic Hypothesis of Alzheimer's Disease: A Review of Progress. *J. Neurol., Neurosurg. Psychiatry* **1999**, *66*, 137−147.

(16) Raina, P.; Santaguida, P.; Ismaila, A.; Patterson, C.; Cowan, D.; Levine, M.; Booker, L.; Oremus, M. Effectiveness of Cholinesterase Inhibitors and Memantine for Treating Dementia: Evidence Review for a Clinical Practice Guideline. *Ann. Intern. Med.* **2008**, *148*, 379−397.

(17) Rountree, S. D.; Chan, W.; Pavlik, V. N.; Darby, E. J.; Siddiqui, S.; Doody, R. S. Persistent Treatment with Cholinesterase Inhibitors and/or Memantine Slows Clinical Progression of Alzheimer Disease. *Alzheimer's Res. Ther.* **2009**, *1*, 7.

(18) Nordberg A.; Ballard C.; Bullock R.; Darreh-Shori T.; Somogyi, M. A Review of Butyrylcholinesterase as a Therapeutic Target in the Treatment of Alzheimer's Disease. *Prim. Care Companion CNS Disord.* **2013**, *15*, DOI: 10.4088/PCC.12r01412.

(19) Arendt, T.; Bruckner, M. K.; Lange, M.; Bigl, V. Changes in Acetylcholinesterase and Butyrylcholinesterase in Alzheimer's Disease Resemble Embryonic Development—A Study of Molecular Forms. *Neurochem. Int.* **1992**, *21*, 381−396.

(20) Giacobini, E. Cholinergic Function and Alzheimer's Disease. *Int. J. Geriatr. Psychiatry* **2003**, *18*, 1−5.

(21) Greig, N. H.; Utsuki, T.; Yu, Q.-S.; Zhu, X.; Holloway, H. W.; Perry, T.; Lee, B.; Ingram, D. K.; Lahiri, D. K. A New Therapeutic Target in Alzheimer's Disease Treatment: Attention to Butyrylcholinesterase. *Curr. Med. Res. Opin.* **2001**, *17*, 159−165.

(22) Grossberg, G. T. Cholinesterase Inhibitors for the Treatment of Alzheimer's Disease: Getting On and Staying On. *Curr. Ther. Res.* **2003**, *64*, 216−235.

(23) Darvesh, S.; Hopkins, D. A.; Geula, C. Neurobiology of Butyrylcholinesterase. *Nat. Rev. Neurosci.* **2003**, *4*, 131−138.

(24) Mesulam, M.-M.; Guillozet, A.; Shaw, P.; Levey, A.; Duysen, E. G.; Lockridge, O. Acetylcholinesterase Knockouts Establish Central Cholinergic Pathways and can Use Butyrylcholinesterase to Hydrolyze Acetylcholine. *Neuroscience* **2002**, *110*, 627−639.

(25) Hartmann, J.; Kiewert, C.; Duysen, E. G.; Lockridge, O.; Greig, N. H.; Klein, J. Excessive Hippocampal Acetylcholine Levels in Acetylcholinesterase-Deficient Mice are Moderated by Butyrylcholinesterase Activity. *J. Neurochem.* **2007**, *100*, 1421−1429.

(26) Furukawa-Hibi, Y.; Alkam, T.; Nitta, A.; Matsuyama, A.; Mizoguchi, H.; Suzuki, K.; Moussaoui, S.; Yu, Q.-S.; Greig, N. H.; Nagai, T.; Yamada, K. Butyrylcholinesterase Inhibitors Ameliorate

(27) Greig, N. H.; Utsuki, T.; Ingram, D. K.; Wang, Y.; Pepeu, G.; Scali, C.; Yu, Q.-S.; Mamczarz, J.; Holloway, H. W.; Giordano, T.; Chen, D.; Furukawa, K.; Sambamurti, K.; Brossi, A.; Lahiri, D. K. Selective Butyrylcholinesterase Inhibition Elevates Brain Acetylcholine, Augments Learning and Lowers Alzheimer β-Amyloid Peptide in Roden. *Proc. Natl. Acad. Sci. U. S. A.* **2005**, *102*, 17213−17218.

(28) Maurice, T.; Strehaiano, M.; Siméon, N.; Bertrand, C.; Chatonnet, A. Learning Performances and Vulnerability to Amyloid Toxicity in the Butyrylcholinesterase Knockout Mouse. *Behav. Brain Res.* **2016**, *296*, 351−360.

(29) Li, B.; Duysen, E. G.; Lockridge, O. The Butyrylcholinesterase Knockout Mouse is Obese on a High-Fat Diet. *Chem.-Biol. Interact.* **2008**, *175*, 88−91.

(30) Iwasaki, T.; Yoneda, M.; Nakajima, A.; Terauchi, Y. Serum Butyrylcholinesterase is Strongly Associated with Adiposity, the Serum Lipid Profile and Insulin Resistance. *Intern. Med.* **2007**, *46*, 1633−1639.

(31) Sato, K. K.; Hayashi, T.; Maeda, I.; Koh, H.; Harita, N.; Uehara, S.; Onishi, Y.; Oue, K.; Nakamura, Y.; Endo, G.; Kambe, H.; Fukuda, K. Serum Butyrylcholinesterase and the Risk of Future Type 2 Diabetes: the Kansai Healthcare Study. *Clin. Endocrinol.* **2014**, *80*, 362−367.

(32) Stojanov, M.; Stefanović, A.; Džingalašević, G.; Mandić-Radić, S.; Prostran, M. Butyrylcholinesterase Activity in Young Men and Women: Association with Cardiovascular Risk Factors. *Clin. Biochem.* **2011**, *44*, 623−626.

(33) Alcântara, V. M.; Chautard-Freire-Maia, E. A.; Scartezini, M.; Cerci, M. S. J.; Braun-Prado, K.; Picheth, G. Butyrylcholinesterase Activity and Risk Factors for Coronary Artery Disease. *Scand. J. Clin. Lab. Invest.* **2002**, *62*, 399−404.

(34) Dougherty, D. A.; Stauffer, D. A. Acetylcholine Binding by a Synthetic Receptor: Implications for Biological Recognition. *Science* **1990**, *250*, 1558−1560.

(35) Brus, B.; Košak, U.; Turk, S.; Pišlar, A.; Coquelle, N.; Kos, J.; Stojan, J.; Colletier, J.-P.; Gobec, S. Discovery, Biological Evaluation, and Crystal Structure of a Novel Nanomolar Selective Butyrylcholinesterase Inhibitor. *J. Med. Chem.* **2014**, *57*, 8167−8179.

(36) Huang, G.; Kling, B.; Darras, F. H.; Heilmann, J.; Decker, M. Identification of a Neuroprotective and Selective Butyrylcholinesterase Inhibitor Derived from the Natural Alkaloid Evodiamine. *Eur. J. Med. Chem.* **2014**, *81*, 15−21.

(37) Takahashi, J.; Hijikuro, I.; Kihara, T.; Murugesh, M. G.; Fuse, S.; Tsumura, Y.; Akaike, A.; Niidome, T.; Takahashi, T.; Sugimoto, H. Design, Synthesis and Evaluation of Carbamate-Modified (−)-N^1-Phenethylnorphysostigmine Derivatives as Selective Butyrylcholinesterase Inhibitors. *Bioorg. Med. Chem. Lett.* **2010**, *20*, 1721−1723.

(38) Groner, E.; Ashani, Y.; Schorer-Apelbaum, D.; Sterling, J.; Herzig, Y.; Weinstock, M. The Kinetics of Inhibition of Human Acetylcholinesterase and Butyrylcholinesterase by Two Series of Novel Carbamates. *Mol. Pharmacol.* **2007**, *71*, 1610−1617.

(39) Yu, Q.; Greig, N. H.; Holloway, H. W.; Brossi, A. Syntheses and Anticholinesterase Activities of (3a*S*)-*N*1, N8-Bisnorphenserine, (3a*S*)-*N1,N8*-Bisnorphysostigmine, their Antipodal Isomers, and Other Potential Metabolites of Phenserine. *J. Med. Chem.* **1998**, *41*, 2371−2379.

(40) Darvesh, S.; Darvesh, K. V.; McDonald, R. S.; Mataija, D.; Walsh, R.; Mothana, S.; Lockridge, O.; Martin, E. Carbamates with Differential Mechanism of Inhibition Toward Acetylcholinesterase and Butyrylcholinesterase. *J. Med. Chem.* **2008**, *51*, 4200−4212.

(41) Chiou, S.-Y.; Huang, C.-F.; Hwang, M.-T.; Lin, G. Comparison of Active Sites of Butyrylcholinesterase and Acetylcholinesterase Based on Inhibition by Geometric Isomers of Benzene-di-*N*-Substituted Carbamates. *J. Biochem. Mol. Toxicol.* **2009**, *23*, 303−308.

(42) Lin, G.; Lee, Y.-R.; Liu, Y.-C.; Wu, Y.-G. *Ortho* Effects for Inhibition Mechanisms of Butyrylcholinesterase by *o*-Substituted Phenyl *N*-Butyl Carbamates and Comparison with Acetylcholinesterase, Cholesterol Esterase, and Lipase. *Chem. Res. Toxicol.* **2005**, *18*, 1124−1131.

(43) Carolan, C. G.; Dillon, G. P.; Khan, D.; Ryder, S. A.; Gaynor, J. M.; Reidy, S.; Marquez, J. F.; Jones, M.; Holland, V.; Gilmer, J. F. Isosorbide-2-benzyl Carbamate-5-salicylate, A Peripheral Anionic Site Binding Subnanomolar Selective Butyrylcholinesterase Inhibitor. *J. Med. Chem.* **2010**, *53*, 1190−1199.

(44) Decker, M.; Krauth, F.; Lehmann, J. Novel Tricyclic Quinazolinimines and Related Tetracyclic Nitrogen Bridgehead Compounds as Cholinesterase Inhibitors with Selectivity Towards Butyrylcholinesterase. *Bioorg. Med. Chem.* **2006**, *14*, 1966−1977.

(45) Darras, F. H.; Wehle, S.; Huang, G.; Sotriffer, C. A.; Decker, M. Amine Substitution of Quinazolinones Leads to Selective Nanomolar AChE Inhibitors with 'Inverted' Binding Mode. *Bioorg. Med. Chem.* **2014**, *22*, 4867−4881.

(46) Decker, M. Homobivalent Quinazolinimines as Novel Nanomolar Inhibitors of Cholinesterases with Dirigible Selectivity Toward Butyrylcholinesterase. *J. Med. Chem.* **2006**, *49*, 5411−5413.

(47) Darras, F. H.; Kling, B.; Heilmann, J.; Decker, M. Neuroprotective Tri- and Tetracyclic BChE Inhibitors Releasing Reversible Inhibitors upon Carbamate Transfer. *ACS Med. Chem. Lett.* **2012**, *3*, 914−919.

(48) Darras, F. H.; Pockes, S.; Huang, G.; Wehle, S.; Strasser, A.; Wittmann, H.-J.; Nimczick, M.; Sotriffer, C. A.; Decker, M. Synthesis, Biological Evaluation, and Computational Studies of Tri- and Tetracyclic Nitrogen-Bridgehead Compounds as Potent Dual-Acting AChE Inhibitors and *h*H$_3$ Receptor Antagonists. *ACS Chem. Neurosci.* **2014**, *5*, 225−242.

(49) Sawatzky, E.; Bukowczan, J.; Decker, M. Investigation into Selective Debenzylation and Ring Cleavage of Quinazoline Based Heterocycles. *Tetrahedron Lett.* **2014**, *55*, 2973−2976.

(50) Zhao, D.; Shen, Q.; Zhou, Y.-R.; Li, J.-X. KO*t*Bu-Mediated Stereoselective Addition of Quinazolines to Alkynes Under Mild Conditions. *Org. Biomol. Chem.* **2013**, *11*, 5908−5912.

(51) Ellman, G. L. A Colorimetric Method for Determining Low Concentrations of Mercaptans. *Arch. Biochem. Biophys.* **1958**, *74*, 443−450.

(52) Ellman, G. L.; Courtney, K. D.; Andres, V.; Featherstone, R. M. A New and Rapid Colorimetric Determination of Acetylcholinesterase Acticity. *Biochem. Pharmacol.* **1961**, *7*, 88−95.

(53) Yücel, Y. Y.; Tacal, Ö.; Özer, I. Comparative Effects of Cationic Triarylmethane, Phenoxazine and Phenothiazine Dyes on Horse Serum Butyrylcholinesterase. *Arch. Biochem. Biophys.* **2008**, *478*, 201−205.

(54) Topliss, J. G. Utilization of Operational Schemes for Analog Synthesis in Drug Design. *J. Med. Chem.* **1972**, *15*, 1006−1011.

(55) O'Boyle, N. M.; Bostrom, J.; Sayle, R. A.; Gill, A. Using Matched Molecular Series as a Predictive Tool to Optimize Biological Activity. *J. Med. Chem.* **2014**, *57*, 2704−2713.

(56) Kier, L. B.; Hall, L. H. Bioisosterism: Quantitation of Structure and Property Effects. *Chem. Biodiversity* **2004**, *1*, 138−151.

(57) Sheridan, R. P. The Most Common Chemical Replacements in Drug-Like Compounds. *J. Chem. Inf. Model.* **2002**, *42*, 103−108.

(58) Cheung, J.; Rudolph, M. J.; Burshteyn, F.; Cassidy, M. S.; Gary, E. N.; Love, J.; Franklin, M. C.; Height, J. J. Structures of Human Acetylcholinesterase in Complex with Pharmacologically Important Ligands. *J. Med. Chem.* **2012**, *55*, 10282−10286.

(59) Harel, M.; Schalk, I.; Ehret-Sabatier, L.; Bouet, F.; Goeldner, M.; Hirth, C.; Axelsen, P. H.; Silman, I.; Sussman, J. L. Quaternary Ligand Binding to Aromatic Residues in the Active-Site Gorge of Acetylcholinesterase. *Proc. Natl. Acad. Sci. U. S. A.* **1993**, *90*, 9031−9035.

(60) Dvir, H.; Wong, D. M.; Harel, M.; Barril, X.; Orozco, M.; Luque, F. J.; Muñoz-Torrero, D.; Camps, P.; Rosenberry, T. L.; Silman, I.; Sussman, J. L. 3D Structure of Torpedo californica Acetylcholinesterase Complexed with Huprine X at 2.1 Å Resolution: Kinetic and Molecular Dynamic Correlates. *Biochemistry* **2002**, *41*, 2970−2981.

(61) Bar-On, P.; Millard, C. B.; Harel, M.; Dvir, H.; Enz, A.; Sussman, J. L.; Silman, I. Kinetic and Structural Studies on the Interaction of Cholinesterases with the Anti-Alzheimer Drug Rivastigmine. *Biochemistry* **2002**, *41*, 3555−3564.

(62) Hosie, L.; Sutton, L. D.; Quinn, D. M. *p*-Nitrophenyl and Cholesteryl-*N*-Alkyl Carbamates as Inhibitors of Cholesterol Esterase. *J. Biol. Chem.* **1987**, *262*, 260−264.

(63) Feaster, S. R.; Lee, K.; Baker, N.; Hui, D. Y.; Quinn, D. M. Molecular Recognition by Cholesterol Esterase of Active Site Ligands: Structure-Reactivity Effects for Inhibition by Aryl Carbamates and Subsequent Carbamylenzyme Turnover. *Biochemistry* **1996**, *35*, 16723−16734.

(64) *GOLD Suite*, version 5.2.2; CCDC Software: Cambridge, U.K.; http://www.ccdc.cam.ac.uk. Jones, G.; Willett, P.; Glen, R. C.; Leach, A. R.; Taylor, R. Development and Validation of a Genetic Algorithm for Flexible Docking. *J. Mol. Biol.* **1997**, *267*, 727−748.

(65) Spitzmüller, A.; Velec, H. F. G.; Klebe, G. MiniMuDS: A New Optimizer using Knowledge-Based Potentials Improves Scoring of Docking Solutions. *J. Chem. Inf. Model.* **2011**, *51*, 1423−1430.

(66) Nicolet, Y.; Lockridge, O.; Masson, P.; Fontecilla-Camps, J. C.; Nachon, F. Crystal Structure of Human Butyrylcholinesterase and of its Complexes with Substrate and Products. *J. Biol. Chem.* **2003**, *278*, 41141−41147.

(67) www.rcsb.org. Berman, H. M.; Westbrook, J.; Feng, Z.; Gilliland, G.; Bhat, T. N.; Weissig, H.; Shindyalov, I. N.; Bourne, P. E. The Protein Data Bank. *Nucleic Acids Res.* **2000**, *28*, 235−242.

(68) Nawaz, S.; Ayaz, M.; Brandt, W.; Wessjohann, L. A.; Westermann, B. Cation-π and π-π Stacking Interactions Allow Selective Inhibition of Butyrylcholinesterase by Modified Quinine and Cinchonidine Alkaloids. *Biochem. Biophys. Res. Commun.* **2011**, *404*, 935−940.

(69) Karlsson, D.; Fallarero, A.; Brunhofer, G.; Mayer, C.; Prakash, O.; Mohan, C. G.; Vuorela, P.; Erker, T. The Exploration of Thienothiazines as Selective Butyrylcholinesterase Inhibitors. *Eur. J. Pharm. Sci.* **2012**, *47*, 190−205.

(70) Basiri, A.; Murugaiyah, V.; Osman, H.; Kumar, R. S.; Kia, Y.; Hooda, A.; Parsons, R. B. Cholinesterase Inhibitory Activity Versus Aromatic Core Multiplicity: A Facile Green Synthesis and Molecular Docking Study of Novel Piperidine Embedded Thiazolopyrimidines. *Bioorg. Med. Chem.* **2014**, *22*, 906−916.

(71) Gao, D.; Zhan, C.-G. Modeling Effects of Oxyanion Hole on the Ester Hydrolysis Catalyzed by Human Cholinesterases. *J. Phys. Chem. B* **2005**, *109*, 23070−23076.

(72) *The PyMOL Molecular Graphics System*, version 1.7.4.3; Schrödinger, LLC.

(73) Berdagué, P.; Herbert-Pucheta, J.-E.; Jha, V.; Panossian, A.; Leroux, F. R.; Lesot, P. Multi-nuclear NMR of Axially Chiral Biaryls in Polypeptide Orienting Solvents: Spectral Discriminations and Enantior-ecognition Mechanisms. *New J. Chem.* **2015**, *39*, 9504−9517.

(74) Lewerenz, J.; Hewett, S. J.; Huang, Y.; Lambros, M.; Gout, P. W.; Kalivas, P. W.; Massie, A.; Smolders, I.; Methner, A.; Pergande, M.; Smith, S. B.; Ganapathy, V.; Maher, P. The Cystine/Glutamate Antiporter System x$_c^-$ in Health and Disease: From Molecular Mechanisms to Novel Therapeutic Opportunities. *Antioxid. Redox Signaling* **2013**, *18*, 522−555.

(75) Murphy, T. H.; Miyamoto, M.; Sastre, A.; Schnaar, R.; Coyle, J. T. Glutamate Toxicity in a Neuronal Cell Line Involves Inhibition of Cystine Transport Leading to Oxidative Stress. *Neuron* **1989**, *2*, 1547−1558.

(76) Fukui, M.; Song, J.-H.; Choi, J.; Choi, H. J.; Zhu, B. T. Mechanism of Glutamate-Induced Neurotoxicity in HT22 Mouse Hippocampal Cells. *Eur. J. Pharmacol.* **2009**, *617*, 1−11.

(77) Tan, S.; Wood, M.; Maher, P. Oxidative Stress Induces a Form of Programmed Cell Death with Characteristics of Both Apoptosis and Necrosis in Neuronal Cells. *J. Neurochem.* **1998**, *71*, 95−105.

(78) *Molecular Operating Environment (MOE)*, versions 2013.0801 and 2014.0901; Chemical Computing Group (1010 Sherbooke St. West, Suite No. 910, Montreal, QC, H3A 2R7, Canada), 2011.

(79) Milletti, F.; Storchi, L.; Sforna, G.; Cruciani, G. J. New and Original pK_a Prediction Method Using Grid Molecular Interaction Fields. *J. Chem. Inf. Model.* **2007**, *47*, 2172−2181.

(80) Jones, G.; Willett, P.; Glen, R. C. Molecular Recognition of Receptor Sites Using a Genetic Algorithm with a Description of Desolvation. *J. Mol. Biol.* **1995**, *245*, 43−53.

(81) Jones, G.; Willett, P.; Glen, R. C.; Leach, A. R.; Taylor, R. Development and Validation of a Genetic Algorithm for Flexible Docking. *J. Mol. Biol.* **1997**, *267*, 727−748.

(82) Neudert, G.; Klebe, G. DSX: A Knowledge-Based Scoring Function for the Assessment of Protein-Ligand Complexes. *J. Chem. Inf. Model.* **2011**, *51*, 2731−2745.

(83) Bartolucci, C.; Siotto, M.; Ghidini, E.; Amari, G.; Bolzoni, P. T.; Racchi, M.; Villetti, G.; Delcanale, M.; Lamba, D. Structural Determinants of *Torpedo californica* Acetylcholinesterase Inhibition by the Novel and Orally Active Carbamates Based Anti-Alzheimer Drug Ganstigmine (CHF-2819). *J. Med. Chem.* **2006**, *49*, 5051−5058.

(84) Halgren, T. A. Merck Molecular Force Field. I. Basis, Form, Scope, Parameterization, and Performance of MMFF94. *J. Comput. Chem.* **1996**, *17*, 490−510.

(85) Dávalos, A.; Gómez-Cordovés, C.; Bartolomé, B. Extending Applicability of the Oxygen Radical Absorbance Capacity (ORAC−Fluorescein) Assay. *J. Agric. Food Chem.* **2004**, *52*, 48−54.

Discovery of Highly Selective and Nanomolar Carbamate-Based Butyrylcholinesterase Inhibitors by Rational Investigation into Their Inhibition Mode

Edgar Sawatzky,[‡] Sarah Wehle,[‡] Beata Kling,[I] Jan Wendrich,[†] Gerhard Bringmann,[†] Christoph A. Sotriffer,[‡] Jörg Heilmann[II] and Michael Decker[‡]*

[‡]Pharmazeutische und Medizinische Chemie, Institut für Pharmazie und Lebensmittelchemie, Universität Würzburg, Am Hubland, D-97074 Würzburg, Germany

[I]Lehrstuhl für Pharmazeutische Biologie, Institut für Pharmazie, Universität Regensburg, Universitätsstraße 31, D-93053 Regensburg, Germany

[†]Lehrstuhl für Organische Chemie I, Institut für Organische Chemie, Universität Würzburg, Am Hubland, D-97074 Würzburg, Germany

Contents:

Experimental Section

General Reaction Procedures:

General Amide Formation Procedure (GP1):

6-Hydroxy-1-methyl-2*H*-benzo[*d*][1,3]oxazine-2,4(1*H*)-dione **5** was dissolved in dry DMF (30 mL) and treated with the corresponding amine (5 equiv) or a mixture of the amine hydrochloride (5 equiv) and triethylamine (5 equiv). The mixture was heated to 40-120 °C (depending on the amine) for 4-5 h. For workup, the mixture was poured into water (100 mL) and the product was extracted with ethyl acetate (5 x 100 mL). The combined organic layers were washed with brine (50 mL), dried over Na_2SO_4 and evaporated to dryness. The crude product was purified by column chromatography to obtain 5-hydroxy-*N*-methyl-2-(alkylamino)benzamides **6a-d**.

General Cyclization Procedure (GP2):

5-Hydroxy-*N*-methyl-2-(alkylamino)benzamides **6a-d** were dissolved in glacial acetic acid (20 mL). The mixture was treated with the corresponding aldehyde (1.2 equiv) and heated to 70 °C for 1-3 h. Then the mixture was poured onto ice water (20 mL), basified with a NaOH-solution (2 M) and the pH was adjusted to 9 with sat. NH_4Cl-solution. The product was extracted with ethyl acetate (3 x 40 mL), the combined organic layers were washed with brine (30 mL), dried over Na_2SO_4 and the solvent was evaporated under reduced pressure. The crude product was either crystallized or purified by column chromatography to obtain dihydroquinazolinones **7a-u** and **8a-c**.

General Reduction Procedure (GP3):

Dihydroquinazolinone **7a-u** and **8a-c** were dissolved in dry THF (30 mL) at 0 °C and $LiAlH_4$ (4 equiv) was added. The mixture was allowed to reach RT and was then heated to reflux temperature for 1-3 h. After cooling to RT, the mixture was poured into ice water (50 mL) followed by the addition of saturated NH_4Cl-solution until pH = 9. The aqueous phase was then extracted with ethyl acetate (3 x 80 mL). The combined organic layers were washed with brine (50 mL), dried over Na_2SO_4 and the solvent was evaporated under reduced pressure. The crude product was purified by column chromatography to obtain the corresponding tetrahydroquinazolines **9a-u** and **10a-c**.

General Carbamate Formation Procedure (GP4):

A solution of tetrahydroquinazolines **9a-n**, **9q-u** and **10a-c** in dry THF (5 mL) were treated with NaH in paraffin oil (60%, 1.2 equiv). The mixture was stirred until the formation of gas stopped. Then, a solution of 4-nitrophenyl-*n*-heptylcarbamate (1.2 equiv) in dry THF (3 mL) was added at once. The mixture was stirred for 2 h. For workup, the mixture was diluted with ethyl acetate (30 mL), washed with water (10 mL) and washed with brine (10 mL). The organic phase was dried over Na_2SO_4 and the solvent was evaporated under reduced pressure. The crude product was purified by column chromatography to obtain the corresponding *n*-heptylcarbamate **2a-n**, **2q-u** and **3a-c**.

Synthesis and Spectral Data:

4-Nitrophenyl-*n*-heptylcarbamate. 4-Nitrophenyl chloroformate (2.1 g, 10 mmol, 1.2 eq.) was dissolved in DCM (30 mL) and treated with triethylamine (1.44 mL, 10.4 mmol, 1.2 eq.). Then heptylamine (1.29 mL, 8.7 mmol, 1 eq.) in DCM (10 mL) was added drop wise over 30 min and the reaction mixture is stirred for 4 h at rt. For workup, the mixture was diluted with DCM (50 mL), washed with 1 M HCl-solution (3 x 30 mL) and washed with brine (30 mL). Then the organic layer was dried over Na_2SO_4, followed by the removal of the solvent under reduced pressure. The crude product was purified by column chromatography (petroleum ether:DCM = 1:1) to yield 4-nitrophenyl-*n*-heptylcarbamate (1.62 g, 67%) as white solid; **mp:** 80-82 °C. **^{1}H NMR** (400 MHz, CDCl$_3$): δ = 8.20 - 8.12 (m, 2H), 7.28 - 7.21 (m, 2H), 5.07 (s, NH), 3.26 - 3.14 (m, 2H), 1.59 - 1.45 (m, 2H), 1.35 - 1.14 (m, 8H), 0.82 (t, J = 6.9 Hz, 3H) ppm. **^{13}C NMR** (101 MHz, CDCl$_3$): δ = 156.03 (CO), 153.10 (arom.), 144.70 (arom.), 125.10 (arom., 2C), 121.93 (arom., 2C), 41.43 (NCH$_2$), 31.71 (CH$_2$), 29.70 (CH$_2$), 28.89 (CH$_2$), 26.67 (CH$_2$), 22.57 (CH$_2$), 14.04 (CH$_3$) ppm. **ESI-MS**: *m/z* calcd: 280.14, found: no mass found.

5-Hydroxy-*N*-*iso*-propyl-2-(methylamino)benzamide 6b. According to GP1, 6-hydroxy-1-methyl-1*H*-benzo[*d*][1,3]oxazine-2,4-dione **5** (800 mg, 4.15 mmol, 1 equiv) and *iso*-propylamine (1.77 mL, 20.73 mmol, 5 equiv) were used to obtain 5-hydroxy-*N*-*iso*-propyl-2-(methylamino)benzamide **6b** (353 mg, 41%) as a yellow solid; mp 144-146 °C. ^{1}H NMR (400 MHz, DMSO-d$_6$): δ = 8.56 (s, OH), 8.01 (d, J = 7.8 Hz, NH), 6.95 (d, J = 2.8 Hz, 1H), 6.79 (dd, J = 8.7, 2.8 Hz, 1H), 6.73 (q, J = 5.2 Hz, NH), 6.48 (d, J = 8.8 Hz, 1H), 4.10 - 3.95

(m, 1H), 2.70 (d, J = 5.1 Hz, 3H), 1.13 (d, J = 6.6 Hz, 6H) ppm. ^{13}C NMR (101 MHz, DMSO-d$_6$): δ = 168.6, 147.0, 143.7, 119.8, 117.8, 115.5, 112.0, 40.9, 30.5, 22.7 (2C) ppm. ESI-MS: m/z calcd: 208.12, found: 209.20 [M+H]$^+$.

5-Hydroxy-2-(methylamino)-*N*-*n*-propylbenzamide 6c. According to GP1, 6-hydroxy-1-methyl-1*H*-benzo[*d*][1,3]oxazine-2,4-dione **5** (800 mg, 4.15 mmol, 1 equiv) and *n*-propylamine (1.70 mL, 20.73 mmol, 5 equiv) were used to obtain 5-hydroxy-2-(methylamino)-*N*-*n*-propylbenzamide **6c** (524 mg, 61%) after column chromatography (petroleum ether:EtOAc= 1:1) as a brown oil; ^{1}H NMR (400 MHz, DMSO-d$_6$): δ = 8.58 (s, OH), 8.21 (t, J = 5.1 Hz, NH), 6.95 (d, J = 2.7 Hz, 1H), 6.86 - 6.69 (m, 1H + NH), 6.48 (d, J = 8.8 Hz, 1H), 3.14 (q, J = 6.6 Hz, 2H), 2.69 (d, J = 5.2 Hz, 3H), 1.50 (sex, J = 7.3 Hz, 2H), 0.88 (t, J = 7.4 Hz, 3H) ppm. ^{13}C NMR (101 MHz, DMSO-d$_6$): δ = 169.4, 147.1, 143.8, 120.0, 117.5, 115.2, 112.1, 41.0, 30.5, 22.8, 11.9 ppm. ESI-MS: m/z calcd: 208.12, found: 209.20 [M+H]$^+$.

N-Benzyl-5-hydroxy-2-(methylamino)benzamide 6d. According to GP1, 6-hydroxy-1-methyl-1*H*-benzo[*d*][1,3]oxazine-2,4-dione **5** (800 mg, 4.15 mmol, 1 equiv) and benzylamine (2.26 mL, 20.73 mmol, 5 equiv) were used to obtain *N*-benzyl-5-hydroxy-2-(methylamino)benzamide **6d** (477 mg, 45%) after column chromatography (petroleum ether:EtOAc = 2:1) as a white solid; mp 161-162 °C. ^{1}H NMR (400 MHz, DMSO-d$_6$): δ = 8.80 (t, J = 5.9 Hz, NH), 8.60 (s, OH), 7.36 - 7.27 (m, 4H), 7.27 - 7.16 (m, 1H), 7.04 (d, J = 2.8 Hz, 1H), 6.88 (q, J = 5.0 Hz, NH), 6.83 (dd, J = 8.8, 2.8 Hz, 1H), 6.51 (d, J = 8.8 Hz, 1H), 4.40 (d, J = 6.0 Hz, 2H), 2.70 (d, J = 5.2 Hz, 3H) ppm. ^{13}C NMR (101 MHz, DMSO-d$_6$): δ = 169.4, 147.0, 144.1, 140.4, 128.7 (2C), 127.6 (2C), 127.1, 120.5, 116.7, 115.2, 112.2, 42.7, 30.5 ppm. ESI-MS: m/z calcd: 256.12, found: 257.15 [M+H]$^+$.

2-(4-Chlorophenyl)-6-hydroxy-1,3-dimethyl-2,3-dihydroquinazolin-4(1*H*)-one   7b. According to GP2, 5-hydroxy-*N*-methyl-2-(methylamino)benzamide **6a** (400 mg, 2.22 mmol, 1 equiv) and 4-chlorobenzaldehyde (375 mg, 2.66 mmol, 1.2 equiv) were used to obtain 2-(4-chlorophenyl)-6-hydroxy-1,3-dimethyl-2,3-dihydroquinazolin-4(1*H*)-one **7b** (538 mg, 80%) after column chromatography (petroleum ether:EtOAc = 1:2) as a yellow solid; mp 196-202 °C. ^{1}H NMR (400 MHz, DMSO-d$_6$): δ = 9.03 (s, OH), 7.43 - 7.34 (m, 2H), 7.22 (d, J = 2.9 Hz, 1H), 7.20 - 7.16 (m, 2H), 6.81 (dd, J = 8.7, 3.0 Hz, 1H), 6.48 (d, J = 8.7 Hz, 1H), 5.71 (s, 1H), 2.90 (s, 3H), 2.73 (s, 3H) ppm. ^{13}C NMR (101 MHz, DMSO-d$_6$): δ = 161.6, 149.8,

139.1, 135.7, 133.3, 128.6 (2C), 128.1 (2C), 121.0, 117.6, 114.4, 113.4, 77.8, 35.8, 32.0 ppm. ESI-MS: *m/z* calcd: 302.08, found: 303.1 [M+H]$^+$.

2-(3-Chlorophenyl)-6-hydroxy-1,3-dimethyl-2,3-dihydroquinazolin-4(1*H*)-one **7c.** According to GP2, 5-hydroxy-*N*-methyl-2-(methylamino)benzamide **6a** (400 mg, 2.22 mmol, 1 equiv) and 3-chlorobenzaldehyde (375 mg, 2.66 mmol, 1.2 equiv) were used to obtain 2-(3-chlorophenyl)-6-hydroxy-1,3-dimethyl-2,3-dihydroquinazolin-4(1*H*)-one **7c** (538 mg, 80%) after column chromatography (petroleum ether:EtOAc = 1:2) as a yellow foam; ^{1}H NMR (400 MHz, DMSO-d$_6$): δ = 9.07 (br, OH), 7.42 - 7.30 (m, 2H), 7.26 - 7.19 (m, 2H), 7.10 (dt, *J* = 7.3, 1.5 Hz, 1H), 6.83 (dd, *J* = 8.7, 3.0 Hz, 1H), 6.50 (d, *J* = 8.7 Hz, 1H), 5.72 (s, 1H), 2.91 (s, 3H), 2.75 (s, 3H) ppm. ^{13}C NMR (101 MHz, DMSO-d$_6$): δ = 162.1, 150.4, 139.9, 139.6, 133.7, 131.1, 129.1, 126.7, 125.2, 121.6, 118.1, 115.1, 113.8, 78.3, 36.4, 32.6 ppm. ESI-MS: *m/z* calcd: 302.08, found: 303.1 [M+H]$^+$.

2-(2-Chlorophenyl)-6-hydroxy-1,3-dimethyl-2,3-dihydroquinazolin-4(1*H*)-one **7d.** According to GP2, 5-hydroxy-*N*-methyl-2-(methylamino)benzamide **6a** (400 mg, 2.22 mmol, 1 equiv) and 2-chlorobenzaldehyde (299 µL, 2.67 mmol, 1.2 equiv) were used to obtain 2-(2-chlorophenyl)-6-hydroxy-1,3-dimethyl-2,3-dihydroquinazolin-4(1*H*)-one **7d** (526 mg, 78%) after crystallization from petroleum ether/DCM as a yellow solid; mp 211-215 °C. ^{1}H NMR (400 MHz, DMSO-d$_6$): δ = 9.13 (s, OH), 7.50 (dd, *J* = 8.0, 1.2 Hz, 1H), 7.34 (td, *J* = 7.7, 1.6 Hz, 1H), 7.27 - 7.19 (m, 2H), 7.06 (dd, *J* = 7.8, 1.6 Hz, 1H), 6.83 (dd, *J* = 8.7, 3.0 Hz, 1H), 6.58 (d, *J* = 8.7 Hz, 1H), 6.06 (s, 1H), 2.87 (s, 3H), 2.79 (s, 3H) ppm. ^{13}C NMR (101 MHz, DMSO-d$_6$): δ = 162.1, 150.9, 139.6, 135.4, 132.6, 130.9, 130.5, 128.3, 127.2, 121.6, 118.8, 116.9, 113.6, 75.6, 38.1, 32.2 ppm. ESI-MS: *m/z* calcd: 302.08, found: 303.1 [M+H]$^+$.

6-Hydroxy-1,3-dimethyl-2-*p*-tolyl-2,3-dihydroquinazolin-4(1*H*)-one **7e.** According to GP2, 5-hydroxy-*N*-methyl-2-(methylamino)benzamide **6a** (400 mg, 2.22 mmol, 1 equiv) and 4-methylbenzaldehyde (314 µL, 2.66 mmol, 1.2 equiv) were used to obtain 6-hydroxy-1,3-dimethyl-2-*p*-tolyl-2,3-dihydroquinazolin-4(1*H*)-one **7e** (472 mg, 75%) after crystallization from a mixture of petroleum ether/DCM as a yellow solid; mp 182-186 °C. ^{1}H NMR (400 MHz, DMSO-d$_6$): δ = 8.97 (s, OH), 7.22 (d, *J* = 2.9 Hz, 1H), 7.11 (d, *J* = 7.9 Hz, 2H), 7.04 (d, *J* = 8.2 Hz, 2H), 6.80 (dd, *J* = 8.7, 3.0 Hz, 1H), 6.44 (d, *J* = 8.7 Hz, 1H), 5.61 (s, 1H), 2.88 (s, 3H), 2.70 (s, 3H), 2.24 (s, 3H) ppm. ^{13}C NMR (101 MHz, DMSO-d$_6$): δ = 161.7, 149.5,

139.4, 138.0, 133.7, 129.1 (2C), 126.2 (2C), 120.8, 117.6, 114.0, 113.4, 78.5, 35.6, 32.0, 20.6 ppm. ESI-MS: *m/z* calcd: 282.14, found: 283.2 [M+H]$^+$.

6-Hydroxy-1,3-dimethyl-2-*m*-tolyl-2,3-dihydroquinazolin-4(1*H*)-one 7f. According to GP2, 5-hydroxy-*N*-methyl-2-(methylamino)benzamide **6a** (400 mg, 2.22 mmol, 1 equiv) and 3-methylbenzaldehyde (314 μL, 2.67 mmol, 1.2 equiv) were used to obtain 6-hydroxy-1,3-dimethyl-2-*m*-tolyl-2,3-dihydroquinazolin-4(1*H*)-one **7f** (380 mg, 61%) after column chromatography (petroleum ether:EtOAc = 1:2) as a yellow foam; ^{1}H NMR (400 MHz, DMSO-d$_6$): δ = 8.98 (s, OH), 7.22 (d, *J* = 2.9 Hz, 1H), 7.18 (t, *J* = 7.5 Hz, 1H), 7.12 (d, *J* = 7.5 Hz, 1H), 7.00 (s, 1H), 6.92 (d, *J* = 7.6 Hz, 1H), 6.81 (dd, *J* = 8.7, 3.0 Hz, 1H), 6.46 (d, *J* = 8.7 Hz, 1H), 5.61 (s, 1H), 2.88 (s, 3H), 2.72 (s, 3H), 2.24 (s, 3H) ppm. ^{13}C NMR (101 MHz, DMSO-d$_6$): δ = 162.2, 150.0, 140.0, 138.1, 137.3, 129.8, 129.0, 127.5, 123.6, 121.4, 118.0, 114.6, 113.8, 79.2, 36.2, 32.6, 21.6 ppm. ESI-MS: *m/z* calcd: 282.14, found: 283.1 [M+H]$^+$.

6-Hydroxy-1,3-dimethyl-2-*o*-tolyl-2,3-dihydroquinazolin-4(1*H*)-one 7g. According to GP2, 5-hydroxy-*N*-methyl-2-(methylamino)benzamide **6a** (400 mg, 2.22 mmol, 1 equiv) and 2-methylbenzaldehyde (308 μL, 2.67 mmol, 1.2 equiv) were used to obtain 6-hydroxy-1,3-dimethyl-2-*o*-tolyl-2,3-dihydroquinazolin-4(1*H*)-one **7g** (283 mg, 45%) after column chromatography (petroleum ether:EtOAc = 1:2) as a yellow solid; mp 207-210 °C. ^{1}H NMR (400 MHz, DMSO-d$_6$): δ = 9.12 (s, OH), 7.22 (d, *J* = 2.9 Hz, 1H), 7.21 - 7.14 (m, 2H), 7.08 - 7.01 (m, 1H), 6.89 (d, *J* = 7.6 Hz, 1H), 6.79 (dd, *J* = 8.6, 3.0 Hz, 1H), 6.61 (d, *J* = 8.7 Hz, 1H), 5.82 (s, 1H), 2.86 (s, 3H), 2.77 (s, 3H), 2.47 (s, 3H) ppm. ^{13}C NMR (101 MHz, DMSO-d$_6$): δ = 162.5, 151.4, 140.4, 137.0, 136.7, 131.5, 128.7, 126.5, 125.7, 121.3, 120.3, 118.7, 113.3, 76.4, 39.6, 32.4, 19.6 ppm. ESI-MS: *m/z* calcd: 282.14, found: 283.2 [M+H]$^+$.

6-Hydroxy-2-(4-methoxyphenyl)-1,3-dimethyl-2,3-dihydroquinazolin-4(1*H*)-one 7h. According to GP2, 5-hydroxy-*N*-methyl-2-(methylamino)benzamide **6a** (400 mg, 2.22 mmol, 1 equiv) and 4-methoxybenzaldehyde (324 μL, 2.66 mmol, 1.2 equiv) were used to obtain 6-hydroxy-2-(4-methoxyphenyl)-1,3-dimethyl-2,3-dihydroquinazolin-4(1*H*)-one **7h** (490 mg, 74%) after column chromatography (petroleum ether:EtOAc = 1:2) as a yellow solid; mp 180-183 °C. ^{1}H NMR (400 MHz, DMSO-d$_6$): δ = 8.97 (s, OH), 7.22 (d, *J* = 2.9 Hz, 1H), 7.12 - 7.03 (m, 2H), 6.89 - 6.83 (m, 2H), 6.80 (dd, *J* = 8.7, 3.0 Hz, 1H), 6.45 (d, *J* = 8.7 Hz, 1H), 5.59 (s, 1H), 3.70 (s, 3H), 2.87 (s, 3H), 2.69 (s, 3H) ppm. ^{13}C NMR (101 MHz, DMSO-d$_6$): δ

= 161.7, 159.4, 149.5, 139.5, 128.7, 127.5 (2C), 120.8, 117.5, 114.0, 113.9 (2C), 113.4, 78.3, 55.0, 35.4, 31.9 ppm. ESI-MS: *m/z* calcd: 298.13, found: 299.15 [M+H]$^+$.

6-Hydroxy-2-(3-methoxyphenyl)-1,3-dimethyl-2,3-dihydroquinazolin-4(1*H*)-one 7i.
According to GP2, 5-hydroxy-*N*-methyl-2-(methylamino)benzamide **6a** (400 mg, 2.22 mmol, 1 equiv) and 3-methoxybenzaldehyde (363 µL, 2.67 mmol, 1.2 equiv) were used to obtain 6-hydroxy-2-(3-methoxyphenyl)-1,3-dimethyl-2,3-dihydroquinazolin-4(1*H*)-one **7i** (375 mg, 57%) after column chromatography (petroleum ether:EtOAc = 1:2) as a yellow foam; ^{1}H NMR (400 MHz, DMSO-d$_6$): δ = 8.99 (s,OH), 7.27 - 7.18 (m, 2H), 6.92 - 6.84 (m, 1H), 6.81 (dd, *J* = 8.7, 2.9 Hz, 1H), 6.77 - 6.67 (m, 2H), 6.47 (d, *J* = 8.7 Hz, 1H), 5.62 (s, 1H), 3.67 (s, 3H), 2.89 (s, 3H), 2.73 (s, 3H) ppm. ^{13}C NMR (101 MHz, DMSO-d$_6$): δ = 162.2, 159.7, 150.1, 140.0, 138.9, 130.3, 121.4, 118.8, 118.0, 114.5, 113.8, 113.8, 113.1, 79.0, 55.4, 36.2, 32.6 ppm. ESI-MS: *m/z* calcd: 298.13, found: 299.2 [M+H]$^+$.

6-Hydroxy-2-(2-methoxyphenyl)-1,3-dimethyl-2,3-dihydroquinazolin-4(1*H*)-one 7j.
According to GP2, 5-hydroxy-*N*-methyl-2-(methylamino)benzamide **6a** (400 mg, 2.22 mmol, 1 equiv) and 2-methoxybenzaldehyde (363 mg, 2.67 mmol, 1.2 equiv) were used to obtain 6-hydroxy-2-(2-methoxyphenyl)-1,3-dimethyl-2,3-dihydroquinazolin-4(1*H*)-one **7j** (631 mg, 95%) after crystallization from petroleum ether/DCM as a yellow solid; mp 216-219 °C. ^{1}H NMR (400 MHz, DMSO-d$_6$): δ = 8.95 (s, OH), 7.32 - 7.24 (m, 1H), 7.22 (d, *J* = 2.9 Hz, 1H), 7.07 (d, *J* = 8.3 Hz, 1H), 6.90 (dd, *J* = 7.7, 1.7 Hz, 1H), 6.83 - 6.76 (m, 2H), 6.47 (d, *J* = 8.7 Hz, 1H), 6.01 (s, 1H), 3.82 (s, 3H), 2.83 (s, 3H), 2.72 (s, 3H) ppm. ^{13}C NMR (101 MHz, DMSO-d$_6$): δ = 162.5, 157.2, 149.9, 140.0, 130.5, 126.5, 125.5, 121.3, 121.0, 117.9, 114.5, 113.7, 112.1, 72.9, 56.1, 36.3, 32.3 ppm. ESI-MS: *m/z* calcd: 298.13, found: 299.15 [M+H]$^+$.

2-(4-Fluorophenyl)-6-hydroxy-1,3-dimethyl-2,3-dihydroquinazolin-4(1*H*)-one 7k.
According to GP2, 5-hydroxy-*N*-methyl-2-(methylamino)benzamide **6a** (400 mg, 2.22 mmol, 1 equiv) and 4-fluorobenzaldehyde (286 µL, 2.67 mmol, 1.2 equiv) were used to obtain 2-(4-fluorophenyl)-6-hydroxy-1,3-dimethyl-2,3-dihydroquinazolin-4(1*H*)-one **7k** (415 mg, 65%) after column chromatography (petroleum ether:EtOAc = 1:2) as a yellow solid; mp: 168-171 °C. ^{1}H NMR (400 MHz, DMSO-d$_6$): δ = 9.01 (s, OH), 7.24 - 7.11 (m, 5H), 6.82 (dd, *J* = 8.7, 3.0 Hz, 1H), 6.48 (d, *J* = 8.7 Hz, 1H), 5.70 (s, 1H), 2.89 (s, 3H), 2.72 (s, 3H) ppm. ^{13}C NMR (101 MHz, DMSO-d$_6$): δ = 162.7 (d, *J* = 244.6 Hz), 162.1, 150.2, 139.7, 133.6 (d, *J* =

3.1 Hz), 128.8 (d, J = 8.4 Hz, 2C), 121.5, 118.1, 115.9 (d, J = 21.4 Hz, 2C), 114.8, 113.9, 78.3, 36.2, 32.5 ppm. ESI-MS: m/z calcd: 286.11, found: 287.1 [M+H]$^+$.

6-Hydroxy-1,3-dimethyl-2-[4-(trifluoromethyl)phenyl]-2,3-dihydroquinazolin-4(1*H*)-one 7l. According to GP2, 5-hydroxy-*N*-methyl-2-(methylamino)benzamide **6a** (400 mg, 2.22 mmol, 1 equiv) and 4-trifluormethylbenzaldehyde (364 µL, 2.67 mmol, 1.2 equiv) were used to obtain 6-hydroxy-1,3-dimethyl-2-[4-(trifluoromethyl)phenyl]-2,3-dihydroquinazolin-4(1*H*)-one **7l** (606 mg, 81%) after column chromatography (petroleum ether:EtOAc = 1:2) as a yellow foam; ^{1}H NMR (400 MHz, DMSO-d$_6$): δ = 9.09 (s, OH), 7.70 (d, J = 8.1 Hz, 2H), 7.38 (d, J = 8.1 Hz, 2H), 7.23 (d, J = 2.9 Hz, 1H), 6.82 (dd, J = 8.7, 2.9 Hz, 1H), 6.50 (d, J = 8.7 Hz, 1H), 5.82 (s, 1H), 2.93 (s, 3H), 2.77 (s, 3H) ppm. ^{13}C NMR (101 MHz, DMSO-d$_6$): δ = 162.2, 150.5, 141.8, 139.6, 129.6 (q, J = 32.0 Hz, 2C), 127.6 (2C), 126.1 (q, J = 3.7 Hz,), 124.5 (q, J = 272.4 Hz), 121.6, 118.3, 115.3, 113.9, 78.3, 36.6, 32.7 ppm. ESI-MS: m/z calcd: 336.11, found: 337.1 [M+H]$^+$.

6-Hydroxy-1,3-dimethyl-2-(pyridin-4-yl)-2,3-dihydroquinazolin-4(1*H*)-one 7m. According to GP2, 5-hydroxy-*N*-methyl-2-(methylamino)benzamide **6a** (400 mg, 2.22 mmol, 1 equiv) and isonicotinaldehyde (251 µL, 2.66 mmol, 1.2 equiv) were used to obtain 6-hydroxy-1,3-dimethyl-2-(pyridin-4-yl)-2,3-dihydroquinazolin-4(1*H*)-one **7m** (483 mg, 81%) after column chromatography (DCM:MeOH = 9:1) as a yellow foam; ^{1}H NMR (400 MHz, DMSO-d$_6$): δ = 9.08 (s, OH), 8.52 (dd, J = 4.5, 1.6 Hz, 2H), 7.22 (d, J = 2.9 Hz, 1H), 7.13 (dd, J = 4.5, 1.6 Hz, 2H), 6.82 (dd, J = 8.7, 3.0 Hz, 1H), 6.53 (d, J = 8.7 Hz, 1H), 5.75 (s, 1H), 2.95 (s, 3H), 2.80 (s, 3H) ppm. ^{13}C NMR (101 MHz, DMSO-d$_6$): δ = 162.2, 150.7, 150.5 (2C), 145.6, 139.6, 121.7 (2C), 121.5, 118.5, 115.5, 113.8, 77.7, 36.9, 32.8 ppm. ESI-MS: m/z calcd: 269.12, found: 270.1 [M+H]$^+$.

6-Hydroxy-1,3-dimethyl-2-(pyridin-3-yl)-2,3-dihydroquinazolin-4(1*H*)-one 7n. According to GP2, 5-hydroxy-*N*-methyl-2-(methylamino)benzamide **6a** (400 mg, 2.22 mmol, 1 equiv) and nicotinaldehyde (250 µL, 2.67 mmol, 1.2 equiv) were used to obtain 6-hydroxy-1,3-dimethyl-2-(pyridin-3-yl)-2,3-dihydroquinazolin-4(1*H*)-one **7n** (395 mg, 66%) as a yellow oil; ^{1}H NMR (400 MHz, DMSO-d$_6$): δ = 9.07 (s, OH), 8.51 (dd, J = 4.8, 1.6 Hz, 1H), 8.43 (d, J = 1.9 Hz, 1H), 7.53 - 7.45 (m, 1H), 7.34 (ddd, J = 7.9, 4.8, 0.7 Hz, 1H), 7.23 (d, J = 2.9 Hz, 1H), 6.83 (dd, J = 8.7, 3.0 Hz, 1H), 6.52 (d, J = 8.7 Hz, 1H), 5.79 (s, 1H), 2.93 (s, 3H), 2.76 (s, 3H) ppm. ^{13}C NMR (101 MHz, DMSO-d$_6$): δ = 161.7, 150.1, 150.0, 147.6,

139.1, 133.7, 132.1, 123.8, 121.0, 117.9, 114.8, 113.3, 76.5, 35.9, 32.1 ppm. ESI-MS: *m/z* calcd: 269.12, found: 270.1 [M+H]$^+$.

6-Hydroxy-1,3-dimethyl-2-(thiophen-3-yl)-2,3-dihydroquinazolin-4(1*H*)-one   **7o.**
According to GP2, 5-hydroxy-*N*-methyl-2-(methylamino)benzamide **6a** (400 mg, 2.22 mmol, 1 equiv) and thiophene-3-carbaldehyde (233 µL, 2.66 mmol, 1.2 equiv) were used to obtain 6-hydroxy-1,3-dimethyl-2-(thiophen-3-yl)-2,3-dihydroquinazolin-4(1*H*)-one **7o** (461 mg, 76%) after crystallization from petroleum ether/DCM as a yellow solid; mp 218-220 °C. ^{1}H NMR (400 MHz, DMSO-d$_6$): δ = 9.00 (s, OH), 7.43 (dd, *J* = 5.0, 3.0 Hz, 1H), 7.33 (dd, *J* = 2.9, 1.1 Hz, 1H), 7.22 (d, *J* = 2.9 Hz, 1H), 6.83 (dd, *J* = 8.7, 3.0 Hz, 1H), 6.71 (dd, *J* = 5.0, 1.3 Hz, 1H), 6.51 (d, *J* = 8.7 Hz, 1H), 5.72 (s, 1H), 2.92 (s, 3H), 2.73 (s, 3H) ppm. ^{13}C NMR (101 MHz, DMSO-d$_6$): δ = 161.7, 149.7, 139.8, 138.2, 127.1, 125.4, 123.6, 120.9, 117.7, 114.0, 113.4, 74.7, 35.5, 31.9 ppm. ESI-MS: *m/z* calcd: 274.08, found: 571.15 [2M+Na]$^+$.

6-Hydroxy-1,3-dimethyl-2-(thiophen-2-yl)-2,3-dihydroquinazolin-4(1*H*)-one   **7p.**
According to GP2, 5-hydroxy-*N*-methyl-2-(methylamino)benzamide **6a** (400 mg, 2.22 mmol, 1 equiv) and thiophene-2-carbaldehyde (249 µL, 2.66 mmol, 1.2 equiv) were used to obtain 6-hydroxy-1,3-dimethyl-2-(thiophen-2-yl)-2,3-dihydroquinazolin-4(1*H*)-one **7p** (428 mg, 70%) after crystallization from ether as a yellow solid; mp 205-208 °C. ^{1}H NMR (400 MHz, DMSO-d$_6$): δ = 9.04 (OH), 7.32 (dd, *J* = 5.0, 1.0 Hz, 1H), 7.21 (d, *J* = 2.9 Hz, 1H), 7.05 (dd, *J* = 3.5, 1.0 Hz, 1H), 6.95 (dd, *J* = 5.0, 3.5 Hz, 1H), 6.86 (dd, *J* = 8.7, 2.9 Hz, 1H), 6.55 (d, *J* = 8.7 Hz, 1H), 5.97 (s, 1H), 2.94 (s, 3H), 2.72 (s, 3H) ppm. ^{13}C NMR (101 MHz, DMSO-d$_6$): δ = 161.5, 150.0, 139.4, 138.7, 127.1, 126.2, 125.9, 121.0, 117.8, 114.6, 113.3, 75.0, 35.4, 31.8 ppm. ESI-MS: *m/z* calcd: 274.08, found: 571.15 [2M+Na]$^+$.

2-(Furan-3-yl)-6-hydroxy-1,3-dimethyl-2,3-dihydroquinazolin-4(1*H*)-one   **7q.**
According to GP2, 5-hydroxy-*N*-methyl-2-(methylamino)benzamide **6a** (400 mg, 2.22 mmol, 1 equiv) and furan-3-carbaldehyde (223 µL, 2.67 mmol, 1.2 equiv) were used to obtain 2-(furan-3-yl)-6-hydroxy-1,3-dimethyl-2,3-dihydroquinazolin-4(1*H*)-one **7q** (323 mg, 56%) after column chromatography (petroleum ether:EtOAc = 1:2) as a yellow foam; ^{1}H NMR (400 MHz, DMSO-d$_6$): δ = 9.00 (s, OH), 7.56 (s, 1H), 7.52 (t, *J* = 1.7 Hz, 1H), 7.20 (d, *J* = 2.9 Hz, 1H), 6.84 (dd, *J* = 8.7, 3.0 Hz, 1H), 6.54 (d, *J* = 8.7 Hz, 1H), 5.96 (dd, *J* = 1.8, 0.8 Hz, 1H), 5.61 (s, 1H), 2.93 (s, 3H), 2.72 (s, 3H) ppm. ^{13}C NMR (101 MHz, DMSO-d$_6$): δ = 162.3,

150.3, 144.3, 141.3, 140.45, 121.5, 121.3, 118.3, 114.6, 113.8, 109.0, 72.3, 35.8, 32.2 ppm. ESI-MS: *m/z* calcd: 258.10, found: 259.1 [M+H]$^+$.

6-Hydroxy-1,3-dimethyl-2-(1*H*-pyrrol-3-yl)-2,3-dihydroquinazolin-4(1*H*)-one   **7r.**

According to GP2, 5-hydroxy-*N*-methyl-2-(methylamino)benzamide **6a** (400 mg, 2.22 mmol, 1 equiv) and 1*H*-pyrrole-3-carbaldehyde (253 mg, 2.67 mmol, 1.2 equiv) were used to obtain 6-hydroxy-1,3-dimethyl-2-(1*H*-pyrrol-3-yl)-2,3-dihydroquinazolin-4(1*H*)-one **7r** (406 mg, 71%) after column chromatography (DCM:MeOH = 95:5) as a yellow solid; mp 222-225 °C. ^{1}H NMR (400 MHz, DMSO-d$_6$): δ = 10.68 (s, NH), 8.88 (s, OH), 7.19 (d, *J* = 2.9 Hz, 1H), 6.80 (dd, *J* = 8.6, 3.0 Hz, 1H), 6.60 - 6.54 (m, 2H), 6.45 (d, *J* = 8.7 Hz, 1H), 5.63 (dd, *J* = 4.2, 2.5 Hz, 1H), 5.45 (s, 1H), 2.89 (s, 3H), 2.68 (s, 3H) ppm. ^{13}C NMR (101 MHz, DMSO-d$_6$): δ = 162.6, 149.7, 141.0, 120.9, 118.7, 118.6, 118.3, 116.7, 114.1, 113.8, 106.2, 74.7, 35.7, 32.3 ppm. ESI-MS: *m/z* calcd: 257.12, found: 258.1 [M+H]$^+$.

6-Hydroxy-1,3-dimethyl-2-(naphthalen-1-yl)-2,3-dihydroquinazolin-4(1*H*)-one   **7s.**

According to GP2, 5-hydroxy-*N*-methyl-2-(methylamino)benzamide **6a** (400 mg, 2.22 mmol, 1 equiv) and 1-naphthalenecarboxaldehyde (362 µL, 2.67 mmol, 1.2 equiv) were used to obtain 6-hydroxy-1,3-dimethyl-2-(naphthalen-1-yl)-2,3-dihydroquinazolin-4(1*H*)-one **7s** (428 mg, 61%) after crystallization from a mixture of DCM/petroleum ether as a yellow solid; mp 228-234 °C. ^{1}H NMR (400 MHz, DMSO-d$_6$): δ = 9.19 (s, OH), 8.48 (d, *J* = 8.5 Hz, 1H), 7.95 (d, *J* = 7.4 Hz, 1H), 7.87 (d, *J* = 8.2 Hz, 1H), 7.63 (ddd, *J* = 8.5, 6.9, 1.4 Hz, 1H), 7.59 - 7.50 (m, 1H), 7.41 - 7.33 (m, 1H), 7.28 (d, *J* = 2.9 Hz, 1H), 7.15 (d, *J* = 6.7 Hz, 1H), 6.77 (dd, *J* = 8.6, 3.0 Hz, 1H), 6.57 (d, *J* = 8.7 Hz, 1H), 6.49 (s, 1H), 2.90 (s, 3H), 2.84 (s, 3H) ppm. ^{13}C NMR (101 MHz, DMSO-d$_6$): δ = 162.8, 151.7, 140.4, 134.1, 133.9, 131.6, 129.6, 129.1, 126.9, 126.4, 125.6, 124.3, 124.2, 121.3, 120.8, 119.2, 113.4, 76.3, 40.2, 32.6 ppm. ESI-MS: *m/z* calcd: 318.14, found: 319.2 [M+H]$^+$.

6-Hydroxy-1,3-dimethyl-2-(naphthalen-2-yl)-2,3-dihydroquinazolin-4(1*H*)-one   **7t.**

According to GP2, 5-hydroxy-*N*-methyl-2-(methylamino)benzamide **6a** (400 mg, 2.22 mmol, 1 equiv) and 2-naphthaldehyde (417 mg, 2.66 mmol, 1.2 equiv) were used to obtain 6-hydroxy-1,3-dimethyl-2-(naphthalen-2-yl)-2,3-dihydroquinazolin-4(1*H*)-one **7t** (494 mg, 70%) after crystallization from DCM as a yellow solid; mp 202-203 °C. ^{1}H NMR (400 MHz, DMSO-d$_6$): δ = 9.02 (s, OH), 7.89 - 7.80 (m, 3H), 7.73 (d, *J* = 1.0 Hz, 1H), 7.54 - 7.48 (m, 2H), 7.27 (d, *J* = 2.9 Hz, 1H), 7.25 (dd, *J* = 8.6, 1.8 Hz, 1H), 6.81 (dd, *J* = 8.7, 3.0 Hz, 1H),

6.49 (d, J = 8.7 Hz, 1H), 5.84 (s, 1H), 2.95 (s, 3H), 2.78 (s, 3H) ppm. ^{13}C NMR (101 MHz, DMSO-d$_6$): δ = 162.2, 150.2, 140.0, 135.0, 133.4, 132.9, 129.0, 128.5, 128.0, 127.0, 126.9, 126.1, 124.2, 121.4, 118.1, 114.8, 113.9, 79.3, 36.4, 32.6 ppm. ESI-MS: *m/z* calcd: 318.14, found: 659.30 [2M+Na]$^+$.

2-(2,6-Dichlorophenyl)-6-hydroxy-1,3-dimethyl-2,3-dihydroquinazolin-4(1*H*)-one 7u.
According to GP2, 5-hydroxy-*N*-methyl-2-(methylamino)benzamide **6a** (400 mg, 2.22 mmol, 1 equiv) and 2,6-dichlorobenzaldehyde (467 mg, 2.67 mmol, 1.2 equiv) were used to obtain 2-(2,6-dichlorophenyl)-6-hydroxy-1,3-dimethyl-2,3-dihydroquinazolin-4(1*H*)-one **7u** (577 mg, 77%) after crystallization from petroleum ether/DCM as a white solid; mp 258-261 °C. ^{1}H NMR (400 MHz, DMSO-d$_6$): δ = 8.84 (s, OH), 7.60 - 7.50 (m, 2H), 7.45 (dd, J = 8.7, 7.3 Hz, 1H), 7.21 (d, J = 3.0 Hz, 1H), 6.82 (dd, J = 8.8, 3.0 Hz, 1H), 6.72 (s, 1H), 6.53 (d, J = 8.8 Hz, 1H), 2.63 (s, 3H), 2.58 (s, 3H) ppm. ^{13}C NMR (101 MHz, DMSO-d$_6$): δ = 161.3, 148.9, 140.6, 135.5, 132.4, 131.8, 130.6 (2C), 121.7, 114.6, 113.5, 111.9, 76.1, 34.4, 30.8 ppm. ESI-MS: *m/z* calcd: 336.04, found: 337.10 [M+H]$^+$.

6-Hydroxy-3-*iso*-propyl-1-methyl-2-phenyl-2,3-dihydroquinazolin-4(1*H*)-one 8a.
According to GP2, 5-hydroxy-*N-iso*-propyl-2-(methylamino)benzamide **6b** (340 mg, 1.96 mmol, 1 equiv) and benzaldehyde (200 µL, 1.63 mmol, 1.2 equiv) were used to obtain 6-hydroxy-3-*iso*-propyl-1-methyl-2-phenyl-2,3-dihydroquinazolin-4(1*H*)-one **8a** (364 mg, 75%) after crystallization from a mixture of DCM and petroleum ether as a pale yellow solid; mp 243-246 °C. ^{1}H NMR (400 MHz, DMSO-d$_6$): δ = 9.01 (s, OH), 7.32 - 7.13 (m, 6H), 6.75 (dd, J = 8.6, 2.9 Hz, 1H), 6.40 (d, J = 8.7 Hz, 1H), 5.73 (s, 1H), 4.70 (hept, J = 6.8 Hz, 1H), 2.77 (s, 3H), 1.25 (d, J = 6.8 Hz, 3H), 0.85 (d, J = 6.9 Hz, 3H) ppm. ^{13}C NMR (101 MHz, DMSO-d$_6$): δ = 161.6, 150.6, 139.4, 139.3, 128.6 (3C), 126.8 (2C), 121.0, 120.5, 115.9, 113.8, 73.1, 45.3, 37.0, 20.8, 20.4 ppm. ESI-MS: *m/z* calcd: 296.15, found: 297.15 [M+H]$^+$.

6-Hydroxy-1-methyl-2-phenyl-3-*n*-propyl-2,3-dihydroquinazolin-4(1*H*)-one 8b.
According to GP2, 5-hydroxy-2-(methylamino)-*N-n*-propylbenzamide **6c** (500 mg, 2.46 mmol, 1 equiv) and benzaldehyde (291 µL, 2.88 mmol, 1.2 equiv) were used to obtain 6-hydroxy-1-methyl-2-phenyl-3-*n*-propyl-2,3-dihydroquinazolin-4(1*H*)-one **8b** (284 mg, 40%) after column chromatography (petroleum ether:EtOAc= 1:1) as a yellow foam; ^{1}H NMR (400 MHz, DMSO-d$_6$): δ = 9.00 (s, OH), 7.33 - 7.23 (m, 3H), 7.23 - 7.15 (m, 3H), 6.79 (dd, J = 8.6, 2.9 Hz, 1H), 6.46 (d, J = 8.7 Hz, 1H), 5.67 (s, 1H), 3.77 (ddd, J = 13.5, 8.7, 6.6 Hz, 1H),

2.82 - 2.69 (m, 4H), 1.68 - 1.55 (m, 1H), 1.55 - 1.42 (m, 1H), 0.85 (t, J = 7.4 Hz, 3H) ppm.
^{13}C NMR (101 MHz, DMSO-d$_6$): δ = 162.0, 150.4, 139.8, 138.0, 129.0, 128.9 (2C), 126.9
(2C), 121.2, 119.0, 115.3, 113.8, 77.3, 46.6, 36.7, 21.2, 11.7 ppm. ESI-MS: *m/z* calcd: 296.15,
found: 297.20 [M+H]$^+$.

3-Benzyl-6-hydroxy-1-methyl-2-phenyl-2,3-dihydroquinazolin-4(1*H*)-one 8c. According
to GP2, *N*-benzyl-5-hydroxy-2-(methylamino)benzamide **6d** (450 mg, 1.76 mmol, 1 equiv)
and benzaldehyde (214 µL, 2.11 mmol, 1.2 equiv) were used to obtain 3-benzyl-6-hydroxy-1-
methyl-2-phenyl-2,3-dihydroquinazolin-4(1*H*)-one **8c** (332 mg, 55%) after column
chromatography (petroleum ether:EtOAc = 1:1) as a yellow foam; ^{1}H NMR (400 MHz,
DMSO-d$_6$): δ = 9.07 (s, OH), 7.38 - 7.32 (m, 4H), 7.32 - 7.25 (m, 5H), 7.23 - 7.15 (m, 2H),
6.83 (dd, J = 8.7, 3.0 Hz, 1H), 6.48 (d, J = 8.7 Hz, 1H), 5.57 (s, 1H), 5.28 (d, J = 15.4 Hz,
1H), 3.77 (d, J = 15.3 Hz, 1H), 2.67 (s, 3H) ppm. ^{13}C NMR (101 MHz, DMSO-d$_6$): δ = 162.2,
150.5, 139.9, 137.8, 137.3, 129.1, 129.97 (2C), 128.96 (2C), 128.0 (2C), 127.7, 127.0 (2C),
121.6, 118.5, 115.4, 114.0, 77.3, 47.6, 36.7 ppm. ESI-MS: *m/z* calcd: 344.15, found: 345.15
[M+H]$^+$.

2-(4-Chlorophenyl)-1,3-dimethyl-1,2,3,4-tetrahydroquinazolin-6-ol 9b. According to
GP3, starting from 2-(4-chlorophenyl)-6-hydroxy-1,3-dimethyl-2,3-dihydroquinazolin-4(1*H*)-
one **7b** (500 mg, 1.65 mmol, 1 equiv) the title compound 2-(4-chlorophenyl)-1,3-dimethyl-
1,2,3,4-tetrahydroquinazolin-6-ol **9b** (415 mg, 87%) was obtained after column
chromatography (petroleum ether:EtOAc = 1:2) as a purple foam; ^{1}H NMR (400 MHz,
DMSO-d$_6$): δ = 8.45 (s, OH), 7.36 (d, J = 8.0 Hz, 2H), 7.16 (d, J = 8.0 Hz, 2H), 6.67 - 6.41
(m, 2H), 6.33 (s, 1H), 4.85 (s, 1H), 3.48 (d, J = 16.2 Hz, 1H), 3.32 (d, J = 16.3 Hz, 1H), 2.84
(s, 3H), 2.36 (s, 3H) ppm. ^{13}C NMR (101 MHz, DMSO-d$_6$): δ = 148.0, 140.1, 136.3, 131.8,
128.8 (2C), 128.1 (2C), 119.0, 114.2, 113.9, 110.3, 80.0, 49.0, 41.6, 36.9 ppm. ESI-MS: *m/z*
calcd: 288.10, found: 289.1 [M+H]$^+$. HPLC (method A): 95%.

2-(3-Chlorophenyl)-1,3-dimethyl-1,2,3,4-tetrahydroquinazolin-6-ol 9c. According to
GP3, starting from 2-(3-chlorophenyl)-6-hydroxy-1,3-dimethyl-2,3-dihydroquinazolin-4(1*H*)-
one **7c** (470 mg, 1.55 mmol, 1 equiv) the title compound 2-(3-chlorophenyl)-1,3-dimethyl-
1,2,3,4-tetrahydroquinazolin-6-ol **9c** (379 mg, 85%) was obtained after column
chromatography (petroleum ether:EtOAc = 1:2) as a red foam; ^{1}H NMR (400 MHz, DMSO-
d$_6$): δ = 8.57 (br, OH), 7.39 - 7.28 (m, 2H), 7.20 - 7.13 (m, 1H), 7.12 - 7.03 (m, 1H), 6.58 (dd,

J = 8.6, 2.6 Hz, 1H), 6.53 (d, J = 8.7 Hz, 1H), 6.34 (d, J = 2.5 Hz, 1H), 4.87 (s, 1H), 3.49 (d, J = 16.3 Hz, 1H), 3.28 (d, J = 16.2, 1H), 2.86 (s, 3H), 2.37 (s, 3H) ppm. ^{13}C NMR (101 MHz, DMSO-d$_6$): δ = 148.5, 144.4, 136.7, 133.3, 130.6, 127.8, 127.3, 126.1, 119.4, 114.7, 114.4, 110.8, 80.5, 49.5, 42.1, 37.5 ppm. ESI-MS: m/z calcd: 288.10, found: 289.1 [M+H]$^+$. HPLC (method A): 99%.

2-(2-Chlorophenyl)-1,3-dimethyl-1,2,3,4-tetrahydroquinazolin-6-ol 9d. According to GP3, starting from 2-(2-chlorophenyl)-6-hydroxy-1,3-dimethyl-2,3-dihydroquinazolin-4(1*H*)-one **7d** (500 mg, 1.66 mmol, 1 equiv) the title compound 2-(2-chlorophenyl)-1,3-dimethyl-1,2,3,4-tetrahydroquinazolin-6-ol **9d** (326 mg, 68%) was obtained after column chromatography (petroleum ether:EtOAc = 2:1) as a yellow solid; ^{1}H NMR (400 MHz, DMSO-d$_6$): δ = 8.47 (s, OH), 7.46 (dd, J = 7.8, 1.2 Hz, 1H), 7.30 (td, J = 7.6, 1.7 Hz, 1H), 7.23 (td, J = 7.5, 1.1 Hz, 1H), 7.01 (dd, J = 7.6, 1.6 Hz, 1H), 6.59 (dd, J = 8.6, 2.7 Hz, 1H), 6.52 (d, J = 8.7 Hz, 1H), 6.38 (d, J = 2.6 Hz, 1H), 5.04 (s, 1H), 3.57 (d, J = 16.3 Hz, 1H), 3.30 (m, 1H), 2.74 (s, 3H), 2.41 (s, 3H) ppm. ^{13}C NMR (101 MHz, DMSO-d$_6$): δ = 148.5, 138.2, 137.1, 133.3, 130.5, 129.7, 127.9, 127.1, 119.2, 114.8, 114.5, 110.2, 78.5, 49.2, 42.3, 36.5 ppm. ESI-MS: m/z calcd: 288.10, found: 289.15 [M+H]$^+$. HPLC (method A): 98%.

1,3-Dimethyl-2-*p*-tolyl-1,2,3,4-tetrahydroquinazolin-6-ol 9e. According to GP3, starting from 6-hydroxy-1,3-dimethyl-2-*p*-tolyl-2,3-dihydroquinazolin-4(1*H*)-one **7e** (450 mg, 1.59 mmol, 1 equiv) the title compound 1,3-dimethyl-2-*p*-tolyl-1,2,3,4-tetrahydroquinazolin-6-ol **9e** (308 mg, 72%) was obtained after column chromatography (petroleum ether:EtOAc = 1:2) as a yellow foam; ^{1}H NMR (400 MHz, DMSO-d$_6$): δ = 8.41 (s, OH), 7.10 (d, J = 7.9 Hz, 2H), 7.02 (d, J = 8.0 Hz, 2H), 6.56 (dd, J = 8.6, 2.6 Hz, 1H), 6.49 (d, J = 8.7 Hz, 1H), 6.32 (d, J = 2.5 Hz, 1H), 4.77 (s, 1H), 3.51 (d, J = 16.1 Hz, 1H), 3.26 (d, J = 16.1 Hz, 1H), 2.81 (s, 3H), 2.34 (s, 3H), 2.26 (s, 3H) ppm. ^{13}C NMR (101 MHz, DMSO-d$_6$): δ = 147.8, 138.0, 136.7, 136.4, 128.6 (2C), 126.9 (2C), 119.2, 114.1, 113.8, 110.1, 80.6, 49.3, 41.6, 36.8, 20.6. ESI-MS: m/z calcd: 268.16, found: 269.2 [M+H]$^+$. HPLC (method A): 96%.

1,3-Dimethyl-2-*m*-tolyl-1,2,3,4-tetrahydroquinazolin-6-ol 9f. According to GP3, starting from 6-hydroxy-1,3-dimethyl-2-*m*-tolyl-2,3-dihydroquinazolin-4(1*H*)-one **7f** (360 mg, 1.28 mmol, 1equiv) the title compound 1,3-dimethyl-2-*m*-tolyl-1,2,3,4-tetrahydroquinazolin-6-ol **9f** (248 mg, 73%) was obtained after column chromatography (petroleum ether:EtOAc = 1:2) as a white foam; ^{1}H NMR (400 MHz, DMSO-d$_6$): δ = 8.41 (s, OH), 7.17 (t, J = 7.5 Hz,

1H), 7.06 (d, J = 7.5 Hz, 1H), 7.00 (s, 1H), 6.90 (d, J = 7.6 Hz, 1H), 6.56 (dd, J = 8.6, 2.7 Hz, 1H), 6.50 (d, J = 8.7 Hz, 1H), 6.32 (d, J = 2.6 Hz, 1H), 4.77 (s, 1H), 3.52 (d, J = 16.1 Hz, 1H), 3.26 (d, J = 16.1 Hz, 1H), 2.82 (s, 3H), 2.34 (s, 3H), 2.26 (s, 3H) ppm. ^{13}C NMR (101 MHz, DMSO-d$_6$): δ = 148.3, 141.7, 137.7, 137.2, 128.5, 128.4, 128.2, 124.4, 119.6, 114.6, 114.4, 110.6, 81.4, 49.8, 42.1, 37.4, 21.6 ppm. ESI-MS: m/z calcd: 268.16, found: 269.2 [M+H]$^+$. HPLC (method A): 97%.

1,3-Dimethyl-2-*o*-tolyl-1,2,3,4-tetrahydroquinazolin-6-ol 9g. According to GP3, starting from 6-hydroxy-1,3-dimethyl-2-*o*-tolyl-2,3-dihydroquinazolin-4(1*H*)-one **7g** (270 mg, 0.96 mmol, 1 equiv) the title compound 1,3-dimethyl-2-*o*-tolyl-1,2,3,4-tetrahydroquinazolin-6-ol **9g** (175 mg, 68%) was obtained after column chromatography (petroleum ether:EtOAc = 1:1) as a yellow foam; ^{1}H NMR (400 MHz, DMSO-d$_6$): δ = 8.39 (br, OH), 7.20 - 7.09 (m, 2H), 7.03 (t, J = 7.8 Hz, 1H), 6.83 (d, J = 7.5 Hz, 1H), 6.57 (dd, J = 8.6, 2.6 Hz, 1H), 6.49 (d, J = 8.7 Hz, 1H), 6.33 (d, J = 2.5 Hz, 1H), 4.91 (s, 1H), 3.55 (d, J = 16.3 Hz, 1H), 3.23 (d, J = 16.3 Hz, 1H), 2.77 (s, 3H), 2.41 (s, 3H), 2.39 (s, 3H) ppm. ^{13}C NMR (101 MHz, DMSO-d$_6$): δ = 148.2, 139.2, 137.5, 136.9, 131.3, 127.7, 125.9, 125.5, 118.8, 114.7, 114.5, 109.7, 78.9, 49.4, 42.1, 36.6, 18.9 ppm. ESI-MS: m/z calcd: 268.16, found: 269.2 [M+H]$^+$. HPLC (method A): 99%.

2-(4-Methoxyphenyl)-1,3-dimethyl-1,2,3,4-tetrahydroquinazolin-6-ol 9h. According to GP3, starting from 6-hydroxy-2-(4-methoxyphenyl)-1,3-dimethyl-2,3-dihydroquinazolin-4(1*H*)-one **7h** (460 mg, 1.54 mmol, 1 equiv) the title compound 2-(4-methoxyphenyl)-1,3-dimethyl-1,2,3,4-tetrahydroquinazolin-6-ol **9h** (282 mg, 64%) was obtained after column chromatography (petroleum ether:EtOAc = 1:2) as a purple foam; ^{1}H NMR (400 MHz, DMSO-d$_6$): δ = 8.42 (s, OH), 7.10 - 7.00 (m, 2H), 6.89 - 6.81 (m, 2H), 6.56 (dd, J = 8.6, 2.7 Hz, 1H), 6.49 (d, J = 8.7 Hz, 1H), 6.32 (d, J = 2.6 Hz, 1H), 4.75 (s, 1H), 3.71 (s, 3H), 3.52 (d, J = 16.1 Hz, 1H), 3.26 (d, J = 16.1 Hz, 1H), 2.80 (s, 3H), 2.33 (s, 3H) ppm. ^{13}C NMR (101 MHz, DMSO-d$_6$): δ = 158.5, 147.8, 136.7, 133.0, 128.1 (2C), 119.2, 114.1, 113.8, 113.4 (2C), 110.1, 80.4, 55.0, 49.3, 41.5, 36.8 ppm. ESI-MS: m/z calcd: 284.15, found: 285.2 [M+H]$^+$. HPLC (method A): 98%.

2-(3-Methoxyphenyl)-1,3-dimethyl-1,2,3,4-tetrahydroquinazolin-6-ol 9i. According to GP3, starting from 6-hydroxy-2-(3-methoxyphenyl)-1,3-dimethyl-2,3-dihydroquinazolin-4(1*H*)-one **7i** (350 mg, 1.17 mmol, 1 equiv) the title compound 2-(3-methoxyphenyl)-1,3-

dimethyl-1,2,3,4-tetrahydroquinazolin-6-ol **9i** (239 mg, 72%) was obtained after column chromatography (petroleum ether:EtOAc = 1:2) as a purple foam; ^{1}H NMR (400 MHz, DMSO-d6): δ = 8.41 (br, OH), 7.21 (t, J = 7.9 Hz, 1H), 6.82 (dd, J = 7.9, 2.2 Hz, 1H), 6.72 (d, J = 7.7 Hz, 1H), 6.69 (d, J = 2.0 Hz, 1H), 6.56 (dd, J = 8.6, 2.7 Hz, 1H), 6.50 (d, J = 8.7 Hz, 1H), 6.32 (d, J = 2.6 Hz, 1H), 4.79 (s, 1H), 3.69 (s, 3H), 3.53 (d, J = 16.2 Hz, 1H), 3.27 (d, J = 16.1 Hz, 1H), 2.83 (s, 3H), 2.36 (s, 3H) ppm. ^{13}C NMR (101 MHz, DMSO-d6): δ = 159.6, 148.4, 143.3, 137.1, 129.6, 119.6 (2C), 114.6, 114.4, 113.3, 112.9, 110.6, 81.1, 55.4, 49.8, 42.1, 37.4 ppm. ESI-MS: m/z calcd: 284.1, found: 285.2 [M+H]$^+$. HPLC (method A): 98%.

2-(2-Methoxyphenyl)-1,3-dimethyl-1,2,3,4-tetrahydroquinazolin-6-ol 9j. According to GP3, starting from 6-hydroxy-2-(2-methoxyphenyl)-1,3-dimethyl-2,3-dihydroquinazolin-4(1*H*)-one **7j** (600 mg, 2.01 mmol, 1 equiv) the title compound 2-(2-methoxyphenyl)-1,3-dimethyl-1,2,3,4-tetrahydroquinazolin-6-ol **9j** (508 mg, 89%) was obtained after column chromatography (petroleum ether:EtOAc = 1:5) as a white foam; ^{1}H NMR (400 MHz, DMSO-d6): δ = 8.42 (s, OH), 7.29 - 7.19 (m, 1H), 7.02 (d, J = 8.1 Hz, 1H), 6.86 (dd, J = 7.5, 1.8 Hz, 1H), 6.80 (t, J = 7.3 Hz, 1H), 6.56 (dd, J = 8.6, 2.7 Hz, 1H), 6.47 (d, J = 8.7 Hz, 1H), 6.37 (d, J = 2.7 Hz, 1H), 5.09 (s, 1H), 3.81 (s, 3H), 3.62 (d, J = 16.1 Hz, 1H), 3.27 (d, J = 16.1 Hz, 1H), 2.65 (s, 3H), 2.33 (s, 3H) ppm. ^{13}C NMR (101 MHz, DMSO-d6): δ = 157.4, 148.3, 137.8, 129.2, 128.5, 126.9, 120.0, 119.6, 114.6, 114.4, 111.8, 110.2, 75.3, 56.0, 49.7, 42.3, 36.4 ppm. ESI-MS: m/z calcd: 284.15, found: 285.20 [M+H]$^+$. HPLC (method A): 97%.

2-(4-Fluorophenyl)-1,3-dimethyl-1,2,3,4-tetrahydroquinazolin-6-ol 9k. According to GP3, starting from 2-(4-fluorophenyl)-6-hydroxy-1,3-dimethyl-2,3-dihydroquinazolin-4(1*H*)-one **7k** (400 mg, 1.40 mmol, 1 equiv) the title compound 2-(4-fluorophenyl)-1,3-dimethyl-1,2,3,4-tetrahydroquinazolin-6-ol **9k** (294 mg, 77%) was obtained after column chromatography (petroleum ether:EtOAc = 2:1) as a yellow foam; ^{1}H NMR (400 MHz, DMSO-d6): δ = 8.44 (br, OH), 7.22 - 7.06 (m, 4H), 6.57 (dd, J = 8.6, 2.6 Hz, 1H), 6.51 (d, J = 8.7 Hz, 1H), 6.33 (d, J = 2.4 Hz, 1H), 4.83 (s, 1H), 3.48 (d, J = 16.2 Hz, 1H), 3.28 (d, J = 16.2 Hz, 1H), 2.83 (s, 3H), 2.35 (s, 3H) ppm. ^{13}C NMR (101 MHz, DMSO-d6): δ = 161.9 (d, J = 243.0 Hz), 148.5, 137.8 (d, J = 2.9 Hz), 136.9, 129.4 (d, J = 8.1 Hz, 2C), 119.5, 115.3 (d, J = 21.3 Hz, 2C), 114.7, 114.4, 110.8, 80.6, 49.6, 42.0, 37.4 ppm. ESI-MS: m/z calcd: 272.13, found: 273.1 [M+H]$^+$. HPLC (method A): 98%.

1,3-Dimethyl-2-(4-(trifluoromethyl)phenyl)-1,2,3,4-tetrahydroquinazolin-6-ol   9l.
According to GP3, starting from 6-hydroxy-1,3-dimethyl-2-(4-(trifluoromethyl)phenyl)-2,3-dihydroquinazolin-4(1*H*)-one **7l** (600 mg, 1.79 mmol, 1 equiv) the title compound 1,3-dimethyl-2-(4-(trifluoromethyl)phenyl)-1,2,3,4-tetrahydroquinazolin-6-ol **9l** (274 mg, 48%) was obtained after column chromatography (petroleum ether:EtOAc = 1:1) as a white foam; ^{1}H NMR (400 MHz, DMSO-d$_6$): δ = 8.59 (br, OH), 7.66 (d, *J* = 8.2 Hz, 2H), 7.35 (d, *J* = 8.1 Hz, 2H), 6.62 - 6.43 (m, 2H), 6.33 (d, *J* = 2.4 Hz, 1H), 4.94 (s, 1H), 3.44 (d, *J* = 16.4 Hz, 1H), 3.28 (d, *J* = 16.4 Hz, 1H), 2.86 (s, 3H), 2.38 (s, 3H) ppm. ^{13}C NMR (101 MHz, DMSO-d$_6$): δ = 148.4, 146.3, 136.7, 128.5 (q, *J* = 31.8 Hz), 128.3 (2C), 125.6 (q, *J* = 3.8 Hz, 2C) 124.7 (q, *J* = 272.0 Hz), 119.4, 114.8, 114.5, 110.9, 80.5, 49.4, 42.4, 37.4 ppm. ESI-MS: *m/z* calcd: 322.13, found: 323.1 [M+H]$^+$. HPLC (method A): 98%.

1,3-Dimethyl-2-(pyridin-4-yl)-1,2,3,4-tetrahydroquinazolin-6-ol 9m. According to GP3, starting from 6-hydroxy-1,3-dimethyl-2-(pyridin-4-yl)-2,3-dihydroquinazolin-4(1*H*)-one **7m** (450 mg, 1.67 mmol, 1 equiv) the title compound 1,3-dimethyl-2-(pyridin-4-yl)-1,2,3,4-tetrahydroquinazolin-6-ol **9m** (226 mg, 53%) was obtained after column chromatography (DCM:MeOH = 9:1) as a yellow foam; ^{1}H NMR (400 MHz, DMSO-d$_6$): δ = 8.50 (dd, *J* = 4.4, 1.6 Hz, 2H), 8.47 (s, OH), 7.12 (dd, *J* = 4.6, 1.2 Hz, 2H), 6.62 - 6.48 (m, 2H), 6.33 (d, *J* = 2.4 Hz, 1H), 4.91 (s, 1H), 3.45 (d, *J* = 16.4 Hz, 1H), 3.31 (d, *J* = 17.1 Hz, 1H), 2.89 (s, 3H), 2.40 (s, 3H) ppm. ^{13}C NMR (101 MHz, DMSO-d$_6$): δ = 150.2, 150.1 (2C), 148.7, 136.6, 122.6 (2C), 119.3, 114.8, 114.4, 110.9, 80.0, 49.5, 42.2, 37.5 ppm. ESI-MS: *m/z* calcd: 255.14, found: 256.2 [M+H]$^+$. HPLC (method A): 99%.

1,3-Dimethyl-2-(pyridin-3-yl)-1,2,3,4-tetrahydroquinazolin-6-ol 9n. According to GP3, starting from 6-hydroxy-1,3-dimethyl-2-(pyridin-3-yl)-2,3-dihydroquinazolin-4(1*H*)-one **7n** (370 mg, 1.38 mmol, 1 equiv) the title compound 1,3-dimethyl-2-(pyridin-3-yl)-1,2,3,4-tetrahydroquinazolin-6-ol **9n** (191 mg, 54%) was obtained after column chromatography (DCM:MeOH = 9:1) as a brown oil; ^{1}H NMR (400 MHz, DMSO-d$_6$): δ = 8.48 (s, OH), 8.46 (dd, *J* = 4.7, 1.5 Hz, 1H), 8.36 (d, *J* = 2.0 Hz, 1H), 7.48 (dt, *J* = 7.8, 1.7 Hz, 1H), 7.33 (dd, *J* = 7.8, 4.8 Hz, 1H), 6.58 (dd, *J* = 8.7, 2.6 Hz, 1H), 6.54 (d, *J* = 8.7 Hz, 1H), 6.34 (d, *J* = 2.4 Hz, 1H), 4.95 (s, 1H), 3.47 (d, *J* = 16.4 Hz, 1H), 3.32 (d, *J* = 16.3 Hz, 1H), 2.87 (s, 3H), 2.39 (s, 3H) ppm. ^{13}C NMR (101 MHz, DMSO-d$_6$): δ = 148.7, 148.6, 148.1, 136.3, 136.2, 134.6, 123.3, 119.0, 114.3, 113.9, 110.6, 78.7, 48.9, 41.5, 36.9 ppm. ESI-MS: *m/z* calcd: 255.14, found: 256.15 [M+H]$^+$. HPLC (method A): 95%.

1,3-Dimethyl-2-(thiophen-3-yl)-1,2,3,4-tetrahydroquinazolin-6-ol 9o. According to GP3, starting from 6-hydroxy-1,3-dimethyl-2-(thiophen-3-yl)-2,3-dihydroquinazolin-4(1H)-one **7o** (430 mg, 1.57 mmol, 1 equiv) the title compound 1,3-dimethyl-2-(thiophen-3-yl)-1,2,3,4-tetrahydroquinazolin-6-ol **9o** (358 mg, 88%) was obtained after column chromatography (petroleum ether:EtOAc = 1:2) as a white foam; ^{1}H NMR (400 MHz, DMSO-d_6): δ = 8.44 (s, OH), 7.44 (dd, J = 4.9, 3.0 Hz, 1H), 7.05 (dd, J = 1.9, 1.0 Hz, 1H), 6.87 (dd, J = 5.0, 1.1 Hz, 1H), 6.55 (dd, J = 8.6, 2.7 Hz, 1H), 6.48 (d, J = 8.7 Hz, 1H), 6.33 (d, J = 2.6 Hz, 1H), 4.87 (s, 1H), 3.56 (d, J = 16.2 Hz, 1H), 3.32 (d, J = 15.3 Hz, 1H), 2.83 (s, 3H), 2.33 (s, 3H) ppm. ^{13}C NMR (101 MHz, DMSO-d_6): δ = 148.1, 142.2, 136.5, 126.8, 126.0, 122.3, 119.4, 114.0, 113.7, 110.7, 77.4, 49.6, 41.2, 36.8 ppm. ESI-MS: m/z calcd: 260.10, found: 261.1 [M+H][+]. HPLC (method A): 96%.

1,3-Dimethyl-2-(thiophen-2-yl)-1,2,3,4-tetrahydroquinazolin-6-ol 9p. According to GP3, starting from 6-hydroxy-1,3-dimethyl-2-(thiophen-2-yl)-2,3-dihydroquinazolin-4(1H)-one **7p** (400 mg, 1.5 mmol, 1 equiv) the title compound 1,3-dimethyl-2-(thiophen-2-yl)-1,2,3,4-tetrahydroquinazolin-6-ol **9p** (249 mg, 66%) was obtained after crystallization from a mixture of EtOAc and Et$_2$O as a yellow solid; ^{1}H NMR (400 MHz, DMSO-d_6): δ = 8.47 (s, OH), 7.40 (dd, J = 5.0, 1.2 Hz, 1H), 6.91 (dd, J = 5.0, 3.5 Hz, 1H), 6.76 (dt, J = 3.4, 0.9 Hz, 1H), 6.55 (dd, J = 8.6, 2.7 Hz, 1H), 6.49 (d, J = 8.7 Hz, 1H), 6.34 (d, J = 2.6 Hz, 1H), 5.09 (s, 1H), 3.70 (d, J = 16.3 Hz, 1H), 3.38 (d, J = 16.3 Hz, 1H), 2.88 (s, 3H), 2.34 (s, 3H) ppm. ^{13}C NMR (101 MHz, DMSO-d_6): δ = 148.6, 144.3, 135.8, 126.2, 125.6, 125.2, 119.4, 114.1, 113.6, 111.2, 77.2, 49.3, 41.0, 37.1 ppm. ESI-MS: m/z calcd: 260.10, found: 261.1 [M+H][+]. HPLC (method A): 100%.

2-(Furan-3-yl)-1,3-dimethyl-1,2,3,4-tetrahydroquinazolin-6-ol 9q. According to GP3, starting from 2-(furan-3-yl)-6-hydroxy-1,3-dimethyl-2,3-dihydroquinazolin-4(1H)-one **7q** (300 mg, 1.16 mmol, 1 equiv) the title compound 2-(furan-3-yl)-1,3-dimethyl-1,2,3,4-tetrahydroquinazolin-6-ol **9q** (221 mg, 78%) was obtained after column chromatography (petroleum ether:EtOAc = 1:2) as a yellow solid; ^{1}H NMR (400 MHz, DMSO-d_6): δ = 8.45 (s, OH), 7.56 (t, J = 1.7 Hz, 1H), 7.36 - 7.23 (m, 1H), 6.53 (dd, J = 8.6, 2.7 Hz, 1H), 6.46 (d, J = 8.7 Hz, 1H), 6.34 (d, J = 2.7 Hz, 1H), 6.19 (dd, J = 1.7, 0.7 Hz, 1H), 4.76 (s, 1H), 3.65 (d, J = 16.2 Hz, 1H), 3.37 (d, J = 16.2 Hz, 1H), 2.79 (s, 3H), 2.32 (s, 3H) ppm. ^{13}C NMR (101 MHz, DMSO-d_6): δ = 148.7, 143.7, 140.9, 137.0, 124.9, 120.2, 114.5, 114.0, 111.7, 110.2, 74.7,

50.2, 41.5, 37.2 ppm. ESI-MS: *m/z* calcd: 244.12, found: 245.2 [M+H]$^+$. HPLC (method A): 97%.

1,3-Dimethyl-2-(1*H*-pyrrol-3-yl)-1,2,3,4-tetrahydroquinazolin-6-ol 9r. According to GP3, starting from 6-hydroxy-1,3-dimethyl-2-(1*H*-pyrrol-3-yl)-2,3-dihydroquinazolin-4(1*H*)-one **7r** (400 mg, 1.56 mmol, 1 equiv) the title compound 1,3-dimethyl-2-(1*H*-pyrrol-3-yl)-1,2,3,4-tetrahydroquinazolin-6-ol **9r** (151 mg, 40%) was obtained after column chromatography (DCM:MeOH = 9:1) as a white solid; ^{1}H NMR (400 MHz, DMSO-d$_6$): δ = 10.53 (br, NH), 8.35 (s, OH), 6.61 (dd, *J* = 4.7, 2.5 Hz, 1H), 6.50 (dd, *J* = 8.6, 2.8 Hz, 1H), 6.41 (d, *J* = 8.7 Hz, 1H), 6.38 (d, *J* = 1.8 Hz, 1H), 6.31 (d, *J* = 2.7 Hz, 1H), 5.77 (dd, *J* = 4.1, 2.5 Hz, 1H), 4.68 (s, 1H), 3.68 (d, *J* = 15.9 Hz, 1H), 3.29 (d, *J* = 16.0 Hz, 1H), 2.74 (s, 3H), 2.28 (s, 3H) ppm. ^{13}C NMR (101 MHz, DMSO-d$_6$): δ = 148.2, 137.9, 122.1, 120.5, 117.9, 116.4, 114.2, 114.0, 111.1, 107.0, 76.8, 50.4, 41.6, 37.2 ppm. ESI-MS: *m/z* calcd: 243.14, found: 244.2 [M+H]$^+$. CHN-anal: calcd: (M + 0.2 H$_2$O) C: 68.10; H: 7.10; N: 17.02; found: C: 68.14; H: 7.10; N: 16.89.

1,3-Dimethyl-2-(naphthalen-1-yl)-1,2,3,4-tetrahydroquinazolin-6-ol 9s. According to GP3, starting from 6-hydroxy-1,3-dimethyl-2-(naphthalen-1-yl)-2,3-dihydroquinazolin-4(1*H*)-one **7s** (400 mg, 1.26 mmol, 1 equiv) the title compound 1,3-dimethyl-2-(naphthalen-1-yl)-1,2,3,4-tetrahydroquinazolin-6-ol **9s** (314 mg, 82%) was obtained after column chromatography (petroleum ether:EtOAc = 2:1) as a yellow foam; ^{1}H NMR (400 MHz, DMSO-d$_6$): δ = 8.47 (br, OH), 8.27 (d, *J* = 7.9 Hz, 1H), 7.96 - 7.87 (m, 1H), 7.82 (d, *J* = 8.2 Hz, 1H), 7.58 - 7.41 (m, 2H), 7.41 - 7.22 (m, 1H), 7.05 (d, *J* = 7.0 Hz, 1H), 6.67 - 6.48 (m, 2H), 6.34 (d, *J* = 2.4 Hz, 1H), 5.50 (s, 1H), 3.50 (d, *J* = 16.3 Hz, 1H), 3.23 (d, *J* = 16.3 Hz, 1H), 2.86 (s, 3H), 2.52 (s, 3H) ppm. ^{13}C NMR (101 MHz, DMSO-d$_6$): δ = 148.3, 137.4, 136.0, 134.4, 131.2, 128.7, 128.6, 126.1, 126.0, 125.4, 125.2, 124.1, 118.6, 114.7, 114.7, 109.9, 79.2, 49.7, 41.9, 36.9 ppm. ESI-MS: *m/z* calcd: 304.16, found: 305.2 [M+H]$^+$. HPLC (method A): 100%.

1,3-Dimethyl-2-(naphthalen-2-yl)-1,2,3,4-tetrahydroquinazolin-6-ol 9t. According to GP3, starting from 6-hydroxy-1,3-dimethyl-2-(naphthalen-2-yl)-2,3-dihydroquinazolin-4(1*H*)-one **7t** (494 mg, 1.55 mmol, 1 equiv) the title compound 1,3-dimethyl-2-(naphthalen-2-yl)-1,2,3,4-tetrahydroquinazolin-6-ol **9t** (410 mg, 87%) was obtained after column chromatography (petroleum ether:EtOAc = 1:1) as a purple foam; ^{1}H NMR (400 MHz,

DMSO-d$_6$): δ = 8.44 (br, OH), 7.91 - 7.83 (m, 2H), 7.83 - 7.77 (m, 1H), 7.58 (s, 1H), 7.51 - 7.43 (m, 2H), 7.40 (dd, J = 8.5, 1.6 Hz, 1H), 6.67 - 6.56 (m, 2H), 6.34 (d, J = 1.9 Hz, 1H), 4.98 (s, 1H), 3.54 (d, J = 16.1 Hz, 1H), 3.30 (d, J = 16.1 Hz, 1H), 2.91 (s, 3H), 2.40 (s, 3H) ppm. ^{13}C NMR (101 MHz, DMSO-d$_6$): δ = 148.4, 139.4, 137.1, 133.0, 133.0, 128.4, 128.3, 127.9, 126.5, 126.3, 126.0, 126.0, 119.7, 114.7, 114.4, 110.8, 81.5, 50.0, 42.2, 37.5 ppm. ESI-MS: m/z calcd: 304.16, found: 305.2 [M+H]$^+$. HPLC (method A): 96%.

2-(2,6-Dichlorophenyl)-1,3-dimethyl-1,2,3,4-tetrahydroquinazolin-6-ol 9u. According to GP3, starting from 2-(2,6-dichlorophenyl)-6-hydroxy-1,3-dimethyl-2,3-dihydroquinazolin-4(1*H*)-one **7u** (520 mg, 1.55 mmol, 1 equiv) the title 2-(2,6-dichlorophenyl)-1,3-dimethyl-1,2,3,4-tetrahydroquinazolin-6-ol **9u** (437 mg, 88%) was obtained after column chromatography (petroleum ether:EtOAc = 1:1) as a pale yellow solid; ^{1}H NMR (400 MHz, DMSO-d$_6$): δ = 8.45 (br, OH), 7.45 (d, J = 7.9 Hz, 2H), 7.38 - 7.26 (m, 1H), 6.54 (dd, J = 8.6, 2.8 Hz, 1H), 6.48 - 6.36 (m, 2H), 5.26 (s, 1H), 3.66 (d, J = 14.8 Hz, 1H), 3.35 (d, J = 15.9 Hz, 1H), 2.58 (s, 3H), 2.23 (s, 3H) ppm. ^{13}C NMR (101 MHz, DMSO-d$_6$): δ = 148.4, 137.7, 135.2, 130.4, 121.4, 114.6, 114.0, 111.1, 80.2, 53.3, 42.0, 35.5 ppm. ESI-MS: m/z calcd: 322.06, found: 323.05 [M+H]$^+$. HPLC (method A): 99%.

3-*iso*-Propyl-1-methyl-2-phenyl-1,2,3,4-tetrahydroquinazolin-6-ol 10a. According to GP3, starting from 6-hydroxy-3-*iso*-propyl-1-methyl-2-phenyl-2,3-dihydroquinazolin-4(1*H*)-one **8a** (340 mg, 1.15 mmol, 1 equiv) the title compound 3-*iso*-propyl-1-methyl-2-phenyl-1,2,3,4-tetrahydroquinazolin-6-ol **10a** (163 mg, 50%) was obtained after column chromatography (petroleum ether:EtOAc= 7:2) as a brown foam; ^{1}H NMR (400 MHz, DMSO-d$_6$): δ = 8.36 (br, OH), 7.34 - 7.25 (m, 2H), 7.25 - 7.19 (m, 1H), 7.15 (d, J = 7.2 Hz, 2H), 6.54 (dd, J = 8.6, 2.7 Hz, 1H), 6.44 (d, J = 8.6 Hz, 1H), 6.32 (d, J = 2.7 Hz, 1H), 5.15 (s, 1H), 3.52 (d, J = 16.7 Hz, 1H), 3.44 (d, J = 16.7 Hz, 1H), 2.85 (s, 3H), 2.84 - 2.75 (m, 1H), 1.14 (d, J = 6.3 Hz, 3H), 1.05 (d, J = 6.4 Hz, 3H) ppm. ^{13}C NMR (101 MHz, DMSO-d$_6$): δ = 148.1, 142.9, 138.0, 128.5 (2C), 127.5, 127.2 (2C), 120.8, 114.4, 113.9, 109.9, 76.9, 50.1, 44.5, 36.9, 22.0, 21.6 ppm. ESI-MS: m/z calcd: 282.17, found: 282.20 [M+H]$^+$. CHN-anal: calcd: C: 76.56; H: 7.85; N: 9.92, found: C: 76.21; H: 7.82; N: 10.13.

1-Methyl-2-phenyl-3-*n*-propyl-1,2,3,4-tetrahydroquinazolin-6-ol 10b. According to GP3, starting from 6-hydroxy-1-methyl-2-phenyl-3-*n*-propyl-2,3-dihydroquinazolin-4(1*H*)-one **8b** (270 mg, 0.91 mmol, 1 equiv) the title compound 1-methyl-2-phenyl-3-*n*-propyl-

1,2,3,4-tetrahydroquinazolin-6-ol **10b** (129 mg, 50%) was obtained after column chromatography (petroleum ether:EtOAc= 7:2) as a brown foam; ^{1}H NMR (400 MHz, DMSO-d$_6$): δ = 8.37 (s, OH), 7.33 - 7.26 (m, 2H), 7.26 - 7.19 (m, 1H), 7.14 (d, J = 7.1 Hz, 2H), 6.55 (dd, J = 8.6, 2.7 Hz, 1H), 6.49 (d, J = 8.7 Hz, 1H), 6.31 (d, J = 2.6 Hz, 1H), 4.96 (s, 1H), 3.47 (d, J = 16.5 Hz, 1H), 3.32 (d, J = 15.9 Hz, 1H), 2.88 (s, 3H), 2.58 - 2.53 (m, 1H), 2.42 (dt, J = 12.3, 7.1 Hz, 1H), 1.55 (hex, J = 7.3 Hz, 2H), 0.92 (t, J = 7.3 Hz, 3H) ppm. ^{13}C NMR (101 MHz, DMSO-d$_6$): δ = 148.1, 142.2, 137.4, 128.6 (2C), 127.6, 127.3 (2C), 119.6, 114.5, 114.5, 110.1, 79.5, 55.1, 47.4, 37.3, 21.2, 12.3 ppm. ESI-MS: *m/z* calcd: 282.17, found: 283.20 [M+H]$^+$. HPLC (method A): 96%.

3-Benzyl-1-methyl-2-phenyl-1,2,3,4-tetrahydroquinazolin-6-ol 10c. According to GP3, starting from 3-benzyl-6-hydroxy-1-methyl-2-phenyl-2,3-dihydroquinazolin-4(1*H*)-one **8c** (320 mg, 0.93 mmol, 1 equiv) the title compound 3-benzyl-1-methyl-2-phenyl-1,2,3,4-tetrahydroquinazolin-6-ol **10c** (155 mg, 50%) was obtained after column chromatography (petroleum ether:EtOAc= 7:2) as a yellow foam; ^{1}H NMR (400 MHz, DMSO-d$_6$): δ = 8.41 (br, OH), 7.43 - 7.35 (m, 4H), 7.32 - 7.20 (m, 4H), 7.15 (d, J = 7.2 Hz, 2H), 6.60 (dd, J = 8.6, 2.5 Hz, 1H), 6.56 (d, J = 8.7 Hz, 1H), 6.28 (d, J = 2.4 Hz, 1H), 4.88 (s, 1H), 3.77 (d, J = 13.3 Hz, 1H), 3.67 (d, J = 13.3 Hz, 1H), 3.51 (d, J = 16.5 Hz, 1H), 3.28 (d, J = 17.0 Hz, 1H), 2.89 (s, 3H) ppm. ^{13}C NMR (101 MHz, DMSO-d$_6$): δ = 148.3, 142.0, 139.6, 137.1, 129.2 (2C), 128.8 (2C), 128.7 (2C), 127.7, 127.5, 127.1 (2C), 119.1, 114.8, 114.5, 110.4, 78.8, 57.3, 47.2, 37.4 ppm. ESI-MS: *m/z* calcd: 330.17, found: 331.20 [M+H]$^+$. HPLC (method A): 97%.

2-(4-Chlorophenyl)-1,3-dimethyl-1,2,3,4-tetrahydroquinazolin-6-yl *n*-heptylcarbamate 2b. According to GP4, starting from 2-(4-chlorophenyl)-1,3-dimethyl-1,2,3,4-tetrahydroquinazolin-6-ol **9b** (150 mg, 0.52 mmol, 1 equiv) the title compound 2-(4-chlorophenyl)-1,3-dimethyl-1,2,3,4-tetrahydroquinazolin-6-yl *n*-heptylcarbamate **2b** (126 mg, 57%) was obtained after column chromatography (petroleum ether:EtOAc = 1:2) as a clear oil; ^{1}H NMR (400 MHz, DMSO-d$_6$): δ = 7.51 (t, J = 5.6 Hz, NH), 7.41 - 7.36 (m, 2H), 7.17 (d, J = 8.4 Hz, 2H), 6.82 (dd, J = 8.7, 2.7 Hz, 1H), 6.63 (d, J = 8.9 Hz, 1H), 6.61 (d, J = 2.7 Hz, 1H), 4.97 (s, 1H), 3.50 (d, J = 16.3 Hz, 1H), 3.34 (d, J = 17.2 Hz, 1H), 3.01 (dd, J = 13.0, 6.7 Hz, 2H), 2.92 (s, 3H), 2.39 (s, 3H), 1.50 - 1.40 (m, 2H), 1.34 - 1.23 (m, 8H), 0.87 (t, J = 6.8 Hz, 3H) ppm. ^{13}C NMR (101 MHz, DMSO-d$_6$): δ = 155.1, 141.1, 140.3, 140.0, 132.0, 128.7 (2C), 128.3 (2C), 120.7, 120.2, 117.9, 109.0, 79.8, 48.4, 41.5, 40.4, 36.7, 31.2, 29.2,

28.4, 26.2, 22.0, 13.9 ppm. ESI-MS: *m/z* calcd: 429.22, found: 430.2 [M+H]$^+$. HPLC (method C): 95%.

2-(3-Chlorophenyl)-1,3-dimethyl-1,2,3,4-tetrahydroquinazolin-6-yl *n*-heptylcarbamate 2c. According to GP4, starting from 2-(3-chlorophenyl)-1,3-dimethyl-1,2,3,4-tetrahydroquinazolin-6-ol **9c** (150 mg, 0.52 mmol, 1 equiv) the title compound 2-(3-chlorophenyl)-1,3-dimethyl-1,2,3,4-tetrahydroquinazolin-6-yl *n*-heptylcarbamate **2c** (117 mg, 53%) was obtained after column chromatography (petroleum ether:EtOAc = 1:1) as a yellow solid; mp 107-109 °C. ^{1}H NMR (400 MHz, DMSO-d$_6$): δ = 7.51 (t, *J* = 5.7 Hz, NH), 7.39 - 7.31 (m, 2H), 7.21 - 7.15 (m, 1H), 7.09 (dt, *J* = 3.6, 1.4 Hz, 1H), 6.83 (dd, *J* = 8.7, 2.7 Hz, 1H), 6.64 (d, *J* = 8.9 Hz, 1H), 6.62 (d, *J* = 2.7 Hz, 1H), 5.01 (s, 1H), 3.51 (d, *J* = 16.4 Hz, 1H), 3.35 (d, *J* = 16.3 Hz, 1H), 3.01 (dd, *J* = 13.0, 6.8 Hz, 2H), 2.94 (s, 3H), 2.40 (s, 3H), 1.49 - 1.39 (m, 2H), 1.33 - 1.22 (m, *J* = 15.4 Hz, 8H), 0.87 (t, *J* = 6.8 Hz, 3H) ppm. ^{13}C NMR (101 MHz, DMSO-d$_6$): δ = 155.6, 144.2, 141.7, 140.7, 133.5, 130.7, 128.0, 127.2, 125.8, 121.2, 120.7, 118.3, 109.6, 80.3, 48.9, 42.0, 40.9, 37.3, 31.7, 29.7, 28.8, 26.7, 22.5, 14.4 ppm. ESI-MS: *m/z* calcd: 429.22, found: 430.2 [M+H]$^+$. HPLC (method C): 98%.

2-(2-Chlorophenyl)-1,3-dimethyl-1,2,3,4-tetrahydroquinazolin-6-yl *n*-heptylcarbamate 2d. According to GP4, starting from 2-(2-chlorophenyl)-1,3-dimethyl-1,2,3,4-tetrahydroquinazolin-6-ol **9d** (150 mg, 0.52 mmol, 1 equiv) the title compound 2-(2-chlorophenyl)-1,3-dimethyl-1,2,3,4-tetrahydroquinazolin-6-yl *n*-heptylcarbamate **2d** (130 mg, 58%) was obtained after column chromatography (petroleum ether:EtOAc = 4:1) as a white solid; mp 140-143 °C. ^{1}H NMR (400 MHz, DMSO-d$_6$): δ = 7.53 (t, *J* = 5.6 Hz, NH), 7.49 (dd, *J* = 7.8, 1.1 Hz, 1H), 7.33 (td, *J* = 7.6, 1.7 Hz, 1H), 7.26 (t, *J* = 7.0 Hz, 1H), 7.01 - 6.94 (m, 1H), 6.85 (dd, *J* = 8.6, 2.6 Hz, 1H), 6.71 - 6.59 (m, 2H), 5.12 (s, 1H), 3.58 (d, *J* = 16.4 Hz, 1H), 3.35 (m, 1H), 3.02 (dd, *J* = 13.0, 6.6 Hz, 2H), 2.81 (s, 3H), 2.43 (s, 3H), 1.49 - 1.40 (m, 2H), 1.34 - 1.21 (m, 8H), 0.87 (t, *J* = 6.7 Hz, 3H) ppm. ^{13}C NMR (101 MHz, DMSO-d$_6$): δ = 155.6, 141.7, 141.1, 138.0, 133.2, 130.7, 129.9, 127.8, 127.2, 121.3, 120.7, 118.1, 109.1, 78.6, 48.5, 42.3, 40.9, 36.3, 31.7, 29.7, 28.8, 26.7, 22.5, 14.4 ppm. ESI-MS: *m/z* calcd: 429.22, found: 430.25 [M+H]$^+$. HPLC (method A): 98%.

1,3-Dimethyl-2-*p*-tolyl-1,2,3,4-tetrahydroquinazolin-6-yl *n*-heptylcarbamate 2e. According to GP4, starting from 1,3-dimethyl-2-*p*-tolyl-1,2,3,4-tetrahydroquinazolin-6-ol **9e** (150 mg, 0.56 mmol, 1 equiv) the title compound 1,3-dimethyl-2-*p*-tolyl-1,2,3,4-

tetrahydroquinazolin-6-yl *n*-heptylcarbamate **2e** (192 mg, 84%) was obtained after column chromatography (petroleum ether:EtOAc = 1:1) as a clear oil; ^{1}H NMR (400 MHz, DMSO-d$_6$): δ = 7.50 (t, *J* = 5.6 Hz, NH), 7.12 (d, *J* = 7.9 Hz, 2H), 7.03 (d, *J* = 8.0 Hz, 2H), 6.81 (dd, *J* = 8.7, 2.6 Hz, 1H), 6.64 - 6.53 (m, 2H), 4.90 (s, 1H), 3.53 (d, *J* = 16.2 Hz, 1H), 3.31 (d, *J* = 16.0 Hz, 1H), 3.01 (dd, *J* = 13.0, 6.7 Hz, 2H), 2.90 (s, 3H), 2.37 (s, 3H), 2.27 (s, 3H), 1.49 - 1.39 (m, 2H), 1.34 - 1.21 (m, 8H), 0.87 (t, *J* = 6.7 Hz, 3H) ppm. ^{13}C NMR (101 MHz, DMSO-d$_6$): δ = 155.1, 140.9, 140.7, 137.9, 136.6, 128.8 (2C), 126.7 (2C), 120.4, 120.1, 118.1, 108.8, 80.4, 48.5, 41.5, 40.4, 36.6, 31.2, 29.2, 28.3, 26.2, 22.0, 20.6, 13.9 ppm. ESI-MS: *m/z* calcd: 409.27, found: 410.3 [M+H]$^+$. HPLC (method C): 97%.

1,3-Dimethyl-2-*m*-tolyl-1,2,3,4-tetrahydroquinazolin-6-yl   *n*-heptylcarbamate   2f. According to GP4, starting from 1,3-dimethyl-2-*m*-tolyl-1,2,3,4-tetrahydroquinazolin-6-ol **9f** (150 mg, 0.49 mmol, 1 equiv) the title compound 1,3-dimethyl-2-*m*-tolyl-1,2,3,4-tetrahydroquinazolin-6-yl *n*-heptylcarbamate **2f** (51 mg, 23%) was obtained after column chromatography (petroleum ether:EtOAc = 1:1) as a yellow oil; ^{1}H NMR (400 MHz, DMSO-d$_6$): δ = 7.50 (t, *J* = 5.6 Hz, NH), 7.19 (t, *J* = 7.6 Hz, 1H), 7.07 (d, *J* = 7.5 Hz, 1H), 7.01 (s, 1H), 6.90 (d, *J* = 8.2 Hz, 1H), 6.81 (dd, *J* = 8.7, 2.6 Hz, 1H), 6.67 - 6.49 (m, 2H), 4.90 (s, 1H), 3.55 (d, *J* = 16.2 Hz, 1H), 3.29 (m, 1H), 3.01 (dd, *J* = 13.0, 6.7 Hz, 2H), 2.91 (s, 3H), 2.38 (s, 3H), 2.27 (s, 3H), 1.50 - 1.37 (m, 2H), 1.35 - 1.22 (m, 8H), 0.87 (t, *J* = 6.7 Hz, 3H) ppm. ^{13}C NMR (101 MHz, DMSO-d$_6$): δ = 155.6, 141.5, 141.4, 141.1, 137.8, 128.7, 128.5, 128.0, 124.2, 121.1, 120.6, 118.5, 109.3, 81.1, 49.1, 42.1, 40.9, 37.2, 31.7, 29.7, 28.8, 26.6, 22.5, 21.6, 14.4 ppm. ESI-MS: *m/z* calcd: 409.27, found: 410.3 [M+H]$^+$. HPLC (method C): 97%.

1,3-Dimethyl-2-*o*-tolyl-1,2,3,4-tetrahydroquinazolin-6-yl   *n*-heptylcarbamate   2g. According to GP4, starting from 1,3-dimethyl-2-*o*-tolyl-1,2,3,4-tetrahydroquinazolin-6-ol **9g** (150 mg, 0.56 mmol, 1 equiv) the title compound 1,3-dimethyl-2-*o*-tolyl-1,2,3,4-tetrahydroquinazolin-6-yl *n*-heptylcarbamate **2g** (135 mg, 59%) was obtained after column chromatography (petroleum ether:EtOAc = 3:1) as a yellow solid; mp 130-133 °C. ^{1}H NMR (400 MHz, DMSO-d$_6$): δ = 7.51 (t, *J* = 5.6 Hz, NH), 7.20 (d, *J* = 6.2 Hz, 1H), 7.16 (td, *J* = 7.3, 1.2 Hz, 1H), 7.09 - 7.00 (m, 1H), 6.85 – 6.78 (m, 2H), 6.63 - 6.56 (m, 2H), 5.01 (s, 1H), 3.56 (d, *J* = 16.4 Hz, 1H), 3.30 (m, 1H), 3.02 (dd, *J* = 13.0, 6.7 Hz, 2H), 2.84 (s, 3H), 2.43 (s, 3H), 2.40 (s, 3H), 1.51 - 1.38 (m, 2H), 1.34 - 1.20 (m, 8H), 0.87 (t, *J* = 6.8 Hz, 3H) ppm. ^{13}C NMR (101 MHz, DMSO-d$_6$): δ = 155.6, 141.5, 141.3, 138.8, 136.9, 131.4, 127.9, 125.7,

125.6, 121.1, 120.7, 117.9, 108.7, 78.9, 48.8, 42.0, 40.9, 36.5, 31.7, 29.8, 28.9, 26.7, 22.5, 18.9, 14.4 ppm. ESI-MS: *m/z* calcd: 409.27, found: 410.3 [M+H]$^+$. HPLC (method C): 95%.

2-(4-Methoxyphenyl)-1,3-dimethyl-1,2,3,4-tetrahydroquinazolin-6-yl

n-**heptylcarbamate 2h.** According to GP4, starting from 2-(4-methoxyphenyl)-1,3-dimethyl-1,2,3,4-tetrahydroquinazolin-6-ol **9h** (150 mg, 0.53 mmol, 1 equiv) the title compound 2-(4-methoxyphenyl)-1,3-dimethyl-1,2,3,4-tetrahydroquinazolin-6-yl *n*-heptylcarbamate **2h** (173 mg, 77%) was obtained after column chromatography (petroleum ether:EtOAc = 1:2) as a clear oil; ^{1}H NMR (400 MHz, DMSO-d$_6$): δ = 7.50 (t, *J* = 5.6 Hz, NH), 7.06 (d, *J* = 8.6 Hz, 2H), 6.87 (d, *J* = 8.7 Hz, 2H), 6.81 (dd, *J* = 8.7, 2.6 Hz, 1H), 6.66 - 6.55 (m, 2H), 4.88 (s, 1H), 3.72 (s, 3H), 3.54 (d, *J* = 16.2 Hz, 1H), 3.31 (d, *J* = 16.0 Hz, 1H), 3.01 (dd, *J* = 12.9, 6.6 Hz, 2H), 2.89 (s, 3H), 2.36 (s, 3H), 1.50 - 1.39 (m, 2H), 1.34 - 1.21 (m, 8H), 0.93 - 0.81 (m, 3H) ppm. ^{13}C NMR (101 MHz, DMSO-d$_6$): δ = 158.6, 155.1, 140.9, 140.7, 132.8, 127.9 (2C), 120.6, 120.0, 118.1, 113.6 (2C), 108.8, 80.2, 55.0, 48.6, 41.4, 40.4, 36.6, 31.2, 29.3, 28.4, 26.2, 22.0, 13.9 ppm. ESI-MS: *m/z* calcd: 425.27, found: 426.3 [M+H]$^+$. HPLC (method C): 98%.

2-(3-Methoxyphenyl)-1,3-dimethyl-1,2,3,4-tetrahydroquinazolin-6-yl

n-**heptylcarbamate 2i.** According to GP4, starting from 2-(3-methoxyphenyl)-1,3-dimethyl-1,2,3,4-tetrahydroquinazolin-6-ol **9i** (150 mg, 0.52 mmol, 1 equiv) the title compound 2-(3-methoxyphenyl)-1,3-dimethyl-1,2,3,4-tetrahydroquinazolin-6-yl *n*-heptylcarbamate **2i** (93 mg, 41%) was obtained after column chromatography (petroleum ether:EtOAc = 1:1) as a clear oil; ^{1}H NMR (400 MHz, DMSO-d$_6$): δ = 7.50 (t, *J* = 5.6 Hz, NH), 7.24 (t, *J* = 7.9 Hz, 1H), 6.88 - 6.78 (m, 2H), 6.75 - 6.67 (m, 2H), 6.65 - 6.56 (m, 2H), 4.92 (s, 1H), 3.70 (s, 3H), 3.56 (d, *J* = 16.3 Hz, 1H), 3.39 - 3.31 (m, 1H), 3.01 (dd, *J* = 13.0, 6.6 Hz, 2H), 2.92 (s, 3H), 2.39 (s, 3H), 1.50 - 1.41 (m, 2H), 1.32 - 1.22 (m, 8H), 0.87 (t, *J* = 6.7 Hz, 3H) ppm. ^{13}C NMR (101 MHz, DMSO-d$_6$): δ = 159.7, 155.6, 143.1, 141.5, 141.1, 129.8, 121.1, 120.6, 119.4, 118.6, 113.2, 113.0, 109.3, 81.0, 55.4, 49.1, 42.1, 40.9, 37.2, 31.7, 29.7, 28.8, 26.7, 22.5, 14.4 ppm. ESI-MS: *m/z* calcd: 425.27, found: 426.3 [M+H]$^+$. HPLC (method B): 98%.

2-(2-Methoxyphenyl)-1,3-dimethyl-1,2,3,4-tetrahydroquinazolin-6-yl

n-**heptylcarbamate 2j.** According to GP4, starting from 2-(2-methoxyphenyl)-1,3-dimethyl-1,2,3,4-tetrahydroquinazolin-6-ol **9j** (150 mg, 0.53 mmol, 1 equiv) the title compound 2-(2-methoxyphenyl)-1,3-dimethyl-1,2,3,4-tetrahydroquinazolin-6-yl *n*-heptylcarbamate **2j**

(159 mg, 71%) was obtained after column chromatography (petroleum ether:EtOAc = 1:2) as a yellow oil; ^{1}H NMR (400 MHz, DMSO-d$_6$): δ = 7.51 (t, J = 5.7 Hz, NH), 7.30 - 7.23 (m, 1H), 7.04 (d, J = 8.2 Hz, 1H), 6.88 - 6.77 (m, 3H), 6.64 (d, J = 2.7 Hz, 1H), 6.58 (d, J = 8.8 Hz, 1H), 5.17 (s, 1H), 3.82 (s, 3H), 3.64 (d, J = 16.2 Hz, 1H), 3.31 (m, 1H), 3.02 (dd, J = 13.0, 6.7 Hz, 2H), 2.73 (s, 3H), 2.36 (s, 3H), 1.53 - 1.41 (m, 2H), 1.34 - 1.22 (m, 8H), 0.87 (t, J = 6.9 Hz, 3H) ppm. ^{13}C NMR (101 MHz, DMSO-d$_6$): δ = 157.4, 155.6, 141.8, 141.4, 129.5, 128.3, 126.7, 121.1, 120.5, 120.1, 118.4, 111.9, 108.9, 75.6, 56.0, 48.9, 42.4, 40.9, 36.2, 31.7, 29.8, 28.9, 26.7, 22.5, 14.4 ppm. ESI-MS: m/z calcd: 425.27, found: 426.30 [M+H]$^+$. HPLC (method A): 98%.

2-(4-Fluorophenyl)-1,3-dimethyl-1,2,3,4-tetrahydroquinazolin-6-yl n-heptylcarbamate 2k. According to GP4, starting from 2-(4-fluorophenyl)-1,3-dimethyl-1,2,3,4-tetrahydroquinazolin-6-ol **9k** (150 mg, 0.55 mmol, 1 equiv) the title compound 2-(4-fluorophenyl)-1,3-dimethyl-1,2,3,4-tetrahydroquinazolin-6-yl n-heptylcarbamate **2k** (93 mg, 41%) was obtained after column chromatography (petroleum ether:EtOAc = 2:1) as a clear oil; ^{1}H NMR (400 MHz, DMSO-d$_6$): δ = 7.51 (t, J = 5.7 Hz, NH), 7.23 - 7.10 (m, 4H), 6.82 (dd, J = 8.7, 2.7 Hz, 1H), 6.62 (d, J = 9.0 Hz, 1H), 6.60 (d, J = 2.8 Hz, 1H), 4.97 (s, 1H), 3.51 (d, J = 16.3 Hz, 1H), 3.32 (m, 1H), 3.01 (dd, J = 13.0, 6.7 Hz, 2H), 2.92 (s, 3H), 2.38 (s, 3H), 1.49 - 1.38 (m, 2H), 1.33 - 1.20 (m, 8H), 0.87 (t, J = 6.8 Hz, 3H) ppm. ^{13}C NMR (101 MHz, DMSO-d$_6$): δ = 161.9 (d, J = 243.3 Hz), 155.6, 141.5, 140.9, 137.6 (d, J = 2.8 Hz), 129.2 (d, J = 8.2 Hz, 2C), 121.1, 120.6, 118.4, 115.5 (d, J = 21.3 Hz, 2C), 109.5, 80.4, 48.9, 42.0, 40.9, 37.2, 31.7, 29.7, 28.8, 26.7, 22.5, 14.4 ppm. ESI-MS: m/z calcd: 413.25, found: 414.3 [M+H]$^+$. HPLC (method C): 100%.

1,3-Dimethyl-2-(4-(trifluoromethyl)phenyl)-1,2,3,4-tetrahydroquinazolin-6-yl n-heptylcarbamate 2l. According to GP4, starting from 1,3-dimethyl-2-(4-(trifluoromethyl)phenyl)-1,2,3,4-tetrahydroquinazolin-6-ol **9l** (150 mg, 0.47 mmol, 1 equiv) the title compound 1,3-dimethyl-2-(4-(trifluoromethyl)phenyl)-1,2,3,4-tetrahydroquinazolin-6-yl n-heptylcarbamate **2l** (154 mg, 72%) was obtained after column chromatography (petroleum ether:EtOAc = 1:1) as a clear oil; ^{1}H NMR (400 MHz, DMSO-d$_6$): δ = 7.70 (d, J = 8.2 Hz, 2H), 7.51 (t, J = 5.6 Hz, NH), 7.38 (d, J = 8.1 Hz, 2H), 6.84 (dd, J = 8.7, 2.6 Hz, 1H), 6.66 (d, J = 8.8 Hz, 1H), 6.61 (d, J = 2.6 Hz, 1H), 5.09 (s, 1H), 3.48 (d, J = 16.5 Hz, 1H), 3.36 (d, J = 17.0 Hz, 1H), 3.01 (dd, J = 13.0, 6.7 Hz, 2H), 2.96 (s, 3H), 2.43 (s, 3H), 1.50 - 1.39 (m, 2H), 1.27 (m, 8H), 0.87 (t, J = 6.8 Hz, 3H) ppm. ^{13}C NMR (101 MHz, DMSO-d$_6$): δ =

155.6, 146.3, 141.7, 140.7, 128.6 (q, J = 31.8 Hz), 128.2 (2C), 125.7 (q, J = 3.8 Hz), 121.3, 120.7, 118.3, 109.6, 80.4, 48.9, 42.1, 40.9, 37.2, 31.7, 29.7, 28.8, 26.7, 22.5, 14.4 ppm. ESI-MS: *m/z* calcd: 463.24, found: 464.2 [M+H]$^+$. HPLC (method B): 99%.

1,3-Dimethyl-2-(pyridin-4-yl)-1,2,3,4-tetrahydroquinazolin-6-yl *n*-heptylcarbamate 2m. According to GP4, starting from 1,3-dimethyl-2-(pyridin-4-yl)-1,2,3,4-tetrahydroquinazolin-6-ol **9m** (150 mg, 0.59 mmol, 1 equiv) the title compound 1,3-dimethyl-2-(pyridin-4-yl)-1,2,3,4-tetrahydroquinazolin-6-yl *n*-heptylcarbamate **2m** (123 mg, 53%) was obtained after column chromatography (DCM:MeOH = 9:1) as a clear oil; ^{1}H NMR (400 MHz, DMSO-d$_6$): δ = 8.53 (dd, J = 4.4, 1.6 Hz, 2H), 7.52 (t, J = 5.7 Hz, NH), 7.16 - 7.11 (m, 2H), 6.84 (dd, J = 8.7, 2.7 Hz, 1H), 6.66 (d, J = 8.9 Hz, 1H), 6.61 (d, J = 2.7 Hz, 1H), 5.04 (s, 1H), 3.48 (d, J = 16.6 Hz, 1H), 3.37 (d, J = 16.4 Hz, 1H), 3.01 (dd, J = 13.1, 6.8 Hz, 2H), 2.97 (s, 3H), 2.43 (s, 3H), 1.48 - 1.38 (m, 2H), 1.32 - 1.21 (m, 8H), 0.87 (t, J = 6.8 Hz, 3H) ppm. ^{13}C NMR (101 MHz, DMSO-d$_6$): δ = 155.5, 150.3 (2C), 150.1, 141.7, 140.6, 122.5 (2C), 121.3, 120.7, 118.2, 109.7, 79.9, 49.0, 42.1, 40.9, 37.3, 31.7, 29.7, 28.8, 26.7, 22.5, 14.4 ppm. ESI-MS: *m/z* calcd: 396.25, found: 397.2 [M+H]$^+$. HPLC (method C): 98%.

1,3-Dimethyl-2-(pyridin-3-yl)-1,2,3,4-tetrahydroquinazolin-6-yl *n*-heptylcarbamate 2n. According to GP4, starting from 1,3-dimethyl-2-(pyridin-3-yl)-1,2,3,4-tetrahydroquinazolin-6-ol **9n** (150 mg, 0.59 mmol, 1 equiv) the title compound 1,3-dimethyl-2-(pyridin-3-yl)-1,2,3,4-tetrahydroquinazolin-6-yl *n*-heptylcarbamate **2n** (134 mg, 58%) was obtained after column chromatography (DCM:MeOH = 9:1) as a clear oil; ^{1}H NMR (400 MHz, DMSO-d$_6$): δ = 8.48 (dd, J = 4.7, 1.4 Hz, 1H), 8.38 (d, J = 1.9 Hz, 1H), 7.55 - 7.46 (m, NH + 1H), 7.35 (dd, J = 7.7, 4.8 Hz, 1H), 6.84 (dd, J = 8.7, 2.6 Hz, 1H), 6.65 (d, J = 8.8 Hz, 1H), 6.62 (d, J = 2.6 Hz, 1H), 5.08 (s, 1H), 3.50 (d, J = 16.4 Hz, 1H), 3.38 (d, J = 16.5 Hz, 1H), 3.01 (dd, J = 13.0, 6.7 Hz, 2H), 2.95 (s, 3H), 2.42 (s, 3H), 1.51 - 1.38 (m, 2H), 1.34 - 1.21 (m, 8H), 0.87 (t, J = 6.7 Hz, 3H) ppm. ^{13}C NMR (101 MHz, DMSO-d$_6$): δ = 155.0, 148.8, 148.5, 141.2, 140.3, 136.1, 134.4, 123.4, 120.8, 120.2, 117.8, 109.3, 78.5, 48.3, 41.5, 40.4, 36.7, 31.2, 29.2, 28.4, 26.2, 22.0, 13.9 ppm. ESI-MS: *m/z* calcd: 396.25, found: 396.9 [M+H]$^+$. HPLC (method B): 99%.

1,3-Dimethyl-2-(thiophen-3-yl)-1,2,3,4-tetrahydroquinazolin-6-yl *n*-heptylcarbamate 2o. A solution of 1,3-dimethyl-2-(thiophen-3-yl)-1,2,3,4-tetrahydroquinazolin-6-ol **9o** (150 mg, 0.58 mmol, 1 equiv) in DCM (5 mL) was treated with *n*-heptyl isocyanate (101 µL,

0.63 mmol, 1.1 equiv) and triethylamine (88 µL, 0.63 mmol, 1.1 equiv). The mixture was stirred for 6 h. For workup, the mixture was diluted with ethyl acetate (30 mL), washed with water (10 mL) and washed with brine (10 mL). The organic phase was dried over Na_2SO_4 and the solvent was evaporated under reduced pressure. The crude product was purified by column chromatography (petroleum ether:EtOAc = 1:1) to yield 1,3-dimethyl-2-(thiophen-3-yl)-1,2,3,4-tetrahydroquinazolin-6-yl *n*-heptylcarbamate **2o** (96 mg, 42%) as a yellow oil; ^{1}H NMR (400 MHz, DMSO-d_6): δ = 7.54 - 7.44 (m, NH + 1H), 7.11 - 7.05 (m, 1H), 6.91 (dd, *J* = 5.0, 1.1 Hz, 1H), 6.80 (dd, *J* = 8.7, 2.7 Hz, 1H), 6.62 - 6.55 (m, 2H), 4.99 (s, 1H), 3.60 (d, *J* = 16.3 Hz, 1H), 3.37 (d, *J* = 16.3 Hz, 1H), 3.01 (dd, *J* = 13.0, 6.7 Hz, 2H), 2.93 (s, 3H), 2.36 (s, 3H), 1.48 - 1.38 (m, 2H), 1.33 - 1.22 (m, 8H), 0.94 - 0.77 (m, 3H) ppm. ^{13}C NMR (101 MHz, DMSO-d_6): δ = 155.6, 143.0, 141.6, 140.9, 127.0, 126.9, 122.9, 121.0, 120.5, 118.6, 109.8, 77.9, 49.4, 41.6, 40.9, 37.1, 31.7, 29.7, 28.8, 26.7, 22.5, 14.4 ppm. ESI-MS: *m/z* calcd: 401.21, found: 402.2 [M+H]$^+$. HPLC (method C): 99%.

1,3-Dimethyl-2-(thiophen-2-yl)-1,2,3,4-tetrahydroquinazolin-6-yl   *n*-heptylcarbamate 2p. A solution of 1,3-dimethyl-2-(thiophen-2-yl)-1,2,3,4-tetrahydroquinazolin-6-ol **9p** (150 mg, 0.58 mmol, 1 equiv) in DCM (5 mL) was treated with *n*-heptyl isocyanate (101 µL, 0.63 mmol, 1.1 equiv) and triethylamine (88 µL, 0.63 mmol, 1.1 equiv). The mixture was stirred for 6 h. For workup, the mixture was diluted with ethyl acetate (30 mL), washed with water (10 mL) and washed with brine (10 mL). The organic phase was dried over Na_2SO_4 and the solvent was evaporated under reduced pressure. The crude product was purified by column chromatography (petroleum ether:EtOAc = 1:1) to yield 1,3-dimethyl-2-(thiophen-2-yl)-1,2,3,4-tetrahydroquinazolin-6-yl *n*-heptylcarbamate **2p** (133 mg, 58%) as a white powder; mp 81 °C. ^{1}H NMR (400 MHz, DMSO-d_6): δ = 7.51 (t, *J* = 5.6 Hz, NH), 7.44 (dd, *J* = 5.0, 1.0 Hz, 1H), 6.93 (dd, *J* = 5.0, 3.5 Hz, 1H), 6.80 (dd, *J* = 8.7, 2.6 Hz, 1H), 6.77 (d, *J* = 3.4 Hz, 1H), 6.65 - 6.56 (m, 2H), 5.21 (s, 1H), 3.76 (d, *J* = 16.5 Hz, 1H), 3.43 (d, *J* = 16.4 Hz, 1H), 3.07 - 2.95 (m, 5H), 2.37 (s, 3H), 1.50 - 1.38 (m, 2H), 1.34 - 1.21 (m, 8H), 0.87 (t, *J* = 6.7 Hz, 3H) ppm. ^{13}C NMR (101 MHz, DMSO-d_6): δ = 155.0, 144.8, 141.4, 139.9, 126.4, 125.9, 125.0, 120.5, 120.0, 118.2, 109.6, 77.1, 48.7, 40.9, 40.4, 36.9, 31.2, 29.2, 28.4, 26.2, 22.0, 13.9 ppm. ESI-MS: *m/z* calcd: 401.21, found: 402.3 [M+H]$^+$. HPLC (method B): 100%.

2-(Furan-3-yl)-1,3-dimethyl-1,2,3,4-tetrahydroquinazolin-6-yl   *n*-heptylcarbamate 2q. According to GP4, starting from 2-(furan-3-yl)-6-hydroxy-1,3-dimethyl-2,3-dihydroquinazolin-4(1H)-one **9q** (150 mg, 0.49 mmol, 1 equiv) the title compound 2-(furan-

3-yl)-1,3-dimethyl-1,2,3,4-tetrahydroquinazolin-6-yl *n*-heptylcarbamate **2q** (71 mg, 30%) was obtained after column chromatography (petroleum ether:EtOAc = 1:2) as a clear oil; ^{1}H NMR (400 MHz, DMSO-d$_6$): δ = 7.58 (dd, J = 8.0, 6.4 Hz, 1H), 7.50 (t, J = 5.6 Hz, NH), 7.34 (s, 1H), 6.78 (dd, J = 8.7, 2.7 Hz, 1H), 6.60 (d, J = 2.6 Hz, 1H), 6.55 (d, J = 8.8 Hz, 1H), 6.25 (d, J = 1.0 Hz, 1H), 4.87 (s, 1H), 3.72 (d, J = 16.4 Hz, 1H), 3.41 (d, J = 16.3 Hz, 1H), 3.01 (dd, J = 13.0, 6.7 Hz, 2H), 2.89 (s, 3H), 2.34 (s, 3H), 1.51 - 1.39 (m, 2H), 1.34 - 1.15 (m, 8H), 0.87 (t, J = 6.8 Hz, 3H) ppm. ^{13}C NMR (101 MHz, DMSO-d$_6$): δ = 155.6, 144.0, 141.7, 141.0, 140.9, 125.6, 120.9, 120.4, 118.8, 110.1, 109.9, 74.7, 49.5, 41.4, 40.9, 36.9, 31.7, 29.7, 28.8, 26.7, 22.5, 14.4 ppm. ESI-MS: *m/z* calcd: 385.24, found: 386.3 [M+H]$^+$. HPLC (method B): 98%.

1,3-Dimethyl-2-(1*H*-pyrrol-3-yl)-1,2,3,4-tetrahydroquinazolin-6-yl *n*-heptylcarbamate 2r. According to GP4, starting from 1,3-dimethyl-2-(1*H*-pyrrol-3-yl)-1,2,3,4-tetrahydroquinazolin-6-ol **9r** (100 mg, 0.49 mmol, 1 equiv) the title compound 1,3-dimethyl-2-(1*H*-pyrrol-3-yl)-1,2,3,4-tetrahydroquinazolin-6-yl *n*-heptylcarbamate **2r** (38 mg, 15%) was obtained after column chromatography (DCM:MeOH = 9:1) as a yellow oil; ^{1}H NMR (400 MHz, DMSO-d$_6$): δ = 10.60 (s, NH), 7.49 (t, J = 5.7 Hz, CONH), 6.76 (dd, J = 8.7, 2.7 Hz, 1H), 6.64 (dd, J = 4.7, 2.4 Hz, 1H), 6.57 (d, J = 2.7 Hz, 1H), 6.51 (d, J = 8.8 Hz, 1H), 6.45 - 6.38 (m, 1H), 5.81 (dd, J = 4.0, 2.4 Hz, 1H), 4.82 (s, 1H), 3.77 (d, J = 16.0 Hz, 1H), 3.35 (m, 1H), 3.01 (dd, J = 13.0, 6.7 Hz, 2H), 2.85 (s, 3H), 2.32 (s, 3H), 1.50 - 1.37 (m, 2H), 1.35 - 1.18 (m, 8H), 0.87 (t, J = 6.8 Hz, 3H) ppm. ^{13}C NMR (101 MHz, DMSO-d$_6$): δ = 155.6, 141.6, 141.3, 122.4, 120.7, 120.2, 119.1, 118.2, 116.4, 109.6, 106.7, 76.8, 49.6, 41.40, 40.9, 37.0, 31.7, 29.8, 28.9, 26.7, 22.5, 14.4 ppm. ESI-MS: *m/z* calcd: 384.25, found: 385.30 [M+H]$^+$. HPLC (method A): 95%.

1,3-Dimethyl-2-(naphthalen-1-yl)-1,2,3,4-tetrahydroquinazolin-6-yl *n*-heptylcarbamate 2s. According to GP4, starting from 1,3-dimethyl-2-(naphthalen-1-yl)-1,2,3,4-tetrahydroquinazolin-6-ol **9s** (150 mg, 0.49 mmol, 1 equiv) the title compound 1,3-dimethyl-2-(naphthalen-1-yl)-1,2,3,4-tetrahydroquinazolin-6-yl *n*-heptylcarbamate **2s** (131 mg, 60%) was obtained after column chromatography (petroleum ether:EtOAc = 7:2) as a clear oil; ^{1}H NMR (400 MHz, DMSO-d$_6$): δ = 8.27 (d, J = 8.1 Hz, 1H), 7.96 - 7.89 (m, 1H), 7.85 (d, J = 8.2 Hz, 1H), 7.60 - 7.48 (m, 2H+NH), 7.42 - 7.34 (m, 1H), 7.03 (d, J = 7.1 Hz, 1H), 6.87 (dd, J = 8.7, 2.7 Hz, 1H), 6.68 (d, J = 8.9 Hz, 1H), 6.61 (d, J = 2.7 Hz, 1H), 5.63 (s, 1H), 3.52 (d, J = 16.5 Hz, 1H), 3.28 (m, 1H), 3.02 (dd, J = 13.0, 6.7 Hz, 2H), 2.94 (s, 3H),

2.56 (s, 3H), 1.51 - 1.39 (m, 2H), 1.33 - 1.22 (m, 8H), 0.87 (t, J = 6.8 Hz, 3H) ppm. ^{13}C NMR (101 MHz, DMSO-d$_6$): δ = 155.6, 141.5, 141.4, 135.8, 134.4, 131.1, 128.7, 128.7, 126.2, 126.1, 125.4, 125.2, 123.9, 121.2, 120.8, 117.7, 108.9, 79.1, 49.1, 41.9, 40.9, 36.8, 31.7, 29.7, 28.8, 26.7, 22.5, 14.4 ppm. ESI-MS: m/z calcd: 445.27, found: 446.3 [M+H]$^+$. HPLC (method B): 97%.

1,3-Dimethyl-2-(naphthalen-2-yl)-1,2,3,4-tetrahydroquinazolin-6-yl

***n*-heptylcarbamate 2t.** According to GP4, starting from 1,3-dimethyl-2-(naphthalen-2-yl)-1,2,3,4-tetrahydroquinazolin-6-ol **9t** (150 mg, 0.49 mmol, 1 equiv) the title compound 1,3-dimethyl-2-(naphthalen-2-yl)-1,2,3,4-tetrahydroquinazolin-6-yl   *n*-heptylcarbamate   **2t** (155 mg, 71%) was obtained after column chromatography (petroleum ether:EtOAc = 1:1) as a clear oil; ^{1}H NMR (400 MHz, DMSO-d$_6$): δ = 7.92 - 7.86 (m, 2H), 7.86 - 7.79 (m, 1H), 7.57 (br, NH), 7.55 - 7.44 (m, 3H), 7.41 (dd, J = 8.5, 1.6 Hz, 1H), 6.86 (dd, J = 8.7, 2.7 Hz, 1H), 6.69 (d, J = 8.9 Hz, 1H), 6.61 (d, J = 2.7 Hz, 1H), 5.12 (s, 1H), 3.56 (d, J = 16.2 Hz, 1H), 3.36 (d, J = 16.1 Hz, 1H), 3.10 - 2.91 (m, 5H), 2.44 (s, 3H), 1.49 - 1.38 (m, 2H), 1.32 - 1.22 (m, 8H), 0.90 - 0.82 (m, 3H) ppm. ^{13}C NMR (101 MHz, DMSO-d$_6$): δ = 155.6, 141.5, 141.1, 139.2, 133.05, 133.0, 128.6, 128.4, 127.9, 126.6, 126.5, 125.8, 125.8, 121.2, 120.6, 118.6, 109.5, 81.3, 49.3, 42.1, 40.9, 37.3, 31.7, 29.7, 28.8, 26.7, 22.5, 14.4 ppm. ESI-MS: m/z calcd: 445.27, found: 446.3 [M+H]$^+$. HPLC (method C): 96%.

2-(2,6-Dichlorophenyl)-1,3-dimethyl-1,2,3,4-tetrahydroquinazolin-6-yl

***n*-heptylcarbamate 2u.** According to GP4, starting from 2-(2,6-dichlorophenyl)-1,3-dimethyl-1,2,3,4-tetrahydroquinazolin-6-ol **9u** (150 mg, 0.47 mmol, 1 equiv) the title compound   2-(2,6-dichlorophenyl)-1,3-dimethyl-1,2,3,4-tetrahydroquinazolin-6-yl   *n*-heptylcarbamate **2u** (64 mg, 30%) was obtained after column chromatography (petroleum ether:EtOAc = 4:1) as a yellow oil; ^{1}H NMR (400 MHz, DMSO-d$_6$): δ = 7.61 - 7.45 (m, 2H+NH), 7.46 - 7.32 (m, 1H), 6.85 (dd, J = 8.7, 2.7 Hz, 1H), 6.75 (d, J = 2.7 Hz, 1H), 6.56 (d, J = 8.8 Hz, 1H), 5.42 (s, 1H), 3.75 (d, J = 15.0 Hz, 1H), 3.46 (d, J = 15.0 Hz, 1H), 3.08 (dd, J = 13.0, 6.7 Hz, 2H), 2.70 (s, 3H), 2.33 (s, 3H), 1.58 - 1.44 (m, 2H), 1.41 - 1.25 (m, 8H), 0.92 (t, J = 6.8 Hz, 3H) ppm. ^{13}C NMR (101 MHz, DMSO-d$_6$): δ = 155.6, 141.8, 141.5, 134.9, 130.5, 121.1, 120.3, 120.1, 109.8, 79.8, 52.5, 42.0, 40.9, 35.2, 31.7, 29.8, 28.9, 26.7, 22.5, 14.4 ppm. ESI-MS: m/z calcd: 463.18, found: 464.20 [M+H]$^+$. HPLC (method A): 96%.

3-*iso*-Propyl-1-methyl-2-phenyl-1,2,3,4-tetrahydroquinazolin-6-yl   *n*-heptylcarbamate 3a. According to GP4, starting from 3-*iso*-propyl-1-methyl-2-phenyl-1,2,3,4-tetrahydroquinazolin-6-ol **10a** (100 mg, 0.35 mmol, 1 equiv) the title compound 3-*iso*-propyl-1-methyl-2-phenyl-1,2,3,4-tetrahydroquinazolin-6-yl *n*-heptylcarbamate **3a** (72 mg, 48%) was obtained after column chromatography (petroleum ether:EtOAc= 5:1) as a white solid; mp 132-133 °C. ^{1}H NMR (400 MHz, DMSO-d$_6$): δ = 7.48 (t, J = 5.7 Hz, NH), 7.36 - 7.28 (m, 2H), 7.28 - 7.21 (m, 1H), 7.16 (d, J = 7.2 Hz, 2H), 6.79 (dd, J = 8.7, 2.7 Hz, 1H), 6.60 (d, J = 2.7 Hz, 1H), 6.56 (d, J = 8.8 Hz, 1H), 5.25 (s, 1H), 3.60 (d, J = 16.4 Hz, 1H), 3.46 (d, J = 16.8 Hz, 1H), 3.01 (dd, J = 13.0, 6.7 Hz, 2H), 2.93 (s, 3H), 2.86 - 2.74 (m, 1H), 1.49 - 1.38 (m, 2H), 1.34 - 1.21 (m, 8H), 1.16 (d, J = 6.3 Hz, 3H), 1.06 (d, J = 6.3 Hz, 3H), 0.87 (t, J = 6.8 Hz, 3H) ppm. ^{13}C NMR (101 MHz, DMSO-d$_6$): δ = 155.6, 142.7, 142.0, 141.2, 128.7 (2C), 127.6, 127.1 (2C), 120.9, 119.9, 119.8, 108.8, 76.8, 50.1, 44.3, 40.9, 36.8, 31.7, 29.8, 28.8, 26.7, 22.5, 22.0, 21.7, 14.4 ppm. ESI-MS: *m/z* calcd: 423.29, found: 424.30 [M+H]$^+$. HPLC (method C): 99%.

1-Methyl-2-phenyl-3-*n*-propyl-1,2,3,4-tetrahydroquinazolin-6-yl   *n*-heptylcarbamate 3b. According to GP4, starting from 1-methyl-2-phenyl-3-*n*-propyl-1,2,3,4-tetrahydroquinazolin-6-ol **10b** (100 mg, 0.35 mmol, 1 equiv) the title compound 1-methyl-2-phenyl-3-*n*-propyl-1,2,3,4-tetrahydroquinazolin-6-yl *n*-heptylcarbamate **3b** (58 mg, 39%) was obtained after column chromatography (petroleum ether:EtOAc= 5:1) as a white solid; mp 106-108 °C. ^{1}H NMR (400 MHz, DMSO-d$_6$): δ = 7.49 (br, NH), 7.37 - 7.29 (m, 2H), 7.29 - 7.19 (m, 1H), 7.19 - 7.09 (m, 2H), 6.81 (d, J = 7.6 Hz, 1H), 6.65 - 6.51 (m, 2H), 5.07 (s, 1H), 3.49 (d, J = 16.3 Hz, 1H), 3.40 (d, J = 17.0 Hz, 1H), 3.06 - 2.88 (m, 5H), 2.46 - 2.37 (m, 2H), 1.57 (dd, J = 13.8, 6.7 Hz, 2H), 1.49 - 1.38 (m, 2H), 1.35 - 1.19 (m, 8H), 0.93 (t, J = 7.0 Hz, 3H), 0.90 - 0.81 (m, 3H) ppm. ^{13}C NMR (101 MHz, DMSO-d$_6$): δ = 155.6, 142.0, 141.4, 141.3, 128.7 (2C), 127.8, 127.1 (2C), 121.0, 120.6, 118.6, 109.1, 79.5, 55.0, 47.0, 40.9, 37.2, 31.7, 29.7, 28.8, 26.7, 22.5, 21.2, 14.4, 12.2 ppm. ESI-MS: *m/z* calcd: 423.29, found: 424.30 [M+H]$^+$. HPLC (method C): 100%.

3-Benzyl-1-methyl-2-phenyl-1,2,3,4-tetrahydroquinazolin-6-yl *n*-heptylcarbamate 3c. According to GP4, starting from 3-benzyl-1-methyl-2-phenyl-1,2,3,4-tetrahydroquinazolin-6-ol **10c** (100 mg, 0.36 mmol, 1 equiv) the title compound 3-benzyl-1-methyl-2-phenyl-1,2,3,4-tetrahydroquinazolin-6-yl *n*-heptylcarbamate **3c** (79 mg, 55%) was obtained after column chromatography (petroleum ether:EtOAc= 5:1) as a white solid; mp 104-106 °C. ^{1}H NMR

(400 MHz, DMSO-d$_6$): δ = 7.50 (t, J = 5.7 Hz, NH), 7.43 - 7.23 (m, 8H), 7.16 (d, J = 7.3 Hz, 2H), 6.85 (dd, J = 8.7, 2.7 Hz, 1H), 6.68 (d, J = 8.8 Hz, 1H), 6.56 (d, J = 2.6 Hz, 1H), 4.96 (s, 1H), 3.78 (d, J = 13.3 Hz, 1H), 3.67 (d, J = 13.3 Hz, 1H), 3.54 (d, J = 16.6 Hz, 1H), 3.37 (d, J = 17.3 Hz, 1H), 3.01 (dd, J = 13.0, 6.7 Hz, 2H), 2.96 (s, 3H), 1.49 - 1.39 (m, 2H), 1.31 - 1.20 (m, 8H), 0.86 (t, J = 6.8 Hz, 3H) ppm. ^{13}C NMR (101 MHz, DMSO-d$_6$): δ = 155.6, 141.7, 141.5, 141.2, 139.4, 129.2 (2C), 128.8 (4C), 127.9, 127.6, 127.0 (2C), 121.3, 120.7, 118.2, 109.4, 78.7, 57.2, 46.9, 40.7, 37.3, 31.7, 29.7, 28.8, 26.7, 22.5, 14.4 ppm. ESI-MS: *m/z* calcd: 471.29, found: 472.30 [M+H]$^+$. HPLC (method C): 97%.

IC$_{50}$Values with Confidence Intervals

Table S1. Cholinesterase inhibition of the synthesized test compounds.[a] Phenols were incubated for 4.5 min and carbamates for 30 min.

Moiety	X = H	IC$_{50}$ [μM] or % inhibition (95% confidence interval)		X = (C=O)NHn-Hept	IC$_{50}$ [μM] or % inhibition (95% confidence interval)	
		BChE	AChE		BChE	AChE
R^1 = Me; R^2 = H	**9a**	39.9 (31.5-50.5)	327.0 (258.2-414.2)	**2a**	0.106 (0.095-0.118)	4%[d]
4-Cl-Ph-	**9b**	13.8 (12.3-15.4)	235.6 (198.7-279.2)	**2b**	0.115 (0.088-0.149)	24%[d]
3-Cl-Ph-	**9c**	2.1 (1.9-2.3)	242.4 (200.9-292.5)	**2c**	0.096 (0.090-0.103)	39%[d]
2-Cl-Ph-	**9d**	56.0 (43.6-71.9)	60%[b]	**2d**	0.474 (0.406-0.555)	48%[e]
4-Me-Ph-	**9e**	22.6 (19.4-26.3)	109.9 (98.4-122.9)	**2e**	0.231 (0.217-0.247)	9%[d]
3-Me-Ph-	**9f**	17.4 (14.2-21.3)	437.0 (376.6-507.1)	**2f**	0.199 (0.181-0.220)	27%[d]
2-Me-Ph-	**9g**	92.4 (79.9-106.8)	143.4 (119.1-172.6)	**2g**	0.251 (0.211-0.298)	18%[e]
4-MeO-Ph-	**9h**	39.5 (27.4-57.0)	103.8 (68.4-157.5)	**2h**	0.875 (0.769-0.997)	14%[d]
3-MeO-Ph-	**9i**	7.8 (5.4-11.2)	61%[b]	**2i**	0.208 (0.185-0.233	10%[d]
2-MeO-Ph-	**9j**	9.9 (8.3-11.8)	192.8 (167.7-221.6)	**2j**	0.238 (0.202-0.281)	47%[e]
4-F-Ph-	**9k**	58.9 (49.6-69.9)	143.4 (119.1-172.6)	**2k**	0.044 (0.035-0.055)	1.61 (0.94-2.77)
4-CF$_3$-Ph-	**9l**	64.6 (56.5-73.9)	nd[c]	**2l**	2.7 (1.7-4.3)	59%[d]
4-pyridyl-	**9m**	2.1 (1.9-2.3)	242.4 (200.9-292.5)	**2m**	0.723 (0.656-0.797)	16%[d]
3-pyridyl-	**9n**	70.7 (57.9-86.2)	61%[b]	**2n**	0.565 (0.478-0.666)	18%[d]
3-thiophenyl-	**9o**	193.7 (148.1-253.4)	52%[b]	**2o**	0.022 (0.021-0.023)	13%[d]
2-thiophenyl	**9p**	63.2 (56.3-71.0)	225.8 (189.1-269.6)	**2p**	0.014 (0.012-0.016) 0.013*	0%[d]

		AChE	AChE		BChE	BChE
						(0.009-0.019)*
3-furyl-	**9q**	196.1	341.7	**2q**	0.083	12%[d]
		(176.1-218.3)	(294.1-397.1)		(0.072-0.095)	
3-pyrrolyl-	**9r**	15.3	115.9	**2r**	0.023	0.852
		(13.2-17.8)	(104.7-128.3)		(0.021-0.026)	(0.75-0.98)
1-naphthyl-	**9s**	2.8	341.7	**2s**	36.2	8%[e]
		(2.6-3.2)	(294.1-397.1)		(25.2-52.1)	
2-naphthyl-	**9t**	16.5	9%[c]	**2t**	0.374	5%[e]
		(14.7-18.5)			(0.315-0.444)	
2,6-dichloro-	**9u**	7.1	13.5	**2u**	0.531	33%[e]
		(6.6-7.8)	(11.2-16.4)		(0.464-0.608)	
$R^2 = Ph; R^1 =$						
i-Pr-	**10a**	55.8	253.0	**3a**	0.021	33%[d]
		(47.7-65.2)	(249.2-256.8)		(0.019-0.024)	
*n*Pr-	**10b**	22.8	279.3	**3b**	0.040	46%[d]
		(20.3-25.5)	(261.9-297.8)		(0.035-0.045)	
benzyl-	**10c**	14.8	16%[c]	**3c**	0.034	17%[e]
		(13.2-16.7)			(0.030-0.038)	
	15	98.1	20%[b]	**16**	1.8	22%[d]
		(82.4-116.8)			(1.2-2.8)	
				physostigmine	0.078	0.032
					(0.073-0.084)	(0.03-0.04)

[a]Experiments were performed in triplicate at AChE from human erythrocytes and BChE from equine serum. [b-e] % Inhibition at a concentration of [b]500 µM; [c]50 µM; [d]100 µM; [e]10 µM.

* Values determined at human BChE.

Enantiomeric Separation of Compound 2p

Enantiomeric resolution was performed on a Jasco HPLC system (pump PU-1580, gradient unit LG-980-02S, degasser DG-2080-53, autosampler AS-2055Plus, UV detector MD-2010Plus; Jasco Deutschland, Gross-Umstadt) equipped with an analytical Chiralpak® IA (Chiral Technologies Europe, 4.6 mm x 250 mm, 5 µm) column and coupled to a J-715 spectropolarimeter (Jasco Deutschland, Gross-Umstadt) for the online-CD measurements (scanning rate: 200 nm/min, bandwith: 5 nm, response time: 1 s). The enantiomeric resolutions were performed at room temperature with an isocratic solvent system of MTBE:MeOH (95:5 containing 0.1% $HNEt_2$) at 1 mL/min. Semi-preparative HPLC was performed on the same system with a semi-preparative Chiralpak® IA (Chiral Technologies Europe, 10 mm x 250 mm, 5 µm) column at 4.7 mL/min.

By HPLC on a chiral phase the racemic mixture (**Figure S1**) of compound **2p** was clearly resolved into its two enantiomers and analyzed chiroptically online, by HPLC-CD coupling (**Figures S2**, **S3** and **S4**). The two enantiomers proved to be configurationally unstable, undergoing rapid isomerization back to the racemic mixture during solvent evaporation.
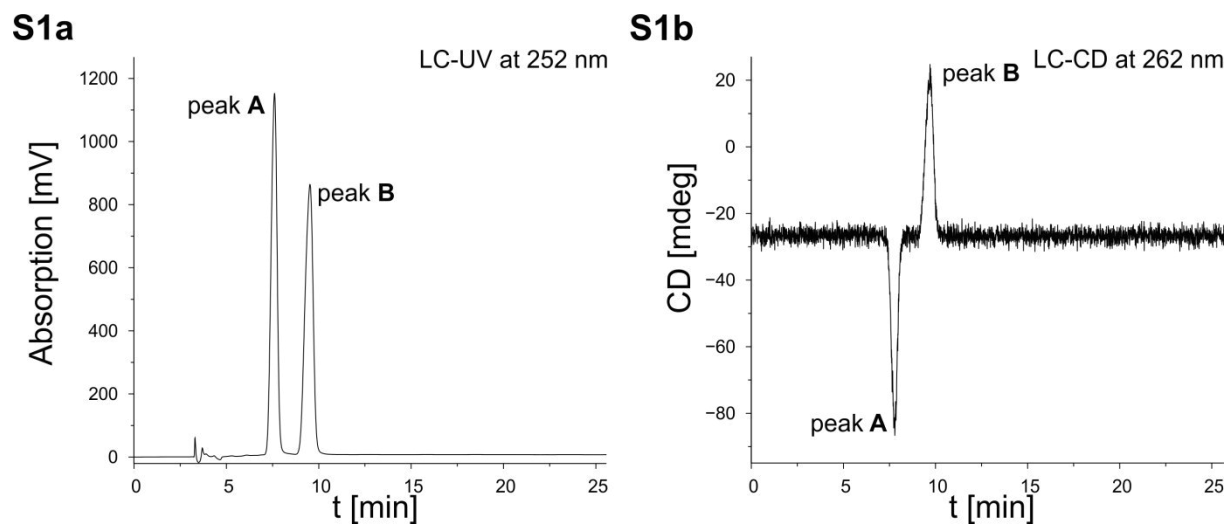

Figure S1. (S1a) HPLC-UVchromatogram of a racemic mixture of compound **2p** and (S1b) the corresponding LC-CD chromatogram.
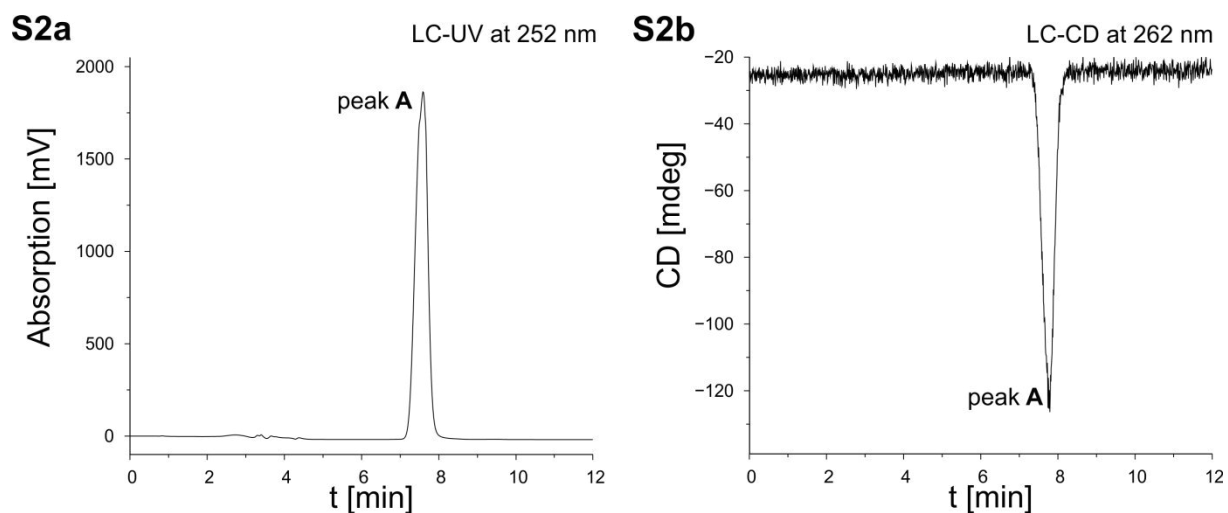
Figure S2. (S2a) HPLC-UV chromatogram of pure separated enantiomer **A** of compound **2p** and (S2b) its LC-CD chromatogram.
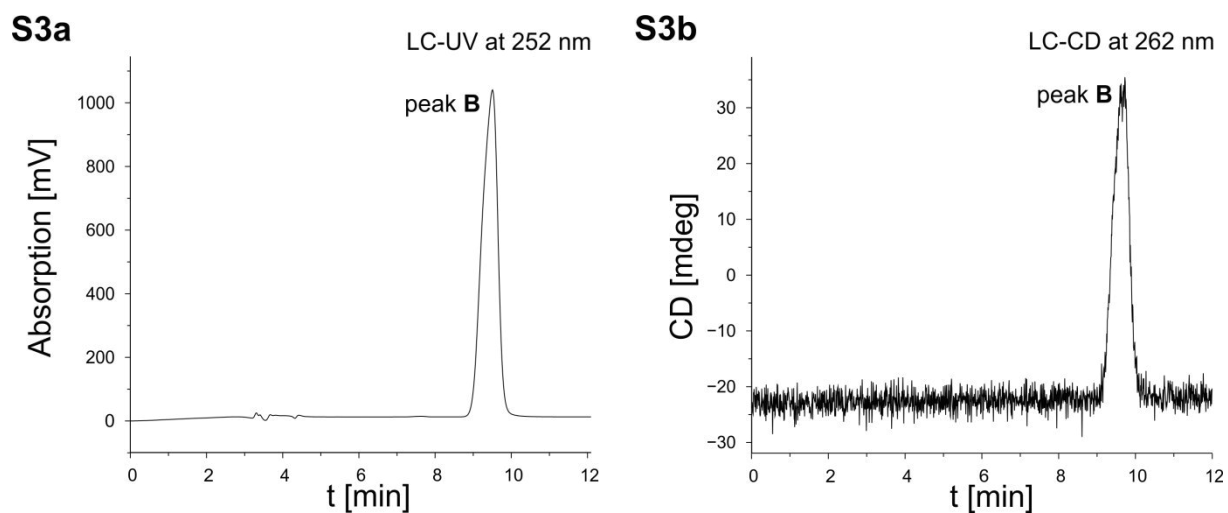

Figure S3. (S3a) HPLC-UV chromatogram of pure separated enantiomer **B** of compound **2p** and (S3b) its LC-CD chromatogram.
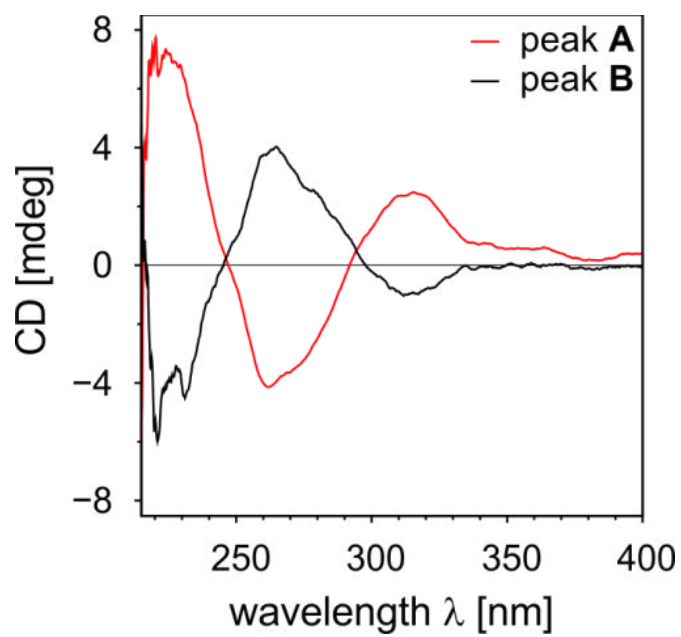
Figure S4. Overlay of the whole CD-spectra of the two separated enantiomers of compound **2p**.

Comparison of the Respective Enantiomeric Forms in the Binding Model

To investigate a possible common enantiomeric preference for binding to BChE by the compounds in the postulated binding mode, the intermolecular interaction scores (obtained from the scoring function DSX[1]) and the conformational strain energies were evaluated and compared. The strain energy ΔE was obtained as the difference between the force field energy of the binding conformation of the ligand and its minimum conformation in the unbound state. As the *n*-heptyl chain was irrelevant in the context of this analysis, it was replaced by a methyl group to restrict the number of conformers and simplify the conformational search. To obtain the global energy minimum of the free ligand, a stochastic search was performed in MOE[2] with the MMFF94s force field[3] and a dielectric constant of 4, using 10,000 iterations and optimization to an rms gradient of 0.01 kcal/(mol·Å). A local 10-step minimization of the binding poses was performed with the Truncated Newton method in MOE using the same force field (MMFF94s). In **Table S2** the obtained ΔE values are shown for both enantiomers along with their DSX scores.

Table S2. Comparison of DSX scores and strain energies for the investigated compounds in the postulated BChE binding mode.
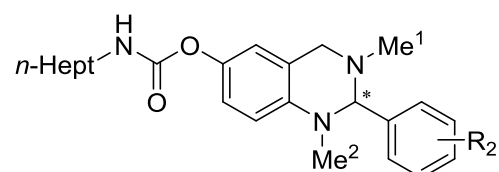
R	*R*-Enantiomer Me^1 "equatorial"		*S*-Enantiomer Me^1 "axial"	
	DSX Score	ΔE [kcal/mol]	DSX Score	ΔE [kcal/mol]
Phe (**2a**)	-125	4.38	-120	2.37
Thiophenyl (**2p**)	-110	4.34	-108	3.30
4-F-Ph- (**2k**)	-125	6.56	-121	2.91
3-Cl-Ph (**2c**)	-118	7.60	-101	1.78
4-OMe-Ph (**2h**)	-121	10.70	-127	1.42
3-OMe-Ph (**2i**)	-127	8.16	-100	3.60
4-CF$_3$-Ph (**2l**)	-113	13.13	-111	2.84
1-Naphthyl (**2s**)	-129	9.42	-110	6.34
Mean	-121	8.04	-112	3.07

On average, the strain energy of the *R*-enantiomers is 5 kcal/mol higher compared to the *S*-enantiomers. In general, this less favorable conformational energy is not counterbalanced by a sufficiently more favorable DSX score. Although a better score is shown by most of the *R*-

enantiomers, the average difference of 9 score units is not significant enough to assume a compensation by improved intermolecular interactions. In fact, as seen in redocking studies, docking poses of the ligands populating the same cluster (i.e., differing by less than 1.5 Å rmsd) show DSX scores varying over a range of 10 units. Accordingly, based on this model and the more favorable conformational energies, the *S*-enantiomers appear as the preferred forms for binding to BChE. However, contributions to activity from the *R*-enantiomers cannot be ruled out, in particular for those compounds where a small difference in the strain energy and a much more favorable (above average) DSX score is observed (i.e., compounds **2i** and **2s**).

Sequence Comparison

The pairwise sequence comparison was carried out using the progam Needle with the EBLOSUM62 matrix of EMBOSS v.6.3.1.[4] For comparison, the BChE and AChE sequences with the numbers D3DNN4 and P22303, respectively, were taken from the UniProt databank.[5]

```
#=======================================
# Aligned_sequences: 2
# 1:P22303_HUMAN
# 2:D3DNN4_HUMAN
# Matrix: EBLOSUM62
# Gap_penalty: 10.0
# Extend_penalty: 0.5
#
# Length: 650
# Identity:     316/650 (48.6%)
# Similarity:   428/650 (65.8%)
# Gaps:          43/650 ( 6.6%)
#=======================================

P22303_HUMAN    1 ---------------MRPPQCLLHTP------------SLASPLLLL-   20
                                 :.|...::.||            ::.|.:.::
D3DNN4_HUMAN    1 MSVQSNLQAGAAAASCISPKYYMIFTPCKLCHLCCRESEINMHSKVTIIC   50

P22303_HUMAN   21 ---LLW--LLGGGVGAEGREDAELLVTVRGGRLRGIRLKTPGGPVSAFLG   65
                     |.|  ||...:|....|| :::::.:.|::||:.|...||.|:||||
D3DNN4_HUMAN   51 IRFLFWFLLLCMLIGKSHTED-DIIIATKNGKVRGMNLTVFGGTVTAFLG   99

P22303_HUMAN   66 IPFAEPPMGPRRFLPPEPKQPWSGVVDATTFQSVCYQYVDTLYPGFEGTE  115
                   ||:|:||:|..||..|:....||.:.:||.:.:|.|.:|..:|||.|:|
D3DNN4_HUMAN  100 IPYAQPPLGRLRFKKPQSLTKWSDIWNATKYANSCCQNIDQSFPGFHGSE  149

P22303_HUMAN  116 MWNPNRELSEDCYLNVWTPYPRPTSPTPVLVWIYGGGFYSGASSLDVYD  165
                   |||||.:|||||||||||.|.|:|.:.| ||:||||||.:|.|||.|||
D3DNN4_HUMAN  150 MWNPNTDLSEDCYLNVWIPAPKPKNAT-VLIWIYGGGFQTGTSSLHVYD  198

P22303_HUMAN  166 GRFLVQAERTVLVSMNYRVGAFGFLALPGSREAPGNVGLLDQRLALQWVQ  215
                   |:||.:.||.::|||||||||.||||||||.|||||:.|||||:||.||:|||||||
D3DNN4_HUMAN  199 GKFLARVERVIVVSMNYRVGALGFLALPGNPEAPGNMGLFDQQLALQWVQ  248

P22303_HUMAN  216 ENVAAFGGDPTSVTLFGESAGAASVGMHLLSPPSRGLFHRAVLQSGAPNG  265
                   :|:|||||:|.|||||||||||||||.:||||.|..||.||:||||:.|.
D3DNN4_HUMAN  249 KNIAAFGGNPKSVTLFGESAGAASVSLHLLSPGSHSLFTRAILQSGSFNA  298

P22303_HUMAN  266 PWATVGMGEARRRATQLAHLVGCPPGGTGGNDTELVACLRTRPAQVLVNH  315
                   |||...:.|||.|...||.|.||    :..|:||::.|||.....|.:::.
D3DNN4_HUMAN  299 PWAVTSLYEARNRTLNLAKLTGC----SRENETEIIKCLRNKDPQEILLN  344

P22303_HUMAN  316 EWHVLPQESVFRFSFVPVVDGDFLSDTPEALINAGDFHGLQVLVGVVKDE  365
                   |..|:|..:.....:|.|.|.||||||:|.|:.|:..|.|...|:||||.|||
D3DNN4_HUMAN  345 EAFVVPYGTPLSVNFGPTVDGDFLTDMPDILLELGQFKKTQILVGVNKDE  394

P22303_HUMAN  366 GSYFLVYGAPGFSKDNESLISRAEFLAGVRVGVPQVSDLAAEAVVLHYTD  415
                   |:.||||||||||||.|:|:|.||..:.:..|.||:...|:::.||||
D3DNN4_HUMAN  395 GTAFLVYGAPGFSKDNNSIITRKEFQEGLKIFFPGVSEFGKESILFHYTD  444

P22303_HUMAN  416 WLHPEDPARLREALSDVVGDHNVVCPVAQLAGRLAAQGARVYAYVFEHRA  465
```
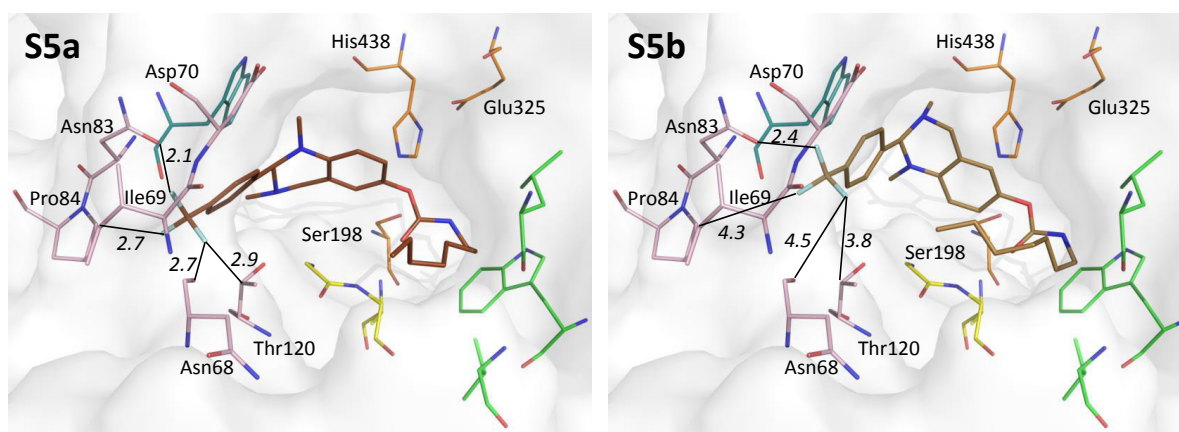
```
                       |:..:.|...||||.|||||:|.:||..:.:..:.:..|...:.|.||||:
D3DNN4_HUMAN 445 WVDDQRPENYREALGDVVGDYNFICPALEFTKKFSEWGNNAFFYYFEHRS 494

P22303_HUMAN 466 STLSWPLWMGVPHGYEIEFIFGIPLDPSRNYTAEEKIFAQRLMRYWANFA 515
                       |.|.||.||||.||||||||:||:||:...|||..|:|.:::.::.|||||
D3DNN4_HUMAN 495 SKLPWPEWMGVMHGYEIEFVFGLPLERRDNYTKAEEILSRSIVKRWANFA 544

P22303_HUMAN 516 RTGDPNEPRDPKAPQWPPYTAGAQQYVSLDLRPLEVRRGLRAQACAFWNR 565
                       :.|:||||.:: .:..||.:.:.:|:|::|:......:...||||.|.||..
D3DNN4_HUMAN 545 KYGNPNETQN-NSTSWPVFKSTEQKYLTLNTESTRIMTKLRAQQCRFWTS 593

P22303_HUMAN 566 FLPKLLSATDTLDEAERQWKAEFHRWSSYMVHWKNQFDHY-SKQDRCSDL 614
                       |.||:|..|..:||||.:|||.||||||::||:.||||||:.| ||::.|..|
D3DNN4_HUMAN 594 FFPKVLEMTGNIDEAEWEWKAGFHRWNNYMMDWKNQFNDYTSKKESCVGL 643
```

Binding Mode of 2l

Figure S5. (S5a) Representation of the binding mode of **2l** (dark brown)in the *R*-enantiomeric form when forced to an analogous binding mode as the most active compound **2p**. (S5b) Representation of the binding mode for the *S*-enantiomer of **2l** (light brown). More clashes with distances below 3 Å are seen between the CF$_3$ group and the protein of the *R*-enantiomer in this rigid binding mode model. This implies that the actual binding mode especially for the *R*-enantiomer of **2l** is likely to differ from the common binding mode suggested for the other compounds. The contribution of the *R*-enantiomer of **2l** to the binding might be very low, whereas for the other compounds the *R*-enantiomeric form of the ligand might have a higher contribution to the activity due to suitable distances from ligand atoms to the protein. Residues of the acyl pocket are shown in green, the oxyanion hole in yellow, the CAS in orange, the choline binding site in turquoise, and parts of the side cavity in pink. Distances (black lines) are shown in italic numbers and are given in Å.

Additional References

[1] Neudert, G.; Klebe G. DSX: A Knowledge-Based Scoring Function for the Assessment of Protein-Ligand Complexes. *J. Chem. Inf. Model.* **2011**, *51*, 2731-2745.

[2] Molecular Operating Environment (MOE), 2013.0801 and 2014.0901; Chemical Computing Group,1010 Sherbooke St. West, Suite #910, Montreal, QC, Canada, H3A 2R7, **2011**.

[3] Halgren, T. A. Merck Molecular Force Field. I. Basis, Form, Scope, Parameterization, and Performance of MMFF94. *J. Comp. Chem.* **1996**, *17*, 490-510.

[4] Rice, P.; Longden, I.; Bleasby, A. EMBOSS: the European Molecular Biology Open Software Suite. *Trends Genet.* **2000**, *16*, 276-277.

[5] The UniProtConsortium. Activities at the Universal Protein Resource (UniProt).*Nucleic Acids Res.* **2014**, *42*, D191-D198.

Appendix 3

Investigation into Selective Debenzylation and Ring Cleavage of Quinazoline Based Heterocycles.

Investigation into selective debenzylation and ring cleavage of quinazoline based heterocycles

Edgar Sawatzky, Jerzy Bukowczan, Michael Decker *

Institut für Pharmazie und Lebensmittelchemie, Universität Würzburg, Am Hubland, 97074 Würzburg, Germany

ARTICLE INFO

ABSTRACT

The selective cleavage of different benzyl bonds within tetrahydroquinazoline and dihydroquinazolinone derived structures can be achieved by the usage of different reduction and debenzylation conditions thereby providing selective removal of O-benzyl protection groups as well as the cleavage of the ring structure within the quinazoline and quinazolinone systems.

© 2014 Elsevier Ltd. All rights reserved.

Over the last decades compounds bearing a quinazoline based structure have been in the focus of different research areas first due to their occurrence as a common core structure in several natural products[1,2] like the alkaloids rutaecarpine **1**, evodiamine **2**, dehydroevodiamine **3**, mackinazolinone **4** and vasicinone **5** (Fig. 1A). And as a result of its promising pharmacological effects in different medicinal applications, the quinazoline core has become to a privileged structure in medicinal chemistry.[3–12]

Therefore, many groups used this nitrogen bridgehead core structure as a key element in the development of numerous experimental therapeutics and prospective drug candidates, also including chemical modifications of the above described natural compounds. Such synthetic compounds are developed for diverse therapeutic applications, such as anticonvulsant agents,[13] in the treatment of cancer,[14,15] as cholinesterase inhibitors for Alzheimer's disease treatment,[16–19] vasodilators,[20] anti-inflammatory agents,[21] as a retrograde transport inhibitor for Shiga toxin treatment[22] or with regard to their effects on different receptors like the serotonin receptor 7 (5-HT$_7$ receptor),[23] the thyroid stimulating hormone (TSH) receptor[24] or the histamine H$_3$ receptor.[25,26] A few examples of recently published compounds bearing quinazoline derived moieties are presented in Figure 1B.

Herein different ways for selective heteroatom (N and O)-carbon-bond cleavage of the different benzyl positions within the tetrahydroquinazoline structure **9** and its precursor dihydroquinazolinone **10** will be described. Both compounds bear a quinazoline derived
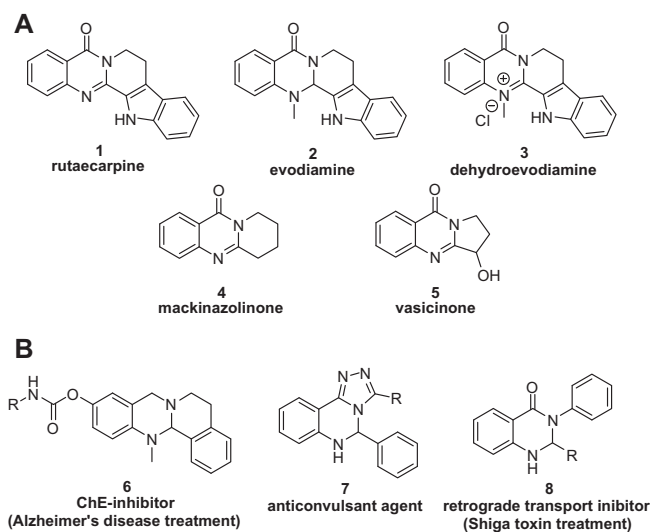

Figure 1. (A) Molecules bearing a quinazoline derived core: (A) The alkaloids rutaecarpine **1**, evodiamine **2**, dehydroevodiamine **3**, mackinazolinone **4** and vasicinone **5**. (B) Examples of some synthetic experimental therapeutics with related chemical structures.[13,16,22]

core structure like the above mentioned natural products and experimental therapeutics. These compounds were used as intermediates for the synthesis of selective butyrylcholinesterase inhibitors[16] and dual-acting AChE inhibitors/hH$_3$ antagonists.[26] In these structures

---

* Corresponding author. Tel.: +49 931 31 89676; fax: +49 931 31 85494.
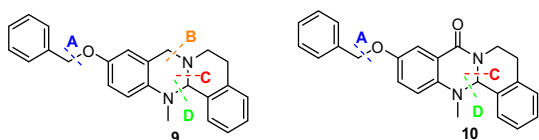 E-mail address: michael.decker@uni-wuerzburg.de (M. Decker).

Figure 2. Illustration of benzyl bonds of tetrahydroquinazoline **9** and dihydroquinazolinone **10** that might be cleaved under debenzylation conditions.

four different benzyl-bonds can be distinguished; **A**: the *O*-benzyl-protection group, **B**: the benzylamine *N–C* bond (only in **9**), **C**: the central *N–C* bond and **D**: the anilinic *N–C* bond (Fig. 2).

This letter shall provide a systematic overview on conditions suitable to selectively cleave and reduce the respective bonds where possible, for example, to induce more flexibility into similar biologically active compounds, and to prevent undesired cleavage reactions during debenzylation and reduction chemistry.

The starting point for this investigation was the synthesis of tetrahydroquinazoline **9** in four steps as described in Scheme 1. Hydroxyl anthranilic acid **11** was treated with triphosgene to yield hydroxy isatoic anhydride **12** quantitatively in high purity, followed by the selective *N*-methylation to yield compound **13**.[16] Compound **13** was then first *O*-benzyl protected and subsequently fused to the tetracyclic dihydroquinazolinone **14** in a two-step one-pot-synthesis with a yield of 53%. Benzylation and ring-fusion can also be performed in two separate steps, but this led to much lower yields. Ring fusion is also possible without protection of the phenol group, but only with a yield of 23%.[16] Tetrahydroquinazoline **9** was synthesized by the reduction of **10** with LiAlH$_4$ in 80% yield.

The described synthetic procedure can of course also be used for other substitution patterns in the aromatic systems of the anthranilic acid derivative as well as for the dihydroisoquinoline compound providing the synthetic basis for performing structure–activity relationship (SAR) investigations in medicinal chemistry approaches.[16,17]

The standard strategy for *O*-debenzylation (cleavage of bond **A**) of dihydroquinazolinone **10** and tetrahydroquinazoline **9** applies the usage of Pd/C and hydrogen in methanol. For compound **10** this procedure led to the desired cleavage of bond **A** to yield the phenolic compound **14** quantitatively (Scheme 2 and Table 1, path *a*). Interestingly, in the case of tetrahydroquinazoline **9**, under these conditions bond **A** was cleaved but additionally also aniline bond **D** was reduced yielding compound **15** in moderate yield (44%). As these conditions were not applicable for the selective *O*-debenzylation of compound **9**, hydrogenation with Pd/C as the catalyst was performed applying different solvent systems. Using EtOH and
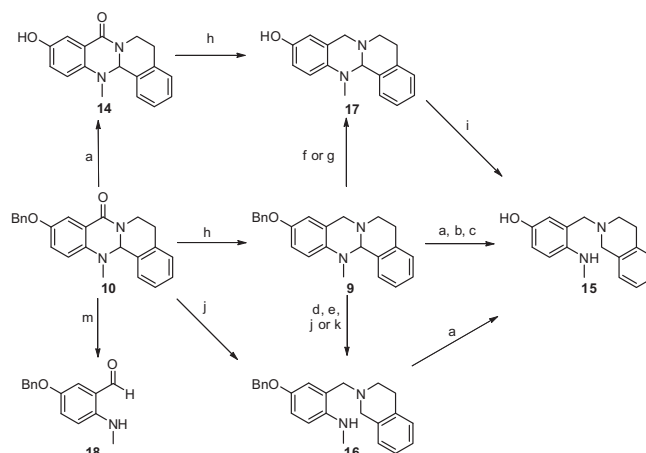

Scheme 2. Reaction pathways during debenzylation and reduction reactions of tetrahydroquinazoline **9** and dihydroquinazolinone **10** towards different products.

Table 1
Reaction conditions for debenzylation strategies via Scheme 2

Path	Starting-material	Product	Conditions	Yield (%)
a	**10**	**14**	H$_2$, Pd/C, methanol, 50 °C	100
a	**16**	**15**	H$_2$, Pd/C, methanol, 50 °C	49
a	**9**	**15**	H$_2$, Pd/C, methanol, 50 °C	44
b	**9**	**15**	H$_2$, Pd/C, ethanol, 50 °C	37
c	**9**	**15**	H$_2$, Pd/C, acetic acid, 50 °C	14
d	**9**	**16**	H$_2$, Pd/C, THF, rt	93
e	**9**	**16**	H$_2$, PtO$_2$, methanol, 50 °C	80
f	**9**	**17**	AlCl$_3$, PhNMe$_2$ CH$_2$Cl$_2$, rt	65
g	**9**	**17**	concd HCl, reflux	80
h	**14**	**17**	LiAlH$_4$, THF, reflux	98
h	**10**	**9**	LiAlH$_4$, THF, reflux	93
i	**17**	**15**	H$_2$, Pd/C, methanol, rt	28
j	**9**	**16**	BH$_3$·THF, THF, reflux	42
j	**10**	**16**	BH$_3$·THF, THF, reflux	47
k	**10**	—	NaBH$_4$, ethanol, reflux	—
k	**9**	**16**	NaBH$_4$, ethanol, reflux	60
l	**10**	—	NaCNBH$_3$, acetic acid, 50 °C	—
m	**10**	**18**	LiAlH$_4$, THF, rt	19

AcOH resulted into the same reaction product as with MeOH (path *b* and *c*). Only the usage of dry THF as the solvent surprisingly led to the selective hydrogenation of the anilinic *N–C*-bond **D** to aniline **16** (path *d*) in excellent yield without affecting the *O*-benzyl bond **A**. A different catalyst for hydrogenation with H$_2$ can also result in different products, but even the usage of PtO$_2$ in MeOH just led to
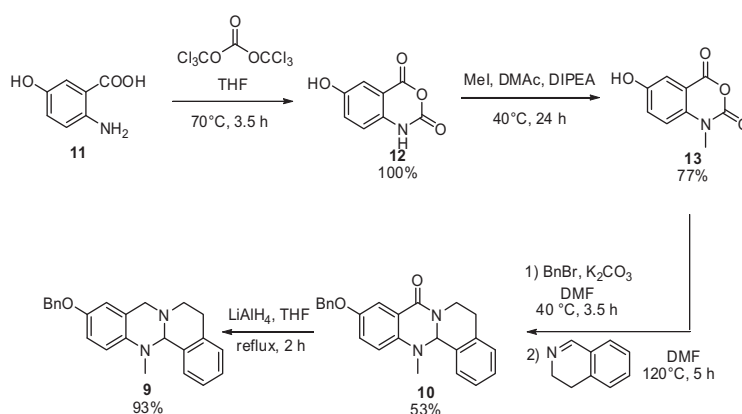
Scheme 1. Synthesis of dihydroquinazolinone **9** and tetrahydroquinazoline **10**.

cleavage of **D** yielding aniline **16** (80%) (path *e*). Cleavage of **A** in the *O*-benzyl protected tetrahydroquinazoline **9** towards the unprotected tetrahydroquinazoline **17** was finally achieved by two different reactions. The conditions of the first one have been reported by Akiyama et al.[27] and used a combined system of the Lewis acid AlCl$_3$ and the Lewis base *N,N*-dimethylaniline in methylene chloride at room temperature and yielded 65% of product **17** (path *f*). The second reaction applied harsher reaction conditions, whereby usage of concentrated HCl under reflux conditions for 16 h gave **17** in a yield of 80% (path *g*). Although both reactions led to the desired product, both have the disadvantage that column chromatography was necessary for purification. Therefore, the synthesis of tetrahydroquinazoline **17** was more easily achieved via reduction of **14** by LiAlH$_4$ (path *h*) in an excellent yield of 98% and without the necessity of column chromatography purification. Altering the sequence of LiAlH$_4$ reduction and debenzylation with hydrogen of **10** (changing pathway *a* followed by *h* into pathway *h* followed by *a*) yields two different products (**15** and **17**). It was further demonstrated that the usage of Pd/C and H$_2$ in MeOH selectively cleaved bond **D** in the case of tetrahydroquinazoline **17** (path *i*) and cleaved bond **A** in the case of aniline **16**, both ultimately leading to compound **15** in low yields. The low yields can be explained by the low stability of **15**, as its *p*-amino phenol structure rapidly undergoes decomposition under oxygen exposure and during heating. GC–MS studies show that bond **D** is also cleaved thereby leading to complete decomposition of the ring system and yielding isoquinoline and dehydroisoquinoline as well as *p*-aminomethyl phenols bearing a methyl group adjacent to the *N*-methyl amino one.

Earlier investigations had already shown how to selectively open the central *N*–*C* bond **C** of quinazolinones **19** and the related structure **21** using BH$_3$·THF to yield medium sized heterocyclic ring systems **20** and **22**[28–30] (Scheme 3).

Therefore, borane reduction was applied for the reductive removal of the amide oxygen and cleavage of the central *N*–*C* bond **C** in dihydroquinazolinone **10** in one step. Interestingly, the usage of BH$_3$·THF did not lead to the expected cleavage of the central *C*–*N* bond **C**, but rather reduced the amide bond and cleaved the anilinic bond **D** to give the ring opened compound **16** in 47% yield (path *j*). As it was expected that milder reducing agents were necessary to break the anilinic bond **D**, quinazolinone **10** was treated with NaBH$_4$ (path *k*) and NaCNBH$_3$ (path *l*), respectively, but in both cases no reaction took place. Besides, for tetrahyroquinazoline **9** cleavage of the anilinic bond **D** to compound **16** was achieved by treatment with BH$_3$·THF in 42% yield (path *j*). Alternatively compound **16** was obtained from **9** using NaBH$_4$ in 60% yield (path *k*). From these results it can be expected that cleavage of the central *C*–*N* bond **C** with BH$_3$·THF is only possible in quinazolinones (Scheme 3) as described in the literature and not in dihydroquinazolinones like compound **10**.

Besides this, the cleavage of the central *C*–*N* bond **C** with LiAlH$_4$ was also applied on tetrahydroquinazoline **10**. Since compound **10** was smoothly reduced to compound **9** by excess of LiAlH$_4$ at high

temperature as described above (path *h*), the product formation at lower temperature was subsequently investigated. Interestingly, reduction towards tetrahydroquinazoline **9** starting from **10** was completely suppressed when only 1 equiv of LiAlH$_4$ was used at room temperature. In this case, besides starting material **10** (63%), only aldehyde **18** (19%) was isolated (path *m*).

In conclusion, first the syntheses of the quinazolin derived structures tetrahydroquinazoline **9** and dihydroquinazolinone **10** were achieved. Both compounds bear different *N*- and *O*-benzyl bonds which were selectively cleaved under different debenzylation and reduction conditions. Thereby the best conditions for the selective cleavage of the *O*-benzyl bond **A** in dihydroquinazolinone **10** was the usage of Pd/C with hydrogen in methanol (path *a*, 100% yield) and for tetrahydroquinazoline **9** the usage of concentrated HCl-solution (path *g*, 80% yield). The cleavage of the anilinic bond **D** was in the case of **10** achieved via reduction with BH$_3$·THF (path *j*, 47%) and in the case of **9** using Pd/C and hydrogen in dry THF (path *d*, 93% yield). Furthermore, it is remarkable, that applying 1 equiv of LiAlH$_4$ on dihydro-quinazolinone **10** led to the cleavage of the amide bond and the benzylamine *N*–*C* bond **C** in one step (path *m*, 19% yield) therefore leading to aldehyde **18**.

Acknowledgements

Supplementary data

Supplementary data (experimental procedures and spectral data) associated with this article can be found, in the online version, at http://dx.doi.org/10.1016/j.tetlet.2014.03.109.

References and notes

1. Lee, S. H.; Son, J.-K.; Jeong, B. S.; Jeong, T.-C.; Chang, H. W.; Lee, E.-S.; Jahng, Y. *Molecules* **2008**, *13*, 272–300.
2. Mhaske, S. B.; Argade, N. P. *Tetrahedron* **2006**, *62*, 9787–9826.
3. Wang, G.-J.; Wu, X.-C.; Chen, C.-F.; Lin, L.-C.; Huang, Y.-T.; Shan, J.; Pang, P. K. T. *J. Pharmacol. Exp. Ther.* **1998**, *289*, 1237–1244.
4. Wei, J.; Ching, L.-C.; Zhao, J.-F.; Shyue, S.-K.; Lee, H.-F.; Kou, Y. R.; Lee, T.-S. *Acta Phys.* **2013**, *207*, 299–307.
5. Haji, A.; Momoser, Y.; Takeda, Y.; Nakanishi, S. *J. Nat. Prod.* **1994**, *57*, 387–389.
6. Kan, S.-F.; Huang, W. J.; Lin, L.-C.; Wang, P. S. *Int. J. Cancer* **2004**, *110*, 641–651.
7. Moon, T. C.; Murakami, M.; Kudo, I.; Son, K. H.; Kim, H. P.; Kang, S. S.; Chang, H. W. *Inflamm. Res.* **1999**, *48*, 621–625.
8. Jia, S.; Hu, C. *Molecules* **2010**, *15*, 1873–1881.
9. Shyu, K.-G.; Lin, S.; Lee, C.-C.; Chen, E.; Lin, L.-C.; Wang, B.-W.; Tsai, S.-C. *Life Sci.* **2006**, *78*, 2234–2243.
10. Yang, J.; Cai, X.; Lu, W.; Hub, C.; Xu, X.; Yu, Q.; Cao, P. *Cancer Lett.* **2012**, *328*, 243–251.
11. Don, M.-J.; Lewis, D. F. V.; Wang, S.-Y.; Tsaia, M.-W. *Bioorg. Med. Chem. Lett.* **2013**, *13*, 2535–2538.
12. Khan, I.; Ibrar, A.; Abbas, N.; Saeed, A. *Eur. J. Med. Chem.* **2014**, *76*, 193–244.
13. Zheng, Y.; Bian, M.; Deng, X.-Q.; Wang, S.-B.; Quan, Z.-S. *Arch. Pharm. Chem. Life Sci.* **2013**, *346*, 119–126.
14. Cao, S.-L.; Feng, Y.-P.; Jiang, Y.-Y.; Liu, S.-Y.; Ding, G.-Y.; Li, R.-T. *Bioorg. Med. Chem. Lett.* **2005**, *15*, 1915–1917.
15. Dong, G.; Wang, S.; Miao, Z.; Yao, J.; Zhang, Y.; Guo, Z.; Zhang, W.; Sheng, C. *J. Med. Chem.* **2012**, *55*, 7593–7613.
16. Darras, F. H.; Kling, B.; Heilmann, J.; Decker, M. *ACS Med. Chem. Lett.* **2012**, *3*, 914–919.
17. Decker, M.; Kraus, B.; Heilmann, J. *Bioorg. Med. Chem.* **2008**, *16*, 4252–4261.
18. Wang, B.; Mai, Y.-C.; Li, Y.; Hou, J.-Q.; Huang, S.-L.; Ou, T.-M.; Tan, J.-H.; An, L.-K.; Li, D.; Gu, L.-Q.; Huang, Z.-S. *Eur. J. Med. Chem.* **2010**, *45*, 1415–1423.
19. Chen, X.; Tikhonova, I. G.; Decker, M. *Bioorg. Med. Chem.* **2011**, *19*, 1222–1235.
20. Chen, Z.; Hua, G.; Li, D.; Chen, J.; Li, Y.; Zhou, H.; Xie, Y. *Bioorg. Med. Chem.* **2009**, *17*, 2351–2359.
21. Bubenyák, M.; Noszál, B.; Kóczián, K.; Takács, M.; Béni, S.; Hermecz, I.; Kökösi, J. *Tetrahedron Lett.* **2008**, *49*, 5711–5713.
22. Noel, R.; Gupta, N.; Pons, V.; Goudet, A.; Garcia-Castillo, M. D.; Michau, A.; Martinez, J.; Buisson, D.-A.; Johannes, L.; Gillet, D.; Barbier, J.; Cintrat, J.-C. *J. Med. Chem.* **2013**, *56*, 3404–3413.
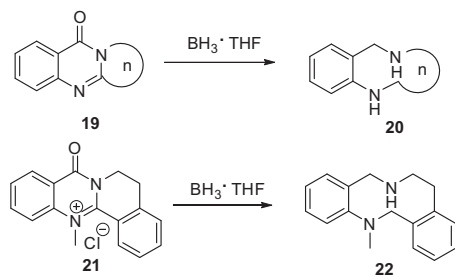
Scheme 3. Selective cleavage of bond **C**.[28–30]

23. Na, Y. H.; Hong, S. H.; Lee, J. H.; Park, W.-K.; Baek, D.-J.; Koh, H. Y.; Cho, Y. S.; Chooa, H.; Paea, A. N. *Bioorg. Med. Chem.* **2008**, *16*, 2570–2578.
24. Englund, E. E.; Neumann, S.; Eliseeva, E.; McCoy, J. G.; Titus, S.; Zheng, W.; Southall, N.; Shinn, P.; Leister, W.; Thomas, C. J.; Inglese, J.; Austin, C. P.; Gershengorn, M. C.; Huang, W. *Med. Chem. Commun.* **2011**, *2*, 1016–1020.
25. Nagase, T.; Mizutani, T.; Ishikawa, S.; Sekino, E.; Sasaki, T.; Fujimura, T.; Ito, S.; Mitobe, Y.; Miyamoto, Y.; Yoshimoto, R.; Tanaka, T.; Ishihara, A.; Takenaga, N.; Tokita, S.; Fukami, T.; Sato, N. *J. Med. Chem.* **2008**, *51*, 4780–4789.
26. Darras, F. H.; Pockes, S.; Huang, G.; Wehle, S.; Strasser, A.; Wittmann, H.-J.; Nimczick, M.; Sotriffer, C. A.; Decker, M. *ACS Chem. Neurosci.* **2014**, *5*, 225–242.
27. Akiyama, T.; Hirofuji, H.; Ozaki, S. *Tetrahedron Lett.* **1991**, *32*, 1321–1324.
28. Decker, M.; Krauth, F.; Lehmann, J. *Bioorg. Med. Chem.* **2006**, *14*, 1966–1977.
29. Wasserman, H. H.; Matsuyama, H. *J. Am. Chem. Soc.* **1981**, *103*, 461–462.
30. Takeuchi, H.; Matsushita, Y.; Eguchi, S. *J. Org. Chem.* **1991**, *56*, 1535–1537.

Investigation into selective debenzylation and ring cleavage of quinazoline based heterocycles

Edgar Sawatzky, Jerzy Bukowcan,and Michael Decker*

Institut für Pharmazie und Lebensmittelchemie, Universität Würzburg, Am Hubland, 97074 Würzburg, Germany

Contents:

General methods:

Common reagents and solvents were obtained from commercial suppliers and used without further purification. Tetrahydrofuran (THF) was distilled from sodium/benzophenone under argon atmosphere.

Reaction progress was monitored using analytical thin layer chromatography (TLC) on precoated silica gel GF_{254} plates(Macherey-Nagel GmbH & Co. KG) and the spots were detected under UV light (254 nm) or through staining with iodine.

Nuclear magnetic resonance spectra were performed with a Bruker AV-400 NMR instrument (Bruker, Karlsruhe, Germany) in DMSO-d_6 or $CDCl_3$. Chemical shifts are expressed in ppm relative to $CDCl_3$ or DMSO-D_6 (7.26/2.50 and 77.16/39.52 ppm for ^{1}H and ^{13}C NMR, respectively).

ESI mass spectral data were acquired on an Agilent 1100 series LC/MSD ion trap mass spectrometer.

Melting points were determined in open capillaries on a Barloworld Scientific Stuart® melting point (SMP3).

IR spectra were measured on a Jasco FT-IR-6100 spectrometer (Jasco, Gross-Umstadt, Germany) with a diamond-ATR unit. The intensity of the absorption is labeled as s = strong, m = medium, w = weak and br = broad. Only the highest wave numbers $\tilde{\nu}$ are presented.

Experimental procedures

Synthesis of tetrahydroquinazoline 9 and dihydroquinazolinone 10

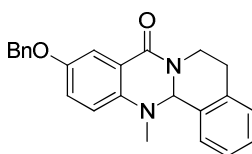*6-Hydroxy-1*H-*benzo[*d*][1,3]oxazine-2,4-dione,***12***:*
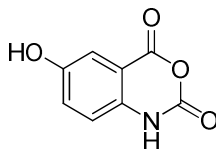
A suspension of 2-amino-5-hydroxy benzoic acid (4 g, 26.1 mmol, 1 eq.) in dry THF (40 mL) was treated with triphosgene (2.94 g, 9.96 mmol, 0.38 eq.). The suspension was heated to 70°C for 3.5 h. Then the mixture was allowed to reach room temperature and the solvent was evaporated under reduced pressure. The residue was suspended in cyclohexane (80 mL) and the precipitate was filtered off to yield 6-hydroxy-1*H*-benzo[*d*][1,3]oxazine-2,4-dione **12**(4.68 g, 100%) as grey solid;**^{1}H-NMR** (400 MHz, DMSO-d_6): δ = 11.49 (s, NH), 9.85 (s, OH), 7.24-7.18 (m, 2H, arom.), 7.05-7.02 (m, 1H, arom.) ppm. Analytical data in accordance with literature data.[1]

*6-Hydroxy-1-methyl-1*H-*benzo[*d*][1,3]oxazine-2,4-dione* **13***:*
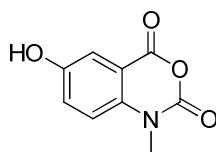
A suspension of 6-hydroxy-1*H*-benzo[*d*][1,3]oxazine-2,4-dione **12** (5.65 g, 31.6 mmol, 1 eq.) in dimethylacetamide (40 mL) was treated with ethyl *N,N*-diisopropylamine (10.7 mL, 63 mmol, 2 eq.) followed by the addition of methyl iodide (7.9 mL, 126 mmol, 4 eq.) after 15 min. The reaction mixture was stirred for 24 h at 40°C. Then ice cold water (100 mL) was added and the mixture was stirred for further 30 min. The precipitated solid was filtered off and then washed with water (30 mL) and cyclohexane (2x 30 mL). After drying in vacuo, 6-hydroxy-1-methyl-1*H*-benzo[*d*][1,3]oxazine-2,4-dione **13**(4.7 g, 77%) was isolated as brown solid;[**1**]**H-NMR** (400 MHz, DMSO-d$_6$): δ = 9.98 (s, OH), 7.35-7.26 (m, 3H, arom.), 3.43 (s, 3H, C*H*$_3$) ppm. Analytical data in accordance with literature data.[1]
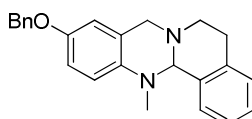
*10-(Benzyloxy)-13-methyl-13,13a-dihydro-5*H-*isoquinolino[1,2-*b*]quinazolin-8(6*H*)-one* **10***:*

6-Hydroxy-1-methyl-1*H*-benzo[*d*][1,3]oxazine-2,4-dione **13**(1.6 g, 8.3 mmol, 1 eq.) was dissolved in dry DMF (20 mL) and treated with potassium carbonate (1.2 g, 8.7 mmol, 1.05 eq.) and benzyl bromide (1.97 mL, 16.6 mmol, 2 eq.). The reaction mixture was stirred for 8 h at 40°C. Then the mixture was allowed to reach room temperature and was filtered off. After treating the filtrate with 3,4-dihydroisoquinoline (1.6 g, 12.4 mmol, 1.5 eq.) the reaction mixture was heated to 120°C for 16 h. The mixture was allowed to reach room temperature, followed by the addition of a NaOH-solution (2 M, 50 mL). After 15 min the aqueous phase was extracted with ethyl acetate (3 x 100 mL) and the combined organic layers were washed with brine (50 mL), dried over Na$_2$SO$_4$ and finally the solvent was removed under reduced pressure. The crude residue was purified by column chromatography (PE:EA = 3:1) to obtain 10-(benzyloxy)-13-methyl-13,13a-dihydro-5*H*-isoquinolino[1,2-*b*]quinazolin-8(6*H*)-one **10** (1.6 g, 53%) as yellow oil;[**1**]**H-NMR** (400 MHz, DMSO-d$_6$): δ = 7.48-7.43 (m, 2H, arom.), 7.43-7.37 (m, 3H, arom.), 7.36-7.24 (m, 5H, arom.), 7.19 (dd, *J* = 8.8, 3.0 Hz, 1H, arom.), 7.12 (d, *J* = 8.8 Hz, 1H, arom.), 5.83 (s, 1H, C*H*), 5.11 (s, 2H, OC*H*$_2$), 4.43 (ddd, *J* = 12.8, 5.6, 3.4 Hz, 1H, NC*H*$_2$CH$_2$), 3.28-3.16 (m, 1H, , NC*H*$_2$CH$_2$), 2.95 (ddd, *J* = 15.9, 7.9, 4.9 Hz, 1H, ArC*H*$_2$CH$_2$), 2.85 (ddd, *J* = 16.0, 4.1, 4.1 Hz, 1H, ArC*H*$_2$CH$_2$), 2.58 (s, 3H, C*H*$_3$) ppm; [**13**]**C-NMR** (101 MHz, DMSO-d$_6$): δ =162.87 (CO), 153.19 (arom.), 143.96 (arom.), 137.08 (arom.), 136.77 (arom.), 133.64 (arom.),

128.60 (arom.), 128.39 (2C, arom.), 127.96 (arom.), 127.74 (arom.), 127.51 (2C, arom.), 126.80 (arom.), 126.48 (arom.), 121.62 (arom.), 121.44 (arom.), 121.31 (arom.), 111.90 (arom.), 71.55 (CH), 69.58 (OCH$_2$), 39.42 (NCH$_2$CH$_2$), 36.73 (CH$_3$), 27.28 (CCH$_2$CH$_2$) ppm; **ESI-MS**: m/z = 371.7 [M+H]$^+$, calc. 370.2; **IR** (ATR): $\tilde{v}$ = 1650 (s, v-C=O), 1609 (m), 1489 (s), 1440 (s), 1416 (m), 1262 (m), 1223 (m), 1018 (m), 739 (m), 696 (m) cm^{-1}.

*10-(Benzyloxy)-13-methyl-6,8,13,13a-tetrahydro-5*H-*isoquinolino[1,2-*b]*quinazoline* ***9***: (path *h*)

10-(Benzyloxy)-13-methyl-13,13a-dihydro-5*H*-isoquinolino[1,2-*b*]quinazolin-8(6*H*)-one **10** (620 mg, 1.68 mmol, 1 eq.) was dissolved in dry THF (5 mL) at 0°C under argon. Then LiAlH$_4$ (198 mg, 5.03 mmol, 3 eq.) was added carefully. The reaction mixture was allowed to reach room temperature and was then refluxed for 2 h. The reaction mixture was poured into ice water (30 mL) and basified with a 2 M NaOH-solution. The product was then extracted with ethyl acetate (3 x 50 mL). The combined organic layers were washed with brine (30 mL) and dried over Na$_2$SO$_4$. After removal of the solvent under reduced pressure, 10-(benzyloxy)-13-methyl-6,8,13,13a-tetrahydro-5*H*-isoquinolino[1,2-*b*]quinazoline **9** (555 mg, 93%) was isolated as yellow solid; **m.p** = 103-108°C; **¹H-NMR** (400 MHz, CDCl$_3$): δ = 7.41-7.38 (m, 1H, arom.), 7.37-7.35 (m, 2H, arom.), 7.33-7.28 (m, 2H, arom.), 7.27-7.20 (m, 1H, arom.), 7.17-7.11 (m, 2H, arom.), 7.09-7.04 (m, 1H, arom.), 6.87 (d, J = 8.8 Hz, 1H, arom.), 6.76 (dd, J = 8.8, 2.9 Hz, 1H, arom.), 6.57 (d, J = 2.9 Hz, 1H, arom.), 4.94 (s, 2H, OCH_2$), 4.66 (s, 1H, C$H$), 3.86 (d, J = 15.3 Hz, 1H, ArCH_2N), 3.80 (d, J = 15.2 Hz, 1H, ArCH_2N), 3.17 (ddd, J = 11.0, 5.1, 3.6 Hz, 1H, NCH_2CH$_2$), 3.05 (ddd, J = 15.5, 10.0, 5.2 Hz, 1H, ArCH_2CH$_2$), 2.69 (ddd, J = 16.0, 3.8, 3.8 Hz, 1H, ArCH_2CH$_2$), 2.64-2.56 (m, 1H, NCH_2CH$_2$), 2.43 (s, 3H, CH_3$) ppm; **¹³C-NMR** (101 MHz, CDCl$_3$): δ = 153.35 (arom.), 143.07 (arom.), 137.41 (arom.), 136.27 (arom.), 134.21 (arom.), 128.62 (arom.), 128.55 (arom., 2C), 128.49 (arom.), 127.85 (arom.), 127.48 (arom., 2C), 127.18 (arom.), 126.78 (arom.), 125.99 (arom.), 122.54 (arom.), 114.35 (arom.), 112.54 (arom.), 77.35 (CH), 70.48 (OCH$_2$), 56.97 (ArCH$_2$N), 48.81 (NCH$_2$CH$_2$), 38.70 (CH$_3$), 28.88 (ArCH$_2$CH$_2$) ppm; **ESI-MS**: m/z = 357.0 [M+H]$^+$, calc. 356.2; **IR** (ATR): $\tilde{v}$ = 1494 (s), 1467 (m), 1453 (m), 1377 (m), 1364 (m), 1284 (m), 1277 (m), 1230 (m), 1161 (m), 1127 (s), 1014 (m), 934 (m), 860 (m), 732 (s), 693 (m) cm^{-1}.

Selective benzyl cleavage reactions:

General hydrogenation procedure:

The corresponding compound was dissolved in either MeOH, EtOH, dry THF or a system of EtOH/AcOH and Pd/C 10% (10 w%) was added. The air atmosphere of the reaction vessel was evaporated and then the vessel was purged with hydrogen. After stirring for 3 h at 50°C, the suspension was filtered off and the filtrate was evaporated to dryness. The residue was suspended in ethyl acetate and filtered over a short silica column. After removal of the solvent the product was directly obtained or purified by column chromatography.
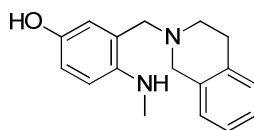
Path a:

*10-Hydroxy-13-methyl-13,13a-dihydro-5*H-*isoquinolino[1,2-*b*]quinazolin-8(6*H*)-one* **14** *from starting material* **10***:*
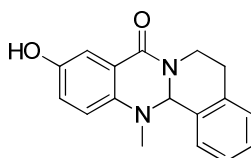
Following the general hydrogenation procedure, starting from10-(benzyloxy)-13-methyl-13,13a-dihydro-5*H*-isoquinolino[1,2-*b*]quinazolin-8(6*H*)-one **10** (2.4 g, 6.5 mmol, 1 eq.) in MeOH (30 mL) the title compound 10-hydroxy-13-methyl-13,13a-dihydro-5*H*-isoquinolino[1,2-*b*]quinazolin-8(6*H*)-one **14** (1.8 g, 100%) was obtained as yellow solid; **m.p.** = 197-108°C; **^{1}H-NMR** (400 MHz, DMSO-d$_6$): δ = 9.38 (s, OH), 7.39-7.34 (m, 1H, arom.), 7.33-7.26 (m, 3H, arom.), 7.25 (d, *J* = 2.8 Hz, 1H, arom.), 7.04 (d, *J* = 8.6 Hz, 1H, arom.), 6.95 (dd, *J* = 8.6, 2.8 Hz, 1H, arom.), 5.77 (s, 1H, C*H*), 4.43 (ddd, *J* = 12.7, 5.2, 3.3 Hz, 1H, NC*H$_2$*CH$_2$), 3.19 (ddd, *J* = 12.8, 10.6, 4.6 Hz, 1H, NC*H$_2$*CH$_2$), 3.01-2.77 (m, 2H, ArC*H$_2$*CH$_2$), 2.42 (s, 3H, C*H$_3$*) ppm; **^{13}C-NMR** (101 MHz, DMSO-d$_6$): δ =162.99 (CO), 152.76 (arom.), 142.83 (arom.), 136.79 (arom.), 133.14 (arom.), 128.48 (arom.), 127.88 (arom.), 127.32 (arom.), 126.58 (arom.), 122.84 (arom.), 122.48 (arom.), 120.85 (arom.), 112.88 (arom.), 71.46 (*C*H), 38.68 (N*C*H$_2$CH$_2$), 36.62 (*C*H$_3$), 27.58 (C*C*H$_2$CH$_2$) ppm; **ESI-MS**: *m/z* = 281.6 [M+H]$^+$, 303.1 [M+Na]$^+$, calc. 280.1; **IR** (ATR): $\tilde{v}$ = 3194 (br,*v*-OH), 1621 (s, *v*-C=O), 1571 (m), 1501 (m), 1462 (m), 1428 (s), 1336 (m), 1282 (m), 1211 (m), 740 (m) cm^{-1}.

*3-((3,4-Dihydroisoquinolin-2(1*H*)-yl)methyl)-4-(methylamino)phenol **15** from starting material **9**:*

Following the general hydrogenation procedure, starting from 10-(benzyloxy)-13-methyl-6,8,13,13a-tetrahydro-5*H*-isoquinolino[1,2-*b*]quinazoline **9** (100 mg, 0.28 mmol, 1 eq.) in MeOH (5 mL) the title compound 3-((3,4-dihydroisoquinolin-2(1*H*)-yl)methyl)-4-(methylamino)phenol**15** (33 mg, 44%) was obtained after column chromatography (DCM:MeOH = 95:5) as yellow solid; **¹H-NMR** (400 MHz, DMSO-d₆): δ = 8.44 (s, OH), 7.15 - 7.06 (m, 3H, arom.), 7.04 - 6.99 (m, 1H, arom.), 6.66 - 6.54 (m, 2H, arom.), 6.40 (d, *J* = 8.4 Hz, 1H, arom.), 5.25 (br, NH), 3.51 (s, 2H, ArC*H*₂N), 3.50 (s, 2H, ArC*H*₂N), 2.80 (t, *J* = 5.7 Hz, 2H, ArC*H*₂CH₂), 2.68 - 2.60 (m, 5H, NC*H*₂CH₂ + C*H*₃) ppm; **¹³C-NMR** (101 MHz, DMSO-d₆): δ =147.91 (arom.), 141.70 (arom.), 134.54 (arom.), 134.05 (arom.), 128.41 (arom.), 126.41 (arom.), 125.99 (arom.), 125.49 (arom.), 122.86 (arom.), 117.54 (arom.), 114.38 (arom.), 110.26 (arom.), 60.64 (Ar*C*H₂N), 55.22 (Ar*C*H₂N), 49.89 (N*C*H₂CH₂), 30.43 (*C*H₃), 28.66 (Ar*C*H₂CH₂) ppm; **ESI-MS**: *m/z* = 269.2 [M+H]⁺, calc. 268.2; **IR** (ATR): $\tilde{v}$ = 3253 (m, *v*-NH), 2953 (br, *v*-OH), 1497 (s), 1476 (m), 1451 (m), 1346 (m), 1272 (m), 1258 (m), 1212 (m), 1162 (m), 1079 (m), 812 (m), 750 (m), 734 (m) cm⁻¹.

*3-((3,4-Dihydroisoquinolin-2(1*H*)-yl)methyl)-4-(methylamino)phenol **15** from starting material **16**:*

Following the general hydrogenation procedure, starting from 4-(benzyloxy)-2-((3,4-dihydroisoquinolin-2(1*H*)-yl)methyl)-*N*-methylaniline **16** (131 mg, 0.37 mmol, 1 eq.)in MeOH (10 mL) the title compound 3-((3,4-dihydroisoquinolin-2(1*H*)-yl)methyl)-4-(methylamino)phenol**15** (48 mg, 49%) was obtained after column chromatography (DCM:MeOH = 95:5) as yellow solid.(Analytical data are summarized in path *a,***15** from starting material **9**)

Path b:

*3-((3,4-Dihydroisoquinolin-2(1*H)-*yl)methyl)-4-(methylamino)phenol **15** from starting material **9**:*

Following the general hydrogenation procedure, starting from 10-(benzyloxy)-13-methyl-6,8,13,13a-tetrahydro-5*H*-isoquinolino[1,2-*b*]quinazoline **9** (70 mg, 0.20 mmol, 1 eq.) in EtOH (5 mL) the title compound 3-((3,4-dihydroisoquinolin-2(1*H*)-yl)methyl)-4-(methylamino)phenol**15** (19 mg, 37%) was obtained after column chromatography (DCM:MeOH = 95:5) as yellow solid. (Analytical data are summarized in path *a,***15** from starting material **9**)

Path c:

*3-((3,4-Dihydroisoquinolin-2(1*H*)-yl)methyl)-4-(methylamino)phenol **15** from starting material **9**:*

Following the general hydrogenation procedure, starting from 10-(benzyloxy)-13-methyl-6,8,13,13a-tetrahydro-5*H*-isoquinolino[1,2-*b*]quinazoline **9** (50 mg, 0.14 mmol, 1 eq.) in a 1:1 mixture of EtOH/AcOH (4 mL) the title compound 3-((3,4-dihydroisoquinolin-2(1*H*)-yl)methyl)-4-(methylamino)phenol**15** (5 mg, 14%) was obtained after column chromatography (DCM:MeOH = 95:5) as yellow solid. (Analytical data are summarized in path *a,***15** from starting material **9**)
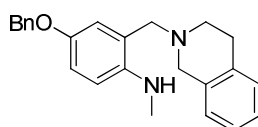
Path d:

*4-(Benzyloxy)-2-((3,4-dihydroisoquinolin-2(1H)-yl)methyl)-N-methylaniline **16** from starting material **9***:

Following the general hydrogenation procedure, starting from 10-(benzyloxy)-13-methyl-6,8,13,13a-tetrahydro-5*H*-isoquinolino[1,2-*b*]quinazoline **9** (200 mg, 0.56 mmol, 1 eq.) in dry THF (3 mL) the title compound 4-(benzyloxy)-2-((3,4-dihydroisoquinolin-2(1*H*)-yl)methyl)-*N*-methylaniline **16** (186 mg, 93%) was obtained as yellow oil;[1]**H-NMR** (400 MHz, DMSO-d$_6$): δ = 7.46 - 7.41 (m, 2H, arom.), 7.41 - 7.35 (m, 2H, arom.), 7.34 - 7.29 (m, 1H, arom.), 7.14 - 7.06 (m, 3H, arom.), 7.04 - 6.98 (m, 1H, arom.), 6.85 (dd, *J* = 8.5, 3.0 Hz, 1H, arom.), 6.82 (d, *J* = 2.9 Hz, 1H, arom.), 6.48 (d, *J* = 8.6 Hz, 1H, arom.), 5.45 (br, N*H*), 5.00 (s, 2H, OC*H*$_2$), 3.55 (s, 2H, ArC*H*$_2$N), 3.51 (s, 2H, ArC*H*$_2$N), 2.80 (t, *J* = 5.7 Hz, 2H, ArC*H*$_2$CH$_2$), 2.66 (s, 3H, C*H*$_3$), 2.63 (t, *J* = 5.9 Hz, 2H, NC*H*$_2$CH$_2$) ppm; **^{13}C-NMR** (101 MHz, DMSO-d$_6$): δ = 149.31 (arom.), 143.29 (arom.), 137.73 (arom.), 134.50 (arom.), 134.03 (arom.), 128.41 (arom.), 128.28 (2C, arom.), 127.55 (2C, arom.), 126.40 (arom.), 126.00 (arom.), 125.51 (arom.), 122.81 (arom.), 117.86 (arom.), 114.19 (arom.), 109.83 (arom.), 69.79 (OCH$_2$), 60.52(ArCH$_2$N), 55.21(ArCH$_2$N), 49.85(NCH$_2$CH$_2$), 30.26 (CH$_3$), 28.63(ArCH$_2$CH$_2$)ppm. **ESI-MS**: *m/z* = 359.3 [M+H]$^+$, calc. 358.2; **IR** (ATR): $\tilde{v}$ = 3302 (br, *v*-NH), 2802 (w), 1514 (m), 1453 (s), 1282 (m), 1270 (m) , 1227 (m), 1168 (w), 1081 (w), 1061 (w), 1025 (m), 736 (m), 695 (m)cm^{-1}.

Path e:

*4-(Benzyloxy)-2-((3,4-dihydroisoquinolin-2(1*H*)-yl)methyl)-*N-*methylaniline **16** from starting material **9***:

PtO$_2$ 10% (10 mg, 10 w%) was dissolved in MeOH (5 mL), the atmosphere of the reaction vessel was evaporated andthen the vessel was purged with hydrogen.After 1 h 10-(benzyloxy)-13-methyl-6,8,13,13a-tetrahydro-5*H*-isoquinolino[1,2-*b*]quinazoline **9** (100 mg, 0.28 mmol, 1 eq.) was added. The mixture was evaporated and purged with hydrogen again. After stirring for 2 h at 50°C, the mixture was filtered off andthe crude product was purified by column chromatography (PE:EE = 5:1) to obtain 4-(benzyloxy)-2-((3,4-dihydroisoquinolin-2(1*H*)-yl)methyl)-*N*-methylaniline **16** (80 mg, 80%) as yellow oil. (Analytical data are summarized in path *d*)

Path f:

*13-Methyl-6,8,13,13a-tetrahydro-5*H*-isoquinolino[1,2-*b*]quinazolin-10-ol **17** from starting material **9***:
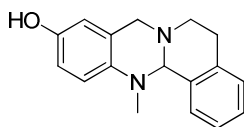
To a solution of 10-(benzyloxy)-13-methyl-6,8,13,13a-tetrahydro-5*H*-isoquinolino[1,2-*b*]quinazoline **9** (50 mg, 0.14 mmol, 1 eq.) and *N,N*-dimethylaniline (71 µL, 0.56 mmol, 4 eq.) in DCM (2 mL) was added AlCl$_3$ (56 mg, 0,42 mmol, 3 eq.). The reaction mixture was stirred for 5 min. Then sat. NH$_4$Cl-solution (10 mL) was added ant the product was extracted with ethyl acetate (3 x 10 mL). The combined organic layers were washed with brine (10 mL) and dried over Na$_2$SO$_4$. After removal of the solvent, the crude product was purified by column chromatography (PE:EA = 1:1) to obtain 13-methyl-6,8,13,13a-tetrahydro-5*H*-isoquinolino[1,2-*b*]quinazolin-10-ol **17**(24 mg, 65%) as yellow solid.Modified protocol from literature;[2]**m.p** = 151 - 156°C; **^{1}H-NMR** (400 MHz, DMSO-d$_6$): δ = 8.91 (s, OH), 7.43-7.38 (m, 1H, arom.), 7.27-7.21 (m, 2H, arom.), 7.21-7.14 (m, 1H, arom.), 6.84 (d, *J* = 8.7 Hz, 1H, arom.), 6.57 (dd, *J* = 8.6, 2.8 Hz, 1H, arom.), 6.43 (d, *J* = 2.7 Hz, 1H, arom.), 4.57 (s, C*H*), 3.86 (d, *J* = 15.3 Hz, 1H, ArC*H$_2$*N), 3.66 (d, *J* = 15.3 Hz, 1H, ArC*H$_2$*N), 3.16 (ddd, *J* = 11.1, 5.0, 3.0 Hz, 1H, NC*H$_2$*CH$_2$), 3.00 (ddd, *J* = 16.0, 10.9, 5.1 Hz, 1H, ArC*H$_2$*CH$_2$), 2.75-2.66 (m, 1H, ArC*H$_2$*CH$_2$), 2.59-2.53 (m, 1H, NC*H$_2$*CH$_2$), 2.34 (s, 3H, C*H$_3$*) ppm; **^{13}C-NMR** (101 MHz, DMSO-d$_6$): δ =151.84 (arom.), 141.02 (arom.), 136.18 (arom.), 134.14 (arom.), 128.48 (arom.), 127.73 (arom.), 127.32 (arom.), 126.92 (arom.), 125.91 (arom.), 123.31 (arom.), 114.16 (arom.), 112.27 (arom.), 76.94 (*C*H), 56.10 (C*C*H$_2$N), 48.40 (N*C*H$_2$CH$_2$), 39.28 (*C*H$_3$), 28.22 (C*C*H$_2$CH$_2$) ppm; **ESI-MS**: *m/z* = 267.0 [M+H]$^+$, calc. 267.1; **IR** (ATR): $\tilde{v}$ = 2937 (br, v-OH), 1509 (m), 1455 (s), 1420 (m), 1364 (m), 1232 (s), 1127 (m), 1110 (s), 1087 (m), 921 (s), 746 (s) cm^{-1}.

Path g:

13-Methyl-6,8,13,13a-tetrahydro-5H-isoquinolino[1,2-b]quinazolin-10-ol 17 from starting material 9:

10-(Benzyloxy)-13-methyl-6,8,13,13a-tetrahydro-5*H*-isoquinolino[1,2-*b*]quinazoline **9** (50 mg, 0.14 mmol, 1 eq.) was dissolved in MeOH (4 mL) at 50°C while stirring and 1 mL of 37% HCl was added. The mixture was stirred under reflux temperature for 24 h. After that, MeOH was evaporated under reduced pressure. The remaining aqueous solution was basified with 1 M NaOH-solution and the pH was adjusted to 9 with a sat. NH₄Cl-solution. The product was extracted with ethyl acetate (3x 30 mL), the combined organic layers were washed with brine and finally dried over Na₂SO₄. The solvent was then evaporated under reduced pressure and the crude product was purified by column chromatography (PE:EA = 1:1) to obtain 13-methyl-6,8,13,13a-tetrahydro-5*H*-isoquinolino[1,2-b]quinazolin-10-ol **17** (30 mg, 80%) as yellow solid. (Analytical data are summarized in path *f*)

Path h:

13-Methyl-6,8,13,13a-tetrahydro-5H-isoquinolino[1,2-b]quinazolin-10-ol 17 from starting material 14:

10-Hydroxy-13-methyl-13,13a-dihydro-5*H*-isoquinolino[1,2-*b*]quinazolin-8(6*H*)-one **14** (1.6 g, 5.71 mmol, 1 eq.) was dissolved in dry THF (40 mL) at 0°C and LiAlH₄ (651 mg, 17.14 mmol, 3 eq.) was added. The mixture was allowed to reach room temperature and was then heated to reflux temperature for 3 h. After cooling to room temperature, the mixture was poured into ice water (50 mL) followed by the addition of saturated NH₄Cl-solution until pH = 9. The aqueous phase was then extracted with ethyl acetate (3 x 200 mL). The combined organic layers were washed with brine (100 mL), dried over Na₂SO₄ and the solvent was evaporated under reduced pressure to obtain 13-methyl-6,8,13,13a-tetrahydro-5*H*-isoquinolino[1,2-b]quinazolin-10-ol **17** (1.5 g, 98%) as yellow solid. (Analytical data are summarized in path *f*)

Path i:

3-((3,4-Dihydroisoquinolin-2(1H)-yl)methyl)-4-(methylamino)phenol 15 from starting material 17:

13-Methyl-6,8,13,13a-tetrahydro-5*H*-isoquinolino[1,2-*b*]quinazolin-10-ol **17** (100 mg, 0.38 mmol, 1 eq.) wasdissolved in methanol at room temperature while stirring and Pd/C 10% (10 mg, 10w%) was added. The reaction vessel was evaporated, purged with hydrogen and the reaction mixture was stirred for 2.5 h. The suspension was filtered off, the filtrate was basified with a 1 M NaOH-solution and finally the pH was adjusted to 9 with a sat. NH₄Cl-solution. The product was then extracted with ethyl

acetate (3 x 20 mL),the combined organic layers were washed with brine (20 mL) and dried over Na$_2$SO$_4$. After removal of the solvent, the crude product was purified by column chromatography (DCM:MeOH = 95:5) to obtain 3-((3,4-dihydroisoquinolin-2(1*H*)-yl)methyl-4-(methylamino)phenol**15** (28 mg, 28%) as yellow solid**.** (Analytical data are summarized in path *a,***15** from starting material **9**)

Path j:

*4-(Benzyloxy)-2-((3,4-dihydroisoquinolin-2(1*H*)-yl)methyl)-*N-*methylaniline **16** from starting material **9***:

10-(Benzyloxy)-13-methyl-6,8,13,13a-tetrahydro-5*H*-isoquinolino[1,2-*b*]quinazoline **9** (50 mg, 0.14 mmol, 1 eq.) was dissolved in dry THF (1 mL), the solution was purged with argon and a 1 M BH$_3$·THF-solution (1.6 mL) was added. The mixture was stirred for 5 h at reflux temperature. Then it was allowed to reach room temperature, water (1.5 mL) was added and the mixture was stirred for 1 h more. The product was extracted with DCM (3x 10 mL), the combined organic layers were washed with brine and dried over Na$_2$SO$_4$. Finally, the solvent was removed under reduced pressure and the crude product was purified by column chromatography (PE:EA = 5:1) to obtain 4-(benzyloxy)-2-((3,4-dihydroisoquinolin-2(1*H*)-yl)methyl)-*N*-methylaniline **16** (21 mg, 42%) as yellow oil. Modified protocol from literature.[3, 4] (Analytical data are summarized in path *d*)

*4-(Benzyloxy)-2-((3,4-dihydroisoquinolin-2(1*H*)-yl)methyl)-*N-*methylaniline **16** from starting material **10***:

10-(Benzyloxy)-13-methyl-13,13a-dihydro-5*H*-isoquinolino[1,2-*b*]quinazolin-8(6*H*)-one**10** (100 mg, 0.27 mmol, 1 eq.) was dissolved in dry THF (2 mL), the solution was purged with argon and a 1 M BH$_3$·THF-solution (3.2 mL) was added. The mixture was stirred for 2.5 h at reflux temperature. Then it was allowed to reach room temperature, water (3 mL) was added and the mixture was stirred for 1 h more. The product was extracted with DCM (3x 20 mL), the combined organic layers were washed with brine and dried over Na$_2$SO$_4$. Finally, the solvent was removed under reduced pressure and the crude product was purified by column chromatography (PE:EA = 5:1) to obtain 4-(benzyloxy)-2-((3,4-dihydroisoquinolin-2(1*H*)-yl)methyl)-*N*-methylaniline **16** (45 mg, 47%) as yellow oil. Modified protocol from literature.[3, 4] (Analytical data are summarized in path *d*)

Path k:

*4-(Benzyloxy)-2-((3,4-dihydroisoquinolin-2(1*H*)-yl)methyl)-N-methylaniline **16** from starting material **9**:*

10-(Benzyloxy)-13-methyl-6,8,13,13a-tetrahydro-5*H*-isoquinolino[1,2-*b*]quinazoline **9** (50 mg, 0.14 mmol, 1 eq) was dissolved in ethanol (3 mL) and NaBH$_4$ (75 mg 1.97 mmol, 14 eq.) was added. The mixture was stirred at reflux temperature for 2.5 h. Then the solvent was evaporated under reduced pressure, water (10 mL) was added and the product was extracted with DCM (3x 10 mL). The combined organic layers were washed with brine, dried over Na$_2$SO$_4$and the solvent was evaporated under reduced pressure to obtain 4-(benzyloxy)-2-((3,4-dihydroisoquinolin-2(1*H*)-yl)methyl)-*N*-methylaniline**16** (30 mg, 60%) as yellow oil. Modified protocol from literature.[5, 6] (Analytical data are summarized in path *d*)

Path m:

*2-Methylamino-5-benzyloxybenzaldehyde **18** from starting material **10**:*
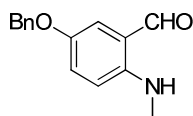
10-(Benzyloxy)-13-methyl-13,13a-dihydro-5*H*-isoquinolino[1,2-*b*]quinazolin-8(6*H*)-one **10** (81 mg, 0.22 mmol, 1 eq.) was dissolved in dry THF (2.5 mL). Then LiAlH$_4$ (8.5 mg, 0.22 mmol, 1 eq) was added at 0°C under argon. The reaction mixture was stirred at room temperature for 24 h. The reaction mixture was poured into ice water (20 mL), basified with a 2 M NaOH-solution and the pH was adjusted to 9 with sat. NH$_4$Cl-solution. The product was then extracted with DCM (3 x 20 mL). The combined organic layers were washed with brine (30 mL) and dried over Na$_2$SO$_4$. The solvent was evaporated under reduced pressure andthe crude product was purified by column chromatography (PE:EE = 2:1) to obtain 2-methylamino-5-benzyloxybenzaldehyde**18** (10 mg, 19%) as yellow oil and the recovered starting material **10**(51 mg, 63%);**1H-NMR** (400 MHz, DMSO-d$_6$): δ = 9.79 (s, 1H, C*H*O), 7.83 (q, 5.0 Hz, NH), 7.45 (dd, *J* = 7.9, 1.0 Hz, 2H, arom.), 7.42 - 7.36 (m, 2H, arom.), 7.36 - 7.29 (m, 2H, arom.), 7.24 (dd, *J* = 9.0, 2.9 Hz, 1H, arom.), 6.72 (d, *J* = 9.1 Hz, 1H, arom.), 5.06 (s, 2H, OC*H*$_2$), 2.85 (d, *J* = 5.1 Hz, 3H, C*H*$_3$) ppm;**13C-NMR** (101 MHz, DMSO-d$_6$): δ = 193.48 (*C*HO), 148.03 (arom.), 146.44 (arom.), 137.24 (arom.), 128.36 (2C, arom.), 127.74 (arom.), 127.68 (2C, arom.), 125.76 (arom.), 119.85 (arom.), 117.58 (arom.), 112.03 (arom.), 70.08 (O*C*H$_2$), 29.14 (*C*H$_3$) ppm; **ESI-MS**: *m/z* = 242.3 [M+H]$^+$, calc. 241.1; **IR** (ATR): $\tilde{v}$ = 3334 (m, *v*-NH), 2926 (m), 1711 (m, *v*-C=O), 1655 (s), 1577 (m), 1516 (s), 1477 (m), 1289 (m), 1255 (m), 1226 (m), 1202 (s), 1152 (s), 1014 (s), 825 (m), 750 (m) cm^{-1}.

NMR-Spectra of 9, 10 and 14-18:
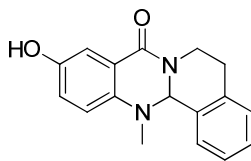
*10-(Benzyloxy)-13-methyl-6,8,13,13a-tetrahydro-5*H-*isoquinolino[1,2-*b*]quinazoline* **9**:

^{1}H-NMR + ^{13}C-NMR

*10-(Benzyloxy)-13-methyl-13,13a-dihydro-5H-isoquinolino[1,2-b]quinazolin-8(6H)-one **10**:*
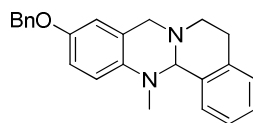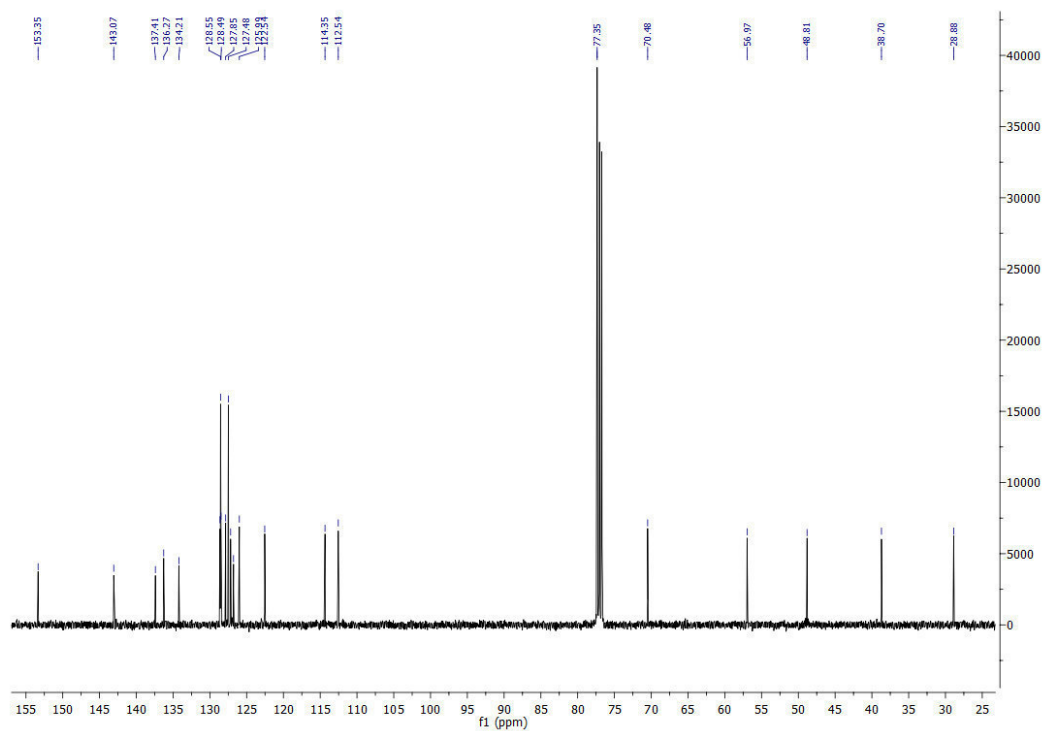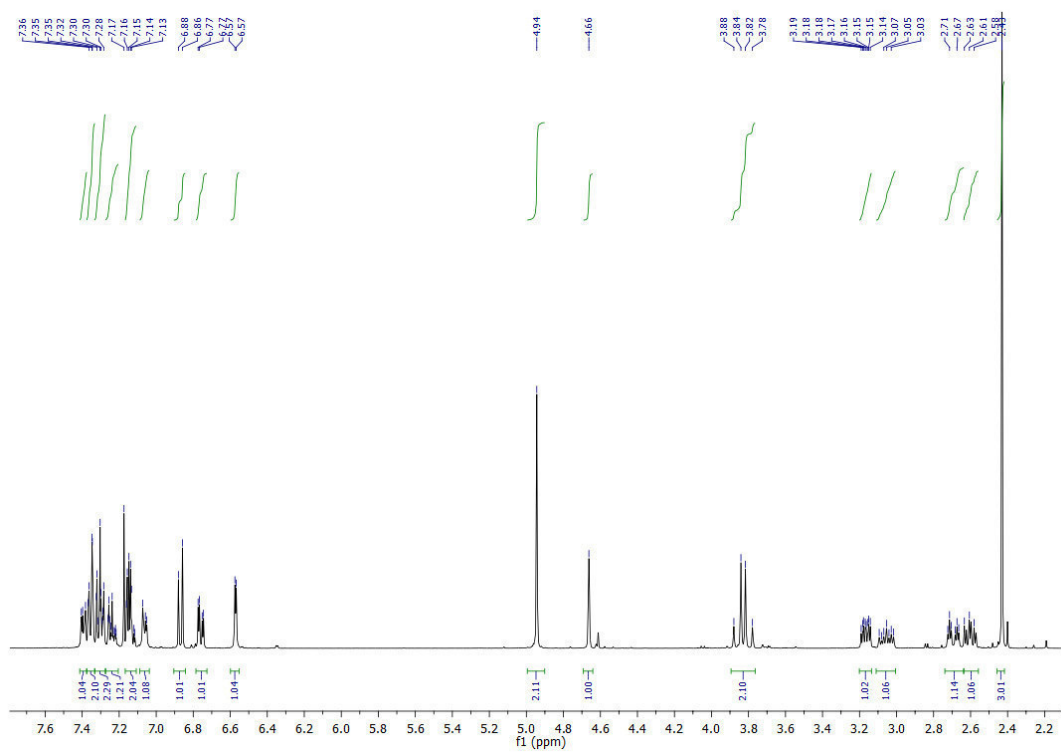
¹H-NMR + ¹³C-NMR

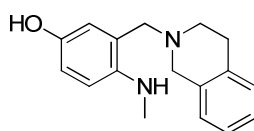*10-Hydroxy-13-methyl-13,13a-dihydro-5H-isoquinolino[1,2-b]quinazolin-8(6H)-one* **14**:

¹H-NMR + ¹³C-NMR
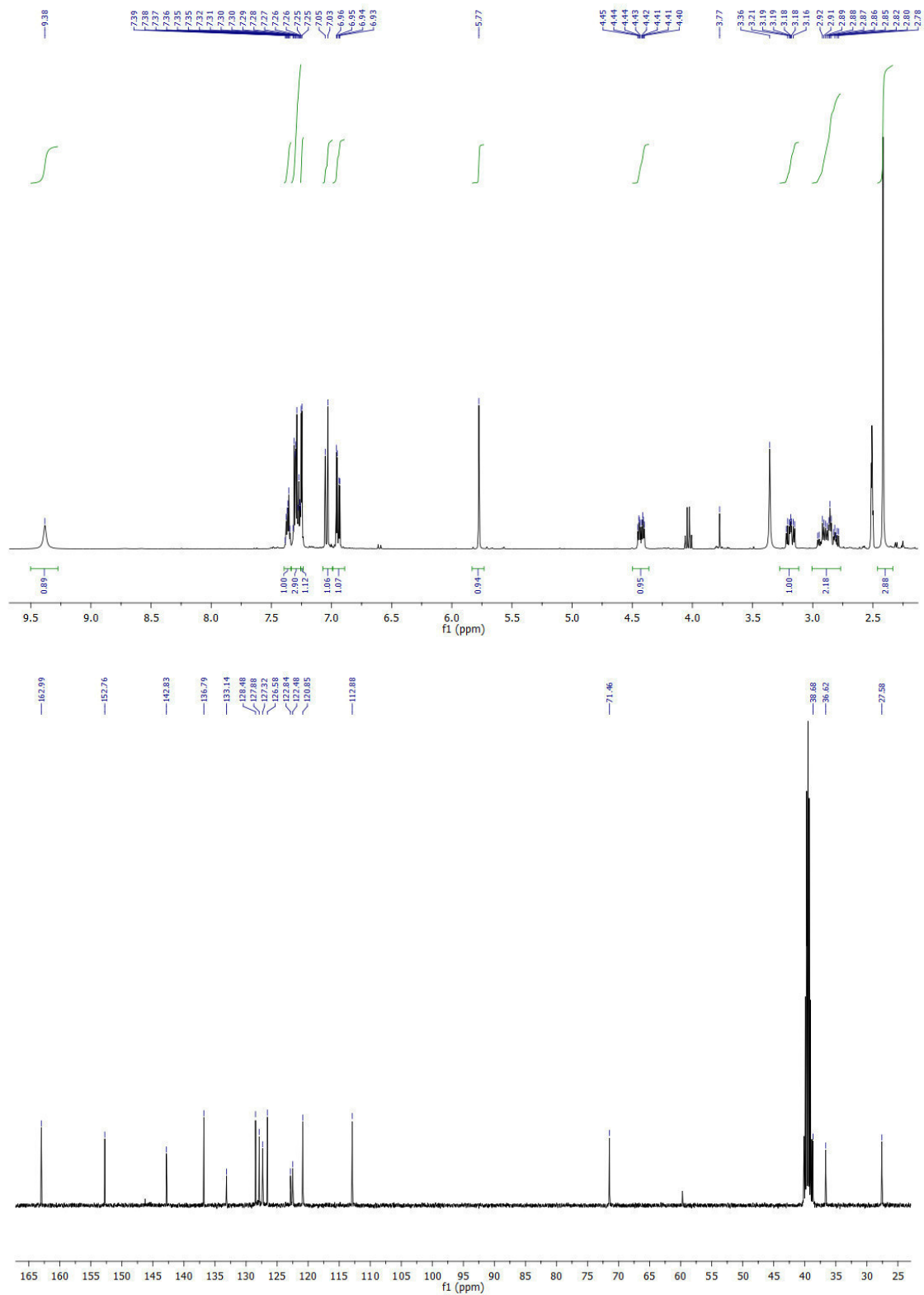
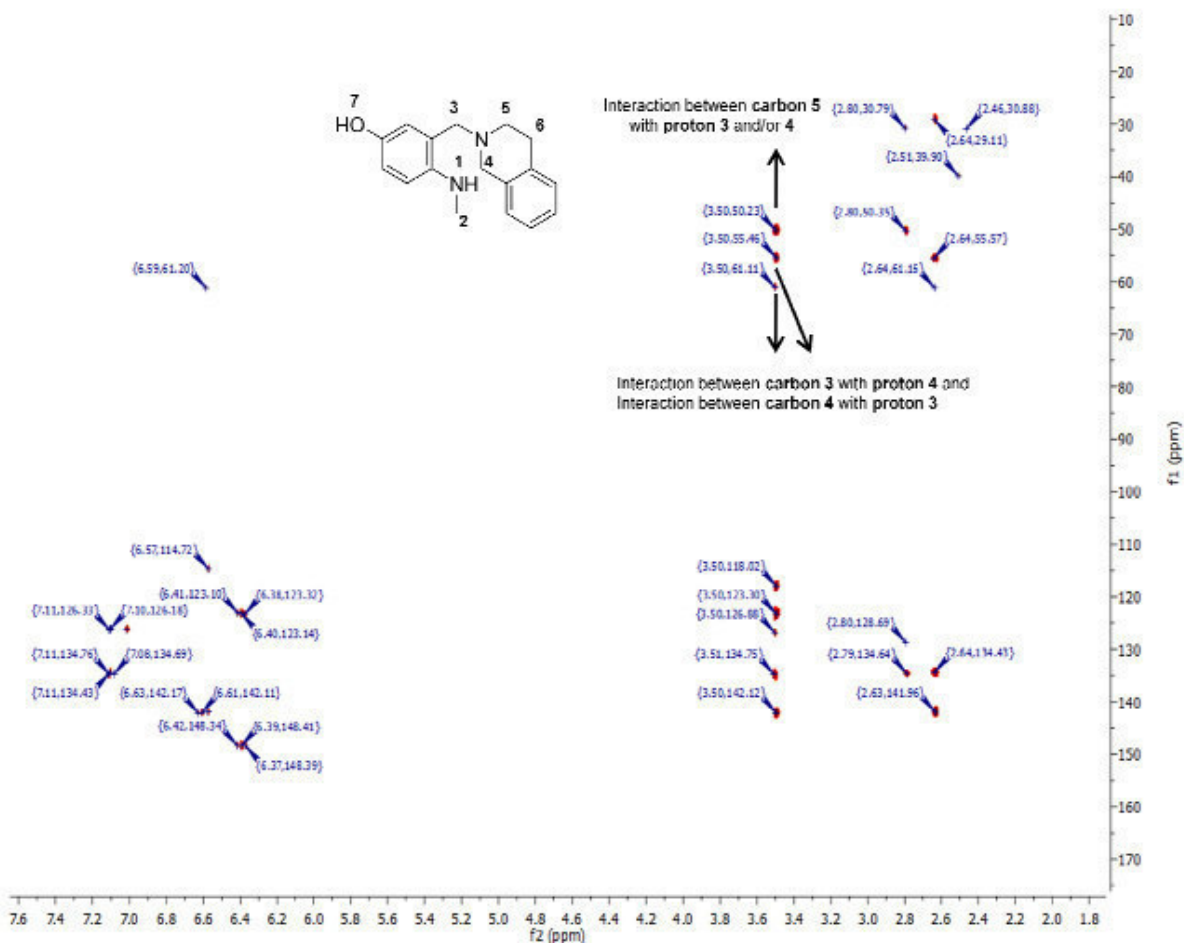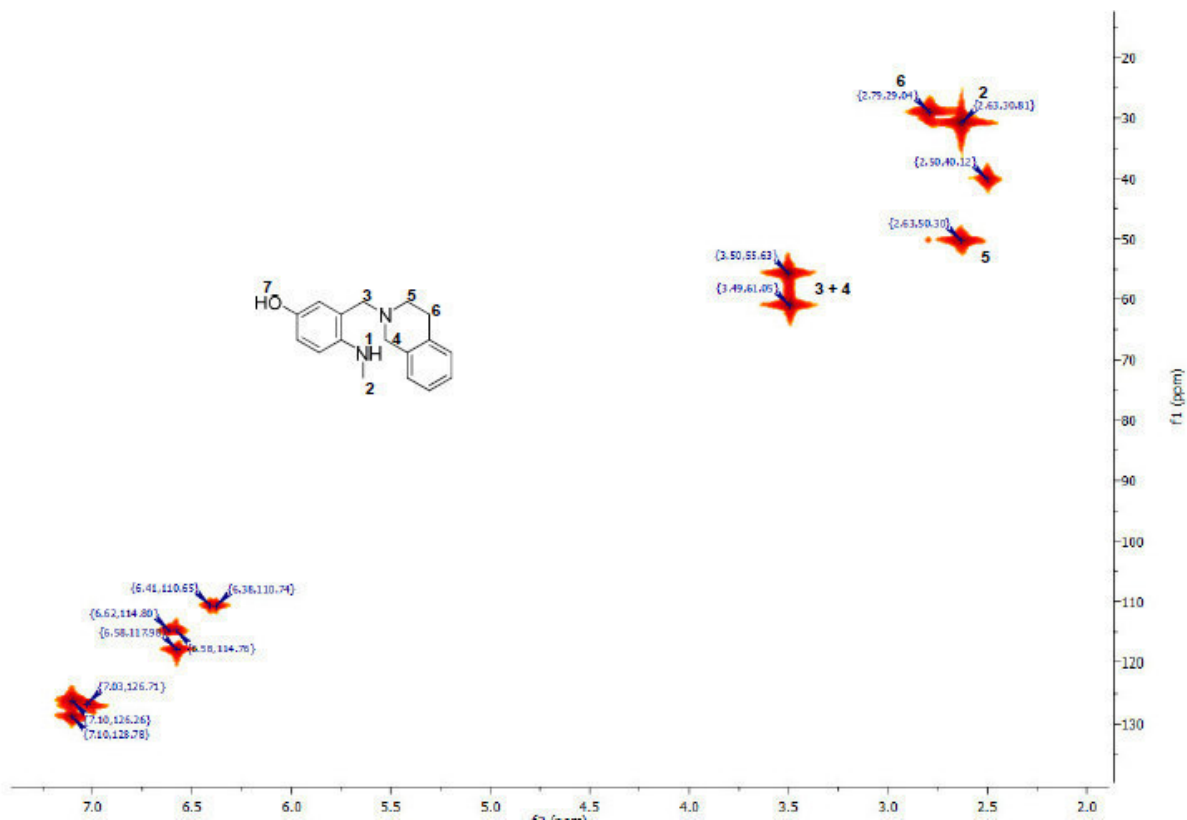*3-((3,4-dihydroisoquinolin-2(1H)-yl)methyl)-4-(methylamino)phenol **15***:

^{1}H-NMR + ^{13}C-NMR + HMQC + HMBC + Interpretation

Interaction between carbon 5 with proton 3 and/or 4

Interaction between carbon 3 with proton 4 and
Interaction between carbon 4 with proton 3

16
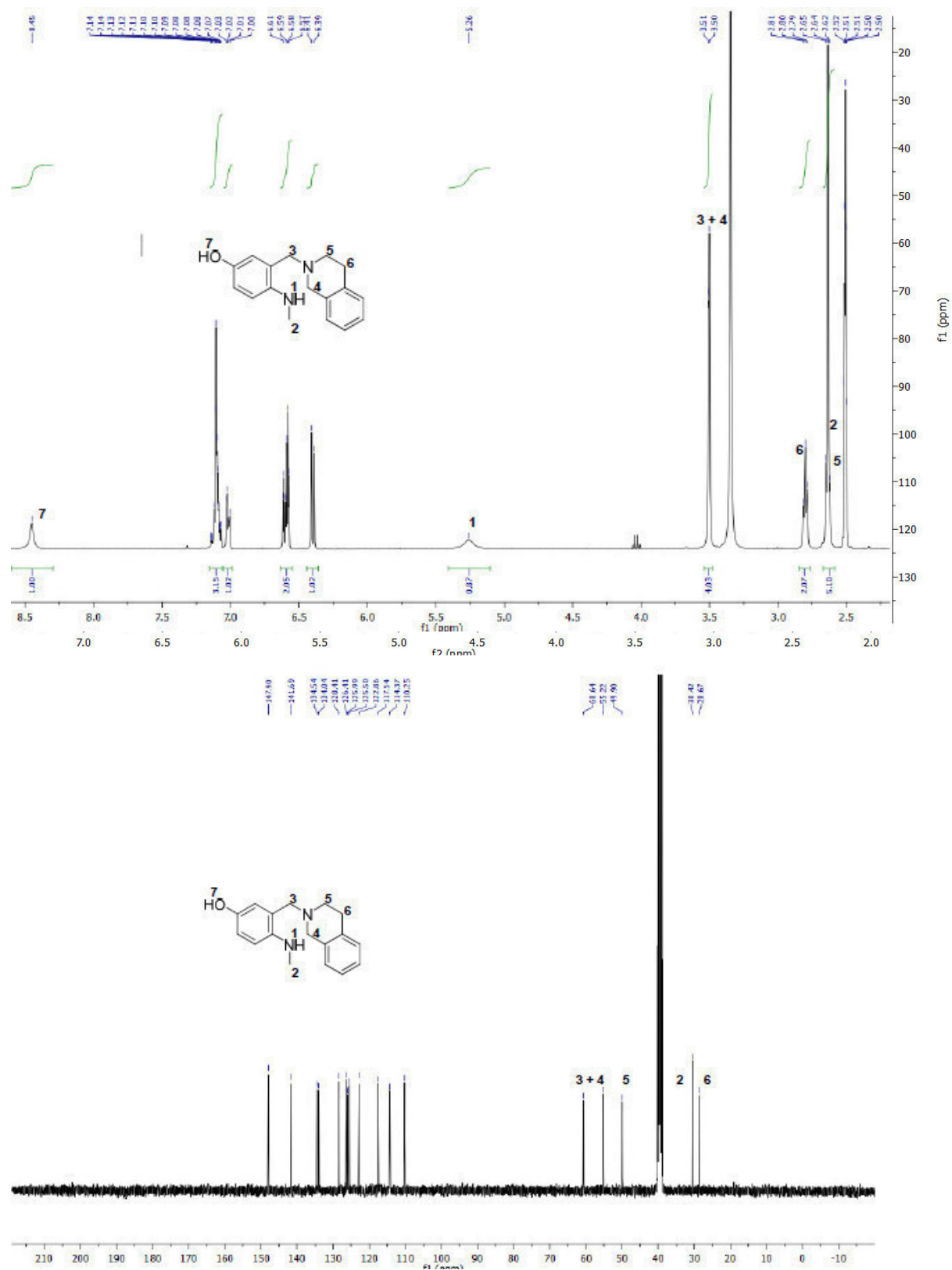
Interpretation of 2D-NMR:
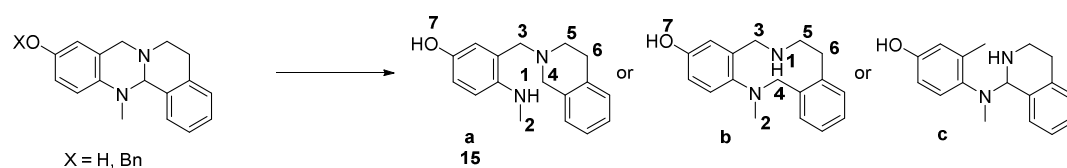
The ESI-MS spectra allows three possibilities for the product formation (**15** = **a**, **b** or **c**, respectively) from the reaction shown above. Structure**c** can be easily excluded by the ¹H-NMR-spectra as it lacks an aromatic CH₃-group. Independently from the product structure, the carbons and protons of the N-*CH₂*-Ar (labeled with number **3** and **4**) can be correlated by HMQC to a combination of ¹H-NMR: δ= 3.50 ppm/¹³C-NMR:δ = 55.63 ppm and ¹H-NMR: δ= 3.49 ppm/¹³C-NMR:δ = 61.05 ppm. Even though a clear assignment of the atoms at position **3** and **4** to the found signals in HMQC is not possible, the HMBC-spectra shows an interactions between the carbon at 55.63 ppm and the proton at 3.49 ppm as well as an interaction between the carbon at 61.05 ppm and the proton at 3.50 ppm. This means the proton at **3** can interact with the carbon **4** and the carbon at **3** can interact with the proton at **4**. As these interactions indicate the formation of product **a**, product **b** misses the core bridge between the benzyl nitrogen and the carbon at position **4** which makes the mentioned interactions possible.

*4-(Benzyloxy)-2-((3,4-dihydroisoquinolin-2(1*H)*-yl)methyl)*-N-*methylaniline **16***:

¹H-NMR + ¹³C-NMR + HMQC + HMBC + Interpretation

Interaction between **carbon 5** with proton 3 and 4

{3.55,50.21} {3.52,50.32}
{3.55,55.63}
{3.51,60.83}

Interaction between **carbon 3** with proton 4 and
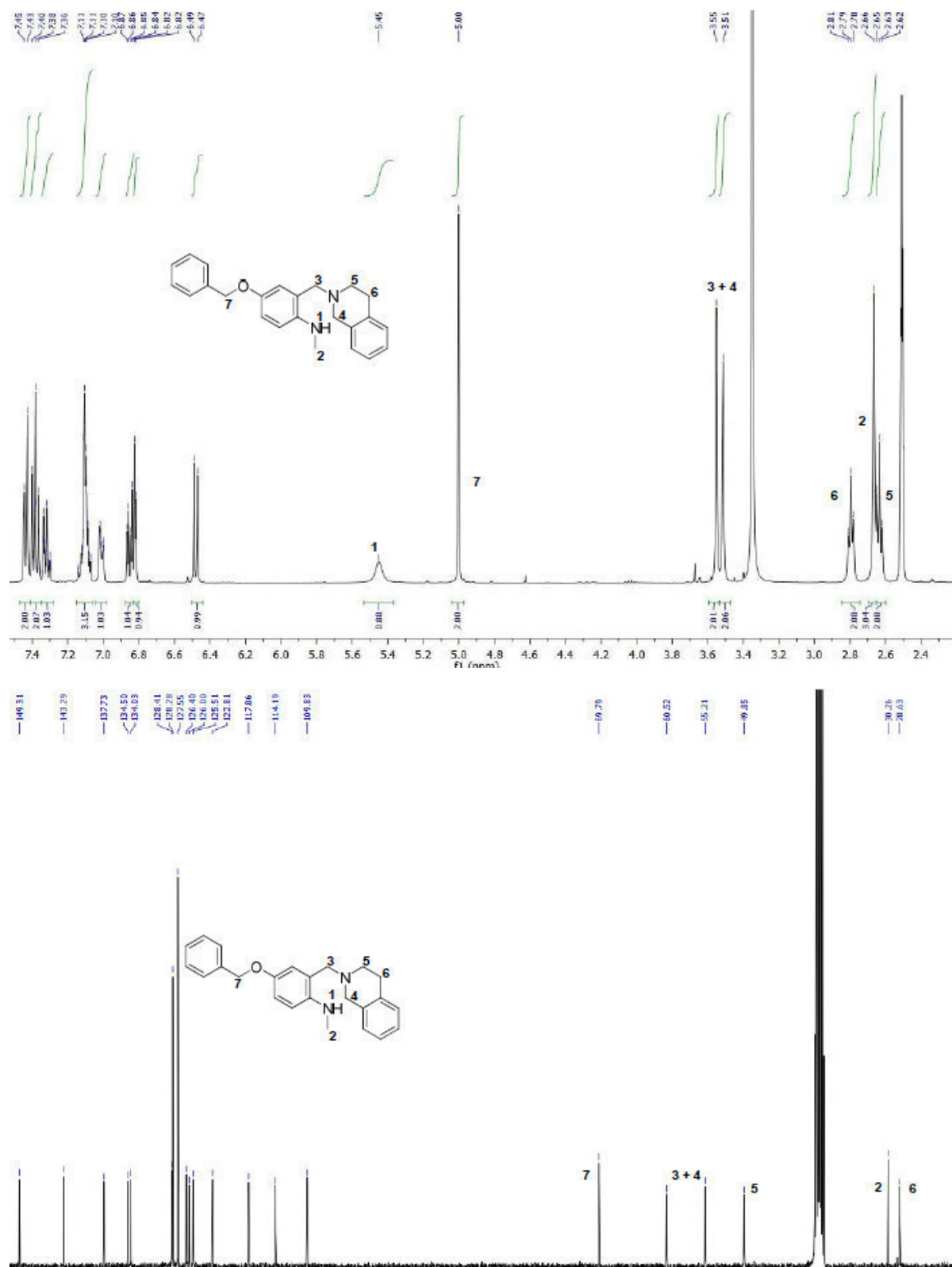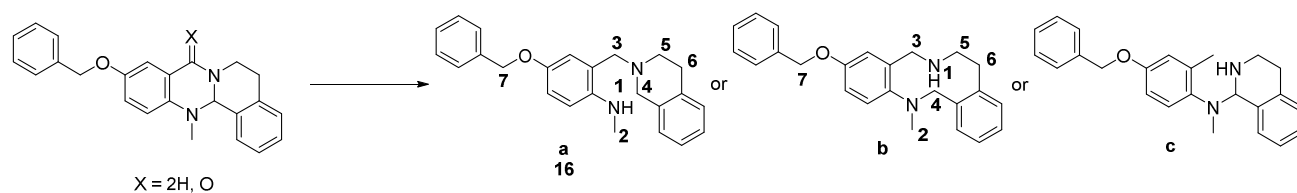Interaction between **carbon 4** with proton 3

Interpretation of 2D-NMR:

X = 2H, O

ESI-MS spectra allows three possibilities for the product formation (a = **16**, **b** or **c**, respectively) in the reaction shown above. Structure**c** can be easily excluded by the ^{1}H-NMR-spectra as it lacks an aromatic CH_3-group. Independent of the product structure, the carbons and protons of the N-CH_2-Ar (labeled with number **3** and **4**) can be correlated by HMQC to a combination of ^{1}H-NMR: δ= 3.51 ppm/^{13}C-NMR:δ = 55.60 ppm and ^{1}H-NMR: δ= 3.55 ppm/^{13}C-NMR:δ = 60.93 ppm. Even though a clear assignment of the atoms at position **3** and **4** to the found signals in HMQC is not possible, the HMBC-spectra shows an interactions between the carbon at 55.60 ppm and the proton at 3.55 ppm as well as an interactions between the carbon at 60.93 ppm and the proton at 3.51 ppm. This means the proton at **3** can interact with carbon **4** and carbon at **3** can interact with the proton at **4**. Besides this, the HMBC-spectra show an interaction between the carbon at position **5** and the proton at position **4** as well as with the proton at position **3**. These interactions indicate the formation of product **a**, product **b** misses the core bridge between the benzyl nitrogen and the carbon at position **4** which makes the mentioned interactions possible.

*13-Methyl-6,8,13,13a-tetrahydro-5*H-*isoquinolino[1,2-b]quinazolin-10-ol* **17:**
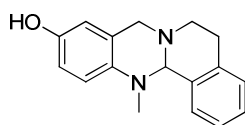
¹H-NMR + ¹³C-NMR
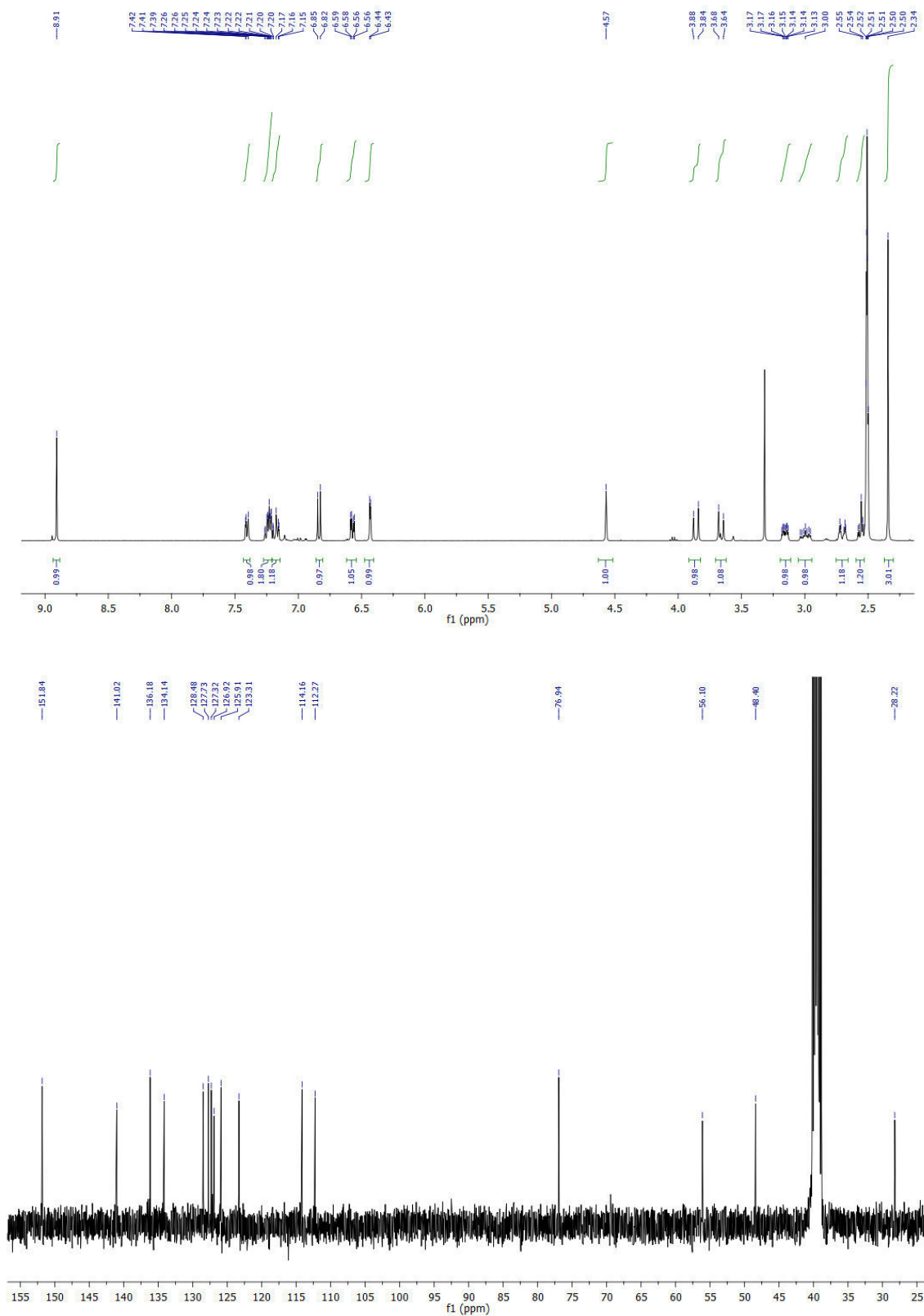
2-Methylamino-5-benzyloxybenzaldehyde *18*:
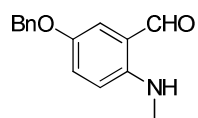
^{1}H-NMR + ^{13}C-NMR
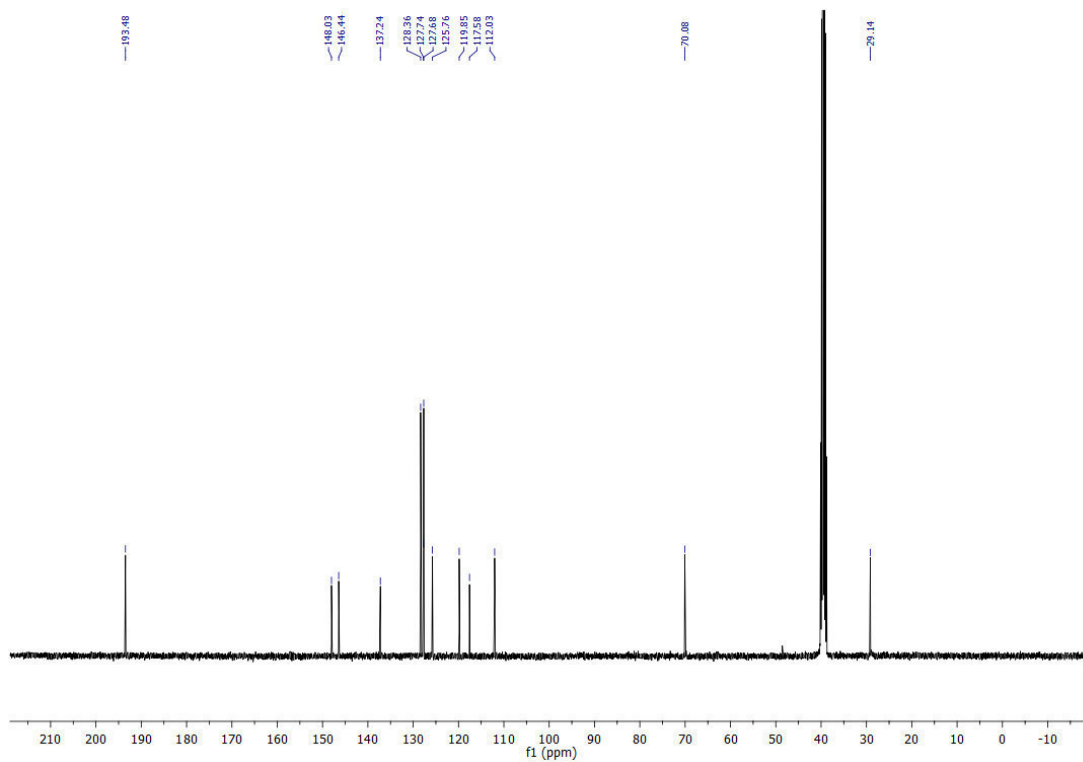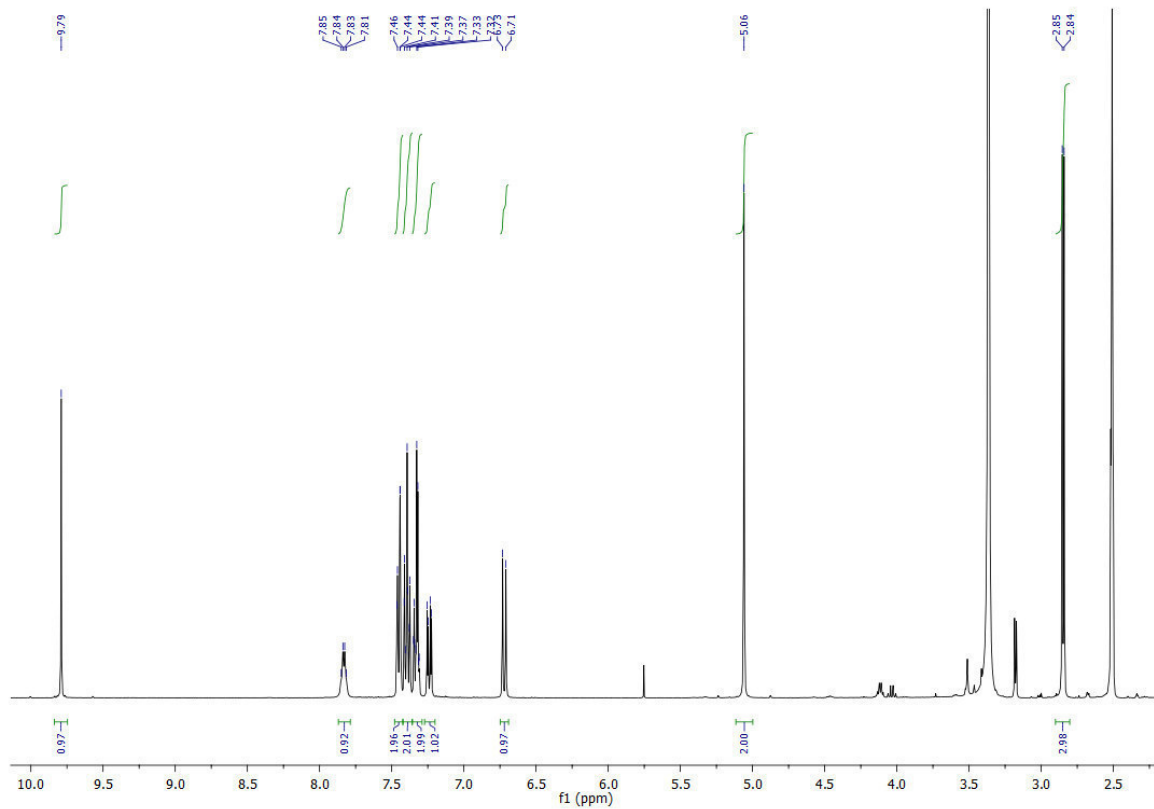
References:

[1] Darras, F. H.; Kling, B.; Heilmann J.; Decker, M. *ACS Med. Chem. Lett.***2012**, *3*, 914-919.

[2] Akiyama, T.; Hirofuji, H.; Ozaki, S. *Tetrahedron Lett.***1991**, 32, 1321-1334.

[3] Wasserman, H. H.; Matsuyama, H. *J. Am. Chem. Soc.***1981**, *103*, 461-462.

[4] Takeuchi, H.; Matsushita, Y.; Eguchi, S. *J. Org. Chem.***1991**, *56*, 1535-1537.

[5] Luo, H.; Lo, J.-M.; Fanwick, P. E.; Stowell, J. G.; Green, M. A. *Inorg. Chem.***1999***38*, 2071-2078.

[6] Pakrashi, S. C. ;Chakravarty, S. C. *J. Org. Chem.***1972**, 37, 3143-3147.

Appendix 4

Experimental and Theoretical Investigations into the Stability of Cyclic Aminals.

(Author's manuscript)

Experimental and Theoretical Investigations into the Stability of Cyclic Aminals

Edgar Sawatzky[1], Antonios Drakopoulos[1], Martin Rölz[1], Christoph Sotriffer[1], Bernd Engels[2], Michael Decker[1]*

Address: [1]Pharmazeutische und Medizinische Chemie, Institut für Pharmazie und Lebensmittelchemie, Julius-Maximilians-Universität Würzburg, Am Hubland, D-97074 Würzburg, Germany. [2]Institut für Physikalische und Theoretische Chemie, Julius-Maximilians-Universität Würzburg, Emil-Fischer-Straße 42, D-97074 Würzburg, Germany.

 * Michael.Decker@uni-wuerzburg.de

Abstract

Background. Cyclic aminals are core features of natural products, drug molecules and important synthetic intermediates. Despite their relevance, systematic investigations into their stability towards hydrolysis depending on the pH value are lacking. **Results**. A set of cyclic aminals was synthesized and their stability quantified by kinetic measurements. Steric and electronic effects were investigated by choosing appropriate groups. Both molecular mechanics (MM) and density functional theory (DFT) based studies were applied to support and explain the results obtained. Rapid decomposition is observed in acidic aqueous media for all cyclic aminals which

occurs as a reversible reaction. Electronic effects do not seem relevant with regard to stability, but the magnitude of the conformational energy of the ring system and pK_a values of the *N*-3 nitrogen atom. **Conclusion**. Cyclic aminals are stable compounds when not exposed to acidic media and their stability is mainly dependent on the conformational energy of the ring system. Therefore, for the preparation and work-up of these valuable synthetic intermediates and natural products, appropriate conditions have to be chosen and for application as drug molecules their sensitivity towards hydrolysis has to be taken into account.

Keywords

hydrolysis, kinetics, molecular mechanics, natural products, quantum mechanics

Introduction

The aminal system (*N,N*-acetal) is the structurally equivalent analog of the *O,O*-acetal. In the literature this moiety is found as a core element in various important structures, for example in the naturally occurring alkaloids tetraponerine T1 to T8 from the venom of the New Guinean ant *Tetraponera sp.*[1,2], in ligands of ruthenium based catalysts for metathesis[3], in imidazolidines acting as anti-protozoal and-bacterial agents[4,5], in Tröger's base derivatives applied in diverse research fields[6-14] (e.g. asymmetric catalysis, supramolecular chemistry, DNA-intercalation, etc.) or synthetic tetrahydroquinazolines as cholinesterase (ChE) inhibitors[15-17] as well as ChE inhibitors based on the scaffold of the naturally occurring alkaloid physostigmine from the calabar bean *physostigma venenosum*[18,19] (**Figure 1**). And this is just a small overview and selection of examples out of numerous compounds incorporating the aminal system as essential structural feature.
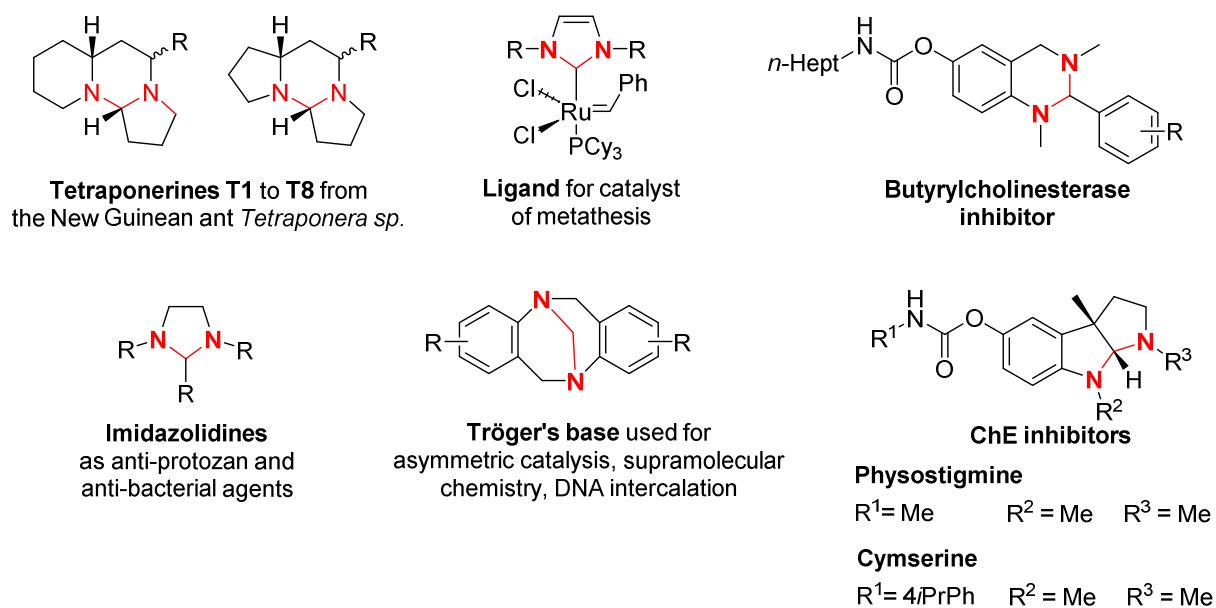
Figure 1: Compounds described in literature containing an aminal core for various applications. The aminal structure is highlighted in red.

Especially the aminal-bearing tetrahydroquinazoline system is of high interest as a structure derived from the quinazolinone and quinazoline cores, which represent privileged structures with various applications in medicinal chemistry[20,21]. Syntheses of tetrahydroquinazolines are well described using different approaches; mostly by direct α-amination of *ortho*-amino benzaldehydes under heating or microwave irradiation conditions[22-24], by condensation of diamines with aldehydes or ketones yielding bicyclic structures[25-27], or by the reduction of corresponding dihydroquinazolinones [15-17] (**Scheme 1**).
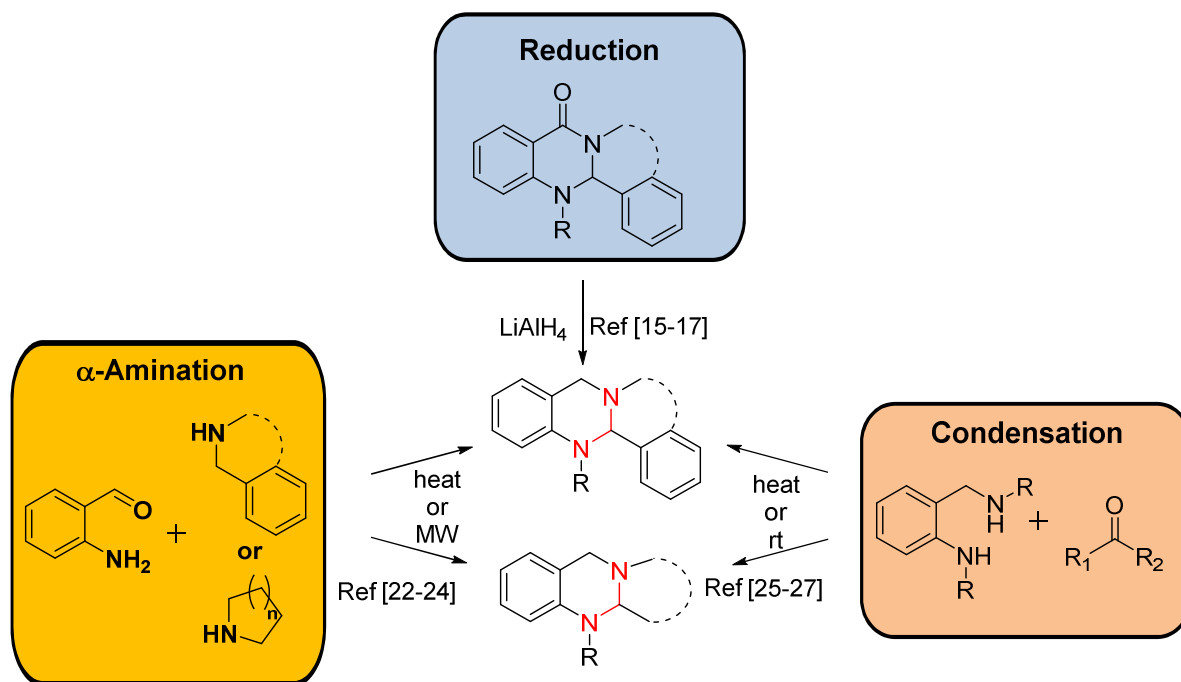
Scheme 1: Synthetic approaches for the formation of the tetrahydroquinazoline moiety. Dashed lines indicate either cyclized or non-cyclized compounds. The aminal structure is highlighted in red.

The aminal templates obtained can be used as starting materials for the synthesis of a broad spectrum of diverse structures. Oxidation reactions with $KMnO_4$ or a mixture of potassium iodide and *tert*-butyl hydroperoxide (TBHP) give access to quinazolinones and have been reported for the synthesis of the naturally occurring alkaloids deoxyvasicinone, mackinazolinone or rutaecarpine [22,28] (**Scheme 2**). Besides total oxidation of the aminal core, also a partial oxidation towards 3,4-dihydroquinazolines is possible promoted either by $Cu(AcO)_2$ as oxidant or by a mixture of elemental iodine and BuLi. These methods allow the synthesis of the partially unsaturated alkaloids vasicine or deoxyvasicine in good yields [22,28] (**Scheme 2**). Furthermore, copper catalyzed reactions or oxidation with sodium hypochlorite were also described to yield the aromatic quinazoline core [26,29,30] (**Scheme 2**). Besides all the oxidation raections described, also reductive conditions applying $NaBH_4$ onto the tetrahydroquinazoline based aminal systems were

investigated, thereby providing the possibility to "open" the rigid aminal core gaining access to sterically more flexible compounds[31-33] (**Scheme 2**).
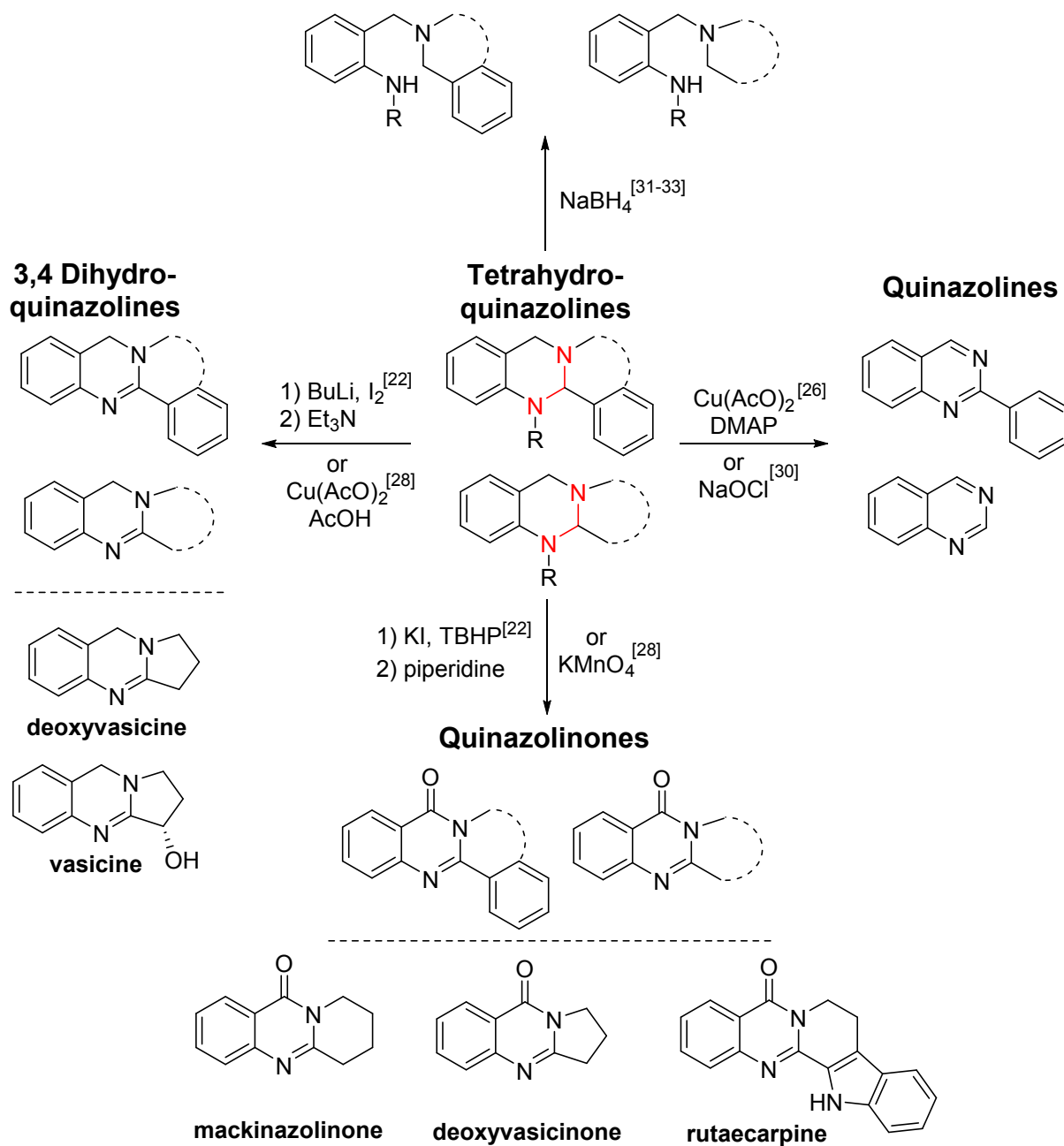
Scheme 2: Oxidation and reduction reactions of tetrahydroquinazolines. Dashed lines indicate either cyclized or non-cyclized compounds. The aminal structure is highlighted in red.

Although the chemistry of aminals - especially concerning tetrahydroquinazolines - is in the focus of current research and includes their preparation and modification, it is highly remarkable that there is only little focus on the pH-stability of these compounds in aqueous media. In general, the aminal moiety is known to undergo (similar to the corresponding O,O-acetal) acidic hydrolysis and can be considered as stable only within a certain pH range. This is of enormous importance especially for aminal bearing compounds which might be exposed to an acidic environment, e. g. drugs that are orally applied and get into direct contact with gastric acid. Also, the pH stability of the aminal system is a key property for synthetic approaches of such compounds to prevent undesired decomposition during reaction or workup. Knowledge about the pH-stability can therefore help to improve the yield during a reaction, or to prevent complete degradation of the product by applying inappropriate conditions. To our knowledge, there is only little data[34,35] describing the stability of the aminal moiety and no study conducted a systematic investigation. The conditions for stability of aminals - especially in tetrahydroquinazolines - are highly important because of the increasing relevance of such compounds in medicinal chemistry.

In the present study, we synthesized and modified tetrahydroquinazolines of the general structure **1** to investigate the pH stability of the aminal core in dependence of the steric and electronic properties of different groups at the 1-N and 3-N nitrogen atoms, as well as at the aromatic residue in position 2 (**Figure 2**). For that purpose, two residues were always kept constant while altering the third one. To investigate the effect of decreasing electron density at the nitrogen sites onto the stability of the aminal core, iPr, nPr, Me-, and Ph-moieties, respectively, were chosen as substituents for both the 1-N and 3-N nitrogen atoms. At the same time the iPr- and Ph-moieties served as bulkier substituents for investigations into steric effects. Similar to the 1-N and 3-N nitrogen atoms, 4-tBu, 4-Me-, 4-F- and 4-CF_3-groups were

incorporated into the aromatic site at position 2 to investigate the influence of decreasing electron density at this position. These substituents were chosen as their influence onto the aromatic residue is mainly determined by inductive effects and therefore no pronounced mesomeric effect has to be considered. In general, to estimate the electron donating effect of all substituents (and therefore the change in electron density at all sides), we used the data reported by Craig[36] for the aromatic side and the data reported by Topliss[37] for the side chains, respectively. Also a disubstituted 2,6-dichloro compound was synthesized to study the influence of steric interactions at this site of the structure, as 2,6-disubstitution of the phenyl ring prevents coplanar orientation.

R^2 = H R^3 = Me
R^1 = iPr, nPr, Me, Ph

R^2 = H R^1 = Me
R^3 = iPr, nPr, Me, Ph

R^1 = R^3 = Me
R^2 = 2,6-Cl, 4-CF_3, 4-F,
     H, 4-Me, 4-tBu
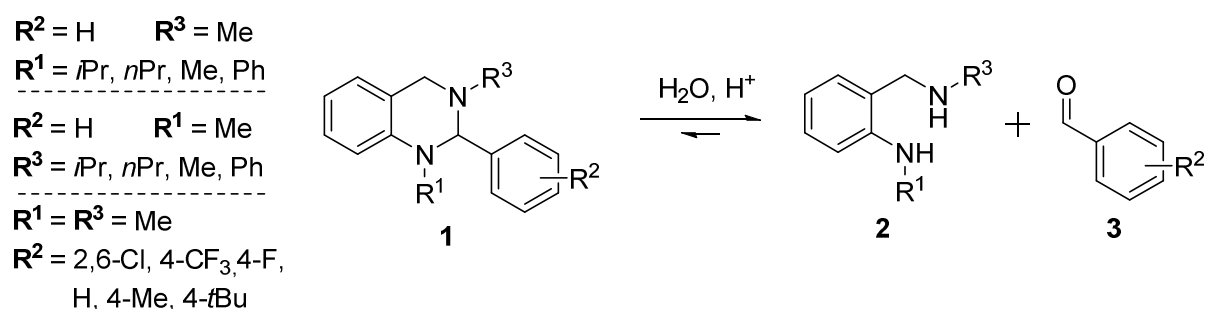
Figure 2: Hydrolysis of the aminal core of tetrahydroquinazolines **1** into the corresponding diamines **2** and aldehydes **3**.

All the compounds synthesized were exposed to aqueous media at defined pH values and time dependent hydrolysis into the corresponding diamines **2** and aldehydes **3** (**Figure 2**) was quantified by reversed phase HPLC. Based on these data, quantum mechanical calculations revealed that hydrolysis of the test compounds is a thermodynamically driven process. Interestingly, we could show that this equilibrium is strongly dependent on the applied reaction conditions and that a change from an acidic to a neutral environment can well induce the formation of tetrahydroquinazolines, instead of their hydrolysis. We also were able to determine

differences in the hydrolysis rate caused by the respective substituents and found the decrease in stability of these compounds to be a result of enthalpic effects.

Results and Discussion

Synthesis of test compounds

The synthesis of tetrahydroquinazolines substituted at the phenyl ring as well as at the 3-*N* nitrogen atom was achieved in 4 steps (**Scheme 3**). Briefly, isatoic anhydride was methylated using MeI to yield compound **4**, followed by formation of amides **5a-d** using the corresponding free amines or their salts. Cyclization towards dihydroquinazolinones **6a-f** and **7a-c** was performed using benzaldehyde derivatives under acidic conditions and gave moderate to excellent yields. Tetrahydroquinazoline target compounds **8a-f** and **9a-c** were finally obtained by reduction with LiAlH$_4$.

R^3 = Me	R^2 = H
8a: R^2 = H	**9a**: R^3 = *n*Pr
8b: R^2 = 4-*t*Bu	**9b**: R^3 = *i*Pr
8c: R^2 = 4-Me	**9c**: R^3 = Ph
8d: R^2 = 4-F	
8e: R^2 = 4-CF$_3$	
8f: R^2 = 2,6 Cl	

R^3 = Me	R^2 = H
6a: R^2 = H	**7a**: R^3 = *n*Pr
6b: R^2 = 4-*t*Bu	**7b**: R^3 = *i*Pr
6c: R^2 = 4-Me	**7c**: R^3 = Ph
6d: R^2 = 4-F	
6e: R^2 = 4-CF$_3$	
6f: R^2 = 2,6 Cl	

5a: R$_3$ = Me
5b: R$_3$ = Ph
5c: R$_3$ = *i*Pr
5d: R$_3$ = *n*Pr
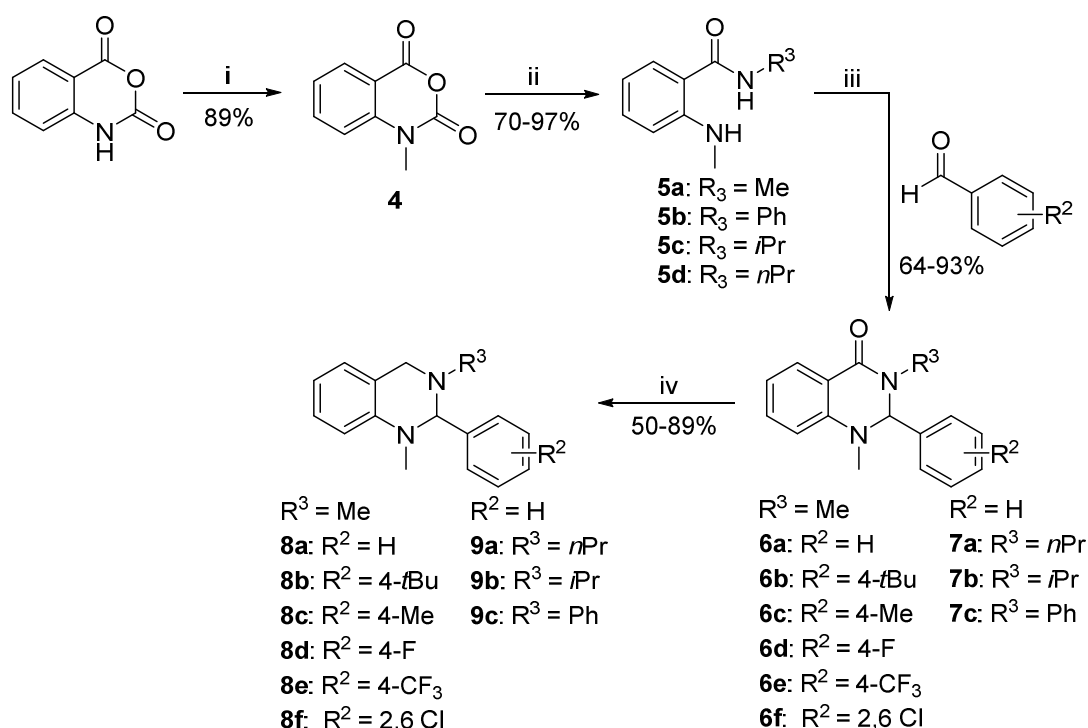
Scheme 3: Reagents and conditions: (i) MeI, DIPEA, DMAc, 40 °C, 24h; (ii) R^1-NH$_2$ or MeNH$_3$Cl and Et$_3$N, DMF, 40-120 °C, 3-6 h; (iii) AcOH, 70 °C, 1-4 h; (iv) LiAlH$_4$, THF, 70 °C, 1-3 h.

Synthesis of different substitution patterns at the 1-*N* nitrogen atom was achieved using two different pathways as shown in **Scheme 4**. Because direct alkylation of isatoic anhydride in the first reaction step with different alkyl halides failed (**Scheme 3**), amide **10** was synthesized using isatoic anhydride and methyl-ammonium hydrochloride (**Scheme 4a**) followed by cyclization under acidic conditions with benzaldehyde to yield dihydroquinazolinone **11**. Unfortunately, introduction of substituents at the *N*-1 in **11** by applying alkyl halides was only successful using *n*-PrBr and the strong non-nucleophilic base *t*BuOK to give compound **12a** and failed in the case of *i*-PrI. Target compound **13a** was then easily obtained through reduction with LiAlH₄. Since substitution reactions using **11** failed applying *i*-PrI, a second synthetic pathway was pursued to alter the substituents at the *N*-1 nitrogen atom of the tetrahydroquinazoline core (**Scheme 4b**). Anthranilic acid was alkylated by reductive amination with acetone and NaBH₄ in two steps to yield the *i*-Pr substituted derivative **14**. Derivative **14** and the commercially available *N*-phenyl anthranilic acid were used to yield amides **15a,b** under standard conditions and were then cyclized with benzaldehyde to yield dihydroquinazolinones **12b,c**. Tetrahydroquinazolines **13b,c** were finally obtained by reduction of **12b,c** with LiAlH₄ (**Scheme 4**).
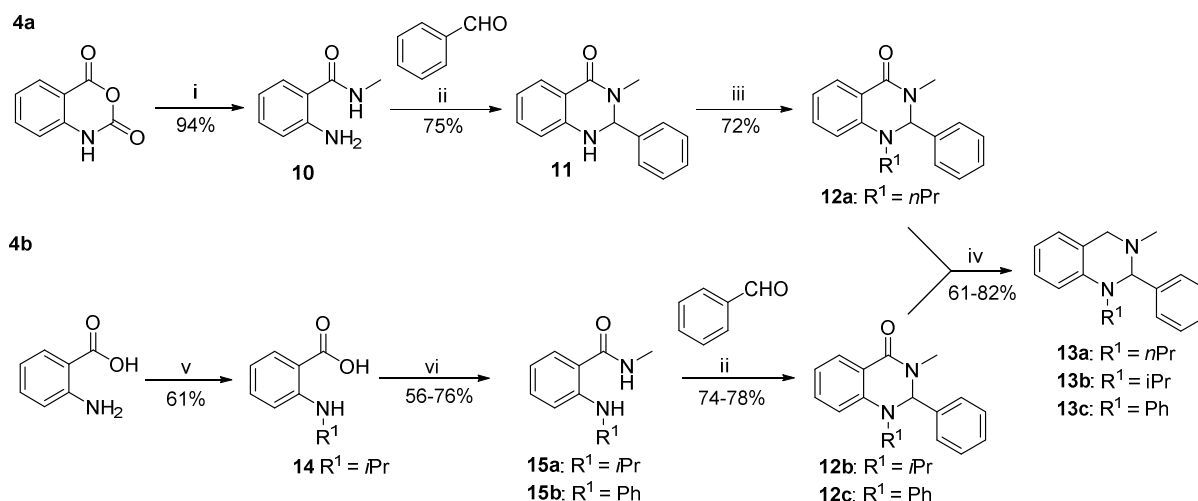
Scheme 4: Reagents and conditions: (4a) (i) MeNH$_3$Cl, Et$_3$N, DMF, 70 °C, 3 h; (ii) AcOH, 70 °C, 4 h; (iii) *n*PrBr, *t*BuOK, DMF, 110°C, 16 h; (iv) LiAlH$_4$, THF, 70 °C, 2-3 h; (4b) (v) 1) Acetone, MeOH, 80 °C, 5h; 2) NaBH$_4$, rt, 3 h; (vi) MeNH$_3$Cl, Et$_3$N, EDCI, HOBt, DMF, 70 °C, 8-14 h.

Stability experiments

All compounds synthesized were exposed to phosphate buffered aqueous systems with defined pH-values between pH = 2 and pH = 12 for 1 h to investigate hydrolysis of the aminal core. After hydrolysis, subsequent reversed phase HPLC analyses were performed to determine the ratio of intact tetrahydroquinazoline **1** and the corresponding aldehyde **3** as cleavage product using calibration curves (a detailed description is given in the Supporting Information). Results of this study are summarized in **Figure 3a-c**.

Compounds **8a-f** (**Figure 3a**) showed no differences in the extent of hydrolysis depending on their substitution pattern. However, a general trend for all of the test compounds was observed: Compounds **8a-f** are stable in a basic or neutral environment down to pH = 6 and only decomposed slowly at pH = 4-5 with less than 20% of hydrolysis after 1 h. Interestingly, at pH = 3 the aminal system is significantly hydrolysed by more than 50%, and at pH = 2 decomposition of the test compounds is

rapidly taking place resulting in complete degradation of the aminal system. These results clearly show a significant pH-dependency for hydrolysis of the aminal core which is accelerated in increasingly acidic media. Different substitution patterns at *N*-1 (**Figure 3b**) significantly alter the sensitivity of the aminal core towards hydrolysis. While a methyl group (compound **8a**) and a *n*Pr residue (compound **13a**) did not alter the hydrolysis rate compared to all compounds of the series **8** (**Figure 3a**), the *i*Pr-residue (**13b**) as well as the Ph-residue (**13c**) increased hydrolysis of the test compounds: The least stable compound **13b** (with the *i*Pr-group) was found to be completely hydrolyzed already at pH = 5 and also at pH = 6 more than 50% of **13b** decomposed. In contrast, compound **13c** (Ph-moiety) completely hydrolysed at pH = 4 and showed ~50% hydrolysis at pH = 5. Different substitution patterns at the *N*-3 position (**Figure 3c**) showed no pronounced differences for the pH-dependent decomposition between an *n*-Pr- (**9a**), a Me- (**8a**) and a Ph- (**9c**) group, respectively. Only the introduction of an *i*Pr residue (**9b**) at *N*-3 led to an increased hydrolysis rate with complete degradation of **9b** already at pH = 4. Finally, also 1,2-dihydroquinazolinone **6a** was tested for its stability towards hydrolysis (data not shown). This compound did not undergo any decomposition in the tested pH-range after 1 h.
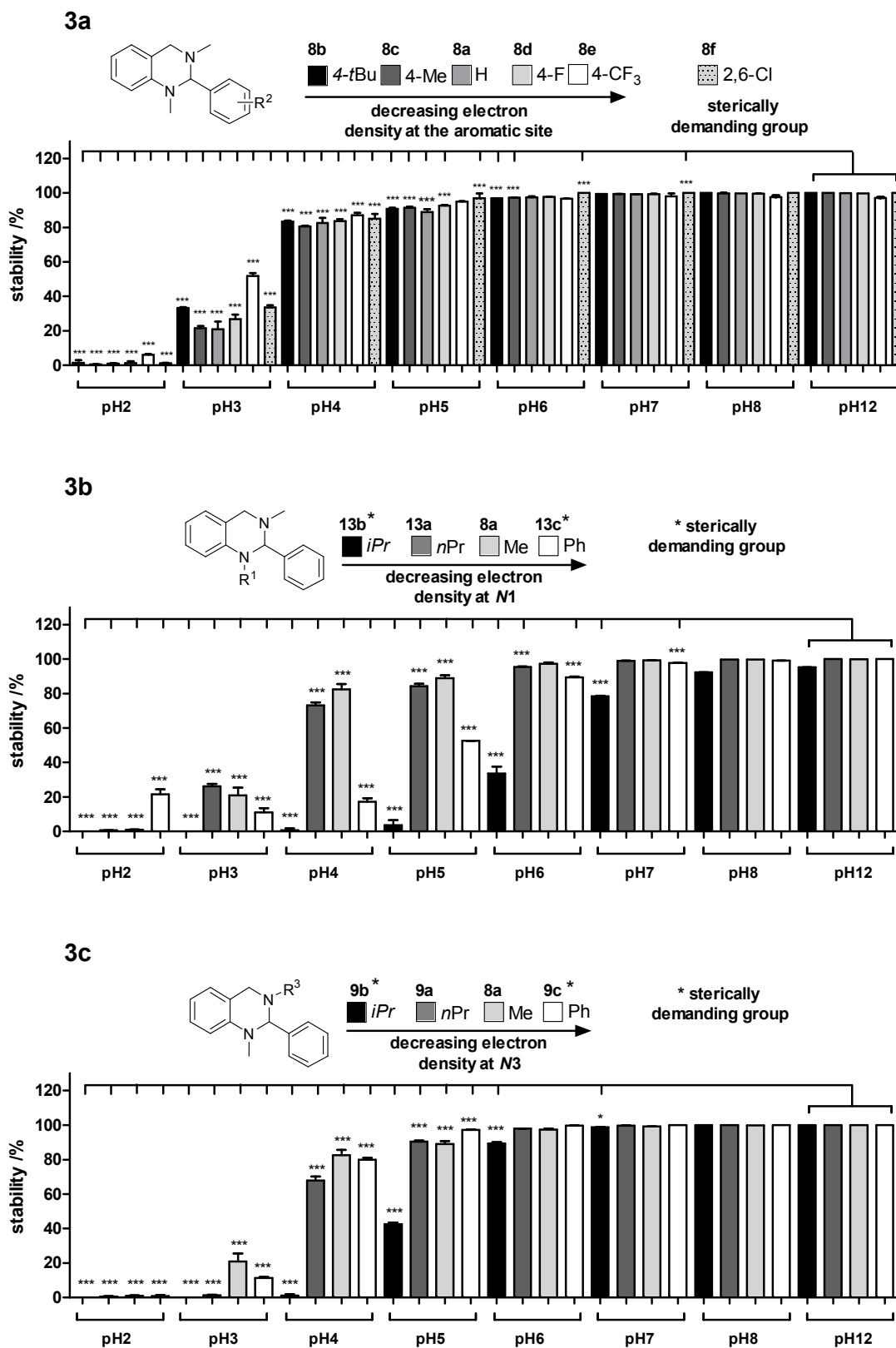
Figure 3: Stability test of the aminal core toward hydrolysis in dependency of different substitution pattern at (3a) the 2-phenyl residue, (3b) the *N*-1 position and (3c) the *N*-3 position. Each experiment was performed in triplicate (mean+SD).

Nevertheless, stability analyses shown in **Figure 3** have to be regarded as snapshots after 1 h of incubation time only. Therefore, the kinetics for this reaction were investigated in greater detail: Under the assumption that hydrolysis of tetrahydroquinazolines (**1**) into the corresponding diamines (**2**) and aldehydes (**3**) is a reversible reaction (*cf.* **Figure 2**), the velocity (v) of the reaction can be described in dependency of time (t) as:

$$v = \frac{d[\mathbf{1}]}{dt} = k_{-1} * [\mathbf{2}] * [\mathbf{3}] - k_1 * [\mathbf{1}] * [H_2O] \qquad \text{(eq. 1)}$$

Furthermore, 1) if the conversion of **2** and **3** into **1** is suppressed as $[H_2O] \gg [\mathbf{2}]$ and [**3**], the term $k_{-1}*[\mathbf{2}]*[\mathbf{3}]$ can be neglected and 2) if water is used as solvent and therefore remains approximately constant during the reaction, the constant $k_2 = k_1 *[H_2O]$ can be introduced. The velocity can then be described as a pseudo first-order kinetic:

$$v = \frac{d[\mathbf{1}]}{dt} = -k_2 * [\mathbf{1}] \qquad \text{(eq. 2)}$$

Finally, rearrangement and integration gives an exponential function from which k_2 can be calculated:

$$[\mathbf{1}] = [\mathbf{1}]_0 e^{-k_2 * t} \qquad \text{(eq. 3)}$$

Kinetic analysis of reference compound **8a** revealed exponential first order kinetic (**Figure 4**) from which k_2 was calculated.

The figure contains a kinetic plot (non-hydrolyzed compound [%] vs t [min]) with a data table:

pH	$k_2 \pm SEM$ [$min^{-1} * 10^{-3}$]	$t_{1/2}$ [min]
2	266.6 ± 10.0	2.6
3	23.9 ± 0.5	29.1
4	2.9 ± 0.03	240.8
5	1.2 ± 0.02	569.9
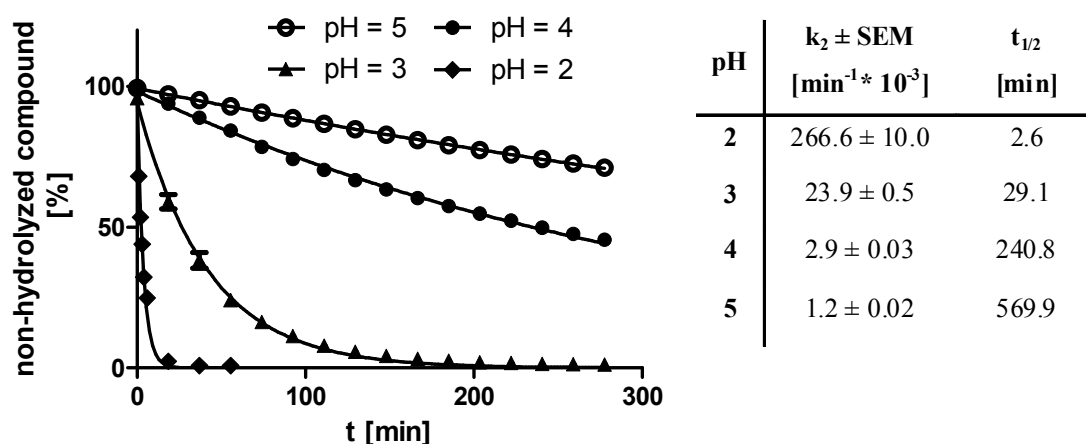
Figure 4: Kinetic analysis of hydrolysis of reference compound **8a** in dependency of different pH-values and calculation of kinetic parameters. Curves and k_2-values were calculated assuming a pseudo-first order kinetic as described in eq. 3. Each experiment was performed in triplicate (mean±SEM).

Interestingly, comparison of the kinetic parameter reveals a ~10fold increase of the k_2-value from pH = 4 to pH = 3 and also from pH = 3 to pH = 2 and therefore a 10fold increase in velocity of hydrolysis per pH unit. Only between pH = 5 and pH = 4 increase by a factor of 2 is observed. Furthermore, it is remarkable that the half life time of compound **8a** at pH = 2 is only 2.6 min and therefore complete hydrolysis of this compound is expected to occur within a couple of minutes.

Computational Studies and Discussion

With regard to the results obtained from the pH-dependent stability test, two factors for hydrolysis need to be investigated. First, the influence of an acidic or a basic environment for the hydrolysis has to be determined due to different hydrolysis rates at different pH-values; and second, the influence of different substitution patterns of

the test compounds should be verified regarding the altered sensitivity towards hydrolysis for some compounds (**9b** and **13b,c**).

Initially, we determined the protonation pattern of the test compounds, as protonation of the tetrahydroquinazoline system should most likely be an essential factor of hydrolysis induction. Theoretically, protonation might occur at the anilinic *N*-1, the aliphatic *N*-3 or by double protonation of *N*-1 and *N*-3. Therefore the pK_a-values of both nitrogens of the test compounds were predicted using the empirical algorithm of MoKa[38] (*cf.* Supporting Information) and validated with density functional theory (DFT) energy calculations of all protonation patterns for compounds **8a** and **13b** (*cf.* Supporting Information). We used the B3LYP-D3 functional[39-41] in combination with the cc-PVTZ basis sets[42,43]. All computations were performed with TURBOMOLE[44]. Solvent effects were mimicked by the Screening Model (COSMO) for water[45]. As expected, *N*-3 was determined to be more basic for all of the test compounds, with the exception of **9c**. Therefore, in the following text, only the molecular forms with protonation of the aliphatic nitrogen *N*-3 will be discussed.

To explore the influence of a basic or an acidic reaction environment on hydrolysis, QM single point energy calculations for the hydrolysis of compound **8a** and the least stable compound **13b** were performed, including the neutral (**8a** and **13b**) and the single protonated forms (**8a'** and **13b'**; -'- indicates *N*-3 protonation in the following) of all reactants and products (*cf.* Supporting Information). The computations include NH_4^+ as proton donor and one water molecule was taken into account for the stoichiometry of the reaction. Interestingly, plotting the data in water (**Figure 5**) as well as in the gas phase (*cf.* Supporting Information) for all relevant fragments revealed an exothermic reaction (-6.7 kcal/mol in water) for the hydrolysis of **8a'** (II in **Figure 5a**) into the protonated fragments (III in **Figure 5a**), while hydrolysis of the neutral form **8a** (I in **Figure 5a**) undergoes an endothermic reaction (3.1 kcal/mol in

water) into the neutral fragments (IV in **Figure 5a**). This indicates that the fragments show greater stability when protonated, while interestingly, the aminal structure is more stable when it is non-protonated. Therefore, protonation of this compound due to an acidic environment might well shift the equilibrium from the non-hydrolyzed compound in neutral media, into its fragments in acidic media (**Figure 5a**). This implies that formation of tetrahydroquinazolines from its fragments is thermodynamically favoured in a neutral or basic environment; and in fact, this is in agreement with data from literature reporting the synthesis of tetrahydroquinazolines to take place in organic solvent[25-27] as well as in non-acidic aqueous media [46]. Indeed, we tried the condensation of the respective diamine **16** and benzaldehyde towards compound **8a** in water as well as in acetonitrile as solvent. In both cases, complete condensation was observed toward compound **8a**. In addition, as larger amounts of benzaldehyde and diamine **16** in water are not soluble, also a mixture of water:acetonitrile (1:1) as solvent was used to dissolve all reactants and to exclude solubility effects on the condensation reaction in water (for details *cf.* Supporting Information). Interestingly, for the least stable compound **13b** (**Figure 5b**) exothermicity of the reaction of the protonated tetrahydroquinazoline (II in **Figure 5b**) into its fragments (III in **Figure 5b**) increased to -11 kcal/mol in aqueous medium, which might explain the increased hydrolysis rate of this compound in acidic media compared to compound **8a'**. In contrast to **8a**, the hydrolysis of the neutral tetrahydroquinazoline **13b** (I in **Figure 5b**) into its neutral fragments (IV in **Figure 5b**) is also exothermic (-4.9 kcal/mol in water), which indicates the hydrolysis of this compound to take place in acidic as well as in neutral environment. These observations are in agreement with the described stability experiments of compound **13b**, which was found to degrade also in neutral environment at pH = 7 (*cf.* **Figure 3b**). It should also be taken into account that calculations of charged

compounds in solutions are less accurate than corresponding calculations of neutral ones. Takano and Houk showed that the mean absolute deviation for single point energy calculations of charged molecules in a continuum solvent model is 3-5 kcal/mol, while 1-3 kcal/mol was computed for neutral ones[47]. Due to the fact that hydrolysis of tetrahydroquinazolines is an equilibrium reaction, the energy differences between the different states are within the range of 10 kcal/mol, which is close to the accuracy of the method for charged molecules. Therefore, the calculation results should be approached in a manner of showing a trend, rather than expecting exact values.
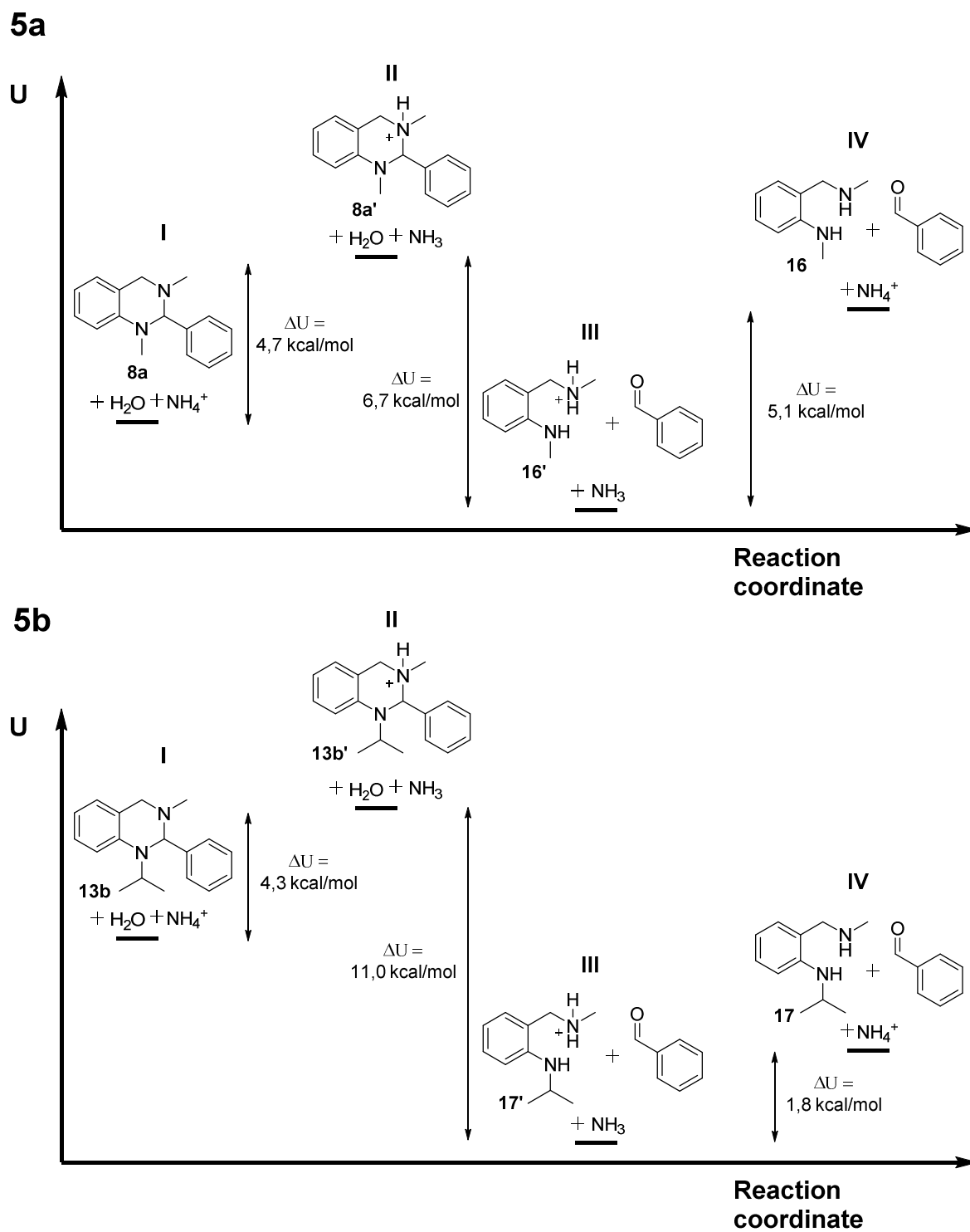
Figure 5. Differences in energy along the reaction coordinate using the functional B3LYP-D3 for the hydrolysis of (5a) compound **8a** and (5b) compound **13b** in water environment.

Taking this data together, it is predicted and experimentally proven, that basic reaction conditions shift the equilibrium towards the formation of tetrahydroquinazolines of the general structure **1** from the respective diamines and aldehydes, while acidic conditions promote hydrolysis of the protonated tetrahydroquinazolines **1'** (**Figure 6**). Therefore, compounds with an increased basicity, like these with a branched alkyl chain at the nitrogen (e.g. compound **9b**), are more sensitive towards hydrolysis due to their accelerated protonation which induces hydrolysis.
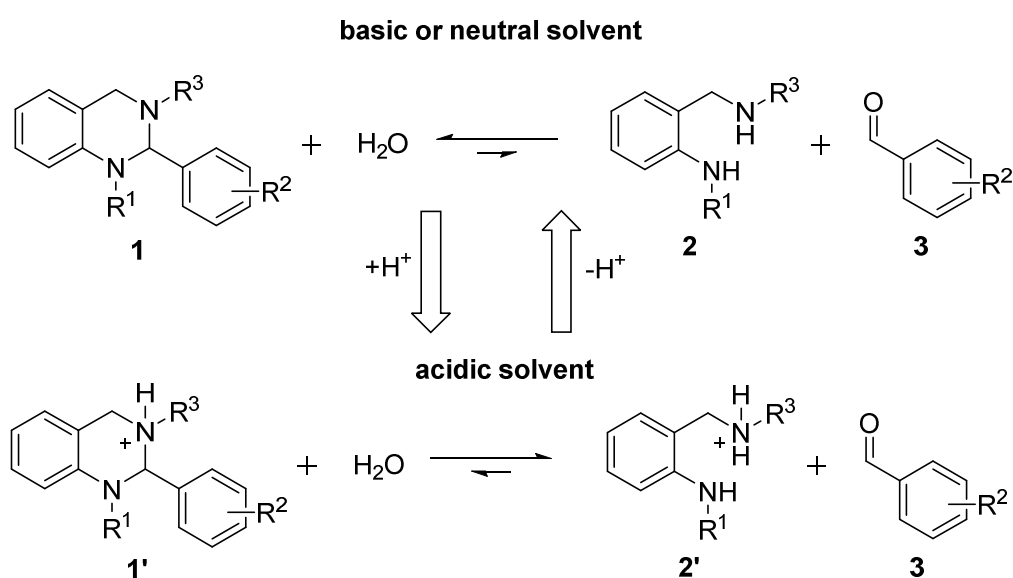
Figure 6: Reaction equilibrium between tetrahydroquinazoline **1**, the corresponding diamine **2** and aldehyde **3** in basic or neutral media as well as the protonated tetrahydroquinazoline **1'** and the corresponding diamine **2'** and aldehyde **3** in acidic media.

Considering the influence of different substitution patterns for an increased hydrolysis rate of some compounds (**9b** and **13b,c**), a systematic conformational search[48] for all compounds was performed to investigate possible differences in the minimum

energy conformation of both the neutral and the protonated forms. The conformational search revealed that the majority of all compounds (neutral form: **8a-c,e**, **9a**, **13a**-**c**; protonated form: **8a'-e'**, **9a'**, **13a'-c'**), shared the same minimum energy conformer in which the phenyl ring in position 2 and the *N*-3 side group are in anti-axial orientation (exemplarily shown for compound **8a** in **Figure 7a**) while the other compounds (neutral form: **8d,f**, **9b**,**c**; protonated form: **8f'**, **9b',c'**) adhere to a conformer of minimal energy where the residues are in equatorial position (exemplarily shown for compound **9b** in **Figure 7b**). Both conformations of minimum energy found in this study are in agreement with crystal structures reported in literature[46,49-52] (CCDC reference numbers for anti-axial motif: 177049[46], 717617[49],778079[50], 722943[51], 820149[52]; and for equatorial motif: 177050, 177052[46]).
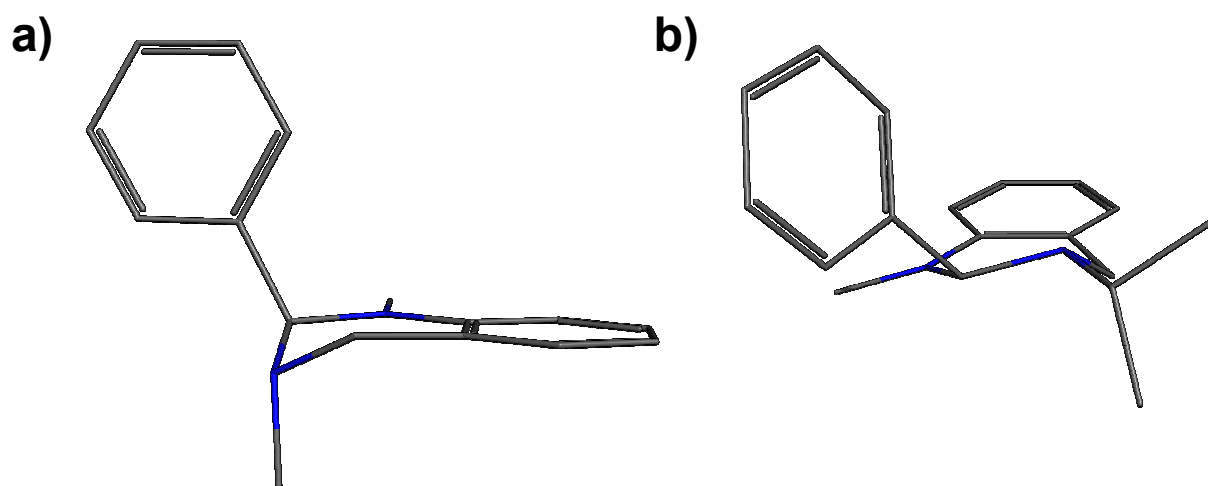
Figure 7: Minimum energy conformers in their neutral form with (7a) an axial orientation of the phenyl system exemplarily shown for compound **8a** and (7b) an equatorial orientation of the phenyl substituent exemplarily shown for **9b**.

Interestingly, the least stable compound **13b** and the significantly more stable compound **8e** were found to share the same anti-axial conformer in the neutral and in the *N*-3 protonated form. Furthermore, the 2,6-dichloro compound **8f** exhibits the same behaviour in terms of stability as the other compounds of the **8** series, even though it adheres to the equatorial minimum energy motif, both in the neutral and in the *N*-3 protonated form. In conclusion, comparison of the conformational search and the experimental data of the hydrolysis experiments proves no coherence between the decreased sensitivity on hydrolysis of **9b** and **13b,c** due to a different conformation of minimal energy; especially as **13b,c** and **13b',c'** are following anti-axial conformation, while **9b** and **9b'** are following equatorial conformation.

To further investigate the increased hydrolysis rates of **9b** and **13b,c**, respectively, energetic differences within the aminal system of these compounds were explored. The cyclic tetrahydroquinazoline system is higher in energy by its conformation in comparison to the non-cyclic diamines and bulky substituents, e.g. Ph- or *i*Pr-residues, might additionally increase the energy in this system (e.g. through strain), thus contributing to its enhanced sensitivity towards hydrolysis. Therefore, a comparison of the energy of the aminal core of the reference compound **8a** with compounds **9b** and **13b,c** was performed using Molecular Mechanics (MM). For this purpose, the conformer of minimal energy for compounds **9b** and **13b,c** was kept frozen, while the *N*-side groups were changed into a methyl residue. The resulting structures were therefore identical with compound **8a**, thus differences in potential energy are attributed to the conformational energy of the tetrahydroquinazoline core. This procedure was followed for all the aforementioned compounds in their neutral and the *N*-3 protonated form. The relative potential energy of the modified compounds (**13b_mod**, **13c_mod** and **9b_mod**) was higher in all cases compared to compound **8a** (**Table 1**) suggesting a correlation of increased conformational energy

of the ring system and increased sensitivity toward hydrolysis. This increase in energy might well be attributed to different geometrical effects including ring strain, strain of the angles or steric repulsion of the side groups. It might be possible that an increased ring-strain at the nitrogens of the tetrahydroquinazoline system could increase the basicity of these compounds and therefore accelerate the induction of hydrolysis, although previous studies showed that the relationship between the magnitude of ring strain and the resulting nitrogen basicity is not straightforward[53,54]. Probably more interesting, the hydrolysis of cyclic geminal ethers was recently reported to be drastically accelerated by introduction of sterically demanding side groups through reduction of the activation barrier [55]. These results are consistent with the herein reported data supporting a preferred elimination of the aldehyde fragment from the respective tetrahydroquinazoline in compounds with increased ring energy. Nevertheless, compound **13c_mod** was computed to be the least stable compound although compound **13b** was experimentally proven to be less stable. Therefore, we assume that additional enthalpic or entropic effects might also be involved in altering the stability of the ring system and an increase in ring energy might be only one part of the puzzle.

In addition, as a proof of concept, also the energy differences between **8a** and the modified compound **8b_mod** as well as the sterically more demanding compound **8f_mod** were calculated. As expected, in the case of **8b_mod** the difference to **8a** is negligible (ΔU < 1 kcal/mol). For the sterically more demanding compound **8f_mod** the energy difference of the protonated form is 1.61 kcal/mol, which is still a moderate value and places it well below compound **9b**. Obviously, an exact correlation of this simple measure with the hydrolytic instability is not to be expected, given the limitations of the molecular mechanical approach and the fact that the hydrolysis rate of the investigated aminal system is not only a function of increased

ring energy but also dependent on other thermodynamic factors, as mentioned above. Nevertheless, a clear trend can be recognized, indicating that the conformational energy of the ring system is at least an important if not the major contribution to the hydrolytic instability of the investigated systems.

Table 1: Calculated differences in potential energy (U) of the modified compounds compared to compound **8a** in water with MM. Differences were calculated by $\Delta U = U(\textbf{Cpd\_mod}) - U(\textbf{8a})$.

	ΔU [kcal/mol]				
	8b_mod	**8f_mod**	**9b_mod**	**13b_mod**	**13c_mod**
neutral	0.74	1.47	2.09	3.05	5.27
protonated	0.73	1.61	2.46	3.5	5.22

Conclusion

The aminal core is a common structural element in various medicinally relevant compounds and naturally occurring alkaloids. However, this system suffers from hydrolysis and therefore might decompose due to inappropriately applied reaction or workup conditions in synthesis, or when being exposed to an acidic environment, e.g. by gastric acid when administered orally.

To systematically investigate the hydrolysis of the aminal system with regard to pH-dependency, tetrahydroquinazolines **8a-f**, **9a-c** and **13a-c** were synthesized and exposed to buffered aqueous media with defined pH-values. A general trend was observed for all compounds with an accelerated hydrolysis rate as a function of decreasing pH value. Additional density functional calculations revealed that protonation of the *N*-3 nitrogen can induce hydrolysis into the corresponding

fragments. Therefore, compounds with a higher pK_a-value at the N-3 nitrogen might increase the hydrolysis sensitivity of these compounds due to their faster protonation, like for compound **9b**. Computational studies as well as experimental data revealed that the formation of tetrahydroquinazolines is favored when exposing their fragments (diamine and aldehyde) to an environment where no protonation occurs (mostly due to a basic environment) and therefore the reaction equilibrium can be shifted to one or the other site by protonating or deprotonating the relevant reactants. Furthermore, different substitution patterns in position 2 (series **8**) of the aromatic system, did not affect the stability because of changes in electron density (**8a-e**) or bulkiness (**8f**) of substituents.

Interestingly, hydrolysis experiments revealed an accelerated decomposition for compounds **9b** and **13b,c**. To investigate these findings, minimum conformational energy calculations were conducted. We found that all compounds adhere to two groups of conformers in accordance with crystal structures reported in literature. Changing the minimum energy conformers of **9b** and **13b,c** into the reference structure **8a** revealed an increase in ring-energy which might accelerate their hydrolysis. However, additional entropic and enthalpic effects may influence stability of such compounds that should be investigated in further studies.

Supporting Information

Detailed synthetic procedures, spectral data, stability analyses and computational investigations.

Acknowledgements (optional)

References

[1] Kim, J. T.; Gevorgyan, V. *Org. Lett.*, **2002**, *4*, 4697-4699.

[2] Bosque, I.; Gonzalez-Gomez, J. C.; Loza, M. I.; Brea, J. *J. Org. Chem.*, **2014**, *79*, 3982-3991.

[3] Scholl, M.; Trnka, T. M.; Morgan, J. P.; Grubbs, R. H. *Tetrahedron Lett.*, **1999**, *40*, 2247-2250.

[4] Sharma, V.; Khan, M. S. Y. *Eur. J. Med. Chem.*, **2001**, *36*, 651-658.

[5] Caterina, M. C.; Perillo, I. A.; Boiani, L.; Pezaroglo, H.; Cerecetto, H.; González, M.; Salerno, A. *Bioorg. Med. Chem.*, **2008**, *16*, 2226-2234.

[6] Veale, E. B.; Frimannsson, D. O.; Lawler, M.; Gunnlaugsson, T. *Org. Lett.*, **2009**, *11*, 4040-4043.

[7] Baldeyrou, B.; Tardy, C.; Bailly, C.; Colson, P.; Houssier, C.; Charmantray, F. *Eur. J. Med. Chem.*, **2002**, *37*, 315-322.

[8] Johnson, R. A.; Gorman, R. R.; Wnuk, R. J.; Crittenden, N. J.; Aiken, J. W. *J. Med. Chem.*, **1993**, 36, 3202-3206.

[9] Goswami, S.; Ghosh, K.; Dasgupta, S. *J. Org. Chem.*, **2000**, *65*, 1907-1914.

[10] Wu, H.; Chen, X.; Wan, Y.; Ye, L.; Xin, H.; Xu, H.; Yue, C.; Pang, L.; Ma, R.; Shi, D. *Tetrahedron Lett.*, **2009**, *50*, 1062-1065.

[11] Harmata, M.; Kahraman, M. *Tetrahedron: Asymmetry*, **2000**, *11*, 2875-2879.

[12] Pardo, C.; Sesmilo, E.; Gutiérrez-Puebla, E.; Monge, A.; Elguero, J.; Fruchier, A. *J. Org. Chem.*, **2001**, *66*, 1607-1611.

[13] Valik, M.; Dolenski, B.; Petrickova, H.; Vasek, P.; Kral, V. *Tetrahedron Lett.*, **2003**, *44*, 2083-2086.

[14] Paul, A.; Maji, B.; Misra, S. K.; Jain, A. K.; Muniyappa, K.; Bhattacharya, S. *J. Med. Chem.*, **2012**, *55*, 7460-7471.

[15] Huang, G.; Kling, B.; Darras, F. H.; Heilmann, J.; Decker, M. *Eur. J. Med. Chem.*, **2014**, *81*, 15-21.

[16] Darras, F. H.; Kling, B.; Heilmann J.; Decker, M. *ACS Med. Chem. Lett.*, **2012**, *3*, 914-919.

[17] Sawatzky, E.; Wehle, S.; Kling, B.; Wendrich, J.; Bringmann, G.; Sotriffer, C. A.; Heilmann, *J. Med. Chem.*, **2016**, *59*, 2067-2082.

[18] Kamal M. A.; Qu, X.; Yu, Q.-S.; Tweedie, D.; Holloway, H. W.; Li, Y.; Tan, Y.; Greig, N. H. *J. Neural Transm.*, **2008**, *115*, 889-898.

[19] Tasso, B.; Catto, M.; Nicolotti, O.; Novelli, F.; Tonelli, M.; Giangreco, I.; Pisani, L.; Sparatore, A.; Boido, V.; Carotti, A.; Sparatore, F. *Eur. J. Med. Chem.*, **2011**, *46*, 2170-2184.

[20] Khan, I.; Ibrar, A.; Abbas, N.; Saeed, A. *Eur. J. Med. Chem.*, **2014**, *76*, 193-244.

[21] Khan, I.; Ibrar, A.; Ahmed, W.; Saeed, A. *Eur. J. Med. Chem.*, **2015**, *90*, 124-169.

[22] Richers, M. T.; Deb, I.; Platonova, A. Y.; Zhang, C.; Seidel, D. *Synthesis*, **2013**, *45*, 1730-1748.

[23] Dieckmann, A.; Richers, M. T.; Platonova, A. Y.; Zhang, C.; Seidel, D.; Houk, K. N. *J. Org. Chem.*, **2013**, *78*, 4132-4144.

[24] Zhang, C.; De, C. K.; Mal, R. Seidel, D. *J. Am. Chem. Soc.*, **2008**, *130*, 416-417.

[25] Sinkkonen, J.; Zelenin, K. N.; Potapov, A.-K. A.; Lagoda, I. V.; Alekseyev, V. V.; Pihlaja, K. *Tetrahedron*, **2003**, *59*, 1939-1950.

[26] Fan, X.; Li, B.; Guo, S.; Wang, Y.; Zhang, X. *Chem. Asian J.*, **2014**, *9*, 739-743.

[27] Schiedler, D. A.; Vellucci, J. K.; Beaudry, C. M. *Org. Lett.*, **2012**, *14*, 6092-6095.

[28] Richers, M. T.; Zhao, C.; Seidel, D. *Beilstein J. Org. Chem.*, **2013**, *9,* 1194-1201.

[29] Han, B.; Yang, X.-L.; Wang, C.; Bai, Y.-W.; Pan, T.-C.; Chen, X.; Yu, W. *J. Org. Chem.*, **2012**, *77*, 1136-1142.

[30] Maheswari, C. U.; Kumar, G. S.; Venkateshwar, M.; Kumar, R. A.; Kantam, M. L.; Reddy, K. R. *Adv. Synth. Catal.*, **2010**, *352*, 341-346.

[31] Mercan, D.; Çetinkaya, E.; Sahin, E. *Inorg. Chim. Acta*, **2013**, *400*, 74-81.

[32] Sawatzky, E.; Bukowczan, J.; Decker, M. *Tetrahedron Lett.*, **2014**, *55*, 2973-2976.

[33] Aga, M. A.; Kumar, B.; Rouf, A.; Shah, B. A.; Andotra, S. S.; Taneja, S. C. *Helv. Chim. Acta*, **2013**, *96*, 969-977.

[34] Greenberg, A.; Molinaro, N.; Lang, M. *J. Org. Chem.*, **1984**, *49*, 1127-1130.

[35] Taylor, P. D. *Talanta*, **1995**, *42*, 243-248.

[36] Craig, P. N. *J. Med. Chem.*, **1971**, *14*, 680-684.

[37] Topliss, J. G. *J. Med. Chem.*, **1972**, *15*, 1006-1011

[38] Milletti, F.; Storchi, L.; Sforna, G.; Cruciani, G. *J. Chem. Inf. Model.*, **2007**, *47*, 2172-2181.

[39] Becke, A. D. *J. Chem. Phys.*, **1993**, *98*, 5648.

[40] Lee, C.; Yang, W.; Parr, R. G. *Phys. Rev. B*, **1988**, *37*, 785-789.

[41] Grimme, S.; Antony, J.; Ehrlich, S.; Krieg, H. *J. Chem. Phys.*, **2010**, *132*, 154104.

[42] Kendall, R. A.; Dunning, T. H.; Harrison, R. J. *J. Chem. Phys.,* **1992**, *96*, 6796.

[43] Schäfer, A.; Huber, C.; Ahlrichs, R. *J. Chem. Phys.,* **1994**, *100*, 5829.

[44] TURBOMOLE V6.2 2010, a development of University of Karlsruhe and Forschungszentrum Karlsruhe GmbH, 1989-2007, TURBOMOLE GmbH, since 2007; available from http://www.turbomole.com.

[45] Klamt, A.; Schüürmann, G. *J. Chem. Soc., Perkin Trans.,* **1993**, *2*, 799–805.

[46] Correa, W. H.; Papadopoulos, S.; Radnidge, P.; Roberts, B. A.; Scott, J. L. *Green Chem.*, **2002**, *4*, 245-251.

[47] Takano, Y.; Houk, K. N. *J. Chem. Theory Comput.*, **2005**, *1*, 70-77.

[48] Goodman, J. M.; Still, W. C. *J. Comput. Chem.*, **1991**, *12*, 1110-1117.

[49] Mori, K.; Ohshima, Y.; Ehara, K.; Akiyama, T. *Chem. Lett.*, **2009**, *38*, 524-525.

[50] Wang, Z.-G.; Xia, Z.-L.; Wang, R.; Wang, M.-L. *Acta Crystallogr. Sect. E. Struct. Rep. Online*, **2010**, *66*, o1205-o1206.

[51] Wang, Z.-G.; Wang, R.; Zhang, Y.; Zhi, F.; Yang, Y.-L. *Acta Crystallogr. Sect. E. Struct. Rep. Online*, **2009**, *65*, o550.

[52] Wang, Z.-G.; Wang, R.; Zhi, F.; Wang, M.-L. *Acta Crystallogr. Sect. E. Struct. Rep. Online*, **2011**, *67*, o808–o809.

[53] Ohwada, T.; Hirao, H.; Ogawa, A. *J. Org. Chem.*, **2004**, *69*, 7486-7494.

[54] Radić, N.; Despotović, I.; Vianello, R. *Croat. Chem. Acta*, **2012**, *85*, 495-504.

[55] Repetto, S. L.; Costello, J. F.; Butts, C. P.; Lam, J. K. W.; Ratcliffe, N. M. *Beilstein J. Org. Chem.*, **2016**, *12*, 1467-1475.

Experimental and Theoretical Investigations into the Stability of Cyclic Aminals

Edgar Sawatzky[1], Antonios Drakopoulos[1], Martin Rölz[1], Christoph Sotriffer[1], Bernd Engels[2], Michael Decker[1*]

[1]Institute of Pharmacy and Food Chemistry, Julius Maximilian University Würzburg, Am Hubland, D-97074 Würzburg, Germany.

[2]Institute for Physical und Theoretical Chemistry, Julius Maximilian University Würzburg, Emil-Fischer-Straße 42, D-97074 Würzburg, Germany.

Contents:

Experimental Section

Chemistry

General

Common reagents and solvents were obtained from commercial suppliers and used without any further purification. Tetrahydrofurane (THF) was distilled from sodium/benzophenone under argon atmosphere. Reaction progress was monitored using analytical thin layer chromatography (TLC) on precoated silica gel GF254 plates (Macherey-Nagel GmbH & Co. KG, Düren, Germany) and spots were detected under UV light (254 nm) or by staining with iodine. Nuclear magnetic resonance spectra were performed with a Bruker AV-400 NMR instrument (Bruker, Karlsruhe, Germany) in DMSO-d6 or CDCl3. Chemical shifts are expressed in ppm relative to CDCl3 or DMSO-d6 (7.26/2.50 and 77.16/39.52 ppm for ^{1}H and ^{13}C NMR, respectively). Melting points were determined in open capillaries on a Büchi B-540 without any further correction. For purity and reaction analyzes, analytic HPLC-analysis was performed on a system from Shimadzu equipped with a DGU-20A3R controller, LC20AB liquid chromatograph, and a SPD-20A UV/Vis detector. Stationary phase was a Synergi 4U fusion-RP (150 x 4.6 mm) column (Phenomenex, Aschaffenburg, Germany). As mobile phase, water (phase A) and MeOH (phase B) were used with 1 mL/min. (conc. B: 5% → 90% from 0 to 8 min; 90% from 8 to 13 min; 90% → 5% from 13 to 15 min; 5% from 15 to 18 min.) ESI mass spectral data were acquired on a Shimadzu LCMS-2020.

General Reaction Procedures

General Amide Formation Procedure (GP1): Isatoic anhydride derivatives were dissolved in dry DMF (30 mL) and treated with the corresponding amine (5 equiv) or a mixture of the amine hydrochloride (5 equiv) and triethylamine (5 equiv). The mixture was heated to 40-120 °C (depending on the amine) for 3-6 h. For workup, the mixture was poured into water (100 mL) and the product was extracted with EtOAc (5 x 100 mL). The combined organic layers were washed with brine (50 mL), dried over Na_2SO_4 and evaporated to dryness. The crude product was purified by column chromatography to obtain benzamide derivatives.

General Cyclization Procedure (GP2): Benzamide derivatives were dissolved in glacial acetic acid (20 mL). The mixture was treated with the corresponding aldehyde (1.2 equiv) and

heated to 70 °C for 1-4 h. Then the mixture was poured onto ice water (20 mL), basified with a NaOH-solution (2 M) and the pH was adjusted to 9 with sat. NH_4Cl-solution. The product was extracted with EtOAc (3 x 40 mL), the combined organic layers were washed with brine (30 mL), dried over Na_2SO_4 and the solvent was evaporated under reduced pressure. The crude product was either crystallized or purified by column chromatography to obtain dihydroquinazolinones.

General Reduction Procedure (GP3): Dihydroquinazolinones were dissolved in dry THF (30 mL) at 0 °C and $LiAlH_4$ (4 equiv) was added. The mixture was allowed to reach rt and was then heated to reflux temperature for 1-3 h. After cooling to rt, the mixture was poured into ice water (50 mL) followed by the addition of saturated NH_4Cl-solution until pH = 9. The aqueous phase was then extracted with EtOAc (3 x 80 mL). The combined organic layers were washed with brine (50 mL), dried over Na_2SO_4 and the solvent was evaporated under reduced pressure. The crude product was purified by column chromatography to obtain the corresponding tetrahydroquinazolines.

Synthesis and Experimental Data

1-Methyl-2*H*-benzo[*d*][1,3]oxazine-2,4(1*H*)-dione **4**: A solution of isatoic anhydride (7.60 g, 46.6 mmol, 1 equiv) in DMAc (100 mL) was treated with DIPEA (16.0 mL, 93.2 mmol, 2 equiv) and methyl iodide (11.6 mL, 186 mmol, 4 equiv). After stirring for 24 h at 40 °C, ice-cold water (100 mL) was added. The formed suspension was stirred for further 40 min. The precipitated solid was filtered off, washed with water (2 x 15 mL), cyclohexane (3 x 15 mL), and dried in vacuo to obtain 1-methyl-2*H*-benzo[*d*][1,3]oxazine-2,4(1*H*)-dione **4** (7.35 g, 89%) as yellow-brown solid; **mp** 174-177 °C. **^{1}H NMR** (DMSO-d$_6$, 400 MHz): δ = 8.01 (dd, *J* = 7.8, 1.4 Hz, 1H), 7.88 - 7.84 (m, 1H), 7.44 (d, *J* = 8.4 Hz, 1H), 7.36 - 7.32 (m, 1H), 3.47 (s, 3H) ppm. **^{13}C NMR** (DMSO-d$_6$, 101 MHz): δ = 159.0, 147.7, 142.2, 137.1, 129.3, 123.5, 114.8, 111.5, 31.6 ppm.

N-Methyl-2-(methylamino)benzamide **5a**: According to GP1, 1-methyl-2*H*-benzo[*d*][1,3]oxazine-2,4(1*H*)-dione **4** (1.50 g, 8.47 mmol, 1 equiv), methylamine hydrochloride (2.86 g, 42.3 mmol, 5 equiv) and triethylamine (5.86 mL, 42.3 mmol, 5 equiv)

were used to obtain *N*-methyl-2-(methylamino)benzamide **5a** (1.28 g, 92%) after column chromatography (petroleum ether:EtOAc = 1:1) as yellow oil; **^{1}H NMR** (CDCl$_3$, 400 MHz): δ = 7.41 (br, NH), 7.31 - 7.27 (m, 2H), 6.65 - 6.63 (d, *J* = 8.1 Hz, 1H), 6.57 - 6.52 (m, 1H), 6.04 (br, NH), 2.92 (d, *J* = 4.8 Hz, 3H), 2.83 (s, 3H) ppm. **^{13}C NMR** (CDCl$_3$, 101 MHz): δ = 170.8, 150.6, 132.9, 127.3, 115.5, 114.7, 111.3, 29.9, 26.7 ppm.

2-(Methylamino)-*N*-phenylbenzamide   **5b**:   According   to   GP1,   1-methyl-2*H*-benzo[*d*][1,3]oxazine-2,4(1*H*)-dione **4** (700 mg, 3.95 mmol, 1 equiv), and aniline (1.80 mL, 19.8 mmol, 5 equiv) were used to obtain 2-(methylamino)-*N*-phenylbenzamide **5b** (625 mg, 70%) after column chromatography (petroleum ether:EtOAc = 2:1) as pale red solid; **mp** 125-127 °C. **^{1}H NMR** (DMSO-d$_6$, 400 MHz): δ = 10.05 (s, NH), 7.72 - 7.70 (m, 2H), 7.67 (dd, *J* = 7.8, 1.3 Hz, 1H), 7.37 - 7.29 (m, 3H+NH), 7.10 - 7.06 (m, 1H), 6.68 (d, *J* = 7.4 Hz, 1H), 6.64 (t, *J* = 7.7 Hz, 1H), 2.80 (d, *J* = 5.0 Hz, 3H) ppm. **^{13}C NMR** (DMSO-d$_6$, 101 MHz): δ = 168.0, 150.0, 139.1, 132.7, 128.8, 128.4 (2C), 123.4, 120.6 (2C), 115.7, 114.0, 110.6, 29.4 ppm.

N-Isopropyl-2-(methylamino)benzamide   **5c**:   According   to   GP1,   1-methyl-2*H*-benzo[*d*][1,3]oxazine-2,4(1*H*)-dione **4** (700 mg, 3.95 mmol, 1 equiv) and *i*-propylamine (1.69 mL, 19.8 mmol, 5 equiv) were used to obtain *N*-isopropyl-2- (methylamino)benzamide **5c** (682 mg, 90%) after column chromatography (petroleum ether:EtOAc = 2:1) as white solid; **mp** 119-121 °C. **^{1}H NMR** (DMSO-d$_6$, 400 MHz): δ = 8.00 (d, *J* = 7.6 Hz, NH), 7.57 (q, *J* = 4.9 Hz, NH), 7.51 (dd, *J* = 7.8, 1.6 Hz, 1H), 7.28 - 7.25 (m, 1H), 6.60 (dd, *J* = 8.4, 0.8 Hz, 1H), 6.56 - 6.52 (m, 1H), 4.12 - 4.00 (m, 1H), 2.76 (d, *J* = 5.1 Hz, 3H), 1.14 (d, *J* = 6.6 Hz, 6H) ppm. **^{13}C NMR** (DMSO-d$_6$, 101 MHz): δ = 168.2, 149.9, 132.0, 128.3, 115.6, 113.8, 110.3, 40.4, 29.2, 22.3 (2C) ppm.

2-(Methylamino)-*N*-propylbenzamide   **5d**:   According   to   GP1,   1-methyl-2H-benzo[*d*][1,3]oxazine-2,4(1*H*)-dione **4** (700 mg, 3.95 mmol, 1 equiv) and *n*-propylamine (973 μL, 11.9 mmol, 3 equiv) were used to obtain 2-(methylamino)-*N*-propylbenzamide **5d** (759 mg, 97%) after column chromatography (petroleum ether:EtOAc = 1:2) as pale yellow solid; **mp** 57-59 °C. **^{1}H NMR** (CDCl$_3$, 400 MHz): δ = 7.40 (br, NH), 7.31 - 7.29 (m, 1H), 7.29 - 7.27 (m, 1H), 6.64 (dd, *J* = 8.6, 0.7 Hz, 1H), 6.58 - 6.54 (m, 1H), 6.01 (br, NH), 3.37 - 3.32 (m, 2H), 2.83 (d, *J* = 4.8 Hz, 3H), 1.60 (sextet, *J* = 7.2 Hz, 2H), 0.96 (t, *J* = 7.4 Hz, 3H)

ppm. ^{13}C NMR (CDCl$_3$, 101 MHz): δ = 170.1, 150.7, 132.9, 127.2, 115.7, 114.6, 111.3, 41.6, 29.9, 23.2, 11.7 ppm.

1,3-Dimethyl-2-phenyl-2,3-dihydroquinazolin-4(1*H*)-one **6a**: According to GP2, *N*-methyl-2-(methylamino)benzamide **5a** (565 mg, 3.44 mmol, 1 equiv) and benzaldehyde (417 µL, 4.13 mmol, 1.2equiv) were used to obtain 1,3-dimethyl-2-phenyl-2,3-dihydroquinazolin-4(1*H*)-one **6a** (628 mg, 73%) after column chromatography (petroleum ether:EtOAc = 2:1) as white solid; **mp** 139-142 °C. ^{1}H NMR (DMSO-d$_6$, 400 MHz): δ = 7.77 (dd, *J* = 7.6, 1.4 Hz, 1H), 7.37 - 7.34 (m, 1H), 7.33 - 7.31 (m, 3H), 7.23 - 7.18 (m, 2H), 6.78 (dt, *J* = 7.6, 0.8 Hz, 1H), 6.59 (d, *J* = 8.1 Hz, 1H), 5.78 (s, 1H), 2.88 (s, 3H), 2.80 (s, 3H) ppm. ^{13}C NMR (DMSO-d$_6$, 101 MHz): δ = 161.6, 146.2, 137.0, 133.7, 128.9, 128.7 (2C), 127.5, 126.0 (2C), 117.3, 115.7, 111.8, 78.3, 34.9, 31.8 ppm. **ESI-MS**: *m/z* calcd: 252.1, found: 253.1 [M+H]$^+$. **HPLC**: 98%.

2-(4-(*tert*-Butyl)phenyl)-1,3-dimethyl-2,3-dihydroquinazolin-4(1*H*)-one **6b**: According to GP2, *N*-methyl-2-(methylamino)benzamide **5a** (200 mg, 1.22 mmol, 1 equiv) and 4-(*tert*-butyl)benzaldehyde (245 µL, 1.45 mmol, 1.2equiv) were used to obtain 2-(4-(*tert*-butyl)phenyl)-1,3-dimethyl-2,3-dihydroquinazolin-4(1*H*)-one **6b** (329 mg, 88%) after column chromatography (petroleum ether:EtOAc = 3:1) as white solid; **mp** 126-129 °C. ^{1}H NMR (400 MHz, DMSO-d$_6$): δ = 7.76 (dd, *J* = 7.6, 1.6 Hz, 1H), 7.41 - 7.24 (m, 3H), 7.13 (d, *J* = 8.3 Hz, 2H), 6.78 (t, *J* = 7.1 Hz, 1H), 6.60 (d, *J* = 8.2 Hz, 1H), 5.75 (s, 1H), 2.88 (s, 3H), 2.81 (s, 3H), 1.23 (s, 9H) ppm. ^{13}C NMR (101 MHz, DMSO): δ = 162.1, 151.7, 146.8, 134.6, 134.2, 127.9, 126.3 (2C), 126.0 (2C), 117.8, 116.3, 112.4, 78.5, 35.5, 34.8, 32.4, 31.5 (3C) ppm.

1,3-Dimethyl-2-(*p*-tolyl)-2,3-dihydroquinazolin-4(1*H*)-one **6c**: According to GP2, *N*-methyl-2-(methylamino)benzamide **5a** (200 mg, 1.22 mmol, 1 equiv) and 4-methylbenzaldehyde (175 µL, 1.45 mmol, 1.2equiv) were used to obtain 1,3-dimethyl-2-(*p*-tolyl)-2,3-dihydroquinazolin-4(1*H*)-one **6c** (287 mg, 88%) after column chromatography (petroleum ether:EtOAc = 3:1) as white solid; **mp** 133-136 °C. ^{1}H NMR (400 MHz, DMSO-d$_6$): δ = 7.76 (dd, *J* = 7.6, 1.7 Hz, 1H), 7.37 - 7.28 (m, 1H), 7.16 - 7.05 (m, *J* = 8.0 Hz, 4H), 6.78 (t, *J* = 7.4 Hz, 1H), 6.58 (d, *J* = 8.2 Hz, 1H), 5.73 (s, 1H), 2.87 (s, 3H), 2.78 (s, 3H), 2.25 (s, 3H) ppm. ^{13}C NMR (101 MHz, DMSO-d$_6$): δ = 162.1, 146.7, 138.8, 134.5, 134.2, 129.8 (2C), 127.9, 126.5 (2C), 117.8, 116.2, 112.3, 78.7, 35.3, 32.3, 21.2 ppm.

2-(4-Fluorophenyl)-1,3-dimethyl-2,3-dihydroquinazolin-4(1*H*)-one **6d**: According to GP2, *N*-methyl-2-(methylamino)benzamide **5a** (200 mg, 1.22 mmol, 1 equiv) and 4-fluorobenzaldehyde (157 μL, 1.45 mmol, 1.2 equiv) were used to obtain 2-(4-fluorophenyl)-1,3-dimethyl-2,3-dihydroquinazolin-4(1*H*)-one **6d** (209 mg, 64%) after crystallization from a mixture of petroleum ether/DCM as white solid; **mp** 134-138 °C. ^{1}H NMR (400 MHz, DMSO-d$_6$): δ = 7.77 (dd, *J* = 7.6, 1.6 Hz, 1H), 7.36 (ddd, *J* = 8.3, 7.3, 1.7 Hz, 1H), 7.28 - 7.21 (m, 2H), 7.21 - 7.13 (m, 2H), 6.79 (td, *J* = 7.5, 0.9 Hz, 1H), 6.60 (d, *J* = 8.2 Hz, 1H), 5.81 (s, 1H), 2.87 (s, 3H), 2.79 (s, 3H) ppm. ^{13}C NMR (101 MHz, DMSO-d$_6$): δ = 162.8 (d, *J* = 244.9 Hz), 162.0, 146.6, 134.3, 133.8 (d, *J* = 3.1 Hz), 128.7 (d, *J* = 8.4 Hz, 2C), 128.0, 118.0, 116.1 (d, *J* = 21.6 Hz, 2C), 116.1, 112.5, 78.0, 35.3, 32.3 ppm.

1,3-Dimethyl-2-(4-(trifluoromethyl)phenyl)-2,3-dihydroquinazolin-4(1*H*)-one **6e**: According to GP2, *N*-methyl-2-(methylamino)benzamide **5a** (200 mg, 1.22 mmol, 1 equiv) and 4-(trifluoromethyl)benzaldehyde (200 μL, 1.46 mmol, 1.2 equiv) were used to obtain 1,3-dimethyl-2-(4-(trifluoromethyl)phenyl)-2,3-dihydroquinazolin-4(1*H*)-one **6e** (354 mg, 91%) after column chromatography (petroleum ether:EtOAc = 1:1) as white solid; **mp** 130-132 °C. ^{1}**H NMR** (CDCl$_3$, 400 MHz): δ = 8.01 - 7.99 (m, 1H), 7.54 (d, *J* = 8.1 Hz, 2H), 7.36 - 7.30 (m, 3H), 6.86 (dt, *J* = 7.6, 0.8 Hz, 1H), 6.48 (d, *J* = 8.3 Hz, 1H), 5.45 (s, 1H), 2.99 (s, 3H), 2.81 (s, 3H) ppm. ^{13}**C NMR** (CDCl$_3$, 101 MHz): δ = 162.6, 146.0, 140.9, 134.2, 131.7 (q, *J* = 32.8 Hz), 128.9, 126.9 (2C), 126.2 (q, *J* = 3.8 Hz, 2C), 124.0 (q, *J* = 273.2 Hz), 118.8, 116.3, 112.0, 80.5, 35.8, 32.7 ppm.

2-(2,6-Dichlorophenyl)-1,3-dimethyl-2,3-dihydroquinazolin-4(1*H*)-one **6f**: According to GP2, *N*-methyl-2-(methylamino)benzamide **5a** (400 mg, 2.44 mmol, 1 equiv) and 2,6-dichlorobenzaldehyde (512 mg, 2.93 mmol, 1.2 equiv) were used to obtain 2-(2,6-dichlorophenyl)-1,3-dimethyl-2,3-dihydroquinazolin-4(1H)-one **6f** (571 mg, 73%) after column chromatography (petroleum ether:EtOAc = 2:1) as white solid; **mp** 195-201 °C. ^{1}H NMR (400 MHz, CDCl$_3$): δ = 7.92 (dd, *J* = 7.7, 1.6 Hz, 1H), 7.32 - 7.28 (m, 2H), 7.26 (ddd, *J* = 8.4, 7.3, 1.7 Hz, 1H), 7.21 - 7.14 (m, 1H), 6.78 (s, 1H), 6.67 (td, *J* = 7.6, 0.9 Hz, 1H), 6.43 (d, *J* = 8.3 Hz, 1H), 2.72 (s, 3H), 2.62 (s, 3H) ppm. ^{13}C NMR (101 MHz, CDCl$_3$): δ = 161.9, 146.5, 136.1 (2C), 133.8, 132.3, 130.4, 128.3, 116.7, 113.6, 109.0, 76.0, 33.7, 30.7 ppm.

<u>1-Methyl-2-phenyl-3-propyl-2,3-dihydroquinazolin-4(1*H*)-one</u> **7a**: According to GP2, 2-(methylamino)-*N*-propylbenzamide **5d** (672 mg, 3.50 mmol, 1 equiv) and benzaldehyde (424 μL, 4.19 mmol, 1.2equiv) were used to obtain 1-methyl-2-phenyl-3-propyl-2,3-dihydroquinazolin-4(1*H*)-one **7a** (649 mg, 66%) after column chromatography (petroleum ether:EtOAc = 3:1) as white solid; **mp** 176-180 °C. **¹H NMR** (DMSO-d₆, 400 MHz): δ = 7.77 (dd, *J* = 7.6, 1.6 Hz, 1H), 7.35 - 7.29 (m, 4H), 7.25 - 7.21 (m, 2H), 6.79 (dt, *J* = 7.5, 0.9 Hz, 1H), 6.57 (d, *J* = 8.1 Hz, 1H), 5.78 (s, 1H), 3.79 - 3.72 (m, 1H), 2.82 (s, 3H), 2.79 - 2.72 (m, 1H), 1.67 - 1.54 (m, 1H), 1.54 - 1.41 (m, 1H), 0.84 (t, *J* = 7.4 Hz, 3H) ppm. **¹³C NMR** (DMSO-d₆, 101 MHz): δ = 161.3, 146.1, 137.7, 133.6, 128.8, 128.6 (2C), 127.5, 126.2 (2C), 117.5, 116.4, 112.1, 76.5, 45.9, 35.0, 20.5, 11.2 ppm.

<u>3-Isopropyl-1-methyl-2-phenyl-2,3-dihydroquinazolin-4(1*H*)-one</u> **7b**: According to GP2, *N*-isopropyl-2-(methylamino)benzamide **5c** (657 mg, 3.42 mmol, 1 equiv) and benzaldehyde (414 μL, 4.1 mmol, 1.2 equiv) were used to obtain 3-isopropyl-1-methyl-2-phenyl-2,3-dihydroquinazolin-4(1*H*)-one **7b** (820 mg, 86%) after column chromatography (petroleum ether:EtOAc = 2:1) as white solid; **mp** 153-155 °C. **¹H NMR** (DMSO-d₆, 400 MHz): δ = 7.96 (dd, *J* = 7.6, 1.5 Hz, 1H), 7.49 - 7.45 (m, 1H), 7.45 - 7.40 (m, 5H), 6.97 (dt, *J* = 7.5, 0.8 Hz, 1H), 6.67 (d, *J* = 8.0 Hz, 1H), 6.00 (s, 1H), 4.84 (septet, *J* = 6.9 Hz, 1H), 3.01 (s, 3H), 1.42 (d, *J* = 6.8 Hz, 3H), 1.03 (d, *J* = 6.9 Hz, 3H) ppm. **¹³C NMR** (DMSO-d₆, 101 MHz): δ = 161.1, 145.7, 138.8, 133.4, 128.4, 128.3 (2C), 127.5, 126.0 (2C), 117.8, 117.7, 112.5, 72.6, 45.2, 35.0, 20.12, 20.11 ppm.

<u>1-Methyl-2,3-diphenyl-2,3-dihydroquinazolin-4(1*H*)-one</u> **7c**: According to GP2, 2-(methylamino)-*N*-phenylbenzamide **5b** (604 mg, 2.67 mmol, 1 equiv) and benzaldehyde (324 μL, 3.20 mmol, 1.2 equiv) were used to obtain 1-methyl-2,3-diphenyl-2,3-dihydroquinazolin-4(1*H*)-one **7c** (772 mg, 93%) after column chromatography (petroleum ether:EtOAc = 3:1) as white solid; **mp** 138–142 °C. **¹H NMR** (DMSO-d₆, 400 MHz): δ = 7.85 (dd, *J* = 7.7, 1.6 Hz, 1H), 7.43 - 7.39 (m, 1H), 7.39 - 7.34 (m, 2H), 7.31 - 7.28 (m, 3H), 7.27 - 7.22 (m, 5H), 6.85 (dt, *J* = 7.6, 0.7 Hz, 1H), 6.67 (d, *J* = 8.0 Hz, 1H), 6.22 (s, 1H), 2.97 (s, 3H) ppm. **¹³C NMR** (DMSO-d₆, 101 MHz): δ = 161.2, 146.3, 140.5, 137.5, 134.2, 128.8 (2C), 128.7, 128.6 (2C), 128.1, 126.53 (2C), 126.48, 126.2 (2C), 117.9, 116.7, 112.8, 79.0, 35.5 ppm.

1,3-Dimethyl-2-phenyl-1,2,3,4-tetrahydroquinazoline **8a**: According to GP3, starting from 1,3-dimethyl-2-phenyl-2,3-dihydroquinazolin-4(1*H*)-one **6a** (250 mg, 0.99mmol, 1 equiv) the title compound 1,3-dimethyl-2-phenyl-1,2,3,4-tetrahydroquinazoline **8a** (208 mg, 89%) was obtained after column chromatography (petroleum ether:EtOAc = 2:1) as brown solid; **mp** 94-96 °C. **^{1}H NMR** (CDCl$_3$, 400 MHz): δ = 7.30 - 7.19 (m, 3H), 7.19 - 7.10 (m, 3H), 6.80 (d, J = 7.3 Hz, 1H), 6.61 - 6.55 (m, 2H), 4.79 (s, 1H), 3.71 (d, J = 16.0 Hz, 1H), 3.30 (d, J = 16.0 Hz, 1H), 2.88 (s, 3H), 2.44 (s, 3H) ppm. **^{13}C NMR** (CDCl$_3$, 101 MHz): δ = 143.8, 141.0, 128.6 (2C), 128.02, 127.95, 127.3 (3C), 118.2, 116.0, 109.0, 82.3, 49.5, 42.5, 36.9 ppm. **ESI-MS**: *m/z* calcd: 238.2, found: 239.1 [M+H]$^{+}$. **HPLC**: 99%.

2-(4-(*tert*-Butyl)phenyl)-1,3-dimethyl-1,2,3,4-tetrahydroquinazoline **8b**: According to GP3, starting from 2-(4-(*tert*-butyl)phenyl)-1,3-dimethyl-2,3-dihydroquinazolin-4(1*H*)-one **6b** (309 mg, 1.00 mmol, 1 equiv) the title compound 2-(4-(*tert*-butyl)phenyl)-1,3-dimethyl-1,2,3,4-tetrahydroquinazoline **8b** (222 mg, 75%) was obtained after column chromatography (petroleum ether:EtOAc = 4:1) as white solid; **mp** 96-99 °C. ^{1}H NMR (400 MHz, DMSO-d$_6$): δ= 7.41 - 7.34 (m, 2H), 7.20 - 7.07 (m, 3H), 6.87 (d, J = 6.5 Hz, 1H), 6.70 (d, J = 7.8 Hz, 1H), 6.59 (td, J = 7.3, 1.0 Hz, 1H), 4.98 (s, 1H), 3.60 (d, J = 16.1 Hz, 1H), 3.35 (d, J = 14.8 Hz, 1H), 2.96 (s, 3H), 2.44 (s, 3H), 1.30 (s, 9H) ppm.^{13}C NMR (101 MHz, DMSO-d$_6$): δ = 150.2, 144.0, 138.5, 128.1, 127.1, 126.9 (2C), 125.4 (2C), 118.0, 115.7, 109.2, 80.9, 49.1, 42.0, 37.0, 34.7, 31.6 (3C) ppm. **ESI-MS**: *m/z* calcd: 294.2, found: 295.1 [M+H]$^{+}$. **HPLC**: 100%.

1,3-Dimethyl-2-(*p*-tolyl)-1,2,3,4-tetrahydroquinazoline **8c**: According to GP3, starting from 1,3-dimethyl-2-(*p*-tolyl)-2,3-dihydroquinazolin-4(1*H*)-one **6c** (269 mg, 1.01 mmol, 1 equiv) the title compound 1,3-dimethyl-2-(*p*-tolyl)-1,2,3,4-tetrahydroquinazoline **8c** (203 mg, 80%) was obtained after column chromatography (petroleum ether:EtOAc = 4:1) as yellow solid; **mp** 34-36 °C. ^{1}H NMR (400 MHz, DMSO-d$_6$): δ = 7.15 - 7.06 (m, 3H), 7.05 - 7.00 (m, J = 8.0 Hz, 2H), 6.82 (d, J = 7.1 Hz, 1H), 6.65 (d, J = 7.9 Hz, 1H), 6.54 (td, J = 7.3, 1.0 Hz, 1H), 4.91 (s, 1H), 3.55 (d, J = 16.0 Hz, 1H), 3.31 (d, J = 16.3 Hz, 1H), 2.88 (s, 3H), 2.37 (s, 3H), 2.26 (s, 3H) ppm.^{13}C NMR (101 MHz, DMSO-d$_6$): δ = 144.0, 138.4, 137.1, 129.2 (2C), 128.1, 127.2 (2C), 127.1, 118.1, 115.7, 109.2, 81.0, 49.1, 42.0, 36.8, 21.1 ppm. **ESI-MS**: *m/z* calcd: 252.2, found: 253.1 [M+H]$^{+}$. **HPLC**: 99%.

2-(4-Fluorophenyl)-1,3-dimethyl-1,2,3,4-tetrahydroquinazoline **8d**: According to GP3, starting from 2-(4-fluorophenyl)-1,3-dimethyl-2,3-dihydroquinazolin-4(1*H*)-one **8c** (200 mg, 0.74 mmol, 1 equiv) the title compound 2-(4-fluorophenyl)-1,3-dimethyl-1,2,3,4-tetrahydroquinazoline **8d** (94 mg, 50%) was obtained after column chromatography (petroleum ether:EtOAc = 2:1) as yellow oil; ^{1}H NMR (400 MHz, DMSO-d_6): δ = 7.21 - 7.03 (m, 5H), 6.84 (d, *J* = 7.2 Hz, 1H), 6.67 (d, *J* = 8.1 Hz, 1H), 6.56 (td, *J* = 7.3, 1.0 Hz, 1H), 4.98 (s, 1H), 3.53 (d, *J* = 16.2 Hz, 1H), 3.33 (d, *J* = 12.3 Hz, 1H), 2.91 (s, 3H), 2.38 (s, 3H) ppm.^{13}C NMR (101 MHz, DMSO-d_6): δ = 161.9 (d, *J* = 243.1 Hz), 143.7, 137.6 (d, *J* = 2.9 Hz), 129.2 (d, *J* = 8.2 Hz, 2C), 128.1, 127.2, 118.0, 115.5 (d, *J* = 21.3 Hz, 2C), 115.4, 109.3, 80.4, 48.9, 42.0, 36.9 ppm. **ESI-MS**: *m/z* calcd: 256.1, found: 257.1 [M+H]$^+$. **HPLC**: 96%.

1,3-Dimethyl-2-(4-(trifluoromethyl)phenyl)-1,2,3,4-tetrahydroquinazoline **8e**: According to GP3, starting from 1,3-dimethyl-2-(4-(trifluoromethyl)phenyl)-2,3-dihydroquinazolin-4(1*H*)-one **6e** (337 mg, 1.05 mmol, 1 equiv) the title compound 1,3-dimethyl-2-(4-(trifluoromethyl)phenyl)-1,2,3,4-tetrahydroquinazoline **8e** (224 mg, 70%) was obtained after column chromatography (petroleum ether:EtOAc = 4:1) as clear oil; **^{1}H NMR** (CDCl$_3$, 400 MHz): δ = 7.53 , (d, *J* = 8.1 Hz, 2H), 7.35 - 7.33 (m, 2H), 7.19 (m, 1H), 6.88 - 6.86 (m, 1H), 6.68 (d, *J* = 8.2 Hz, 1H), 6.66 (dt, *J* = 7.3, 1.0 Hz, 1H), 4.88 (s, 1H), 3.70 (d, 16.2 Hz, 1H), 3.39 - 3.35 (m, 1H), 2.96 (s, 3H), 2.51 (s, 3H) ppm. **^{13}C NMR** (CDCl$_3$, 101 MHz): δ = 145.2, 143.4, 130.2 (q, *J* = 32.4 Hz, 2C), 128.2, 127.7 (2C), 127.4, 125.6 (q, *J* = 3.8 Hz), 124.4 (q, *J* = 273.7 Hz), 118.0, 116.5, 109.3, 81.9, 49.4, 42.6, 37.1 ppm. **ESI-MS**: *m/z* calcd: 306.1, found: 307.0 [M+H]$^+$. **HPLC**: 97%.

2-(2,6-Dichlorophenyl)-1,3-dimethyl-1,2,3,4-tetrahydroquinazoline **8f**: According to GP3, starting from 2-(2,6-dichlorophenyl)-1,3-dimethyl-2,3-dihydroquinazolin-4(1*H*)-one **6f** (520 mg, 1.63 mmol, 1 equiv) the title compound 2-(2,6-dichlorophenyl)-1,3-dimethyl-1,2,3,4-tetrahydroquinazoline **8f** (386 mg, 78%) was obtained after column chromatography (petroleum ether:EtOAc = 5:1) as white solid; **mp** 78-79 °C. ^{1}H NMR (400 MHz, CDCl$_3$): δ = 7.24 (br, 2H), 7.14 - 7.04 (m, 2H), 6.89 (d, *J* = 7.2 Hz, 1H), 6.57 (td, *J* = 7.3, 1.0 Hz, 1H), 6.49 (d, *J* = 8.1 Hz, 1H), 5.40 (d, *J* = 0.9 Hz, 1H), 3.83 (d, *J* = 15.0 Hz, 1H), 3.41 (d, *J* = 15.0 Hz, 1H), 2.68 (s, 3H), 2.36 (s, 3H) ppm.^{13}C NMR (101 MHz, CDCl$_3$): δ = 144.2, 135.2, 129.0, 128.0, 126.5, 119.3, 115.7, 109.0, 79.9, 52.6, 42.2, 34.7 ppm. **ESI-MS**: *m/z* calcd: 306.1, found: 307.0 [M+H]$^+$. **HPLC**: 99%.

1-Methyl-2-phenyl-3-propyl-1,2,3,4-tetrahydroquinazoline **9a**: According to GP3, starting from 1-methyl-2-phenyl-3-propyl-2,3-dihydroquinazolin-4(1*H*)-one **7a** (350 mg, 1.25 mmol, 1 equiv) the title compound 1-methyl-2-phenyl-3-propyl-1,2,3,4-tetrahydroquinazoline **9a** (277 mg, 84%) was obtained after column chromatography (petroleum ether:EtOAc = 3:1) as beige solid; **mp**: 46-48 °C. **¹H NMR** (CDCl₃, 400 MHz): δ = 7.24 - 7.20 (m, 2H), 7.19 - 7.13 (m, 3H), 7.13 - 7.09 (m, 1H), 6.79 (d, J = 7.2 Hz, 1H), 6.59 - 6.53 (m, 2H), 4.90 (s, 1H), 3.68 (d, J = 16.3 Hz, 1H), 3.37 - 3.32 (m, 1H), 2.90 (s, 3H), 2.57 - 2.42 (m, 2H), 1.56 (sextet, J = 7.3 Hz, 2H), 0.89 (t, J = 7.3 Hz, 3H) ppm. **¹³C NMR** (CDCl₃, 101 MHz): δ = 144.2, 141.6, 128.6 (2C), 127.9, 127.7, 127.24 (2C), 127.16, 118.6, 115.7, 108.7, 80.4, 55.6, 47.6, 37.0, 21.6, 12.1 ppm. **ESI-MS**: *m/z* calcd: 266.2, found: 267.2 [M+H]⁺. **HPLC**: 100%.

3-Isopropyl-1-methyl-2-phenyl-1,2,3,4-tetrahydroquinazoline **9b**: According to GP3, starting from 3-isopropyl-1-methyl-2-phenyl-2,3-dihydroquinazolin-4(1*H*)-one **7b** (300 mg, 1.07 mmol, 1 equiv) the title compound 3-isopropyl-1-methyl-2-phenyl-1,2,3,4-tetrahydroquinazoline **9b** (247 mg, 87%) was obtained after column chromatography (petroleum ether: EtOAc = 4:1) as yellow solid; **mp**: 40-42 °C. **¹H NMR** (CDCl₃, 400 MHz): δ = 7.31 - 7.28 (m, 1H), 7.27 - 7.26 (m, 1H), 7.24 - 7.20 (m, 3H), 7.18 - 7.13 (m, 1H), 6.85 - 6.83 (m, 1H), 6.62 - 6.58 (m, 2H), 5.19 (s, 1H), 3.73 (d, J = 16.6 Hz, 1H), 3.62 (d, J = 16.6, 1H), 2.94 (s, 3H), 2.87 (septet, J = 6.3 Hz, 1H), 1.20 (d, J = 6.3 Hz, 3H), 1.23 (d, J = 6.4 Hz, 3H) ppm. **¹³C NMR** (CDCl₃, 101 MHz): δ = 144.9, 142.3, 128.6 (2C), 127.9, 127.5, 127.2 (2C), 126.6, 119.5, 115.6, 108.5, 77.6, 50.0, 44.7, 36.6, 22.1, 21.7 ppm. **ESI-MS**: *m/z* calcd: 266.2, found: 267.1 [M+H]⁺. **HPLC**: 99%.

1-Methyl-2,3-diphenyl-1,2,3,4-tetrahydroquinazoline **9c**: According to GP3, starting from 1-methyl-2,3-diphenyl-2,3-dihydroquinazolin-4(1*H*)-one **7c** (310 mg, 0.99mmol, 1 equiv) the title compound 1-methyl-2,3-diphenyl-1,2,3,4-tetrahydroquinazoline **9c** (178 mg, 61%) was obtained after crystallization from petroleum ether/DCM as pale yellow solid; **mp** 132-134 °C. **¹H NMR** (CDCl₃, 400 MHz): δ = 7.25 - 7.22 (m, 1H), 7.22 - 7.17 (m, 4H), 7.17 - 7.14 (m, 2H), 7.10 - 7.06 (m, 1H), 7.00 - 6.97 (m, 2H), 6.86 - 6.84 (m, 1H), 6.80 (tt, J = 7.3, 1.0 Hz, 1H), 6.60 - 6.56 (m, 2H), 5.77 (s, 1H), 4.16 (d, J = 16.4 Hz, 1H), 4.10 (d, J = 16.2 Hz, 1H), 2.96 (s, 3H) ppm. **¹³C NMR** (CDCl₃, 101 MHz): δ = 150.5, 144.4, 140.5, 129.4 (2C), 128.7 (2C), 128.1, 128.0, 127.1 (2C), 126.4, 120.8, 120.0, 118.6 (2C), 116.6, 110.2, 78.8, 46.7, 37.2 ppm. **ESI-MS**: *m/z* calcd: 300.2, found: 301.1 [M+H]⁺. **HPLC**: 99%.

2-Amino-*N*-methylbenzamide **10**: According to GP1, isatoic anhydride (1.00 g, 6.13 mmol, 1 equiv), methylamine hydrochloride (2.07 g, 30.7 mmol, 5 equiv) and triethylamine (4.25 mL, 30.7 mmol, 5 equiv) were used to obtain 2-amino-*N*-methylbenzamide **10** (862 mg, 94%) after column chromatography (petroleum ether:EtOAc = 1:1) as white solid; **mp**: 80-82 °C. ^{1}**H NMR** (CDCl$_3$, 400 MHz): δ = 7.27 (dd, J = 7.8, 1.48 Hz, 1H), 7.20 - 7.16 (m, 1H), 6.66 (dd, J = 8.2, 0.8 Hz, 1H), 6.64 - 6.60 (m, 1H), 6.02 (br, NH), 5.47 (br, NH$_2$), 2.95 (d, J = 4.8 Hz, 3H) ppm. ^{13}**C NMR** (CDCl$_3$, 101 MHz): δ = 170.2, 148.8, 132.4, 127.2, 117.5, 116.8, 116.5, 26.7 ppm.

3-Methyl-2-phenyl-2,3-dihydroquinazolin-4(1*H*)-one **11**: According to GP2, 2-amino-*N*-methylbenzamide **10** (529 mg, 3.52 mmol, 1 equiv) and benzaldehyde (436 μL, 4.23 mmol, 1.2 equiv) were used to obtain 3-methyl-2-phenyl-2,3-dihydroquinazolin-4(1*H*)-one **11** (628 mg, 75%) after crystallization from a mixture of petroleum ether/DCM as white solid; **mp** 165-167 °C. ^{1}**H NMR** (DMSO-d$_6$, 400 MHz): δ = 7.65 (dd, J = 7.6, 1.4 Hz, N*H*), 7.39 - 7.35 (m, 2H), 7.34 - 7.30 (m, 4H), 7.22 - 7.18 (m, 1H), 6.67 - 6.62 (m, 2H), 5.82 (d, J = 2.3 Hz, 1H), 2.85 (s, 3H) ppm. ^{13}**C NMR** (DMSO-d$_6$, 101 MHz): δ = 162.5, 146.4, 140.6, 133.2, 128.6 (2C), 128.5, 127.3, 126.1 (2C), 116.9, 114.3, 114.0, 72.0, 32.0 ppm.

3-Methyl-2-phenyl-1-propyl-2,3-dihydroquinazolin-4(1*H*)-one **12a**: Starting from 3-methyl-2-phenyl-2,3-dihydroquinazolin-4(1*H*)-one **11** (236 mg, 0.99 mmol, 1 equiv) dissolved in dry DMF (10 mL), *n*-propyl bromide (452 μL, 4.96 mmol, 5 equiv) and *t*BuOK (557 mg, 4.96 mmol, 5 equiv) were added successively. The reaction mixture was stirred for 16 h at 110 °C. Ice-cold water (30 mL) was then added and the mixture was stirred for further 30 min. The product was extracted with EtOAc (3 x 30 mL), the combined organic layers were washed with brine (30 mL), dried over Na$_2$SO$_4$ and the solvent was evaporated under reduced pressure to yield 3-methyl-2-phenyl-1-propyl-2,3-dihydroquinazolin-4(1*H*)-one **12a** (200 mg, 72%) after column chromatography (petroleum ether:EtOAc = 1:1) as white solid; **mp** 116-119 °C. ^{1}**H NMR** (CDCl$_3$, 400 MHz): δ = 7.97 (dd, J = 7.7, 1.5 Hz, 1H), 7.32 - 7.24 (m, 4H), 7.23 - 7.20 (m, 2H), 6.80 - 6.76 (m, 1H), 6.57 (d, J = 8.2 Hz, 1H), 5.43 (s, 1H), 3.35 - 3.28 (m, 1H), 3.05 - 2.97 (m, 4H), 1.72 - 1.59 (m, 1H), 1.57 - 1.46 (m, 1H), 0.92 (t, J = 7.4 Hz, 3H) ppm. ^{13}**C NMR** (CDCl$_3$, 101 MHz): δ = 162.8, 146.1, 139.0, 133.7, 129.2, 129.0 (2C), 128.9, 126.5 (2C), 118.0, 116.7, 112.6, 79.6, 51.4, 32.9, 20.7, 11.6 ppm.

2-(Isopropylamino)benzoic acid 14: To a solution of 2-aminobenzoic acid (1 g, 7.3 mmol, 1 equiv) in methanol (20 mL) was added acetone (643 µL, 8.76 mmol, 1.2 equiv). The mixture was heated to reflux temperature and stirred for 5 h. After cooling to room temperature, NaBH$_4$ (333 mg, 8.76 mmol, 1.2 equiv) was added portion wise and stirring was continued for further 3 h. The solvent was then evaporated to dryness and suspended in water. The product was extracted with DCM (3 x 150 mL), the organic layer was dried over Na$_2$SO$_4$ and the solvent was removed. The crude product was purified by column chromatography (petroleum ether:EtOAc = 4:1) to yield 2-(isopropylamino)benzoic acid 14 (794 mg, 61%) as white solid; mp 110-112 °C. ^{1}H NMR (400 MHz, DMSO-d$_6$): δ = 12.52 (br, COOH), 7.78 (dd, J = 8.0, 1.6 Hz, 1H), 7.35 (ddd, J = 8.7, 7.1, 1.8 Hz, 1H), 6.74 (d, J = 8.5 Hz, 1H), 6.52 (ddd, J = 8.0, 7.1, 1.1 Hz, 1H), 3.72 (hept, J = 6.2 Hz, 1H), 1.19 (d, J = 6.3 Hz, 6H) ppm. ^{13}C NMR(101 MHz, DMSO-d$_6$): δ = 170.5, 150.5, 134.9, 132.3, 114.3, 112.1, 110.2, 43.0, 23.1 (2C) ppm.

2-(Isopropylamino)-N-methylbenzamide 15a: A mixture of 2-(isopropylamino)benzoic acid 14 (770 mg, 4.3 mmol, 1 equiv), methylamine hydrochloride (1.45 g, 21.5 mmol, 5 equiv), triethylamine (2.98 mL, 21.5 mmol, 5 equiv), EDCI hydrochloride (991 mg, 5.16 mmol, 1.2 equiv) and HOBT (697 mg, 5.16 mmol, 1.2 equiv) in DMF (50 mL) were heated to 70 °C for 14 h. The mixture was then poured into water (150 mL) and extracted with EtOAc (4 x 100 mL). The combined organic layers were washed with brine (100 mL), dried over Na$_2$SO$_4$ and the solvent was removed under reduced pressure. The crude product was purified by column chromatography (petroleum ether:EtOAc = 4:1) to yield 2-(isopropylamino)-N-methylbenzamide 15a (627 mg, 76%) as clear oil; ^{1}H NMR (400 MHz, CDCl$_3$): δ = 7.66 (br, NH), 7.35 - 7.25 (m, 2H), 6.73 (d, J = 8.4 Hz, 1H), 6.62 - 6.47 (m, 1H), 6.12 (br, NH), 3.68 (hept, J = 6.3 Hz, 1H), 2.97 (d, J = 4.8 Hz, 3H), 1.27 (d, J = 6.3 Hz, 6H) ppm. ^{13}C NMR (101 MHz, CDCl$_3$): δ = 170.6, 148.7, 132.6, 127.4, 115.0, 114.3, 112.3, 43.5, 26.5, 22.7 (2C) ppm.

N-Methyl-2-(phenylamino)benzamide 15b: To a solution of 2-(phenylamino)benzoic acid (1.00 g, 4.69 mmol, 1 equiv) in dry DMF (40 mL), 1-HOBt (761 mg, 5.63 mmol, 1.2 equiv), EDCI hydrochloride (1.08 g, 5.63 mmol, 1.2 equiv), methylamine hydrochloride (1.59 g, 23.5 mmol, 4 equiv), and triethylamine (3.25 mL, 23.5 mmol, 5 equiv) were added successively. After stirring for 8 h at ambient temperature, the reaction mixture was poured

onto water (60 mL) and extracted with EtOAc (3 x 30 mL). The combined organic layers were washed with a 0.1 M HCl (2 x 20 mL), brine (30 mL), and dried over Na_2SO_4. The solvent was evaporated under reduced pressure and the crude product was purified by column chromatography (petroleum ether:EtOAc = 2:1) to obtain the title compound **15b** (584 mg, 56%) as white solid; **mp** 85-87 °C. **^{1}H NMR** (CDCl$_3$, 400 MHz): δ = 9.22 (br, N*H*), 7.32 (dd, *J* = 7.8, 1.6 Hz, 1H), 7.29 - 7.24 (m, 1H), 7.23 - 7.16 (m, 3H), 7.13 - 7.10 (m, 2H), 6.92 (tt, *J* = 7.3, 1.2 Hz, 1H), 6.70 - 6.66 (m, 1H), 6.09 (br, N*H*), 2.91 (d, *J* = 4.9 Hz, 3H) ppm. **^{13}C NMR** (CDCl$_3$, 101 MHz): δ = 170.4, 145.5, 141.8, 132.3, 129.5 (2C), 127.6, 122.5, 120.9 (2C), 118.8, 118.1, 115.7, 26.8 ppm.

1-Isopropyl-3-methyl-2-phenyl-2,3-dihydroquinazolin-4(1*H*)-one **12b**: According to GP2, 2-(isopropylamino)-*N*-methylbenzamide **15a** (600 mg, 3.13 mmol, 1 equiv) and benzaldehyde (379 µL, 3.75 mmol, 1.2 equiv), were used to obtain 1-isopropyl-3-methyl-2-phenyl-2,3-dihydroquinazolin-4(1*H*)-one **12b** (648 mg, 74%) after column chromatography (petroleum ether:EtOAc = 3:1) as white solid; **mp** 107-109 °C. **^{1}H NMR** (400 MHz, CDCl$_3$): δ = 7.92 - 7.84 (m, 1H), 7.23 (ddd, *J* = 8.3, 7.3, 1.7 Hz, 1H), 7.18 - 7.08 (m, 5H), 6.87 - 6.79 (m, 2H), 5.46 (s, 1H), 3.87 (hept, *J* = 6.7 Hz, 1H), 3.10 (s, 3H), 1.29 (d, *J* = 6.8 Hz, 3H), 1.14 (d, *J* = 6.6 Hz, 3H) ppm. **^{13}C NMR** (101 MHz, CDCl$_3$): δ =163.3, 146.6, 140.2, 132.9, 128.5 (2C), 128.1, 127.9, 126.3 (2C), 121.8, 120.8, 119.6, 71.9, 55.0, 33.1, 21.8, 20.3 ppm.

3-Methyl-1,2-diphenyl-2,3-dihydroquinazolin-4(1*H*)-one **12c**: According to GP2, *N*-methyl-2-(phenylamino)benzamide **15b** (454 mg, 2.01 mmol, 1 equiv) and benzaldehyde (244 µL, 2.41 mmol, 1.2 equiv) were used to obtain 3-methyl-1,2-diphenyl-2,3-dihydroquinazolin-4(1*H*)-one **12c** (488 mg, 78%) after crystallization from a mixture of petroleum ether/DCM as white solid; **mp** 158-160 °C. **^{1}H NMR** (CDCl$_3$, 400 MHz): δ = 8.00 - 7.99 (m, 1H), 7.35 - 7.32 (m, 2H), 7.31 - 7.26 (m, 5H), 7.26 - 7.22 (m, 1H), 7.17 - 7.14 (m, 2H), 7.14 - 7.12 (m, 1H), 6.96 - 6.92 (m, 1H), 6.84 - 6.81 (m, 1H), 5.93 (s, 1H), 3.16 (s, 3H) ppm. **^{13}C NMR** (CDCl$_3$, 101 MHz): δ = 162.8, 146.3, 144.1, 139.5, 133.1, 129.9 (2C), 129.0 (2C), 128.9, 128.7, 126.6 (2C), 125.0, 123.5 (2C), 121.4, 120.6, 118.9, 80.2, 34.3 ppm.

3-Methyl-2-phenyl-1-propyl-1,2,3,4-tetrahydroquinazoline **13a**: According to GP3, starting from 3-methyl-2-phenyl-1-propyl-2,3-dihydroquinazolin-4(1*H*)-one **12a** (180 mg, 0.64mmol, 1 equiv) the title compound 3-methyl-2-phenyl-1-propyl-1,2,3,4-tetrahydroquinazoline **13a**

(140 mg, 82%) was obtained after column chromatography (petroleum ether:EtOAc = 3:1) as grey solid; **mp** 45-46 °C. **¹H NMR** (CDCl$_3$, 400 MHz): δ = 7.31 - 7.21 (m, 5H), 7.16 - 7.12 (m, 1H), 6.85 - 6.83 (m, 1H), 6.67 (d, J = 8.2 Hz, 1H), 6.59 (dt, J = 7.3, 1.0 Hz, 1H), 4.91 (s, 1H), 3.76 (d, J = 16.2 Hz, 1H), 3.52 - 3.41 (m, 1H), 3.30 (dd, J = 16.2, 1.0 Hz, 1H), 2.97 - 2.85 (m, 1H), 2.51 (s, 3H), 1.74 - 1.54 (m, 2H), 0.92 (t, J =7.4 Hz, 3H) ppm. **¹³C NMR** (CDCl$_3$, 101 MHz): δ = 142.9, 141.6, 128.5 (2C), 127.89, 127.86, 127.7, 127.4 (2C), 117.6, 115.5, 108.9, 80.9, 50.9, 49.2, 42.5, 20.7, 11.6 ppm. **ESI-MS**: m/z calcd: 266.2, found: 267.1 [M+H]$^+$. **HPLC**: 99%.

1-Isopropyl-3-methyl-2-phenyl-1,2,3,4-tetrahydroquinazoline **13b**: According to GP3, starting from 1-isopropyl-3-methyl-2-phenyl-2,3-dihydroquinazolin-4(1H)-one **12b** (300 mg, 1.07 mmol, 1 equiv) the title compound 1-isopropyl-3-methyl-2-phenyl-1,2,3,4-tetrahydroquinazoline **13b** (174 mg, 61%) was obtained after column chromatography (petroleum ether:EtOAc = 3:1) as clear oil; **¹H NMR** (400 MHz, CDCl$_3$): δ = 7.25 - 7.13 (m, 5H), 7.13 - 7.07 (m, 1H), 6.83 - 6.73 (m, 2H), 6.55 (td, J = 7.3, 0.9 Hz, 1H), 5.04 (s, 1H), 4.18 (hept, J = 6.6 Hz, 1H), 3.71 (d, J = 16.2 Hz, 1H), 3.25 (d, J = 16.1 Hz, 1H), 2.40 (s, 3H), 1.20 (d, J = 6.5 Hz, 3H), 1.00 (d, J = 6.8 Hz, 3H) ppm. **¹³C NMR** (101 MHz, CDCl$_3$): δ =142.9, 142.3, 128.2 (2C), 127.9, 127.7, 127.5, 127.3 (2C), 117.4, 115.2, 109.3, 74.2, 49.0, 46.6, 42.1, 20.7, 19.9 ppm. **ESI-MS**: m/z calcd: 266.2, found: 267.1 [M+H]$^+$. **HPLC**: 94%.

3-Methyl-1,2-diphenyl-1,2,3,4-tetrahydroquinazoline **13c**: According to GP3, starting from 3-methyl-1,2-diphenyl-2,3-dihydroquinazolin-4(1H)- one **12c** (200 mg, 0.64mmol, 1 equiv) the title compound 3-methyl-1,2-diphenyl-1,2,3,4-tetrahydroquinazoline **13c** (153 mg, 81%) was obtained after column chromatography (petroleum ether:EtOAc = 3:1) as pale yellow solid; **mp** 107-109 °C. **¹H NMR** (CDCl$_3$, 400 MHz): δ = 7.47 - 7.44 (m, 2H), 7.33 - 7.29 (m, 2H), 7.28 - 7.25 (m, 3H), 7.25 - 7.22 (m, 2H), 7.10 - 7.06 (m, 1H), 7.06 - 7.01 (m, 2H), 6.87 (dd, J = 7.5 Hz, 0.6 Hz, 1H), 6.73 (dt, J = 7.2, 1.3 Hz, 1H), 5.32 (s, 1H), 3.89 (d, J = 16.4 Hz, 1H), 3.47 (d, J = 16.7 Hz, 1H), 2.63 (s, 3H) ppm. **¹³C NMR** (CDCl$_3$, 101 MHz): δ = 147.7, 141.4, 141.1, 129.5 (2C), 128.7 (2C), 127.8 (2C), 127.5 (2C), 127.0, 123.7, 123.4 (2C), 119.7, 118.9, 115.2, 82.4, 49.3, 42.4 ppm. **ESI-MS**: m/z calcd: 300.2, found: 301.1 [M+H]$^+$. **HPLC**: 99%.

N-Methyl-2-((methylamino)methyl)aniline **16**: N-methyl-2-(methylamino)benzamide **5a** (300 mg, 1.83 mmol, 1 equiv) was dissolved in dry THF (20 mL) and treated with LiAlH$_4$ (278 mg, 7.32 mmol, 4 equiv) under ice cooling. The mixture was heated for 24 h to reflux temperature under argon

atmosphere. The mixture was then poured into water (30 mL) and extracted with DCM (3 x 30 mL). The combined organic layers were extracted with a 1 M HCl-solution (3 x 30 mL). The aqueous phase was wahed with DCM (1 x 30 mL), basified with concentrated NH$_3$-solution and extracted with DCM (3 x 30 mL). The combined organic layers were dried over Na$_2$SO$_4$ and the solvent was evaporated under reduced pressure to obtain *N*-methyl-2-((methylamino)methyl)aniline **16** (247 mg, 90%) as a yellow liquid; . **^{1}H NMR** (CDCl$_3$, 400 MHz): δ = 7.13 (td, *J* = 7.7, 1.6 Hz, 1H), 6.97 - 6.92 (m, 1H), 6.58 - 6.52 (m, 2H), 3.65 (s, 2H), 2.76 (s, 3H), 2.33 (s, 3H) ppm.**^{13}C NMR** (CDCl$_3$, 101 MHz): δ = 149.41, 129.53, 128.64, 123.70, 115.99, 109.60, 55.60, 36.07, 30.21 ppm. **ESI-MS**: *m/z* calcd: 150.1, found: 151.2 [M+H]$^+$.

Stability Tests

Preparation of Phosphate Buffered Systems

For the preparation of phosphate buffered solutions with defined pH values, 0.1 M H_3PO_4 was titrated with a 0.3 M NaOH solution while monitoring the pH value on a Metohm 744 pH Meter (Metrohm GmbH & Co. KG, Filderstadt, Germany). Using this procedure, phosphate buffered systems were obtained with pH = 2,3,4,5,6,7,8 and 12.

Hydrolysis Experiments

A calibration line for each test compound and their respective aldehydes as hydrolysis product was recorded (see calibration lines).

For stability analyzes, 300 µL of a solution of the test compound (333 µg/mL) in acetonitrile was thoroughly mixed with 700 µL of a phosphate buffered solution with defined pH-value to give a solution with a final test concentration of 100 µg/mL (a certain amount of acetonitrile is necessary to keep the compound in solution). The reaction mixture was incubated for 1 h before it was directly analyzed with HPLC by injecting a volume of 20 µL of the test solution. Analytic HPLC-analysis were performed on a system from Shimadzu equipped with a DGU-20A3R controller, LC20AB liquid chromatograph, and a SPD-20A UV/Vis detector. Stationary phase was a Synergi 4U fusion-RP (150 x 4.6 mm) column (Phenomenex, Aschaffenburg, Germany). As mobile phase, water (phase A) and MeOH (phase B) were used with 1 mL/min. (conc. B: 5% → 90% from 0 to 8 min; 90% from 8 to 13 min; 90% → 5% from 13 to 15 min; 5% from 15 to 18 min.). Using the beforehand recorded calibration lines, it was possible to calculate the ration between the intact tetrahydroquinazoline as well as the respective aldehyde as its hydrolysis product. Data were subjected to one way ANOVA followed by Dunnett's multiple comparison post testusing GraphPad Prism 4 Software(levels of significance * $p < 0.05$; ** $p < 0.01$; *** $p < 0.001$). Each experiment was performed three times with three independently prepared test solutions.

Kinetic monitoring of the hydrolysis of compound **8a** at different pH values (3,4 and 5) was followed the above mentioned procedure after t = 0, 18.5, 37, 55.5, 74, 92,5 111, 129.5, 148, 166.5, 185, 203.5, 222, 240.5, 259 and 277.5 min. Due to the fast hydrolysis at pH = 2, the time interval was shortened to t = 0, 1, 2, 3, 4, 6, 18.5, 37 and 55.5 min. Calculation of k_2 was performed under assumption of a pseudo first order kinetics using

$Y = (Y_0) * \exp(-k_2 * t)$

With Y = amount of non-hydrolyzed test compound (%) in dependency of time and Y_0 = amount of non-hydrolyzed test compound (%) at t = 0 min. All data were analyzed using GraphPad Prism 4 Software.

Aminal Condensation Experiments:

To proof that acid mediated hydrolysis of the described tetrahydroquinazolines can be reversed by changing the reaction conditions to basic ones, the synthesis of tetrahydroquinazoline **8a** was performed using *N*-methyl-2-((methylamino)methyl)aniline **16** and benzaldehyde:
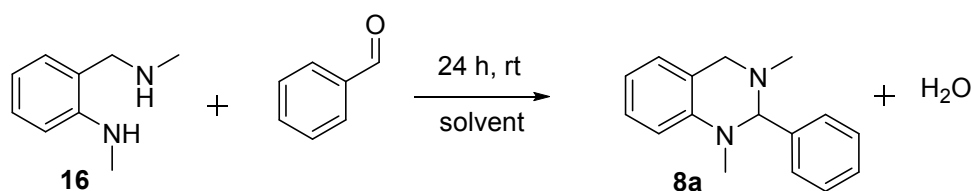
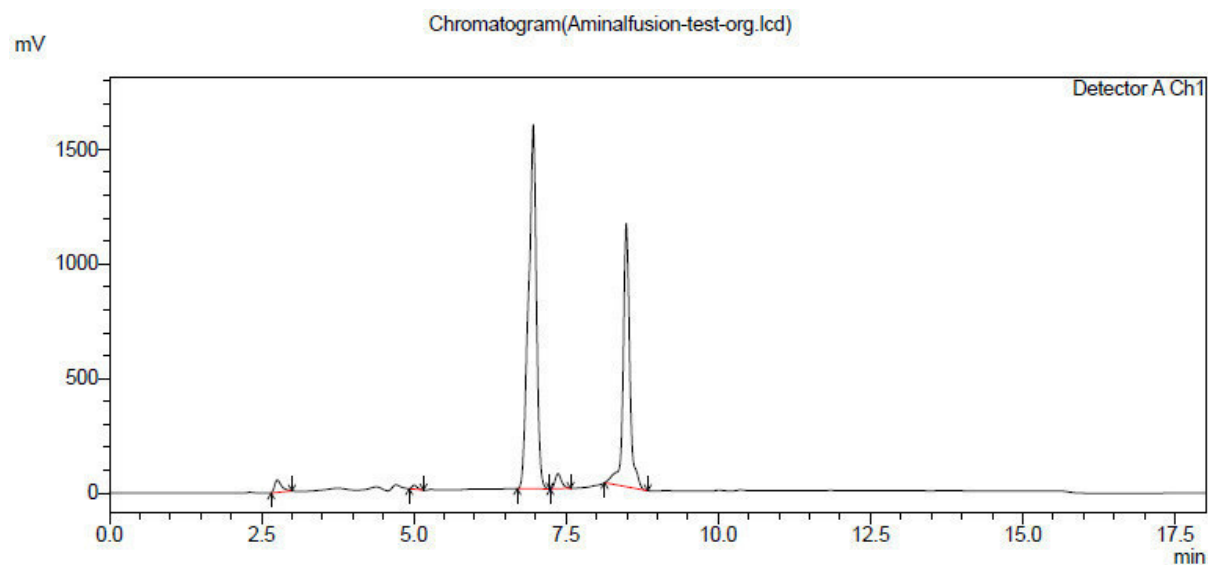Therefore, *N*-methyl-2-((methylamino)methyl)aniline **16** (100 mg, 0.67 mmol, 1 equiv) and benzaldehyde (1.2 equiv) were mixed at room temperature in either a) acetonitrile (1 mL) as reference for the condensation, b) water (1 mL) and c) water/acetonitrile (1:1, 1 mL). After 24 h the reaction mixtures were directly analyzed by LCMS (*cf.* general part).
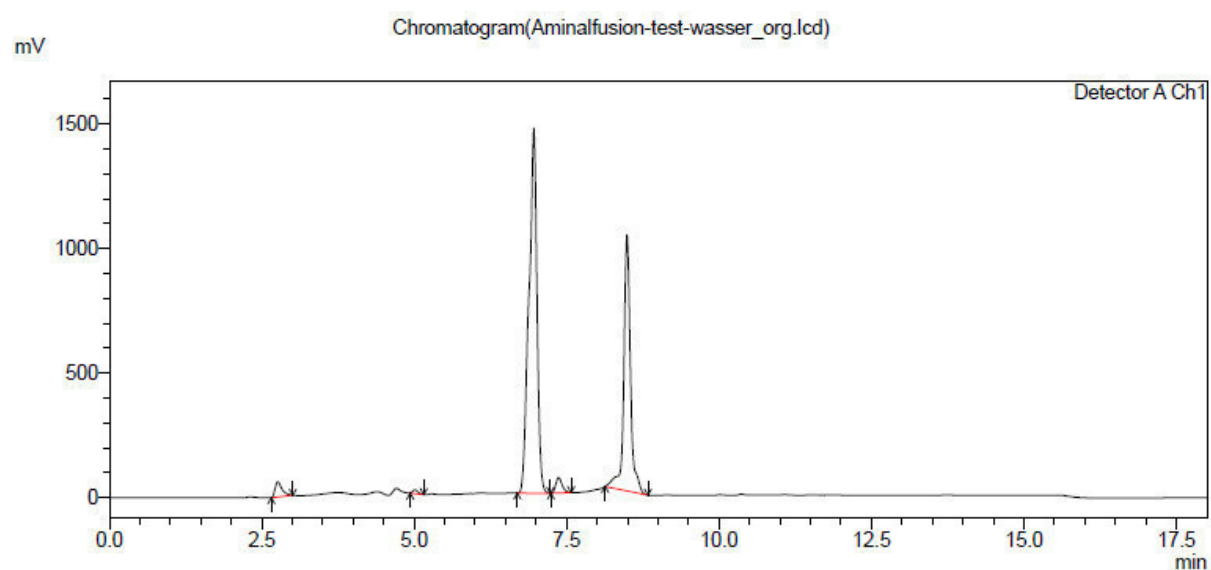
Chromatogram for the reaction in water:
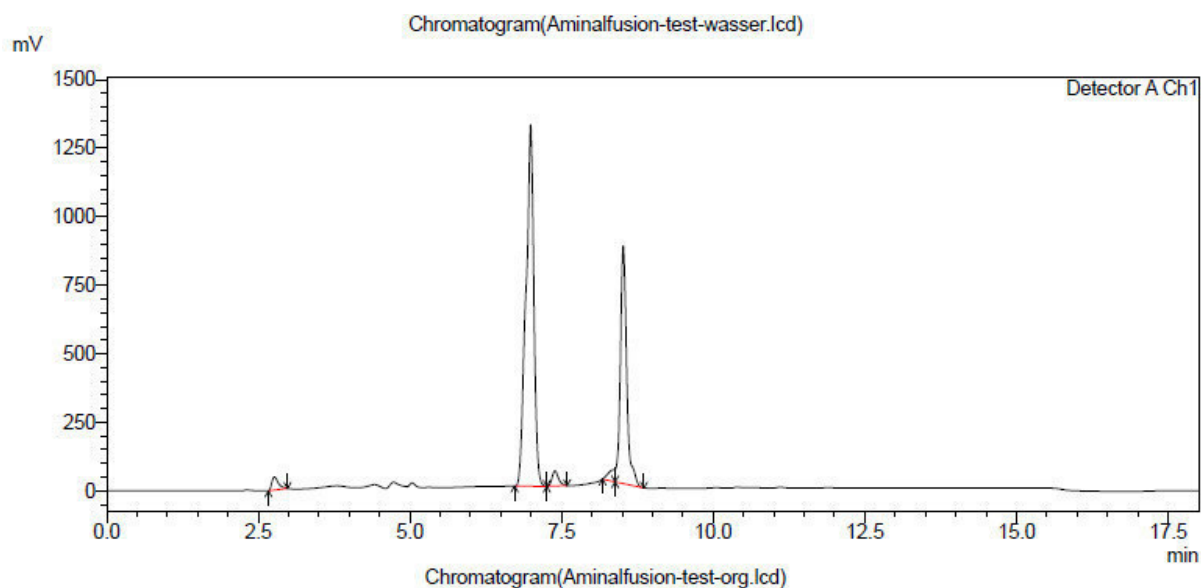
Chromatogram for the reaction in acetonitrile:

Chromatogram(Aminalfusion-test-org.lcd)

Chromatogram for the reaction in acetonitrile/water:

Chromatogram(Aminalfusion-test-wasser_org.lcd)

Interestingly, all reactions showed the same result with complete consumption of *N*-methyl-2-((methylamino)methyl)aniline **16** at $t_R \approx 5$ min and benzyldehyde at $t_R = 2.2$ min while forming the tetrahydroquinazoline **8a** ($t_R \approx 7$ min). It is remarkable, that there is another peak at $t_R \approx 8$ min for all cases which could not be identified by mass spectrometry. This peak might be a byproduct from the reaction of benzaldehyde due to the fact, that benzaldehyde is completely consumed although being used in excess. However, these results clearly indicated, that the condensation of diamines and aldehydes is possible in neutral aqueous media, while the hydrolysis is promoted in acidic aqueous media (see the main manuscript).

Computational Section

Materials and Methods

Conformational search: All compounds prior to the conformational search were minimized in MOE[1] using the MMFF94x forcefield[2] in gas phase ($\varepsilon = 1$) and an RMS-gradient of 0.0001 kcal/molÅ.

The systematic search was conducted in Macromodel 10.3 (Schrodinger 2014-1 platform) using the Systematic Pseudo Monte Carlo (SPMC) method[3]. The conformational search was conducted in MMFF94s forcefield[4] and the potential treatment was set according to the Macromodel built-in module for water ($\varepsilon = 7.8000E+1$). The convergence threshold for minimization was set at 0.0001 kcal/molÅ and the maximum iteration limit was set at 25000. Miscellaneous technical characteristics: Maximum number of steps 100000; steps per rotational bond 10000; energy window 478.01 kcal/mol; Maximum atom deviation cutoff: 0.01Å

MM relative ring strain comparison: The transformation of the structures and the potential energy calculation was conducted in the Schrodinger 2014-1 platform environment, using the MMFF94s forcefield. The potential treatment for calculations in water environment was set according to the Macromodel built-in module for water as previously described.

QM single point energy calculations: All tetrahydroquinazoline structures used were results of the aforementioned MM systematic conformational search. All other structures were designed and minimized in Maestro (Schrodinger platform) using the MMFF94s forcefield. The Brønsted acid was simulated by an ammonium cation to facilitate the calculations.

The single point calculations were performed with DFT using the functional B3LYP-D3[5–9] (grid m4[10]) in Turbomole (dscf[11,12]). The basis set used was cc-pVTZ[13,14].

Calculations were performed in water environment ($\varepsilon = 78.5$) and in gas phase. The Conductor-Like Screening Model (COSMO)[15] was used to form the implicit water continuum solvation model. The studied structures were optimized in water and gas phase respectively.

MoKa[16] Calculations

Structure	N1pK$_a$	SD	QualityParameter	N3 pK$_a$	SD	QualityParameter
8a	-0,86	0,51	-0,40	6,31	0,60	0,00
8c	-0,86	0,51	-0,40	6,31	0,60	0,00
8d	-1,00	0,51	-0,40	6,06	0,60	0,00
8b	-0,92	0,51	-0,40	6,25	0,60	0,00
8e	-0,51	0,51	-0,40	6,66	0,60	0,00
8f	-1,00	0,51	-0,40	4,84	0,60	0,00
9a	-0,82	0,51	-0,40	6,35	0,60	0,00
9b	-0,56	0,51	-0,40	6,61	0,60	0,00
9c	8,85	0,51	0,00	2,41	0,51	0,00
13a	-0,72	0,51	-0,40	6,45	0,60	0,00
13b	-0,69	0,51	-0,40	6,48	0,60	0,00
13c	-1,00	0,51	-0,40	6,00	0,60	0,00
6a	1,98	0,51	-0,04	NA	NA	NA

Quality parameter (QP): The quality parameter can be used to check whether the compound contains features that MoKa cannot take into account when it predicts the specific pK$_a$.

QP = 0 indicates that all the chemical groups in the compound have appropriate parameters to calculate the specific pK$_a$.

QP< or > indicates that the effect of one or more chemical groups on the specific pK$_a$ is unknown. The higher the absolute value of the QP, the higher is the expected effect of these groups on pK$_a$. The +/- sign before QP specifies whether these groups are expected to shift pK$_a$ upwards or downwards.

QM calculations

Absolute Energies of all Reactants

Table 1: Absolute energy values.

	B3LYP-D3 water (kcal/mol)	B3LYP-D3 gas (kcal/mol)
H_2O	-47962,92	-47955,99
NH_4^+	-35780,86	-35698,10
NH_3	-35489,63	-35484,54
PhCHO	-216805,79	-216799,60
8a_neutral	-457969,49	-457963,11
8a_N3	-458256,03	-458205,26
8a_N1	-458247,24	-458200,30
8a_N1_N3	-458515,90	-458347,50
N-methyl-2-[(methylamino)methyl]aniline_neutral	-289123,51	-289116,71
N-Methyl-2-[(methylamino)methyl]aniline_N1	-289416,51	-289365,03
N-Methyl-2-[(methylamino)methyl]aniline_N3	-289419,85	-289366,17
N-Methyl-2-[(methylamino)methyl]aniline_N1_N3	-289693,03	-289505,43
13b_neutral	-507287,54	-507281,09
13b_N3	-507574,42	-507524,90
13b_N1	-507564,37	-507520,02
13b_N1_N3	-507832,45	-507672,01
N-Isopropyl-2-[(methylamino)methyl]aniline_neutral	-338449,55	-338444,20
N-Isopropyl-2-[(methylamino)methyl]aniline_N1	-338738,70	-338690,85
N-Isopropyl-2-[(methylamino)methyl]aniline_N3	-338742,54	-338690,41
N-Isopropyl-2-[(methylamino)methyl]aniline_N1_N3	-339015,83	-338836,56

Determining the Protonation Pattern:

Energy differences between the different protonation patterns for compounds **8a** and **13b** in water revealed that protonation is most likely at the *N*-3 nitrogen.
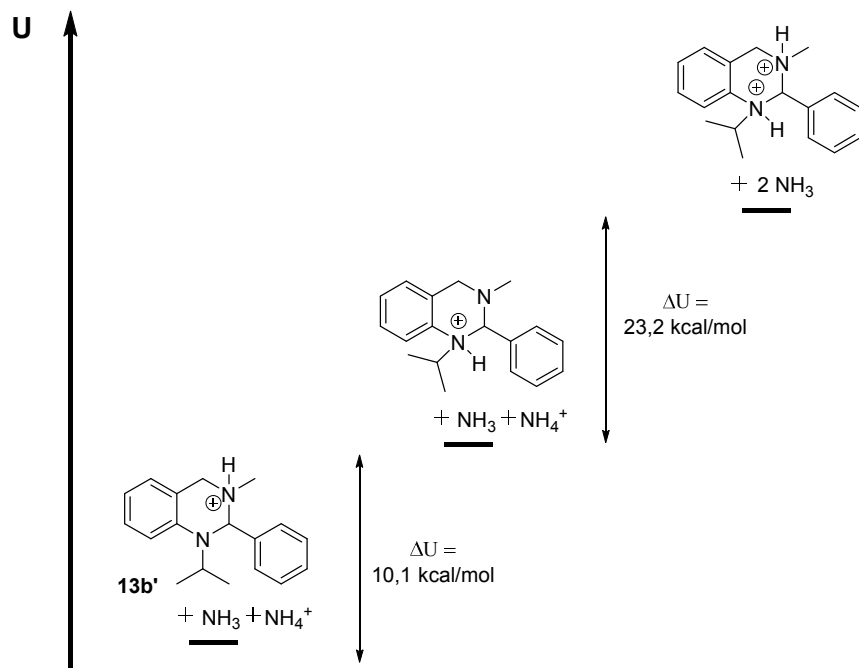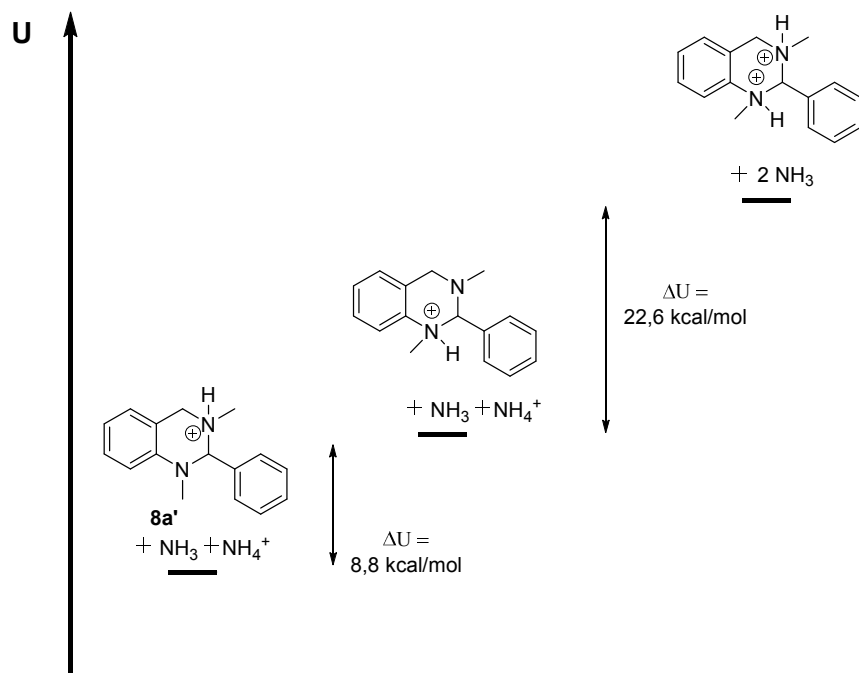
QM Summary

The scheme below depicts a reaction pathway. The energy difference ($\Delta U = U_2 - U_1$) between different reaction states (**A** to **H**) for compounds **8a** and **13b** is presented in Table 2. $\Delta U < 0$ indicates that the respective reaction is spontaneous (exothermic) while $\Delta U > 0$ indicates that it is not (endothermic).The energy of each state is calculated from the absolute energies of the molecules that comprise it, which are presented in Table 1.
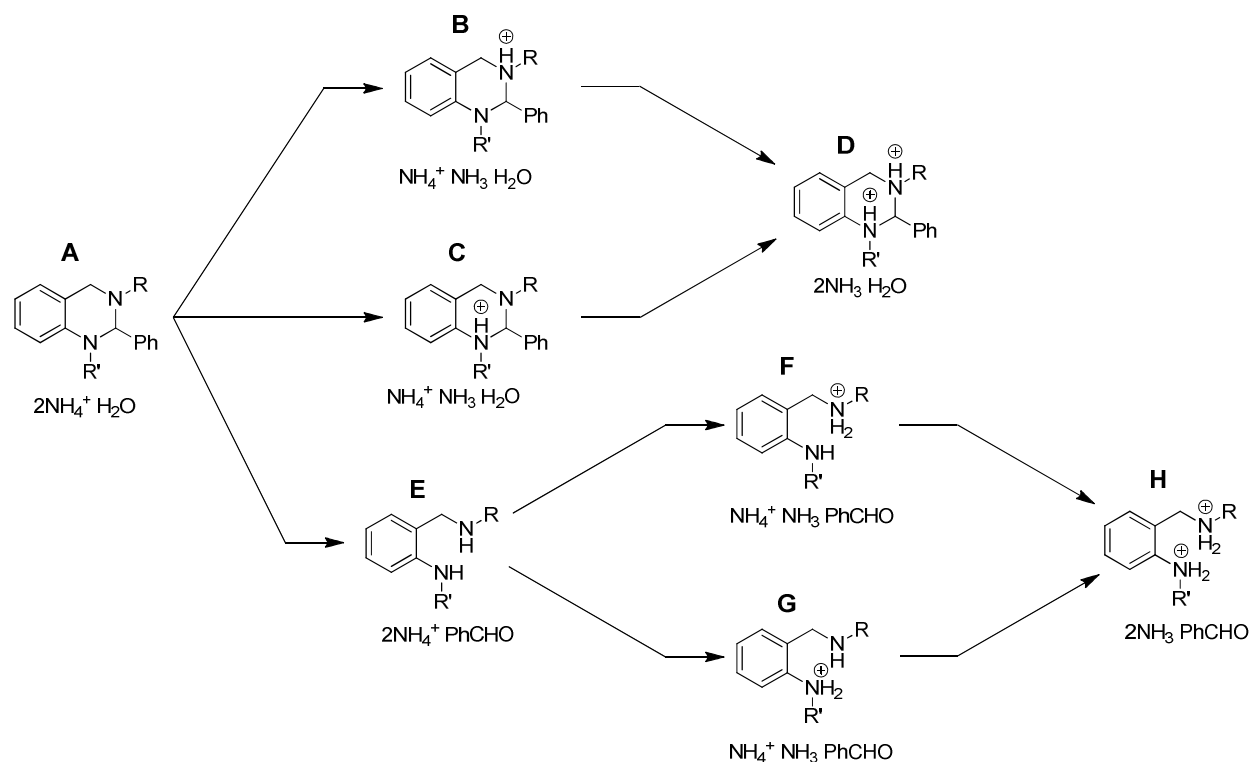

Table 2: Energy differences between states along the reaction pathway.

ΔU	Compound 8a:R = R′ = Me		Compound 13b: R = Me, R′ = i-Pr	
	B3LYP-D3 water (kcal/mol)	B3LYP-D3 gas (kcal/mol)	B3LYP-D3 water (kcal/mol)	B3LYP-D3 gas (kcal/mol)
B - A	4,68	-28,58	4,34	-30,24
C - A	13,47	-23,63	14,39	-25,36
D - B	31,36	71,33	33,19	66,46
D - C	22,56	66,37	23,15	61,58
E - A	3,11	2,78	-4,88	-6,72
F - E	-5,12	-35,89	-1,76	-32,64
G - E	-1,78	-34,75	2,08	-33,08
H - F	18,05	74,31	17,93	67,42
H - G	14,71	73,17	14,09	67,85
H - D	-20,00	-1,54	-26,25	-8,16
F - B	-6,69	-4,53	-10,99	-9,12
G - C	-12,14	-8,34	-17,20	-14,43

It is worthy to mention that in all calculations for both compounds, the N1 protonated open-ring diamine forms an intramolecular H bond, while the N3 protonated open-ring diamine of both compounds formed an intramolecular H bond only in the DFT optimization in gas phase.

MM Conformational Search:
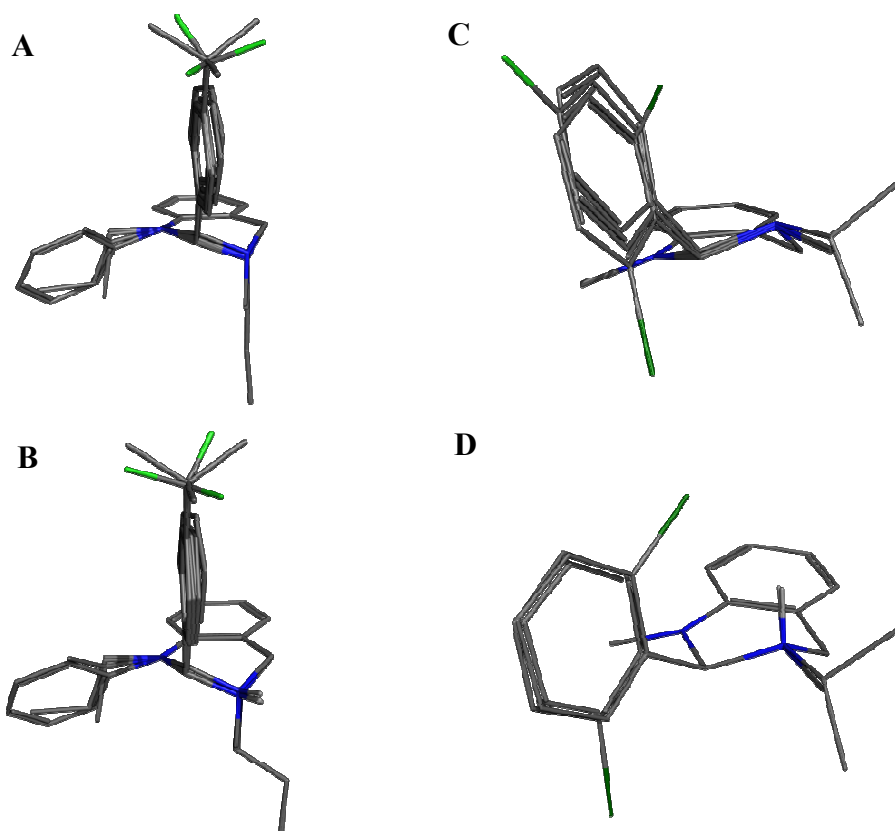
A: anti-axial conformation of minimal energy for neutral compounds (**8a-c,e**, **9a**, **13a-c**)
B: anti-axial conformation of minimal energy forN3 protonated compounds (**8a'-e'**, **9a'**, **13a'-c'**)
C: equatorial conformation of minimal energy for neutral compounds (**8d,f**, **9b**)
D: equatorial conformation of minimal energy for N3 protonated compounds (**8f'**, **9b'**)

| Compounds	Number of Conformers	RMSD (Å)$^\alpha$	Motif of minimum energy conformation$^\beta$
8a	2	0.0311	i (A)
8c	4	0.0207	i (A)
8d	2	0.0314	ii (C)
8b	4	0.0206	i (A)
8e	6	0.0187	i (A)
8f	5	0.0256	ii (C)
9a	74	0.0230	i (A)
9b	24	0.0331	ii (C)
9c	32	0.0208	i (E)
13a	69	0.0198	i (A)
13b	32	0.0283	i (A)
13c	27	0.0333	i (A)
8a'	4	0.0185	i (B)
8c'	9	0.0140	i (B)
8d'	4	0.0188	i (B)
8b'	9	0.0157	i (B)
8e'	9	0.0158	i (B)
8f'	3	0.0188	ii (D)
9a'	40	0.0115	i (B)
9b'	11	0.0178	ii (D)
9c N1 prot	22	0.0368	(F)
13a'	35	0.0156	i (B)
13b'	23	0.0216	i (B)
13c'	14	0.0298	i (B)
8a N1 prot	6	0.0258	(G)
13b N1 prot	20	0.0464	(G)
8a diprot (anti)	3	0.0494	(H)
13b diprot (anti)	13	0.0580	(H)

α: Mean value of the RMS for every conformer individually compared to the conformer of minimum energy after superposition.

β: i = anti-axial motif as described in the manuscript, ii = equatorial motif as described in the manuscript, () = letter corresponding to relative figure as presented in the Supporting Information.

Both the anti-axial and the equatorial conformers are found in all compounds, usually as next optimal conformation after the one of minimal energy. The energy difference between the respective other conformation is 2-5 kcal/mol.

In neutral compound **9c** the structure of minimal energy follows the anti-axial conformational motif, although N3 is more planar due to the presence of the phenyl group. The N1 protonated form of compound **9c** could not be superimposed with the rest of the compounds, as the protonation occurs in different atoms.

Conformers of minimal energy for **9c** neutral (**E**) and N1 protonated (**F**)
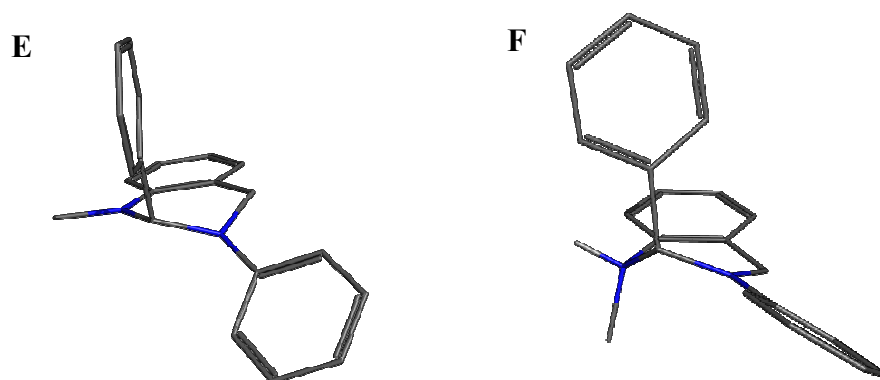
The systematic conformational search of the diprotonated compounds retained the protonated N stereoisomerism, therefore the syn- and anti- form of the N^+-H were both submitted for a conformational search and their minimal energy conformers were compared. The anti-conformer was of lower energy than the syn-, thus it was selected for the QM calculations.

Conformers of minimal energy for **8a** and **13b** N1 protonated (**G**) and anti-diprotonated (**H**)
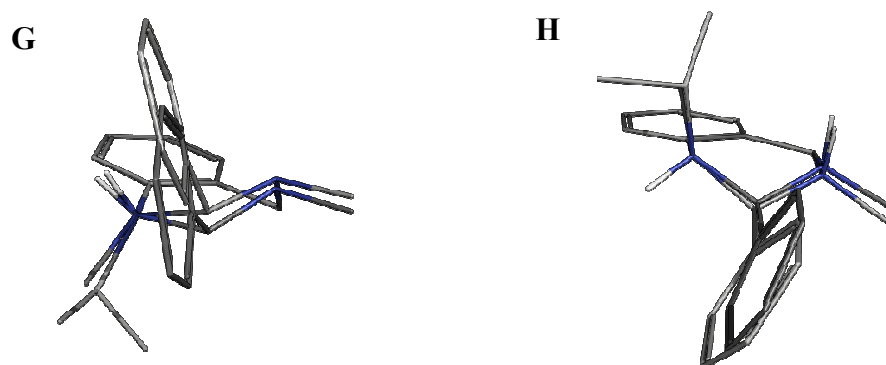
It is noteworthy to highlight that both the reference compound **8a** and the least stable compound **13b** share the same conformational motif in all cases - neutral from, N3 protonation, N1 protonation, diprotonation.

MM Ring Strain Comparison in Gas Phase

The energy values presented are calculated by: $\Delta U = U(\mathbf{Cpd\_mod}$ or $\mathbf{Cpd\_mod'}) - U(\mathbf{8a}$ or $\mathbf{8a'})$.

	8b_mod	8f_mod	9b_mod	13b_mod	13c_mod
ΔU [kcal/mol]					
gas					
neutral	0.71	3.61	3.74	3.09	4.90
protonated	0.81	0.48	0.74	3.6	5.84

	U (kcal/mol) gas	U (kcal/mol) water
8a	-4.46	-11.09
8a'	-58.85	-106.01
8b	13.72	8.99
8b_mod	-3.75	-10.35
8b'	-41.02	-86.19
8b'_mod	-58.04	-105.28
8f	-16.45	-23.88
8f_mod	-0.85	-9.62
8f'	-84.20	-127.68
8f'_mod	-58.37	-104.40
9b	-1.65	-8.52
9b_mod	-0.72	-9.00

9b'	-54.64	-97.10
9b'_mod	-58.11	-103.55
13b	1.28	-4.04
13b_mod	-1.37	-8.04
13b'	-52.27	-97.41
13b'_mod	-55.21	-102.51
13c	38.41	33.76
13c_mod	0.44	-5.82
13c'	-13.02	-60.89
13c'_mod	-53.01	-100.79

Additional References

[1]   Molecular Operating Environment (MOE), 2013.08; Chemical Computing Group Inc., 1010 Sherbooke St. West, Suite #910, Montreal, QC, Canada, H3A 2R7, 2015.

[2]   Halgren, T. A. *J. Comput. Chem.* **1996**, *17*, 490–519.

[3]   Goodman, J. M.; Still, W. C. *J. Comput. Chem.* **1991**, *12*, 1110–1117.

[4]   Halgren, T. A. *J. Comput. Chem.* **1999**, *20*, 720–729.

[5]   Becke, A. D. *J. Chem. Phys.* **1993**, *98*, 5648.

[6]   Lee, C.; Yang, W.; Parr, R. G. *Phys. Rev. B* **1988**, *37*, 785–789.

[7]   Vosko, S. H.; Wilk, L.; Nusair, M. *Can. J. Phys.* **1980**, *58*, 1200–1211.

[8]   Stephens, P. J.; Devlin, F. J.; Chabalowski, C. F.; Frisch, M. J. *J. Phys. Chem.* **1994**, *98*, 11623–11627.

[9]   Grimme, S.; Antony, J.; Ehrlich, S.; Krieg, H. *J. Chem. Phys.* **2010**, *132*, 154104.

[10]   Eichkorn, K.; Weigend, F.; Treutler, O.; Ahlrichs, R. *Theor. Chem. Accounts Theory, Comput. Model. (Theoretica Chim. Acta)* **1997**, *97*, 119–124.

[11]   Häser, M.; Ahlrichs, R. *J. Comput. Chem.* **1989**, *10*, 104–111.

[12]   Treutler, O.; Ahlrichs, R. *J. Chem. Phys.* **1995**, *102*, 346.

[13]   Kendall, R. A.; Dunning, T. H.; Harrison, R. J. *J. Chem. Phys.* **1992**, *96*, 6796.

[14]   Schäfer, A.; Huber, C.; Ahlrichs, R. *J. Chem. Phys.* **1994**, *100*, 5829.

[15]   Klamt, A.; Schüürmann, G. *J. Chem. Soc., Perkin Trans. 2,* **1993**, 799–805.

[16]   Milletti, F.; Storchi, L.; Sforna, G.; Cruciani, G. *J. Chem. Inf. Model.* **2007**, *47*, 2172–2181.